UNIVERSIDAD DE LAS PALMAS
DE GRAN CANARIA

Departamento de Química
y
Departamento de Bioquímica y Biología Molecular,
Fisiología, Genética e Inmunología

TESIS DOCTORAL

EVALUACIÓN DE NUEVOS COMPUESTOS COMO POTENCIALES AGENTES ANTILEUCÉMICOS

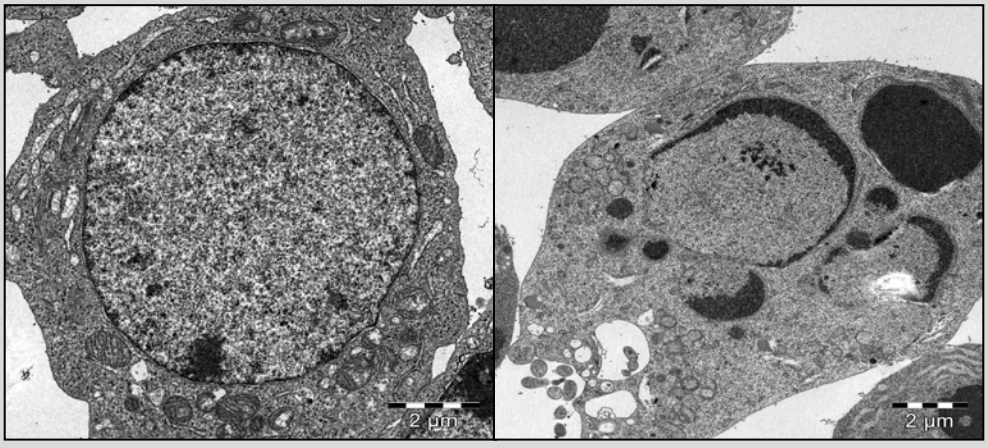

Fernando Torres Andón

Las Palmas de Gran Canaria
2010

UNIVERSIDAD DE LAS PALMAS
DE GRAN CANARIA

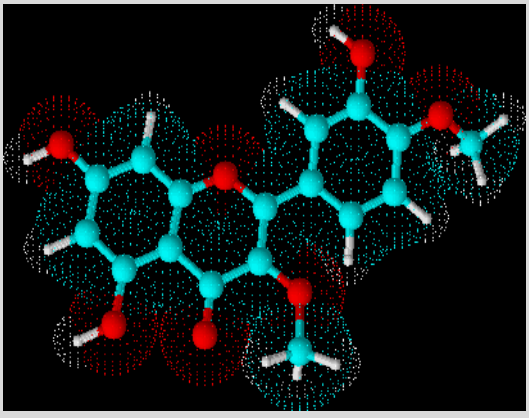

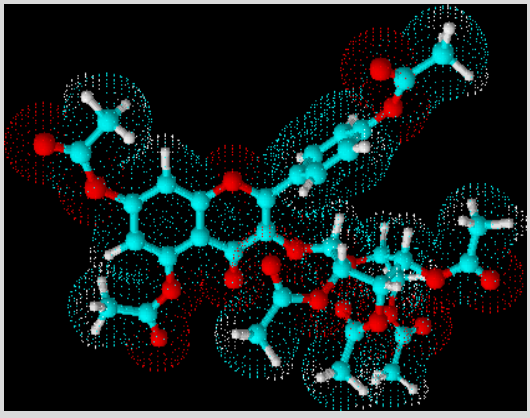

El tratamiento del cáncer ha evolucionado mucho en los últimos años y aunque se ha conseguido aumentar la supervivencia frente a algunos tipos de cáncer, no se ha logrado la efectividad deseada debido fundamentalmente a una limitada actividad terapéutica o a una excesiva toxicidad. La lucha contra esta enfermedad sólo podrá solucionarse seleccionando las mejores dianas terapéuticas. Las neoplasias hematológicas forman uno de los grupos de cáncer más estudiados y el análisis de los mecanismos implicados en la supervivencia o muerte de estas células tumorales ha proporcionado en numerosas ocasiones nuevas dianas terapéuticas eficaces en el tratamiento de éste y otros tipos de cáncer.

Los principios activos obtenidos de fuentes naturales o sus derivados semisintéticos han dado lugar a los principales fármacos utilizados contra el cáncer. Los flavonoides son compuestos con una estructura fenilbenzo-γ-pirona de origen natural, que abundan en frutas, verduras y bebidas derivadas de plantas, y además poseen propiedades antitumorales. Los datos del presente estudio proporcionan evidencias acerca del mecanismo por el que el trifolín acetato y la 3´,5,7-trihidroxi-3,4´-dimetoxiflavona inducen apoptosis en diferentes líneas celulares tumorales humanas y sientan las bases científicas para la utilización de estos compuestos en el desarrollo de nuevos fármacos antitumorales.

UNIVERSIDAD DE LAS PALMAS
DE GRAN CANARIA

Departamento de Química

UNIVERSIDAD DE
LAS PALMAS DE GRAN CANARIA
DPTO. DE QUÍMICA
12 ABR. 2010
Número 74
SALIDA

Dª ZORAIDA SOSA FERRERA, SECRETARIA DEL DEPARTAMENTO DE QUÍMICA DE LA UNIVERSIDAD DE LAS PALMAS DE GRAN CANARIA,

CERTIFICA,

Que en la comisión de Doctores del departamento en su sesión de fecha 09 de Abril de 2010 tomó el acuerdo de dar el consentimiento para su tramitación, a la tesis doctoral titulada *"EVALUACIÓN DE NUEVOS COMPUESTOS COMO POTENCIALES AGENTES ANTILEUCÉMICOS"*

Cuya memoria está escrita en castellano e incluye un resumen en inglés en forma y estructura de acuerdo con el artículo 2º del reglamento vigente para la elaboración, tribunal, defensa y evaluación de tesis doctorales con opción a la solicitud de acreditación de doctorado europeo de la Universidad de Las Palmas de Gran Canaria.

Presentada por el doctorando D. FERNANDO TORRES ANDÓN y dirigida por los doctores D. FRANCISCO ESTÉVEZ ROSAS Y D. JOSE QUINTANA AGUIAR.

Y para que así conste, y a efectos de lo previsto en el Artº 73.2 del Reglamento de Estudios de Doctorado de esta Universidad, firmo la presente en

Las Palmas de Gran Canaria, a 12 de abril de 2010

UNIVERSIDAD DE LAS PALMAS DE GRAN CANARIA
DPTO DE QUIMICA

UNIVERSIDAD DE LAS PALMAS
DE GRAN CANARIA

UNIVERSIDAD DE LAS PALMAS DE GRAN CANARIA

Departamento:

DEPARTAMENTO DE QUÍMICA
Y
DEPARTAMENTO DE BIOQUÍMICA Y BIOLOGÍA MOLECULAR, FISIOLOGÍA, GENÉTICA E INMUNOLOGÍA

Programa de Doctorado:

Obtención, Preparación y Evaluación Biológica de Fármacos de Origen Marino y Terrestre
(Programa Interdepartamental)

TÍTULO

EVALUACIÓN DE NUEVOS COMPUESTOS COMO POTENCIALES AGENTES ANTILEUCÉMICOS

Title

EVALUATION OF NEW COMPOUNDS AS POTENTIAL ANTILEUKEMIA AGENTS

Memoria para optar al grado de Doctor por la Universidad de Las Palmas de Gran Canaria presentada por el Licenciado: D. Fernando Torres Andón

---

El Doctorando	El Director	El Director
D. Fernando Torres Andón	**Dr. Francisco Estévez Rosas**	**Dr. José Quintana Aguiar**

Las Palmas de Gran Canaria, a 26 de Marzo de 2010

D. FRANCISCO ESTÉVEZ ROSAS, PROFESOR TITULAR DEL DEPARTAMENTO DE BIOQUÍMICA Y BIOLOGÍA MOLECULAR, FISIOLOGÍA, GENÉTICA E INMUNOLOGÍA DE LA UNIVERSIDAD DE LAS PALMAS DE GRAN CANARIA.

CERTIFICA,

Que D. Fernando Torres Andón, licenciado en Farmacia por la Universidad de Santiago de Compostela, ha realizado bajo mi dirección y asesoramiento el trabajo de investigación titulado:

EVALUACIÓN DE NUEVOS COMPUESTOS COMO POTENCIALES AGENTES ANTILEUCÉMICOS

Una vez revisada la presente memoria, escrita en castellano y que incluye un resumen en inglés en forma y estructura acorde con el artículo 2º del reglamento vigente para la elaboración, tribunal, defensa y evaluación de tesis doctorales de la Universidad de Las Palmas de Gran Canaria, la encuentra apta para su defensa pública ante tribunal para la obtención del título de Doctor con mención de Doctorado Europeo por la Universidad de Las Palmas de Gran Canaria.

Para que así conste y surta los efectos oportunos, extiende la presente certificación en

Las Palmas de Gran Canaria, a 26 de Marzo de 2010.

Fdo. D. Francisco Estévez Rosas

D. JOSÉ QUINTANA AGUIAR, PROFESOR TITULAR DEL DEPARTAMENTO DE BIOQUÍMICA Y BIOLOGÍA MOLECULAR, FISIOLOGÍA, GENÉTICA E INMUNOLOGÍA DE LA UNIVERSIDAD DE LAS PALMAS DE GRAN CANARIA.

CERTIFICA,

Que D. Fernando Torres Andón, licenciado en Farmacia por la Universidad de Santiago de Compostela, ha realizado bajo mi dirección y asesoramiento el trabajo de investigación titulado:

EVALUACIÓN DE NUEVOS COMPUESTOS COMO POTENCIALES AGENTES ANTILEUCÉMICOS

Una vez revisada la presente memoria, escrita en castellano y que incluye un resumen en inglés en forma y estructura acorde con el artículo 2º del reglamento vigente para la elaboración, tribunal, defensa y evaluación de tesis doctorales de la Universidad de Las Palmas de Gran Canaria, la encuentra apta para su defensa pública ante tribunal para la obtención del título de Doctor con mención de Doctorado Europeo por la Universidad de Las Palmas de Gran Canaria.

Para que así conste y surta los efectos oportunos, extiende la presente certificación en

Las Palmas de Gran Canaria, a 26 de Marzo de 2010.

Fdo. D. José Quintana Aguiar

“¿Que cómo veo el futuro?...

El futuro no se ve, el futuro se hace.”

J. M. Keynes

Este trabajo ha sido financiado por:

- Ministerio de Educación y Ciencia de España y FEDER. Plan Nacional de Biomedicina. SAF 2004-07928 y SAF 2007-62536.
- Subvención para equipamiento e infraestructura científico-tecnológica.Dirección General de Universidades e Investigación. Resoluciones de 21 de diciembre de 2006 y 21 de diciembre de 2007.
- Beca del Gobierno Autónomo de Canarias. Resolución de 30 de diciembre de 2005. BOC 7 feb 2006.
- Consejería de Educación, Cultura y Deportes. Gobierno de Canarias y FEDER. GRUP 2004-44.
- Agencia Canaria de Investigación, Innovación y Sociedad de la Información del Gobierno de Canarias. PI 2007/045.
- Instituto Canario de Investigación del Cáncer. RED PRODNATCANCER- 2008 y 2009.

Ilustración de portada: Microfotografías de una célula HL-60 normal (izquierda) y una célula en apoptosis (derecha) obtenida mediante microscropía electrónica de transmisión.

Ilustración de contraportada: Estructura química de la 3´,5,7-trihidroxi-3,4´-dimetoxiflavona (izquierda) y del trifolín acetato (derecha).

ÍNDICE

AGRADECIMIENTOS

En primer lugar, me gustaría dar las gracias a mis directores de tesis, Dr. Francisco Estévez Rosas y Dr. José Quintana Aguiar, por introducirme en el mundo de la investigación. Gracias por haber compartido conmigo sus conocimientos y su pasión por la investigación, por su ayuda y dedicación en el trabajo diario.

Quiero agradecer a todos los que son o han sido compañeros de laboratorio, personas que han seguido más de cerca y saben perfectamente lo que conlleva la lectura de esta tesis. Hago especial mención a Sara y a Gledy por su amistad y ayuda a lo largo de estos años. Gracias a Olga, Carol, Ana, Cristina, Fabio, Mayte, Dionisio y Juan, por haberme acompañado durante estos años, por su ayuda, amistad y por traer el buen humor a estas cuatro paredes.

Merci à mes collègues de la Faculté de Pharmacie de l'Université Paris-Sud 11, Aida, Jöel e spécialement à la Dr. Jacqueline Bréard par vivre chaque découverte comme un grand événement et de m'avoir contaminés sa illusion.

Gracias al Dr. Javier Cabrera, y al Dr. Juan Francisco Loro por su inestimable ayuda y consejos en los inicios de mi trabajo, a la Dra. Mª del Pino Santana, a la Dra. Inmaculada Servanda Hernández, al Dr. Ignacio Javier González, al Dr. Enrique Castro, al Dr. Germán Gallardo, y al Dr. Carlos Tabraue por haber sido un gran apoyo en estos años, por sus consejos y por haberme ayudado a resolver todo tipo de problemas. También quiero agradecer su ayuda a Jose Manuel Pérez y Olivia Rodriguez, del Servicio de Microscopía Electrónica.

Grazas aos meus amigos, Fernando, Fran, Luis, David y Joana, Pipo, Juanma, Iván, Jacobo, Mariña, Jose Carlos, Pedro y Marcos… porque hai cousas mellores que o traballo. Y sobre todo gracias a lo mejor que me pasó durante esta tesis, gracias Ana por cada segundo que estás conmigo, por tu cariño, alegría y por todo lo que nos queda por vivir. Gracias por ayudarme tanto y por hacerme conocer a tu familia, que me hacen sentir uno más.

Finalmente, quero dar as grazas á miña familia, que sempre me axudou, aínda dende a distancia. Grazas Suso e Nati, porque grazas ao voso esforzo puiden chegar ata aquí. Grazas David pola túa paciencia e por axudarme sempre que o necesitei. Grazas aos meus avós, Xosé e Concha, Suso e Benjamina; e aos meus tíos, Conchi, Pili e Manel, por ser parte da miña educación e da miña vida. Grazas a Luís Miguel, Bruno, Pedro e Sara por renovar a ledicia da familia.

ABREVIATURAS

$\Delta\Psi_m$	Potencial de membrana mitocondrial
μM	Micromolar
ADN	Ácido desoxirribonucleico
AIF	Factor inductor de apoptosis
Akt	Quinasa involucrada en la supervivencia celular
Apaf-1	Factor activador de proteasas apoptóticas
ARC	Inhibidor general de la apoptosis
ARN	Ácido ribonucleico
ATP	Adenosín trifosfato
Bad	Proteína pro-apoptótica perteneciente a la familia Bcl-2
Bak	Proteína pro-apoptótica perteneciente a la familia Bcl-2
Bax	Proteína pro-apoptótica perteneciente a la familia Bcl-2
Bcl-2	Proteína anti-apoptótica
Bcl-x_L	Proteína anti-apoptótica perteneciente a la familia Bcl-2
Bid	Proteína pro-apoptótica
BIR	Dominio de interacción proteína-proteína presente en las IAP_S
CAK	Proteína quinasa constitutiva activadora de CDK
CARD	Dominio de reclutamiento de caspasa
CAT	Catalasa
CCCP	Carbonil Cianuro m-Clorofenil- Hidrazona
CDK	Proteína quinasa dependiente de ciclina
CIP	Proteínas inhibidoras de CDKs
CKI	Inhibidores de las quinasas dependientes de ciclinas
CoA	Coenzima A
DAG	Diacilglicerol
DED	Dominio efector de muerte
DETAPAC	Ácido dietilen-triamina-penta-acético
DEVD-*p*NA	Sustrato específico de caspasa -3/-7
DGK	Diacilglicerol quinasa
DISC	Complejo inductor de muerte
DMSO	Dimetilsulfóxido
DNA-PK	Proteína quinasa dependiente de ADN
DTT	Ditiotreitol
EDTA	Ácido etilen-diamin-tetra-acético
EGFR	Receptores del factor de cremiento epidérmico
EGTA	Ácido etilenglicol-bis-N,N'-tetraacético
ERK1/2	Proteína quinasa regulada por señales extracelulares 1 y 2
ETO	Etopósido
FADD	Dominio de muerte asociado a Fas
Fas	Receptor de muerte, también llamado Apo1 o CD95
FasL	Ligando del receptor de muerte Fas
FBS	Suero bovino fetal
GlcCer	Glucosilceramida
GPCR	Receptor asociado a proteína G
GTP	Guanosín trifosfato
GW4869	Inhibidor de la esfingomielinasa neutra
H_2-DCF-DA	Diacetato 2´,7´-dicloro-dihidro-fluoresceína
HEPES	N-[2-hidroxietil] piperazino N'-[2-etanosulfanílico]
IAP	Proteína inhibidora de apoptosis
IC_{50}	Concentración de producto que inhibe el crecimiento celular a la mitad
IP	Yoduro de propidio
JC-1	Yodurode5,5',6,6'–tetracloro-1,1',3,3'-tetraetilbenzimidazolocarbocianina

JNK	Proteína quinasa N-terminal de jun
Jun	Factor de transcripcion de la familia de AP-1
MAPK	Proteina quinasa activada por mitógenos
MEK	Proteína quinasa MAPK
MIF	Factor inhibitorio de la migración
MK	Proteínas quinasas activadas por MAPKs
MKP	MAP quinasas fosfatasas
MMP	Metaloproteinasa de la matriz extracelular
MSK	Proteína quinasa activada por mitógenos y estrés
MTT	Bromuro de 3-[4,5- Dimetiltiazol-2-il]-2,5-difeniltetrazolio
MYT1	Factor de transcripción de mielina
Na_3VO_4	Ortovanadato sódico
NAC	N-acetil-L-cisteína
NaCl	Cloruro de sodio
NADPH	Nicotinamida adenina dinucleótido fosfato
NaOH	Hidróxido de sodio
NF-κB	Factor nuclear - κB
NO	
p21	Inhibidor de quinasas dependientes de ciclinas
$p38^{MAPK}$	
p53	Proteína supresora de tumores
PA	Plasminógeno tisular
PARP-1	Poli (ADPribosa) polimerasa-1
PBMC	Células mononucleares humanas de sangre periférica
PBS	Tampón fosfato salino
PD98059	Inhibidor específico de la quinasa reguladora MEK1
PHA	Fitohemaglutinina
PI3K	Fosfatidil inositol 3quinasa
PK	Proteína quinasa
PL	Fosfolipasa
PMSF	Fluoruro de metilsulfonilfenilo
pRB	Proteína retinoblastoma
PVDF	Fluoruro de Poli-vinilideno
Raf	MAPKKK
Ras	Proteína G pequeña
RING	Dominio interacción proteína-proteína
RIP	Proteína de interacción con el receptor
ROS	Especies reactivas de oxígeno
RTK	Receptores de tirosina quinasas
S1P	Esfingosina 1-fosfato
SB203580	Inhibidor específico de $p38^{MAPK}$
SDS	Dodecil sulfato sódico
Ser	Serina
SIDA	Síndrome de inmunodeficiencia adquirida
SK	Esfingosina quinasa
Smac	Segundo activador de caspasas derivado de la mitocondria
SMasa	Esfingomielinasa
SOD	Superóxido dismutasa
SOS	Factor de intercambio de nucleótidos de guanina
SP600125	Inhibidor específico de JNK
TA	Trifolín heptaacetato
TBST	20 mM Tris-HCl (pH 7,5), 137 mM NaCl, 0,1 % Tween-20
TEMED	N,N,N,N,-tetrametil-etilendiamina
THDF	3´,5,7-Trihidroxi-3,4´-dimetoxiflavona

Thr	Treonina
TLC	Cromatografia en capa fina.
TNF	Factor de necrosis tumoral
TNFR1	Receptor 1 del factor necrótico tumoral
TRADD	Dominio de muerte asociado al TNFR
TRAF2	Factor asociado a al receptor de TNF
TRAIL	Ligando inductor de apoptosis relacionado con TNF
U0126	Inhibidor selectivo de las quinasa reguladoras MEK1 y MEK2
UV	Ultravioleta
VEGF	Factor de crecimiento endotelial vascular
Wee1	Tirosina quinasa Wee1
XIAP	Proteína inhibidora de la apoptosis
z-DEVD-fmk	Inhibidor específico de caspasa-3 y -7
z-IETD-fmk	Inhibidor específico de caspasa-8
z-LEHD-fmk	Inhibidor específico de caspasa-9
z-VAD-fmk	Inhibidor general de caspasas
z-VDVAD-fmk	Inhibidor específico de caspasa-2
z-VEID-fmk	Inhibidor específico de caspasa-6
z-YVAD-fmk	Inhibidor específico de caspasa-1

FIGURAS Y TABLAS

INTRODUCCIÓN

RESULTADOS

INTRODUCCIÓN

El cáncer puede ser considerado una epidemia. Su incidencia y prevalencia están aumentando rápidamente, debido entre otras causas, al crecimiento y envejecimiento de la población. Alrededor de 2,3 millones de nuevos casos de cáncer se contabilizaron en la Unión Europea en el año 2006, y el número de casos aumenta cada año. Una de cada cuatro muertes en la Unión Europea se atribuye al cáncer, y en el rango de edad entre 45 y 64 años, la proporción es cercana al 50% [1]. Proporciones similares se han observado en los Estados Unidos, dónde se detectaron en el año 2009 un total de 1,5 millones de casos y alrededor de 500.000 muertes [2]. La Organización Mundial de la Salud ha estimado que alrededor de 12 millones de personas morirán, en todo el mundo, a causa de esta enfermedad en el año 2030 [3].

El cáncer se produce como consecuencia de una acumulación de errores en el material genético de las células, que adquieren la capacidad de propagarse de forma indefinida (generando sus propias señales mitógenas), en su localización normal o en otras zonas (invadiendo otros tejidos y/o produciendo metástasis), como consecuencia de una pérdida de control de su proliferación, diferenciación o de la respuesta ante señales de apoptosis (muerte celular programada).

Existen más de 200 tipos diferentes de cáncer, la mayoría de los cuales deben su nombre al órgano o al tejido en el que se forman, y pueden ser agrupados en las siguientes categorías:

- **Carcinoma** – tejido epitelial.
- **Sarcoma** – tejido conjuntivo (hueso, cartílago, grasa, músculo, vasos sanguíneos u otros).
- **Glioma** – tejido nervioso.
- **Neoplasias hematológicas (Leucemia, Linfoma y Mieloma)** – tejido sanguíneo, médula ósea y ganglios linfáticos.
- **Otros** – melanoma, hepatoma, etc.

En la mayoría de estos tipos de cáncer las células no se mueren y se forman nuevas células innecesarias para el organismo, formando una masa llamada tumor (“tumor maligno”). En cambio algunos tipos de cáncer, como la leucemia, pueden no formar un tumor.

La leucemia es un grupo de enfermedades de la médula ósea y de la sangre, que implica un aumento incontrolado de glóbulos blancos (leucocitos). Es el cáncer más frecuente en los

niños menores de 15 años a nivel mundial [4], y en Estados Unidos en hombres menores de 40 años y mujeres menores de 20 años [2]. De acuerdo con la población leucocitaria que afecten, se clasifican en: leucemia mieloide crónica, leucemia linfoide crónica, leucemia linfoide aguda, leucemia mieloide aguda ó leucemia de células pilosas.

1. Tratamiento del cáncer.

1.1. Selección de nuevas dianas terapéuticas.

El tratamiento del cáncer ha evolucionado mucho en los últimos años, y se ha conseguido aumentar la supervivencia frente a algunos tipos de cáncer (por ejemplo, leucemias o linfomas), pero no se ha conseguido la efectividad deseada debido fundamentalmente a una insuficiente actividad terapéutica (30%) ó a una excesiva toxicidad (30%). Estos problemas sólo podrán solucionarse seleccionando las mejores dianas terapeúticas y mediante el uso de biomarcadores para identificar a los pacientes apropiados para recibir cada tratamiento [5,6].

El conocimiento de los mecanismos moleculares implicados en el cáncer ha mejorado de forma significativa, y actualmente, el desarrollo de nuevos fármacos antitumorales está dirigido al estudio de los mecanismos moleculares y genéticos implicados, con el objetivo de desarrollar una medicina “personalizada”. La activación de oncogenes y la inactivación de genes supresores de tumores en la célula tumoral implican una modificación de las vías de señalización induciendo: la falta de respuesta frente a factores homeostáticos, la pérdida del control del ciclo celular y la proliferación descontrolada, el aumento de la supervivencia celular, la disminución de la apoptosis, la inmortalización y la estimulación de procesos como invasión, angiogénesis y metástasis (propagación a otras partes del cuerpo por vía sanguínea o linfática). Todos estos procesos presentan potenciales dianas desde el punto de vista de una intervención terapéutica [7].

El gran avance que se ha producido en el conocimiento de la muerte celular por apoptosis, mecanismo mediante el cual las células son eliminadas con el propósito de controlar la proliferación celular ó en respuesta a un daño en el ADN, nos proporciona las líneas a seguir en el desarrollo de nuevas terapias dirigidas, induciendo la muerte de las células tumorales de forma específica o sensibilizándolas frente a los tratamientos antitumorales actuales.

Las neoplasias hematológicas forman uno de los grupos de cáncer más estudiados. En 1980 se descubrió que los glucocorticoides inducen fragmentación del ADN y apoptosis en los timocitos, y desde entonces el sistema hematopoyético ha desvelado numerosas situaciones en

las que los mecanismos de muerte celular resultan clave en el control de la homeostasis. El análisis de este mecanismo ha proporcionado nuevas dianas terapéuticas eficaces en el tratamiento de este y otros tipos de cáncer [8]. Entre las neoplasias hematológicas, la leucemia mieloide crónica es una de las más estudiadas, y constituye uno de los mejores ejemplos de cómo una enfermedad puede ser tratada mediante una terapia dirigida a una diana molecular específica. El tratamiento con Imatinib ha supuesto una importante mejora en la lucha contra la enfermedad y además ha sido utilizado en el tratamiento de otros tipos de cáncer [9,10] (tumores del estroma gastrointestinal).

El esfuerzo realizado en la identificación de nuevas dianas terapéuticas ha tenido en los últimos años múltiples frutos, ejemplos de ello son: el Bortezomib, tratamiento de elección en mieloma múltiple, el Trastuzumab de aplicación en cáncer de mama, ó el Cetuximab que se utiliza en el tratamiento del cáncer de colon metastásico con sobreexpresión de receptores del factor de crecimiento epidérmico (EGFR) [7].

1.2. Utilización de fármacos de origen natural.

En la búsqueda de nuevos fármacos antitumorales no debemos olvidarnos de los productos naturales. Las plantas han sido utilizadas con fines médicos durante miles de años y la búsqueda de nuevos compuestos activos de origen natural se ha intensificado en la última década [11]. De todos los fármacos antitumorales descubiertos entre 1940 y 2002, el 40% fueron productos naturales o derivados.

El área de la fitoterapia tiene una influencia cada vez mayor en la nutrición y en el control de enfermedades. Los compuestos fitoquímicos, también llamados compuestos bioactivos, tienen efectos beneficiosos para la salud cuando se usan de forma adecuada con el objetivo de modificar ciertas actividades fisiológicas ó celulares, y presentan la gran ventaja, de que se consideran seguros farmacológicamente. No son esenciales para la vida, aparecen en pequeñas cantidades en los alimentos y sus efectos sobre la salud son sutiles. Debido a su potencial aplicación en la prevención y curación de algunas enfermedades crónicas, existe un gran interés en el estudio de sus efectos sobre la salud y la elucidación de los mecanismos que median sus efectos [12].

Desde la secuenciación del genoma humano, se han identificado miles de nuevas dianas moleculares en diferentes enfermedades [13], que junto con los ensayos de alto rendimiento,

hacen que el análisis de las dianas moleculares sobre las que pueden actuar estos compuestos resulte esencial para la identificación de nuevos fármacos.

A lo largo de la historia se ha identificado una gran variedad de compuestos químicos en frutas, verduras y semillas [14], y de entre ellos, los flavonoides son los compuestos fitoquímicos más abundantes. Su amplia bioactividad y su elevada presencia en nuestra dieta los hace merecedores de la atención de la investigación farmacológica.

2. Flavonoides.

Los flavonoides son un grupo de compuestos con una estructura común fenil benzo–γ-pirona (C6-C3-C6), que podemos encontrar en muchas plantas, como producto de su metabolismo secundario, siendo abundantes en las *Poligonaceae, Rutaceae, Leguminosae, Umbelliferae* y *Compositae*. Podemos clasificarlos fijándonos en los carbonos que forman la estructura común: antocianidinas (rojo, púrpura o azul), flavanonas, flavanoles (o catequinas), flavonas, flavonoles y sus glucósidos (amarillo pálido ó color marfil); e isoflavonas (sin color) [15].

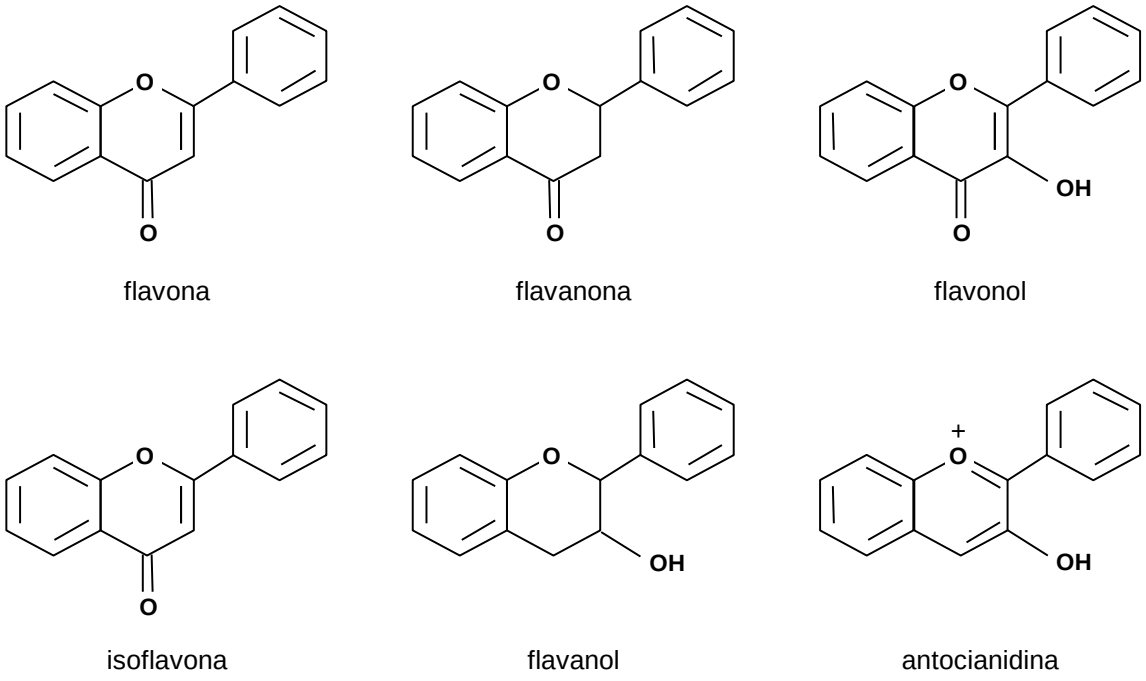

Figura 1. Clasificación de los flavonoides.

En las plantas los flavonoides se encuentran en estado libre o unidos a azúcares formando heterósidos, que es lo más frecuente debido a que les confiere una mayor estabilidad química.

Estos heterósidos son polares por lo tanto son generalmente solubles en agua; se extraen y se solubilizan en disolventes polares: agua o etanol.

2.1. Fuentes de flavonoides y su presencia en la dieta.

Se han identificado alrededor de 9.000 flavonoides [16], que podemos encontrar en frutas, verduras, semillas y flores, así como en cerveza, vino, té verde, té negro y soja, los cuales se consumen en la dieta humana de forma habitual y también se utilizan en forma de suplementos nutricionales, junto con ciertas vitaminas y minerales. Los flavonoides se encuentran también en extractos de plantas como arándano, Gingko biloba, cardo-mariano o crataegus. Se ubican principalmente en las partes aéreas de las plantas, a excepción de los tubérculos de cebolla, que contienen una gran cantidad de quercetina.

Los hábitos alimenticios son muy diversos en el mundo, pero el valor medio de ingesta de flavonoides se estima en torno a 23 mg/día [17], predominando los flavonoles, especialmente la quercetina. Las fuentes alimenticias principales de flavonoles son: el té negro, las cebollas, las manzanas, la pimienta negra y bebidas alcohólicas como el vino y la cerveza. En la dieta, el té es una de las fuentes principales de quercetina, principalmente en Japón y los Países Bajos, el vino tinto lo es en Italia, Francia, España y las cebollas en los Estados Unidos y Grecia.

La ingesta promedio de flavonoles y flavonas se sitúa entre los 20 y 26 mg/día [18,19,20], excediendo a la de otros antioxidantes en la dieta, como el beta-caroteno (2-3 mg/día) y la vitamina E (7-10 mg/día) mientras que es aproximadamente un tercio de la vitamina C (70-100 mg/día). Así, pues los flavonoides representan una contribución importante al potencial antioxidante de la dieta humana.

2.2. Absorción, metabolismo y actividad.

Los flavonoides que ingerimos en la dieta son absorbidos en el tracto gastrointestinal, mientras que los utilizados con fines médicos son administrados directamente en el tejido enfermo si es accesible, y luego son excretados en heces y sobre todo en orina. La transformación de los flavonoides tiene lugar en dos localizaciones: en primer lugar en el hígado, por medio de reacciones de biotransformación de fase I en las que se introducen o exponen grupos polares; en segundo lugar en el colon mediante reacciones de biotransformación de fase II, en las que los microorganismos degradan los flavonoides no absorbidos [18]. La conjugación con el ácido glucurónico, sulfatos, o glicina, parecen tener

lugar tanto para los flavonoides como para sus metabolitos procedentes del colon, y los conjugados, solubles en agua, pueden excretarse por la orina [21]. La biodisponibilidad es uno de los factores más importantes a tener en cuenta al evaluar los efectos biológicos de los flavonoides, así como de cualquier fármaco o componente alimenticio.

En cuanto a su actividad, los flavonoides cumplen funciones metabólicas importantes en las plantas: protección frente a la luz UV, defensa ante los herbívoros, regulación del transporte de la hormona auxina, atracción de animales polinizadores, atracción de presas, inducción de la nodulación por parte de las bacterias fijadoras de nitrógeno, protección contra hongos [22].

En los seres humanos, muestran un gran espectro de actividades biológicas, haciéndose posible su aplicación en [22,23]: hipertensión y microedemas, inflamación, diabetes, como antioxidantes, como anestésicos locales, pérdida de tejido conectivo, alergia, asma, úlceras gastrointestinales, enfermedades reumáticas, infecciones bacterianas, propiedades antivirales, alzheimer, regeneración tisular, hipercolesterolemia, estimulación del sistema inmune, profilaxis o terapia del síndrome de inmunodeficiencia adquirida (SIDA), o fertilidad. Sus aplicaciones más importantes, y más estudiadas son las relacionadas con las enfermedades cardiovasculares [24,25] y el cáncer, enfermedades que según la última clasificación de la Organización Mundial de la Salud son la primera y la tercera causas de muerte en el mundo [26].

2.3. Utilización de flavonoides contra el cáncer.

Una amplia variedad de alimentos, especialmente frutas, contienen flavonoides que poseen propiedades contra el cáncer [23,27]. Numerosos estudios epidemiológicos han demostrado que existe una relación inversa entre el consumo de flavonoides y el riesgo de desarrollar un cáncer [28,29,30,31]. Estudios experimentales y ensayos clínicos han indicado que poseen efectos importantes en la prevención y tratamiento del cáncer, siendo capaces de interferir en las cuatro etapas de la carcinogénesis: iniciación, promoción, progresión e invasión [32].

Los flavonoides modulan la acción y biosíntesis de varios citocromos P450 (CIPs) que están implicados en el cáncer y en el metabolismo de fármacos, aumentando su interés como potenciales agentes terapéuticos [12]. Existen estudios que afirman que son capaces de inhibir la activación de la carcinogénesis, inhibir la proliferación de las células cancerígenas, inducir parada del ciclo celular, inducir apoptosis de forma selectiva en las células tumorales, inducir diferenciación celular, inhibir la metástasis y la angiogénesis, activar la respuesta inmune

frente a las células tumorales, y además, pueden presentar efectos antioxidantes y/o modular la resistencia a fármacos [32].

Algunos de los mecanismos mediante los cuales inducen los anteriores efectos implican: inhibición de la actividad ADN topoisomerasa I/II, modificación de la generación de especies reactivas de oxígeno (ROS), indución de la oxidación y fragmentación del ADN, modulación de las vías celulares de supervivencia y/o proliferación, liberación de citocromo *c* al citoplasma celular con la consiguiente activación de caspasa-9 y caspasa-3, aumento de los niveles de caspasa-8 y t-Bid, disminución de la expresión de las proteínas Bcl-2 y Bcl-x_L y aumento de la expresión de Bax y Bak, aumento del plasminógeno tisular (PA) y u-PA, disminución del factor de crecimiento endotelial vascular (VEGF) y/o los niveles de metaloproteinasas de la matriz extracelular (MMPs), aumento del factor inhibitorio de la migración (MIF), y modulación del factor nuclear κB (NF-κB) [33].

En este contexto, la apoptosis constituye un mecanismo fisiológico para la eliminación de células anormales, y la indución de este tipo de muerte celular en un tumor, junto con la inhibición de su proliferación, son las principales metas en la lucha contra el cáncer [33,34,35].

3. Inhibición de la proliferación celular.

3.1. Inducción de la parada del ciclo celular.

En los últimos años, el avance en el conocimiento de las relaciones moleculares entre muerte, supervivencia y ciclo celular ha sido espectacular. El ciclo celular de una célula eucariota está dividido en cuatro fases [36]:

- En la fase G_1 la célula se está preparando para la síntesis de ADN, la célula está creciendo y las células diploides tienen 2n cromosomas.

- En la siguiente fase, S, se produce la duplicación del ADN (4n).

- En la fase G_2 se produce un crecimiento celular y las células se preparan para su división.

- En la fase M (mitosis), las células se separan en dos células hijas.

Las células en fase G_0 (quiescentes), permanecen fuera del ciclo celular. Existen mecanismos de control para evitar una proliferación inadecuada, y las proteínas clave en la regulación del

paso de una fase del ciclo celular a la siguiente son las quinasas dependientes de ciclina (CDKs), una familia de serina/treonina proteínquinasas que se activan en puntos específicos del ciclo celular mediante fosforilación y asociación a las ciclinas [37].

Los niveles de ciclinas activas van cambiando en las diferentes fases del ciclo celular, mientras los niveles de CDKs permanecen estables [38]. La expresión de las ciclinas D1, D2, D3 y C aumenta en la transición desde la fase G_0 a la S. Las ciclinas D1, D2 y D3 se unen a CDK4 y CDK6, mientras la ciclina C se une a CDK8. La progresión a través de la fase G_1 está mediada por las diferentes isoformas de la ciclina D y CDK2, CDK4 y CDK6 [38]. La ciclina E se activa durante la transición de la fase G_1 a S y activa a la CDK2. La ciclina A aumenta durante la fase S y se une a CDK1 y CDK2. Las ciclinas tipo B están presentes al final de la fase G_2 y promueven la entrada en mitosis, estando asociadas a CDK1. Las ciclinas tipo G y T están asociadas con CDK5 y CDK9, respectivamente [36].

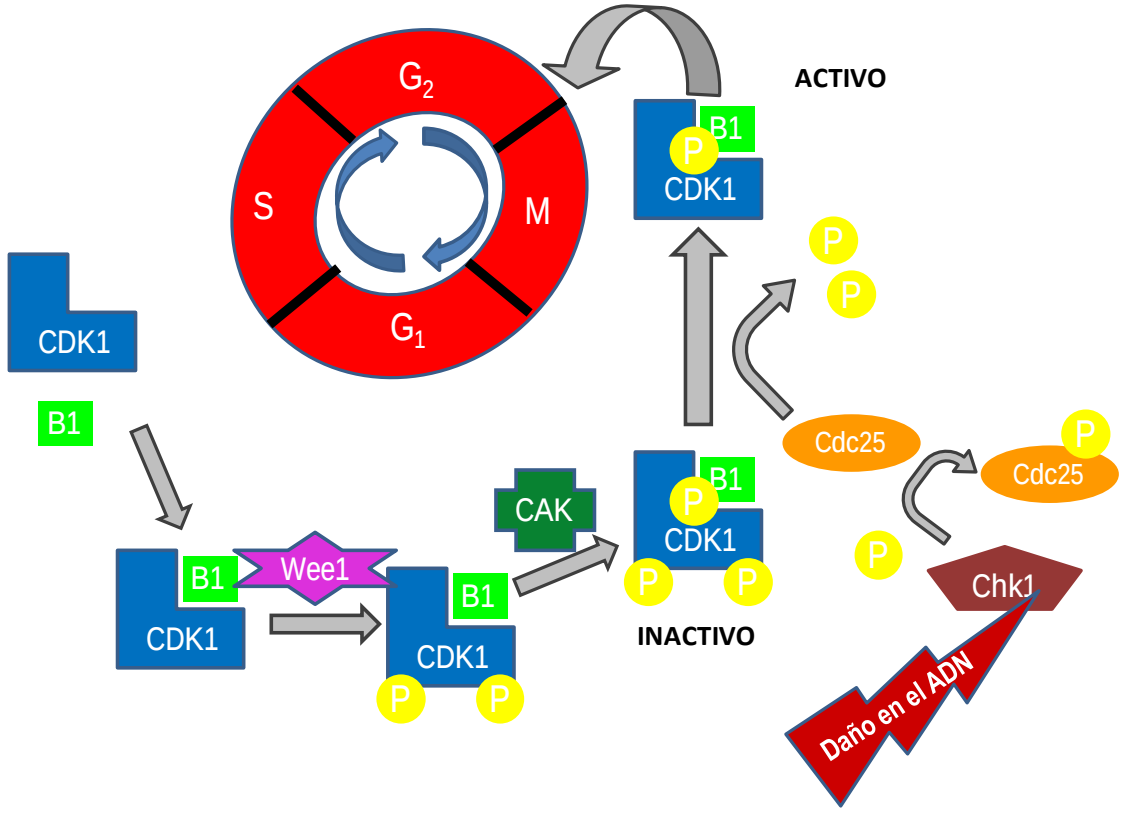

F*igura 2: Esquema de las quinasas dependientes de ciclina implicadas en la transición de la fase G_2 a la mitosis.*

Las moléculas inhibidoras de CDKs impiden su actividad uniéndose a ellas y frenan la progresión del ciclo celular. Se pueden dividir en dos familias, la familia del inhibidor de la CDK4 (INK4), como p15, p16, p18 y p19 que inhiben específicamente CDK4 y CDK6 [39] y

la familia inhibidora de CDK (CIP/KIP) como p21, p27 y p57 que son capaces de inhibir a todas las CDKs [40] en todas las fases del ciclo. Además, la activación de las CDKs puede estar inhibida mediante fosforilación por las quinasas Wee1 y MYT1. Las moléculas inhibidoras se unen a las CDKs e inhiben su actividad, regulando negativamente la progresión del ciclo [41,42].

La CDK1, que es la única proteína no-redundante de su familia (Figura 2), para ser activada deberá formar un complejo con la ciclina B1 (CDK1-ciclina B1), y ser fosforilada por una quinasa (CAK). Aún así, su actividad será inhibida por la fosforilación de un par de aminoácidos en el sitio activo llevado a cabo por la proteína Wee1. Esta inhibición sólo podrá suprimida por las fosfatasas Cdc25C que pueden desfosforilar estos residuos aumentando la actividad CDK. CHK1 inactiva Cdc25C mediante su fosforilación. Este efecto de CHK1 previene la desfosforilación de CDK1, manteniendo el complejo CDK1-ciclina B1 en un estado inactivo. Un daño en el ADN activa CHK1, que luego inactivará Cdc25C dejando al complejo CDK1-ciclina B1 en un estado inactivo fosforilado. Por lo tanto, la activación de la proteína Cdc25C, es un evento muy importante en la progresión del ciclo celular desde la fase G_2 a la fase M [43]. Además, los inhibidores de CDK1 son capaces de parar el ciclo celular en este punto induciendo una acumulación de células, y posterior muerte por apoptosis.

Cuando se produce un error o un daño en el ADN, como hemos visto, la célula dispone de puntos de control que permiten detectarlo y detener la progresión del ciclo celular, poniéndo en marcha el sistema de reparación. En el caso de no producirse la reparación la célula induce su propia muerte por apoptosis. La apoptosis se convierte así, una vez más, en un proceso esencial para la correcta progresión del ciclo celular, protegiendo a los organismos multicelulares y permitiéndoles una eliminación selectiva de las células dañadas [36].

Un amplio porcentaje de cánceres humanos (25-30%) está asociado con hiperactividad de las CDKs, cuya expresión suele estar aumentada como resultado de una mutación [44]. La alteración y pérdida de regulación en la actividad de las CDKs son marcas inequívocas de neoplasia [45].

Los inhibidores o moduladores de las CDKs representan un nuevo arsenal de agentes terapéuticos contra el cáncer [45], entre ellos, algunos flavonoides como la quercetina, la silimarina, la daidzeina, la luteolina, kaempherol, la apigenina y la genisteína, que presentan actividad inhibitoria sobre varias quinasas [46,47].

3.2. Interacción con los microtúbulos.

Los microtúbulos son polímeros dinámicos en continua polimerización y despolimerización que juegan un papel crucial en funciones celulares como: el crecimiento, la división celular, la movilidad, la fagocitosis, el transporte o la localización intracelular de orgánulos. Los filamentos del citoesqueleto interaccionan con un gran número de proteínas que en condiciones normales podrían estar secuestrando e inhibiendo su función. Al producirse cualquier cambio en la dinámica de los microtúbulos, estas proteínas pueden liberarse y participar de forma decisiva en la modulación de múltiples procesos de señalización celular [48].

El papel vital de los microtúbulos en la mitosis unido a que son la única diana celular con la que interaccionan directamente los agentes que afectan a los microtúbulos, los convierte en una diana muy atractiva para el desarrollo de fármacos antitumorales. Estos fármacos poseen un gran interés y se utilizan habitualmente en quimioterapia. Los microtúbulos juegan un papel crucial en la regulación de la mitosis, y su desorganización puede inducir la parada del ciclo celular en la fase M, formación de un huso mitótico anormal y muerte celular por apoptosis [49].

Teniendo en cuenta su función, estos compuestos pueden clasificarse en:

- Inhibidores de la polimerización: colchicina, dolastatina, nocodazol y alcaloides de la Vinca (vincristina y vinblastina).

- Potenciadores o estabilizantes de la polimerización: taxanos (paclitaxel) y epotilonas.

Además, podríamos aguparlos basándonos en sus sitios de unión a la tubulina. Los taxanos y el nocodazol se unen a la β-tubulina; los alcaloides de la Vinca, se unen en un lugar cercano al sitio de unión del GTP en la β-tubulina, y la colchicina en la interfase entre los dímeros de α- y β-tubulina.

Aunque el mecanismo de acción de estos fármacos no se conoce con detalle, todos ellos inducen una acumulación de células mitóticas asociada y muerte celular.

El daño de los microtúbulos inhibe la degradación de la ciclina B1 por el proteasoma e induce la expresión de CDK1, originando una activación continuada del complejo CDK1-ciclina B1 y parada del ciclo celular en G_2/M. La inhibición de CDK1 por olomoucina o la inhibición de CDKs por medio del inhibidor endógeno p21, previenen la apoptosis inducida por taxol. La

activación de CDK1-ciclina B1 es necesaria para la fosforilación de Bcl-2, poniendo de manifiesto la vinculación entre la alteración de la dinámica de los microtúbulos, la activación de CDKs y proteínas reguladoras de la apoptosis. Bcl-2 se inactiva por fosforilación, y Bax o Bad se pueden activar disparando la apoptosis por via mitocondrial [50].

El tratamiento con agentes que afectan a los microtúbulos también provoca un aumento de la expresión de p53 y del inhibidor de quinasas dependientes de ciclinas p21, activación de proteínquinasas como Ras/Raf y MAPKs, aumento en la expresión de c-Mos, Mcl-1, DR4 y DR5, COX-2 y TNF-α [51,52,53]; y una disminución de los niveles de c-FLIPL o XIAP [54].

Estos compuestos pueden inducir apoptosis, o sensibilizar las células tumorales frente a otras drogas ancancerígenas.

Algunos flavonoides ejercen su actividad antiproliferativa mediante interacción con la tubulina [55], siendo uno de los requerimientos estructurales la presencia de un grupo metoxilo en C-3. Por ejemplo, la casticina que se comporta como inhibidor de la polimerización produciendo una parada en la fase G_2/M y activando la apoptosis. No obstante, esta no parece ser una condición indispensable, ya que existen ejemplos como la quercetina que no cumple esta condición, y sin embargo, es capaz de unirse a la tubulina impidiendo así la polimerización de los microtúbulos. Se ha descrito que la quercetina se comporta como el antimitótico colchicina, tiene afinidad por el mismo sitio de unión, induce la actividad GTPasa de la tubulina soluble y perturbando la polimerización de los microtúbulos por inducción de cambios conformacionales en la tubulina [56].

4. Apoptosis.

Los organismos multicelulares dependen de la apoptosis para un apropiado desarrollo y mantenimiento de sus tejidos. Este proceso permite la eliminación de las células que no están en su sitio, que no se necesitan o que están dañadas de manera irreparable [57].

La apoptosis se puede definir como el conjunto de reacciones bioquímicas que tienen lugar en la célula, que concluyen con la muerte de la célula de una forma ordenada y silenciosa, sin producir ningún tipo de alteración en el resto del tejido. La apoptosis es un proceso de autodestrucción celular controlada, que permite al organismo su correcta morfogénesis y la eliminación de las células que amenacen su supervivencia, además de ser necesaria para evitar la sobreproducción celular. Este proceso es de vital importancia, tanto durante el desarrollo embrionario como en la vida adulta [58,59], y podemos observar su aparición en algunas

reacciones inmunes, o cuando las células son dañadas por alguna enfermedad o por la acción de un agente nocivo [60].

Existe una gran variedad de estímulos y condiciones, fisiológicas o patológicas, que pueden desencadenar la apoptosis: ligandos que actúan sobre receptores específicos (TRAIL ó TNF), carencia de factores de crecimiento, la radiación, golpe de calor, hipoxia, toxinas, fármacos, la luz ultravioleta, la presencia de radicales libres, una infección viral o bacteriana, o un desprendimiento de la célula de su tejido habitual [61]. Pero no todas las células mueren irremediablemente en respuesta a estos estímulos. Los corticoesteroides inducen apoptosis en timocitos, mientras otras células no resultan afectadas. La sensibilidad de la célula a un estímulo dependerá del equilibrio entre la expresión de proteínas pro- y anti-apoptóticas, de la potencia del estímulo y del estado del ciclo celular en el que se encuentre la célula.

La función crítica de la apoptosis en la regulación de la homeostasis tisular tiene importantes implicaciones en la salud. Niveles excesivos de apoptosis contribuyen al desarrollo de múltiples patologías, como el SIDA [62], trastornos neurodegenerativos como el Alzheimer [63] y la enfermedad de Huntington [64], isquemia cardíaca [65] y daño renal [66], mientras que la deficiencia de apoptosis es clave en el desarrollo de enfermedades autoinmunes [67] y del cáncer [68]. Esto hace que todos los estudios que contribuyan al conocimiento y manipulación de la apoptosis tengan un inmenso potencial, siendo la búsqueda de nuevos fármacos antitumorales una de las áreas más prolíficas.

Durante la apoptosis, la célula sufre una serie de cambios bioquímicos que afectan en último término a la morfología celular:

- Cambios bioquímicos: Se produce hidrólisis de proteínas, jugando un papel esencial las caspasas, y rotura del ADN en fragmentos de 180 a 200 pares de bases. También se produce la externalización de fosfatidilserina, anexina I y calreticulina que actúan como marcadores de fagocitosis. Aumentan los niveles de calcio iónico libre y hay una deshidratación celular [69].

- Cambios morfológicos: En el inicio de la apoptosis temprana podemos observar una contracción celular y la condensación y fragmentación de la cromatina. Las células se hacen más pequeñas, el citoplasma más denso y los orgánulos están más apretados. En la membrana plasmática se van formando evaginaciones, el núcleo se fragmenta y se forman cuerpos apoptóticos, fragmentos de la membrana celular que incluyen citoplasma con orgánulos densamente empaquetados con o sin fragmentos nucleares. Estos cuerpos apoptóticos son

rápidamente fagocitados por macrófagos o por células vecinas debido a la exposición de marcadores de fagocitosis en la superficie celular como la fosfatidilserina, evitando la exposición del material intracelular al sistema inmune que podría desencadenar una respuesta inflamatoria [57].

La activación de la apoptosis es controlada por dos vías de señalización diferentes pero interrelacionadas, las vías extrínseca e intrínseca.

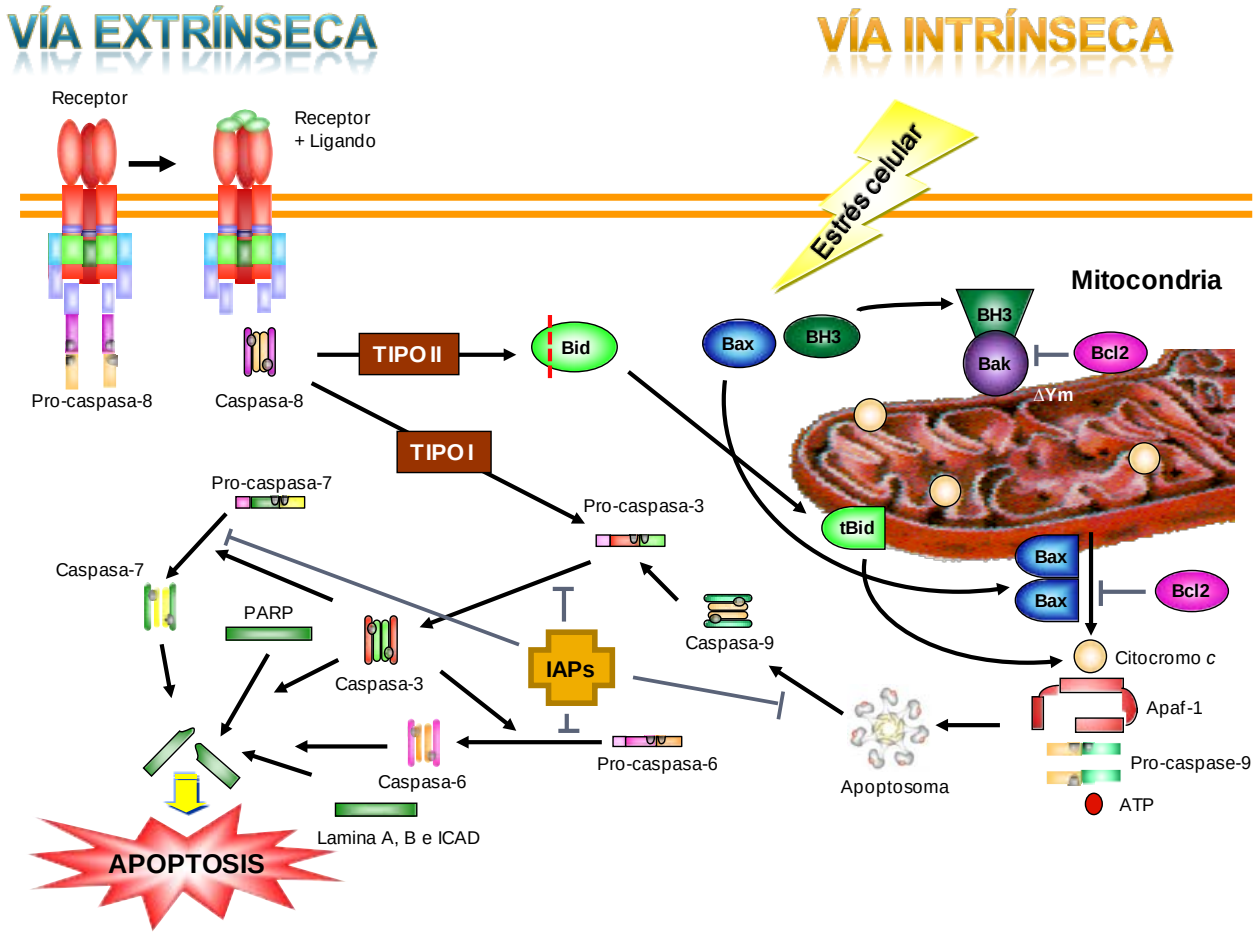

Figura 3: Vías de activación de la apoptosis.

4.1. Vía extrínseca: receptores de muerte celular.

La activación de la vía extrínseca se inicia mediante la unión de ligandos específicos a sus receptores de muerte, provocando la agregación del receptor y el reclutamiento de proteínas adaptadoras, que mediante la interacción proteína-proteína transmiten la señal de muerte hasta las moléculas efectoras.

Los receptores de muerte pertenecen a la superfamilia del receptor del factor de necrosis tumoral (TNF), cuyos miembros tienen en común un dominio extracelular rico en cisteína y un dominio intra-celular que permite al receptor acoplarse con el resto de la maquinaría apoptótica. Los receptores de muerte mejor caracterizados y sus correspondientes ligandos son: TNFR1/TNF-α, FasR/FasL, DR3/Apo3L, DR4/TRAIL y DR5/TRAIL [70,71,72,73,74].

4.1.1. Receptor Fas (CD95).

Cuando se une FasR y Fas-L se produce la trimerización del complejo ligando/receptor, reclutando otras moléculas adaptadoras asociadas al dominio de muerte como FADD (proteína con dominio de muerte asociado a Fas) o RIP (proteína de interacción con el receptor). Estas últimas, a su vez promueven el reclutamiento de las procaspasas iniciadoras -8 y -10, formándose así el complejo inductor de muerte (DISC).

En la vía extrínseca existen dos mecanismos de señalización intracelular, que dependen del tipo celular [75,76]:

- Tipo I: la expresión de caspasa-8 es suficiente para activar las caspasas efectoras (-3, -6 y -7) y llevar a la célula a su muerte por apoptosis. Este tipo de inducción no precisa la mitocondria y por tanto no está inhibida por factores como Bcl-2 o Bcl-x_L, ya que no requiere la amplificación de la señal mediante factores pro-apoptóticos mitocondriales.

- Tipo II: la expresión de caspasa-8 no es suficiente para activar eficientemente otras caspasas y se hace necesaria la amplificación de la señal. En estas células la caspasa-8 provoca la activación proteolítica de Bid, que se trasloca a la mitocondria e interacciona con moléculas anti-apoptóticas de la familia Bcl-2 como son Bax y Bak, induciendo la liberación de citocromo *c* y otros factores pro-apotóticos al citosol. En este compartimento, el citocromo *c* se une al dominio C-terminal de la proteína Apaf-1 (factor de activación de la apoptosis) y esta unión produce un cambio conformacional en Apaf-1 que es ahora más flexible, facilitando la unión del ATP a sus dominios de unión a nucleótidos. Se forma así el apoptosoma, un complejo formado por siete moléculas de Apaf-1 interaccionando por los extremos N-terminal, a las que se une dATP, citocromo *c* y, finalmente caspasa-9 en su zona central por interacción de dominios CARD (dominios de reclutamiento de caspasas), provocando un cambio conformacional a una forma activa, capaz de activar a caspasas ejecutoras (-3, -6 y -7) [77].

4.1.2. Receptor de TNF-α: TNFR1.

El receptor de TNF-α (TNFR1) es una proteína de aproximadamente 55 kDa que se expresa en la mayoría de las líneas celulares. Comparte con CD95 los tres subdominios ricos en cisteina situados en la región extracelular, pero a diferencia de la pareja formada por CD95/CD95L, el par TNFR1/TNF-α es capaz de trasmitir a la célula dos tipos de señales muy distintas entre sí. Tras la unión de TNF-α a su receptor, el dominio intracelular es reconocido por una molécula que lleva un dominio de muerte asociado, TRADD, la cual puede unirse a FADD, RIP o a TRAF-2 (TNF-R-asociado al factor 2). FADD se une a caspasa -8/-10 activándola mediante autoproteolísis e induciendo apoptosis. TRAF2 recluta proteínas inhibidoras de la apoptosis como cIAP-1 y cIAP-2, aunque tambien puede activar MAPKKKs, activando la cascada de quinasas y JNK. Si TRADD se une a la proteina RIP se induce la transcripción de los factores NF-kB y AP-1 promoviendo la inducción de genes de carácter proinflamatorio e inmunomodulador, oponiéndose a la acción pro-apoptótica del TNF. La unión del ligando al receptor puede dar lugar a dos tipos de complejos: Complejo I formado por TRADD unido a RIP y a TRAF2 que dará lugar a la señalizacion de NF-kB, y Complejo II: formado por TRADD unido a FADD que induce la autoproteolísis de caspasa -8/10 promoviendo la apotosis.

Los niveles de c-FLIP van a determinar la activación de una vía u otra. En el caso de TNFR1, la unión de su ligando sólo induce apoptosis en algunas líneas celulares cuando la síntesis de proteínas ha sido bloqueada. De aquí se deduce la existencia de algún factor que bloquea las señales apoptóticas derivadas de TNFR1, por lo que se podría sugerir que la expresión de este factor estará probablemente controlada a través de NFkB y JNK/AP-1[78]. Además TNFR1, como veremos más adelante, puede activar dos tipos de esfingomielinasas (SMasas) [79] que a su vez podrían activar una serie de MAP-quinasas que activan la ruta de las caspasas.

4.2. Vía intrínseca: inicio de la señal de apoptosis en la mitocondria.

La vía intrínseca, puede ser activada por una gran variedad de estímulos, como compuestos citotóxicos, radiación, estrés celular o la ausencia de factores de crecimiento [80], que actúan directamente sobre la mitocondria o a través de moléculas mediadoras. Además, la mitocondria como hemos visto, puede ser esencial en la amplificación de la señal apoptótica de la vía extrínseca. Esta vía es controlada por el equilibrio entre los miembros pro- y anti-apoptóticos de la familia de proteínas Bcl-2.

Los miembros pro-apoptóticos pueden provocar la permeabilización de la membrana mitocondrial externa y liberar moléculas solubles al citosol, como:

- Citocromo *c*: estimula la formación del apoptosoma, seguida de la activación de caspasa-9 e hidrólisis de las caspasas efectoras -3, -6 y -7 [81].
- Smac/DIABLO: se une a las proteínas inhibidoras de la apoptosis (IAPs) impidiendo su unión a las caspasas [82].
- Endonucleasa G: principal nucleasa responsable de la degradación del ADN, se transloca al núcleo tras su liberación de la mitocondria, está involucrada en la fragmentación del ADN y junto con exonucleasas y ADNasa I, producen el típico patrón en escalera [83].
- Htr/Omi: serínproteasa que funciona también como inhibidor de IAPs, mediante la inactivación por corte [84].

Como resultado se produce la ruptura de la cadena de transporte de electrones, la liberación de iones superóxido [85,86] y la hiperpolarización de la membrana mitocondrial interna (que puede terminar con la dilatación de la matriz y la ruptura de la membrana). Además, se abren los poros mitocondriales permitiendo la entrada de agua y solutos a la matriz, produciéndose un choque osmótico y la liberación del factor inductor de apoptosis (AIF), que se transloca al núcleo y provoca la condensación y rotura del ADN en fragmentos de alto peso molecular (50Kb). A nivel de la membrana celular, AIF activa a la flipasa e inhibe a la translocasa haciendo que la fosfatidilserina que en células normales se encuentran en la cara interna de la membrana se exponga ahora al exterior [87]. La actividad de AIF es inhibida por la sobreexpresión de Bcl-2, pero no por los inhibidores de caspasas, es decir su efecto es indedependiente de las caspasas [88]. También se induce la activación de Bax que puede formar un canal en la membrana mitocondrial.

Además, de estas dos vías, existen señales apoptóticas que tienen su origen en el núcleo celular. La más importante, es la proteína supresora de tumores p53, que se activa en el contexto de un daño celular irreparable, en respuesta a diferentes tipos de estrés. Esta proteína nuclear puede inducir la expresión de numerosos factores pro-apoptóticos (ej. Puma, noxa, Bax, Apaf-1, Fas y DR5) [89].

4.3. Proteínas reguladoras de la apoptosis.

4.3.1. Proteínas de la familia Bcl-2.

El primer miembro y que da nombre a la familia, Bcl-2, fue clonado a partir del punto de corte en la translocación cromosomal t(14:18), presente en el 85% de los linfomas foliculares de células B humanas, y se caracteriza por inhibir la muerte celular por apoptosis [80]. Posteriormente, fue identificada toda una familia de proteínas relacionadas por su homología de secuencia y su participación en el control de la apoptosis. Los factores Bcl-x_L, Bcl-w, Mcl-1, Bcl-B y Bfl-1 comparten con Bcl-2 una actividad anti-apoptótica y una homología estructural en cuatro regiones α-hélice homólogas a Bcl-2, BH1-BH4. Bax, Bak y Bok, con función pro-apoptótica, comparten sólo los dominios BH1, BH2 y BH3. Finalmente, Bid, Bim, Bad, Bik, Puma, Noxa, Bmf, Hrk, Bk1, BNIP3 y Skipe, sólo poseen el dominio BH3 necesario y suficiente para promover la apoptosis [90].

Los miembros de la familia Bcl-2 interactúan de forma dinámica para regular la apoptosis, mediante homo/hetero-dimerización o mediante fosforilación y desfosforilación. Los miembros que sólo poseen el dominio BH3, necesitan heterodimerizar para ejercer su acción, uniéndose a las proteínas anti-apoptóticas. Además, los miembros pro-apoptóticos como Bax pueden heterodimerizar con los anti-apoptóticos como Bcl-2 ó Bcl-x_L y bloquear su actividad anti-apoptótica. Cuando Bcl-2 está en exceso, las células están protegidas de la muerte celular, y cuando Bax está en exceso la célula está avocada a entrar en apoptosis. Por tanto la relación de los niveles de expresión entre los miembros pro- y anti-apoptóticos de la familia Bcl-2 determina el destino celular [80].

Estas proteínas, poseen localizaciones subcelulares diferentes. Los miembros anti-apoptóticos suelen aparecer como proteínas integrales en las membranas del núcleo, del retículo endoplásmico y fundamentalmente de la mitocondria, estabilizando la membrana mitocondrial y evitando la liberación de citocromo *c*. En cambio los miembros pro-apoptóticos se encuentran en el citosol o asociados al citoesqueleto. En respuesta a un estímulo de muerte estos sufren un cambio conformacional que les permite integrarse en la membrana mitocondrial externa donde interactúan con los miembros anti-apoptóticos, inhibiéndolos, permeabilizando la membrana mitocondrial externa y activando la apoptosis [91].

Miembros anti-apoptóticos más representativos de la familia Bcl-2:

- Bcl-2*:* es la proteína prototipo de la familia, su peso molecular es de 26 KDa y posee los cuatro dominios que la definen (BH1-BH4). Es una proteína integral y forma una estructura similar a un poro, pudiendo modificar el flujo de moléculas o proteínas pequeñas de un lado a otro de la membrana. Su sobre-expresión puede evitar, o retrasar, la muerte celular inducida por la carencia de factores de crecimiento, irradiación, glucocorticoides y drogas quimioterápicas, y promover la tumorigénesis mediante la prevención de la muerte celular [92].

- Bcl-$x_{L:}$ es una proteína muy similar a Bcl-2, tanto en su estructura como en su función. Posee los cuatro dominios BH y su peso molecular es de 30 KDa. Su sobre-expresión puede mediar una resistencia significativa a la muerte celular por apoptosis dependiente de una deprivación de factores de crecimiento. Bcl-x_L puede ejercer su acción anti-apoptótica mediante la interacción con moléculas pro-apoptóticas como Bax. Además, puede regular la permeabilidad de la membrana mitocondrial impidiendo la liberación del citocromo *c* al citosol [93].

Miembros pro-apoptóticos más representativos de la familia Bcl-2:

- Subfamilia Bax: Bax es uno de los miembros pro-apoptóticos más importantes, su peso molecular es de 21 KDa y posee los dominios BH1, BH2 y BH3, aunque son BH1 y BH2 los que guardan una estrecha homología con Bcl-2. En condiciones normales Bax se encuentra en el citosol o en el citoesqueleto en forma monomérica, y en respuesta a estímulos apoptóticos se transloca a la membrana mitocondrial externa o interna, formando homo- o hetero-oligómeros con Bak, y puede ser que con otros factores. No está claro su mecanismo pero sí que su regulación se lleva a cabo mediante fosforilación, y que su sobre-expresión acelera la apoptosis mediante la permeabilización de la membrana mitocondrial externa [80].

Subfamilia BH3: son proteínas pro-apoptóticas, que sólo muestran homología con Bcl-2 por su dominio BH3. Para ejercer su actividad pueden formar heterodímeros con los miembros anti-apoptóticos de la familia: Bcl-2 y Bcl-x_L. Para ello, el dominio BH3 de los miembros de este grupo puede introducirse en el hueco hidrofóbico formado por la asociación de las regiones BH1, BH2 y BH3 de los miembros anti-apoptóticos. Bad se activa mediante des-fosforilación, cuando está fosforilada se encuentra inactiva en el citosol pudiendo estar unida a la proteína 14-3-3. La hidrólisis de la proteína 14-3-3 durante la apoptosis promueve la

muerte celular mediante la liberación de Bad, facilitando su translocación a la mitocondria y su interacción con Bcl-x_L. Bid y Bik pueden actuar sobre la mitocondria, induciendo la liberación de citocromo *c* [94]. Bid y Bim, inducen la permeabilización de la membrana mitocondrial en un modelo dependiente de Bax y/o Bak, induciendo su oligomerización [80]. Bid es la proteína que interrelaciona las dos vías apoptóticas (vía extrínseca e intrínseca), la activación de caspasa-8 induce la hidrólisis de Bid formando un fragmento truncado tBid que se transloca a la membrana mitocondrial e induce la liberación de citocromo *c*.

La pérdida de la regulación sobre los miembros de la familia Bcl-2 está estrechamente vinculada a la tumorogénesis, los miembros anti-apoptóticos parecen funcionar como onco-proteínas y los pro-apoptóticos como supresores de tumores.

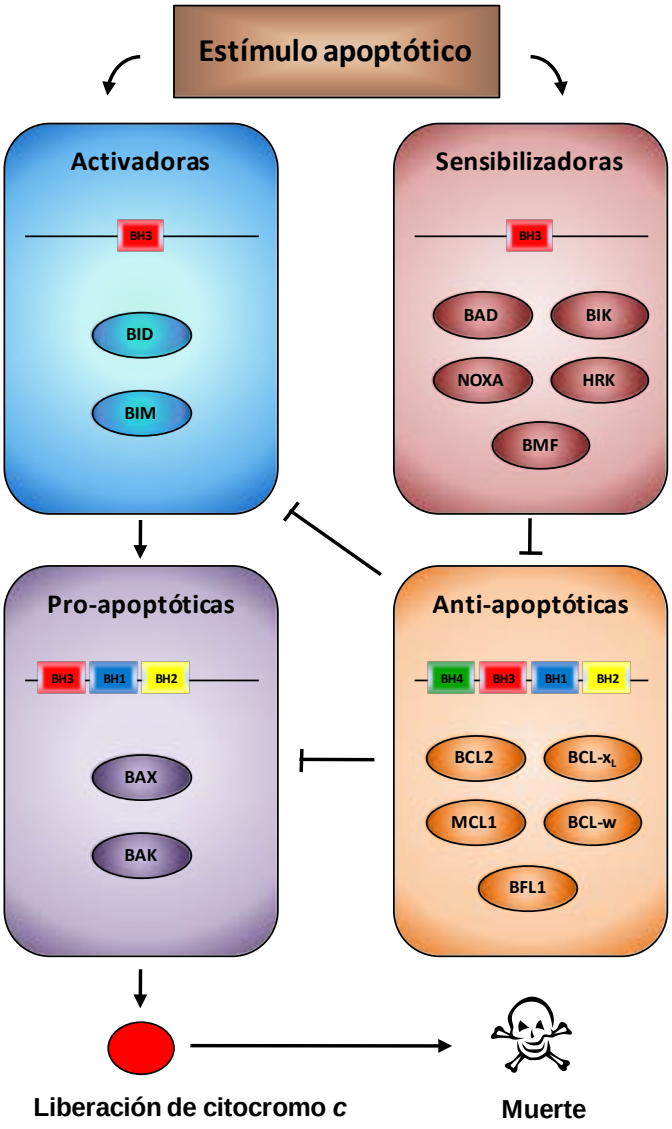

Figura 4. Interacciones entre los miembros más importantes de la familia Bcl-2.

4.3.2. Proteínas de la familia de las caspasas.

Las caspasas (cisteín-proteasas específicas de aspartato) poseen funciones centrales en las vías de señalización de la apoptosis y de la inflamación. La familia de las caspasas se compone de 15 miembros en mamíferos que se agrupan en dos grandes sub-familias: las caspasas relacionadas con la inflamación y las apoptóticas. En humanos se han descrito 11 caspasas: -1, -2, -3, -4, -5, -6, -7, -8, -9, -10, -12 y -14. Todas ellas se encuentran en forma de zimógenos o proenzimas con una estructura bien definida: a) un dominio N-terminal muy variable tanto en su secuencia como en su longitud, con funciones de regulación y activación, b) y una región catalítica formada por dos dominios, uno grande (20 Kda) y otro pequeño (10 Kda), que darán lugar a las dos subunidades de la enzima una vez activada [96].

Las caspasas se dividen en dos grupos según la longitud de su región reguladora N-terminal o prodominio. Las caspasas con prodominio largo son la -1, -2, -4, -5, -8, -9 y -10, y están involucradas en funciones de regulación de la activación de la cascada (iniciadoras). Las procaspasas -8 y -10 contienen en sus prodominios repeticiones de una secuencia de interacción proteína-proteína llamada dominio efector de muerte (DED), mientras que las procaspasas -1, -2, -4, -5 y -9 contienen dominios de reclutamiento de caspasas (CARDs); estos dominios facilitan la interacción con proteínas que contienen los mismos dominios. Las caspasas con prodominio corto (efectoras) son las caspasas -3, -6 y -7, son activadas por alguna de las caspasas iniciadoras e hidrolizan numerosas proteínas celulares. Las caspasas -1, -4, -5 y -12 están implicadas en la regulación de señales inflamatorias, mientras -2, -3, -6, -7, -8, -9 y -10 están más implicadas en la apoptosis [97].

El inicio de la activación de las caspasas puede ocurrir a través de la vía intrínseca de la apoptosis, formándose el apoptosoma y activándose la caspasa-9 debido a un cambio conformacional, o a través de la vía extrínseca que puede inducir la activación de la caspasa-8 (Tipo I) de forma directa, ó a través de la activación de caspasa-9 (Tipo II). La activación de las caspasas se inicia por un procesamiento proteolítico entre sus dominios mayor y menor, que puede ser llevado a cabo por ellas mismas, o por otras caspasas, formando un heterodímero y dando lugar a una conformación activa. Luego, estas caspasas iniciadoras, son capaces de activar a otras caspasas. Para ejercer su función, normalmente se produce la dimerización de dos caspasas heterodímeras formando heterotetrámeros. Una caspasa activa a la otra cortando entre sus dominios, amplificándose así la señal pro-apoptótica y culminando con la activación de las caspasas efectoras que inducen la proteólisis que acaba con la célula por apoptosis [96,97].

Además de estas vías principales de activación de caspasas, también se pueden activar vía retículo endoplasmático, inducida por agentes que perturban la homeostasis del ión calcio provocando la translocación de la caspasa-7 a la superficie del retículo endoplasmático, que a su vez activa la caspasa-12, activando a la caspasa-9 que activa las caspasas efectoras -3, -6 y -7, sin producirse la liberación del citocromo *c* [98]. En los linfocitos T citotóxicos y las células NK, se puede inducir la activación de caspasas vía Granzima B, proteína que es capaz de hidrolizar a las caspasas -3 y -7, iniciando la apoptosis [99].

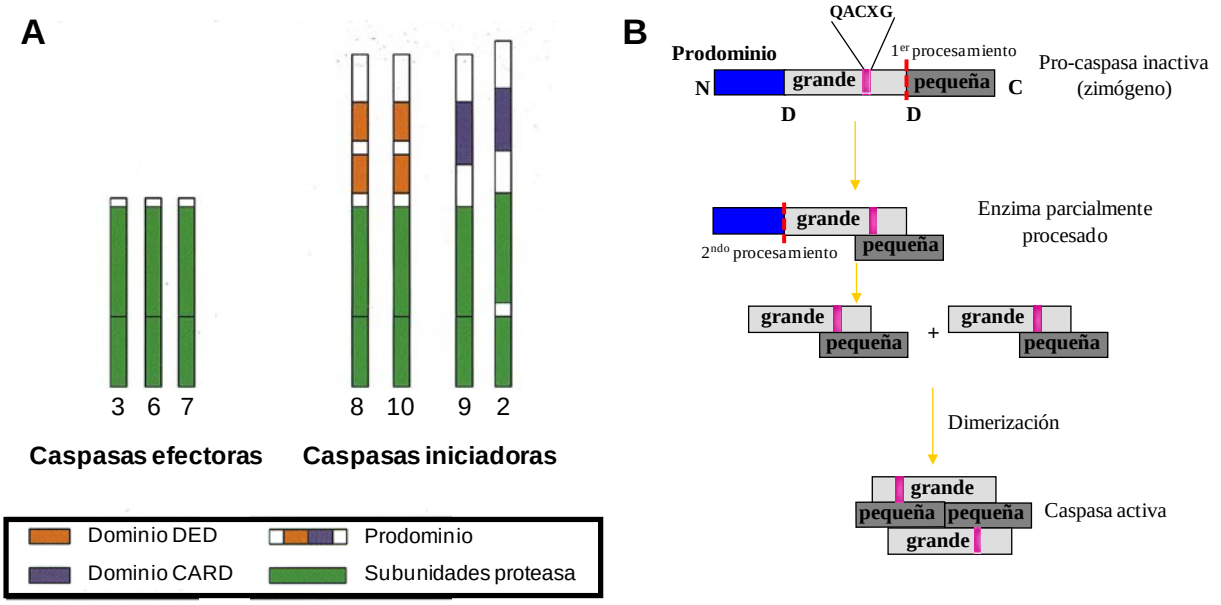

Figura 5. (A) Estructura de las caspasas implicadas en la apoptosis. (B)Activación de las caspasas por procesamiento proteolítico.

4.3.2.1. Sustratos de las caspasas.

Las caspasas organizan de forma coordinada la destrucción de las estructuras y orgánulos de las células mediante la hidrólisis de sustratos específicos. En conjunto, estos eventos proteolíticos inducen en la célula los cambios fenotípicos característicos de la apoptosis. Se conocen más de 200 sustratos hidrolizados por las caspasas y pueden clasificarse en: proteínas citoplasmáticas (actina, gelsolina, componentes de unión ϕ -cateninas), proteínas nucleares (lamina-A, B, receptor de lamina B, proteínas nucleares del aparato mitótico, proteínas asociadas a ribonucleoproteínas, proteínas de unión a la estructura del cromosoma), proteínas relacionadas con el metabolismo y reparación del ADN (PARP, DNA-PKcs, proteínas de replicación del ADN, ADN-topoisomerasas), proteínquinasas (PKC y sus isoformas, MAPK, ERK, Akt, Wee1), proteínas implicadas en las vías de señalización (citoquinas, pro-

interleukinas y fosfolipasas), proteínas del ciclo celular y proliferación celular (p21, p27, pRb, ubiquitinas) [96].

4.3.2.2. Mecanismos inhibidores de las caspasas.

Las proteínas inhibidoras de la apoptosis (IAPs) constituyen una familia de factores proteicos que son liberados por la mitocondria y ejercen su acción inhibiendo directamente a las caspasas. Se han identificado cinco IAPs en humanos: NAIP, XIAP, c-IAP1, c-IAP2 y ML-IAP. Todas ellas pueden presentar: a) al menos un dominio BIR, mediante el que se unen a las caspasas inhibiendo su acción, b) dominios RING, que actúan como una ubiquitín-ligasa induciendo su autodegradación y la degradación de la caspasa unida a él por el proteasoma y c) dominios CARD, que pueden permitir la regulación de la degradación de las caspasas por interacción entre dominios de este tipo. Los inhibidores XIAP, c-IAP1 y c-IAP2 suprimen la actividad de las caspasas -3, -7 y -9. Dentro de esta familia de proteínas, la mejor estudiada es XIAP. Su estructura está formada por tres dominios BIR y un dominio RING, el dominio BIR2 inhibe las caspasas -3 y -7, mientras que el dominio BIR3 inhibe la caspasa-9. Los antagonistas de XIAP pueden unirse a BIR2, bloquear su efecto inhibidor y activar directamente a la caspasa-3, que a su vez activa a las caspasas -8 y -9 como consecuencia del bucle de amplificación de la señal apoptótica. Además, el efecto apoptótico inducido por el antagonista de XIAP sólo se observa en células tumorales, debido a que sus niveles de expresión son mayores que en las células normales. La proteína *survivina* sólo posee un dominio BIR, y aunque fue considerada como una IAP, no inhibe a las caspasas directamente, sino que es una proteína nuclear importante en la mitosis celular [96].

La proteína c-FLIPL posee dos regiones homólogas a los dominios efectores de muerte (DED) en su extremo amino, asemejándose a la estructura de las caspasas -8 y -10. Esto le permite impedir la formación del complejo inductor de muerte (DISC), y también mediante la unión a la caspasa-8 por sus dominios DED formar un heterodímero caspasa-8/c-FLIPL, que promueve la proteolisis parcial de ambos. Esta proteólisis incompleta mantiene a las dos proteínas unidas al receptor, impidiendo la liberación de la forma activa de la caspasa-8 [100].

Las caspasas pueden, además ser modificadas covalentemente por fosforilación. Por ejemplo, Akt, quinasa involucrada en la supervivencia celular y mediador de PI3K, fosforila el centro activo de la caspasa-9 inhibiendo su función [101].

4.4. Vía de las MAPKs.

Las proteínas quinasas activadas por mitógenos (MAPKs) forman una familia de serina/treonina quinasas con un papel fundamental en la transducción de señales desde la membrana hasta el núcleo celular, a través de cascadas de fosforilación. Son activadas por un gran número de estímulos, y modulan eventos importantísimos en la célula como son: la expresión génica, la migración celular, la supervivencia, la progresión del ciclo celular, la diferenciación celular y la apoptosis [102].

Las MAPKs se encuentran en el citoplasma de las células y existen 6 grupos en mamíferos: p38 (p38 α/β/γ/δ), ERK1/2 (quinasa reguladora de señales extracelulares), JNK1/2/3 (c -Jun NH2 quinasa terminal), ERK7/8, ERK3/4 y ERK5. Los grupos más estudiados son los de ERK1/2, JNKs y p38 quinasas.

La cascada de señalización de las MAPKs se encuentra organizada de forma jerárquica en tres etapas, a través de fosforilación y desfosforilación de las proteínas que sirven de sustrato (quinasas, fosfolipasas, factores de trascripción y/o proteínas del citoesqueleto), induciendo su activación o represión.

Las MAPKKK o MAP3K se activan interaccionando con una familia de pequeñas GTP-asas y/o con otras quinasas que conectan las MAPKs con los receptores de superficie o con estímulos externos [103]. Los receptores acoplados a proteínas G (GPCR) son activados por una gran variedad de estímulos externos, que inducen un cambio de GDP por GTP y desencadenan diversas cascadas de señalización. Las señales producidas hacia el citoesqueleto acopladas a GPCR, integrinas y receptores de tirosina quinasas, tienen distintos efectos en la actividad celular. Estos efectos son provocados por cambios extracelulares en el medio, la matriz, la comunicación intercelular y/o la presencia o ausencia de factores de crecimiento.

La regulación intracelular tiene lugar mediante una serie de cascadas en las que participa la familia de GTPasas Rho (Rho, Rac, cdc42) y sus activadores. Estas cascadas convergen pudiendo afectar al citoesqueleto, mediante la alteración de la polimerización de proteínas de los microtúbulos, produciéndose un aumento del dinamismo y de la movilidad celular, pudiendo afectar a la supervivencia. Esto ocurre cuando se producen aberraciones en las señales de control, produciéndose entonces la desconexión de la respuesta celular ante los estímulos, situación común en patologías inmunes y en el desarrollo de cáncer [102].

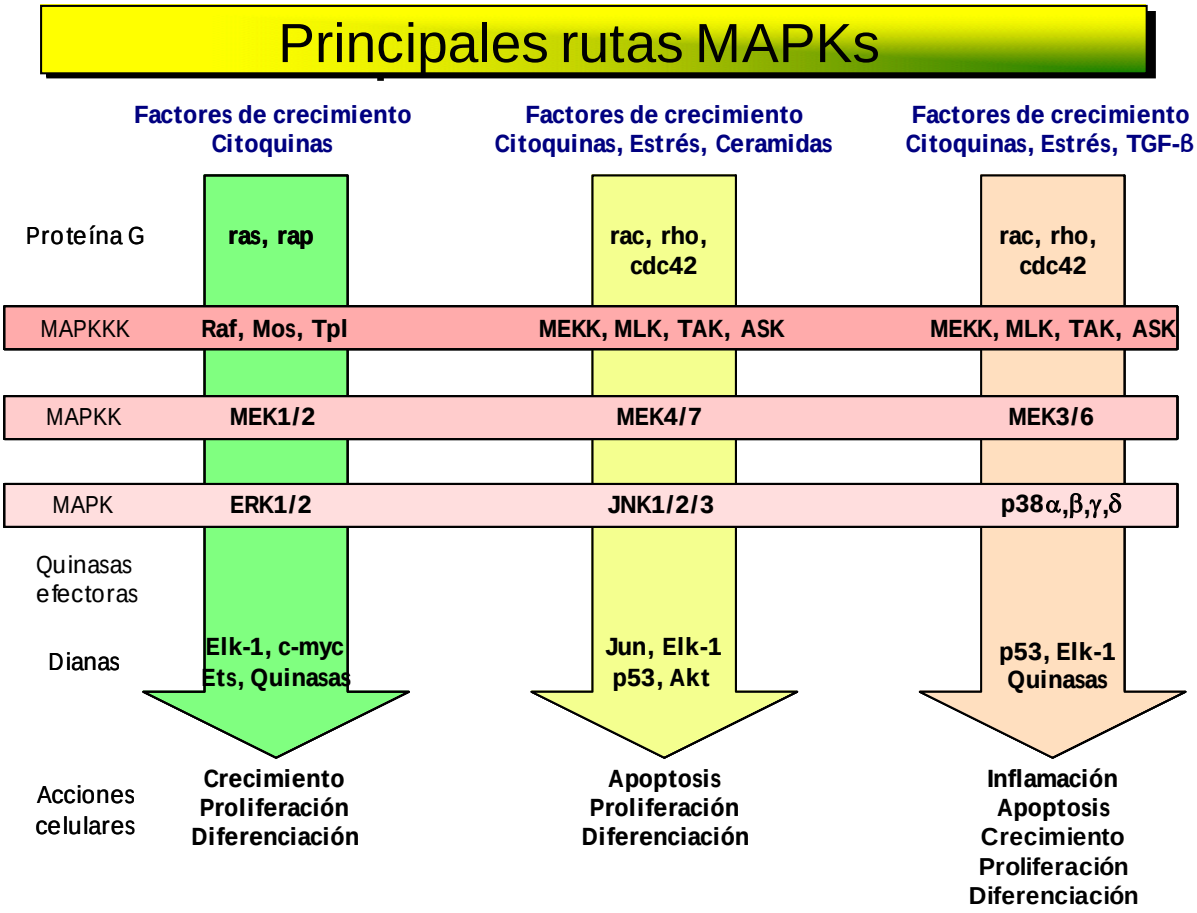

Figura 6. Vías de activación de las MAPKs.

La activación de las MAPKs determina la inducción de varias respuestas celulares que será diferente en función de la vía MAPK activada. La especificidad de las señales trasmitidas dependerá de varios factores, como: el estímulo, su duración y fuerza, la interacción con diferentes proteínas adaptadoras, la localización subcelular, la presencia de varias isoformas en cada nivel de la cascada, las conexiones entre la vía de las MAPKs y otras vías y modificaciones post-traduccionales distintas a la fosforilación [104].

4.4.1. ERK1/2 (p42/44 MAPK).

La vía ERK1/2 (p42/44 MAPK) es activada por un gran número de estímulos, tanto intracelulares como extracelulares: factores de crecimiento, el suero, los ésteres de forbol, los ligandos de receptores acoplados a proteína G, las citoquinas, el estrés osmótico y la desorganización de los microtúbulos. La señalización de ERK1/2 está implicada principalmente en la proliferación celular y, por esta razón, los inhibidores de esta vía se ensayan como potenciales fármacos antitumorales, aunque en algunas circunstancias regula también la diferenciación celular [104].

Existen dos isoformas, ERK1 y ERK2, que presentan diferentes niveles de expresión en diferentes tejidos y pueden actuar sobre más de 150 sustratos diferentes en todos los compartimentos celulares, incluyendo proteínas citosólicas y de membrana, sustratos nucleares y proteínas del citoesqueleto. Además ERK1/2 puede fosforilar y activar otras quinasas.

La activación de la vía ERK1/2 estimula los factores de transcripción implicados en la síntesis de ciclinas tipo D, y también puede controlar su expresión a nivel post-transcripcional. Estabiliza mediante fosforilación a c-myc, un factor de transcripción, que desempeña un papel importante en la regulación del crecimiento y la progresión del ciclo celular y la apoptosis, a través de un aumento de la expresión de ciclina D, p21 y cdc25, proteínas ribosómicas y factores de traducción, disminuyendo la expresión de genes antiproliferativos [105].

La vía ERK1/2 no funciona normalmente en aproximadamente un tercio de los cánceres humanos, una mutación activadora en los genes implicados provoca la oncogénesis [104].

Además de en la proliferación celular, otros sustratos de ERK1/2 juegan un papel clave en la angiogénesis, la migración celular, la invasión y la metástasis. La señalización de ERK1/2 puede promover más el fenotipo maligno del cáncer, interrumpiendo las vías de señalización Rho, fosforilando proteínas implicadas en la migración celular y regulando la expresión de proteasas implicadas en la degradación de la membrana basal. Una alta actividad de ERK1/2 reduce la tasa de apoptosis de las células del carcinoma de colon e induce la detención del ciclo celular al aumentar los niveles de inhibidores de CDK, p21 y p27. ERK1/2 puede inhibir la activación de las caspasas citosólicas y la liberación del citocromo *c* de la mitocondria. Además, ERK1/2 puede fosforilar a Bad, secuestrándolo en el citosol e impidiéndole actuar en la mitocondria previniendo la apoptosis [104].

La activación de ERK1/2 está implicada además, en la muerte celular inducida por factores tales como las especies reactivas de oxígeno (ROS), las toxinas de E.coli, y el zinc, y también por la deprivación de factores de supervivencia. Los inhibidores de MEK-ERK como U0126 o PD98059 suprimen la apoptosis inducida por la quercetina en células A549 [106], mientras que PD98059 aumenta la resistencia al cisplatino en células de carcinoma cervical humano SiHa y en células de hepatoblastoma HepG2 [107]. Los mecanismos mediante los cuales la vía ERK1/2 media la apoptosis no se conocen en detalle, pero parece producirse a diferentes niveles. ERK1/2 puede actuar antes de la liberación del citocromo *c* y de la activación de la caspasa -3 como se ha observado con cisplatino. ERK1/2 puede aumentar los niveles de Bax y

p53, e incluso fosforilar directamente a p53, aumentando la apoptosis [108,109,110]. ERK1/2 puede tener un papel relevante en la inducción de la apoptosis por vía extrínseca aumentando la respuesta a TNF-α e induciendo la activación de caspasa-8. La promoción de la muerte celular por esta vía también puede ser el resultado de la represión de la señal de supervivencia mediada por Akt [104,111].

4.4.2. Familia JNK.

La vía JNK posee una actividad principalmente pro-apoptótica [112]. Las MAPKKs que activan JNK, son MKK4 y MKK7, las cuales pueden ser activadas por una gran diversidad de estímulos externos: citoquinas, radiación ultravioleta, agentes que dañan el ADN, y en menor medida, en respuesta a receptores acoplados a proteína G, suero, y factores de crecimiento. La activación de la vía puede producir la translocación de JNK del citoplasma al núcleo y producir alteraciones en la expresión de los genes, en la muerte y/o en la proliferación celular [104].

Entre los sustratos de JNK se encuentran principalmente factores de transcripción y receptores nucleares de hormonas, que tienen un efecto directo en la expresión génica: proteínas nucleares, receptores nucleares de hormonas, proteínas no nucleares, proteínas mitocondriales de la familia Bcl-2, proteínas del citoesqueleto y Akt [104].

JNK tiene un papel muy importante en la degradación de proteínas y en la tumorogénesis. Una función importante de c-Jun es la represión transcripcional de p53, y su pérdida o la mutación de alguno de sus sitios de fosforilación para JNK puede reducir el número y tamaño de algunos tumores [113].

El mecanismo mediante el cual JNK induce la apoptosis depende del estímulo y del tipo celular implicados. JNK se une y degrada a p53 por ubiquitinización [116-117], pero la activación de JNK por estrés inhibe la degradación dependiente de ubiquitina debido a la formación de un complejo estable. JNK inhibe mediante fosforilación a las proteínas anti-apoptóticas Bcl-2 y Bcl-x_L, y activa Bax y 14-3-3, pro-apoptóticas. JNK está involucrado en la degradación del inhibidor de la caspasa-8, c-FLIPL, y en la activación de la variante de histona 2 (H2AX), que es esencial en la fragmentación del ADN. Y además, la caspasa-3 puede amplificar la activación de JNK, mediante la activación de MEKK1 [104].

Aunque JNK está asociado con acciones pro-apoptóticas [112] y señales que inhiben el crecimiento [114], también existen evidencias de que JNK puede actuar como señal de

supervivencia en células de carcinoma hepático [115] y en líneas celulares de cáncer gástrico y colorrectal [116]. Otra hipótesis, es que la activación prolongada de JNK pueda inducir apoptosis, mientras que la activación transitoria promociona la supervivencia celular, debido a la duración o a la magnitud de la activación de la vía y en parte a la activación de otras vías de supervivencia [117].

4.4.3. Familia p38.

La vía p38 regula principalmente la apoptosis, la respuesta inflamatoria y transmite señales inhibidoras del crecimiento, estando implicada en respuestas a estímulos de estrés extracelular, en la regulación del ciclo celular y en la osmorregulación. La vía p38, al igual que la vía JNK, se activa por estrés ambiental, y citoquinas inflamatorias, y es activada de forma contraria en menor medida por la insulina y factores de crecimiento; pero a diferencia de JNK, p38 también se activa en la isquemia por reperfusión [118].

Se conocen cuatro isoformas de p38 (α, β, γ y δ) y sus sustratos son: factores de transcripción, otras quinasas y proteínas citosólicas como fosfolipasa A2, proteínas de movilidad, Tau (proteína asociada a microtúbulos) y queratina 8, entre otros [104].

p38 está presente tanto en el núcleo como en el citoplasma de las células quiescentes, y aunque existen evidencias de que a raíz de su activación se transloca del citoplasma al núcleo, p38 también está presente en el citoplasma [119]. p38 también participa en la respuesta de los macrófagos y neutrófilos, la quimiotaxis, la exocitosis granular, la adhesión, y la apoptosis; y también en la diferenciación y apoptosis de células T [120].

El papel de p38 en la apoptosis depende de la línea celular y del estímulo inducido [121]. La activación de p38 es necesaria para la apoptosis inducida por cadmio, retirada de factor trófico e isquemia [122,123,124,125], sin embargo, su activación no se produce en la apoptosis inducida por la radiación ultravioleta en células U937 [126] ni por S-nitrosoglutatión en macrófagos RAW 264.7 [127] ni en células Jurkat T tratadas con Fas y/o UV [128]. Muchos agentes quimioterapéuticos inducen la apoptosis mediante la activación de p38 [129,130], mientras que la supresión de su activación aumenta la apoptosis en respuesta al daño del ADN inducido por la doxorrubicina o el cisplatino [131].

p38 es activada por diferentes tipos de estrés celular y actúa en un paso previo a la disfunción de la mitocondria y a la activación de la cascada de caspasas. Sin embargo, p38 también puede funcionar como un supresor de tumores, posiblemente mediante la activación de p53

[104]. En células endoteliales, p38 induce fosforilación y disminución de los niveles de Bcl-x_L y aumenta la expresión de p53. Además, p38 es uno de los potenciales reguladores de Bax [132] y un mediador de la respuesta a los puntos de control de G_2/M [133,134]. El punto de unión entre p38 y el control del ciclo celular parece ser la regulación de los sustratos HBP1 y p21 [135]. Muchos de los efectos de p38 sobre el ciclo celular están mediados por otras quinasas, las cuales fosforilan diversos sustratos que influyen en la expresión génica.

4.5. Esfingolípidos.

Los esfingolípidos son una familia de lípidos presentes en la membrana que contribuyen a la regulación de su fluidez y a su estructura de bicapa lipídica. Además, los esfingolípidos bioactivos, como son la ceramida, la glucosilceramida y la esfingosina generalmente median respuestas antiproliferativas como inhibición del crecimiento, parada del ciclo celular, senescencia y apoptosis. Mientras que la esfingosina 1-fosfato (S1P) juega un papel opuesto induciendo la supervivencia y la proliferación celular. El equilibrio entre los niveles intracelulares de cada uno de estos esfingolípidos está controlado por las enzimas que los producen. La esfingosina quinasa (SK) es uno de los reguladores esenciales de este balance, cataliza la formación del metabolito pro-supervivencia esfingosina 1-fosfato y reduce el contenido de los metabolitos pro-apoptóticos [136]. Existen varias rutas de entrada a la vía de los esfingolípidos que convergen en la formación de ceramidas, que desempeña un papel clave en la generación de otros esfingolípidos activos:

- La primera ruta de entrada es la biosíntesis *de novo:* la serina y el palmitoil CoA se condensan y conducen a la formación de ceramida en el retículo endoplásmico y en el aparato de Golgi. La ceramida puede ser convertida en esfingosina, S1P, o bien formar esfingomielina y glicoesfingolípidos complejos. Esta es la única ruta bioquímica de eliminación de ceramidas y demás esfingolípidos de la célula, ya que se requiere la transformación final en S1P, mediada por la SK. Esta vía puede ser activada por agentes quimioterápicos, choque térmico y LDL oxidadas. La ceramida formada *de novo* está involucrada en la respuesta al estrés y en la apoptosis.

- La segunda ruta implica la hidrólisis de esfingomielina por acción de las esfingomielinasas. La hidrólisis de esfingomielina es considerada la principal vía para la producción de ceramida como transductor de señales que regulan la muerte celular [6, 141][137]. En primer término se forma ceramida, que es hidrolizada por la acción de

ceramidasas para formar esfingosina, que a su vez es transformada por la SK en S1P. Esta vía es estimulada en respuesta al TNF-α, al ligando Fas o al estrés oxidativo [137,138].

- Un tercer mecanismo más complejo de formación y acumulación de ceramidas, es la vía de salvamento. Este mecanismo se relaciona con el catabolismo de esfingolípidos complejos que se transforman en esfingosina, y mediante reacilación son reutilizados para producir ceramida. Está mediada por una serie de enzimas claves: esfingomielinasas, posiblemente glucocerebrosidasas (ácidoβ -glucosidasa), ceramidasas, y (dihidro) ceramida sintasas. La ceramida generada por esta vía es transformada por la ceramidasa ácida para formar esfingosina y ácidos grasos libres, que son capaces de dejar el lisosoma [7, 143][139], mientras la ceramida no sale del lisosoma. Una vez liberados de los lisosomas pueden entrar en la vía de la síntesis de ceramida o en la síntesis de S1P (mediante esfingosina quinasas). Esta vía, se cree que es la responsable de las funciones de la ceramida generada en situaciones como la detención del crecimiento, la apoptosis, y la señalización celular [140].

La diferente activación de cada una de las vías de formación de ceramidas es posible gracias a la separación espacial de las enzimas que contribuyen a su formación. El metabolismo de los esfingolípidos, es específico del tipo celular, y es regulado a diferentes niveles, mediante la expresión de enzimas, modificaciones post-traduccionales y mecanismos alostéricos.

4.5.1. Ceramidas.

La ceramida también se conoce como lípido supresor de tumores, debido a su efecto apoptótico en respuesta a estímulos de estrés celular, y su acumulación en respuesta a agentes pro-apoptóticos [141]. Está implicada en la regulación de parada del ciclo y muerte celular, y/o apoptosis, actuando sobre fosfatasas y quinasas como Akt, proteínquinasa C (PKC), MAPKs, la proteína retinoblastoma Rb, la quinasa dependiente de ciclina p21 y la quinasa dependiente de ciclina CDK2. Su influencia en la senescencia se atribuye a fallos en la vía fosfolipasa C/proteínquinasa C, enzimas que son inhibidas por ceramida [142].

La hidrólisis de esfingomielina da lugar a la liberación de ceramidas, y se han identificado al menos cinco subtipos diferentes de esfingomielinasas dependiendo de su pH óptimo, su localización subcelular y su dependencia de cationes: Smasa neutra dependiente de magnesio y unida a membrana (N-SMasa), SMasa neutra independiente de magnesio, SMasa ácida presente en los lisosomas (A-SMasa), una forma secretada y soluble de SMasa ácida

dependiente de zinc y una SMasa alcalina. El papel específico de cada una no se conoce con detalle siendo la N-SMasa y la A-SMasa las más estudiadas.

La N-SMasa es activada por el receptor de TNF a través de una proteína adaptadora denominada FAN asociándose al dominio NSD del receptor [6, 141][137], y provocando la atracción y activación de numerosas proteínas implicadas en rutas de señalización [137].

La A-SMasa, puede ser también activada por el receptor de TNF a través de otras proteínas adaptadoras como FADD y TRADD que se unen al dominio de muerte (DED) del receptor [143], y su expresión es imprescindible para que se produzca la muerte celular en respuesta a una gran variedad de estímulos que inducen la acumulación de ceramidas como: la luz ultravioleta, la irradiación y el estrés. En respuesta a estos estímulos se produce una translocación de la A-SMasa desde las vesículas intracelulares en que se encuentra a la membrana celular donde se fusiona con la misma y se produce una liberación de ceramidas [144].

Estudios recientes señalan a la mitocondria como un lugar de generación y actuación de las ceramidas [145,146,147]. La ceramida mitocondrial parece generarse a través de la vía de síntesis de novo, y/o a través de la actividad de la A-SMasa, que se encuentra entre la membrana externa e interna de la mitocondria [148]. En la mitocondria, la apoptosis inducida por la ceramida puede ser bloqueada por Bcl-2, indicando que la produción de ceramidas en la apoptosis es un evento anterior al punto de control de Bcl-2 [146]. La ceramida está implicada en la formación de poros mitocondriales que favorecen la salida de factores pro-apoptóticos como el citocromo *c*, AIF, Smac/Diablo y la Endonucleasa G; así como en la activación de numerosas vías de transducción de señales, mediante la interacción con diferentes proteínas.

Otro mecanismo por el cual la ceramida puede inducir apoptosis es la regulación del potencial redox, induciendo estrés oxidativo a través de la disfunción mitocondrial, sobreexpresión de NO sintasa, activación de la NADPH oxidasa y desregulación de enzimas antioxidantes.

OBJETIVOS

1. Evaluar la actividad antitumoral de una serie de flavonoides utilizando como modelo de estudio diversas líneas celulares tumorales humanas.

2. Seleccionar los compuestos más citotóxicos e investigar su mecanismo de acción.

MATERIAL Y MÉTODOS

1. Agentes farmacológicos.

Los estudios correspondientes al aislamiento, elucidación estructural y derivatizaciones de los productos naturales fueron llevados a cabo en el Instituto Universitario de Bio-Orgánica "Antonio González", La Laguna, Tenerife, bajo la dirección del Dr. Jesús M. González Díaz. Los compuestos naturales utilizados en este estudio se aislaron de *Consolida oliveriana* (DC) Schrod, que fue recogida e identificada en el este de Turquía (Pazarkik) a una altitud de 980 metros por el Prof. Julián Molero Briones, del Departamento de Botánica, de la Facultad de Farmacia de la Universidad de Barcelona, donde ha sido depositado un espécimen (BCF-37810) [149].

Partiendo de las partes aéreas de *Consolida oliveriana* se aislaron los siguientes compuestos: hiperósido, 2´-acetilhiperósido **(2)**, 6´-acetilhiperósido **(3)**, kaempferol, quercetina, trifolín, 7-glucotrifolín, robinina y biorobinina. A partir de algunos de ellos, mediante acetilación, se obtuvieron los siguientes compuestos: hiperósido acetato **(1)**, kaempferol tetraacetato **(5)**, trifolín hexaacetato **(11)**, trifolín heptaacetato **(12)**, glucotrifolín decaacetato **(13)**, quercetín pentaacetato **(15)**, biorobina nonaacetato y robinina undecaacetato. Finalmente, mediante metilación del trifolín se obtuvo el heptametiltrifolín **(14)**.

La identificación de las estructuras se realizó por espectroscopía de resonancia magnética nuclear (^{1}H-NMR y ^{13}C-NMR) y espectrometría de masas de alta resolución (HR-MS), la pureza de todos los compuestos fue del 99%.

Los compuestos de origen sintético fueron los siguientes: kaempferol **(4)**, 3´,4´,7,8-tetrahidroxiflavona **(6)**, 3´,4´,5-trihidroxi-6,7-dimetoxiflavona **(7)**, 3´,5,7-Trihidroxi-3,4´-dimetoxiflavona **(8)**, 3-metoxiflavona **(9)**, 6-metoxiflavonol **(10)**, quercetín-3,7,3´,4´-tetrametiléter **(16)**, robinetina **(17)**, siringetina **(18)**, tamarixetina **(19)** y tangeretina **(20)**, todos ellos suministrados por Extrasynthese (Lyon Nord, France).

2. Productos y material:

Los medios de cultivo RPMI 1640 y Dulbecco´s MEM (DMEM), el suero bovino fetal (FBS), la tripsina, el HEPES (N-[2-hidroxietil] piperazino N'-[2-etanosulfanílico]), la L-glutamina, el azul de tripán, el bicarbonato sódico y los antibióticos (estreptomicina, gentamicina y penicilina G) fueron de Sigma Chemical Co. (St. Louis, MO, USA). Las botellas de cultivo de 75 cm^2 y las placas de 48 y 96 pocillos estériles, así como el resto del material estéril utilizado fueron de Becton-Dickinson.

El yoduro de propidio, la RNasa A, la proteinasa K, el paraformaldehído, la bisbenzimida (Hoechst nº 33258) y el fenol fueron suministradas por Sigma Chemical Co. El cloroformo y alcohol isoamílico se obtuvieron de BDH (Poole, Inglaterra). La agarosa se obtuvo de Bio-Rad (Madrid, España) y el bromuro de etidio de Sigma/Aldrich (España). Se utilizó un microscopio de fluorescencia LSM 5 PASCAL de ZEISS.

La anexina V se obtuvo de BD PharmigenTH (Annexin V-FITC Apoptosis Detection Kit). Los fluorocromos H_2-DCF-DA (diacetato 2´,7´-dicloro-dihidro-fluoresceína) y JC-1 (yoduro de 5,5', 6,6'–tetracloro-1,1', 3,3'-tetraetil-benzimidazolo-carbocianina) se obtuvieron de Molecular Probes (Invitrogen Corporation Carlsbad, CA). Los inhibidores de caspasas: z-VAD-fmk (benziloxi-carbonil-Val-Ala-Asp (OME)-fluoro metil cetona), z-DEVD-fmk (Benziloxicarbonil-Asp-Glu-Val-Asp-(OME) fluorometil cetona), z-LEHD-fmk (Benziloxicarbonil-Leu-Glu-His-Asp (OME) fluorometil cetona), z-IETD-fmk (Benziloxicarbonil-Ile-Glu-Thr-Asp(OME) fluorometil cetona), z-VDVAD-fmk (Benziloxicarbonil-Val-Asp-Val-Ala-Asp(OME) fluorometil cetona) fueron obtenidos de Sigma, mientras que los inhibidores z-YVAD-fmk (Benziloxicarbonil-Tyr-Val-Ala-Asp(OME) fluorometil cetona) y z-VEID-fmk (Benziloxicarbonil-Val-Glu-Ile-Asp(OME) fluorometil cetona fueron obtenidos de Calbiochem.

El nocodazol, desipramina, miriocina, fumonisina B1, GW4869, SP600125, PD98059, SB203580, wortmanina, Trolox, N-acetil-L-cisteína (NAC), Tocoferol (vitamina E), ditiotreitol (DTT), alopurinol, ácido ascórbico (vitamina C), hidroxibutilanisol (BHA), pirrolidín ditiocarbamato (PDTC), catalasa (CAT) y superóxido dismutasa (SOD), U0126 y el resto de inhibidores fueron obtenidos de Sigma Chemical Co.

El sustrato específico utilizado para determinar la actividad caspasa -3/-7 fue N-acetil-Asp-Glu-Val-Asp-p-nitroanilina (DEVD-pNA) obtenido de Sigma, y la paranitroanilina (pNA) fue obtenida de Calbiochem.

La acrilamida (bis N,N'-metilen-bis-acrilamida), persulfato amónico, TEMED (N,N,N,N,-tetrametil-etilendiamina), SDS (dodecil sulfato sódico) y los marcadores de pesos moleculares se obtuvieron de Bio-Rad. El azul de bromofenol, el BSA (albumina de suero bovino) y el β-mercaptoetanol fueron de Sigma. Las membranas (PVDF) y el sustrato de revelado por quimioluminiscencia se obtuvieron de Millipore (Billerica, MA, USA). Las placas para autorradiografía se adquirieron de Kodak.

Los productos utilizados en la obtención del lisado celular, fueron: aprotinina (inhibidor de serínproteasas que inhibe tripsina, quimiotripsina y plasmina), leupeptina (inhibidor de cisteín y serínproteasas. Inhibe plasmina, tripsina, papaína y catepsina B), pepstatina A (inhibidor potente de proteasas ácidas), PMSF (inhibe cisteín, serínproteasas y acetilcolinesterasa), ditiotreitol (DTT: agente reductor estereoselectivo para puentes disulfuro en complejos moleculares), ortovanadato sódico (inhibidor de fosfatasas alcalinas) y el detergente tritón X-100 fueron obtenidos de Sigma Chemical Co.

Los anticuerpos para PARP, caspasa -3, caspasa -6, caspasa -7, caspasa -8, caspasa -9, citocromo *c*, BCL-2 se obtuvieron de Stressgen (Victoria, British Columbia, Canada). El anticuerpo para BAX, α-tubulina y anti-β-actina se obtuvieron de Sigma/Aldrich.

Los anticuerpos para fosfo-$p38^{MAPK}$ (Thr^{180}/Tyr^{182}), $p38^{MAPK}$, fosfo-JNK (Thr^{183}/Tyr^{185}), JNK, fosfo-ERK1/2 (Thr^{202}/Tyr^{204}) y ERK1/2 fueron obtenidos de New England Biolabs (Cell Signaling Technology, Beverly, MA, USA). Los anticuerpos anti-ciclina B1, anti-fosfo-ciclina B1, anti-cox IV, anti-cdc25c, anti-fosfo-cdc25c, anti-CDK 1, anti-fosfo-CDK1, anti-p21 y anti-MPM2 se obtuvieron de Abcam (Cambridge, UK). Los anticuerpos secundarios se obtuvieron de Amersham Biosciences.

El anticuerpo anti-α-tubulina, el suero normal de cabra (NGS), la colchicina y el paclitaxel fueron obtenidos de Sigma Chemical Co., el BSA (albumina de suero bovino) de Sigma/Aldrich y el Anti –IgG de ratón (H+L)-Cy2™ (cabra) de Jackson Immuno Research Laboratories, Inc. (West Grove, PA, USA). El VECTASHIELD® con DAPI (Vector Laboratories, INC. Burlingame, CA 94010) y se utilizó un microscopio de fluorescencia LSM 5 PASCAL de ZEISS. El CytoDYNAMIX ScreenTM3 (CDS-03) fue adquirido de Cytoskeleton Inc. (Denver, CO). Los filtros de DEAE-celulosa (DE81) fueron obtenidos de Whatman (Maidstone, UK),

La N-metil-^{14}C-esfingomielina (actividad específica 56.6 mCi/mmol) y el [γ-^{32}P] 5´-trifosfato de adenosina (actividad específica 3000 Ci/mmol) fueron obtenidos de Perkin Elmer (Madrid, Spain) y sn-1,2-Diacilglicerol quinasa fue obtenido de Calbiochem (Darmstadt, Germany). Las placas de TLC (placas de silica gel de 250 μm de espesor) fueron obtenidos de Whatman (Maidstone, UK).

El agua desionizada y bidestilada se obtuvo con un equipo Mili-Q (Water Purification System, Millipore Ibérica, Madrid, Spain). El dimetilsulfóxido (DMSO), EDTA, EGTA,

NaCl, glicerol, trizma base, trizma-HCl, azida sódica, bromuro de 3-[4,5- dimetiltiazol-2-il]-2,5-difeniltetrazolio (MTT), la sacarosa, tween 20, hidróxido de sodio, ácido clorhídrico y otros compuestos utilizados en la preparación de reactivos y tampones se adquirieron de Sigma Chemical Co. o de BDH (Carlo Erba, E Merck y Fluka).

3. *Modelo experimental.*

Las células se contaron en un hematocitómetro y la viabilidad siempre fue superior al 95% utilizando el método de exclusión de azul de tripán.

3.1. Cultivo de células leucémicas humanas HL-60, JURKAT y MOLT-3, y células de linfoma histiocítico humano U937.

Las células HL-60, JURKAT, MOLT-3 y U937 se obtuvieron de la colección europea de cultivos celulares (European Collection of Cell Cultures, ECACC) y se cultivaron en medio RPMI 1640 suplementado con 10% (v/v) de suero bovino fetal (FBS) inactivado por calor y antibiótico (100 unidades/ml de penicilina y 100 μg/ml estreptomicina) en una atmósfera humidificada (37 ºC y 5% $CO_{2)}$ y a una densidad no superior a 0.5 x 10^6 células/ml [150,151]. A las células se les cambió el medio de cultivo tres veces por semana y se dividieron aproximadamente cada 24 horas.

3.2. Cultivo de células de melanoma humanas SK-MEL-1.

Las células de melanoma humano SK-MEL-1 se obtuvieron de la colección alemana de cultivos celulares (DMSZ), se cultivaron en medio RPMI 1640 en las mismas condiciones que las anteriores. Aunque las células crecen lentamente producen sin embargo una rápida acidificación del medio por lo que el medio de cultivo se cambió tres veces por semana [150,151].

3.3. Cultivo de células A549.

Las células de cáncer de pulmón humano A549 se obtuvieron de la colección alemana de cultivos celulares (DMSZ) y se cultivaron en medio DMEM conteniendo 10% de suero bovino fetal inactivado por calor, 100 unidades/ml de penicilina y 100 μg/ml estreptomicina, en placas Falcon de 100 mm. Estas células son adherentes y crecen rápidamente, por lo que se pasaron dos o tres veces en semana utilizando 0,25 % tripsina-EDTA durante 5 minutos y las células obtenidas por centrifugación (500 g durante 5 minutos) se resuspendieron a una

densidad de [1×10^4] células/ml. Se mantuvieron en una atmósfera humidificada (37 ºC y 5% CO_2) [150,151].

3.4. Cultivo de células HL-60 transfectadas con el gen humano Bcl-x_L y con el vector control, y de células U937 que expresan niveles elevados del gen humano Bcl-2.

Las células HL-60 fueron transfectadas con el plasmido pSFFV-neo (HL-60/neo) o con el plasmido pSFFV-Bcl-x_L (HL-60/Bcl-x_L) que fueron establecidos por el Dr. Kapil N Bhalla (Medical College of Georgia Cancer Center, GA, USA) y fueron obtenidas por donación de Dra. Angelika Vollmar (Department of Pharmacy, University of Munich, Germany). Las células HL-60/Bcl-x_L y HL-60/neo fueron cultivadas igual que en el caso de las células HL-60, añadiendo 0,1 mM de aminoácidos no esenciales y 1 mM de piruvato de sodio (Invitrogen) al medio de cultivo. Además añadimos gentamicina (1mg/ml) al medio de cultivo cada quinto pase, y las células con gentamicina no fueron empleadas para los experimentos.

Las células U937/Bcl-2 fueron proporcionadas por la Dra. Jacqueline Bréard (INSERM U749, Faculté de Pharmacie Paris-Sud, Châtenay-Malabry, France). Las células se cultivaron en RPMI 1640 con glutamax y 25mM de HEPES, 1% MEM piruvato de sodio, complementado con un 10% de suero bovino fetal inactivado por calor, 100 unidades /ml de penicilina y 100 μg/ml estreptomicina, en una atmósfera humidificada a 37 ºC y 5% CO_2.

A las células se les cambió el medio de cultivo tres veces por semana y se duplicaron cada 24 horas [150,151].

3.5. Células mononucleares de sangre periférica de origen humano.

Las células mononucleares de sangre periférica de origen humano (PBMC) fueron aisladas de sangre obtenida de voluntarios sanos, recogidas en tubos heparinizados para evitar la coagulación y se aislaron mediante centrifugación con Ficoll-Paque Plus (Amersham Biosciences). Una parte de las PBMCs obtenidas se estimularon con fitohemaglutinina (PHA, 2 mg / ml) durante 48 h antes del tratamiento experimental.

3.6. Tratamiento con los compuestos.

Los productos se prepararon a una concentración de 10-100 mM en dimetilsulfóxido (DMSO) y las alícuotas se mantuvieron a –20º C. Las diluciones necesarias se hicieron en medio de cultivo justo antes del experimento y el porcentaje de DMSO no excedió del 0,3%,

concentración no tóxica para las células. La misma proporción de DMSO fue añadida a las células control.

4. Métodos:

4.1. Evaluación de la citotoxicidad in vitro y estudios de la proliferación celular: MTT.

Se realizó, mediante el ensayo de la reducción metabólica del bromuro de 3-[4,5-dimetiltiazol-2-il]-2,5-difeniltetrazolio (MTT) por la actividad deshidrogenasa mitocondrial [152].

Las células se cultivaron en placas de 96 pocitos, por triplicado, a una densidad de $1x10^4$ células/pocito en 0,2 ml de medio de cultivo y en presencia de diferentes concentraciones de los flavonoides durante 72 h. Las placas se centrifugaron (500 g, 10 min) a temperatura ambiente y el medio se eliminó por aspiración. A cada pocito se le añadió 100 μl de MTT (0,5 mg/ml en medio de cultivo con antibiótico pero sin suero) y las placas se incubaron durante 4 h a 37 ^oC. La reacción se paró añadiendo 100 μl de SDS (20%) con HCl 0.02 N e incubando la mezcla hasta la mañana siguiente. La cuantificación de la conversión del MTT (amarillo) en su forma reducida (púrpura) por la deshidrogenasa mitocondrial se determinó a 570 nm en un lector de microplacas (modelo 680 Bio-Rad) utilizando como blancos pocitos sin células a los que se les añadió medio. Los datos se analizaron con el programa informático Prism 2.0 (GraphPad) y se determinó la concentración de producto que inhibe el crecimiento celular a la mitad (IC_{50}) [150,153].

4.2. Estudio de la apoptosis celular:

La apoptosis celular se determinó mediante diversos criterios:

4.2.1 Tinción con el fluorocromo bisbenzimida.

Método cuantitativo, basado en la capacidad del fluorocromo para unirse al ADN, permitiendo visualizar la existencia de cambios morfológicos del núcleo como son la condensación de la cromatina y su compactación a lo largo de la periferia del núcleo y la segmentación del núcleo. Una vez finalizados los tratamientos, las células (~$5x10^5$) se lavaron con PBS (10 mM fosfato sódico, 150 mM NaCl, pH 7,4) y se fijaron con 70 μl de paraformaldehído (3% en PBS) durante 10 minutos a temperatura ambiente. A continuación se centrifugaron (12.000 g, 1 minuto), se eliminó el paraformaldehído y las células se tiñeron

con 20 µl de una disolución que contenía 20 µg/mL de bisbenzimida (Hoechst 33258) en PBS durante 15 minutos a temperatura ambiente y en la oscuridad. Una alícuota (10 µl) se fijó en un porta y se analizó la morfología nuclear de 500 células con un microscopio de fluorescencia (Zeiss-Axiovert). Se consideraron células apoptóticas aquellas cuyos núcleos presentaron condensación de la cromatina, su compactación a lo largo de la periferia y/o la fragmentación nuclear en tres o más cuerpos apoptóticos [150].

4.2.2. Fragmentación del ADN.

Método cualitativo, basado en la detección de la fragmentación internucleosómica del ADN y visualización como una escalera discontinua de bandas multiméricas de 185-200 pares de bases, características del proceso apoptótico.

Las células (5 x 10^5 células/ml) después de ser tratadas con los distintos flavonoides se recolectaron por centrifugación (12.000 g, 1 minuto) y se lavaron dos veces con PBS frío. Las células se resuspendieron con 30 µl de tampón de lisis [50 mM Tris-HCl (pH 8,0), 10 mM EDTA, 0,5% SDS] y se incubaron sucesivamente con 1 µg/µl de RNasa A (1 hora a 37 ºC) y con 1 µg/ µl de Proteinasa K (1h a 50ºC). Se añadió a cada muestra 2 µl de azul bromofenol (0,25%) y el ADN se extrajo con 100 µl de una mezcla fenol:cloroformo:alcohol isoamílico (24:24:1). Las muestras se centrifugaron (12.000 g, 1 min.) a temperatura ambiente y la fase acuosa (azul) se lavó nuevamente con 100 µl de cloroformo. A las muestras se les añadió 5 µl de tampón de carga (10 mM EDTA, pH 8,0, conteniendo 1% (p/v) de agarosa de bajo punto de fusión y 40% de sacarosa) y se incubaron a 70ºC durante 5-10 minutos. Finalmente 30 µl de cada muestra se sometieron a electroforesis (5 V/cm) durante 3-4 h en geles de agarosa al 1,8 %. Los geles se tiñeron con bromuro de etidio (1 µg/ml durante 20 min), los fragmentos de ADN se visualizaron a 260 nm en un transiluminador y la imagen se captó con una cámara digital (DC290, Kodak) y se analizó con el software Quantity One (Bio-Rad).

4.2.3. Cuantificación de células hipodiploides por citometría de flujo. Cuantificación de la fracción SubG_1, G_1, S y G_2/M mediante el análisis del contenido en ADN.

Método cuantitativo basado en la fluorescencia emitida por diferentes fluorocromos capaces de unirse al ADN (Ej. yoduro de propidio). Se puede detectar el porcentaje de células en cada fase del ciclo celular en función de su contenido en ADN. Las células en fase G_1 forman el primer pico, en la fase S las células están sintetizando ADN y en fase G_2/M las células

presentan el doble de contenido en ADN que una célula normal y aparecerán como un segundo pico. Las células que contienen ADN hipodiploide (menor contenido de ADN que el contenido diploide de las células normales) son consideradas apoptóticas, y se localizan a la izquierda del pico G_1 constituyendo la fracción $SubG_1$ [150].

Después de los tratamientos, las células se lavaron con PBS frío y se fijaron durante al menos una hora en etanol al 70 %, a -20ºC. A continuación se lavaron dos veces con PBS, se centrifugaron a 500 g durante 10 minutos y se incubaron con 1 ml de PBS (1h a 37ºC en oscuridad) conteniendo 100 μg/ml de RNasa A y 50 μg/ml de yoduro de propidio. La sonda fue excitada a 488nm y la fluorescencia emitida por el complejo propidio-ADN (617nm) se determinó en un citómetro Coulter Epics XL-MCL, (Beckman Coulter) usando el detector FL3 (620±15nm). Se analizaron 10.000 células en cada muestra y los resultados se analizaron con el software EXPO 32 ADC Sofware^{tm} (Beckman Coulter) [153]..

4.2.4. Determinación de las células apoptóticas mediante el análisis de la externalización de fosfatidilserina.

La fosfatidilserina es un fosfolípido que normalmente se encuentra en la cara interna de la membrana plasmática y se transloca a la cara externa de dicha membrana en los estadíos tempranos del proceso de apoptosis. La proteína Anexina V se une a fosfatidilserina en presencia de Ca^{2+} y permite detectar las células apoptóticas por citometria de flujo, previa incubación de las células con Anexina V unida a un fluorocromo (FITC). De esta manera distinguimos: a) células viables, no unen anexina V y excluyen yoduro de propidio, b) células en apoptosis temprana, unen anexina V y excluyen yoduro de propidio, c) células en apoptosis tardía, unen anexina V e incorporan yoduro de propidio y d) células necróticas, unen anexina V e incorporan yoduro de propidio, o sólo incorporan yoduro de propidio.

Las células ($1x10^6$ por muestra) una vez tratadas se lavaron con PBS frío, y se resuspendieron en el tampón 1X (10 mM Hepes/NaOH, pH 7,4, 140 mM NaCl, 2,5 mM $CaCl_2$). Se transfirieron 100 μl de la suspensión (1×10^5 células) a un tubo de cultivo de 5 ml, y se le añadió 5 μl de Anexina V-FITC y 5 μl de yoduro de propidio. Mezclamos suavemente las células e incubamos durante 15 minutos a temperatura ambiente (25°C) en la oscuridad. Se añadió 400 μl del anterior tampón 1X a cada tubo, y se analizó cada muestra por citometría de flujo.

Cuando las células en cultivo sufren apoptosis, al no poder ser fagocitadas, sufren necrosis

secundaria al proceso apoptótico, por lo que puede aumentar el número de células que dan positivo a yoduro de propidio.

4.2.5. Microscopía Electrónica de Transmisión (MET).

Para el procesado de muestras en microscopía electrónica de transmisión, las células se centrifugaron, se resuspendieron y se fijaron en glutaraldehído al 2.5 % en tampón fosfato (0.1M, pH 7,2) durante 24 horas. La post-fijación se realizó en OsO_4 al 1% en tampón fosfato. Las células se deshidrataron con una serie de concentraciones crecientes de etanol. El sedimento se incluyó en resina EMBed 812 que polimerizó a 70º C. Los cortes fueron realizados con un ultramicrotomo *Reichert Ultracut s (Leica).* Los cortes semifinos fueron teñidos con azul de toluidina, mientras que los ultrafinos fueron contrastados con acetato de uranilo y plomo. Las fotografías fueron tomadas en un microscopio electrónico de transmisión *Zeiss EM 910 (Carl ZEISS, Germany*) equipado con cámara digital *Proscan Slow-scan CCD-Camera for TEM (Fa. Proscan Elektronische Systeme GmbH, Germany)* y software *Soft Imaging System (Germany)* del *Servicio de Microscopía Electrónica de la Universidad de Las Palmas de Gran Canaria*.

4.3. Determinación de la actividad caspasa.

Las células tratadas se centrifugaron a 1.000 g durante 5 min a 4 °C, se lavaron con PBS y se incubaron en hielo. Las células se resuspendieron en tampón de lisis (50 mM HEPES, pH 7,4, 1 mM dithiothreitol, 0,1 mM EDTA, 0.1% Chaps) y se dejaron 5 min en hielo. Se centrifugaron durante 10 min at 16.000 g a 4°C, se determinó la concentración de proteínas en los sobrenadantes mediante el método de Bradford y se almacenaron a −20 °C hasta que se usaron para el estudio de la actividad enzimática de las caspasas. Se utilizó una cantidad equivalente de proteínas de los diferentes tratamientos (~20 µg). El incremento de la absorbancia a 405 nm después de la incubación a 37 °C durante 1 hora fue indicativo de la actividad enzimática de las caspasas. El sustrato colorimétrico específico utilizado en el ensayo para la actividad caspasa -3/7 fue N-acetil-Asp-Glu-Val-Asp-p-nitroanilina (DEVD-pNA).

4.4. Inmunodetección de proteínas (western blot).

Las células (1-10 x 10^6) se incubaron en medio de cultivo con los productos de interés durante distintos tiempos a 37 ºC. A continuación se recolectaron por centrifugación (500 g, 10 minutos, 4ºC) y se lavaron dos veces con PBS. En este punto, las células se procesaron de

distinta forma: en función de si se necesitaba el lisado celular o las diferentes fracciones subcelulares (fracción nuclear, citosólica y mitocondrial).

- *Obtención del lisado celular:*

El precipitado celular se resuspendió en 100 µl de tampón de lisis [Tris-HCl (pH 7,4), 2 mM EDTA, 137 mM cloruro sódico, 10% glicerol, 1% Triton X-100, 2 mM de pirofosfato de sodio, 20 mM glicerofosfato de sodio, 10 mM fluoruro sódico, 2 mM ortovanadato sódico, 1 mM PMSF, leupeptina (5 µg/ml), aprotinina (5 µg/ml) y pepstatina A (5 µg/ml)] e incubó durante 15 min a 4ºC. Los lisados se sonicaron (cuatro ciclos de cinco segundos) y se centrifugaron a 11,000 x g durante 10 min a 4ºC. El precipitado resultante (membranas y demás restos celulares) se descartó, mientras el sobrenadante se analizó [150,152].

- *Fraccionamiento subcelular:*

El precipitado celular (~ 10^7 células) se resuspendió en 100 µl de tampón de homogeneización [20 mM HEPES-KOH (pH 7,5), 10 mM KCl, 1,5 mM $MgCl_2$, 1 mM EDTA, 1 mM EGTA, 1 mM DTT, 250 mM sacarosa] con inhibidores de proteasas (0,1 mM PMSF, 10 µg/ml de leupeptina, 10 µg/ml aprotinina y 10 µg/ml pepstatina A), y se incubó durante 15 min a 4 ºC. Las células se lisaron usando una aguja de 21G y el extracto resultante se centrifugó a 1.000 x g durante 5 min a 4 ºC. El precipitado (fracción nuclear) se resuspendió en 100 µl de tampón de homogeneización y se sonicó 3 veces durante 10 segundos a 4 ºC. El sobrenadante resultante se centrifugó a 22.000 x g durante 20 minutos a 4ºC. El precipitado (fracción mitocondrial) se resuspendió en 50 µl de tampón de homogeneización mientras que el sobrenadante fue utilizado como fracción citosólica. Las diferentes fracciones se congelaron a -20 ºC hasta su utilización [150].

La concentración de proteínas se determinó por el método de Bradford, y todas las muestras se ajustaron a la misma concentración utilizando el tampón anterior. Los lisados celulares se hirvieron en tampón de electroforesis [50 mM Tris-HCl (pH 6,8), 15% sacarosa, 2 mM EDTA, 3% SDS, 5 mM β-mercaptoetanol y 0,01% azul de bromofenol] a 100 ºC durante 5 min [150].

Las muestras se sometieron a electroforesis en un gel de poliacrilamida (del 7,5% al 15%, dependiendo del peso molecular de la proteína a estudiar) conteniendo 0,1% SDS y se transfirieron a membranas de PVDF. Las membranas se bloquearon con 10% de leche

desnatada en tampón TBST [20 mM Tris-HCl (pH 7,5), 137 mM NaCl, 0,1 % Tween-20] durante 1 h a temperatura ambiente (o toda la noche a 4 ºC), seguido de una incubación con el anticuerpo específico.

Los anticuerpos utilizados en este estudio se diluyeron en TBST conteniendo 3% de leche desnatada y las membranas se incubaron en presencia del anticuerpo de interés, durante 24 h con agitación suave y a 4 ºC. Las membranas se lavaron con TBST tres veces durante 15 min cada vez y se incubaron con el anticuerpo secundario apropiado durante 1 h a temperatura ambiente. Finalmente las membranas se lavaron nuevamente con TBST en las mismas condiciones anteriores y la detección de las proteínas específicas se determinó por emisión de quimioluminiscencia, utilizando un kit comercial y posterior exposición de las membranas sobre películas de autorradiografía. Las imágenes fueron capturadas con un escáner y analizadas con el programa Adobe Photoshop 7.0.

Como control de que se ha cargado y transferido la misma cantidad de proteínas, las distintas muestras se analizaron con un anticuerpo específico anti-β-actina.

4.5. Análisis de la tubulina por western blot.

Las células (~ $0{,}5x10^6$ células) se incubaron a las concentraciones indicadas de 3´,5,7-Trihidroxi-3,4´-dimetoxiflavona (THDF), paclitaxel y colchicina durante el tiempo seleccionado. Las células se recolectaron por centrifugación (500 g, 10 min, 4 ºC) y se lavaron tres veces con PBS. Los precipitados celulares se resuspendieron en 100 µl de tampón de homogeneización [20 mM Tris-HCl (pH 6,8), 1 mM $MgCl_2$, 2 mM EGTA, 5 µg/ml leupeptina, 5 µg/ml aprotinina, 1 mM PMSF, 1 mM ortovanadato y 0,5% Nonidet], se incubaron a 4 º C durante 5 min y se centrifugaron a 15.000 g durante 10 min a 4 ºC. En el sobrenadante obtenido tendremos la tubulina soluble y en el precipitado la tubulina insoluble. La fracción insoluble se solubilizó con 100 µl de tampón de homogeneización mediante sonicación. Se determinó la concentración de proteínas en cada una de las fracciones obtenidas mediante el método de Bradford y se igualaron posteriormente las concentraciones de todas las muestras. Cantidades equivalentes de cada muestra se mezclaron con tampón de electroforesis [50 mM Tris-HCl (pH 6,8), 15% sacarosa, 2mM EDTA, 3% SDS, 5 mM β-mercaptoetanol y 0,01% azul de bromofenol] y se hirvieron a 100 ºC durante 3 minutos. Las muestras se sometieron a electroforesis en gel de SDS-poliacrilamida al 10% y las proteínas se transferieron a membranas de PVDF. Las membranas se bloquearon con 5% leche desnatada en tampón TBST [50 mM Tris-HCl (pH 7,4), 150 mM NaCl] con 1% Tween 20,

fueron incubadas con un anticuerpo monoclonal anti-α-tubulina (Sigma) y luego con un anticuerpo secundario (GE Healthcare Bio-Sciences AB, Uppsala, Sweden). El complejo antígeno-anticuerpo se visualizó mediante quimioluminiscencia [150].

4.6. Determinación de la generación de especies reactivas de oxígeno intracelular.

La generación de especies reactivas de oxígeno (ROS) intracelular se midió fluorimétricamente usando la sonda diacetato 2´,7´-dicloro-dihidro-fluoresceína (H_2-DCF-DA). Las células fueron expuestas a los tratamientos correspondientes y se incubaron con 8 μM de H_2-DCF-DA durante los últimos 30 minutos antes de finalizar el ensayo, a 37 ºC. Inmediatamente después, las muestras se analizaron mediante citometría de flujo con el equipo Coulter Epics XL-MCL (Beckman Coulter), excitando la sonda con un láser de argón a 488 nm y recogiendo la emisión fluorescente de la diclorofluoresceína (529 nm), con el detector FL1 (525±20 nm). La distinta intensidad de la emisión fluorescente indica la mayor o menor presencia de ROS en el interior de la célula. Los resultados se analizaron con el EXPO 32 ADC Sofware^{tm} (Beckman Coulter) [154,155].

4.7. Análisis de la despolarización de la membrana mitocondrial (ΔΨm).

Las células HL-60 (1 x 10^6 células) se incubaron a 37 ºC en la oscuridad, con la sonda JC-1 (10 μg/ml) durante los últimos 30 minutos antes de finalizar el ensayo y se analizaron mediante citometría de flujo utilizando el canal FL1 (527 nm) para detectar la fluorescencia verde de los monómeros de la sonda y el canal FL2 (590 nm) para la fluorescencia roja de los agregados. La cuantificación de la despolarización mitocondrial (ΔΨm) se obtuvo a partir de la representación gráfica de los datos recogidos por el detector FL1 frente a los recogidos por el detector FL2. La división de las gráficas en cuadrantes permite estimar el porcentaje de células con potencial de membrana intacto (cuadrantes superiores) de aquellas que sufren despolarización mitocondrial (cuadrantes inferiores).

El ionóforo de protones carbonil cianuro *m*-clorofenil hidrazona (CCCP) se utilizó como control positivo de la disipación del potencial de membrana. La despolarización de la membrana mitocondrial inducida por CCCP (10 μM) se ve reflejada por un incremento del número de células que emiten mayor fluorescencia verde y menos roja respecto a las células control y que se sitúan en el cuadrante inferior derecho. Para el análisis se usó citómetro Coulter Epics XL-MCL (Beckman Coulter).

4.8. Análisis de la red de microtúbulos por microscopía de fluorescencia.

Las células (~1x10^6) se lavaron con PBS y se fijaron con 70 µl de paraformaldehído (3%, en PBS) durante 10 minutos a temperatura ambiente. A continuación se centrifugaron (16.000 g, 1 min), se lavaron con PBS y se bloquearon con una disolución de PBS conteniendo un 3 % de BSA (albúmina de suero bovino) y 0,1% de triton X-100 durante 1 hora a 4°C. Las células se lavaron dos veces durante 5 minutos con PBS y se incubaron durante 24 h a 4 ºC con anti-α-tubulina (1/2000) en PBS, 3% BSA, 2% NGS (suero normal de cabra). Las células se lavaron con PBS, se añadió el anticuerpo secundario (1/200), Anti–IgG de ratón (H+L)-Cy2™, (de cabra) en PBS, 3% BSA, 2% NGS e incubaron durante 1 h a 4 ºC. Se realizaron tres lavados con PBS durante 10 minutos y se añadió 10 µL VECTASHIELD®. Tras una incubación de 15 minutos se fijaron las células en un portaobjetos y se analizó la morfología nuclear (en azul se tiñeron los núcleos) y la red de microtúbulos (en verde se visualizó la tubulina), en un microscopio de fluorescencia LSM 5 PASCAL de ZEISS.

4.9. Análisis de la polimerización de tubulina in vitro.

La tubulina (>99% de pureza) a una concentración final de 3 mg/ml fue resuspendida en 100 µl de tampón [80 mM PIPES, pH 6,9, 2 mM $MgCl_2$, 0,5 mM EGTA, 1 mM GTP, 10,2% glicerol] en ausencia o presencia del compuesto ensayado a 4ºC. La mezcla se transfirió a una placa de 96 pocillos a 37ºC, y la polimerización de tubulina se determinó midiendo los cambios en la absorbancia a 340 nm cada minuto durante 100 minutos en un lector de fluorescencia (DTX 880 Multimode Detector, Beckman Coulter).

4.10. Ensayo de competición por la unión a tubulina.

La unión de la [^{3}H] colchicina a la tubulina se determinó utilizando filtros de DEAE-celulosa (DE81), tal y como fue descrito previamente [156]. El ensayo se llevó a cabo en 100 µl de mezcla, conteniendo 1 mM (0,1 mg/ml) tubulina, 1 M glutamato monosódico, 0,1 M glucosa-1-fosfato, 1 mM $MgCl_2$, 1 mM GTP, 0,5 mg/ml albúmina de suero bovino, 5% (v/v) dimetilsulfóxido, 5,0 µM [^{3}H] colchicina (75,5 Ci/mmol, Perkin-Elmer), en ausencia o presencia de diferentes concentraciones del compuesto estudiado. Estas condiciones de reacción se llevaron a cabo para estabilizar fuertemente la unión de la tubulina y la colchicina [157]. Incubamos las muestras durante 10 minutos a 37ºC, y para lavar la [^{3}H] colchicina no unida utilizamos 2 ml de agua fría 5 veces. Finalmente la colchicina retenida por el filtro se

midió usando un contador de centelleo líquido. Cada determinación se realizó 3 veces por triplicado.

4.11. Determinación de la actividad esfingomielinasa ácida y neutra.

Los ensayos de determinación la actividad SMasa se realizaron utilizando [^{14}C-metil-colina] esfingomielina [158]. Las células HL-60 se trataron por triplicado en ausencia o en presencia del compuesto. A los tiempos indicados de tratamiento se paró por inmersión en un baño de hielo seco con metanol, las células se centrifugaron a 1500 rpm durante 5 min a 4ºC y se lavaron dos veces con PBS, separando la mitad de las células para determinar la actividad SMasa ácida y la otra mitad para la actividad SMasa neutra.

- *Determinación de la actividad esfingomielinasa neutra.*

Las células se resuspendieron en 50 µl de tampón que contenía 20 mM Hepes (pH 7,4), 10 mM $MgCl_2$, 2 mM EDTA, 5 mM DTT, 0,1 mM ortovanadato sódico, 0,1 mM molibdato sódico, 30 mM p-nitrofenilfosfato, 10 mM β-glicerofosfato, 750 µM ATP, 1 mM PMSF, 10 µM de leupeptina, 10 µM pepstatina y 0,2% Triton X-100. Después de incubar durante 5 minutos a 4ºC, las células se homogeneizaron con una aguja de 21G y se obtuvo la fracción citosólica mediante centrifugación. Se determinó la concentración de proteínas mediante el método de Bradford y aproximadamente 30 µg de cada muestra se incubó durante 2 horas a 37ºC en un tampón que contenía 20 mM HEPES (pH 7,4), 1 mM $MgCl_2$, 2,25 µl de [N-metil-^{14}C] esfingomielina (0,2 µCi/ml, con una actividad específica de 56,6 mCi/mmol). La cantidad de [^{14}C] esfingomielina hidrolizada no excedió del 10% de la cantidad de esfingomielina radiactiva añadida. La fosforilcolina fue extraída con 800 µl de cloroformo: metanol 2:1 (v/v) y 250 µl de agua. La fosforilcolina radiactiva producida a partir de [^{14}C] esfingomielina fue determinada en la fase acuosa utilizando un contador de centelleo líquido.

- *Determinación de la actividad esfingomielinasa ácida.*

Las células se resuspendieron en 50 µl de 0,2% Triton X-100 y fueron incubadas durante 5 minutos a 4ºC. Las células se homogeneizaron con una aguja de 21G y se obtuvo la fracción citosólica mediante centrifugación. Todas las muestras se ajustaron a la misma concentración de proteínas (~30 µg) y se incubaron durante 2 h a 37 ºC en un tampón que contenía 250 mM acetato de sodio (PH 5,0), 1 mM EDTA, y 2,25 µl de [N-metil-^{14}C] esfingomielina. La cantidad de fosforilcolina producida a partir de [^{14}C] esfingomielina fue determinada en la fase acuosa mediante un contador de centelleo líquido.

4.12. Determinación de la cantidad de ceramidas.

Las células se incubaron a 37 ºC durante diferentes tiempos con THDF. Para determinar la cantidad de ceramidas intracelulares recogemos las células totales, mientras que para estudiar la fracción mitocondrial procederemos a la separación como hemos indicado en la sección de western blot (fraccionamiento subcelular) quedándonos sólo con la fracción mitocondrial.

En ambos casos, el contenido lipídico (1×10^6 células por tubo) se extrajo en tubos de cristal de 12x75mm, con 1 ml de "solución de parada" ($CHCl_3$ 500:MeOH 500:1N HCl 5), 270 µl de tampón salino (135 mM NaCl, 4,5 mM KCl, 1,5 mM $CaCl_2$, 0,5 mM $MgCl_2$, 5,6 mM glucosa y 10 mM HEPES pH 7,2) y 30 µl de EDTA 100 mM. Todo ello se mezcló y se separó mediante centrifugación 500 g 5 min a 4ºC. La fase orgánica (400 µl) se transfirió a tubos de cristal de 12x75 mm que se secaron bajo nitrógeno.

La cantidad de ceramida generada se determinó mediante cromatografía en capa fina después de su conversión a [^{32}P] ceramida-1-fosfato por la diacilglicerol quinasa de *Escherichia coli* [159,160].

- *Hidrólisis alcalina.*

En cada tubo se añadieron 500 µl de 0.1M KOH/MeOH y se incubaron durante 1 hora y media a 37 ºC) para eliminar los glicerofosfolípidos. Los lípidos se extrajeron con 500 µl de $CHCl_3$, 270 µl de tampón salino y 30 µl de EDTA 100 mM, colocando la fase lipídica en nuevos tubos de cristal de 13x100 mm que se secaron bajo nitrógeno.

- *Ensayo diacilglicerol quinasa.*

En un tubo de cristal, preparamos la siguiente mezcla (µl por muestra): añadimos 6 µl de cardiolipina (25 mg/ml) y lo secamos con nitrógeno, luego añadimos 20 µl de DETAPAC 1 mM (ácido dietilenetriamina-pentaacético) y los lípidos se solubilizaron mediante sonicación durante 2 minutos en un baño, posteriormente añadimos 6,2 µl de una disolución acuosa de Octyl-β-D-glucopiranósido (825 mM), 50 µl de tampón de reacción 2X (100 mM imidazol, 100 mM NaCl, 2 mM EDTA, 25 mM $MgCl_2$, pH 6,5), 8 µl de imidazol/DETAPAC (10 mM/1 mM), 2 µl de DTT 100 mM, 1 µl de ATP 100 mM, 8,3 µl de agua bidestilada y 3,5 µl de diacilglicerol quinasa (1 mg/ml). Mezclamos e incubamos durante 30 minutos a temperatura de laboratorio y luego añadimos 1 µl [γ-^{32}P] ATP (3.000 Ci/mmol).

De la mezcla final, añadimos 100 µl por muestra e incubamos a temperatura ambiente durante 30 minutos. Paramos la reacción añadiendo 1 ml de solución de parada, 170 µl de tampón salino y 30 µl de EDTA 100 mM. Extraemos la fase orgánica que colocamos en nuevos tubos (13x100mm) y la secamos bajo nitrógeno. Luego, resuspendimos cada muestra en 50 µl de $CHCl_3$/MeOH y separamos los lípidos mediante cromatografía en capa fina (TLC) desarrollada en $CHCl_3$/MeOH/HAc (65:15:5) durante 45-75 min. Las placas cromatográficas fueron reveladas por autorradiografía y se extrajeron las bandas correspondientes a ceramida, para determinar la radiactividad mediante un contador de centelleo líquido.

5. Métodos estadísticos.

En todos los casos las determinaciones para cada grupo experimental se realizaron por triplicado o cuadruplicado, y los valores representados se corresponden a datos de tres experimentos como mínimo (Media ± S.E.M). La comparación entre los distintos tratamientos se realizó por el método de la t de Student o análisis de la varianza, considerando significativos los valores de $P < 0,05$.

RESULTADOS

1. Los derivados de la fenilbenzopirona inhiben el crecimiento y la viabilidad de las líneas celulares estudiadas.

En esta Tesis hemos evaluado la potencial actividad antitumoral de 20 flavonoides (Tabla 1 y 2), sobre una serie de líneas celulares tumorales de origen humano.

Entre ellos tenemos una serie de flavonoides extraídos directamente de las partes aéreas de la especie *Consolida oliveriana* (**2** y **3**) y otros obtenidos mediante modificaciones semisintéticas, acetilaciones **(1, 5, 11, 12**, **13, 15)** o metilaciones **(14)** en los compuestos extraídos de esta fuente natural. Su citotoxicidad se evaluó en tres líneas celulares tumorales.

Además estudiamos una serie de 11 compuestos obtenidos mediante síntesis **(4, 6, 7, 8, 9, 10, 16, 17, 18, 19, 20)** que comparten con los anteriores la misma estructura básica, y se diferencian tan sólo en la presencia o ausencia de grupos metoxilo o hidroxilo en diferentes partes del esqueleto básico. Hemos estudiado la actividad citotóxica de estos compuestos en cuatro líneas celulares tumorales.

Los estudios antiproliferativos en células HL-60, U937, SK-MEL-1 y A549, nos permiten identificar los compuestos que presentan unas propiedades antitumorales interesantes y los que son incapaces de inhibir el crecimiento de las células tumorales.

Todos los compuestos estudiados comparten un mismo esqueleto fenilbenzo-γ-pirona (C6-C3-C6), es decir, un anillo aromático unido a una cadena propánica que está unida a su vez a otro anillo aromático.

En los estudios antiproliferativos identificamos la 3´,5,7-Trihidroxi-3,4´-dimetoxiflavona (THDF) ó Quercetín-3,4´-dimetiléter, compuesto obtenido de síntesis, como el más interesante, ya que presenta las IC_{50} más bajas en todas las líneas celulares ensayadas. Y al fijarnos en los compuestos extraídos de una fuente natural y sus derivados obtenidos por semisíntesis, destacamos el trifolín heptaacetato (TA) como el compuesto más citotóxico en la mayoría de las líneas tumorales ensayadas.

En general podemos llegar a la conclusión de que entre las cuatro líneas celulares utilizadas las células de leucemia mieloide humana, HL-60 y U937, son las más sensibles a la citotoxicidad inducida por la mayoría de los flavonoides, mientras que las células de cáncer de pulmón humano, A549 son las más resistentes, y sólo los compuestos **7, 8** y **19** son capaces de inhibir su proliferación.

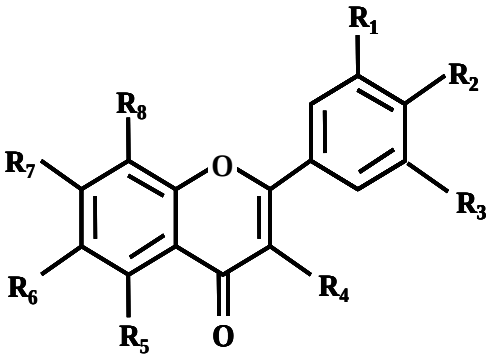

Compuesto	R_1	R_2	R_3	R_4	R_5	R_6	R_7	R_8
1. Hiperósido acetato	H	OAc	OAc	OGalAc	OAc	H	OAc	H
2. 2´-Acetilhiperósido	H	OH	OH	OGal-2´-Ac	OH	H	OH	H
3. 6´-Acetilhiperósido	H	OH	OH	OGal-6´-Ac	OH	H	OH	H
4. Kaempferol	H	OCH_3	H	OH	OH	H	OH	H
5. Kaempferol tetraacetato	H	OAc	H	OAc	OAc	H	OAc	H
6. 3´,4´,7,8-Tetrahidroxiflavona	OH	OH	H	H	H	H	OH	OH
7. 3´,4´,5-Trihidroxi-6,7-dimetoxiflavona	OH	OH	H	H	OH	OCH_3	OCH_3	H
8. 3´,5,7-Trihidroxi-3,4´-dimetoxiflavona	OH	OCH_3	H	OCH_3	OH	H	OH	H
9. 3-Metoxiflavona	H	H	H	OCH_3	H	H	H	H
10. 6-Metoxiflavonol	H	H	H	OH	H	OCH_3	H	H
11. Trifolín hexaacetato (5-OH)	H	OAc	H	OGalAc	OH	H	OAc	H
12. Trifolín heptaacetato	H	OAc	H	OGalAc	OAc	H	OAc	H
13. Glucotrifolín decaacetato	H	OAc	H	OGalAc	OAc	H	OGluAc	H
14. Heptametiltrifolín	H	OMe	H	OGalOMe	OMe	H	OMe	H
15. Quercetín pentaacetato	H	OAc	OAc	OAc	OAc	H	OAc	H
16. Quercetín-3,7,3´,4´-tetrametiléter	OCH_3	OCH_3	H	OCH_3	OH	H	OCH_3	H
17. Robinetina	OH	OH	OH	OH	H	H	OH	H
18. Siringetina	OCH_3	OH	OCH_3	OH	OH	H	OH	H
19. Tamarixetina	OH	OCH_3	H	OH	OH	H	OH	H
20. Tangeretina	H	OCH_3	H	H	OCH_3	OCH_3	OCH_3	OCH_3

Gal = β-galactopiranosa. Glu = β-glucopiranosa

Tabla 1. Estructura química de los flavonoides evaluados.

COMPUESTO	IC_{50} (μM)			
	HL-60	**U937**	**SK-MEL-1**	**A549**
1	15 ± 1	19 ± 2	23 ± 2	>100
2	>100	>100	>100	ND
3	>100	>100	>100	ND
4	>100	>100	>100	>100
5	45 ± 3	48 ± 17	37 ± 8	ND
6	85,2 ± 6,8	19,9 ± 4,3	14,7 ± 5,2	>100
7	39,4 ± 3,9	14,9 ± 4,6	>100	28,2 ± 13,3
8	0,31 ± 0,02	1,4 ± 0,5	13,9 ± 2,5	10,8 ± 2,4
9	>100	84,4 ± 5,9	>100	>100
10	>100	>100	>100	>100
11	20 ± 5	13 ± 7	16 ± 1	ND
12	21 ± 8	10 ± 2	15 ± 2	ND
13	>100	>100	>100	ND
14	88 ± 9	>100	>100	ND
15	38 ± 6	25 ± 11	58 ± 7	ND
16	>100	>100	>100	>100
17	9,1 ± 1,9	>100	>100	>100
18	>100	>100	>100	>100
19	10 ± 3,1	5,3 ± 3,8	27,2 ± 0,9	22,4 ± 4,2
20	32 ± 4,2	45,3 ± 9,9	>100	>100

Tabla 2. Efecto de los flavonoides sobre el crecimiento de células tumorales humanas. Las células se cultivaron durante 72 horas y el valor de la IC_{50} se determinó mediante un ensayo colorimétrico con MTT. Los datos representan la media ± S.E.M. de 3-5 experimentos independientes con tres determinaciones en cada uno.

2. Trifolín acetato induce apoptosis en células de leucemia mieloide humana HL-60.

El trifolín acetato (TA), compuesto obtenido por acetilación del producto natural trifolín, induce un claro efecto antiproliferativo sobre las tres líneas celulares ensayadas ($IC_{50} \cong 10$ µM a 72h).

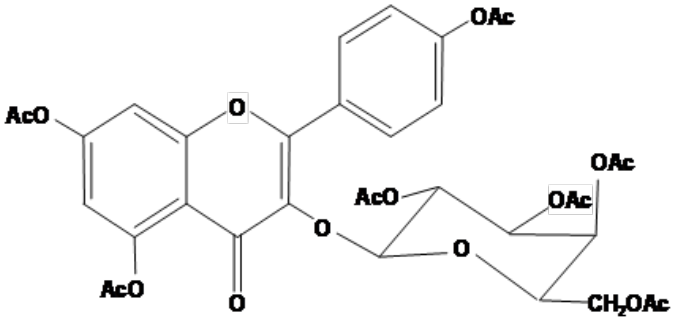

Figura 7. Estructura química del trifolín acetato.

Con el fin de evaluar su mecanismo de acción, determinamos si TA induce apoptosis, utilizando tres métodos complementarios: tinción con el fluorocromo bisbenzimida, cuantificación de células hipodiploides y evaluación de la fragmentación del ADN.

Mediante microscopía de fluorescencia (Figura 8A) podemos observar que el tratamiento con TA promueve condensación y fragmentación de la cromatina nuclear, cambios morfológicos característicos de la muerte celular por apoptosis.

El análisis del número de células hipodiploides mediante citometría de flujo (Figura 8B) nos muestra que el porcentaje de células apoptóticas aumentó seis veces después de cultivar las células HL-60 con TA 30 µM durante 6 horas.

Mediante electroforesis en un gel de agarosa (Figura 8C), podemos observar la degradación del ADN y su fragmentación internucleosómica visualizada como una escalera discontinua de bandas multiméricas de 185-200 pares de bases, característica de la apoptosis y que se diferencia de la fragmentación aleatoria típica de la necrosis.

Al tratar las células HL-60 y U937 con TA, el ADN mostró el patrón característico de hidrólisis internucleosomal, que no parece ser claro en el caso de las células SK-MEL-1 lo cual sugiere la posible existencia de otros factores implicados (Figura 8C). Uno de ellos podría ser el factor inductor de apoptosis (AIF), una flavoproteína que al liberarse de la

mitocondria se transloca al núcleo y es capaz de producir la condensación y rotura del ADN en fragmentos de alto peso molecular (50Kb) [88].

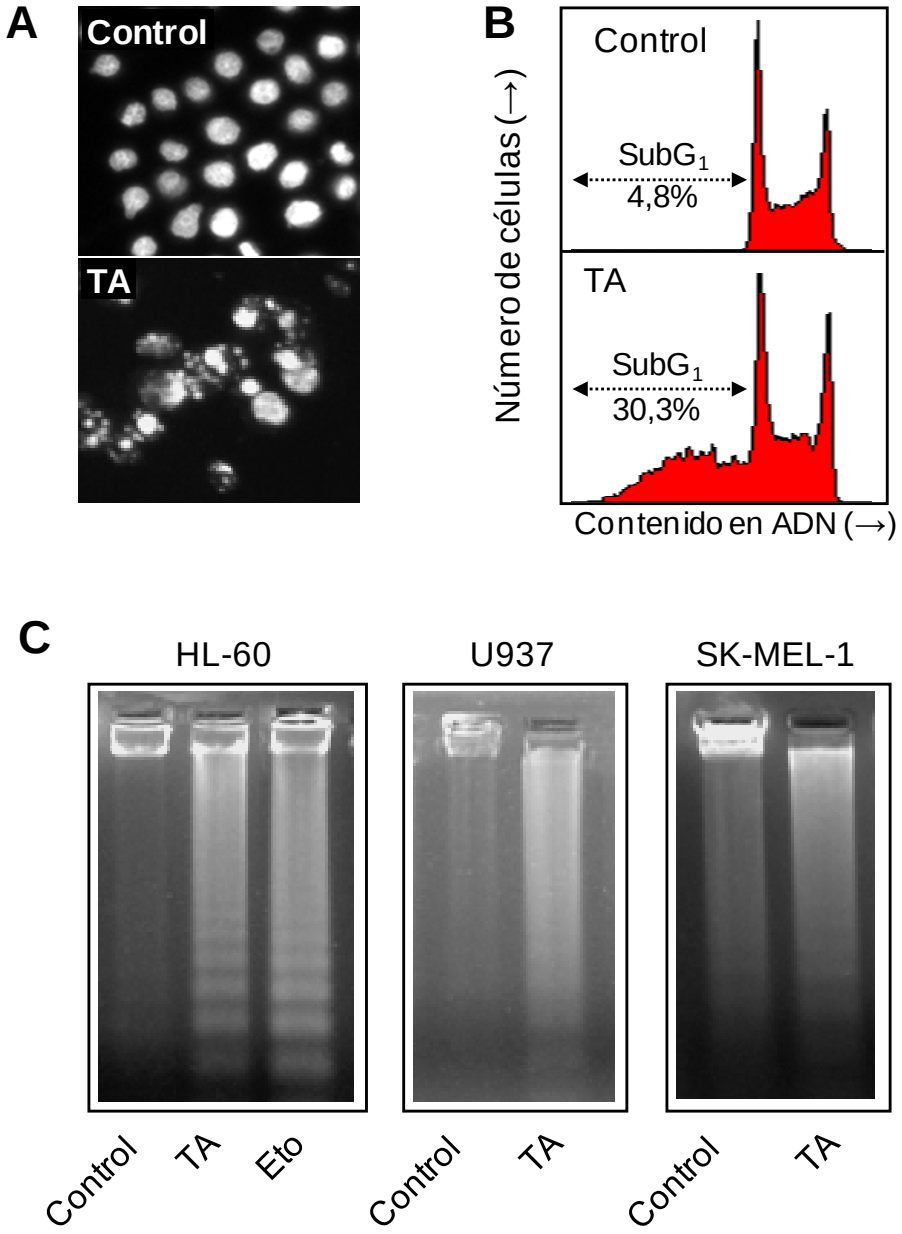

Figura 8. Efecto del TA sobre la inducción de apoptosis. (A) Microfotografías de campos representativos de células HL-60 teñidas con bisbenzimida para evaluar la condensación de la cromatina nuclear, tras ser tratadas durante 6 h con 30 µM de trifáh acet ato (TA). (B) Las células HL-60 se incubaron con TA como en el apartado anterior y se analizaron por citometría de flujo usando ioduro de propidio. La región marcada con una flecha indica las células hipodiploides (células en apoptosis). (C) Evaluación de la fragmentación del ADN en células tumorales humanas. Las células se trataron con TA (10 µM) durante 24 h y el ADN genómico se extrajo y se separó por electroforesis en un gel de agarosa y se visualizó bajo luz UV previa tinción con bromuro de etidio. El etopósido (Eto) se incluyó como control positivo.

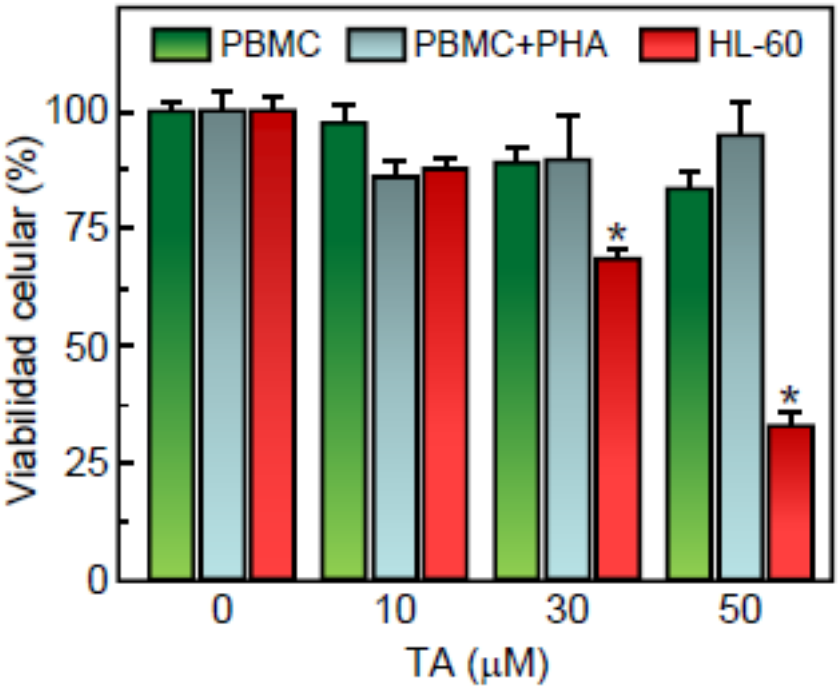

Figura 9. Efecto del TA sobre la proliferación de células mononucleares humanas de sangre periférica (PBMC) y de células HL-60. Se cultivaron células HL-60, células quiescentes PBMC y células PBMC activadas con fitohemaglutinina en presencia de las concentraciones indicadas de TA durante 24 horas. Los valores representan la media ± SE de dos experimentos independientes por triplicado. *P < 0,05 significativamente diferente al control.

En conjunto, estos resultados indican que el trifolín acetato es un potente inductor de apoptosis en células tumorales humanas, y sería interesante evaluar su efecto sobre células normales. El estudio con linfocitos humanos extraídos de voluntarios sanos (células mononucleares de sangre periférica, PBMC) indica que el TA no muestra citotoxicidad hasta una concentración de 50 μM, independientemente de si son quiescentes o proliferantes. Como control positivo se incluyó células HL-60 (Figura 9).

3. Trifolín acetato induce muerte celular mediada por la activación de caspasas.

Para confirmar que la apoptosis inducida por el TA requiere la activación de las caspasas, pretratamos las células HL-60 con concentraciones crecientes del inhibidor general de caspasas, z-VAD-fmk. Los resultados indican que el inhibidor bloquea totalmente la apoptosis inducida por el TA y, por lo tanto, que la muerte celular es dependiente de la activación de caspasas (Figura 10A).

Para identificar las caspasas involucradas en el efecto citotóxico inducido por el trifolín acetato, empleamos una serie de inhibidores de caspasas: el inhibidor específico de caspasa -9 (z-LEHD-fmk), el inhibidor específico de las caspasas -3 y -7 (z-DEVD-fmk), el inhibidor

selectivo de caspasa -1 (z-YVAD-fmk), el inhibidor selectivo de caspasa -2 (z-VDVAD-fmk), el inhibidor selectivo de caspasa -6 (z-VEID-fmk) y el inhibidor selectivo de caspasa -8 (z-IETD-fmk).

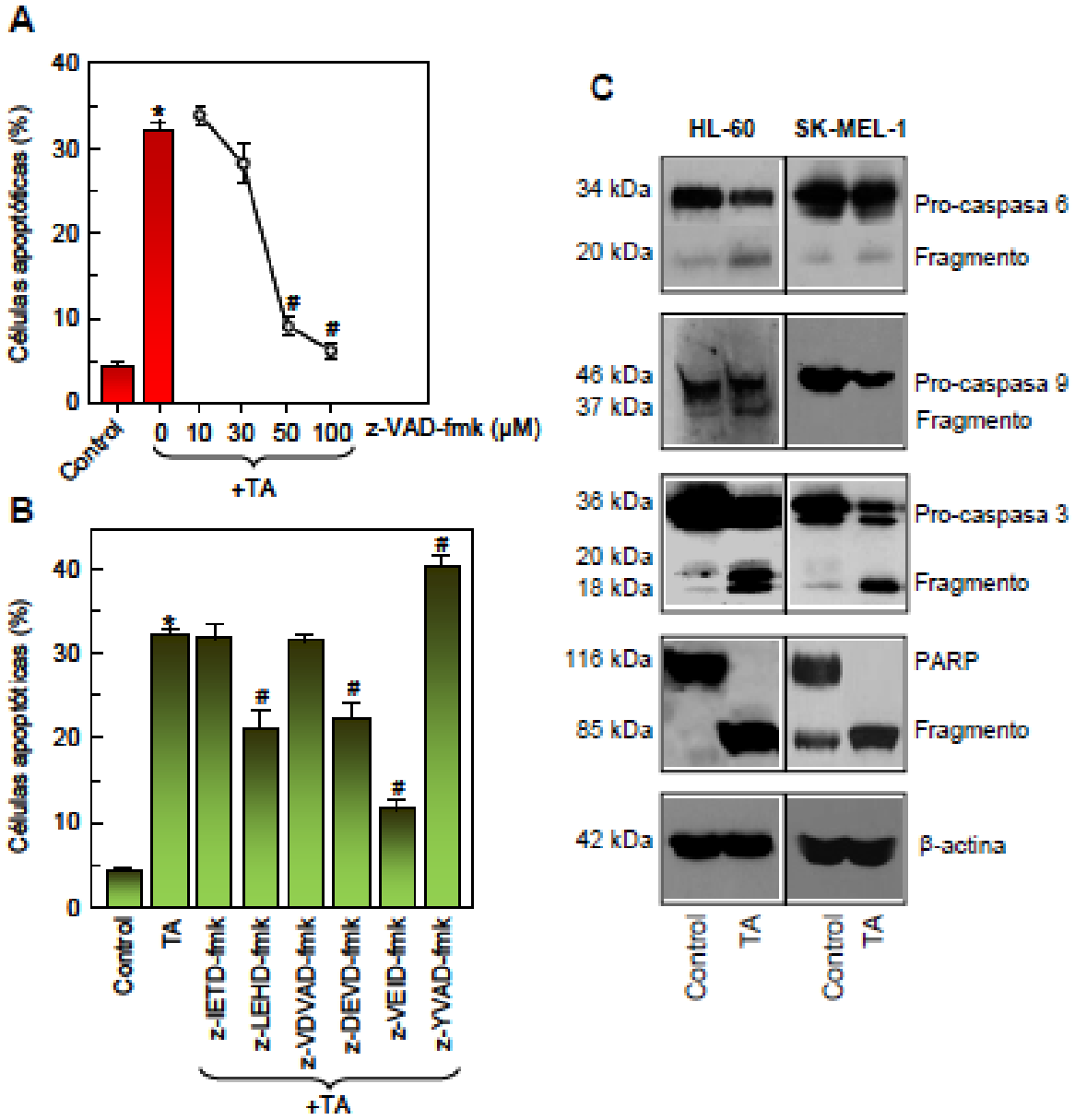

Figura 10. Influencia de la activación de caspasas en la apoptosis inducida por TA en células tumorales. (A) Células HL-60 se pretrataron con diferentes concentraciones de z-VAD-fmk y luego se les añadió TA (10 μM). El porcentaje de células apoptóticas se determinó mediante citometría de flujo. (B) Las células se incubaron con TA (10 μM) durante 12 horas, en ausencia o presencia del inhibidor de caspasa -8 (z-IETD-fmk, 50 μM), el inhibidor de caspasa -2 (z-VDVAD-fmk, 50 μM), el inhibidor de caspasa-9 (z-LEHD-fmk, 50 μM), el inhibidor de caspasa -6 (z-VEID-fmk, 50 μM), el inhibidor de las caspasas -3 y -7 (z-DEVD-fmk, 50 μM) y el inhibidor de caspasa -1 (z-YVAD-fmk, 50 μM). Las células apoptóticas fueron determinadas mediante citometria de flujo. Los valores representan las medias ± SE de dos experimentos realizados por triplicado. *P < 0,05, significativamente diferentes del control sin tratar. (C) Células HL-60 y SK-MEL-1 se incubaron en presencia de TA (10 μM) y los lisados celulares se analizaron mediante western blot para determinar la hidrólisis de procaspasa -9, -6, -3 y PARP. La β-actina fue usada como control de carga. #P< 0,05, significativamente diferentes del tratamiento con TA solo.

Los resultados (Figura 10B) revelaron que las células pretratadas con z-LEHD-fmk, z-DEVD-fmk o z-VEID-fmk son significativamente más resistentes a sufrir apoptosis por el TA. El porcentaje de células hipodiploides disminuyó desde 33 ± 2 % en las células tratadas con TA hasta un 20 ± 2 % en las células pretratadas con z-LEHD-fmk o z-DEVD-fmk, y el efecto del inhibidor z-VEID-fmk resultó ser el más importante cuantitativamente reduciendo el porcentaje de apoptosis hasta un 10 ± 1 %.

El pretratamiento con los inhibidores, z-IETD-fmk y z-VDVAD-fmk no mostró ningún efecto, lo cual nos indica que las caspasas -8 y -2 no están implicadas en la muerte celular inducida por el TA. Sorprendentemente el pretratamiento con z-YVAD-fmk sensibilizó las células HL-60 frente a la apoptosis inducida por el TA.

Teniendo en cuenta los resultados anteriores, estudiamos el efecto del TA sobre la activación de las caspasas en células HL-60 y SK-MEL-1 mediante western blot, y demostramos que el TA promueve la hidrólisis de las procaspasas -3, -6 y -9 en ambas líneas celulares (Figura 10C).

Para determinar si el procesamiento de procaspasa -3 está asociado con un aumento de la actividad enzimática examinamos también la hidrólisis de PARP, sustrato de caspasa -3 que juega un papel fundamental en la reparación del ADN. Los resultados demuestran que TA induce el procesamiento de PARP (116 kDa), dando lugar a la aparición de un fragmento de 85 kDa (Figura 10C).

4. Trifolín acetato induce liberación de citocromo c al citosol, sin producir cambios en el potencial de membrana mitocondrial.

La liberación de citocromo *c* de la mitocondria al citosol es uno de los eventos principales en la vía intrínseca de la apoptosis. Para determinar si esta vía está implicada en la apoptosis inducida por TA en células HL-60 y SK-MEL-1, realizamos experimentos variando el tiempo de tratamiento y analizamos los extractos citosólicos mediante western blot. Como se muestra en la Figura 11, detectamos un aumento de citocromo *c* en el citosol a las 6 horas de tratamiento, que persiste tras 12 horas en ambas líneas celulares.

Para determinar si la liberación de citocromo *c* está asociada con una pérdida del potencial de membrana mitocondrial ($\Delta\Psi_m$), tratamos las células HL-60 durante diferentes tiempos (3, 6, 12 y 24 h) con TA, a continuación con la sonda JC-1 durante 30 minutos y finalmente analizamos las células mediante citometría de flujo. Los resultados indican que el $\Delta\Psi_m$

permanece intacto por lo menos durante las primeras 24 h de tratamiento (Figura 12A), en contraste con la caída del potencial de membrana producida por el ionóforo de protones carbonil cianuro *m*-clorofenil hidrazona (CCCP), sugiriendo que la alteración del potencial de membrana no está implicada en la apoptosis inducida por TA.

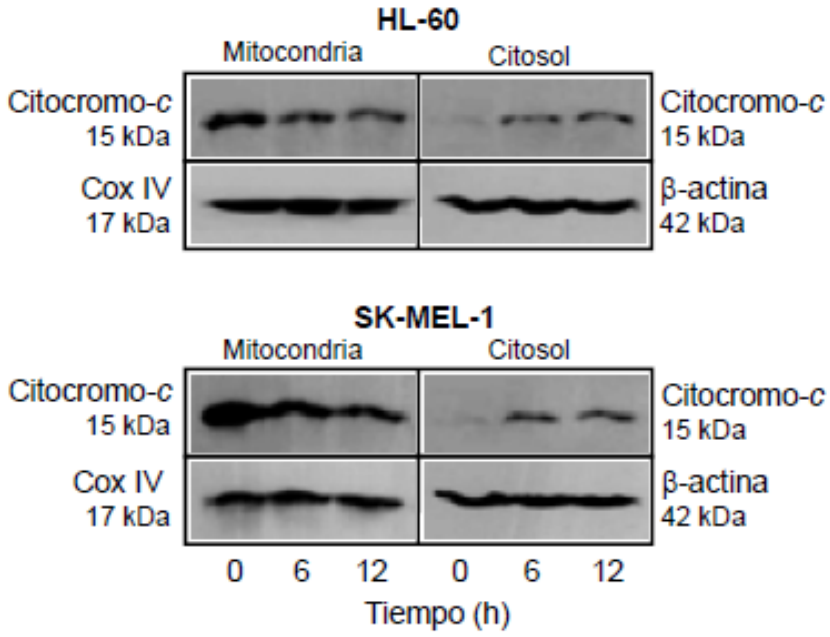

Figura 11. El tratamiento con TA induce liberación de citocromo c en células tumorales. Las células se incubaron en presencia de TA (10 µM) durante los tiempos indicados y los extractos citosólicos y mitocondriales se ensayaron mediante western blot para determinar la liberación de citocromo *c*. β-actina y citocromo *c* oxidasa (COX IV) se usaron como controles de carga en la fracción citosólica y mitocondrial, respectivamente.

5. Trifolín acetato no induce apoptosis en líneas celulares de leucemia humana que sobreexpresan Bcl-2 o Bcl-x_L

Bcl-2 y Bcl-x_L pertenecen a una familia de proteínas que inhiben la apoptosis, regulando el potencial de membrana mitocondrial e impidiendo la liberación de citocromo *c* necesaria para la activación de caspasa -9 [161,162]. Por tanto, investigamos si estas proteínas son capaces de proteger a las células frente al efecto citotóxico del TA. Para ello usamos líneas celulares que expresan altos niveles de las proteínas anti-apoptóticas Bcl-x_L (HL-60 / Bcl-x_L) o Bcl-2 (U937 / Bcl-2). La cuantificación del número de células hipodiploides nos indica que efectivamente, ambas proteínas confieren protección a las líneas celulares ensayadas (Figura 12B).

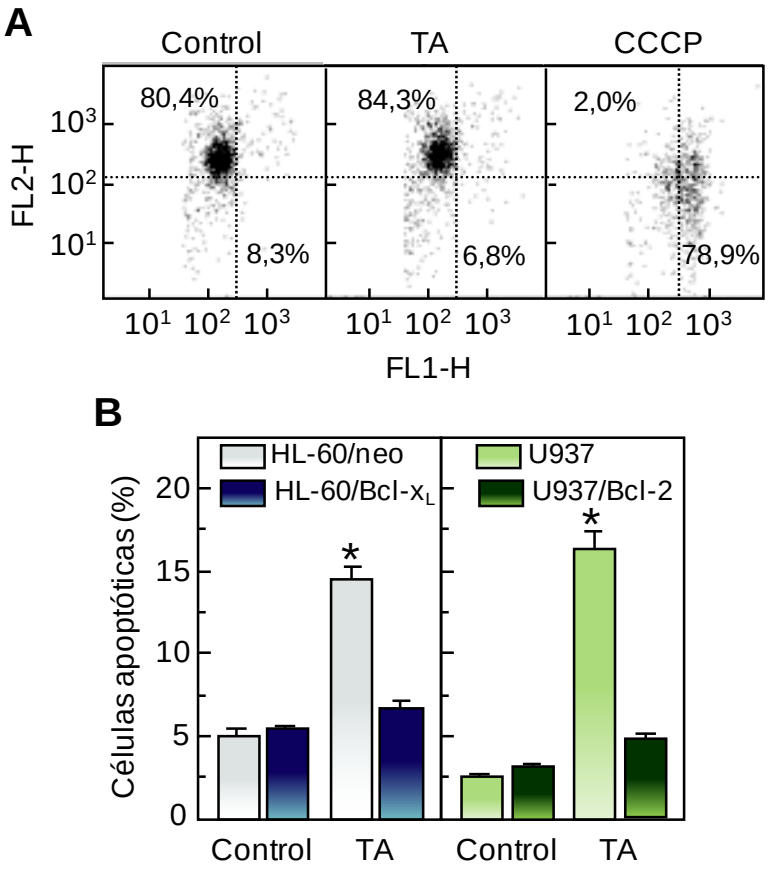

Figura 12. (A) *El TA no afecta al potencial de membrana mitocondrial ($\Delta\Psi_m$).* Las células fueron incubadas con TA durante 24 h y el $\Delta\Psi_m$ se analizó por citometría de flujo utilizando la sonda JC-1. Resultados similares fueron obtenidos en dos experimentos independientes realizados por triplicado. Como control positivo se utilizó 10 µM de CCCP. (B) *El TA no es capaz de inducir apoptosis en líneas celulares que sobreexpresan Bcl-2 y Bcl-x_L.* Comparación de la apoptosis inducida por TA en células HL-60/neo y HL-60/Bcl-x_L, así como en células U937 y U937/Bcl-2. Las células se incubaron durante 24 h, en ausencia o presencia de TA. El porcentaje de células hipodiploides se determinó mediante citometría de flujo. Los valores representan la media ± SE de tres experimentos independientes realizados por triplicado. *P < 0.01, significativamente diferente del control.

6. Trifolín acetato activa la vía MAPKs.

La vía de las MAPKs actúa como mediadora de una serie de señales que promueven o inhiben el crecimiento de células leucémicas. Las quinasas ERK, JNK y p38 juegan un importante papel en el crecimiento y la proliferación celular, la diferenciación y la apoptosis. Por lo tanto estudiamos el efecto del TA sobre la activación de estas proteínas (Figura 13A).

Los resultados muestran que se produjo una fosforilación rápida (<15 min) de ERK1/2, JNK y $p38^{MAPK}$ en células HL-60 y U937. La fosforilación de ERK1/2 y JNK permaneció elevada en ambas líneas celulares durante al menos 6 horas, mientras la activación de p38 disminuyó a partir de las 4 horas en células HL-60, pero no en células U937. El tratamiento de las células

HL-60 y U937 con TA produjo una activación de ERK1/2, JNK y p38, siguiendo cinéticas similares.

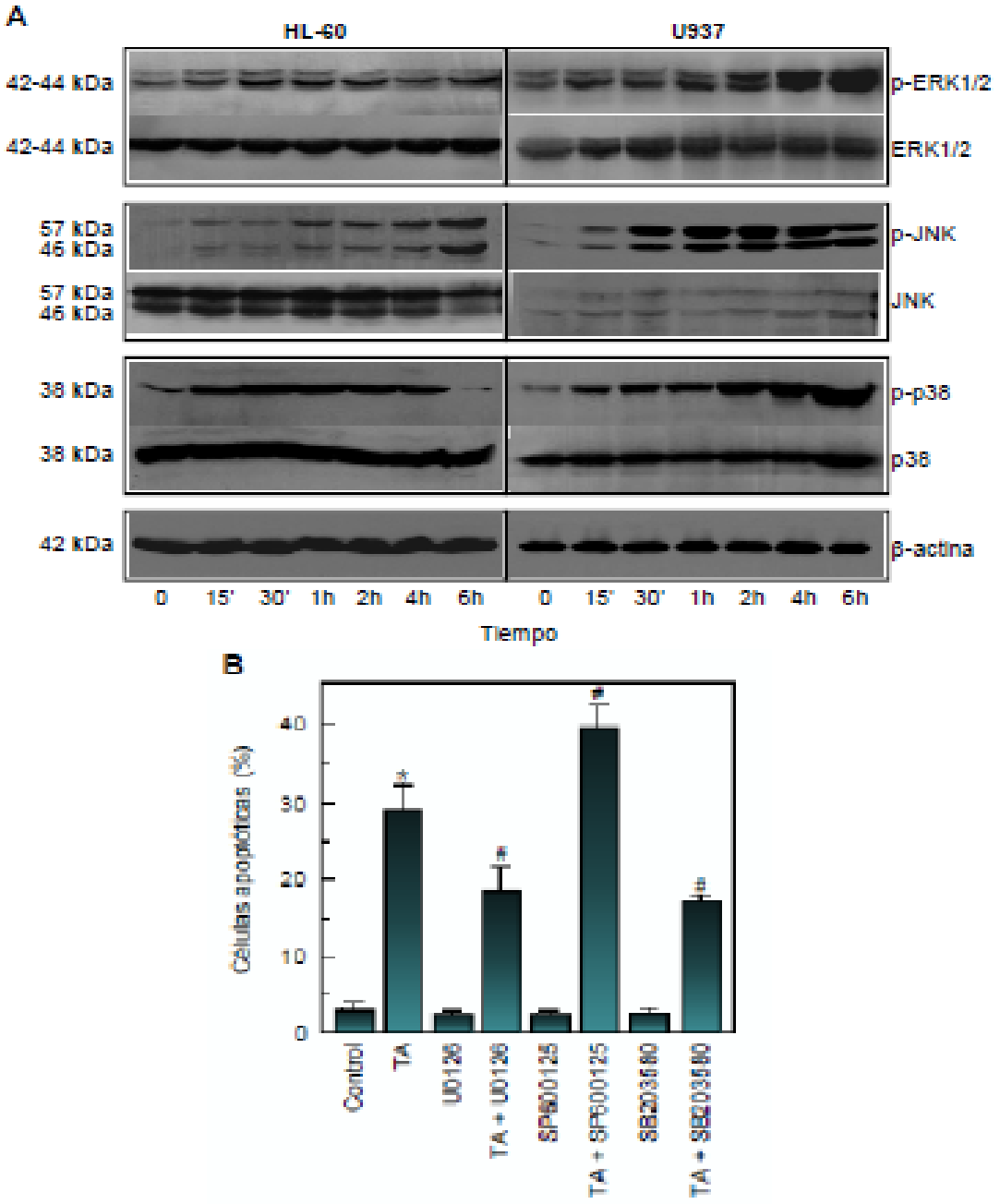

Figura 13. Papel de la vía de las MAPKs en la apoptosis inducida por TA en células HL-60. (A) TA induce la fosforilación dependiente del tiempo de ERK 1/2, JNK y p38. Las células se trataron con TA a los tiempos indicados y los extractos de proteínas se analizaron mediante inmunoblot utilizando anticuerpos específicos para determinar la fosforilación de las diferentes MAPKs. -actina fue utilizada como control de carga. (B) Las células se preincubaron con U0126 (10 µM), SP600125 (10 µM) y SB203580 (2 µM) durante 1 h y se trataron posteriormente con TA. El porcentaje de células apoptóticas se cuantificó mediante citometria de flujo. Los valores representan las medias ± SE de tres experimentos realizados por triplicado. *P < 0,05, significativamente diferentes del control. #P< 0,05, significativamente diferentes del tratamiento con TA solo.

Para determinar si la fosforilación de las MAPKs juega un papel importante en la apoptosis inducida por TA, examinamos el efecto de los inhibidores específicos de cada una de las MAPKs en células HL-60 (Figura 13B). El tratamiento con U0126 (10 μM), un inhibidor específico de la quinasa reguladora MEK1/2 que bloquea la activación de ERK1/2, redujo parcialmente la apoptosis inducida por TA, lo cual sugiere que ERK1/2 está implicado en la citotoxicidad inducida por TA. En contraste con estos resultados, existen estudios previos que demuestran los efectos sinérgicos entre diferentes agentes quimioterápicos y fármacos que inhiben la activación de MAPKs, inhibiendo el crecimiento e induciendo apoptosis en células leucémicas [163,164]. Además, mediante experimentos llevados a cabo en nuestro laboratorio, se ha demostrado que los inhibidores específicos de ERK1/2 pueden aumentar la sensibilidad de las células leucémicas frente a la apoptosis inducida por el tetraacetato de 3-metil-éter de quercetina [155].

La inhibición farmacológica de p38 usando el inhibidor SB203580 disminuyó la muerte celular inducida por el TA desde un 30% hasta un 15%, sugiriendo que la activación de p38 puede estar implicada en la apoptosis inducida por TA.

El pretratamiento de células HL-60 con SP600125, inhibidor específico de JNK, parece exhibir efectos sinérgicos con la apoptosis desencadenada por el TA. Este resultado es sorprendente, ya que la vía de JNK ha sido descrito que es activada por varios agentes quimioterápicos que inducen apoptosis y son utilizados habitualmente en el tratamiento de la leucemia aguda [165,166]. Este resultado sugiere que la inhibición de la vía de JNK podría sensibilizar las células tumorales al TA.

7. Las especies reactivas de oxígeno no están involucradas en la muerte celular inducida por el trifolín acetato.

Dado que las especies reactivas de oxígeno (ROS) pueden dar lugar a la activación de las MAPKs y provocar la muerte celular [167,168,169,170], estudiamos su implicación en la apoptosis inducida por TA mediante el uso de la sonda fluorescente diacetato 2´,7´-dicloro-dihidro-fluoresceína (H_2-DCF-DA). Los resultados demuestran que el trifolín acetato induce generación de ROS después de 1 h de tratamiento (Figura 14A).

Para determinar si la generación de ROS está implicada en la muerte celular inducida por TA se estudió el efecto de los siguientes antioxidantes: ácido ascórbico (vitamina C, 100 μM), el precursor de glutatión N-acetil-L-cisteína (NAC, 10 mM), α-tocoferol (vitamina E, 25 μM), el

derivado hidrosoluble de la vitamina E trolox (2 mM), el inhibidor de xantina oxidasa alopurinol (100 µM) y la superóxido dismutasa (SOD, 400 unidades/ml). Ninguno de estos antioxidantes fue capaz de bloquear la muerte celular, indicando que la apoptosis inducida por el TA es independiente de la producción de ROS (Figura 14B).

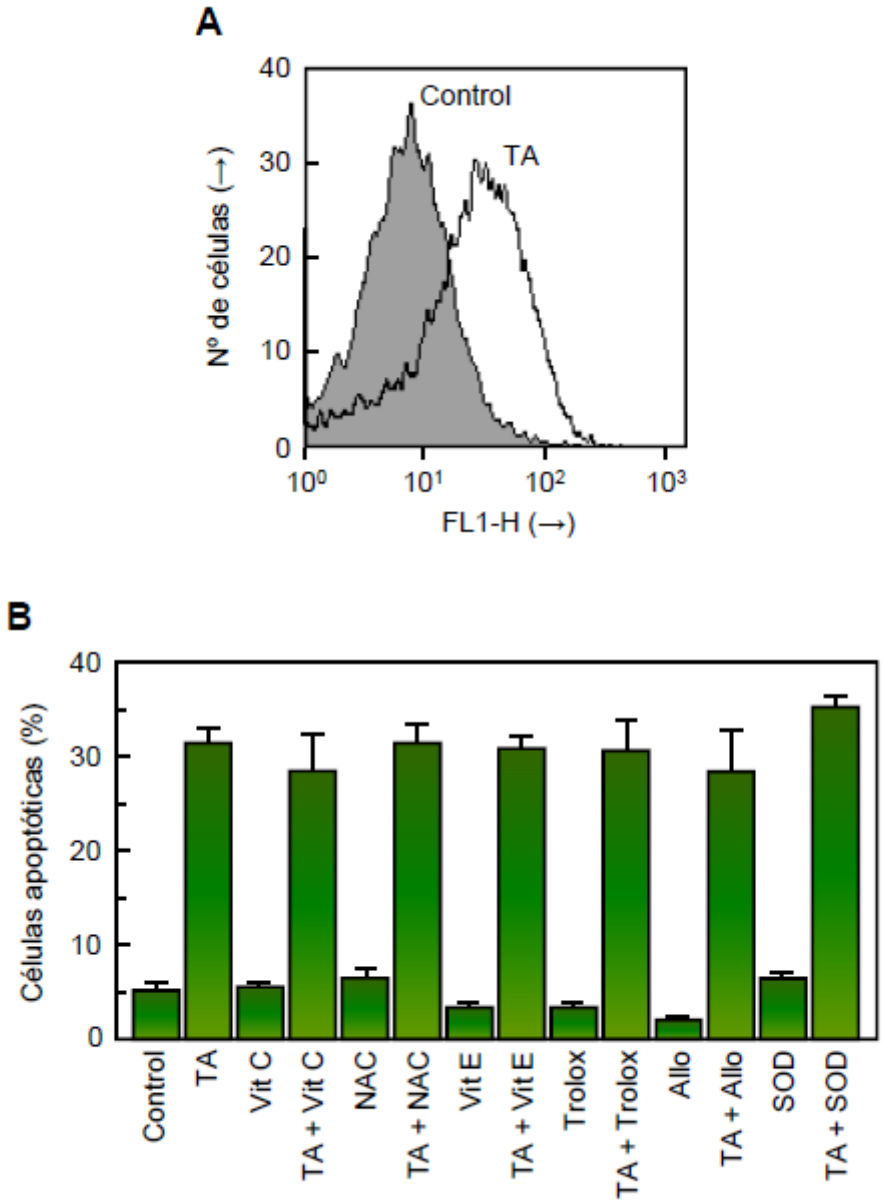

Figura 14. TA induce la generación de ROS en células HL-60. (A) Las células se incubaron durante 1 h en presencia de TA y la fluorescencia obtenida por la oxidación de H_2-DCF-DA fue determinada mediante citometria de flujo. (B) Las células se pretrataron con ácido ascórbico (vitamina C, 100 µM), el precursor de glutatión N-acetil-L-cisteína (NAC, 10 mM),α -tocoferol (vitamina E, 25 µM), trolox (2 mM), alopurinol (100 µM) y superóxido dismutasa (SOD, 400 unidades/ml) durante 1 h y luego tratadas con TA (10 µM, 24 h). Las células también fueron incubadas con cada inhibidor en ausencia de TA. El porcentaje de células apoptóticas se evaluó mediante citometría de flujo. Los valores representan la media ± SE de tres experimentos independientes realizados por triplicado.

8. THDF inhibe la viabilidad de células tumorales humanas y no presenta citotoxicidad frente a linfocitos normales.

De todos los compuestos estudiados, la 3´,5,7-trihidroxi-3,4´-dimetoxiflavona (THDF) resultó ser el más citotóxico. Estudiamos su efecto sobre el crecimiento de nueve líneas celulares tumorales humanas (Figura 15) y observamos que presenta actividad citotóxica frente a todas ellas (Tabla 3).

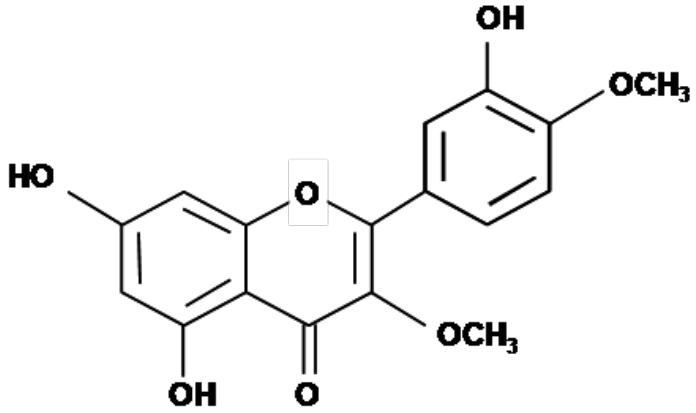

Figura 15. Estructura química del THDF.

Tabla 3. Efecto del THDF sobre la proliferación de células tumorales humanas.

IC_{50} (μM)								
HL-60	HL-60/neo	HL-60/Bcl-x_L	U937	U937/Bcl-2	Jurkat	Molt-3	SK-MEL-1	A549
0,3 ± 0,02	0,59 ± 0,02	3,0 ± 1,2	1,4 ± 0,5	4,3 ± 1,7	0,43 ± 0,05	0,27 ± 0,01	13,9 ± 2,5	10,8 ± 2,4

Las células fueron cultivadas durante 72 h y los valores de IC_{50} se calcularon como se describe en la sección de material y métodos. Los datos representan la media ± S.E.M. de 3-5 experimentos independientes con tres determinaciones en cada uno.

Las líneas celulares tumorales mieloides de origen humano (HL-60 y U937) y linfoides (Jurkat y Molt-3), junto con las líneas celulares que sobreexpresan las proteínas Bcl-2 (U937/Bcl-2) y Bcl-x_L (HL-60/Bcl-x_L) son altamente sensibles al efecto citotóxico del THDF, mientras que las células de adenocarcinoma humano A549 (IC_{50}= 10,8 ± 2,4 μM) y las células de melanoma humano SK-MEL-1 (IC_{50}= 13,9 ± 2,5 μM) son las más resistentes (Figura 16A). Como experimento control usamos células mononucleares de sangre periférica (PBMC) quiescentes, que se encuentran en un estado G_0. Además usamos PBMC cultivados en presencia de fitohemaglutinina (PHA) que actúa como mitógeno induciendo una respuesta proliferativa en los linfocitos [171]. Los resultados nos indican que el THDF no es citotóxico

hasta una concentración de 10µM durante 24 h en los linfocit os quiescentes, mientras que concentraciones superiores a 3 µM inhiben el crecimiento de los linfocitos que proliferan (Figura 16B).

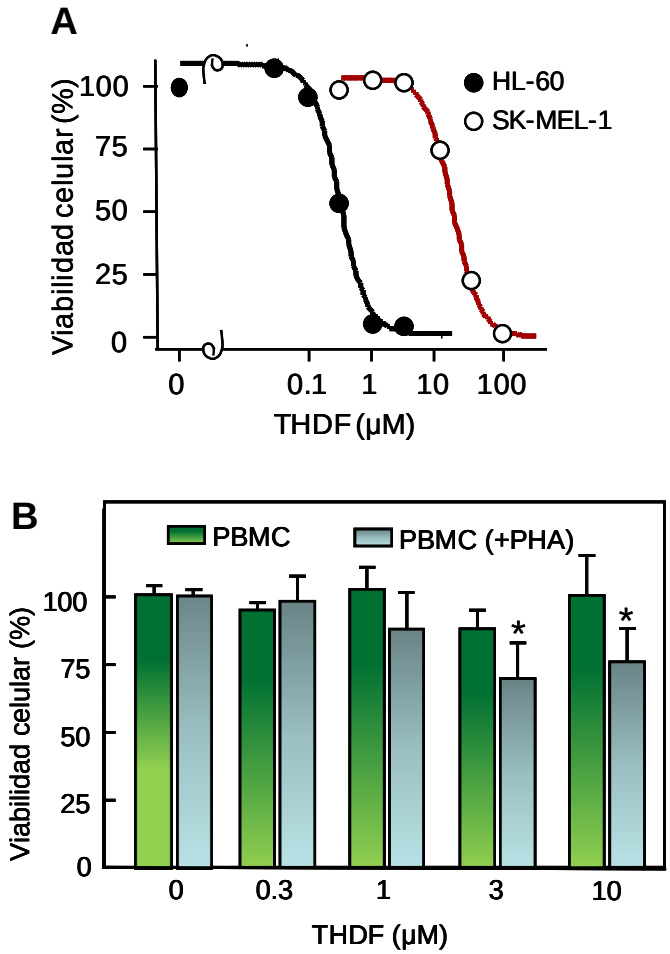

Figura 16. (A) *Efecto del THDF sobre la viabilidad de las células HL-60 y SK-MEL-1*. Las células se trataron con las concentraciones de THDF indicadas durante 72 h y la viabilidad celular fue determinada por el ensayo del MTT, tal como se describe en la sección de material y métodos. Se muestran los valores de un experimento representativo en el que cada punto representa la media de tres determinaciones. (B) *Efecto del THDF sobre la proliferación de células mononucleares humanas de sangre periférica*. Se cultivaron células quiescentes PBMC y células PBMC activadas con fitohemaglutinina (+PHA) en presencia de las concentraciones indicadas de THDF durante 24 h. Los valores representan la media ± SE de dos experimentos independientes realizados por triplicado. *P < 0,05 significativamente diferente al control.

9. THDF induce apoptosis en células de leucemia mieloide humana.

Para evaluar si la apoptosis está implicada en el efecto citotóxico inducido por el THDF en las células de leucemia mieloide humana HL-60 y U937, utilizamos una serie de métodos complementarios.

El análisis mediante citometría de flujo revela que ambas líneas celulares sufren apoptosis (Figura 17). El porcentaje de células hipodiploides (fracción $SubG_1$) aumentó en las células

HL-60 y U937, desde un 4,4% y un 3,2% hasta un 21,5% y 27,6%, respectivamente, después del tratamiento con 3µM de THDF durante 24 h.

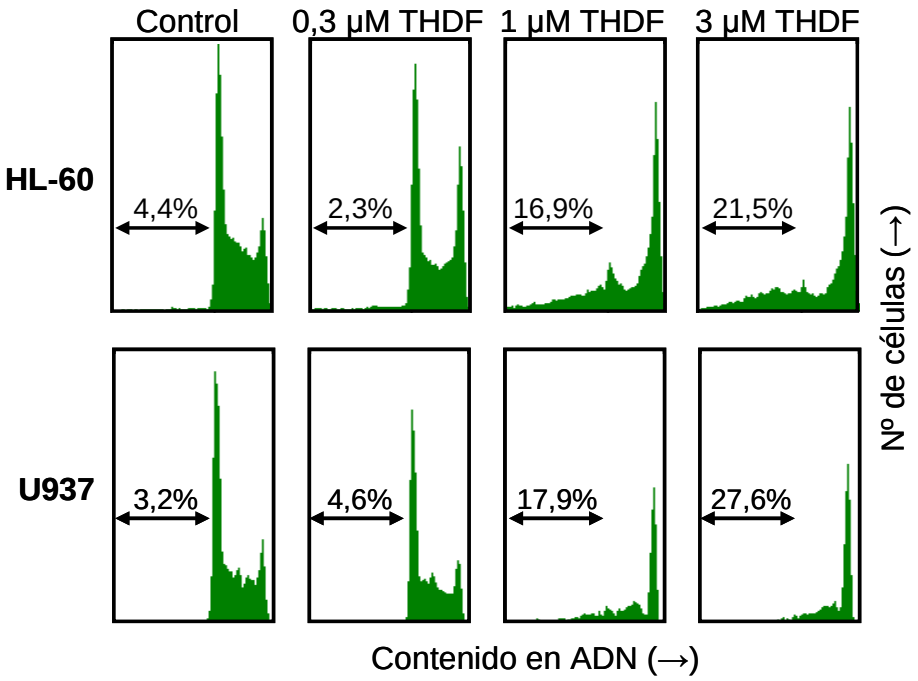

Figura 17. Evaluación mediante citometría de flujo del efecto del THDF sobre la inducción de apoptosis en células HL-60 y U937. Las células fueron tratadas con las concentraciones indicadas de THDF durante 24 h, y analizadas usando ioduro de propidio. La región marcada con una flecha indica las células hipodiploides (% de células apoptóticas).

El análisis del ADN por electroforesis en gel de agarosa, muestra un patrón de fragmentación típico (hidrólisis de cromatina internucleosómica) en las células tratadas con THDF, confirmando el efecto sobre la inducción de la apoptosis en ambas líneas celulares (Figura 18ª).

Mediante microscopía de fluorescencia (Figura 18B) detectamos cambios morfológicos característicos de las células apoptóticas (condensación y fragmentación de la cromatina).

El THDF provoca la externalización de fosfatidilserina desde la cara interna de la membrana plasmática, evaluado mediante citometría de flujo con tinción con Anexina-V en ambas líneas celulares (Figura 19A).

Por último, mediante microscopía electrónica de transmisión visualizamos con mayor detalle los cambios que se producen en una célula apoptótica. En la Figura 19B podemos ver la fragmentación y condensación nuclear acompañada de una densa condensación perinuclear y la abundancia de vacuolas en las células tratadas con THDF.

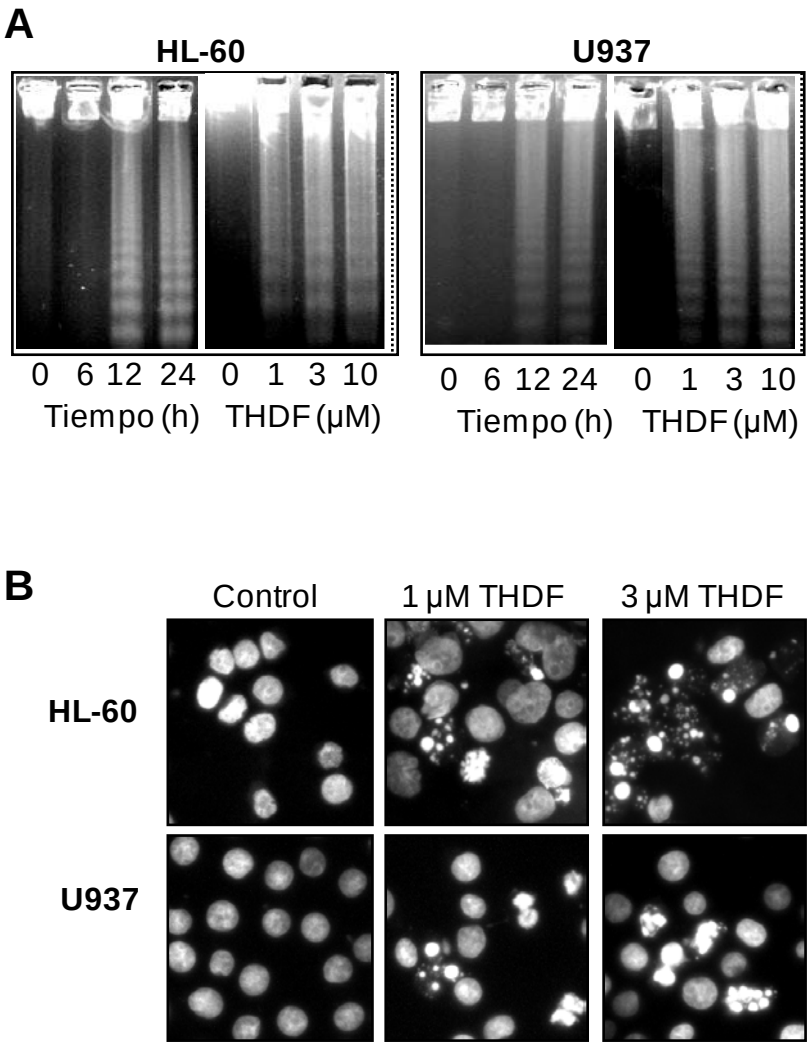

Figura 18. Efecto del THDF sobre la inducción de apoptosis en células HL-60 y U937. (A) Evaluación de la fragmentación del ADN. Las células se trataron con diferentes concentraciones de THDF durante 24 h y con una concentración 3 μM de THDF durante diferentes tiempos. (B) Microfotografías de campos representativos de células teñidas con bisbenzimida para evaluar la condensación de la cromatina nuclear después del tratamiento durante 24 h con 3 μM de THDF.

10. THDF induce muerte celular a través de la activación de caspasas.

Para determinar si las caspasas están involucradas en la respuesta de las células HL-60 y U937 al THDF, examinamos si este flavonoide induce activación de las caspasas e hidrólisis de PARP (Figura 20A). Para ello se trataron las células con 3 μM de THDF durante diferentes tiempos, o con concentraciones crecientes de THDF durante 24 horas, y analizamos mediante western blot el efecto sobre las caspasas iniciadoras (-8 y -9) y ejecutoras (-3, -6 y -7). Utilizamos concentraciones entre 3 y 10 veces los valores de IC_{50} para identificar así las dianas y mecanismos de acción que se activan rápidamente como respuesta al estímulo inducido por THDF.

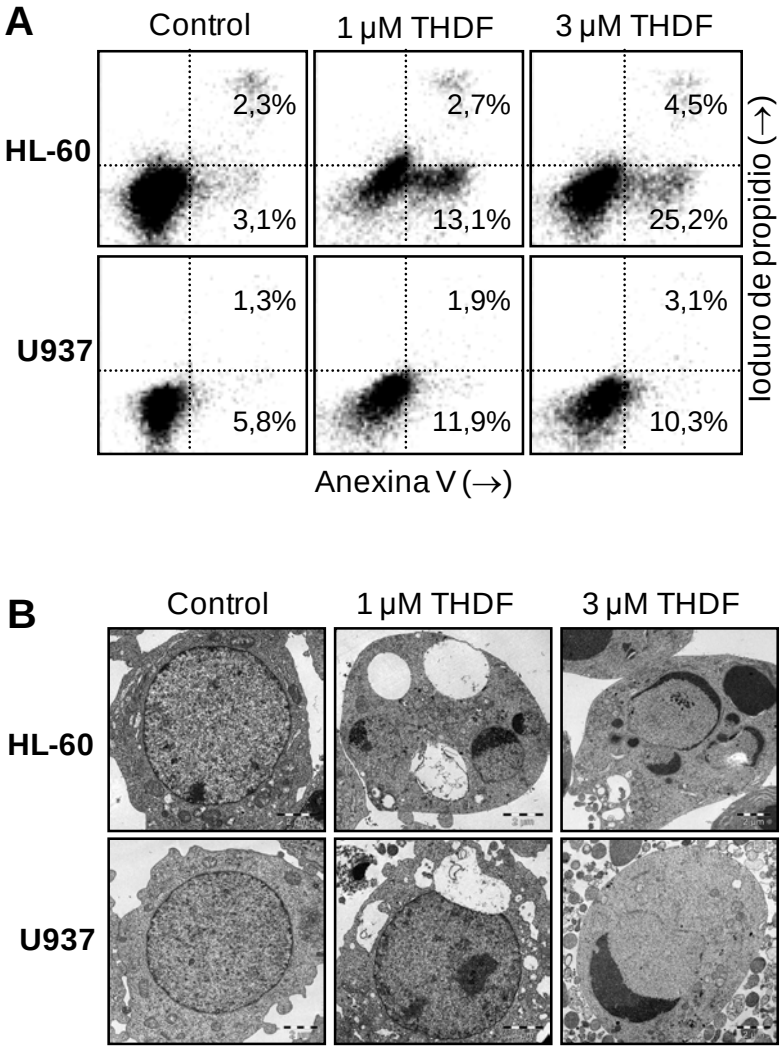

Figura 19. Estudio de la apoptosis inducida por THDF en células HL-60 y U937. (A) Análisis de la externalización de fosfatidilserina por citometría de flujo con Anexina V-FITC y tinción con yoduro de propidio, después de 24 h de tratamiento con THDF. Los datos son representativos de tres experimentos independientes. (B) Análisis de la morfología nuclear mediante microscopía electrónica de transmisión después de 24 h de incubación con las concentraciones indicadas de THDF**.**

Los resultados indican que tras 12 h de tratamiento con THDF se produce en ambas líneas celulares hidrólisis de procaspasa-9 (inactiva) dando lugar a los correspondientes fragmentos activos de 35-37 kDa (Figura 20A).

Posteriormente evaluamos la contribución de la vía extrínseca de la apoptosis, y como podemos observar (Figura 20A), el THDF no produce una activación significativa de procaspasa-8 y su hidrólisis sólo se puede detectar en los tratamientos prolongados (24 h) y con la concentración más alta (10 µM).

La hidrólisis de la procaspasa-3 en fragmentos de 18-20 kDa aumentó significativamente en las células tratadas con THDF (Figura 20A) y de acuerdo con este resultado detectamos también hidrólisis del sustrato de caspasa-3, PARP, proteína de 116 kDa implicada en la reparación del ADN y que da lugar a un fragmento de 85 kDa. Además, THDF induce el procesamiento de las procaspasas -6 y -7 en ambas líneas celulares.

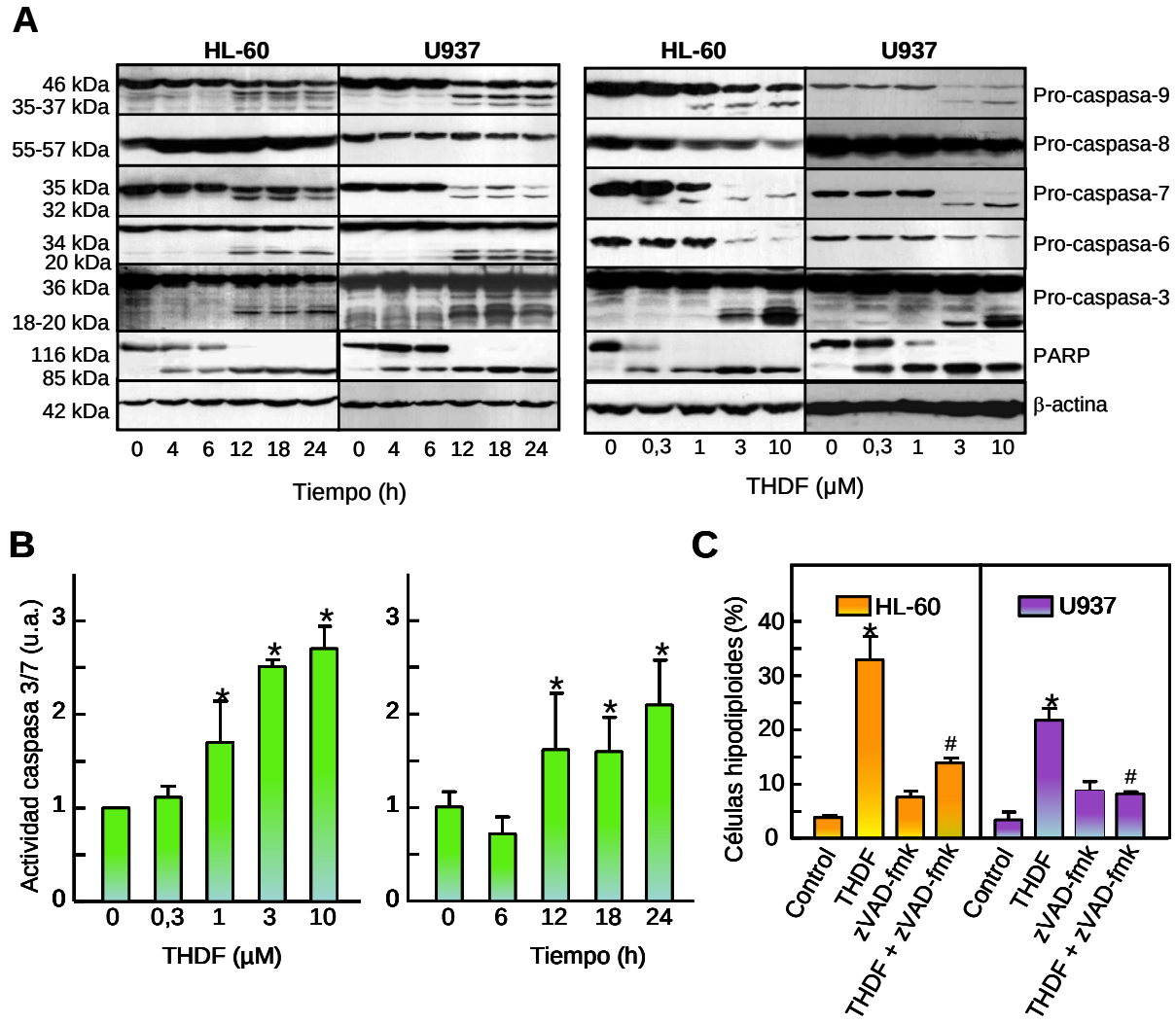

Figura 20. Evaluación de la activación de caspasas en células de leucemia HL-60 y U937. (A) Las células se incubaron en presencia de THDF (3 μM) durante los tiempos indicados o con las concentraciones señaladas durante 24 h. Los extractos celulares se analizaron por western blot y la β-actina fue usada como control de carga. (B) Evaluación de la actividad de las caspasas-3 y -7 en células HL-60. Los lisados totales se utilizaron para medir la actividad caspasa -3 y -7 usando el sustrato colorimétrico DEVD-pNA. Los resultados se expresan en incrementos de actividad comparada con el control. Los valores representan la media ± S.E. Este histograma es representativo de dos experimentos independientes cada uno realizado por triplicado. Los asteriscos indican una diferencia significativa (*P < 0,05) en comparación con los controles. (C) Las células se pretrataron con z-VAD-fmk (100 μM) y luego se les añadió THDF (3 μM) durante 24 h. El porcentaje de células apoptóticas se determinó mediante citometría de flujo. Los valores representan las medias ± SE de dos experimentos realizados por triplicado. *P < 0,05, significativamente diferentes del control sin tratar. #P< 0,05, significativamente diferentes respecto al tratamiento con THDF solo.

Ya que el procesamiento de las caspasas no siempre está relacionado con su activación, evaluamos la actividad enzimática de la caspasa -3/-7 en las células HL-60 tratadas a diferentes tiempos y diferentes concentraciones de THDF, utilizando el tetrapéptido DEVD-*p*NA como sustrato específico. La activación de caspasa -3 es evidente a partir de las 12 h de incubación con 3 µM de THDF, y al tratar las células durante 24 h observamos aumento de con concentraciones mayores de 1 µM de THDF (Figura 20B).

Finalmente, analizamos el efecto del inhibidor de caspasas de amplio espectro z-VAD-fmk (Figura 20C). Utilizando una concentración de 100 µM de dicho inhibidor, suprimimos completamente la apoptosis inducida por THDF en ambas líneas celulares, lo cual confirma que su citotoxicidad es dependiente de la activación de caspasas.

11. THDF induce liberación de citocromo c mitocondrial y disminución de Bax citosólico.

La liberación de citocromo *c* desde la mitocondria al citosol es un evento central en la señalización apoptótica. Para determinar si en la apoptosis inducida por THDF se produce la liberación de citocromo *c*, analizamos los extractos citosólicos y mitocondriales mediante western blot, tanto en células HL-60 como en U937.

Los resultados obtenidos nos indican que al aumentar la concentración de THDF o el tiempo de tratamiento, se produce un aumento proporcional de citocromo *c* en el citosol que está relacionado con una disminución de citocromo *c* mitocondrial (Figura 21A).

La vía intrínseca de la apoptosis está controlada por las proteínas de la familia Bcl-2. Dentro de esta familia, Bcl-2 y Bax inhiben y promueven la apoptosis, respectivamente. Por lo tanto, estudiamos su expresión en las células tratadas con THDF.

Aunque no se producen cambios significativos en los niveles de Bcl-2, sí observamos en ambas líneas celulares hidrólisis de este factor anti-apoptótico (Figura 21A). Por su parte, Bax desempeña un papel crucial en el proceso apoptótico a través de diferentes mecanismos y Bcl-2 o Bcl-x_L son capaces de contrarrestar el efecto de Bax formando heterodímeros con él. Numerosos estudios han demostrado que el ratio entre los miembros pro-apoptóticos y anti-apoptóticos de la familia Bcl-2 juega un papel muy importante, determinando la susceptibilidad de las células a los estímulos apoptóticos [172,173].

Cuando las células HL-60 y U937 son tratadas con THDF se produce una disminución en los niveles de Bax citosólico, pero no se observan cambios significativos en la fracción mitocondrial en las condiciones del ensayo empleadas (Figura 21A).

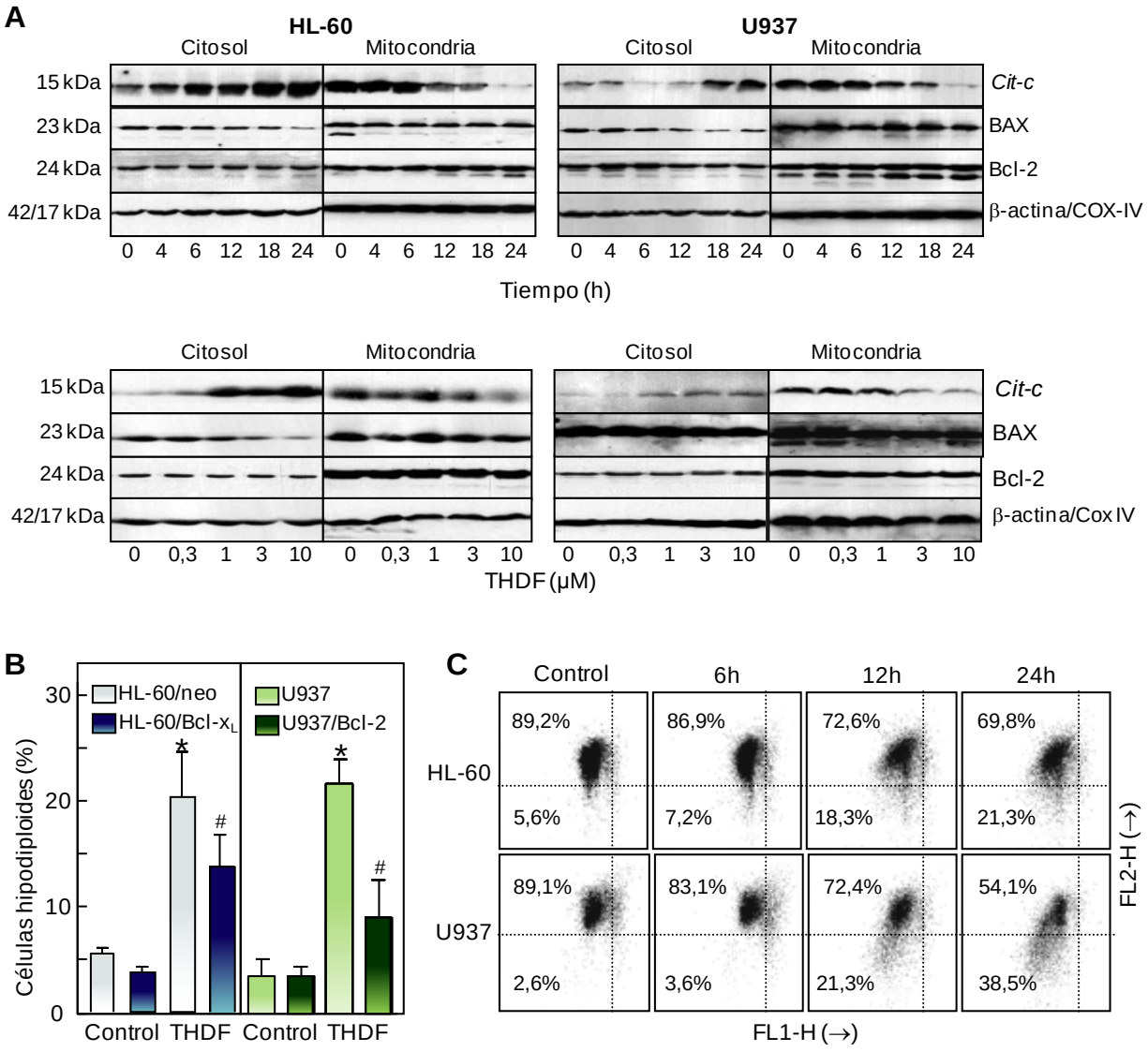

Figura 21. Evaluación del papel de las mitocondrias en la apoptosis inducida por THDF en células HL-60 y U937. (A) Las células se incubaron en presencia de THDF (3 μM) durante los tiempos indicados o con las concentraciones señaladas durante 24 h. Los extractos citosólicos y mitocondriales se ensayaron por western blot. β-actina y Cox IV (citocromo *c* oxidasa) se usaron como controles de carga en la fracción citosólica y mitocondrial, respectivamente. (B) *Comparación del efecto sobre la apoptosis inducida por THDF en células HL-60/neo y HL-60/Bcl-x_L, así como en células U937 y U937/Bcl-2.* El porcentaje de células hipodiploides fue determinado mediante citometría de flujo tras 24 h en ausencia o presencia de 3 μM de THDF. Los valores representan la media ± SE de tres experimentos independientes realizados por triplicado. *P < 0,05, significativamente diferente respecto al control. (C) *El THDF disminuye el potencial de membrana mitocondrial ($\Delta\Psi_m$).* Las células fueron incubadas con 1 μM de THDF durante los tiempos indicados y el $\Delta\Psi_m$ se analizó con la sonda JC-1. La intensidad de fluorescencia de JC-1 se determinó mediante citometría de flujo. Resultados similares fueron obtenidos en dos experimentos independientes realizados por triplicado.

12. La expresión de niveles elevados de las proteínas mitocondriales Bcl-2 y Bcl-x_L confiere resistencia parcial a la apoptosis inducida por THDF.

Bcl-2 y Bcl-x_L son proteínas que inhiben la apoptosis regulando el potencial de membrana mitocondrial y la liberación de citocromo *c* necesaria para la activación de caspasa -9. Para determinar si estas proteínas protegen a las células de la acción del THDF, usamos líneas celulares que sobreexpresan Bcl-x_L (HL-60/Bcl-x_L) o Bcl-2 (U937/Bcl-2). Los resultados nos indican que las células que expresan niveles elevados de ambas proteínas son más resistentes al efecto citotóxico (Tabla 3) y proapoptótico (Figura 21B) del THDF que sus correspondientes células control.

13. THDF induce cambios en el potencial de membrana mitocondrial ($\Delta\Psi_m$).

La disipación del gradiente electroquímico ($\Delta\Psi_m$) creado por las proteínas de la cadena respiratoria localizadas en la membrana mitocondrial interna es un elemento clave en la vía intrínseca de la apoptosis. Al estudiar si los cambios en el $\Delta\Psi_m$ son necesarios para que se produzca la liberación de citocromo *c*, se observa (Figura 21C) una disminución significativa en el $\Delta\Psi_m$ después de 12 h de tratamiento, lo cual nos sugiere que los cambios del potencial de membrana mitocondrial están implicados en la apoptosis inducida por THDF.

14. THDF activa las proteínas quinasas activadas por mitógenos (MAPKs).

Puesto que las MAPKs juegan un papel crucial en el destino de la célula, evaluamos el efecto del THDF en la activación de esta vía de señalización. Sólo estudiamos el efecto del THDF en la fosforilación de las MAPKs durante las primeras 6 h de tratamiento para evitar los efectos citotóxicos inducidos por el THDF que aparecen después de las 12 h de tratamiento, y al estudiar tratamientos más largos nos podríamos encontrar cambios inespecíficos asociados a la apoptosis.

Como se puede ver en la Figura 22A, el THDF induce la fosforilación de JNK, p38 en HL-60 y U937, mientras que la fosforilación de ERK1/2 sólo se observa en HL-60. La fosforilación de p38 se detectó a los 15 minutos, y se mantuvo elevada durante al menos 6 h (Figura 22A). Sin embargo, la activación de JNK no se observó hasta 1 h y 2 h en U937 y HL-60, respectivamente, bajo las mismas condiciones experimentales (Figura 29A). Los niveles de fosfo-ERK1/2 en las células HL-60 aumentaron después de 15 minutos y volvieron a los niveles del control después de 1 h (pico inicial). A partir de las 2 h de tratamiento, los niveles

de ERK1/2 fosforilada aumentaron de nuevo y se mantuvieron por lo menos durante 6 h (Figura 22A).

Estos resultados indican que la vía de ERK1/2 se activa rápidamente en respuesta al tratamiento con THDF en las células HL-60 y que la activación ocurre de forma bifásica. El THDF induce la activación de JNK, p38 y ERK1/2 siguiendo diferentes cinéticas. Para establecer si la fosforilación de las MAPKs juega un papel fundamental en la apoptosis inducida por este compuesto, examinamos los efectos de una serie de inhibidores específicos.

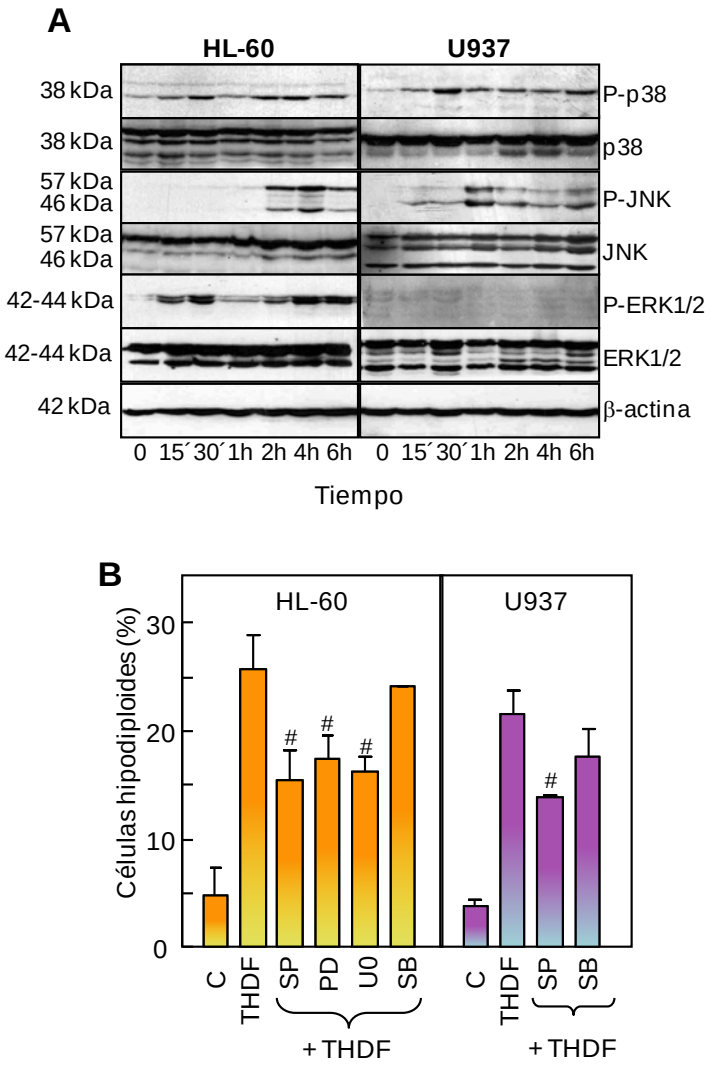

Figura 22. (A) *THDF induce la fosforilación de las MAPKs.* Las células HL-60 y U937 se trataron con THDF (10 µM) a los tiempos indicados y los extractos de proteínas se analizaron mediante western blot usando anticuerpos específicos para determinar la fosforilación de las diferentes MAPKs. Las membranas se analizaron también con anticuerpos de ERK1/2, JNK y p38 total, como control de carga. (B) *Impacto de los inhibidores de las MAPKs en la apoptosis inducida por THDF*. Las células fueron preincubadas con SP600125 (SP, 10 µM), PD98059 (PD, 10 µM), U0126 (U0, 10 µM) y SB203580 (SB, 2 µM) durante 1 h y luego fueron tratadas con THDF (3 µM, 24 h). La apoptosis se cuantificó por citometría de flujo, y las barras representan la media ± SE de tres experimentos independientes cada uno de ellos realizado por triplicado. *P < 0,05, significativamente diferente del control sin tratar. #P < 0,05, significativamente diferente del tratamiento con THDF solo.

El pretratamiento de células HL-60 y U937 con SB203580 (2 μM) no altera significativamente el porcentaje de apoptosis inducido por THDF (Figura 22B), lo cual sugiere que la activación de $p38^{MAPK}$ no está involucrada en la apoptosis inducida por THDF.

Sin embargo, el pretratamiento con el inhibidor específico de JNK SP600125 (10 μM) bloqueó parcialmente la apoptosis inducida por THDF en ambas líneas celulares.

Finalmente estudiamos el impacto de ERK1/2 en la muerte celular inducida por THDF en las células HL-60 usando los inhibidores específicos de la quinasa extracelular activada por mitógenos 1/2 (MEK1/2) y observamos que tanto PD98059 como U0126 atenúan los niveles de muerte celular inducida por THDF (Figura 22B).

15. THDF aumenta los niveles de las especies reactivas de oxígeno intracelulares.

La producción de especies reactivas de oxígeno (ROS) es considerada como uno de los mediadores claves en la apoptosis inducida por la mayoría de los agentes antitumorales. Evaluamos entonces la generación de estas especies químicas en células HL-60 mediante el uso de la sonda fluorescente sensible a la oxidación diacetato 2´,7´-dicloro-dihidro-fluoresceína (H_2-DCF-DA). Los resultados muestran una rápida generación de ROS a los 15 min de tratamiento con THDF (resultados no mostrados), aunque los niveles más altos (~2,2 veces los niveles del control) se alcanzaron tras 1 h de tratamiento (Figura 23).

Para determinar si la generación de ROS es esencial en la apoptosis inducida por THDF pretratamos las células con diferentes antioxidantes: trolox (2 mM), NAC (10 mM), vitamina E (25 μM), alopurinol (100 μM), ácido ascórbico (100 μM) y las enzimas degradantes de ROS catalasa (400 unidades/ml) y superóxido dismutasa (400 unidades/ml). El trolox fue el único antioxidante capaz de disminuir la generación de ROS, pero no evitó la muerte celular (Figuras 23B y 23C). En conjunto, estos resultados sugieren que la apoptosis inducida por THDF es independiente de la producción de ROS.

16. THDF induce parada del ciclo celular en fase M.

Fijándonos en el análisis por citometría de flujo (ver Figura 17), podemos ver que THDF acumula células en la fase G_2-M del ciclo celular, a expensas de un descenso en la cantidad de células en fase G_1. Al tratar las células HL-60 y U937 con una dosis de 3 μM de THDF y observando lo que pasa a lo largo del tiempo (Tabla 4), vemos que este efecto se produce ya a las 6-12 h de tratamiento en ambas líneas celulares.

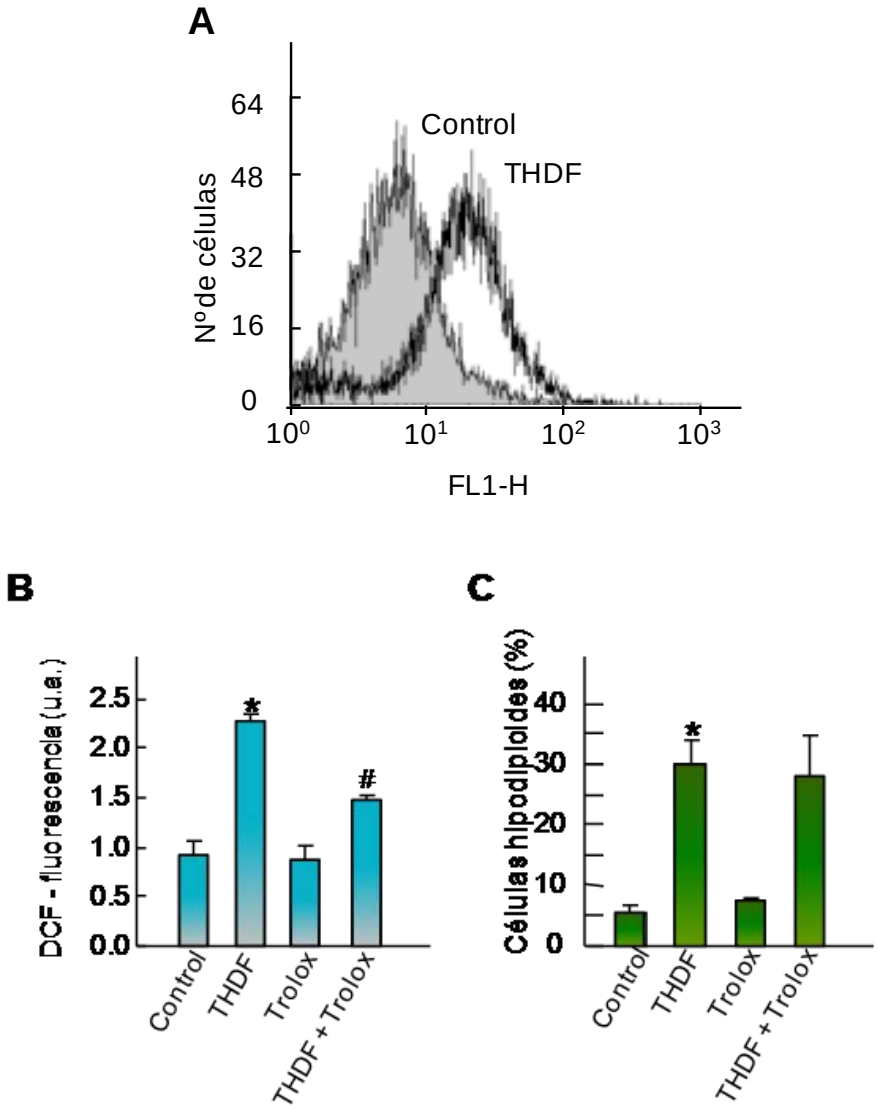

Figura 23. ROS no está involucrado en la muerte celular inducida por THDF. (A) Las células HL-60 se incubaron durante 1 h en presencia de 10 μM THDF y la fluorescencia obtenida por la oxidación de H_2-DCF-DA se determinó mediante citometria de flujo. Resultados similares se obtuvieron en tres experimentos independientes. (B) Las células se preincubaron con trolox (2 mM) durante 1 h y posteriormente incubadas con THDF (10 μM) durante 1 h. Los niveles de ROS se determinaron mediante citometría de flujo usando la sonda H_2-DCF-DA. (C) Las células se pretrataron con trolox y tratadas con THDF (3 μM) durante 24 h, la apoptosis se determinó mediante citometria de flujo. Los valores representan la media ± S.E. de tres experimentos independientes realizados por triplicado. *P < 0,05, significativamente diferente del control. $^{\#}P$ < 0,05, significativamente diferente del tratamiento con THDF solo.

En HL-60 el porcentaje de células en fase G_2-M aumenta desde un ~ 25% (control), hasta un ~ 44% después del tratamiento con THDF durante 12 h. Mientras que el porcentaje de células hipodiploides (fracción $SubG_1$) se multiplica por 5 en las células tratadas con 3 μM de THDF en comparación con las células control tras 24 h (Figura 17).

		% $SubG_1$	% G_1	% S	% G_2-M
HL-60					
6h	Control	5,7 ± 0,6	40,6 ± 2,4	21,6 ± 0,8	33,3 ± 3,6
	THDF	6,3 ± 2,2*	28,4 ± 4,5*	23,1 ± 2,2	42,8 ± 4,8*
12h	Control	4,3 ± 1,5	46,6 ± 3,3	24,9 ± 2,6	25,1 ± 3,1
	THDF	11,3 ± 3,4*	22,5 ± 2,5*	16,5 ± 5,1	44,3 ± 0,5*
24h	Control	4,4 ± 1,8	46,8 ± 3,1	23,9 ± 2,3	25,4 ± 2,9
	THDF	21,5 ± 3,8*	30,6 ± 1,7*	17,8 ± 3,9*	26,5 ± 1,0*
U937					
6h	Control	4,9 ± 1,9	48,8 ± 3,6	20,4 ± 1,5	24,1 ± 4,6
	THDF	5,0 ± 1,3	36,5 ± 2,1*	22,6 ± 0,8	33,4 ± 5,3*
12h	Control	4,8 ± 1,1	51,8 ± 5,2	20,3 ± 2,5	22,4 ± 3,0
	THDF	23,6 ± 4,8*	20,5 ± 5,5*	10,1 ± 3,6	38,6 ± 8,7*
24h	Control	5,4 ± 1,5	51,3 ± 3,6	19,7 ± 2,4	22,6 ± 2,1
	THDF	21,4 ± 0,6*	20,9 ± 0,6*	14,6 ± 4,6	35,8 ± 3,2*

Tabla 4. Efecto del THDF sobre las diferentes fases del ciclo celular en HL-60 y U937. Las células se incubaron con THDF (3 μM) a los periodos de tiempo mencionados y la distribución en cada fase del ciclo celular se determinó por citometría de flujo. Los valores representan la media ± S.E. de dos experimentos independientes. Los asteriscos indican una diferencia significativa (*P < 0,05) en comparación con los controles correspondientes.

En las células U937 la acumulación de células en fase G_2-M se mantiene hasta las 24 h y los niveles máximos de apoptosis (aproximadamente 5 veces con respecto al control) se pueden observar a las 12 h de tratamiento (Tabla 4).

Para determinar si las células HL-60 se acumulan en la fase M, sincronizamos las células tratándolas con nocodazol (100 ng/ml) durante 24 h. De este modo se obtiene una población rica en células en fase M (aproximadamente el 90%). Luego, liberamos las células del bloqueo en fase M, lavando con RPMI y resuspendiendo las células en nuevo medio de cultivo con o sin THDF (3 μM). El análisis mediante citometría de flujo indica que las células tratadas con THDF no son capaces de continuar el ciclo celular (Figura 24), lo cual sugiere que el THDF bloquea las células en fase M.

Para confirmar estos resultados, cultivamos las células HL-60 y U937 con 3 μM de THDF durante 6, 12 y 24 h y el porcentaje de células en mitosis lo cuantificamos mediante microscopía de fluorescencia, tras realizar una tinción con Hoechst 33258 (Figura 25).

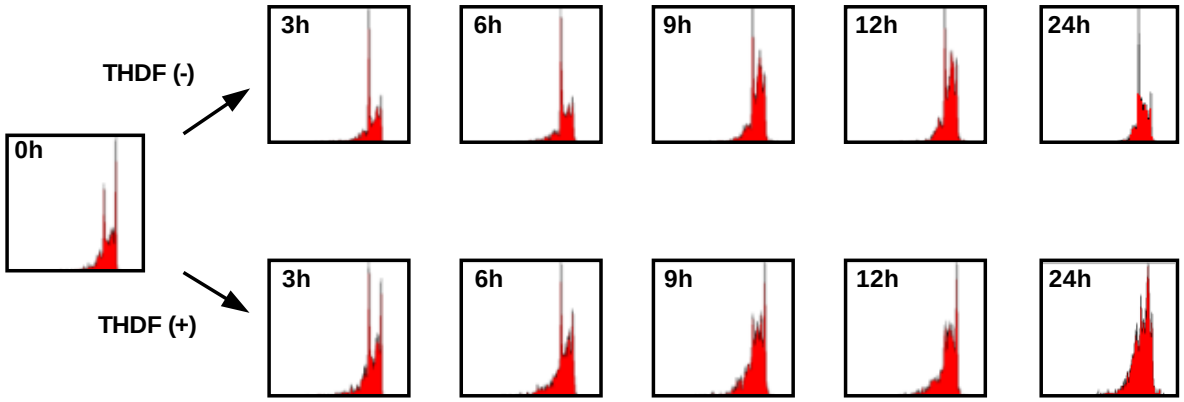

Figura 24. Distribución del ciclo celular durante la incubación en presencia o ausencia de THDF en células HL-60 previamente sincronizadas en fase M. Las células fueron sincronizadas en mitosis mediante tratamiento con nocodazol (100 ng/ml) durante 24 h, se lavaron con medio de cultivo y se incubaron con 0,03% DMSO o 3 µM de THDF a los tiempos indicados. El análisis del ciclo celular fue determinado mediante citometría de flujo.

El porcentaje de células HL-60 en mitosis aumentó desde un 7 ± 3,1 % (control) hasta un 26,0 ± 5,7 % (~4 veces) y un 25,5 ± 10 % (3,6 veces) al tratarlas con THDF durante 6 y 12 h, respectivamente. En las células U937, el porcentaje de células en mitosis aumentó desde un 3,6 ± 0,6 % (control) hasta un 27,0 ± 4,0 % (~8 veces) y 42,0 ± 6,2 % (~12 veces) después de 6 y 12 h de tratamiento con THDF, respectivamente.

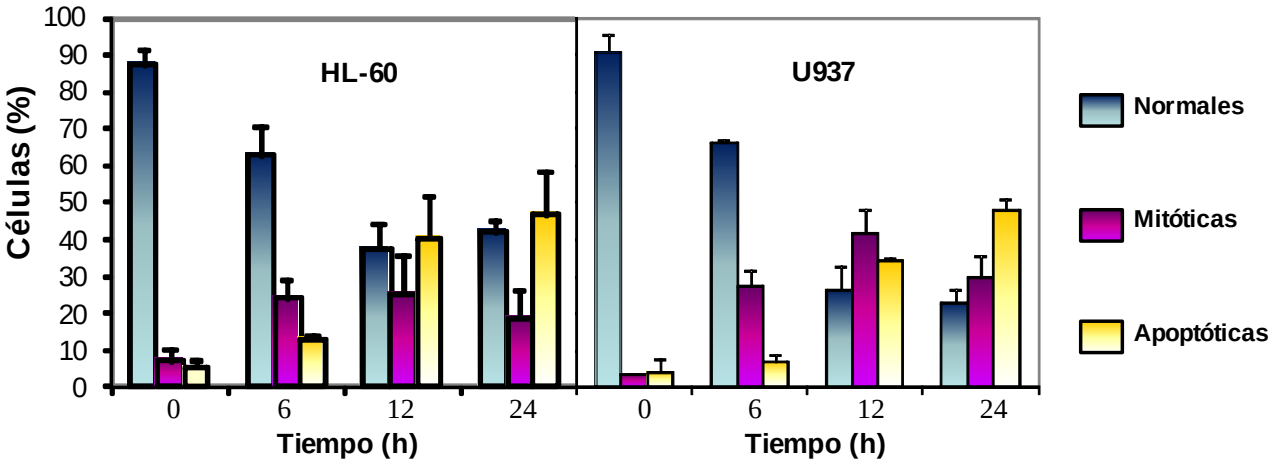

Figura 25. THDF induce parada en mitosis. (A) Las células HL-60 y U937 fueron cultivadas en presencia de 3 µM de THDF a los tiempos indicados. El porcentaje de células normales, mitóticas y apoptóticas fue analizado mediante microscopía de fluorescencia usando Hoechst 33258, y los porcentajes se calcularon después de contar 500 células. Los datos representan la media de los valores obtenidos de tres experimentos independientes y las barras representan las desviaciones estándar.

17. Efectos del THDF sobre la expresión y fosforilación de las proteínas reguladoras de la fase M.

Teniendo en cuenta que THDF inhibe la proliferación de las células de leucemia HL-60 y U937 induciendo parada del ciclo celular en fase M, estudiamos la expresión de las proteínas reguladoras de esta fase del ciclo celular.

Mediante western blot (Figura 26) podemos observar que los niveles de ciclina B1, fosfo-ciclina B1 (fosfo S126) y el inhibidor de CDK p21 aumentaron en las células HL-60 después de 4 h de tratamiento con 3 μM de THDF mientras que en U937 los niveles de ciclina B1 y fosfo-ciclina B1 aumentaron a partir de las 6 h. El efecto del THDF sobre la expresión y fosforilación de ciclina B1 es dependiente de la concentración.

El aumento de la expresión de p21 tras el tratamiento de las células HL-60 y U937 con THDF, concuerda perfectamente con el hecho, demostrado previamente (Figura 25), de que THDF activa la vía MEK 1/2 / ERK 1/2, ya que la transcripción de p21 es ERK 1/2 dependiente [13].

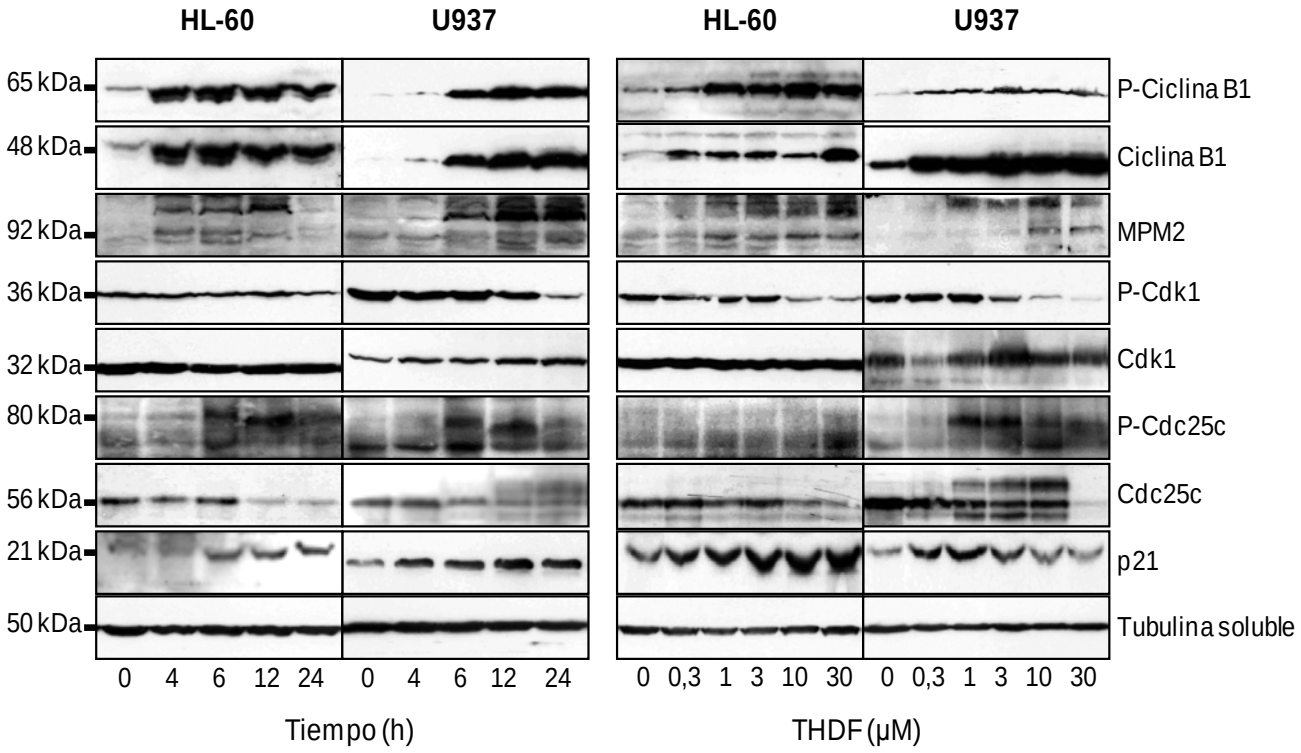

Figura 26. Efecto del THDF sobre la expresión de las proteínas que regulan el ciclo celular. Las células HL-60 y U937 se incubaron en presencia de THDF durante 24 h utilizando las concentraciones indicadas, y con 3 μM de THDF a los tiempos indicados. Se recolectaron las células y los lisados totales se analizaron mediante western blot. Se muestran los resultados de un experimento representativo. Se usó α-tubulina como control positivo.

La disminución de los niveles de Cdc25c es consistente con el aumento de la fosforilación de esta proteína, que podemos detectar usando un anticuerpo específico fosfo-Cdc25c (Thr^{48}).

La activación de CDK1 se controla en diferentes etapas, incluyendo la unión de ciclinas y la fosforilación de la treonina 161. No obstante, un paso crítico en la activación de CDK1 durante la mitosis es la desfosforilación de T14 e Y15, función que desempeña la fosfatasa de actividad dual Cdc25c. Al usar un anticuerpo que reconoce la forma fosforilada de la CDK1 (pTpY 14/15), demostramos que THDF induce desfosforilación en ambas líneas celulares y consecuentemente activación de CDK1 (Figura 26).

El uso del anticuerpo MPM-2 nos permite evaluar el estado de polipéptidos fosforilados que sólo se encuentran en las células mitóticas. Este anticuerpo reconoce un epítopo (ST/T)P que aparece en fosfoproteínas como MAP2, HSP70, Cdc25c y ADN topoisomerasa IIα, la mayoría de las cuales se fosforilan en la mitosis.

Los experimentos dependientes del tiempo muestran un aumento de las proteínas MPM-2 a partir de las 4 h y 6 h en las células HL-60 y U937, respectivamente. Mientras que después de 24 h de tratamiento con THDF, podemos observar un aumento significativo de los niveles de MPM-2 a partir de una concentración de 1 μM en ambas líneas celulares.

18. THDF desestabiliza la polimerización de los microtúbulos.

Ya que THDF produce una acumulación de células en la fase M del ciclo celular, estudiamos si este compuesto afecta a la polimerización de tubulina en células HL-60 y U937. El análisis mediante western blot nos muestra que una baja concentración de THDF (3 μM) es suficiente para inhibir la polimerización de tubulina en ambas líneas celulares (Figura 27A). Como controles positivos de la inhibición y estimulación de la polimerización de tubulina utilizamos colchicina y paclitaxel, respectivamente. Además, examinamos el efecto del THDF sobre la red de microtúbulos celular mediante inmunofluorescencia. Como se observa en la Figura 27B, el tratamiento con 3 μM de THDF provoca una disminución de la red de microtúbulos similar a la inducida por la colchicina, mientras que el paclitaxel aumenta la densidad de los microtúbulos.

19. THDF inhibe la polimerización de la tubulina in vitro.

Estudiamos el efecto del THDF sobre la formación de los microtúbulos evaluando la polimerización de la tubulina *in vitro* mediante los cambios en la absorbancia de la mezcla de

reacción. Los resultados indican que THDF inhibe la polimerización de tubulina y que es dependiente de la concentración de compuesto utilizado (Figura 28A). Este resultado indica que la actividad biológica del THDF es debida al menos en parte a su interacción con la tubulina.

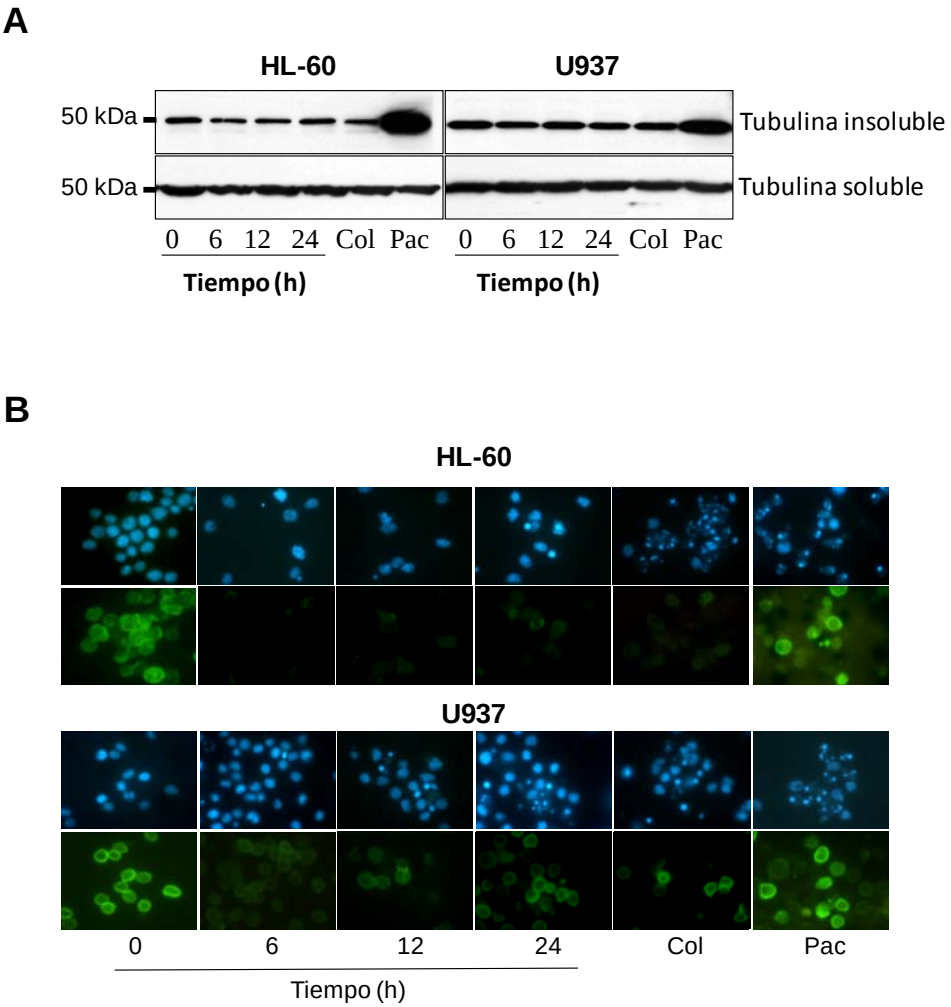

Figura 27. THDF inhibe la polimerización de la tubulina en células HL-60 y U937. Las células fueron incubadas en ausencia o presencia de 3 µM de THDF a los tiempos indicados, colchicina (50 nM) o paclitaxel (100 nM) durante 24 h. (A) Las células fueron lisadas y los microtúbulos polimerizados se separaron de los dímeros de tubulina mediante centrifugación. Se detectó la α-tubulina mediante western blot. (B) Las células se recolectaron y se fijaron, para ser incubadas con el anticuerpo monoclonal anti-α-tubulina a temperatura ambiente durante 2 h y posteriormente con un anticuerpo secundario conjugado con Cy2™. La red de microtúbulos celular se analizó usando un microscopio fluorescente Zeiss. Las microfotografías son representativas de tres experimentos independientes. Colchicina y paclitaxel fueron utilizados como controles positivos, como agentes despolimerizante y polimerizante de microtúbulos, respectivamente.

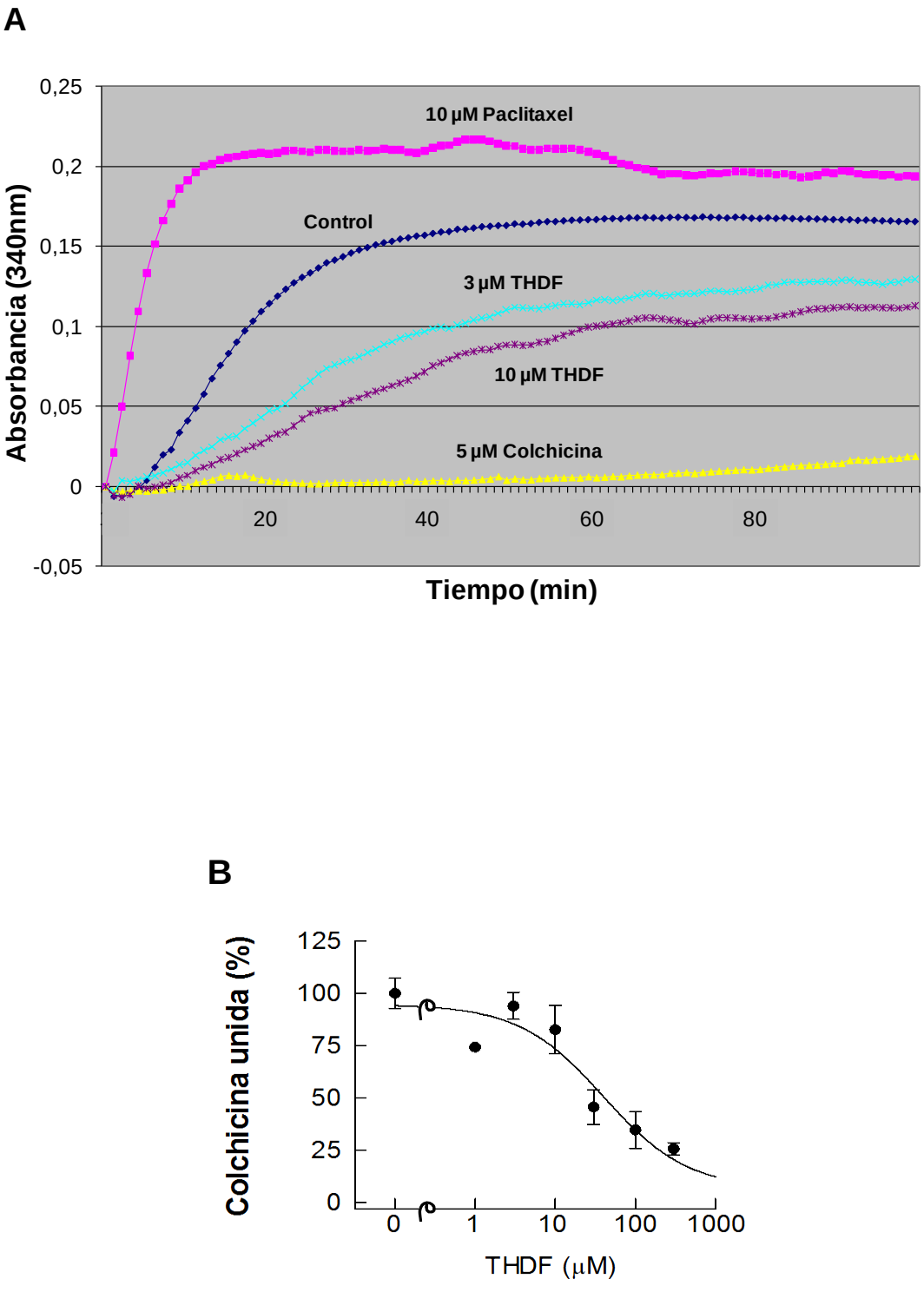

Figura 28. (A) THDF inhibe la polimerización de la tubulina "in vitro". Tubulina purificada se incubó en el tampón de reacción a 37 ºC en ausencia (control) o en presencia de paclitaxel (10 µM), colchicina (5 µM) o diferentes concentraciones de THDF (3-10 µM). El aumento de absorbancia a 340 nm se midió en un lector de microplacas (DTX 880 Multimode Reader, Beckman Coulter). (B) *Ensayo de competición entre [^{3}H]-colchicina y THDF por la unión a la tubulina.* Se muestran los valores de un experimento representativo en el que cada punto representa la media de tres determinaciones.

20. THDF se une específicamente al sitio de unión de la colchicina.

En un intento de precisar el sitio de acción del THDF, evaluamos su capacidad de competir con la unión de la [^{3}H]-colchicina a la tubulina. Como podemos observar en la Figura 28B, THDF inhibió la unión de la colchicina a la tubulina de forma dosis dependiente, con una IC_{50} de aproximadamente 40 μM.

21. THDF induce la generación de ceramidas y la activación de SMasa.

Evaluamos la capacidad de este compuesto de inducir cambios en los niveles de ceramida endógena en las células de leucemia humana HL-60.

El ensayo de la diacilglicerol quinasa es un método ampliamente utilizado para estimar el contenido de ceramidas en los extractos lipídicos. Para ello, tratamos las células con 3 μM de THDF durante diferentes tiempos y cuantificamos la cantidad de ceramidas. Cualquier aumento de ceramidas en los extractos lipídicos sería indicativo de la producción celular de ceramidas. Como podemos observar (Figura 29A), THDF indujo un aumento significativo en la concentración de ceramidas intracelulares a partir de las 2 h de tratamiento que permaneció elevado por lo menos hasta las 24 h.

Para evaluar si la acumulación de ceramidas se produce, por lo menos en parte, en la mitocondria, tratamos las células HL-60 con THDF, y determinamos los niveles de ceramidas en la fracción mitocondrial. Como observamos en la Figura 29B, los niveles de ceramidas de la fracción mitocondrial de las células tratadas con THDF fue significativamente mayor que el de las células control.

Además, evaluamos la implicación de las esfingomielinasas (SMasas), tanto la SMasa ácida como la neutra están implicadas en la generación de ceramidas en respuesta al estrés. Tratamos las células HL-60 con 3 μM de THDF durante diferentes períodos de tiempo y analizamos los lisados libres de núcleos a pH 5,0 ó 7,4 para determinar la actividad esfingomielinasa ácida (A-SMasa) y la actividad esfingomielinasa neutra (N-SMasa), respectivamente.

Como se muestra en la Figura 29C, los resultados revelan que el THDF induce activación de A-SMasa a partir de las 2 h de tratamiento, que continúa aumentando hasta las 24 h. En cambio no detectamos cambios en la actividad N-SMasa en el mismo marco de tiempo aunque sí con TNFα utilizado como control positivo.

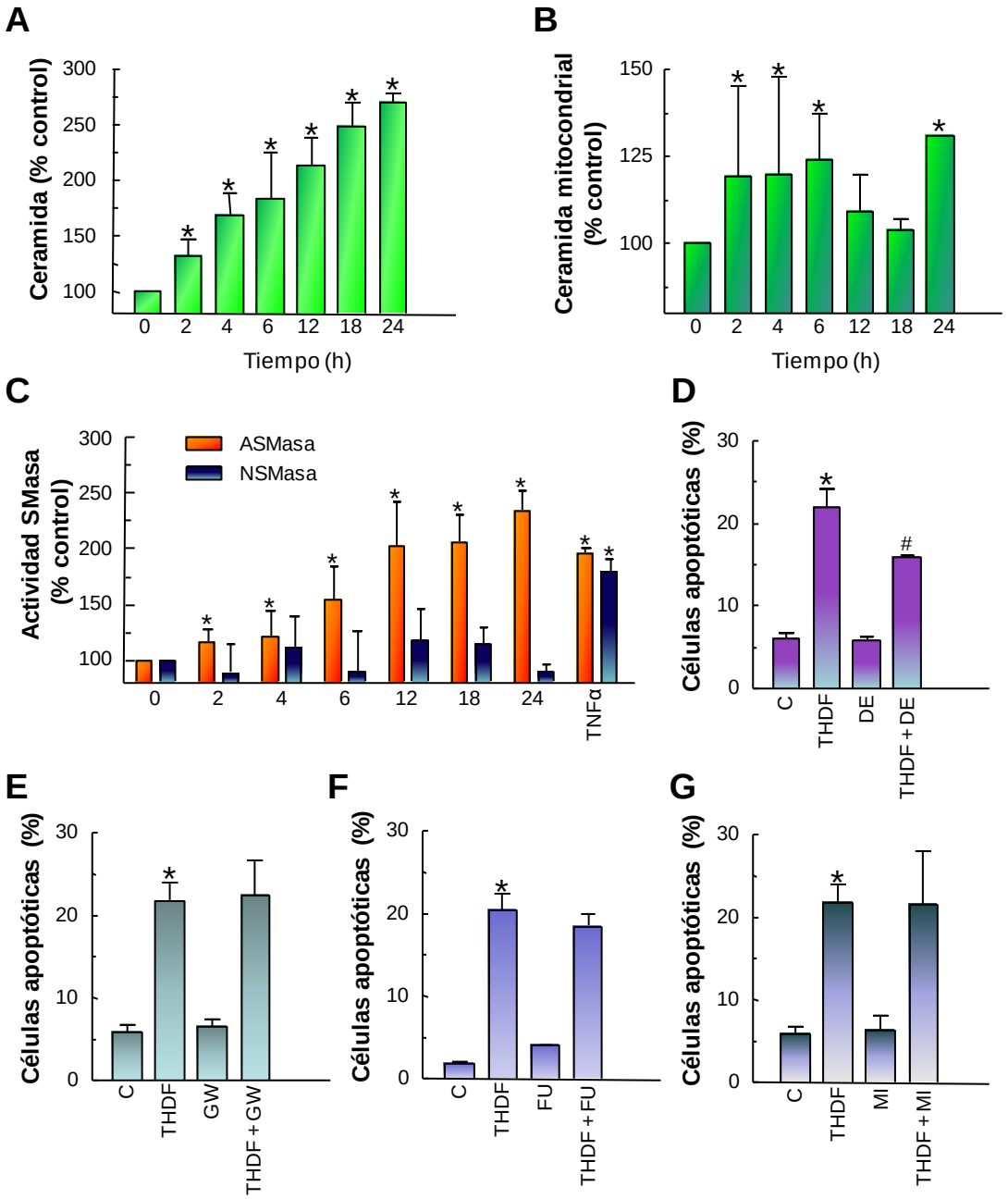

Figura 29. Efecto de THDF sobre la vía de la esfingomielina en células HL-60. (A) Incremento de los niveles intracelulares de ceramidas después del tratamiento con 3 μM de THDF durante los tiempos indicados, el contenido en ceramidas se determinó mediante el ensayo de la diacilglicerol quinasa. Los datos representan la media ± S.E. de tres experimentos independientes. (B) El análisis de los niveles de ceramida mitocondrial se realizó igual que en el apartado anterior, separando previamente las mitocondrias. (C) Se analizó la actividad de SMasa ácida y neutra después de tratar las células con 3 μM de THDF a los tiempos indicados. TNFα se usó como control positivo. (D, E, F y G) Las células se trataron con o sin 3 μM de THDF durante 24 h en presencia o ausencia de desipramina (DE, 10 μM), GW4869 (GW, 20 μM), fumonisina B1 (FU, 100 μM) o miriocina (MI, 5 μM), el porcentaje de células apoptóticas se cuantificó mediante citometria de flujo. *P < 0,05, significativamente diferente del control sin tratar. #P < 0,05, significativamente diferente del tratamiento con THDF solo.

Ya que la ceramida está implicada en la regulación de la apoptosis en las células tumorales, usamos la desipramina, inhibidor de la esfingomielinasa ácida, para determinar si la ceramida generada a través de la activación de A-SMasa está implicada en la apoptosis inducida por THDF [174]. El pretratamiento de las células HL-60 con 10 µM de desipramina inhibió significativamente la muerte celular después de un tratamiento de 24 h con 3 µM de THDF (Figura 29D). Sin embargo el inhibidor de la esfigomielinasa neutra, GW4869, no tuvo ningún efecto en la muerte celular inducida por el flavonoide (Figura 29E).

Tampoco observamos una disminución de la muerte celular al usar miriocina, un inhibidor selectivo de la serina palmitoil-transferasa [175], que es capaz de bloquear de forma selectiva la síntesis de ceramida por la vía *de novo*. Además usamos la fumonisina B1 (100 µM) para inhibir la dihidroceramida sintasa, una enzima implicada en la vía *de novo* y en la vía de salvamento de ceramida [176]. Los resultados revelan que ni la mioricina ni la fumonisina B1 bloquean la apoptosis inducida por el THDF en las células HL-60 (Figura 29F y 29G), indicando que ni vía de salvamento ni la biosíntesis *de novo* están implicadas en la muerte celular inducida por el THDF.

Globalmente, estos resultados nos sugieren que la generación de ceramidas en respuesta a THDF en células HL-60 es un evento que se produce antes de la activación de caspasas y que implica la activación de esfingomielinasa ácida.

DISCUSIÓN

El tratamiento del cáncer ha evolucionado mucho en los últimos años y se ha conseguido aumentar la supervivencia frente a algunos tipos de cáncer (por ejemplo, leucemias o linfomas), pero no se ha conseguido la efectividad deseada debido fundamentalmente a una limitada actividad terapéutica (30%) o a una excesiva toxicidad (30%). Existen cada vez más evidencias de que no se pueden tratar todos los tipos de cáncer de igual forma y la lucha contra esta enfermedad sólo podrá solucionarse seleccionando las mejores dianas terapéuticas [5,6].

Nuestro estudio hace especial hincapié en la lucha contra la leucemia. Aunque existen tratamientos eficaces frente a la leucemia linfoide aguda, leucemia linfoblástica y leucemia mieloide crónica necesitamos tratamientos más efectivos frente a otros tipos de leucemia aguda. Además, las neoplasias hematológicas forman uno de los grupos de cáncer más estudiados y el análisis de los mecanismos implicados en la supervivencia o muerte de estas células tumorales ha proporcionado nuevas dianas terapéuticas eficaces en el tratamiento de este y otros tipos de cáncer [8].

Los principios activos obtenidos de fuentes naturales o sus derivados semisintéticos han dado lugar a los principales medicamentos utilizados contra el cáncer [177]. Los flavonoides son compuestos con una estructura fenilbenzo-γ-pirona de origen natural, que abundan en las dietas ricas en frutas, verduras y bebidas derivadas de plantas [22], y además poseen propiedades antitumorales [178].

En estudios previos llevados a cabo por nuestro grupo de investigación, se ha demostrado que diferentes compuestos con una estructura fenilbenzo-γ-pirona obtenidos mediante semisíntesis a partir de fuentes naturales inducen citotoxicidad en células de leucemia mieloide humana (HL-60) [153]. En concreto, se ha demostrado que la metilación del grupo hidroxilo en la posición C3 de la quercetina da lugar a un compuesto con una importante actividad antiproliferativa en diversas líneas celulares tumorales, y que el 3-metil éter de betuletol, un flavonoide de origen natural, es un potente inhibidor de la proliferación que muestra una alta actividad citotóxica [153].

Los estudios realizados con el trifolín, compuesto obtenido de una fuente natural indican que no presenta actividad citotóxica en ninguna de las líneas celulares ensayadas, mientras que el trifolín acetato obtenido mediante semisíntesis exhibe propiedades citotóxicas frente a todas las líneas celulares ensayadas, con valores de IC_{50} entorno a 15 µM.

TRIFOLÍN ACETATO

Teniendo en cuenta que la selectividad hacia las células tumorales es un criterio muy importante en la utilización o desarrollo de un nuevo agente anticancerígeno, hemos comparado el efecto del TA en células tumorales humanas y en linfocitos humanos (PBMC). Los resultados nos indican que tanto las PBMC quiescentes como las PBMC proliferantes son altamente resistentes frente al TA.

La mayoría de los agentes antitumorales inducen la muerte celular por apoptosis, por lo tanto, evaluamos el efecto del TA sobre esta vía utilizando diferentes líneas celulares tumorales humanas. Los resultados obtenidos nos indican que el TA induce muerte celular por apoptosis. Este tipo de muerte celular puede llevarse a cabo con o sin la activación de caspasas, proteínas que juegan un papel fundamental en la apoptosis y en la activación de citoquinas. La activación de caspasas, además, depende del estímulo apoptótico y de la línea celular estudiada. Al estudiar el efecto del TA en las células pretratadas con el inhibidor general de caspasas z-VAD-fmk, podemos observar que no se produce apoptosis indicándonos que estamos ante un mecanismo de muerte celular dependiente de caspasas.

Existen dos vías apoptóticas bien caracterizadas en las células de mamíferos, la vía de los "receptores de muerte" (extrínseca) y la vía mitocondrial (intrínseca), que generalmente son las responsables de la apoptosis dependiente de caspasas. Su implicación en la muerte celular inducida por el TA fue evaluada mediante el uso de inhibidores selectivos de caspasa-8 (z-IETD-fmk) y caspasa-9 (z-LEHD-fmk), que son las principales caspasas iniciadoras de las vías extrínseca e intrínseca, respectivamente.

Demostramos que la vía de "los receptores de muerte" no juega un papel importante, ya que el z-IETD-fmk es incapaz de prevenir la muerte celular inducida por el TA. Este resultado está de acuerdo con la ausencia de hidrólisis de procaspasa-8, evaluada por inmunoblot (datos no mostrados). En cambio, el porcentaje de células apoptóticas disminuyó de forma significativa en presencia de z-LEHD-fmk, lo cual indica que la vía mitocondrial desempeña una función importante en la muerte celular inducida por el TA. Este resultado concuerda con el aumento en la hidrólisis de la procaspasa-9 observado en los lisados de células tratadas con TA.

También evaluamos si la caspasa-2 está implicada en la apoptosis inducida por el TA. Esta caspasa parece actuar en un nivel anterior a la mitocondria, aumentando la liberación de citocromo *c* en diferentes líneas [179,180,181]. Mediante el uso del inhibidor específico z-

VDVAD-fmk, hemos observado que la caspasa-2 no es necesaria para que se produzca la apoptosis inducida por el TA y descartamos su posible implicación en la activación de la caspasa-9. Este hecho apoya una función preeminente de la caspasa-9 como caspasa apical que se activa en respuesta al tratamiento por TA.

La caspasa-2 es única, en cuanto está presente en el núcleo de forma constitutiva y parece ser necesaria para el comienzo de la apoptosis provocada por agentes promotores de daño en el ADN como el etopósido, el cisplatino y la luz ultravioleta [179,182]. Aunque son necesarios experimentos adicionales, los resultados obtenidos sugieren que el TA induce muerte celular a través de un mecanismo que parece ser independiente del daño en el ADN.

Una vez activadas, la mayoría de las caspasas iniciadoras activan por proteólisis la cascada de las caspasas y las caspasas efectoras hidrolizan sustratos celulares específicos produciéndose una disminución del tamaño nuclear, la aparición de evaginaciones esféricas en la membrana plasmática (“blebbing”) y la condensación de la cromatina.

Los estudios con inhibidores selectivos para caspasa-3 (z-DEVD-fmk) y caspasa-6 (z-VEID-fmk) sugieren que ambas caspasas son muy importantes en la apoptosis inducida por el TA. El inhibidor z-VEID-fmk resultó ser más efectivo que el z-DEVD-fmk en la prevención de la apoptosis inducida por el TA. Este resultado indica que la caspasa-6 podría jugar un papel importante en la activación de la cascada apoptótica, similar al descrito previamente para el resveratrol en líneas celulares de leucemia humana [183] y contrasta con un gran número de estudios que sugieren que la caspasa-6 es una caspasa efectora y que es activada después de la caspasa-3 [77,184]. De todas formas, no podemos descartar otras posibilidades como podrían ser las diferencias en la accesibilidad de los inhibidores a las caspasas celulares [185] y/o la implicación de proteasas apicales no identificadas con una actividad similar a las caspasas, como se ha sugerido recientemente en la apoptosis inducida por estrés térmico en células Jurkat [186].

En este contexto, la caspasa-1 además de poseer una función en el procesamiento de las citoquinas proinflamatorias IL-1b e IL-18 [187] parece estar implicada en la muerte celular, tal y como se ha demostrado en fibroblastos [188], células neuronales [189] y en la apoptosis inducida en macrófagos por una bacteria [190]. Existen evidencias de que la caspasa-1 activa a la caspasa-6 en neuronas humanas cultivadas en ausencia de suero y provoca la muerte de las células neuronales [191]. Paradógicamente, nos hemos encontrado que el porcentaje de células hipodiploides aumenta de manera significativa en presencia del inhibidor de caspasa-1

z-YVAD-fmk, lo que sugiere que la caspasa-1 está involucrada en la supervivencia de las células estimuladas con el TA.

Existen estudios que demuestran que la caspasa-1 promueve la supervivencia celular mediante un mecanismo en el que están implicadas las proteínas de unión a elementos que regulan el esterol (SREBPs) y la biogénesis lipídica. La inhibición selectiva de la caspasa-1 con z-YVAD-fmk o mediante ARN de interferencia aumentó la muerte celular en respuesta a toxinas formadoras de poros [192]. Por lo tanto, sería un interesante objeto de estudio la implicación de la caspasa-1 en la biogénesis lipídica en células tratadas con TA.

Tal y como esperábamos, las procaspasas -3 y -6 se hidrolizan dando lugar a las formas activas de las enzimas en respuesta al TA. También se induce la hidrólisis de la proteína nuclear PARP, reconocido sustrato de caspasa-3 que está implicado en la reparación del ADN y que es importante en el mantenimiento de la viabilidad celular [193,194,195]. Puesto que la hidrólisis de PARP garantiza el desensamblaje celular, este parece ser un elemento regulador clave en la apoptosis inducida por el TA [195].

La mitocondria juega un papel clave en la muerte celular cuando su membrana externa se permeabiliza [196], y los miembros de la familia Bcl-2 regulan la permeabilización de la membrana mitocondrial externa que constituye un punto de regulación crítica en la vía intrínseca de la apoptosis [197]. Los resultados demuestran que el TA induce la redistribución de citocromo *c* al citosol que podemos detectar a las 6 h de tratamiento. No obstante, este evento temprano no está asociado con una pérdida en el $\Delta\Psi m$, ya que no detectamos cambios por lo menos en las primeras 24 h de tratamiento. En este aspecto, estudios previos han demostrado que los cambios en el $\Delta\Psi m$ no son imprescindibles para que se produzca la liberación de citocromo *c* desde la membrana mitocondrial externa [198]. La activación de Bax y/o Bak puede conducir a la formación de poros en la membrana mitocondrial externa [199].

Para profundizar en el estudio del papel de la mitocondria en la acción citotóxica del TA, utilizamos células HL-60 y U937 que sobreexpresan proteínas anti-apoptóticas. Las células HL-60/Bcl-x_L y U937/Bcl-2 resultaron ser completamente resistentes al compararlas con las líneas celulares parentales, lo cual sugiere que la mitocondria desempeña un papel central en la muerte celular inducida por el TA.

En conjunto, nuestros resultados indican que el TA induce apoptosis por un mecanismo que implica la vía mitocondrial y que la caspasa-6 parece activarse antes que la caspasa-9.

Las MAP quinasas forman parte fundamental de la maquinaria de transducción de señales y desempeñan un papel esencial en el crecimiento celular, la diferenciación y la muerte celular.

Aunque JNK está asociado con acciones pro-apoptóticas [112] y con señales que inhiben el crecimiento [114], hemos demostrado que el TA induce la activación de JNK y que la utilización del inhibidor SP600125, para suprimir su actividad, aumenta la apoptosis. Estudios previos han demostrado que el efecto pro-apoptótico del inhibidor de la histona deacetilasa D1 aumenta en presencia de SP600125 en líneas celulares de leucemia mieloide humana aguda [200]. Evidencias adicionales de que JNK pueda actuar como señal de supervivencia las podemos encontrar en células de carcinoma hepático [115] y en líneas celulares de cáncer gástrico y colorrectal [116].

La muerte celular en algunas líneas celulares está directamente asociada con la activación de p38, aunque también se ha descrito que esta proteína promueve la supervivencia, el crecimiento celular y la diferenciación. Así pues, el papel de p38 en la apoptosis depende de la línea celular y del estímulo [121]. La p38 parece estar implicada en la activación de la apoptosis inducida por el TA ya que el inhibidor específico SB203580 atenua la muerte celular. La activación de p38 es también necesaria para la apoptosis inducida por cadmio y en la isquemia [122,123,124,125].

Nuestros datos, también indican que el inhibidor U0126 atenua el efecto apoptótico del TA, sugiriendo que ERK1/2 está implicado en la señalización de la muerte celular. Resultados similares han sido descritos por otros autores con la quercetina en células A549 [106]. Además, la supresión de la vía de señalización MEK-ERK utilizando el inhibidor PD98059 produjo un aumento de la resistencia al cisplatino en células de carcinoma cervical humano SiHa y en células de hepatoblastoma HepG2 [107]. Además, la acroleína, un aldehído α,β -insaturado altamente reactivo generado por peroxidación lipídica, induce fosforilación de ERK mientras que la inhibición de su actividad con PD98059 y U0126 bloquea la apoptosis inducida por la acroleína [201]. A modo de comparación, el tetraacetato de 3-metil éter de quercetina, compuesto químicamente muy similar al TA, aumenta la activación de la vía MEK/ERK [155] y los inhibidores de ERK potencian los efectos apoptóticos del tetraacetato de 3-metil éter de quercetina. Esto demuestra que compuestos estructuralmente muy similares pueden activar diferentes vías de señalización en el mismo modelo celular.

La producción de ROS en células de leucemia, podría ser la causa de la activación de las MAPKs [167,168,169]. Aunque la generación de ROS intracelular es evidente con tan sólo 1 h de tratamiento con TA, no parece estar implicada en la apoptosis inducida por el TA, ya que diferentes antioxidantes fueron incapaces de proteger a las células.

5,7,3´-TRIHIDROXI-3,4´-DIMETOXIFLAVONA

En este estudio hemos seleccionado, además, un análogo del 3-metil éter de quercetina, THDF, que contiene un grupo metoxilo adicional en la posición 4´ del núcleo fenilbenzo-γ-pirona y hemos evaluado su actividad citotóxica en nueve líneas celulares tumorales.

Los resultados claramente demuestran que el THDF presenta propiedades citotóxicas frente a todas las líneas celulares ensayadas, pero con diferente intensidad. Las células de leucemia humana (HL-60, U937, Molt-3 and Jurkat) fueron las más sensibles, mientras que las células SK-MEL-1 y A549 presentaron una resistencia. La realización de experimentos con linfocitos humanos quiescentes (PBMC) nos reveló que son más resistentes al THDF que los linfocitos humanos proliferantes, tratados con fitohemaglutinina.

El análisis del ciclo celular nos demuestra que la inhibición de la viabilidad celular inducida por el THDF está asociada con una significante acumulación de células en la fase G_2-M, y con un aumento en la fracción $SubG_1$ y externalización de fosfatidilserina, características de la muerte celular por apoptosis. Estos resultados son similares a los obtenidos recientemente con el derivado semisintético tetraacetato de 3-metil éter de quercetina en células de leucemia humana [155], ambos compuestos inducen apoptosis y parada del ciclo celular en fase G_2-M, pero es interesante destacar que la potencia del THDF es significativamente mayor.

Nuestros resultados, además, revelan que el efecto antiproliferativo inducido por el THDF es dependiente de la activación de caspasas, ya que la muerte celular puede ser inhibida por el inhibidor general de caspasas z-VAD-fmk. Además, el THDF inicia la redistribución del citocromo *c* al citosol, que se correlacionará con la disipación del $\Delta\Psi_m$ y con la activación de caspasa -9 y caspasa -3, enfatizando que la vía intrínseca juega un papel muy importante en la muerte celular.

El THDF también estimula el procesamiento proteolítico y consecuentemente la activación de otras caspasas ejecutoras, como la caspasa-7 y la caspasa-6, así como la disminución de los niveles citosólicos de Bax. Sin embargo, los niveles de Bcl-2 permanecen inalterados en la mitocondria y en el citosol.

En conjunto, parece que el mecanismo citotóxico inducido por el THDF es claramente diferente al causado por otras fenilbenzo-γ-pironas estudiadas previamente, como el 3-metil éter de betuletol que induce apoptosis en células HL-60 a través de un mecanismo dependiente de la activación de caspasa-8 [202].

Estudios previos han demostrado que un aumento en la expresión de Bcl-2 y/o Bcl-x_L está asociado con la aparición de quimiorresistencia, particularmente en el caso de las enfermedades hematológicas [203] y que el pronóstico empeora notablemente al verse aumentada la expresión de Bcl-x_L [204]. Para determinar con más detalle el papel de la mitocondria en la citotoxicidad inducida por el THDF, incluimos en el estudio células HL-60 y U937 que sobreexpresan factores anti-apoptóticos. Así, las células HL-60/Bcl-x_L y U937/Bcl-2 demostraron ser parcialmente resistentes respecto a las líneas celulares parentales, confirmando que la mitocondria desempeña una función central en la muerte celular inducida por el THDF. No obstante, la protección parcial que proporcionan estas proteínas podría ser explicada por diferentes mecanismos, como la inactivación de Bcl-2 o la activación de la vía extrínseca de la apoptosis. El hecho de que el THDF también sea capaz de inducir la muerte celular de células de leucemia que sobreexpresan las proteínas Bcl-2 y Bcl-x_L tiene gran interés como potencial agente terapéutico.

Es bien conocido que las MAPKs como JNK y p38 juegan un importante papel provocando la apoptosis como respuesta a diferentes tipos de estrés celular, incluyendo el estrés oxidativo [205]. La p38 es activada por la luz ultravioleta, hiperosmolaridad, golpe de calor o citoquinas proinflamatorias, y actúa en un paso previo a la disfunción de la mitocondria y a la activación de la cascada de caspasas. Además, la p38 es uno de los potenciales reguladores de Bax [132] y un mediador de la respuesta a los puntos de control de G_2-M [133]. En relación con esto, la activación de p38 en las células de mamíferos como respuesta al desbaratamiento del citoesqueleto, induce cambios en los puntos de control de G_2-M [134], y estudios previos han demostrado que flavonoides con un grupo 3-metoxilo podrían inhibir la polimerización de la tubulina [206]. Aunque nuestros estudios indican que la activación de p38 no está implicada en la muerte celular inducida por el THDF, podría estar implicada en el papel fundamental del punto de control de G_2-M mediante una perturbación de los microtúbulos.

Se ha descrito un papel pro-apoptótico de JNK en la apoptosis inducida por diferentes agentes quimioterápicos, como la vinblastina, la doxorubicina y el etopósido [207,208]. Además, la apoptosis inducida por el 2-metoxiestradiol es inhibida por SP600125 en células de mieloma múltiple [209].

En nuestro estudio, demostramos que la muerte celular inducida por el THDF está asociada con la fosforilación de diferentes miembros de las MAPKs siguiendo diferentes cinéticas, y este efecto es dependiente de la línea celular, ya que la activación de ERK1/2 se detectó en células HL-60 pero no en U937.

El THDF induce una fosforilación bifásica de ERK1/2, aunque no conocemos el mecanismo que provoca esta respuesta. Una posible explicación podría ser la implicación de alguna de las fosfatasas de espeficidad dual (MKPs), que están codificadas por genes cuya transcripción es activada por ERK1/2 creándose un bucle de retroalimentación que disminuye la actividad de ERK1/2 [210]. Además, la actividad enzimática de las MKPs es sensible a la oxidación e inactivación reversible debida a la presencia de un residuo de cisteína en la hendidura catalítica [211], mediada por la generación de especies reactivas de oxígeno como H_2O_2 [212]. THDF induce ROS y podría inhibir a las MKPs explicándose así el segundo pico de fosforilación de ERK1/2 inducida por el THDF. Otra posible explicación podría ser que una rápida activación de ERK1/2 aumente la expresión de potenciales dianas que amplifiquen la respuesta al THDF produciéndose así una fosforilación de ERK1/2 secundaria, al igual que ocurre con el factor de crecimiento TGF-β [213].

Aunque la vía de JNK está íntimamente relacionada con la apoptosis [214], ello depende del tipo celular y del estímulo. En las células HL-60 el porcentaje de células hipodiploides en respuesta al THDF es atenuado mediante la utilización de inhibidores específicos de JNK y ERK 1/2, sugiriendo que ambas MAPKs están implicadas en la muerte celular. Estos resultados están de acuerdo con trabajos previos donde se demuestra que la inhibición de MEK-ERK con U0126 o PD98059 suprime la apoptosis inducida por la quercetina en las células A549 [106]. Además, la inhibición de ERK1/2 también atenuó la muerte celular inducida por el trifolín acetato.

Las especies reactivas de oxígeno (ROS) están implicadas como segundos mensajeros en múltiples vías de señalización celular [215]. Aunque el efecto antiproliferativo del THDF está asociado con un aumento de los niveles intracelulares de ROS, esto no parece jugar un papel crucial en el proceso apoptótico. La generación de especies reactivas de oxígeno no es una característica general de los compuestos polifenólicos que contienen un núcleo fenilbenzo-γ-pirona, tal y como sucede con el tetraacetato de 3-metil éter de quercetina que induce apoptosis en células de leucemia humana sin producirse generación de ROS [155], mientras que el trifolín acetato induce ROS, pero no es necesario para la indución de la muerte celular.

El estudio de la influencia del THDF sobre el ciclo celular en células tumorales, indica que la inhibición de la viabilidad celular está causada por una parada del ciclo celular en la fase M y posterior muerte celular por apoptosis. Entre las posibles causas de la acumulación de las células en la fase M del ciclo celular están la inhibición de la formación de los microtúbulos y también una inducción de cambios en la expresión y/o actividad de proteínas clave en la regulación del ciclo celular en esa fase M. Estas proteínas reguladoras son la quinasa dependiente de ciclina-1 (CDK1), el inhibidor de la quinasa dependiente de ciclina (p21) y las isoformas de ciclina tipo B y Cdc25C.

Los agentes antitumorales que afectan a las propiedades dinámicas de los microtúbulos poseen un gran interés y se utilizan habitualmente en quimioterapia. Los microtúbulos juegan un papel crucial en la regulación de la mitosis y su desorganización puede inducir la parada del ciclo celular en la fase M, formación de un huso mitótico anormal y muerte celular por apoptosis [49]. El bioflavonoide mejor estudiado, la quercetina, inhibe la proliferación celular reduciendo los microtúbulos celulares e inhibiendo su polimerización al unirse a la tubulina [56]. De modo similar, el THDF, análogo de la quercetina, inhibe la polimerización de la tubulina e induce cambios en la red de microtúbulos celular siguiendo un patrón similar a la colchicina.

El THDF induce además fosforilación de la ciclina B1, acumulación de p21, y activación de CDK1 mediante la desfosforilación de fosfoT14-Y15.

Estudios previos indican que la desorganización de la estructura de los microtúbulos mediante el uso de agentes que se unen a la tubulina conduce a una inducción de diferentes proteínas, entre ellas p21 [49]. El aumento de la expresión de p21 es un evento importante en el efecto antiproliferativo inducido por el THDF y conforma una vía independiente de p53, ya que las células HL-60 y U937 carecen de p53 funcional. Este hecho, aumenta el interés del THDF como potencial agente quimiopreventivo o quimioterapéutico destinado al tratamiento del cáncer, ya que aproximadamente el 50% de los tumores humanos poseen mutaciones de p53 [216,217].

Además, el aumento en la expresión de la quinasa dependiente de ciclina p21 concuerda con la activación de ERK1/2 inducida por THDF, ya que la transcripción de p21 es dependiente de ERK1/2 [218].

Al tratar las células de leucemia mieloide humana con THDF se inicia una cascada de fosforilación, activando la fosfatasa de especificidad dual Cdc25C [219] y estimulando directamente su actividad fosfatasa. Esta fosforilación es necesaria para activar los complejos CDK1-ciclina B que regulan importantes eventos durante la transición por la fase G_2-M [220] y durante la progresión de la mitosis [221].

Los cambios en la actividad CDK1 y Cdc25C inducidos por THDF coinciden con la aparición de fosfoepítopos reconocidos por un marcador de mitosis, MPM-2, anticuerpo que reconoce polipéptidos fosforilados que sólo podemos encontrar en las células mitóticas [222]. Estos cambios en la fosforilación de las proteínas concuerdan con la parada del ciclo celular en mitosis inducido por algunos agentes anti-tubulina [223].

La vía de la esfingomielinasa, la vía *de novo* y la vía de salvamento, son tres vías que contribuyen de forma individual o de forma coordinada a la síntesis de ceramidas. La ceramida, un esfingolípido que actúa como segundo mensajero se origina por la hidrólisis de la esfingomielina asociada a la membrana, promueve la muerte celular por apoptosis en las células de leucemia mieloide humana [224] y a menudo se genera después de la exposición a agentes quimioterapéuticos mediante la activación de SMasa [141,225,226].

El THDF induce un aumento importante de los niveles de ceramida celular y mitocondrial, activación de A-SMasa pero no de N-SMasa. El inhibidor de la esfingomielinasa, desipramina, es capaz de disminuir la apoptosis inducida por el THDF, sugiriendo que la muerte celular implica la activación de la esfingomielinasa ácida y aumenta la producción de ceramidas.

Estudios recientes señalan a la mitocondria como un lugar de generación y actuación de las ceramidas [145,146,147]. En la mitocondria, la apoptosis inducida por las ceramidas puede ser bloqueada por Bcl-2, indicando que la produción de ceramidas en la apoptosis es un evento anterior al punto de control de Bcl-2 [146]. Aunque THDF es capaz de inducir apoptosis en células U937 que sobreexpresan Bcl-2, lo que indica que aunque se incremente la expresión de Bcl-2, la generación de ceramidas inducida por el THDF podría ser capaz de desencadenar la apoptosis.

CONCLUSIONES

1. Hemos evaluado la actividad antitumoral de 20 flavonoides en cuatro líneas tumorales humanas y seleccionado los más citotóxicos. Las líneas de leucemia mieloide humana fueron, en general, las que mostraron mayor sensibilidad a estos compuestos.

2. Los flavonoides, 3´,5,7-trihidroxi-3,4´-dimetoxiflavona y trifolín acetato, exhiben propiedades citotóxicas selectivas frente a células tumorales, a concentraciones que se podrían alcanzar in vivo, mientras no afectan a los linfocitos normales humanos.

3. El trifolín acetato induce apoptosis a través de un mecanismo que es dependiente de la actividad caspasa. Las caspasas -3 y -9, y fundamentalmente la caspasa -6, desempeñan un papel principal, mientras que las caspasas -8 y -2 no están involucradas.

4. La apoptosis inducida por el trifolín acetato está asociada con la liberación de citocromo *c* a través de un mecanismo que es independiente de la despolarización de la membrana mitocondrial, y puede ser inhibida mediante la expresión de niveles elevados de Bcl-2 y Bcl-x_L.

5. La vía de las proteínas quinasas activadas por mitógenos juega un papel muy importante en la apoptosis inducida por el trifolín acetato, induciendo una rápida fosforilación de ERK1/2 y $p38^{MAPK}$ que desempeñan en este caso una función pro-apoptótica, mientras que la también rápida fosforilación de JNK promueve la supervivencia celular.

6. La fosforilación de las proteínas quinasas activadas por mitógenos es independiente de la generación de especies reactivas de oxígeno, ya que la utilización de diferentes antioxidantes es incapaz de proteger a las células de la apoptosis inducida por el trifolín acetato.

7. La 3´,5,7-trihidroxi-3,4´-dimetoxiflavona induce apoptosis, en las líneas celulares de leucemia mieloide humana HL-60 y U937, a través de un mecanismo que implica activación de las caspasas -3, -6, -7 y -9.

8. La 3´,5,7-trihidroxi-3,4´-dimetoxiflavona induce liberación de citocromo *c* mitocondrial, disminución de los niveles de Bax citosólico, y disipación del potencial de membrana mitocondrial ($\Delta\Psi_m$), mientras que la expresión de niveles elevados de las proteínas mitocondriales Bcl-2 y Bcl-x_L confiere resistencia parcial frente a la apoptosis inducida por este compuesto.

9. La 3´,5,7-trihidroxi-3,4´-dimetoxiflavona activa a las proteínas quinasas activadas por mitógenos siguiendo diferentes cinéticas, por un mecanismo independiente de la generación de especies reactivas de oxígeno, ya que la utilización de diferentes antioxidantes es incapaz de proteger a las células de la apoptosis inducida por este compuesto.

10. La 3´,5,7-trihidroxi-3,4´-dimetoxiflavona induce acumulación de las células HL-60 y U937 en la fase M del ciclo celular y aumento de los niveles de ciclina B1, fosfo-ciclina B1, p21 y MPM-2. Además, promueve la fosforilación de Cdc25C y la desfosforilación y activación de CDK1.

11. La 3´,5,7-trihidroxi-3,4´-dimetoxiflavona desestabiliza la polimerización de los microtúbulos *in vivo*, e inhibe la polimerización de tubulina *in vitro*, uniéndose específicamente al sitio de unión de la colchicina.

12. La 3´,5,7-trihidroxi-3,4´-dimetoxiflavona induce aumento de los niveles de ceramida celular y mitocondrial y activación de la esfingomielinasa ácida en las células HL-60, pero no induce activación de la esfingomielinasa neutra.

13. Puesto que las líneas celulares HL-60 y U937 carecen de p53 funcional, nuestros resultados indican que la apoptosis inducida por el trifolín acetato y la 3´,5,7-trihidroxi-3,4´-dimetoxiflavona se produce de forma independiente a los eventos celulares mediados por p53.

Los datos del presente estudio proporcionan evidencias acerca del mecanismo por el que el trifolín acetato y la 3´,5,7-trihidroxi-3,4´-dimetoxiflavona inhiben el crecimiento de las células tumorales mieloides humanas e inducen apoptosis, sugiriendo que estos flavonoides podrían ser utilizados para el desarrollo de futuros fármacos antitumorales.

SUMMARY

Despite many therapeutic successes, cancer is the third-most frequent cause of death in the World and is set to become the most common in the relatively near future. Cancer comes in many different forms, both anatomically and molecularly, and whereas in several of these drug therapy can markedly increase survival, in many of the common adult epithelial tumors the impact is modest at best. Reasons for the failure of candidate drugs for cancer are now insufficient therapeutic activity (30%) and toxicity (30%). These risks can be reduced by identifying better predictive and molecularly defined animal models of cancer and *in vitro* models of mechanism-based and offtarget toxicity. However, drugs acting on new molecular targets are inherently risky. Risk can be minimized by selecting only the best targets, and by using biomarkers to identify the most appropriate subjects and to demonstrate proof of concept for the intended mechanism of action [7].

Our study focuses primarily on the fight against leukemia. While there are effective treatments for acute lymphocytic leukemia and for chronic myelogenous leukemia, more effective treatments for other forms of acute leukemia are needed. Furthermore, hematologic malignancies are one of the most studied groups of cancer, and analysis of the mechanisms involved in the survival or death of these tumor cells has repeatedly provided new therapeutic targets effective in treating this and other type of cancers [8].

The use of naturally occurring substances for prevention and treatment of cancer represents a realistic option in the fight against the disease. Plant-derived active principles and their semi-synthetic and synthetic analogs have served as a major route to new anticancer compounds [177]. Flavonoids are naturally occurring phenylbenzo-γ-pyrones found in abundance in diets rich in fruits, vegetables and plant derived beverages [22], that display a vast array of biological activities and are among the most promising anticancer agents [178]. So, an understanding of the mechanisms involved in cell growth inhibition is an important step in determining the potential of flavonoids as anticancer agents. Some flavonoids have been shown to induce cell cycle arrest and apoptosis, a kind of cell death which is thought to be an important response to most chemotherapeutic agents in leukemia cells.

Most antitumoral compounds induce apoptosis, a kind of cell death defined by characteristic changes in the nuclear morphology. This form of cell death can occur with or without the activation of caspases [227], a family of conserved cysteine aspartate-specific proteases, generally synthesized as inactive proenzymes or zymogens which are activated by proteolytic cleavage. In general, two major pathways for apoptosis have been described [228]. The extrinsic (or death receptor) pathway involves apoptosis mediated by death receptors, such as

Fas or tumor necrosis factor receptors [229], that is dependent on the initiator caspase-8. Active caspase-8 activates the downstream effector caspases (caspase-3, -6 and -7), inducing a cascade of caspases. In the intrinsic (or mitochondrial) pathway, diverse proapoptotic signals lead to the release of cytochrome *c* from mitochondria to cytoplasm that promotes the assembly of apoptosome and caspase-9 activation, which cleaves and activates downstream caspases. This mitochondrial pathway of apoptosis may be inhibited by antiapoptotic factors of the Bcl-2 family, which interfere with the relocalization of cytochrome *c* resulting in inhibition of the binding of this protein to apoptotic protease activating factor-1 [162,230]. Although caspase-3 is the main effector caspase, it seems to be dispensable for cell death induced by a variety of stimuli, such as tumor necrosis factor or anticancer drugs, since other effector caspases, such as caspase-6 or -7 can compensate for the lack of caspase-3 [231].

Mitogen-activated protein kinases (MAPKs) are a family of serine/threonine protein kinases that are activated by mitogens or stress conditions, and play an essential role in a diverse array of cellular functions, including proliferation, differentiation, stress responses and apoptosis [232]. Mammalian MAPKs comprise three major groups, which are classified on the basis of sequence similarity, differential activation by agonists and substrate specificity. These are the extracellular signal-regulated kinases (ERK) 1/2, the c-Jun N-terminal kinases/stress-activated protein kinases (JNK) and the p38 mitogen-activated protein kinases ($p38^{MAPK}$). Activation of MAPKs requires dual-phosphorylation of threonine and tyrosine residues in the catalytic domain by specific MAPK kinases (MAPKKs). ERK 1/2 is predominantly activated by growth factors or mitogens leading to cell differentiation, growth and survival. In contrast, JNK and p38 are preferentially activated in response to stress conditions and are often associated with apoptosis [233], although under certain conditions both kinases may induce antiapoptotic, proliferative and cell survival signals [214].

Antitumor agents that affect microtubule dynamics are of great medical interest and are widely used in current chemotherapy regimens [234]. Tubulin-containing structures such as microtubules are cytoskeletal components present in all eukaryotic cells and are involved in cell division by forming the mitotic spindle during mitosis. Since microtubules play essential roles in the regulation of the mitotic apparatus, disruption of microtubules can induce cell-cycle arrest in M phase and triggering apoptotic cell death. The progression from one phase of the cell cycle to the next is controlled by the activation of a family of heterodimeric serine/threonine protein kinases, the cyclin-dependent kinases (CDKs). Different CDKs govern different phases of the cell cycle such as G_1 by CDK4 and CDK6, late G_1 to early S by

CDK2, and G_2-M by CDK1. The protein kinase activity of CDKs is controlled by their regulatory subunits known as cyclins, which form a complex with their catalytic subunit CDKs and are activated at a specific phase of the cell cycle. The other important components that control CDK activity are cyclin-dependent kinase inhibitors (CKIs) which include the INK4 family and the Cip and Kip family [45]. These families inhibit the kinase activity of CDK-cyclin complexes which are essential for various cell cycle transitions. The CKI p21 can induce a G_1 arrest and may also take part in a G_2-M arrest through its interactions with cyclin-CDK complexes. The G_2 to M phase progression is governed by the cyclin B1-CDK1 complex. Cyclin B1 is expressed during late S and G_2 phase and immediately binds to and activates CDK1. Moreover, CDK1 is activated by phosphorylation at Thr-161 by the CDK-activating kinase CAK. Cyclin B1-CDK1 complexes are negatively regulated until M phase by phosphorylation of Thr-14 and Tyr-15 in the ATP binding domain. The activation of the cyclin-dependent kinase (CDK) complex CDK1-cyclin B1 depends on the dephosphorylation of Thr-14 and Tyr-15 residues by the dual specificity phosphatase Cdc25C. This dephosphorylation/activation has been demonstrated to be an absolute requirement for the onset of mitosis [235].

The sphingomyelin cycle is a signal transduction pathway that has attracted a lot of attention because it is involved in an apoptotic response. In this pathway, the hydrolysis of sphingomyelin through the action of either acid or neutral sphingomyelinase can generate ceramide, which has been implicated in mediating or regulating many cellular processes, including cell cycle arrest and apoptosis [236].

In previous studies with naturally occurring and semi-synthetic phenylbenzo-γ-pyrones, our group has showed that some derivatives induce cytotoxicity in human myeloid leukemia HL-60 cells. Specifically, that methylation of hydroxyl group at position C3 of quercetin yields a compound with a higher antiproliferative activity in several cancer cell lines, and that betuletol 3-methyl ether, a natural flavonoid, is a potent inhibitor of proliferation which displays high cytotoxic activity on human myeloid leukemia HL-60 cells [202].

Anti-proliferative studies performed with the naturally occurring flavonoid trifolin, isolated from the aerial parts of *Consolida oliveriana*, indicated that this compound did not display cytotoxic activity in all cell lines tested (data not shown). In contrast, trifolin acetate (TA), obtained by acetylation, displayed cytotoxic properties in all assayed cell lines, with an IC_{50} value of about 15 µM on human leukemia (HL-60 and U937) and melanoma (SK-MEL-1) cell lines.

TRIFOLIN ACETATE

Therefore, further studies were carried out with TA. As for all of the agents used or developed for cancer treatment, selectivity toward cancer cells is an important criterion. We therefore compared the effects of TA between human tumor cells and human PBMC. Interestingly, dose-response studies revealed that quiescent PBMC and proliferating PBMC were highly resistant toward TA.

Since many antitumoral compounds are apoptotic inducers we initiated studies to evaluate whether TA stimulates apoptosis in human cell lines. Ours results clearly indicate that TA induces cell death by apoptosis. This form of cell death that can occur with or without activation of caspases, a family of cysteine proteases that plays critical roles in mammalian apoptosis or proteolytic activation of cytokine. Thus, the utilization of these mechanisms is stimulus- and cell type-dependent.

In order to know whether the cell death is associated to caspase activation, a general caspase inhibitor (z-VAD-fmk) was used. The results indicate that TA-induced apoptosis was completely abolished in z-VAD-fmk pretreated cells which supported a caspase dependent cell death mechanism.

There are two well-characterized apoptotic pathways in mammalian cells, referred to as the death receptor (extrinsic) and mitochondrial (intrinsic) pathways. They are widely considered as being responsible for most, if not all, caspase-dependent apoptosis. Therefore, we decided to evaluate which apoptotic pathway was involved in TA-induced cell death by using selective inhibitors against caspase-8 (z-IETD-fmk) and caspase-9 (z-LEHD-fmk), the main initiator (apical) caspases for the extrinsic- and intrinsic- pathway, respectively.

We demonstrated that the death receptor pathway does not play any role since z-IETD-fmk was unable to prevent TA-induced cell death. This result is also concordant with those obtained from immunoblotting analyses which indicated absence of hydrolysis of inactive procaspase-8 (data not shown). In contrast, the percentage of apoptotic cells significantly decreased in the presence of z-LEHD-fmk which indicates that the mitochondrial pathway plays an important role in TA-induced cell death. This result is consistent with an increase in the hydrolysis of the inactive pro-caspase-9 observed in lysates from TA-treated cells. In a previous study in HL-60 cells, z-IETD-fmk, but not by z-LEHD-fmk, has blocked betuletol 3-methyl ether induced-apoptosis, supporting a caspase-8 mediated mechanism [7,237].

Therefore, different apoptotic pathways can be activated in this cell line in response to compounds containing the same basic structure (phenylbenzo-γ-pyrones) such as TA and betuletol 3-methyl ether.

We also evaluated whether caspase-2 is involved in TA-induced cell death since this caspase appears to act upstream of mitochondria to promote cytochrome *c* release in different cell systems [179,180,181]. Our results, by using the specific inhibitor z-VDVAD-fmk, indicate that caspase-2 is not necessary for TA-induced apoptosis and that its involvement in caspase-9 activation can be ruled out. It also supports a preeminent function of caspase-9 as the apical caspase which is activated in response to TA. Thus, caspase-2 is the only pro-caspase constitutively present in the nucleus and appears to be necessary for the onset of apoptosis triggered by agents that promote DNA damage such as etoposide, cis-platin and ultraviolet-light [179,182]. Although more experimental evidences are necessary, the results showed herein also suggest that TA triggers cell death through a mechanism that seems to be independent of DNA damage.

Once activated, most initiator caspases proteolytically activate the downstream effector caspases, which in turn cleave specific cellular substrates resulting in chromatin condensation, membrane blebbing and cell shrinkage. To further characterize the effector caspases that are involved in TA-induced apoptotic process, selective inhibitors against caspase-3 (z-DEVD-fmk) and caspase-6 (z-VEID-fmk) were used. Therefore, we demonstrated that both caspases are important to promote apoptosis triggered by TA. Interestingly we found that z-VEID-fmk was significantly more effective than z-DEVD-fmk to prevent apoptosis upon treatment with TA. This result suggests that caspase-6 might play an important upstream role, as previously described for resveratrol-induced apoptosis in human T-cell leukemia cell lines [183] and in contrast with a large number of studies which suggest that caspase-6 is an effector caspase that is activated downstream of caspase-3 during apoptosis [77,184]. However, other explanations can not be ruled out and could be related to differences in the accessibilities of inhibitors to cellular caspases [185] and/or implication of non identified apical protease with caspase-like activity, as recently suggested for heat shock induced-apoptosis in Jurkat cells [186].

In this context caspase-1, in addition to the well-characterized function in the processing of proinflammatory cytokines IL-1b and IL-18 [187], appears to be involved in cell death as demonstrated in fibroblasts [188], neuronal cells [189] and is also required for the induction of apoptosis in macrophages by certain bacteria [190]. Moreover, previous work has shown

that caspase-1 activates caspase-6 in serum-deprived human neurons and results in neuronal cell death [191]. Paradoxically, we find that the percentage of hypodiploid cells significantly increased in presence of the caspase-1 inhibitor z-YVAD-fmk, which suggests a survival role of caspase-1 in TA-stimulated cells. Interestingly, caspase-1 has been reported to promote cell survival through a mechanism that involves activation of sterol regulatory element binding proteins (SREBPs) and lipid biogenesis. Thus, selective inhibition of caspase-1 by z-YVAD-fmk or si-RNA mediated knockdown resulted in higher levels of cell death in response to pore-forming toxins [192]. Whether caspase-1 is activated in TA-stimulated cells and displays a mechanism that involves lipid biogenesis remains to be elucidated.

As expected, given the roles of caspases-3 and -6 in TA-induced cell death, there was also an increase in the proteolytic processing of both pro-enzymes to form activated enzymes. Thus, apoptosis was accompanied by cleavage of the nuclear protein PARP, a recognized caspase-3 substrate which is involved in DNA repair and it is important for maintaining cell viability [193,194,195]. Therefore, hydrolysis of PARP guarantees cellular disassembly and supports a role for this protein as a key regulator of apoptosis in TA-treated cells [195].

Mitochondria play a key role in cell death when their membranes become permeabilized [196]. Outer mitochondrial membrane permeabilization is regulated by different members of the Bcl-2 family which constitutes a critical cellular checkpoint in the intrinsic pathway of apoptosis [197]. Here we have shown that TA initiated redistribution of cytochrome *c* into the cytosol which was already detected at 6 h. However, this early event is not associated with a loss in $\Delta\Psi m$ which remains unchanged for at least 24 h. In this regard, previous studies have shown that changes in $\Delta\Psi m$ are not required for the complete release of cytochrome *c* upon the mitochondrial outer membrane permeabilization [198].

To further investigate the role of mitochondria upon treatment with TA, HL-60 and U937 cells over-expressing antiapoptotic factors were included in the study. HL-60/Bcl-x_L and U937/Bcl-2 were completely resistant compared with the parental cell lines, which suggest a central role of mitochondria in TA-induced cell death.

Taken together, our results suggest that TA induces apoptosis through a mechanism that involves the mitochondrial pathway in which caspase-6 seems to operate upstream to caspase-9.

In addition to apoptosis, MAP kinases regulate diverse cellular programs including proliferation and differentiation. Although the JNK has generally been associated with pro-apoptotic actions [112] and growth inhibitory signals [114], here we show that TA induces JNK activation and its inhibition by SP600125 enhances apoptotic cell death. Previous studies have shown that the pro-apoptotic effect of the histone deacetylase inhibitor D1 increased in the presence of SP600125 in human acute myeloid leukemia cell lines [200]. Additional evidence that JNK can be a prosurvival signal has been also demonstrated in hepatocellular carcinoma cells [115] and in gastric and a colorectal cancer cell lines [116].

Cell death is promoted by p38 signaling in some cell lines, and also enhances survival, cell growth and differentiation. Therefore, the role of p38 in apoptosis is dependent on cell type and stimulus [121]. The p38 appears to be involved in the activation of TA-induced apoptosis, since the specific inhibitor SB203580 attenuated cell death. Activation of p38 is also a prerequisite for apoptosis induced by cadmium, trophic factor withdrawal and ischemia [122,123,124,125]. However, the activation of p38 is not involved in apoptosis induced by ultraviolet radiation in U937 cells [126] or by S-nitrosoglutathione in RAW 264.7 macrophages [127] and/or in Fas- and ultraviolet-treated Jurkat T cells [128].

Our data also indicate that the inhibitor U0126 attenuated the apoptotic effects of TA, which suggested that ERK1/2 is involved in cell death signals. Our results are in agreement with previous work that has shown that inhibition of MEK-ERK activation with U0126 or PD98059 abolishes quercetin-induced apoptosis in A549 cells [106]. In addition, the suppression of MEK-ERK signal pathway by the MEK inhibitor PD98059 resulted in an increase in cisplatin-resistance in human cervical carcinoma SiHa cells and hepatoblastoma HepG2 cells [107]. Moreover, acrolein, a highly reactive α,β-unsaturated aldehyde generated by lipid peroxidation, induced phosphorylation of ERK and the inhibition of its activity by PD98059 and U0126 blocked acrolein-induced apoptosis [201]. Quercetin 3-methyl ether acetate, which is chemically similar to TA, enhances the activation of the MEK/ERK pathway [155]. In contrast, ERK inhibitors potentiate the apoptotic effects of quercetin 3-methyl ether. Therefore, different pathways can be activated in the same cell line by these similar compounds.

Previous reports have demonstrated that production of ROS in leukaemic cells may lead to cell death via MAPKs activation [167,169,238]. Although intracellular ROS generation was observed within 1 h after exposure to TA, different anti-oxidants were unable to abrogate cell

death. These results indicate that ROS generation does not seem to be involved in TA triggered apoptosis.

3´,5,7-TRIHYDROXY-3,4´-DIMETHOXIFLAVONE

In addition, we have specifically selected an analog of quercetin 3-methyl ether, THDF, which contains an additional methoxyl group on position 4´ of the phenylbenzo-γ-pyrone core and evaluated its potential cytotoxic properties using nine tumor cell lines.

Interestingly, we found that THDF displays cytotoxic properties in a cell-type specific manner. Human leukemia cells (HL-60, U937, Molt-3 and Jurkat) were highly sensitive to THDF cytotoxicity while SK-MEL-1 and A549 cells were more resistant than hematopoietic cells. Moreover, dose-response studies revealed that PBMC were more resistant to THDF than PBMC treated with phytohemaglutinine.

Cell cycle analysis showed that inhibition of cell viability by THDF was caused by a significant cell cycle arrest at the G_2-M phase, accompanied by an increase in sub-G_1 fraction and phosphatidylserine externalization, indicating apoptotic cell death. Similar results were recently reported by the semi-synthetic quercetin 3-methyl ether tetracetate in human leukemia cells [155], although the potency of THDF was the highest, both in arresting the cells at the G_2-M phase and as an apoptotic inducer.

Our results also indicate that THDF´s antiproliferative effect is dependent on caspase, since cell death was inhibited by the general caspase inhibitor z-VAD-fmk. The intrinsic apoptotic pathway (mitochondrial pathway) involves the release of cytochrome *c* and the assembly of apoptosome. THDF initiated redistribution of cytochrome *c* into the cytosol which was correlated with the dissipation of $\Delta\Psi m$ and caspase-3 activation. We also observed a concentration- and time-dependent activation of caspases-9 and -3, in accordance with the cytochrome *c* release experiments, emphasizing that the intrinsic pathway plays an important role in the cell death.

Moreover, THDF induced PARP cleavage, a hallmark of apoptosis that indicates activation of caspase. Although PARP is also degraded in other forms of cell death like necrosis [239], this did not seem to be the case with THDF in accordance with the fluorescence microscopy and the flow cytometric analyses of Annexin V-FITC and propidium iodide-stained cells experiments. The results clearly demonstrate that THDF also stimulates the proteolytic processing of other executioner caspases, namely caspase-7 and caspase-6 to form activated

enzymes. There was also a clear concentration- and time-dependent decrease of the Bax levels in the cytosol in both cell lines. However, the levels of Bcl-2 in mitochondria and in cytosol remain unchanged.

Therefore, it appears that the mechanism of cytotoxicity displayed by THDF is clearly different to that caused by previously described phenylbenzo-γ-pyrones, such as betuletol 3-methyl ether which induces apoptosis in HL-60 cells by a caspase-8 dependent mechanism [153]. In contrast, quercetin 3-methyl ether tetracetate, a flavonoid obtained by acetylation of the natural product quercetin 3-methyl ether, triggers apoptosis which is prevented by the general caspase inhibitor z-VAD-fmk, but not by the specific caspase-8 inhibitor [155].

Previous studies have shown that increased expression of Bcl-2 and/or Bcl-x_L is associated with chemoresistance particularly in the case of hematologic malignancies [203] and there is also poor prognostic outcome with increased Bcl-x_L expression [204]. To further investigate the role of mitochondria in THDF-induced cytotoxicity, HL-60 and U937 cells overexpressing antiapoptotic factors were included in this study. Our results indicate that HL-60/Bcl-x_L and U937/Bcl-2 were partially resistant compared with the parental cell lines, which suggest that mitochondria play an important role in THDF-induced cell death. However, the partial protection by these proteins could be explained by various mechanisms, including inactivation of Bcl-2 or the activation of the extrinsic apoptotic pathway. The fact that THDF induces cell death also in leukemic cells over-expressing Bcl-2 and Bcl-x_L could have important clinical implications for the use of this compound as potential therapeutic agent.

Recent studies suggest that MAPKs such as JNK and p38 play a key role in triggering apoptosis in response to various cellular stressors including oxidative stress [205].

The p38 is activated by a variety of cellular stresses including ultraviolet light, hyperosmolarity, heat shock and proinflammatory cytokines, and acts at early step prior to dysfunction of mitochondria and caspase activation. Moreover, p38 is a potential upstream regulator of Bax [132] and a mediator of the G_2-M checkpoint response [133]. In this regard, activation of p38 in mammalian cells in response to the disruption of the microtubule cytoskeleton initiates G_2-M checkpoint [134] and also previous studies have shown that flavonoids containing a 3-methoxyl group may inhibit tubulin polymerization [206]. Although our studies indicate that the activation of p38 is not involved in THDF-induced cell death, this

could be involved in the initiation of the G_2-M checkpoint through a perturbation of the microtubules.

A proapoptotic role of JNK has been described in apoptosis induced by different chemotherapeutic agents, such as vinblastine, doxorubicin and etoposide [207,208]. Furthermore, 2-methoxyestradiol-induced apoptosis was inhibited by SP600125 in multiple myeloma cells [209].

In our study, we show that THDF-induced cell death was also associated with the phosphorylation of the members of MAPKs following different kinetics and this effect was cell specific, since ERK1/2 activation was observed in HL-60 but not in U937 cells. Moreover, THDF induced a biphasic phosphorylation of ERK1/2. Although the mechanisms by which THDF caused this response is unkown, one possible explanation could be the involvement of dual specificity threonine/tyrosine MAPK phosphatases (MKPs) because some of these MKPs are encoded by genes that are transcriptionally activated by ERK1/2 and this can provide a feedback loop to downregulate ERK1/2 activity [210]. In addition, the enzymatic activity of MKPs is sensitive to reversible oxidation and inactivation due to the presence of the catalytic cysteine residue in the catalytic cleft [211]. The reversible oxidation of this cysteine residue that inactivates the phosphatase may be mediated by the generation of reactive oxygen species such as H_2O_2 [212]. THDF induces ROS and might inhibit the MKPs and therefore explain the second peak of ERK activation triggered by THDF. Another possible explanation could be that the early activation of ERK1/2 may enhance the expression of potential targets which amplify the THDF response and induce a secondary phosphorylation of ERK1/2, as previously reported for transforming growth factor-β-1 [213].

Although the JNK pathway has been shown to be closely linked to apoptosis [214], its exact role seems to depend on the cell type and stimulus. Interestingly, in HL-60 the percentage of hypodiploid cells in response to THDF was attenuated by inhibition of JNK and by inhibition of ERK1/2, which suggests that both MAPKs are required for cell death. Our results also indicate that the mitogen-activated extracellular kinases (MEK) 1/2 inhibitors PD98059 and U0126 attenuated the apoptotic effects of THDF, which suggest that ERK1/2 is involved in cell death signals. These findings are in agreement with previous work that has shown that inhibition of MEK-ERK activation with U0126 or PD98059 abolishes quercetin induced apoptosis in A549 cells [106]. In addition, as we have seen previously, the inhibition of ERK1/2 attenuates cell death induced by trifolin acetate.

Reactive oxygen species (ROS) have been implicated as second messengers in multiple signaling pathways [215]. Although the antiproliferative effect of THDF is associated with an increase in the intracellular level of ROS, this did not seem to play a pivotal role in the apoptotic process. The generation of reactive oxygen species is not a general feature of polyphenolic compounds containing a phenylbenzo-γ-pyrone core. In this regard, we have previously demonstrated that quercetin 3-methyl ether tetracetate induces apoptosis in human leukemia cells without ROS formation [155], while that trifolin acetate induces ROS, but they are not necessary to trigger cell death.

Antitumor agents that affect microtubule dynamics are of great interest and are now commonly used in current chemotherapy. Microtubules play crucial roles in the regulation of mitosis, and the disruption of microtubules can induce cell cycle arrest in M phase, formation of abnormal mitotic spindles and apoptotic cell death [49]. The best-studied bioflavonoid quercetin has been shown to inhibit cancer cell proliferation by depleting cellular microtubules and inhibiting microtubule polymerization through tubulin binding [56]. Since THDF is an analogue of quercetin, the cell cycle phase arrest might be explained by the inhibition of microtubule formation. We demonstrated herein that THDF inhibits tubulin polymerization and promotes changes on cellular microtubule network following a similar pattern to the microtubule-targeting drug colchicine.

In this study we found that THDF blocks the cell cycle in the M phase which was associated with induction and phosphorylation of cyclin B1, accumulation of p21, and also activation of Cdk1 via dephosphorylation of phosphoT14-Y15.

The marked up-regulation of the Cdk inhibitor, p21, might be the consequence of tubulin disorganization. In this regard, previous studies indicate that the disruption of microtubule structure by tubulin-binding agents results in induction of different proteins including p21 [49]. Up-regulation of p21 appears to be an important event in THDF-induced antiproliferative effect and involves a p53-independent pathway, since HL-60 and U937 cells lack functional p53. These results might have important implications for developing THDF as a chemopreventive or as a chemotherapeutic agent in treatment of cancer, because approximately 50% of human cancers harbor p53 mutations [216,217].

Up-regulation of the cyclin-dependent kinase inhibitor p21 is in accordance with our previous studies of ERK1/2 activation by THDF, since p21 transcription is ERK1/2 dependent [218].

THDF treatment initiates a phosphorylation cascade resulting in the phosphorylation of the dual-specificity phosphatase Cdc25C [219]. This phosphorylation directly stimulates its phosphatase activity and this is necessary to activate Cdk1-cyclin B complexes which regulate several events during both the G_2-M transition [220] and progression through mitosis [221].

There was also a clear concentration- and time-dependent decrease of the P-Cdk1 levels in both cell lines. The changes in Cdk1 and Cdc25C induced by THDF coincide with the appearance of phosphoepitopes recognized by a marker of mitosis, MPM-2, which is an antibody that recognizes phosphorylated polypeptides found only in mitotic cells [222]. These changes in protein phosphorylation are consistent with cell cycle arrest in mitosis induced by anti-tubulin agents [223].

Three pathways, the SMase pathway, the *de novo* pathway and the salvage pathway, individually or coordinately contribute to ceramide synthesis. Ceramide, a sphingolipid second messenger generated by the hydrolysis of membrane-associated sphingomyelin, promotes apoptotic cell death in the human myeloid leukemia cells [224] and is often generated after exposure to chemotherapeutic agents [141] through the activation of SMase [225,226].

In our study we show that THDF led to a very pronounced increase in both, cellular and mitochondrial ceramide levels, induces activation of ASMase, but not NSMase and the ability of the sphingomyelinase inhibitor, desipramine, to diminish THDF-mediated apoptosis confirms that the cell death involves activation of acidic sphingomyelinase and enhanced ceramide production.

Recent studies point to the mitochondria as a site of ceramide generation and action [145,146,147]. In the mitochondria, ceramide-induced apoptosis could be blocked by Bcl-2, indicating that ceramide production is upstream of the Bcl-2 control point [146]. As we have seen previously, THDF effectively induces apoptosis in U937 cells over-expressing Bcl-2, suggesting that ceramide generation induced by THDF could trigger apoptosis in Bcl-2 over-expressing cells.

CONCLUSIONS

1. We have evaluated the antitumoral activity of 20 flavonoids in four human tumor cell lines and selected the most cytotoxic. Myeloid leukemia cell lines were, in general, the most sensitive to these compounds.

2. 3´,5,7-Trihydroxy-3,4´-dimethoxyflavone and trifolin acetate showed selectively citotoxic properties against tumoral cells, since human peripheral blood mononuclear cells were resistant to used concentrations with both compounds.

3. Trifolin acetate induces apoptosis through a caspase-dependent mechanism. The caspase-3, -9 and primarily caspase-6 play an important role in that mechanism, while caspase-8 and -2 are not involved.

4. Apoptosis-induced by trifolin acetate is associated with cytochrome *c* release, which was not accompanied by dissipation of the mitochondrial membrane potential ($\Delta\Psi_m$), and could be inhibited by overexpression of Bcl-2 and Bcl-x_L.

5. Mitogen-activated protein kinases play an important role in trifolin acetate-triggered apoptosis, inducing a fast phosphorylation of ERK1/2 and p38 associated with pro-apoptotic actions, while the fast phosphorylation of JNK enhances cell survival.

6. Phosphorylation of mitogen-activated protein kinases is independent of reactive oxygen species generation, since different anti-oxidants were unable to abrogate trifolin acetate-induced cell death.

7. 3´,5,7-Trihydroxy-3,4´-dimethoxyflavone induces apoptosis, in the human leukemia cell lines HL-60 and U937, through a mechanism dependent on caspases -3, -6, -7 and -9.

8. 3´,5,7-Trihydroxy-3,4´-dimethoxyflavone induces release of mitochondrial cytochrome *c*, decrease of Bax levels in the cytosol, and dissipation of the mitochondrial membrane potential ($\Delta\Psi_m$), while overexpression of the protective mitochondrial proteins Bcl-2 and Bcl-x_L conferred partial resistance to apoptosis.

9. 3´,5,7-Trihydroxy-3,4´-dimethoxyflavone activated mitogen-activated protein kinases following different kinetics, through a mechanism independent of reactive oxygen species generation, since different anti-oxidants were unable to abrogate apoptosis.

10. 3´,5,7-Trihydroxy-3,4´-dimethoxyflavone induced cell cycle arrest in M phase in HL-60 and U937 cells, increasing the levels of cyclin B1, phospho-cyclin B1, p21 and MPM-2. Moreover, THDF induced Cdc25C phosphorylation with dephosphorylation and activation of Cdk1.

11. 3´,5,7-Trihydroxy-3,4´-dimethoxyflavone induces disruption of microtubules *in vivo,* and inhibits *in vitro* tubulin polymerization by binding specifically at the colchicine binding site.

12. 3´,5,7-Trihydroxy-3,4´-dimethoxyflavone led to a very pronounced increase in both cellular and mitocondrial ceramide levels, and induced acidic sphingomyelinase, but not neutral sphingomyelinase, activation in HL-60 cells.

13. Since HL-60 and U937 cell lines lack functional p53, our results suggest that trifolin acetate and 3´,5,7-trihydroxy-3,4´-dimethoxyflavone induced apoptosis involve a p53-independent pathway.

These studies provide new insights into the signaling pathways by which trifolin acetate and 3´,5,7-trihydroxy-3,4´-dimethoxyflavone inhibit human leukemia cells growth, induce apoptosis and suggest that these compounds have an important potential in the development of preventive chemotherapy and probably as new therapeutic agents against cancer.

BIBLIOGRAFÍA

1. Albreht T, McKee M, Alexe DM, Coleman MP, Martin-Moreno JM (2008) Making progress against cancer in Europe in 2008. Eur J Cancer 44: 1451-1456.
2. Jemal A, Siegel R, Ward E, Hao Y, Xu J, et al. (2009) Cancer statistics, 2009. CA Cancer J Clin 59: 225-249.
3. Salud OMS (2009) Cancer. Nota descriptiva Nº297.
4. Langholz B, Ebi KL, Thomas DC, Peters JM, London SJ (2002) Traffic density and the risk of childhood leukemia in a Los Angeles case-control study. Ann Epidemiol 12: 482-487.
5. Benson JD, Chen YN, Cornell-Kennon SA, Dorsch M, Kim S, et al. (2006) Validating cancer drug targets. Nature 441: 451-456.
6. Sawyers CL (2003) Opportunities and challenges in the development of kinase inhibitor therapy for cancer. Genes Dev 17: 2998-3010.
7. Collins I, Workman P (2006) New approaches to molecular cancer therapeutics. Nat Chem Biol 2: 689-700.
8. Reed JC, Pellecchia M (2005) Apoptosis-based therapies for hematologic malignancies. Blood 106: 408-418.
9. Melo JV, Barnes DJ (2007) Chronic myeloid leukaemia as a model of disease evolution in human cancer. Nat Rev Cancer 7: 441-453.
10. Kantarjian H, O'Brien S, Cortes J, Wierda W, Faderl S, et al. (2008) Therapeutic advances in leukemia and myelodysplastic syndrome over the past 40 years. Cancer 113: 1933-1952.
11. Balunas MJ, Kinghorn AD (2005) Drug discovery from medicinal plants. Life Sci 78: 431-441.
12. Kale A, Gawande S, Kotwal S (2008) Cancer phytotherapeutics: role for flavonoids at the cellular level. Phytother Res 22: 567-577.
13. Kramer R, Cohen D (2004) Functional genomics to new drug targets. Nat Rev Drug Discov 3: 965-972.
14. Liu RH (2003) Health benefits of fruit and vegetables are from additive and synergistic combinations of phytochemicals. Am J Clin Nutr 78: 517S-520S.
15. Ross JA, Kasum CM (2002) Dietary flavonoids: bioavailability, metabolic effects, and safety. Annu Rev Nutr 22: 19-34.
16. Williams CA, Grayer RJ (2004) Anthocyanins and other flavonoids. Nat Prod Rep 21: 539-573.
17. Hollman PC, Hertog MG, Katan MB (1996) Role of dietary flavonoids in protection against cancer and coronary heart disease. Biochem Soc Trans 24: 785-789.
18. Rimm EB, Katan MB, Ascherio A, Stampfer MJ, Willett WC (1996) Relation between intake of flavonoids and risk for coronary heart disease in male health professionals. Ann Intern Med 125: 384-389.
19. Hollman PC, Katan MB (1998) Bioavailability and health effects of dietary flavonols in man. Arch Toxicol Suppl 20: 237-248.
20. Knekt P, Jarvinen R, Reunanen A, Maatela J (1996) Flavonoid intake and coronary mortality in Finland: a cohort study. BMJ 312: 478-481.
21. Rowland M (1986) Scheele lecture. Pharmacokinetics: concepts, insights and applications. Acta Pharm Suec 23: 173-190.
22. Havsteen BH (2002) The biochemistry and medical significance of the flavonoids. Pharmacol Ther 96: 67-202.
23. Yao LH, Jiang YM, Shi J, Tomas-Barberan FA, Datta N, et al. (2004) Flavonoids in food and their health benefits. Plant Foods Hum Nutr 59: 113-122.
24. Hooper L, Kroon PA, Rimm EB, Cohn JS, Harvey I, et al. (2008) Flavonoids, flavonoid-rich foods, and cardiovascular risk: a meta-analysis of randomized controlled trials. Am J Clin Nutr 88: 38-50.

25. Geleijnse JM, Hollman P (2008) Flavonoids and cardiovascular health: which compounds, what mechanisms? Am J Clin Nutr 88: 12-13.
26. WHO (2008) The top ten causes of death. WHO Media centre: Fact sheet 310.
27. Passamonti S, Terdoslavich M, Franca R, Vanzo A, Tramer F, et al. (2009) Bioavailability of flavonoids: a review of their membrane transport and the function of bilitranslocase in animal and plant organisms. Curr Drug Metab 10: 369-394.
28. Le Marchand L, Murphy SP, Hankin JH, Wilkens LR, Kolonel LN (2000) Intake of flavonoids and lung cancer. J Natl Cancer Inst 92: 154-160.
29. Yang CS, Landau JM, Huang MT, Newmark HL (2001) Inhibition of carcinogenesis by dietary polyphenolic compounds. Annu Rev Nutr 21: 381-406.
30. Knekt P, Kumpulainen J, Jarvinen R, Rissanen H, Heliovaara M, et al. (2002) Flavonoid intake and risk of chronic diseases. Am J Clin Nutr 76: 560-568.
31. Yang CS, Lambert JD, Ju J, Lu G, Sang S (2007) Tea and cancer prevention: molecular mechanisms and human relevance. Toxicol Appl Pharmacol 224: 265-273.
32. Ren W, Qiao Z, Wang H, Zhu L, Zhang L (2003) Flavonoids: promising anticancer agents. Med Res Rev 23: 519-534.
33. Ramos S (2007) Effects of dietary flavonoids on apoptotic pathways related to cancer chemoprevention. J Nutr Biochem 18: 427-442.
34. Reed JC (2006) Drug insight: cancer therapy strategies based on restoration of endogenous cell death mechanisms. Nat Clin Pract Oncol 3: 388-398.
35. Ashkenazi A (2008) Directing cancer cells to self-destruct with pro-apoptotic receptor agonists. Nat Rev Drug Discov 7: 1001-1012.
36. Maddika S, Ande SR, Panigrahi S, Paranjothy T, Weglarczyk K, et al. (2007) Cell survival, cell death and cell cycle pathways are interconnected: implications for cancer therapy. Drug Resist Updat 10: 13-29.
37. Collins I, Garrett MD (2005) Targeting the cell division cycle in cancer: CDK and cell cycle checkpoint kinase inhibitors. Curr Opin Pharmacol 5: 366-373.
38. Vermeulen K, Berneman ZN, Van Bockstaele DR (2003) Cell cycle and apoptosis. Cell Prolif 36: 165-175.
39. Carnero A, Hannon GJ (1998) The INK4 family of CDK inhibitors. Curr Top Microbiol Immunol 227: 43-55.
40. Pavletich NP (1999) Mechanisms of cyclin-dependent kinase regulation: structures of Cdks, their cyclin activators, and Cip and INK4 inhibitors. J Mol Biol 287: 821-828.
41. Harper JW, Elledge SJ, Keyomarsi K, Dynlacht B, Tsai LH, et al. (1995) Inhibition of cyclin-dependent kinases by p21. Mol Biol Cell 6: 387-400.
42. Roberts JM, Koff A, Polyak K, Firpo E, Collins S, et al. (1994) Cyclins, Cdks, and cyclin kinase inhibitors. Cold Spring Harb Symp Quant Biol 59: 31-38.
43. DiPaola R (2002) To arrest or not to G(2)-M Cell-cycle arrest : commentary re: A. K. Tyagi et al., Silibinin strongly synergizes human prostate carcinoma DU145 cells to doxorubicin-induced growth inhibition, G(2)-M arrest, and apoptosis. Clin. cancer res., 8: 3512-3519, 2002. Clin Cancer Res 8: 3311-3314.
44. Iida H, Towatari M, Tanimoto M, Morishita Y, Kodera Y, et al. (1997) Overexpression of cyclin E in acute myelogenous leukemia. Blood 90: 3707-3713.
45. Malumbres M, Barbacid M (2001) To cycle or not to cycle: a critical decision in cancer. Nat Rev Cancer 1: 222-231.
46. Zi X, Feyes DK, Agarwal R (1998) Anticarcinogenic effect of a flavonoid antioxidant, silymarin, in human breast cancer cells MDA-MB 468: induction of G1 arrest through an increase in Cip1/p21 concomitant with a decrease in kinase activity of cyclin-dependent kinases and associated cyclins. Clin Cancer Res 4: 1055-1064.
47. Choi JA, Kim JY, Lee JY, Kang CM, Kwon HJ, et al. (2001) Induction of cell cycle arrest and apoptosis in human breast cancer cells by quercetin. Int J Oncol 19: 837-844.

48. Mollinedo F, Gajate C (2003) Microtubules, microtubule-interfering agents and apoptosis. Apoptosis 8: 413-450.
49. Wang LG, Liu XM, Kreis W, Budman DR (1999) The effect of antimicrotubule agents on signal transduction pathways of apoptosis: a review. Cancer Chemother Pharmacol 44: 355-361.
50. Ling YH, Tornos C, Perez-Soler R (1998) Phosphorylation of Bcl-2 is a marker of M phase events and not a determinant of apoptosis. J Biol Chem 273: 18984-18991.
51. Subbaramaiah K, Hart JC, Norton L, Dannenberg AJ (2000) Microtubule-interfering agents stimulate the transcription of cyclooxygenase-2. Evidence for involvement of ERK1/2 AND p38 mitogen-activated protein kinase pathways. J Biol Chem 275: 14838-14845.
52. Blagosklonny MV, Schulte TW, Nguyen P, Mimnaugh EG, Trepel J, et al. (1995) Taxol induction of p21WAF1 and p53 requires c-raf-1. Cancer Res 55: 4623-4626.
53. Chadebech P, Truchet I, Brichese L, Valette A (2000) Up-regulation of cdc2 protein during paclitaxel-induced apoptosis. Int J Cancer 87: 779-786.
54. Schmidt M, Bastians H (2007) Mitotic drug targets and the development of novel anti-mitotic anticancer drugs. Drug Resist Updat 10: 162-181.
55. Hanahan D, Weinberg RA (2000) The hallmarks of cancer. Cell 100: 57-70.
56. Gupta K, Panda D (2002) Perturbation of microtubule polymerization by quercetin through tubulin binding: a novel mechanism of its antiproliferative activity. Biochemistry 41: 13029-13038.
57. Elmore S (2007) Apoptosis: a review of programmed cell death. Toxicol Pathol 35: 495-516.
58. Kerr JF, Wyllie AH, Currie AR (1972) Apoptosis: a basic biological phenomenon with wide-ranging implications in tissue kinetics. Br J Cancer 26: 239-257.
59. Jacobson MD, Weil M, Raff MC (1997) Programmed cell death in animal development. Cell 88: 347-354.
60. Norbury CJ, Hickson ID (2001) Cellular responses to DNA damage. Annu Rev Pharmacol Toxicol 41: 367-401.
61. Gulbins E, Jekle A, Ferlinz K, Grassme H, Lang F (2000) Physiology of apoptosis. Am J Physiol Renal Physiol 279: F605-615.
62. Casella CR, Finkel TH (1997) Mechanisms of lymphocyte killing by HIV. Curr Opin Hematol 4: 24-31.
63. Rohn TT, Head E, Nesse WH, Cotman CW, Cribbs DH (2001) Activation of caspase-8 in the Alzheimer's disease brain. Neurobiol Dis 8: 1006-1016.
64. Gil JM, Rego AC (2008) Mechanisms of neurodegeneration in Huntington's disease. Eur J Neurosci 27: 2803-2820.
65. Hayakawa K, Takemura G, Koda M, Kawase Y, Maruyama R, et al. (2002) Sensitivity to apoptosis signal, clearance rate, and ultrastructure of fas ligand-induced apoptosis in in vivo adult cardiac cells. Circulation 105: 3039-3045.
66. Becherucci F, Mazzinghi B, Ronconi E, Peired A, Lazzeri E, et al. (2009) The role of endothelial progenitor cells in acute kidney injury. Blood Purif 27: 261-270.
67. Prasad KV, Prabhakar BS (2003) Apoptosis and autoimmune disorders. Autoimmunity 36: 323-330.
68. Gerl R, Vaux DL (2005) Apoptosis in the development and treatment of cancer. Carcinogenesis 26: 263-270.
69. Hengartner MO (2000) The biochemistry of apoptosis. Nature 407: 770-776.
70. Chicheportiche Y, Bourdon PR, Xu H, Hsu YM, Scott H, et al. (1997) TWEAK, a new secreted ligand in the tumor necrosis factor family that weakly induces apoptosis. J Biol Chem 272: 32401-32410.

71. Ashkenazi A, Dixit VM (1998) Death receptors: signaling and modulation. Science 281: 1305-1308.
72. Suliman A, Lam A, Datta R, Srivastava RK (2001) Intracellular mechanisms of TRAIL: apoptosis through mitochondrial-dependent and -independent pathways. Oncogene 20: 2122-2133.
73. Zapata JM, Pawlowski K, Haas E, Ware CF, Godzik A, et al. (2001) A diverse family of proteins containing tumor necrosis factor receptor-associated factor domains. J Biol Chem 276: 24242-24252.
74. Rubio-Moscardo F, Blesa D, Mestre C, Siebert R, Balasas T, et al. (2005) Characterization of 8p21.3 chromosomal deletions in B-cell lymphoma: TRAIL-R1 and TRAIL-R2 as candidate dosage-dependent tumor suppressor genes. Blood 106: 3214-3222.
75. Scaffidi C, Fulda S, Srinivasan A, Friesen C, Li F, et al. (1998) Two CD95 (APO-1/Fas) signaling pathways. EMBO J 17: 1675-1687.
76. Ozoren N, El-Deiry WS (2002) Defining characteristics of Types I and II apoptotic cells in response to TRAIL. Neoplasia 4: 551-557.
77. Slee EA, Harte MT, Kluck RM, Wolf BB, Casiano CA, et al. (1999) Ordering the cytochrome c-initiated caspase cascade: hierarchical activation of caspases-2, -3, -6, -7, -8, and -10 in a caspase-9-dependent manner. J Cell Biol 144: 281-292.
78. Micheau O, Tschopp J (2003) Induction of TNF receptor I-mediated apoptosis via two sequential signaling complexes. Cell 114: 181-190.
79. Obeid LM, Linardic CM, Karolak LA, Hannun YA (1993) Programmed cell death induced by ceramide. Science 259: 1769-1771.
80. Letai A (2005) Pharmacological manipulation of Bcl-2 family members to control cell death. J Clin Invest 115: 2648-2655.
81. Henry-Mowatt J, Dive C, Martinou JC, James D (2004) Role of mitochondrial membrane permeabilization in apoptosis and cancer. Oncogene 23: 2850-2860.
82. Roberts DL, Merrison W, MacFarlane M, Cohen GM (2001) The inhibitor of apoptosis protein-binding domain of Smac is not essential for its proapoptotic activity. J Cell Biol 153: 221-228.
83. Li LY, Luo X, Wang X (2001) Endonuclease G is an apoptotic DNase when released from mitochondria. Nature 412: 95-99.
84. Gray CW, Ward RV, Karran E, Turconi S, Rowles A, et al. (2000) Characterization of human HtrA2, a novel serine protease involved in the mammalian cellular stress response. Eur J Biochem 267: 5699-5710.
85. Kroemer G, Reed JC (2000) Mitochondrial control of cell death. Nat Med 6: 513-519.
86. Kroemer G, Zamzami N, Susin SA (1997) Mitochondrial control of apoptosis. Immunol Today 18: 44-51.
87. Susin SA, Daugas E, Ravagnan L, Samejima K, Zamzami N, et al. (2000) Two distinct pathways leading to nuclear apoptosis. J Exp Med 192: 571-580.
88. Susin SA, Lorenzo HK, Zamzami N, Marzo I, Snow BE, et al. (1999) Molecular characterization of mitochondrial apoptosis-inducing factor. Nature 397: 441-446.
89. Vousden KH, Lu X (2002) Live or let die: the cell's response to p53. Nat Rev Cancer 2: 594-604.
90. Cory S, Adams JM (2002) The Bcl2 family: regulators of the cellular life-or-death switch. Nat Rev Cancer 2: 647-656.
91. Hsu YT, Wolter KG, Youle RJ (1997) Cytosol-to-membrane redistribution of Bax and Bcl-X(L) during apoptosis. Proc Natl Acad Sci U S A 94: 3668-3672.
92. Reed JC (1998) Bcl-2 family proteins. Oncogene 17: 3225-3236.

93. Boise LH, Gonzalez-Garcia M, Postema CE, Ding L, Lindsten T, et al. (1993) bcl-x, a bcl-2-related gene that functions as a dominant regulator of apoptotic cell death. Cell 74: 597-608.
94. Scorrano L, Korsmeyer SJ (2003) Mechanisms of cytochrome c release by proapoptotic BCL-2 family members. Biochem Biophys Res Commun 304: 437-444.
95. Letai AG (2008) Diagnosing and exploiting cancer's addiction to blocks in apoptosis. Nat Rev Cancer 8: 121-132.
96. Chowdhury I, Tharakan B, Bhat GK (2008) Caspases - an update. Comp Biochem Physiol B Biochem Mol Biol 151: 10-27.
97. Taylor RC, Cullen SP, Martin SJ (2008) Apoptosis: controlled demolition at the cellular level. Nat Rev Mol Cell Biol 9: 231-241.
98. Nakagawa T, Zhu H, Morishima N, Li E, Xu J, et al. (2000) Caspase-12 mediates endoplasmic-reticulum-specific apoptosis and cytotoxicity by amyloid-beta. Nature 403: 98-103.
99. Sutton VR, Wowk ME, Cancilla M, Trapani JA (2003) Caspase activation by granzyme B is indirect, and caspase autoprocessing requires the release of proapoptotic mitochondrial factors. Immunity 18: 319-329.
100. Thome M, Schneider P, Hofmann K, Fickenscher H, Meinl E, et al. (1997) Viral FLICE-inhibitory proteins (FLIPs) prevent apoptosis induced by death receptors. Nature 386: 517-521.
101. Hermann C, Assmus B, Urbich C, Zeiher AM, Dimmeler S (2000) Insulin-mediated stimulation of protein kinase Akt: A potent survival signaling cascade for endothelial cells. Arterioscler Thromb Vasc Biol 20: 402-409.
102. Schaeffer HJ, Weber MJ (1999) Mitogen-activated protein kinases: specific messages from ubiquitous messengers. Mol Cell Biol 19: 2435-2444.
103. Whitmarsh AJ, Cavanagh J, Tournier C, Yasuda J, Davis RJ (1998) A mammalian scaffold complex that selectively mediates MAP kinase activation. Science 281: 1671-1674.
104. Krishna M, Narang H (2008) The complexity of mitogen-activated protein kinases (MAPKs) made simple. Cell Mol Life Sci 65: 3525-3544.
105. Pelengaris S, Khan M, Evan G (2002) c-MYC: more than just a matter of life and death. Nat Rev Cancer 2: 764-776.
106. Nguyen TT, Tran E, Nguyen TH, Do PT, Huynh TH, et al. (2004) The role of activated MEK-ERK pathway in quercetin-induced growth inhibition and apoptosis in A549 lung cancer cells. Carcinogenesis 25: 647-659.
107. Yeh PY, Chuang SE, Yeh KH, Song YC, Ea CK, et al. (2002) Increase of the resistance of human cervical carcinoma cells to cisplatin by inhibition of the MEK to ERK signaling pathway partly via enhancement of anticancer drug-induced NF kappa B activation. Biochem Pharmacol 63: 1423-1430.
108. Kim GS, Hong JS, Kim SW, Koh JM, An CS, et al. (2003) Leptin induces apoptosis via ERK/cPLA2/cytochrome c pathway in human bone marrow stromal cells. J Biol Chem 278: 21920-21929.
109. Park BG, Yoo CI, Kim HT, Kwon CH, Kim YK (2005) Role of mitogen-activated protein kinases in hydrogen peroxide-induced cell death in osteoblastic cells. Toxicology 215: 115-125.
110. Brown L, Benchimol S (2006) The involvement of MAPK signaling pathways in determining the cellular response to p53 activation: cell cycle arrest or apoptosis. J Biol Chem 281: 3832-3840.
111. Sinha D, Bannergee S, Schwartz JH, Lieberthal W, Levine JS (2004) Inhibition of ligand-independent ERK1/2 activity in kidney proximal tubular cells deprived of

soluble survival factors up-regulates Akt and prevents apoptosis. J Biol Chem 279: 10962-10972.
112. Cross T, Scheel-Toellner D, Henriquez N, Deacon E, Salmon M, et al. (2000) Serine/threonine protein kinases and apoptosis. Exp Cell Res 256: 34-41.
113. Schreiber M, Kolbus A, Piu F, Szabowski A, Mohle-Steinlein U, et al. (1999) Control of cell cycle progression by c-Jun is p53 dependent. Genes Dev 13: 607-619.
114. Platanias LC (2003) Map kinase signaling pathways and hematologic malignancies. Blood 101: 4667-4679.
115. Kuntzen C, Sonuc N, De Toni EN, Opelz C, Mucha SR, et al. (2005) Inhibition of c-Jun-N-terminal-kinase sensitizes tumor cells to CD95-induced apoptosis and induces G2/M cell cycle arrest. Cancer Res 65: 6780-6788.
116. Xia HH, He H, De Wang J, Gu Q, Lin MC, et al. (2006) Induction of apoptosis and cell cycle arrest by a specific c-Jun NH2-terminal kinase (JNK) inhibitor, SP-600125, in gastrointestinal cancers. Cancer Lett 241: 268-274.
117. Ventura JJ, Hubner A, Zhang C, Flavell RA, Shokat KM, et al. (2006) Chemical genetic analysis of the time course of signal transduction by JNK. Mol Cell 21: 701-710.
118. Kyriakis JM, Avruch J (2001) Mammalian mitogen-activated protein kinase signal transduction pathways activated by stress and inflammation. Physiol Rev 81: 807-869.
119. Raingeaud J, Gupta S, Rogers JS, Dickens M, Han J, et al. (1995) Pro-inflammatory cytokines and environmental stress cause p38 mitogen-activated protein kinase activation by dual phosphorylation on tyrosine and threonine. J Biol Chem 270: 7420-7426.
120. Dong C, Davis RJ, Flavell RA (2002) MAP kinases in the immune response. Annu Rev Immunol 20: 55-72.
121. Zarubin T, Han J (2005) Activation and signaling of the p38 MAP kinase pathway. Cell Res 15: 11-18.
122. Galan A, Garcia-Bermejo ML, Troyano A, Vilaboa NE, de Blas E, et al. (2000) Stimulation of p38 mitogen-activated protein kinase is an early regulatory event for the cadmium-induced apoptosis in human promonocytic cells. J Biol Chem 275: 11418-11424.
123. Rockwell P, Martinez J, Papa L, Gomes E (2004) Redox regulates COX-2 upregulation and cell death in the neuronal response to cadmium. Cell Signal 16: 343-353.
124. Kummer JL, Rao PK, Heidenreich KA (1997) Apoptosis induced by withdrawal of trophic factors is mediated by p38 mitogen-activated protein kinase. J Biol Chem 272: 20490-20494.
125. Mackay K, Mochly-Rosen D (1999) An inhibitor of p38 mitogen-activated protein kinase protects neonatal cardiac myocytes from ischemia. J Biol Chem 274: 6272-6279.
126. Franklin CC, Srikanth S, Kraft AS (1998) Conditional expression of mitogen-activated protein kinase phosphatase-1, MKP-1, is cytoprotective against UV-induced apoptosis. Proc Natl Acad Sci U S A 95: 3014-3019.
127. Callsen D, Brune B (1999) Role of mitogen-activated protein kinases in S-nitrosoglutathione-induced macrophage apoptosis. Biochemistry 38: 2279-2286.
128. Juo P, Kuo CJ, Reynolds SE, Konz RF, Raingeaud J, et al. (1997) Fas activation of the p38 mitogen-activated protein kinase signalling pathway requires ICE/CED-3 family proteases. Mol Cell Biol 17: 24-35.
129. Olson JM, Hallahan AR (2004) p38 MAP kinase: a convergence point in cancer therapy. Trends Mol Med 10: 125-129.
130. Bradham C, McClay DR (2006) p38 MAPK in development and cancer. Cell Cycle 5: 824-828.

131. Losa JH, Parada Cobo C, Viniegra JG, Sanchez-Arevalo Lobo VJ, Ramon y Cajal S, et al. (2003) Role of the p38 MAPK pathway in cisplatin-based therapy. Oncogene 22: 3998-4006.
132. Ghatan S, Larner S, Kinoshita Y, Hetman M, Patel L, et al. (2000) p38 MAP kinase mediates bax translocation in nitric oxide-induced apoptosis in neurons. J Cell Biol 150: 335-347.
133. Bulavin DV, Higashimoto Y, Popoff IJ, Gaarde WA, Basrur V, et al. (2001) Initiation of a G2/M checkpoint after ultraviolet radiation requires p38 kinase. Nature 411: 102-107.
134. Matsusaka T, Pines J (2004) Chfr acts with the p38 stress kinases to block entry to mitosis in mammalian cells. J Cell Biol 166: 507-516.
135. Yee AS, Paulson EK, McDevitt MA, Rieger-Christ K, Summerhayes I, et al. (2004) The HBP1 transcriptional repressor and the p38 MAP kinase: unlikely partners in G1 regulation and tumor suppression. Gene 336: 1-13.
136. Saddoughi SA, Song P, Ogretmen B (2008) Roles of bioactive sphingolipids in cancer biology and therapeutics. Subcell Biochem 49: 413-440.
137. Andrieu-Abadie N, Levade T (2002) Sphingomyelin hydrolysis during apoptosis. Biochim Biophys Acta 1585: 126-134.
138. Futerman AH, Hannun YA (2004) The complex life of simple sphingolipids. EMBO Rep 5: 777-782.
139. Riboni L, Prinetti A, Bassi R, Viani P, Tettamanti G (1998) The effects of exogenous sphingosine on Neuro2a cells are strictly related to the overall capacity of cells to metabolize sphingosine. J Biochem 124: 900-904.
140. Kitatani K, Idkowiak-Baldys J, Hannun YA (2008) The sphingolipid salvage pathway in ceramide metabolism and signaling. Cell Signal 20: 1010-1018.
141. Jaffrezou JP, Levade T, Bettaieb A, Andrieu N, Bezombes C, et al. (1996) Daunorubicin-induced apoptosis: triggering of ceramide generation through sphingomyelin hydrolysis. EMBO J 15: 2417-2424.
142. Uchida Y, Nardo AD, Collins V, Elias PM, Holleran WM (2003) De novo ceramide synthesis participates in the ultraviolet B irradiation-induced apoptosis in undifferentiated cultured human keratinocytes. J Invest Dermatol 120: 662-669.
143. Schwandner R, Wiegmann K, Bernardo K, Kreder D, Kronke M (1998) TNF receptor death domain-associated proteins TRADD and FADD signal activation of acid sphingomyelinase. J Biol Chem 273: 5916-5922.
144. Grassme H, Jekle A, Riehle A, Schwarz H, Berger J, et al. (2001) CD95 signaling via ceramide-rich membrane rafts. J Biol Chem 276: 20589-20596.
145. Birbes H, El Bawab S, Obeid LM, Hannun YA (2002) Mitochondria and ceramide: intertwined roles in regulation of apoptosis. Adv Enzyme Regul 42: 113-129.
146. Birbes H, El Bawab S, Hannun YA, Obeid LM (2001) Selective hydrolysis of a mitochondrial pool of sphingomyelin induces apoptosis. FASEB J 15: 2669-2679.
147. Decaudin D, Marzo I, Brenner C, Kroemer G (1998) Mitochondria in chemotherapy-induced apoptosis: a prospective novel target of cancer therapy (review). Int J Oncol 12: 141-152.
148. Bionda C, Portoukalian J, Schmitt D, Rodriguez-Lafrasse C, Ardail D (2004) Subcellular compartmentalization of ceramide metabolism: MAM (mitochondria-associated membrane) and/or mitochondria? Biochem J 382: 527-533.
149. Diaz JG, Carmona AJ, Torres F, Quintana J, Estevez F, et al. (2008) Cytotoxic activities of flavonoid glycoside acetates from Consolida oliveriana. Planta Med 74: 171-174.
150. Rivero A, Quintana J, Eiroa J, López M, Triana J, et al. (2003) Potent induction of apoptosis by germacranolide sesquiterpene lactones on human myeloid leukemia cells. Eur J Pharmacol 482: 77-84.

151. Cabrera J, Quintana J, Reiter R, Loro J, Cabrera F, et al. (2003) Melatonin prevents apoptosis and enhances HSP27 mRNA expression induced by heat shock in HL-60 cells: possible involvement of the MT2 receptor. J Pineal Res 35: 231-238.
152. Bradford MM (1976) A rapid and sensitive method for the quantitation of microgram quantities of protein utilizing the principle of protein-dye binding. Anal Biochem 72: 248-254.
153. Rubio S, Quintana J, López M, Eiroa J, Triana J, et al. (2006) Phenylbenzopyrones structure-activity studies identify betuletol derivatives as potential antitumoral agents. Eur J Pharmacol 548: 9-20.
154. Haridas V, Higuchi M, Jayatilake GS, Bailey D, Mujoo K, et al. (2001) Avicins: triterpenoid saponins from Acacia victoriae (Bentham) induce apoptosis by mitochondrial perturbation. Proc Natl Acad Sci U S A 98: 5821-5826.
155. Rubio S, Quintana J, Eiroa J, Triana J, Estévez F (2007) Acetyl derivative of quercetin 3-methyl ether-induced cell death in human leukemia cells is amplified by the inhibition of ERK. Carcinogenesis 28: 2105-2113.
156. Kang GJ, Getahun Z, Muzaffar A, Brossi A, Hamel E (1990) N-acetylcolchinol O-methyl ether and thiocolchicine, potent analogs of colchicine modified in the C ring. Evaluation of the mechanistic basis for their enhanced biological properties. J Biol Chem 265: 10255-10259.
157. Hamel E, Lin CM (1981) Stabilization of the colchicine-binding activity of tubulin by organic acids. Biochim Biophys Acta 675: 226-231.
158. Wiegmann K, Schutze S, Machleidt T, Witte D, Kronke M (1994) Functional dichotomy of neutral and acidic sphingomyelinases in tumor necrosis factor signaling. Cell 78: 1005-1015.
159. Birbes H, Luberto C, Hsu YT, El Bawab S, Hannun YA, et al. (2005) A mitochondrial pool of sphingomyelin is involved in TNFalpha-induced Bax translocation to mitochondria. Biochem J 386: 445-451.
160. Okazaki T, Bell RM, Hannun YA (1989) Sphingomyelin turnover induced by vitamin D3 in HL-60 cells. Role in cell differentiation. J Biol Chem 264: 19076-19080.
161. Kang CD, Yoo SD, Hwang BW, Kim KW, Kim DW, et al. (2000) The inhibition of ERK/MAPK not the activation of JNK/SAPK is primarily required to induce apoptosis in chronic myelogenous leukemic K562 cells. Leuk Res 24: 527-534.
162. Yang J, Liu X, Bhalla K, Kim C, Ibrado A, et al. (1997) Prevention of apoptosis by Bcl-2: release of cytochrome c from mitochondria blocked. Science 275: 1129-1132.
163. Jarvis WD, Fornari FA, Jr., Tombes RM, Erukulla RK, Bittman R, et al. (1998) Evidence for involvement of mitogen-activated protein kinase, rather than stress-activated protein kinase, in potentiation of 1-beta-D-arabinofuranosylcytosine-induced apoptosis by interruption of protein kinase C signaling. Mol Pharmacol 54: 844-856.
164. Yu C, Wang S, Dent P, Grant S (2001) Sequence-dependent potentiation of paclitaxel-mediated apoptosis in human leukemia cells by inhibitors of the mitogen-activated protein kinase kinase/mitogen-activated protein kinase pathway. Mol Pharmacol 60: 143-154.
165. Laurent G, Jaffrézou J (2001) Signaling pathways activated by daunorubicin. Blood 98: 913-924.
166. Yu R, Shtil A, Tan T, Roninson I, Kong A (1996) Adriamycin activates c-jun N-terminal kinase in human leukemia cells: a relevance to apoptosis. Cancer Lett 107: 73-81.
167. Chen Y, Wang W, Kong A, Tan T (1998) Molecular mechanisms of c-Jun N-terminal kinase-mediated apoptosis induced by anticarcinogenic isothiocyanates. J Biol Chem 273: 1769-1775.
168. Shiah SG, Chuang SE, Chau YP, Shen SC, Kuo ML (1999) Activation of c-Jun NH2-terminal kinase and subsequent CPP32/Yama during topoisomerase inhibitor beta-

lapachone-induced apoptosis through an oxidation-dependent pathway. Cancer Res 59: 391-398.
169. Watabe M, Kakeya H, Osada H (1999) Requirement of protein kinase (Krs/MST) activation for MT-21-induced apoptosis. Oncogene 18: 5211-5220.
170. Zhuang S, Demirs J, Kochevar I (2000) p38 mitogen-activated protein kinase mediates bid cleavage, mitochondrial dysfunction, and caspase-3 activation during apoptosis induced by singlet oxygen but not by hydrogen peroxide. J Biol Chem 275: 25939-25948.
171. Kaczmarek L, Calabretta B, Baserga R (1985) Expression of cell-cycle-dependent genes in phytohemagglutinin-stimulated human lymphocytes. Proc Natl Acad Sci U S A 82: 5375-5379.
172. Zhang L, Yu J, Park BH, Kinzler KW, Vogelstein B (2000) Role of BAX in the apoptotic response to anticancer agents. Science 290: 989-992.
173. Perlman H, Zhang X, Chen MW, Walsh K, Buttyan R (1999) An elevated bax/bcl-2 ratio corresponds with the onset of prostate epithelial cell apoptosis. Cell Death Differ 6: 48-54.
174. Hundal RS, Gomez-Munoz A, Kong JY, Salh BS, Marotta A, et al. (2003) Oxidized low density lipoprotein inhibits macrophage apoptosis by blocking ceramide generation, thereby maintaining protein kinase B activation and Bcl-XL levels. J Biol Chem 278: 24399-24408.
175. Miyake Y, Kozutsumi Y, Nakamura S, Fujita T, Kawasaki T (1995) Serine palmitoyltransferase is the primary target of a sphingosine-like immunosuppressant, ISP-1/myriocin. Biochem Biophys Res Commun 211: 396-403.
176. Becker KP, Kitatani K, Idkowiak-Baldys J, Bielawski J, Hannun YA (2005) Selective inhibition of juxtanuclear translocation of protein kinase C betaII by a negative feedback mechanism involving ceramide formed from the salvage pathway. J Biol Chem 280: 2606-2612.
177. Lee KH (1999) Novel antitumor agents from higher plants. Med Res Rev 19: 569-596.
178. Middleton E, Jr., Kandaswami C, Theoharides TC (2000) The effects of plant flavonoids on mammalian cells: implications for inflammation, heart disease, and cancer. Pharmacol Rev 52: 673-751.
179. Lassus P, Opitz-Araya X, Lazebnik Y (2002) Requirement for caspase-2 in stress-induced apoptosis before mitochondrial permeabilization. Science 297: 1352-1354.
180. Guo Y, Srinivasula SM, Druilhe A, Fernandes-Alnemri T, Alnemri ES (2002) Caspase-2 induces apoptosis by releasing proapoptotic proteins from mitochondria. J Biol Chem 277: 13430-13437.
181. Robertson JD, Enoksson M, Suomela M, Zhivotovsky B, Orrenius S (2002) Caspase-2 acts upstream of mitochondria to promote cytochrome c release during etoposide-induced apoptosis. J Biol Chem 277: 29803-29809.
182. Zhivotovsky B, Samali A, Gahm A, Orrenius S (1999) Caspases: their intracellular localization and translocation during apoptosis. Cell Death Differ 6: 644-651.
183. Bernhard D, Tinhofer I, Tonko M, Hubl H, Ausserlechner MJ, et al. (2000) Resveratrol causes arrest in the S-phase prior to Fas-independent apoptosis in CEM-C7H2 acute leukemia cells. Cell Death Differ 7: 834-842.
184. Srinivasula SM, Ahmad M, Fernandes-Alnemri T, Alnemri ES (1998) Autoactivation of procaspase-9 by Apaf-1-mediated oligomerization. Mol Cell 1: 949-957.
185. Scoltock AB, Cidlowski JA (2004) Activation of intrinsic and extrinsic pathways in apoptotic signaling during UV-C-induced death of Jurkat cells: the role of caspase inhibition. Exp Cell Res 297: 212-223.
186. Milleron RS, Bratton SB (2006) Heat shock induces apoptosis independently of any known initiator caspase-activating complex. J Biol Chem 281: 16991-17000.

187. Gracie JA, Robertson SE, McInnes IB (2003) Interleukin-18. J Leukoc Biol 73: 213-224.
188. Miura M, Zhu H, Rotello R, Hartwieg EA, Yuan J (1993) Induction of apoptosis in fibroblasts by IL-1 beta-converting enzyme, a mammalian homolog of the C. elegans cell death gene ced-3. Cell 75: 653-660.
189. Friedlander RM (2003) Apoptosis and caspases in neurodegenerative diseases. N Engl J Med 348: 1365-1375.
190. Saleh M (2006) Caspase-1 builds a new barrier to infection. Cell 126: 1028-1030.
191. Guo H, Petrin D, Zhang Y, Bergeron C, Goodyer CG, et al. (2006) Caspase-1 activation of caspase-6 in human apoptotic neurons. Cell Death Differ 13: 285-292.
192. Gurcel L, Abrami L, Girardin S, Tschopp J, van der Goot FG (2006) Caspase-1 activation of lipid metabolic pathways in response to bacterial pore-forming toxins promotes cell survival. Cell 126: 1135-1145.
193. Virag L, Szabo C (2002) The therapeutic potential of poly(ADP-ribose) polymerase inhibitors. Pharmacol Rev 54: 375-429.
194. Oliver FJ, de la Rubia G, Rolli V, Ruiz-Ruiz MC, de Murcia G, et al. (1998) Importance of poly(ADP-ribose) polymerase and its cleavage in apoptosis. Lesson from an uncleavable mutant. J Biol Chem 273: 33533-33539.
195. Nicholson DW, Thornberry NA (1997) Caspases: killer proteases. Trends Biochem Sci 22: 299-306.
196. Green DR, Kroemer G (2004) The pathophysiology of mitochondrial cell death. Science 305: 626-629.
197. Danial NN, Korsmeyer SJ (2004) Cell death: critical control points. Cell 116: 205-219.
198. Goldstein JC, Munoz-Pinedo C, Ricci JE, Adams SR, Kelekar A, et al. (2005) Cytochrome c is released in a single step during apoptosis. Cell Death Differ 12: 453-462.
199. Green DR, Evan GI (2002) A matter of life and death. Cancer Cell 1: 19-30.
200. Rovida E, Gozzini A, Barbetti V, Giuntoli S, Santini V, et al. (2006) The c-Jun-N-terminal-Kinase inhibitor SP600125 enhances the butyrate derivative D1-induced apoptosis via caspase 8 activation in Kasumi 1 t(8;21) acute myeloid leukaemia cells. Br J Haematol 135: 653-659.
201. Tanel A, Averill-Bates DA (2007) P38 and ERK mitogen-activated protein kinases mediate acrolein-induced apoptosis in Chinese hamster ovary cells. Cell Signal 19: 968-977.
202. Rubio S, Quintana J, Lopez M, Eiroa JL, Triana J, et al. (2006) Phenylbenzopyrones structure-activity studies identify betuletol derivatives as potential antitumoral agents. Eur J Pharmacol 548: 9-20.
203. Amundson SA, Myers TG, Scudiero D, Kitada S, Reed JC, et al. (2000) An informatics approach identifying markers of chemosensitivity in human cancer cell lines. Cancer Res 60: 6101-6110.
204. Addeo R, Caraglia M, Baldi A, D'Angelo V, Casale F, et al. (2005) Prognostic role of bcl-xL and p53 in childhood acute lymphoblastic leukemia (ALL). Cancer Biol Ther 4: 32-38.
205. Tobiume K, Matsuzawa A, Takahashi T, Nishitoh H, Morita K, et al. (2001) ASK1 is required for sustained activations of JNK/p38 MAP kinases and apoptosis. EMBO Rep 2: 222-228.
206. Beutler JA, Hamel E, Vlietinck AJ, Haemers A, Rajan P, et al. (1998) Structure-activity requirements for flavone cytotoxicity and binding to tubulin. J Med Chem 41: 2333-2338.
207. Brantley-Finley C, Lyle CS, Du L, Goodwin ME, Hall T, et al. (2003) The JNK, ERK and p53 pathways play distinct roles in apoptosis mediated by the antitumor agents vinblastine, doxorubicin, and etoposide. Biochem Pharmacol 66: 459-469.

208. Mingo-Sion AM, Marietta PM, Koller E, Wolf DM, Van Den Berg CL (2004) Inhibition of JNK reduces G2/M transit independent of p53, leading to endoreduplication, decreased proliferation, and apoptosis in breast cancer cells. Oncogene 23: 596-604.
209. Chauhan D, Li G, Hideshima T, Podar K, Mitsiades C, et al. (2003) JNK-dependent release of mitochondrial protein, Smac, during apoptosis in multiple myeloma (MM) cells. J Biol Chem 278: 17593-17596.
210. Owens DM, Keyse SM (2007) Differential regulation of MAP kinase signalling by dual-specificity protein phosphatases. Oncogene 26: 3203-3213.
211. Kamata H, Honda S, Maeda S, Chang L, Hirata H, et al. (2005) Reactive oxygen species promote TNFalpha-induced death and sustained JNK activation by inhibiting MAP kinase phosphatases. Cell 120: 649-661.
212. Tonks NK (2005) Redox redux: revisiting PTPs and the control of cell signaling. Cell 121: 667-670.
213. Lien SC, Usami S, Chien S, Chiu JJ (2006) Phosphatidylinositol 3-kinase/Akt pathway is involved in transforming growth factor-beta1-induced phenotypic modulation of 10T1/2 cells to smooth muscle cells. Cell Signal 18: 1270-1278.
214. Davis RJ (2000) Signal transduction by the JNK group of MAP kinases. Cell 103: 239-252.
215. Apel K, Hirt H (2004) Reactive oxygen species: metabolism, oxidative stress, and signal transduction. Annu Rev Plant Biol 55: 373-399.
216. Hollstein M, Rice K, Greenblatt MS, Soussi T, Fuchs R, et al. (1994) Database of p53 gene somatic mutations in human tumors and cell lines. Nucleic Acids Res 22: 3551-3555.
217. Hollstein M, Sidransky D, Vogelstein B, Harris CC (1991) p53 mutations in human cancers. Science 253: 49-53.
218. Ciccarelli C, Marampon F, Scoglio A, Mauro A, Giacinti C, et al. (2005) p21WAF1 expression induced by MEK/ERK pathway activation or inhibition correlates with growth arrest, myogenic differentiation and onco-phenotype reversal in rhabdomyosarcoma cells. Mol Cancer 4: 41.
219. Karlsson-Rosenthal C, Millar JB (2006) Cdc25: mechanisms of checkpoint inhibition and recovery. Trends Cell Biol 16: 285-292.
220. Nigg EA (2001) Mitotic kinases as regulators of cell division and its checkpoints. Nat Rev Mol Cell Biol 2: 21-32.
221. Hoffmann I, Clarke PR, Marcote MJ, Karsenti E, Draetta G (1993) Phosphorylation and activation of human cdc25-C by cdc2--cyclin B and its involvement in the self-amplification of MPF at mitosis. EMBO J 12: 53-63.
222. Davis FM, Tsao TY, Fowler SK, Rao PN (1983) Monoclonal antibodies to mitotic cells. Proc Natl Acad Sci U S A 80: 2926-2930.
223. Scatena CD, Stewart ZA, Mays D, Tang LJ, Keefer CJ, et al. (1998) Mitotic phosphorylation of Bcl-2 during normal cell cycle progression and Taxol-induced growth arrest. J Biol Chem 273: 30777-30784.
224. Jarvis WD, Kolesnick RN, Fornari FA, Traylor RS, Gewirtz DA, et al. (1994) Induction of apoptotic DNA damage and cell death by activation of the sphingomyelin pathway. Proc Natl Acad Sci U S A 91: 73-77.
225. Marchesini N, Hannun YA (2004) Acid and neutral sphingomyelinases: roles and mechanisms of regulation. Biochem Cell Biol 82: 27-44.
226. Pettus BJ, Chalfant CE, Hannun YA (2002) Ceramide in apoptosis: an overview and current perspectives. Biochim Biophys Acta 1585: 114-125.
227. Kroemer G, El-Deiry WS, Golstein P, Peter ME, Vaux D, et al. (2005) Classification of cell death: recommendations of the Nomenclature Committee on Cell Death. Cell Death Differ 12 Suppl 2: 1463-1467.

228. Boatright KM, Salvesen GS (2003) Mechanisms of caspase activation. Curr Opin Cell Biol 15: 725-731.
229. Nagata S (1997) Apoptosis by death factor. Cell 88: 355-365.
230. Kluck RM, Bossy-Wetzel E, Green DR, Newmeyer DD (1997) The release of cytochrome c from mitochondria: a primary site for Bcl-2 regulation of apoptosis. Science 275: 1132-1136.
231. Essmann F, Engels IH, Totzke G, Schulze-Osthoff K, Janicke RU (2004) Apoptosis resistance of MCF-7 breast carcinoma cells to ionizing radiation is independent of p53 and cell cycle control but caused by the lack of caspase-3 and a caffeine-inhibitable event. Cancer Res 64: 7065-7072.
232. Raman M, Chen W, Cobb MH (2007) Differential regulation and properties of MAPKs. Oncogene 26: 3100-3112.
233. Verheij M, Bose R, Lin XH, Yao B, Jarvis WD, et al. (1996) Requirement for ceramide-initiated SAPK/JNK signalling in stress-induced apoptosis. Nature 380: 75-79.
234. Checchi PM, Nettles JH, Zhou J, Snyder JP, Joshi HC (2003) Microtubule-interacting drugs for cancer treatment. Trends Pharmacol Sci 24: 361-365.
235. Pines J, Rieder CL (2001) Re-staging mitosis: a contemporary view of mitotic progression. Nat Cell Biol 3: E3-6.
236. Kolesnick R, Hannun YA (1999) Ceramide and apoptosis. Trends Biochem Sci 24: 224-225; author reply 227.
237. Teillet F, Boumendjel A, Boutonnat J, Ronot X (2008) Flavonoids as RTK inhibitors and potential anticancer agents. Med Res Rev 28: 715-745.
238. Zhuang S, Demirs JT, Kochevar IE (2000) p38 mitogen-activated protein kinase mediates bid cleavage, mitochondrial dysfunction, and caspase-3 activation during apoptosis induced by singlet oxygen but not by hydrogen peroxide. J Biol Chem 275: 25939-25948.
239. Soldani C, Scovassi AI (2002) Poly(ADP-ribose) polymerase-1 cleavage during apoptosis: an update. Apoptosis 7: 321-328.

ANEXOS

PUBLICACIONES:

Autores: León F, Brouard I, Rivera A, **Torres F,** Rubio S, Quintana J, Estévez F, Bermejo J.
Título: Isolation, Structure Elucidation, Total Synthesis, and Evaluation of New Natural and Synthetic Ceramides on Human SK-MEL-1 Melanoma Cells.
Revista : Journal of Medicinal Chemistry Volumen: 49 Páginas: 5830-39 Fecha: 2006

Autores: León F, Brouard I, **Torres F**, Quintana J, Rivera A, Estévez F, Bermejo J.
Título: A new ceramide from *Suillus luteus* and its cytotoxic activity against human SK-MEL-1 melanoma cells.
Revista: Chemistry & Biodiversity Volumen: 5 Páginas: 120-5 Fecha: 2008

Autores: Díaz JG, Carmona AJ, **Torres F**, Quintana J, Estévez F, Herz W.
Título: Cytotoxic Activities of Flavonoid Glycoside Acetates from *Consolida oliveriana*.
Revista: Planta Medica Volumen: 74 Páginas: 171-4 Fecha: 2008

Autores: Hernández JC, León F, Brouard I, **Torres F**, Rubio S, Quintana J, Estévez F, Bermejo J.
Título: Synthesis of novel spirostanic saponins and their cytotoxic activity.
Revista: Bioorganic & Medicinal Chemistry.Volumen: 16 Páginas: 2063-76 Fecha: 2008

Autores: **Torres F**, Quintana J, Díaz JG, Carmona AJ, Estévez F.
Título: Trifolin acetate-induced cell death in human leukemia cells is dependent on caspase-6 and activates the MAPK pathway.
Revista: Apoptosis Volumen: 13 Páginas: 716-28 Fecha: 2008

Autores: **Torres F**, Quintana J, Cabrera J, Loro JF, León F, Bermejo J, Estévez F.
Título: Induction of G_2-M phase arrest and apoptosis by α-methylene-γ-butyrolactones in human leukemia cells.
Revista: Cancer Letters Volumen: 269 Páginas: 139-47 Fecha: 2008

Autores: Triana J, Eiroa JL, Ortega JJ, León F, Brouard I, **Torres F**, Quintana J, Estévez F, Bermejo J.
Título: Sesquiterpene lactones from *Gonospermun gomerae* and *Gonospermun fruticosum* and their cytotoxic activities.
Revista: Journal of Natural Products Volumen: 71 Páginas: 2015-20 Fecha: 2008

Autores: **Torres F**, Quintana J, Estévez F.
Título: 5,7,3´-Trihydroxy-3,4´-dimethoxyflavone-induced cell death in human leukemia cells is dependent on caspases and activates the MAPK pathway.
Revista: Molecular Carcinogenesis DOI 10.1002/mc.20619

CONTRIBUCIONES A CONGRESOS:

Autores: **Fernando Torres**, Javier Cabrera, Juan Loro, Sara Rubio, José Quintana, Francisco León, Jaime Bermejo, Francisco Estévez.
Título: Síntesis y evaluación de compuestos con un agrupamiento alfa-metilén-gamma-butirolactona como potenciales compuestos antitumorales.
Tipo de participación: Póster
Congreso: X Congreso Nacional de la Asociación Española de Investigación sobre el Cáncer.
Publicación: Clinical & Translational Oncology Vol 7, Suppl. 3, 52, 2005.
Lugar celebración: Pamplona Fecha: 13 al 16 de octubre de 2005

Autores: Juan Loro, Sara Rubio, Javier Cabrera, Francisco Estévez, **Fernando Torres**, José Quintana.
Título: Efecto Antitumoral de la Melatonina en células promielocíticas humanas HL-60.
Tipo de participación: Póster
Congreso: X Congreso Nacional de la Asociación Española de Investigación sobre el Cáncer.
Publicación: Clinical & Translational Oncology Vol 7, Suppl. 34, 2005.
Lugar celebración: Pamplona Fecha: 13 al 16 de octubre de 2005

Autores: **Fernando Torres**, José Quintana, Jesús G.Díaz, Armando J.Carmona y Francisco Estévez.
Título: Efectos citotóxicos e inducción de apoptosis por compuestos derivados de la fenilbenzopirona.
Tipo de participación: Póster
Congreso: XXIX Congreso de la Sociedad Española de Bioquímica y Biología Molecular.
Publicación: Libro de resúmenes del Congreso
Lugar celebración: Elche Fecha: 7 al 10 de septiembre de 2006

Autores: **Fernando Torres**, José Quintana, Jesús G.Díaz, Armando J.Carmona y Francisco Estévez.
Título: Inducción de apoptosis en células leucémicas humanas por el acetato de trifolin: papel de las MAP quinasas.
Tipo de participación: Póster
Congreso: X Semana Científica "Antonio González".
Lugar celebración: La Laguna (Tenerife) Fecha: 2 al 6 de octubre de 2006

Autores: **Fernando Torres**, Juan C.Hernández, Francisco León, Ignacio Brouard, Sara Rubio, José Quintana, Francisco Estévez and Jaime Bermejo.
Título: Synthesis and evaluation of saponins on human tumoral cells.
Tipo de participación: Póster
Congreso: 3rd Meeting of Young Cancer Investigators of the Canaries **(3rd YCIC)** & 1st Meeting of Young Biomedical Investigators of the Macaronesia **(1st YBIM)**.
Lugar celebración: La Laguna (Tenerife) Fecha: 9 al 10 de noviembre de 2006

Autores: Juan C. Hernández, Francisco León, Ignacio Brouard, **Fernando Torres**, Sara Rubio, José Quintana, Francisco Estévez, Jaime Bermejo.
Título: Síntesis de Nuevas Saponinas Espirostánicas y su Actividad Citotóxica.
Tipo de participación: Póster
Congreso: XI Semana Científica "Antonio González".
Publicación: Libro de resúmenes del Congreso.
Lugar celebración: La Laguna (Tenerife) Fecha: 1 al 5 de octubre de 2007

Autores: Jesús G. Díaz, Armando J. Carmona, **Fernando Torres**, José Quintana, Francisco Estévez, Werner Herz.
Título: Actividad Citotóxica de Acetatos de Flavonol Glicosidos de Consolida oliveriana.
Tipo de participación: Póster
Congreso: XI Semana Científica "Antonio González".
Publicación: Libro de resúmenes del Congreso.
Lugar celebración: La Laguna (Tenerife). Fecha: 1 al 5 de octubre de 2007

Autores: **Fernando Torres**, José Quintana y Francisco Estévez.
Título: Signalling pathways triggered by THDF in human leukaemic cell lines.
Tipo de participación: Póster
Congreso: XXXI Congreso de la Sociedad Española de Bioquímica y Biología Molecular.
Publicación: Libro de resúmenes del Congreso
Lugar celebración: Bilbao Fecha: 10 al 13 de septiembre de 2008

Autores: **Fernando Torres**, José Quintana, Javier Cabrera, Juan F. Loro, Francisco León, Jaime Bermejo y Francisco Estévez.
Título: α-Metilén-γ-Butirolactonas inducen parada del ciclo celular en la fase G_2-M y apoptosis en células leucémicas humanas.
Tipo de participación: Póster
Congreso: XII Semana Científica "Antonio González".
Publicación: Libro de resúmenes del Congreso.
Lugar celebración: La Laguna (Tenerife) Fecha: 6 al 10 de octubre de 2008

Autores: José Quintana, Sara Rubio, Gledy Negrín, **Fernando Torres**, Javier Cabrera, Juan F. Loro y Francisco Estévez.
Título: Búsqueda de nuevos compuestos antitumorales y evaluación de su mecanismo de acción.
Tipo de participación: Póster
Congreso: Semanas de la Ciencia y la Innovación en Canarias 2008.
Lugar celebración: Las Palmas de Gran Canaria Fecha: 3 al 18 de noviembre de 2008

Autores: **Fernando Torres**, José Quintana y Francisco Estévez.
Título: THDF is a microtubule inhibitor and a selective apoptosis inducer in leukaemic cells.
Tipo de participación: Póster
Congreso: XXXII Congreso de la Sociedad Española de Bioquímica y Biología Molecular.
Lugar celebración: Oviedo Fecha: 23 al 26 de septiembre de 2009

Autores: Fabio Nicolini, **Fernando Torres**, José Quintana y Francisco Estévez.
Título: Induction of G2/M phase arrest and apoptosis by the flavonoid Tamarixetin on human leukaemia cells.
Tipo de participación: Póster
Congreso: 6th Meeting of the Young Cancer Investigators of the Canary Islands.
Lugar celebración: Las Palmas de Gran Canaria Fecha: 10 al 13 de diciembre de 2009

ESTANCIA EN CENTRO EXTRANJERO:

Centro: Faculté de Pharmacie Paris-Sud, INSERM U749
Localidad: Paris País: Francia Fecha: 19/09/2008 Duración (semanas): 13
Tema: Mecanismos de resistencia a anoikis de las células de cáncer de colon metastático humanas.

Isolation, Structure Elucidation, Total Synthesis, and Evaluation of New Natural and Synthetic Ceramides on Human SK-MEL-1 Melanoma Cells

Francisco León,[†,‡] Ignacio Brouard,[†] Augusto Rivera,[⊥] Fernando Torres,[§] Sara Rubio,[§] José Quintana,[§] Francisco Estévez,[§] and Jaime Bermejo*,[†]

Instituto de Productos Naturales y Agrobiología, C.S.I.C., Instituto Universitario de Bio-Orgánica "Antonio González", Avda. Astrofísico F. Sánchez 3, 38206 La Laguna, Tenerife, Spain, Instituto Canario de Investigación del Cáncer, Avda. Astrofísico F. Sánchez 2, 38206 La Laguna, Tenerife, Spain, Departamento de Bioquímica y Biología Molecular, Centro de Ciencias de la Salud, Universidad de Las Palmas de Gran Canaria, Avenida S. Cristóbal, 35016 Las Palmas de Gran Canaria, Spain, and Departamento de Química, Facultad de Ciencias, Universidad Nacional de Colombia, Apartado Aéreo 14490, Bogotá, D.C., Colombia

Received May 8, 2006

Two new long-chain ceramides, trametenamides A (**1**) and B (**2**), were isolated from the methanolic extract of the fruiting body of the fungus *Trametes menziesii*. The structures were elucidated by spectroscopic analyses and chemical transformations, and the absolute stereochemistry of trametenamide B (**2**) was determined by stereoselective total synthesis of four possible diastereomers. The acetyl derivative of the natural ceramide (**1a**) and synthetic ceramides (**24**−**27**) showed cytotoxicity on the human melanoma cell line SK-MEL-1, which was caused by induction of apoptosis as determined by DNA fragmentation, poly-(ADP-ribose) polymerase cleavage, and procaspase-9 and -8 processing.

Introduction

Programmed cell death or apoptosis is triggered by a variety of stimuli, including cell surface receptors such as FAS, the mitochondrial response to stress, and factors released from cytotoxic T cells. It is well established that mitochondria play a central role in the process of apoptosis. Numerous signals converge on this intracellular organelle across the activation of diverse proapoptotic Bcl-2 family members that include Bak, Bad, Bid, and Bax. In response to apoptotic stimuli these proteins are redistributed from the cytosol to the mitochondria and result in the permeabilization of the outer mitochondrial membrane.

Cytochrome *c* is an essential component of the mitochondrial respiratory chain, and it is localized in the intermembrane space. Release of cytochrome *c* from the mitochondria provides the signal for the initiation of the assembly of the apoptosome, a large multisubunit complex formed from constitutive proteins. This complex recruits and activates procaspase-9, which then activates downstream effector caspases.[1] Caspase-3 is one of the key executioners of apoptosis, being responsible either partially or totally for the proteolytic cleavage of many key proteins, such as the nuclear enzyme poly(ADP-ribose) polymerase.[2] Other mitochondrial proteins such as the protein Smac and its murine homologue DIABLO have been described that promote caspase activation by eliminating IAP (inhibitor of apoptosis proteins) inhibition of caspases. IAPs inhibit apoptosis primarily by direct inhibition of distinct caspases.

Ceramides have been proposed as a second messenger for events as diverse as differentiation, senescence, proliferation, and cell cycle arrest, although most research has focused on their role in apoptosis.[3] In addition, ceramides are involved in the processes of neuronal death during the development of neurodegenerative diseases.[4] In some cells, apoptosis induction requires ceramide generation at the plasma membrane,[5] and ceramide generation probably drives the clustering of sphingolipid rafts into platforms.[6] Recently, a mitochondrial sphingomyelinase activity has been described that generates enough ceramide in this organelle to activate the apoptotic pathway.[7] Ceramides also seem to be involved in the mitochondrial membrane permeabilization allowing the exit of proapoptotic factors such as cytochrome *c*, AIF, Smac/DIABLO, and the endonuclease Endo G.[8] Recent evidence suggests that ceramides can also induce apoptosis by a caspase-independent mechanism.[9]

In the course of our research on biologically active metabolites from higher fungi, we recently described a series of new triterpene compounds isolated from *Ganoderma lucidum*,[10] *G. concinna*,[11] *G. australe*,[12] and *Laetiporus sulphureus*[13] as well as their biological activities. The present work deals with the chemical study of the fungus *Trametes menziesii*, which is mainly distributed in tropical and subtropical regions (American Samoa region) and has not hitherto been chemically investigated. Two new ceramides were isolated and characterized as their peracetylated derivatives, trametenamide A (**1**) and trametenamide B (**2**), the latter being synthesized along with three of its diastereomers and analyzed as bioactive compounds.

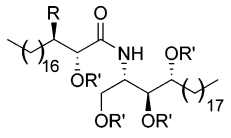

1. R = H; R' = H **1a**. R = H; R' = Ac
2. R = OH; R' = H **2a**. R = OAc; R' = Ac

This fungus belongs to a group of fungi (Polyporaceae) that break down woody plants into their basic elements and are a critical part of the tropical ecosystem including Colombia.[14] Although few species of Polyporaceae fungi have been evaluated for biological activity, most of the tested polypore fungi have shown significant antimicrobial activity as well as antiviral, cytotoxic, and/or antineoplastic activities properties. Therefore, these fungi may constitute a good source for the development of new drugs.[15] To assess whether acetylated ceramides (**1a** and

* To whom correspondence should be addressed. Phone: (34) 922-318583. Fax: (34) 922-318571. E-mail: jbermejo@ull.es.
† Instituto de Productos Naturales y Agrobiología, C.S.I.C.
‡ Instituto Canario de Investigación del Cáncer.
⊥ Universidad Nacional de Colombia.
§ Universidad de Las Palmas de Gran Canaria.

10.1021/jm0605334 CCC: $33.50 © 2006 American Chemical Society
Published on Web 08/22/2006

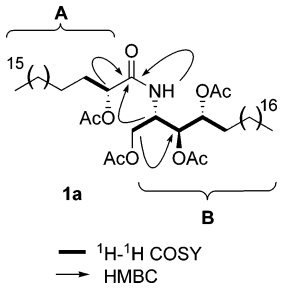

Figure 1. ^{1}H−^{1}H COSY and HMBC correlations for **1a**.

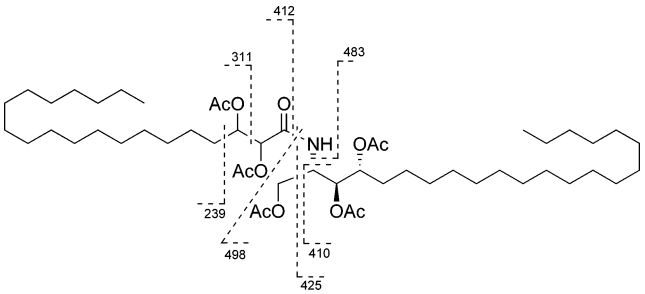

Figure 2. EIMS fragmentation of **1a**.

24−**27**) display cytotoxic activities, we studied their effects on the viability of the human melanoma cell line SK-MEL-1.

Results and Discussion

Isolation and Structural Elucidation. The fungus was collected in the Valencia region (Córdoba, Colombia). The ethanolic extract of the fresh fruiting bodies of the fungus was separated by extensive column chromatography over silica gel to yield five known products, linoleic acid, ergosta-7,22-diene-3-one,[11] ergosta-7,22-diene-3β-ol,[11] ergosterol peroxide,[12] and cerevisterol,[13] as well as an inseparable mixture of two compounds. Acetylation of this mixture and purification of the products by gradient flash silica gel chromatography gave pure compounds **1a** and **2a**. The structures of the known compounds were determined by a combination of spectroscopic analysis and comparison with reported data.

Compound **1a** gave a $[M]^+$ ion at *m*/*z* 851.6778 in HR-FABMS appropriate for a molecular formula of $C_{50}H_{93}NO_9$. The typical IR absorptions at 1667 and 1530 cm^{-1} suggested that compound **1a** contains a secondary amide, which was supported by the presence of a nitrogen-attached carbon signal at δ 46.9 and a carbonyl signal at δ 169.1 in the ^{13}C NMR spectrum. The ^{1}H and ^{13}C NMR spectra of **1a** showed the presence of two terminal methyls, aliphatic methylenes, three oxygenated methines, one oxygenated methylene, a nitrogenous methine, four acetates, and a carbon and a proton of an amide function. The ^{1}H−^{1}H COSY, HSQC, and HBMC spectra of **1a** afforded two partial regions **A** and **B** (Figure 1). ^{1}H−^{1}H COSY experiment correlations from the nitrogeneous methine to the oxygenated methylene and to one oxygenated methine together with correlations from this methine to another one gave the partial structure of sphingosine **B**. The correlations in the ^{1}H−^{1}H COSY experiment from an oxygenated methine to an aliphatic methylene gave the partial structure of acyl chain **A**. The HMBC correlations of the amide carbonyl with the oxygenated methine proton of C-2′ and with the nitrogenous methine proton of C-2 gave the connectivity between partial structures **A** and **B**.

Amide **1a** was subjected to basic methanolysis in order to determine the nature of the alkyl chains of the ceramide (Scheme 1). Two products were separated chromatographically affording an acid and a sphingosine. The fatty acid was methylated with CH_2N_2 to give the methyl ester **3**, which was directly analyzed by GC−MS and identified as the methyl ester of unbranched 2-hydroxy fatty acid comprising 20 carbon atoms. The presence of this methyl ester **3** was supported by a HR-FABMS ion peak at *m*/*z* 366.2540. The second product from the methanolysis was identified as the aminotriol **4** having 22 carbon atoms based on an ion peak at *m*/*z* 396.3371 as well as major peak fragments at 377, 307, and 289. The stereochemistry of the molecule was established by comparison of ^{1}H NMR and optical rotation data from a similar analogue isolated by Lourenço et al.[16] On the basis of the above data, compound **1** was identified as (2*S*,3*S*,4*R*,2′R)-2-(2′-hydroxyeicosanoylamino)docosane-1,3,4-triol and named as trametenamide A (**1**).

Compound **2**, isolated as the peracetylated derivative **2a**, showed an ion peak at *m*/*z* 932.8060 in the HR-FABMS spectrum. This mass spectrometric datum is in accordance with the molecular formula $C_{52}H_{95}NO_{11}$, suggesting that **2a** should possess an extra acetoxy group compared to peracetate ceramide **1a**. This hypothesis was corroborated by the observation of an additional acetyl methyl singlet in the ^{1}H NMR spectrum of **2a**, as well as an additional oxymethine signal in its ^{13}C NMR spectrum. In the EIMS data of **2a**, characteristic fragment peaks were observed at *m*/*z* 498, 483, 425, 412, 410, 311, and 239, which were rationalized according to the pattern shown in Figure 2 indicating a C_{22} long chain for the sphingosine and a C_{20} long chain for the acid including two acetoxy groups.

Furthermore, the chemical shifts and coupling constants of the sphinganine protons are almost identical to those of the corresponding protons in peracetate ceramide **1a**, thus indicating the same relative stereochemistry in **2a**. As a consequence of those data and on the basis of the results of ^{1}H−^{1}H COSY and HMBC experiments, the additional oxygenated function could only be located at the C-3 position of the acyl chain. However, we could not determine the stereochemistry at C-2′ and C-3′ in the fatty acid chain because a minute amount of compound **2a** hampered further chemical transformation and 2D NMR studies. To unambiguously fully characterize compound **2a**, we carried out the total synthesis of the four possible diastereomers of 2,3-dihydroxyeicosanoic acid. Subsequent coupling of these acids with synthetic common sphingosine **4** will lead us to four peracetylated ceramides and will resolve the remaining absolute stereochemistry of **2a** and, ultimately, provide access to additional material for biological evaluation. Compound **2** is one of the few examples of natural ceramides that contain that particular hydroxylation profile in the fatty acid region.[17] To the best of our knowledge, there is no example of a complete stereochemical characterization of such compounds.

Chemical Synthesis. The first step was the preparation of common sphingosine **4**. The construction of this optically pure amine was achieved by application of the strategy developed by Asai et al.[18] starting from β-D-galactose pentaacetate (Scheme 2) employing a 17-carbon alkylphosphonium salt in the synthesis of compound **8**. Subsequent derivatization of alkene **8** afforded sphingosine **4**.

The four acid partners were synthesized following two different strategies depending on the threo or erythro series. For the threo series we took advantage of the Sharpless asymmetric dihydroxylation process performed using both AD-mix-α and AD-mix-β separately. As starting material we used α,β-unsaturated ester **14** obtained from the Horner−Wadsworth−Emmons reaction (HWE) over octadecanal **13** (Scheme 3). Treatment of ester **14** with AD-mix-α and AD-mix-β gave access to diols **15a** and **15b**, respectively, each with a relatively

Scheme 1[a]

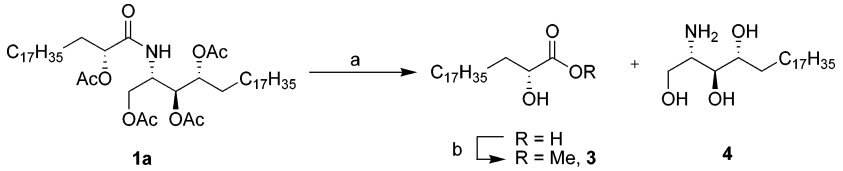

[a] Reagents and conditions: (a) KOH, MeOH, room temp; (b) CH_2N_2, Et_2O, room temp.

Scheme 2[a]

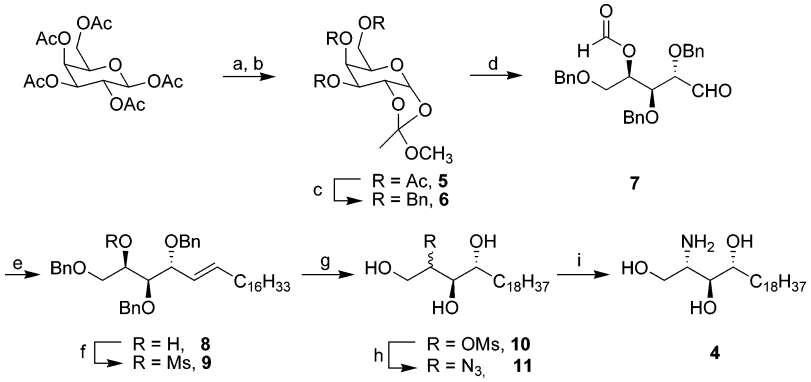

[a] Reagents and conditions: (a) HBr/AcOH (30%); (b) MeOH, Et_3N, $ClCH_2CH_2Cl$; (c) KOH, BnBr, toluene; (d) $NaIO_4$, $EtOH/H_2O$; (e) phosphonium salt, *n*-BuLi, THF; (f) MsCl, Py; (g) H_2, 10% Pd/C, EtOH; (h) NaN_3, DMF; (i) H_2, 10% Pd/C, EtOH.

Scheme 3[a]

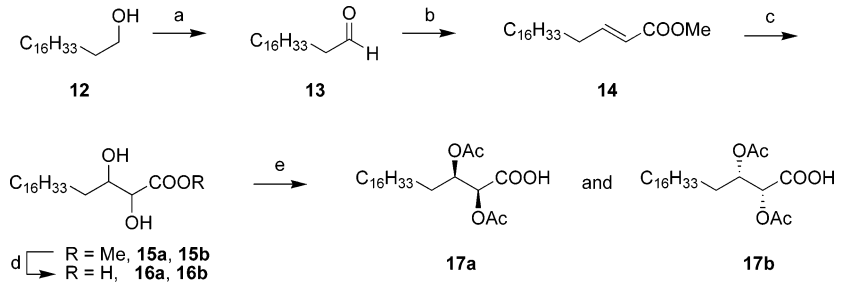

[a] Reagents and conditions: (a) PCC, CH_2Cl_2, room temp; (b) methyl phosphonoacetate, NaH, benzene; (c) AD-mix-β or *t*-BuOH−H_2O, methanesulfonamide; (d) NaOH, H_2O, THF; (e) Ac_2O, Py, room temp.

Scheme 4[a]

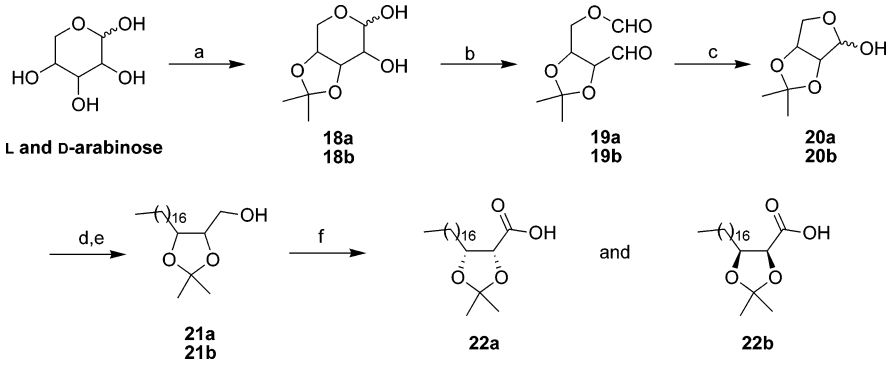

[a] Reagents and conditions: (a) dimethoxypropane, DMF, room temp; (b) $NaIO_4$, CH_2Cl_2−EtOH−H_2O, room temp; (c) K_2CO_3, MeOH, room temp; (d) phosphonium salt, *n*-BuLi, THF, −20 °C; (e) H_2, Pd/C (10%), room temp; (f) $RuCl_3$, $NaIO_4$, $CHCl_3$, room temp.

poor yield, presumably due to solubility problems. Subsequent basic hydrolysis followed by alcohol protection as acetates gave efficient access to the pair of threo enantiomeric acids **17a** and **17b** in a very straightforward manner.

We next explored the synthesis of the erythro acid series via Sharpless asymmetric epoxidation of the allylic alcohol derived from reduction of the above-mentioned ester **14**. Unfortunately, attempts to achieve regioselective epoxide opening induced by Ti(*i*-PrO)$_4$ in the presence of AcOH and subsequent selective protection led us to an unseparable mixture of transesterification byproducts. In our reasoning, the low solubility of the long-chain intermediates could be partly responsible for the inefficiency of this process.

As an alternative, we examined a new strategy using arabinose as starting material (Scheme 4), which contains the appropriate stereochemistry for both chiral centers in the acid chain. Treatment of commercially available D- and L-arabinose, separately, with 2,2-dimethoxypropane afforded diols **18a** and

Scheme 5[a]

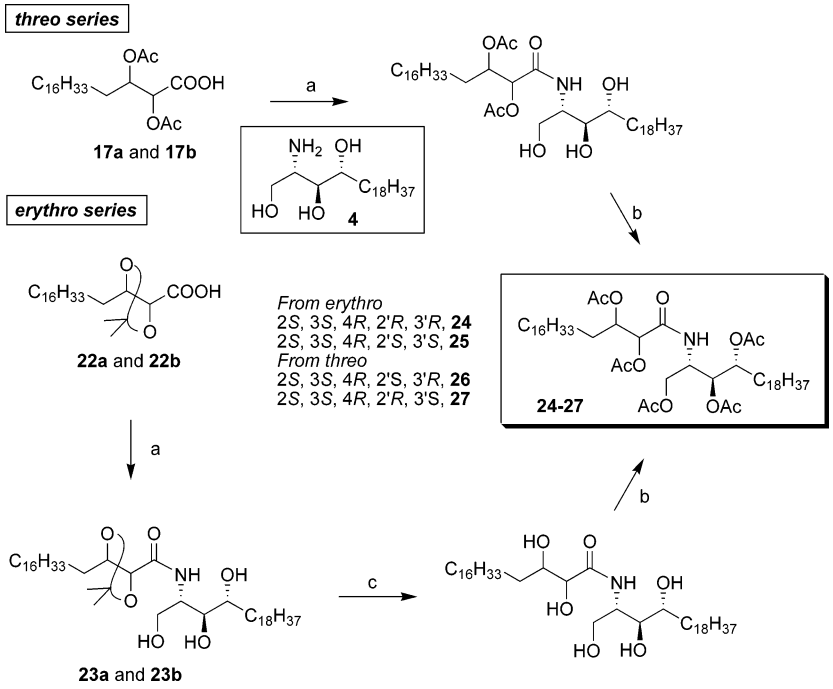

[a] Reagents and conditions: (a) HOBt, EDCI or *N*-hydroxysuccinimide, sphingosine **4**; (b) Ac_2O, Py, room temp; (c) HCl (3 N), MeOH, room temp.

Table 1. Effects of Natural and Synthetic Ceramides on the Growth of Human Melanoma Cell Line SK-MEL-1[a]

ceramide	IC_{50} (μM)
1a	7.7 ± 0.8
24	5.6 ± 0.5
25	10.2 ± 3.2
26	3.9 ± 0.9
27	7.1 ± 0.5

[a] The data shown represent the mean ± SEM of two independent experiments with three determinations in each. The IC_{50} values were calculated from experiments such as those shown in Figure 3 using the methodology described in the Experimental Section.

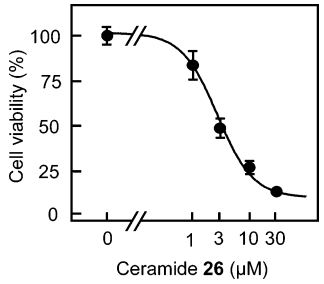

Figure 3. Effect of ceramide **26** on human SK-MEL-1 cell viability. Cells were cultured in the presence of the indicated concentrations (doses) of ceramide **26** for 72 h, and thereafter, cell viability was determined by the MTT assay as described in the Experimental Section. The results of a representative experiment are shown. Each point represents the average of triplicate determinations.

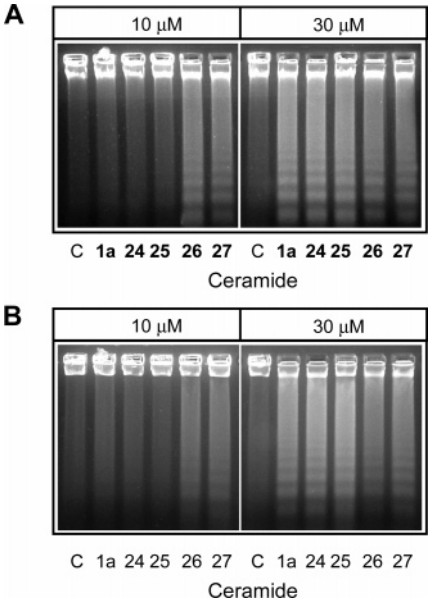

Figure 4. DNA fragmentation. Qualitative assessment of apoptotic DNA damage. SK-MEL-1 human melanoma cells were incubated in absence (C, control) or presence of 10−30 μM of the indicated ceramides for 6 h (A) or 12 h (B). Laddered electrophoretic patterns of oligonucleosomal DNA fragments were resolved by conventional agarose gel electrophoresis, stained with ethidium bromide and visualized under UV light.

18b[19] as their respective anomeric mixtures. Oxidative fragmentation employing $NaIO_4$ followed by basic hydrolysis furnished dimethyl ketal protected erythroses **20a** and **20b**. Both compounds were submitted separately to the Wittig coupling reaction with the phosphonium bromide salt generated from 1-hexadecanol to provide the complete carbon chain. Subsequent hydrogenation of the double bond led us to alcohols **21a** and **21b**, which were oxidated to acids **22a** and **22b** in moderate yields using $RuCl_3$−$NaIO_4$.[20]

With these four fatty acids **17a**, **17b**, **22a**, and **22b** in hand, we turned our attention to the amide generation by coupling amine **4**, separately, with each acid. Toward this end we first applied the reaction conditions used by Schultz et al.[21] in the synthesis of a wide combinatorial ceramide library. This methodology consists of the activation of the acid as a resin-bound ester derived from nitrophenol. To our dismay, attempts to couple activated acid **17a** with the amine partner **4** proved to be unrewarding. When the same coupling was performed using stearic acid, the reaction occurred easily. We therefore

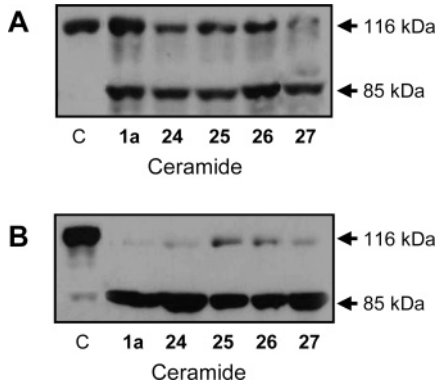

Figure 5. Western blot analysis for the cleavage of poly(ADP-ribose) polymerase (PARP). Control lanes refer to untreated cells. In the other lanes, SK-MEL-1 cells were treated with 10 μM (upper panel, A) or 30 μM (lower panel, B) of the indicated ceramides for 12 h. Cell lysates were subjected to SDS−PAGE followed by blotting with an anti-poly-(ADP-ribose) polymerase that also recognizes the 85 kDa fragment.

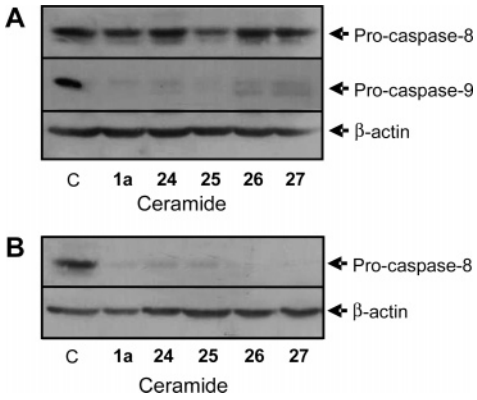

Figure 6. Western blot analysis for procaspase-8 and -9. SK-MEL-1 cells were cultured in the presence of 10 μM (A) or 30 μM (B) ceramides and harvested at 12 h. Total cell lysates were then analyzed by immunoblotting with anti-procaspase-8 or anti-procaspase-9 antibodies. β-Actin was used as loading control.

assumed that the presence of the acetoxy groups close to the reaction center creates a negative effect during the coupling process.

In light of the above, we turned to the acid activation employing either *N*-hydroxysuccinimide or HOBT/EDCI (Scheme 5). In all four cases acetylated ceramides **24**−**27** were obtained in similar and moderate yields. Comparison of the ^{1}H and ^{13}C NMR spectra and physical data of synthetic compound **24** and the peracetylated isolated ceramide **2a** confirmed the absolute configuration of trametenamide B **2** as (2*S*,3*S*,4*R*,2′*R*,3′*R*)-2-(2′,3′-dihydroxyeicosanoylamino)docosane-1,3,4-triol.

Induction of Apoptosis by Ceramides. We also report here on the cytotoxic activity of the acetyl derivative of natural ceramide (**1a**) and synthetic ceramides (**24**−**27**) against human melanoma SK-MEL-1 cells (Table 1, Figure 3), using the 3-[4,5-dimethylthiazol-2-yl]-2,5-diphenyltetrazolium bromide (MTT) dye-reduction assay. These ceramides show similar IC_{50} values (3−10 μM), indicating that the configurations at carbons C-2′ and C-3′ of the ceramide skeleton do not play a significant role in cytotoxic activity (Table 1, Figure 3). Similar results were obtained in the human myeloid leukaemia cell line HL-60 (results not shown).

To determine whether the decrease in human SK-MEL-1 cell viability (Table 1) observed after treatment with ceramides **1a** and **24**−**27** occurs by apoptosis, we performed DNA fragmentation and poly(ADP-ribose) polymerase cleavage experiments. DNA fragmentation is considered the end point of the apoptotic pathway, and poly(ADP-ribose) polymerase cleavage is a hallmark of apoptosis that indicates activation of caspase.

We observed the appearance of internucleosomal DNA fragmentation in SK-MEL-1 cells treated with ceramides **1a** and **24**−**27**. As illustrated in Figure 4, SK-MEL-1 cells underwent apoptosis in a dose-dependent fashion after treatment with ceramides. These ceramides also induced poly(ADP-ribose) polymerase cleavage; the typical 85 kDa band was observed after treatment with ceramides **1a** and **24**−**27** (Figure 5). By use of Western blot analysis, the cleavage of procaspase-9 (46−50 kDa) and procaspase-8 (55−57 kDa) was observed after exposure to ceramides. Procaspase-9 processing exhibited a higher level than procaspase-8 processing at 10 μM ceramides (Figure 6).

Conclusions

The polyporaceae fungus *Trametes menziesii* has been chemically studied for the first time, and two new long-chain ceramides have been identified along with five known compounds. One of these ceramides contains an unusual dihydroxylation profile for sphingolipids. The scarcity of novel isolated ceramide **2** encouraged us to develope the synthesis of such a compound, together with three of its diastereomers, to fully determine the stereochemistry of the chiral centers in the fatty acid chain and to provide enough material to perform biological assays. For the first time in the literature an example of this kind of ceramides is unambiguously described.

The exposure of SK-MEL-1 cells to ceramides **1a** and **24**−**27** described in this work elicits a strong antiproliferative effect and induces apoptosis. These ceramides induced internucleosomal DNA fragmentation and poly(ADP-ribose) polymerase cleavage characteristic of apoptotic cell death. It was found that the induction of apoptosis by ceramides **1a** and **24**−**27** in SK-MEL-1 melanoma cells correlated with enhanced poly(ADP-ribose) polymerase cleavage and procaspase-9 and -8 processing. The results of the biological experiments allow us to conclude that the stereochemistry of the hydroxyl groups in fatty acids has no significant influence on the antiproliferative activity of the ceramides.

Experimental Section

General Experimental Procedures. Melting points were determined on a Büchi B-540 apparatus and are uncorrected. Optical rotations were recorded in a Perkin-Elmer model 343 polarimeter. ^{1}H NMR and ^{13}C NMR spectra were obtained on Bruker models AMX-400, Avance 400, and Avance 300 spectrometers with standard pulse sequences operating at 400 and 300 MHz in ^{1}H NMR and at 100 and 75 MHz in ^{13}C NMR. $CDCl_3$ and C_5D_5N were used as solvents. EIMS, HR-EIMS, FABS, and HR-FABS data were taken on a Micromass model Autospec (70 eV) spectrometer. Column chromatography was carried out on silica gel 60 (Merck 230−400 mesh) and preparative TLC on silica gel 60 $PF_{254+366}$ plates (20 cm × 20 cm, 1 mm thickness) and Sephadex LH-20 (Aldrich).

Plant Material. The fungus *Trametes menziesii* (Berk) Ryv. was collected in the region of Valencia, Córdoba Department, Colombia, in May 2000. The fungus was identified by Professor Luis G. Henao of the Instituto de Ciencias Naturales, Universidad Nacional de Colombia, where a voucher specimen is deposited (Col. 344005).

Extraction and Isolation. The body fungi (380 g) were ground and steeped in EtOH (96%) for a week. The ethanolic extract (3.62 g) was chromatographed on silica gel (400 g), the fractions were eluted with *n*-hexane, *n*-hexanes−EtOAc mixtures (9:1; 4:1; 7:3; 1:1), and EtOAc (each 200 mL), yielding six fractions. Fraction 1 (150 mg) was rechromatographed over silica gel, eluting with

n-hexanes−EtOAc (9:1) to yield linoleic acid (50 mg). Fraction 2 (200 mg) and fraction 3 (500 mg) were further chromatographed with a Sephadex LH-20 column, eluting with *n*-hexane-$CHCl_3$-MeOH (3:3:1), and preparative TLC was carried out with toluene−acetone (9:1) and three elutions, affording ergosta 7,22-dien-3-one (90 mg) and ergosta 7,22-dien-3β-ol (130 mg). Fraction 4 (200 mg) was rechromatographed on preparative TLC with *n*-hexanes−EtOAc (8:2) and four elutions, yielding ergosterol peroxide (70 mg). Fraction 5 (150 mg) was chromatographed by column silica gel, eluting with $CHCl_3$−MeOH (50:1), and preparative TLC was carried out with *n*-hexanes−EtOAc (7:3) and three elutions, affording cerevisterol (2 mg). Fraction 6 (300 mg), after acetylation with Ac_2O/pyridine and subsequent purification by preparative TLC chromatography with *n*-hexanes−EtOAc (4:1), eluting twice, afforded tetraacetyltrametenamide A (**1**) (10 mg) and pentaacetyltrametenamide B (**2**) (3 mg).

(2*S*,3*S*,4*R*,2′*R*)-2-[2′-Acetoxyeicosanoylamino]-1,3,4-triacetoxydocosane (1a). Amorphous solid; $[\alpha]^{25}_D$ +25.0 (*c* 0.08, $CHCl_3$); IR ν_{max} (film, NaCl) 3341, 2920, 2850, 1737, 1667, 1530, 1470,1374, 1229, 1040 cm^{-1}; ^1H NMR (δ, $CDCl_3$) 0.87 (6H, t, *J* = 7.1 Hz, Me-22 and Me-20′), 1.27−1.41 (64H, br s, 32-CH_2), 1.60 (4H, m, CH_2-5 and CH_2-3′), 2.02 (3H, s, OAc), 2.05 (3H, s, OAc), 2.08 (3H, s, OAc), 2.18 (3H, s, OAc), 4.00 (1H, dd, *J* = 3.2, 11.8 Hz, H_a-1), 4.33 (1H, dd, *J* = 6.4, 11.2 Hz, H_b-1), 4.44 (1H, ddd, *J* = 3.2, 7.3, 9.7 Hz, H-2), 4.94 (1H, dd, *J* = 3.3, 10.0 Hz, H-2′), 5.09 (1H, m, H-3), 5.09 (1H, m, H-4), 6.60 (1H, d, *J* = 9.1 Hz, N−H); ^{13}C NMR (δ, $CDCl_3$) 13.2 (C-22 and C-20′), 19.8 (OAc), 19.9 (OAc), 20.0 (OAc), 20.1 (OAc), 21.8−31.0 [C-(5−21) and C-(3′-19′)], 46.9 (C-2), 61.5 (C-1), 71.4 (C-3), 71.8 (C-2′), 73.1 (C-4), 169.1 (C-1′), 169.1 (2 × C═O), 170.0 (C═O), 170.4 (C═O); FABMS *m*/*z* (relative intensity) 875 $[M + Na]^+$ (9), 852 $[M + H]^+$ (30), 851 $[M]^+$ (1), 820 (20), 806 (25), 792 (55), 790 (11), 264 (13), 154 (70), 137 (70), 107 (22), 69 (60), 54 (100); HR-FABMS 851.6778 ($C_{50}H_{93}NO_9$, calcd 851.6850).

Basic Hydrolysis of 1a. A solution of 1 N KOH in MeOH−H_2O (9:1) (5 mL) was added to acetylated trametenamide A (4 mg), and the mixture was maintained at 80 °C under argon with constant stirring. After 24 h, the mixture was diluted with H_2O and extracted with CH_2Cl_2. The organic phase was removed in vacuo, and the residue was subjected to preparative TLC and eluted with $CHCl_3$−methanol (5:1) to give phytosphingosine **4** (1.0 mg) as an amorphous solid. $[\alpha]^{25}_D$ +12.3 (*c* 0.008, pyridine); ^1H NMR (δ, pyridine-d_5) 0.85 (3H, t, *J* = 5.5 Hz, CH_3-22), 1.1−1.3 (30H, br s, 15-CH_2 (7−21)), 1.61 (1H, m, H_b-6), 1.82 (2H, m, H_a-6 and H_b-5), 2.20 (1H, m, H_a-5), 4.03 (1H, d, *J* = 4.7 Hz, H-2), 4.18 (1H, t, *J* = 8.0 Hz, H-4), 4.33 (1H, dd, *J* = 5.4, 7.6 Hz, H-3), 4.49 (2H, m, 2 × H-1); FABMS *m*/*z* (relative intensity) 396 $[M + Na]^+$ (11), 377 $[M + Na - H_2O]^+$ (9), 307 (28), 289 (13), 176 (8), 154 (100), 137 (66), 107 (17); HR-FABMS 396.3371 ($C_{22}H_{47}NO_3Na$ calcd 396.3453). The aqueous phase was then acidified with 5% H_2SO_4, extracted with CH_2Cl_2, and concentrated. The residue was treated with CH_2N_2 in diethyl ether, and the mixture was kept at room temperature for 12 h. Concentration of the reaction mixture under vacuo furnished methyl (2*R*)-2-hydroxyeicosanoate (0.6 mg) as an oil. $[\alpha]^{25}_D$ −2.3 (*c* 0.048, $CHCl_3$); ^1H NMR (δ, $CDCl_3$) 0.96 (3H, t, *J* = 7.4 Hz), 1.25 (30H, s br, 15-CH_2), 1.42 (2H, m), 1.71 (2H, m), 3.66 (3H, s, OMe), 4.10 (1H, dd, *J* = 6.8, 10.1 Hz); HR-FABMS *m*/*z* (relative intensity) 366.2540 ($C_{21}H_{43}O_3Na$ calcd 366.2489) $[M + Na + H]^+$ (11), 327 (5), 313 (18), 311 (17), 299 (7), 284 (5).

(2*S*,3*S*,4*R*,2′*R*,3′*R*)-2-[2′,3′-Diacetoxyeicosanoylamino]-1,3,4-triacetoxydocosane (2a). Amorphous solid; IR ν_{max} (film, NaCl) 2923, 2853, 1747, 1697, 1660, 1546, 1371, 1225, 1047 cm^{-1}; ^1H NMR (δ, $CDCl_3$) 0.87 (6H, t, *J* = 6.8 Hz, Me-22 and Me-20′), 1.20−1.50 (62H, br s, 31-CH_2), 1.60 (4H, m, CH_2-5 and CH_2-4′), 2.02 (3H, s, OAc), 2.05 (3H, s, OAc), 2.06 (3H, s, OAc), 2.08 (3H, s, OAc), 2.09 (3H, s, OAc), 4.02 (1H, dd, *J* = 3.4, 11.8 Hz, H_a-1), 4.28 (1H, dd, *J* = 6.4, 11.8 Hz, H_b-1), 4.82 (1H, ddd, *J* = 3.2, 6.8, 9.6 Hz, H-2), 4.98 (1H, dt, *J* = 3.2, 6.6 Hz, H-4), 5.11 (1H, dd, *J* = 4.0, 7.4 Hz, H-3), 5.25 (1H, dt, *J* = 4.0, 7.4 Hz, H-3′), 5.36 (1H, d, *J* = 3.2 Hz, H-2′), 6.78 (1H, d, *J* = 9.2 Hz, N−H); ^{13}C NMR (δ, $CDCl_3$) 14.1 (C-22 and C-20′), 20.5 (OAc), 20.6 (OAc), 20.7 (OAc), 20.9 (OAc), 21.0 (OAc), 22.6−31.9 [C-(5−21) and C-(4′-19′)], 47.9 (C-2), 62.5 (C-1), 72.1 (C-3), 72.8 (C-3′), 72.9 (C-4), 73.7 (C-2′), 166.6 (C-1′), 169.3 (C═O), 170.0 (C═O), 170.5 (C═O), 170.8 (C═O), 171.2 (C═O); EIMS (70 eV) *m*/*z* (relative intensity 498 (4), 483 (7), 439 (24), 425 (35), 424 (35), 412 (7), 410 (26), 369 (23), 341 (8), 325 (6), 311 (18), 239 (4); HR-FABMS *m*/*z* (relative intensity) 932.8060 $[M + Na]^+$ (5), 911 $[M + H]^+$ (3), 910 $[M]^+$ (7), 864 (3 850 (7), 790 (4), 308 (3), 264 (8), 154 (10), 137 (22), 107 (22), 69 (60), 54 (100).

Synthesis of Phytosphingosine 4. 3,4,6-Tri-*O*-acetyl-1,2-*O*-(1-methoxyethylidene)-α-D-galactopyranose (5). To penta-*O*-acetyl-β-D-galactopyranose (16.0 g, 41.0 mmol) was added 30% HBr/AcOH (30 mL), and the mixture was stirred for 3 h at room temperature and then evaporated with toluene under reduced pressure to afford the bromide derivative (∼90%). ^1H NMR (δ, $CDCl_3$) 1.97 (3H, s, OAc), 2.01 (3H, s, OAc), 2.07 (3H, s, OAc), 2.11 (3H, s, OAc), 4.07 (1H, dd, *J* = 6.8, 11.4 Hz, H_a-6), 4.15 (1H, dd, *J* = 6.3, 11.4 Hz, H_b-6), 4.45 (1H, t, *J* = 6.6 Hz, H-5), 5.00 (1H, dd, *J* = 3.9, 10.6 Hz, H-2), 5.36 (1H, dd, *J* = 3.2, 10.6 Hz, H-3), 5.48 (1H, dd, *J* = 1.1, 3.2 Hz, H-4), 6.66 (1H, d, *J* = 3.9 Hz, H-1); ^{13}CNMR (δ, $CDCl_3$) 20.4−20.6 (4 × OAc), 60.7 (C-6), 66.9 (C-4), 67.6 (C-2), 67.9 (C-3), 70.9 (C-5), 88.0 (C-1), 169.7−170.3 (4 × OAc). This compound, without purification, was dissolved in 1,2-dichloroethane (150 mL), and triethylamine (12 mL, 86.0 mmol), methanol (1.82 mL, 45.0 mmol), and tetrabutylammonium bromide (6.8 g, 21.2 mmol) were added. The mixture was stirred for 20 h at 45 °C, and the precipitated salt was removed by filtration. The filtrate was washed with brine and concentrated in vacuo. The residue was chromatographed over silica gel and eluted with *n*-hexanes−EtOAc (7:3) to give **5** (12 g, 33.0 mmol, 80%). The physical and spectroscopic data were identical to those reported in the literature.[18]

3,4,6-Tri-*O*-benzyl-1,2-*O*-(1-methoxyethylidene)-α-D-galactopyranose (6). To a stirred solution of **5** (11.0 g, 30.3 mmol) in toluene (250 mL) were added KOH (17.5 g, 310.0 mmol) and benzyl bromide (25 mL, 35.9 g, 210.2 mmol). The mixture was gradually heated and refluxed for 4 h. It was then diluted with toluene and washed with water and brine. The organic phase was concentrated in vacuo, chromatographed over silica gel, and eluted with *n*-hexanes−EtOAc (4:1) to afford compound **6** (9.96 g, 19.69 mmol, 65%). The physical and spectroscopic data were identical to those reported in the literature.[18]

(2*S*,3*S*,4*R*)-2,3,5-Tribenzyloxy-4-formyloxypentanal (7). To a stirred solution of **6** (9.0 g, 17.77 mmol) in 1,4-dioxane was added 1 M H_2SO_4 (40 mL), and the mixture was refluxed for 3 h. The reaction mixture was cooled to room temperature, and then solid $NaHCO_3$ was carefully added until the mixture was neutralized. The precipitated salts were removed by filtration, and the filtrate was evaporated to dryness. The resulting residue was dissolved in $CHCl_3$ and washed with brine and concentrated. This residue was dissolved in EtOH−H_2O (4:1, 80 mL). Sodium metaperiodate (7.5 g, 35.34 mmol) was added, and the mixture was stirred for 24 h at room temperature. Then the solution was diluted with ether, washed with brine, and dried over $MgSO_4$ and the solvent was evaporated to give aldehyde **7** (6.52 g, 14.57 mmol, 82%) as an oil. $[\alpha]^{25}_D$ −3.2 (*c* 0.06, $CHCl_3$); IR ν_{max} (film, NaCl) 3429, 3063, 2927, 1790, 1734, 1698, 1501, 1496, 1454, 1250, 738, 698 cm^{-1}; ^1H NMR (δ, $CDCl_3$) 3.70 (2H, m, H_2-4), 4.02 (1H, dd, *J* = 1.7, 4.5 Hz, H-1), 4.17 (1H, dd, *J* = 4.6, 4.7 Hz, H-2), 4.47−4.76 (6H, m, 3-CH_2-benz), 5.44 (1H, dd, *J* = 5.0, 10.1 Hz, H-3), 7.28−7.41 (15H, m, 15CH-aromatic), 8.03 (1H, s, OCHO), 9.64 (1H, s, CHO); ^{13}C NMR (δ, $CDCl_3$) 67.8 (C-4), 71.8 (C-3), 73.0 (CH_2-benz), 73.2 (CH_2-benz), 74.2 (CH_2-benz), 77.5 (C-2), 82.6 (C-1), 127.0−128.6 (15C-aromatic), 136.8, 137.2, 137.5 (3C-aromatic), 160.3 (OCHO), 200.9 (CHO); HR-EIMS (70 eV) *m*/*z* (relative intensity) $[M]^+$ (absent), 327.1215 $[M - C_8H_{10}O]^+$ ($C_{19}H_{19}O_5$, calcd 327.1232) (3), 253 (8), 181 (7), 122 (5), 107 (7), 105 (15), 91 (100), 77 (9).

(2*R*,3*S*,4*R*)-1,3,4-Tribenzyloxy-5-docosen-2-ol (8). A suspension of heptadecyltriphenylphosphonium bromide (23.35 g, 40.2 mmol, prepared by the method of Duclos[22]) in THF (160 mL) was

stirred at 0 °C. *n*-BuLi (2.0 M in cyclohexane, 14 mL) was added dropwise. The resulting solution was stirred for 30 min, and then a solution of **7** (6.0 g, 13.4 mmol) in THF (10 mL) was added dropwise. The mixture was warmed to room temperature and stirred for 1 h. The reaction was quenched by adding water and extracted with ether, and the organic phase was dried over Na_2SO_4 and concentrated in vacuo. The residue was chromatographed over silica gel and eluted with *n*-hexanes−EtOAc (4:1), giving olefin **8** (4.39 g, 6.93 mmol, 51%) as an oil. $[\alpha]^{25}_D$ −13.3 (*c* 0.08, $CHCl_3$); IR ν_{max} (film, NaCl) 3446, 3031, 2922, 2853, 1723, 1604, 1496, 1454, 1270, 1091, 1027, 734, 697 cm^{-1}; ^1H NMR (δ, $CDCl_3$) 0.94 (3H, t, J = 6.3 Hz, CH_3-22), 1.2−1.4 (28H, br s, $14CH_2$ (8−21)), 2.00 (2H, m, H_2-7), 3.58 (2H, d, J = 5.8 Hz, 2 × H-1), 3.63 (1H, dd, J = 2.8, 5.5 Hz, H-3), 4.17 (1H, m, H-2), 4.40 (1H, d, J = 11.7 Hz, 1H-benz), 4.51 (4H, m, 3H-benz and H-4), 4.69 (1H, d, J = 11.3 Hz, 1H-benz), 4.77 (1H, d, J = 10.6 Hz, 1H-benz), 5.52 (1H, dd, J = 9.4, 10.5 Hz, H-5), 5.80 (1H, m, H-6), 7.26−7.36 (15H, m, 15CH-aromatic); ^{13}C NMR, (δ, $CDCl_3$) 14.1 (C-22), 22.7, 28.0, 29.3, 29.6, 29.7, 32.0 (C-7-C-21), 69.9 (C-2), 70.2 (CH_2-benz), 71.1 (C-1), 73.3 (CH_2-benz), 73.8 (CH_2-benz), 74.6 (C-4), 80.2 (C-3), 127.0 (C-5), 127.6−128.4 (15C-aromatic), 136.3 (C-6), 136.9, 138.2, 138.3 (3C-aromatic); HR-EIMS (70 eV) *m*/*z* (relative intensity) $[M]^+$ (absent), 491.3937 $[M - C_9H_{11}O_2]^+$ ($C_{34}H_{51}O_2$, calcd 491.3889) (1), 443 (1), 384 (2), 371 (3), 293 (2), 279 (3), 181 (7), 108 (4), 91 (100), 79 (6).

(5*E*)-(2*R*,3*R*,4*R*)-1,3,4-Tribenzyloxy-2-methanesulfonyloxy-5-docosene (9). A solution of **8** (4.2 g, 6.53 mmol) in pyridine (10 mL) was ice-cooled at 0 °C, and then mesyl chloride (1.05 mL, 13.57 mmol) was added. The mixture was stirred for 8 h at room temperature, then toluene was added, and the solution was concentrated in vacuo. The resulting residue was dissolved in ether, and the solution was washed successively with water and brine. The organic phase was dried over Na_2SO_4 and evaporated to dryness, and the residue was chromatographed over silica gel and eluted with *n*-hexanes−EtOAc (9:1) to afford sulfonate **9** (4.6 g, 6.38 mmol, 97%) as an oil. $[\alpha]^{25}_D$ +3.3 (*c* 0.008, $CHCl_3$); IR ν_{max} (film, NaCl) 2924, 2853, 1454, 1359, 1174, 1092, 971, 920, 803, 736, 698, 526 cm^{-1}; ^1H NMR (δ, $CDCl_3$) 0.88 (3H, t, J = 6.4 Hz, CH_3-22), 1.2−1.4 (30H, br s, $15CH_2$ (8−21)), 2.00 (2H, m, H_2-7), 2.94 (3H, s, SO_3CH_3), 3.51 (1H, dd, J = 3.6, 10.9 Hz, H_a-1), 3.67 (1H, dd, J = 4.0, 7.0 Hz, H_b-1), 3.78 (1H, dd, J = 4.1, 6.4 Hz, H-3), 4.17 (3H, m, 2 × benz and H-4), 4.51 (3H, m, benz), 4.77 (1H, d, J = 11.2 Hz, benz), 5.06 (1H, ddd, J = 3.8, 7.0, 7.4 Hz, H-2), 5.50 (1H, dd, J = 9.6, 10.9 Hz, H-5), 5.81 (1H, ddd, J = 7.2, 10.8, 11.2 Hz, H-6), 7.26−7.36 (15H, m, 15CH-aromatic); ^{13}C NMR (δ, $CDCl_3$) 14.1 (C-22), 22.7, 28.0, 29.3, 29.6, 29.7, 31.9 (C-7-C-21), 38.6 ($C-SO_3CH_3$), 69.5 (C-1), 70.0 (CH_2-benz), 73.4 (C-4), 73.4 (CH_2-benz), 74.8 (CH_2-benz), 79.3 (C-3), 80.8 (C-2), 126.3 (C-5), 127.5−128.4 (15C-aromatic), 137.4 (C-aromatic), 137.8 (C-aromatic), 138.3 (C-aromatic), 155.2 (C-6); EIMS (70 eV) *m*/*z* (relative intensity) 720 $[M]^+$ (absent), 371 (3), 279 (3), 253 (36), 181 (6), 91 (100).

(2*R*,3*R*,4*R*)-2-Methanesulfonyloxy-1,3,4-docosanetriol (10). To a solution of **9** (4.34 g, 6.02 mmol) in EtOH (40 mL) was added 10% Pd/C (0.5 g). The mixture was stirred for 24 h under a hydrogen atmosphere at room temperature and filtered through a pad of Celite, and the filtrate was concentrated to give **10** (2.6 g, 5.7 mmol, 95%) as an amorphous solid. $[\alpha]^{25}_D$ +16.8 (*c* 0.006, pyridine); IR ν_{max} (film, NaCl) 3367, 3209, 2915, 2849, 1166, 1020, 950, 920, 483 cm^{-1}; ^1H NMR (δ, pyridine-d_5) 0.74 (3H, t, J = 6.4 Hz, CH_3-22), 1.1−1.3 (32H, br s, $16CH_2$ (6−21)), 1.82 (2H, m, CH_2-5), 3.32 (3H, s, SO_3CH_3), 4.11 (1H, ddd, J = 2.1, 8.2, 10.5 Hz, H-4), 4.18 (1H, dd, J = 2.0, 8.5 Hz, H-3), 4.40 (2H, m, CH_2-1), 5.62 (1H, dt, J = 1.9, 5.9 Hz, H-2); ^{13}C NMR (δ, pyridine-d_5) 15.2 (C-22), 23.8, 26.9, 30.5, 30.9, 31.1, 33.0, 35.5 (C-(7−21)), 39.4 ($C-SO_3CH_3$), 63.2 (C-1), 71.7 (C-4), 74.9 (C-3), 85.7 (C-2); HR-EIMS (70 eV) *m*/*z* (relative intensity) $[M]^+$ (absent), 356.3282 $[M - OMs]^+$ ($C_{22}H_{44}O_3$, calcd 356.3290) (3), 338 (21), 325 (13), 320 (47), 281 (100), 264 (15), 151 (16), 137 (12), 123 (28), 113 (13).

(2*S*,3*S*,4*R*)-2-Azido-1,3,4-docosanetriol (11). Sodium azide (81.9 g, 29.38 mmol) was added to a solution of **10** (2.49 g, 5.51 mmol) in DMF (65 mL) at room temperature. The mixture was slowly heated to 100 °C, stirred for 3 h, then diluted with EtOAc and washed with water and brine. The organic phase was dried on Na_2SO_4 and concentrated in vacuo. The resulting residue was chromatographed over silica gel with $CHCl_3$−MeOH (9:1) to give triol **11** (1.45 g, 3.65 mmol, 66%) as an amorphous solid. $[\alpha]^{25}_D$ +26.6 (*c* 0.01, pyridine); IR ν_{max} (film, NaCl) 3339, 2915, 2848, 2113, 1463, 1350, 1200 cm^{-1}; ^1H NMR (δ, pyridine-d_5) 0.71 (3H, t, J = 6.5 Hz, CH_3-22), 1.1−1.3 (30H, m, $15CH_2$ (7−21)), 1.51 (1H, m, H_b-6), 1.75 (2H, m, H_a-6, H_b-5), 2.02 (1H, m, H_a-5), 4.08 (1H, br d, J = 6.0 Hz, H-4), 4.16 (1H, br d, J = 5.4 Hz, H-3), 4.26 (1H, br t, J = 2.5 Hz, H-2), 4.40 (1H, m, H_b-1), 4.52 (1H, m, H_a-1); ^{13}C NMR (δ, pyridine-d_5) 15.5 (C-22), 24.2, 27.6, 30.8, 31.3, 31.5, 33.3 (C-(6−21)), 35.4 (C-5), 63.2 (C-1), 67.9 (C-2), 73.6 (C-4), 77.3 (C-3); HR-EIMS (70 eV) *m*/*z* (relative intensity) $[M]^+$ (absent), 340.3352 $[M - OH - N_3]^+$ ($C_{22}H_{44}O_2^+$, calcd 340.3341) (11), 322 (10), 313 (18), 283 (15), 281 (88), 264, 137 (8), 123 (14), 109 (26). Anal. ($C_{22}H_{45}N_3O_3$) C, H, N.

(2*S*,3*S*,4*R*)-2-Amino-1,3,4-docosanetriol (4). To a solution of azide **11** (1.3 g, 3.25 mmol) in EtOH (100 mL) was added 10% Pd/C (0.3 g). The mixture was stirred for 24 h under a hydrogen atmosphere at room temperature. The Pd/C was then removed by filtration through a pad of Celite, and the filtrate was concentrated in vacuo. The resulting residue was chromatographed over silica gel with $CHCl_3$−MeOH−H_2O−25% NH_4OH (8:2:0.15:0.05) to give amine **4** (0.95 g, 2.54 mmol, 78%) as an amorphous solid. $[\alpha]^{25}_D$ +10.6 (*c* 0.01, pyridine); IR ν_{max} (film, NaCl) 3250, 3019, 2916, 2846, 1216, 757, 658 cm^{-1}; ^1H NMR (δ, pyidine-d_5) 0.82 (3H, t, J = 5.5 Hz, CH_3-22), 1.1−1.3 (30H, br s, $15CH_2$ (7−21)), 1.61 (1H, m, H_b-6), 1.80 (2H, m, H_a-6 and H_b-5), 2.23 (1H, m, H_a-5), 4.01 (1H, d, J = 4.5 Hz, H-2), 4.16 (1H, t, J = 8.0 Hz, H-4), 4.31 (1H, dd, J = 5.3, 7.6 Hz, H-3), 4.47 (2H, m, CH_2-1); ^{13}C NMR (δ, pyridine-d_5) 15.5 (C-22), 24.2, 27.3, 30.8, 31.2, 31.5, 33.4 (C-6−C-21), 36.1 (C-5), 58.7 (C-2), 63.6 (C-1), 75.2 (C-4), 76.0 (C-3); HR-EIMS (70 eV) *m*/*z* (relative intensity) $[M]^+$ (absent), 342.3383 $[M - CH_2OH]^+$ ($C_{21}H_{44}NO_2^+$, calcd 342.3372) (6), 324 (8), 308 (8), 90 (10), 60 (100). Anal. ($C_{22}H_{47}NO_3$) C, H, N.

Synthesis of Threo Series of Acids. Methyl (2*E*)-Eicosenoate (14). To a suspension of pyridinium chlorochromate (PCC) (17 g, 83.24 mmol) in anhydrous CH_2Cl_2 was added 1-octadecanol (15 g, 55.49 mmol). The mixture was stirred for 40 min. Then ether was added and the supernatant decanted from the black gum. The insoluble residue was washed with ether four times whereupon it became a black granular solid. The combined organic solutions were passed through a pad of Celite, and the filtrate was concentrated yielding the crude aldehyde **13**, which was used without further purification in the following reaction. To a nitrogen-flushed solution of NaH (1.33 g, 110.98 mmol) in 250 mL of freshly distilled benzene at 0 °C, trimethyl phosphonoacetate (110.98 mmol, 17.95 mL) was injected dropwise. After the solution was stirred for 30 min, crude aldehyde (∼15 g, 55.5 mmol) in benzene (10 mL) was added. The reaction mixture was stirred vigorously at room temperature until full consumption of the aldehyde (3 h) was observed (TLC). The mixture was diluted with EtOAc and washed with water and brine. The organic phase was dried over Na_2SO_4 and concentrated in vacuo. The resulting residue was chromatographed over silica gel with *n*-hexanes−EtOAc (19:1) to give **14** (10.48 g, 32.33 mmol, 58%) as an amorphous solid. IR ν_{max} (film, NaCl) 2916, 2850, 1722, 1656, 1471, 1436, 1266, 975, 716 cm^{-1}; ^1H NMR (δ, $CDCl_3$) 0.84 (3H, t, J = 6.5 Hz, CH_3-20), 1.2−1.4 (30H, br s, $15CH_2$ (5−19)), 2.17 (2H, m, CH_2-4), 3.68 (3H, s, OMe), 5.78 (1H, d, J = 15.6 Hz, H-2), 6.93 (1H, ddd, J = 6.9, 14.4, 15.6 Hz, H-3); ^{13}C NMR (δ, $CDCl_3$) 14.1 (C-20), 22.6, 29.1, 29.3, 29.5, 29.7, 31.9, 32.2 (C-(4−19)), 51.2 (OMe), 120.8 (C-2), 149.7 (C-3), 167.0 (C-1); HR-EIMS (70 eV) *m*/*z* (relative intensity) 324.3011 $[M]^+$ ($C_{21}H_{40}O_2$, calcd 324.3028) (20), 311 (21), 292 (100), 250 (21), 227 (28), 113 (18), 97 (14), 87 (32).

General Experimental Procedure for Asymmetric Dihydroxylation of α,β-Unsaturated Ester (14). A solution of 0.88 g of AD-mix-β (or AD-mix-α) in *t*-BuOH−H_2O (1:1, 50 mL) was stirred vigorously at room temperature for 30 min. Then methane-

sulfonamide (73.4 mg, 0.77 mmol) was added, and the stirring was continued for 10 min. After the reaction mixture was cooled to 0 °C, ester **14** (215 mg, 0.66 mmol) was added and the reaction mixture was stirred vigorously at this temperature until no change was observed by TLC (4 days). Then a solution of sodium sulfite was added to quench the reaction and stirring was continued for 60 min while the reaction mixture was allowed to warm to room temperature. The mixture was diluted with EtOAc and washed with water and brine. The organic phase was dried over Na_2SO_4 and concentrated in vacuo. The resulting residue was chromatographed over silica gel with *n*-hexanes−EtOAc (3:1) to give diol **15a** (92.4 mg, 0.25 mmol, 37%).

Methyl (2*S*,3*R*)-2,3-Dihydroxyeicosanoate (15a). Amorphous solid; $[\alpha]^{25}_D$ +6.0 (*c* 0.004, $CHCl_3$); IR ν_{max} (film, NaCl) 3382, 2916, 2848, 1731, 1454, 1278, 1116, 1071, 721, 495, 479 cm^{-1}; ^1H NMR (δ, $CDCl_3$) 0.90 (3H, t, J = 5.5 Hz, CH_3-20), 1.10−1.30 (28H, br s, 14CH_2 (5−18)), 1.63 (3H, m, CH_2-19 and H_a-4), 1.91 (1H, d, J = 8.3 Hz, H_b-4), 3.85 (3H, s, OMe), 3.89 (1H, m, H-3), 4.12 (1H, dd, J = 1.9, 5.2 Hz, H-2); ^{13}C NMR (δ, $CDCl_3$) 14.1 (C-20), 22.7, 25.7, 29.3, 29.4, 29.5, 29.7, 31.9, 33.7 (C-(4−19)), 52.8 (OMe), 72.4 (C-3), 73.0 (C-2), 174.1 (C-1); HR-EIMS (70 eV) *m*/*z* (relative intensity) 358.3054 $[M]^+$ ($C_{21}H_{42}O_4$, calcd 358.3083) (0.1), 340 (6), 299 (6), 281 (11), 269 (3), 125 (2), 119 (2), 111 (4), 97 (8), 90 (100), 83 (9), 71 (5), 69 (8).

Methyl (2*R*,3*S*)-2,3-Dihydroxyeicosanoate (15b). Amorphous solid; $[\alpha]^{25}_D$ −4.4 (*c* 0.006, $CHCl_3$). The IR, MS, and ^1H and ^{13}C NMR data were identical to those of **15a**.

General Experimental Procedure for the Preparation of Diacetoxy Acids. To a solution of **15a** (90 mg, 0.25 mmol) in THF was added a solution of 1 M NaOH, and the mixture was stirred at 50 °C for 24 h. Then the mixture was acidified with 5% HCl, extracted with ether, washed with water, dried over $MgSO_4$, and concentrated affording acid **16a**, which was treated with acetic anhydride in pyridine. The solution was stirred for 16 h at room temperature. The product was dried under vacuo to furnish **17a**.

(2*S*,3*R*)-2,3-Diacetoxyeicosanoic Acid (17a). Amorphous solid (95 mg, 0.22 mmol, 88%); $[\alpha]^{25}_D$ +16.0 (*c* 0.002, $CHCl_3$); IR ν_{max} (film, NaCl) 3417, 3063, 2919, 2872, 1722, 1651, 1496, 1459, 1362, 1275, 1207, 1071, 1026, 737, 698 cm^{-1}; ^1H NMR (δ, $CDCl_3$) 0.86 (3H, t, J = 6.8 Hz, CH_3-20), 1.10−1.30 (30H, br s, 15CH_2 (5−19)), 1.64 (1H, m, H_a-4), 1.70 (1H, m, H_b-4), 2.09 (OAc), 2.21 (OAc), 5.19 (1H, s, H-2), 5.39 (1H, br s, H-3); ^{13}C NMR (δ, $CDCl_3$) 14.1 (C-20), 20.4 (OAc), 20.8 (OAc), 22.7, 25.2, 29.2, 29.3, 29.4, 29.5, 29.7, 30.3, 31.9 (C-4 and C-19), 72.0 (C-3), 72.1 (C-2), 170.3 (OAc), 170.6 (OAc), 171.7 (C-1); HR-EIMS (70 eV) *m*/*z* (relative intensity) 428.3144 $[M]^+$ ($C_{24}H_{44}O_6$, calcd 428.3138) (0.2), 383 (10), 369 (4), 354 (3), 350 (7), 341 (11), 326 (52), 325 (4), 311 (8), 308 (72), 295 (9), 290 (10), 281 (36), 264 (8), 135 (9), 125-(11), 118 (17), 100 (100).

(2*R*,3*S*)-2,3-Diacetoxyeicosanoic Acid (17b). Amorphous solid; $[\alpha]^{25}_D$ −12.0 (*c* 0.003, $CHCl_3$). The IR, MS, and ^1H and ^{13}C NMR data were identical to those of **17a**.

Synthesis of Erythro Series of Acids. General Experimental Procedure for the Preparation of Alcohols 21a and 21b. Hexadecylphosphonium bromide (850 mg, 1.5 mmol) and anhydrous tetrahydrofuran (10 mL) were mixed in a round-bottom flask at −20 °C under argon atmosphere. *n*-Butyllithium (1.7 M in *n*-hexane, 0.93 mL, 1.5 mmol) was added dropwise to the solution. After 30 min at 0 °C, the mixture was cooled to −20 °C, followed by the addition of **20a** (80 mg, 0.5 mmol) in THF (5 mL). After 1 h at −20 °C, the mixture was allowed to warm to room temperature. The mixture was extracted with CH_2C1_2 (10 mL) and then washed with water (10 mL). The organic layers were dried over $MgSO_4$. Removal of the solvent afforded the crude olefin, which was further purified by silica gel column chromatography to yield a cis−trans mixture of the olefin (145 mg, 78%). A suspension of this alcohol (120 mg, 0.326 mmol) and Pd/C (10% w/w, 5 mg) in MeOH (10 mL) was stirred for 12 h under an atmosphere of hydrogen. Then the catalyst was filtered off and carefully rinsed with CH_2Cl_2. The combined filtrates were evaporated and the crude product was purified by flash chromatography to give compound **21a** (120 mg, 99%).

(2*S*,3*R*)-2,3-*O*-Isopropylideneicosanol (21a). Amorphous solid; $[\alpha]^{25}_D$ −6.0 (*c* 0.015, $CHCl_3$); IR ν_{max} (film, NaCl) 3443, 2919, 2852, 1464, 1375, 1246, 1217, 1044 cm^{-1}; ^1H NMR (δ, $CDCl_3$, 400 MHz) 0.84 (3H, br s), 1.22−1.30 (32H, m), 1.36 (3H, s), 1.44 (3H, s), 3.57 (1H, br s), 4.11 (1H, br s); ^{13}C NMR (δ, $CDCl_3$) 13.8, 22.4, 25.2, 26.4, 28.0, 28.6, 29.1, 29.2, 29.3, 29.4, 31.6, 61.5, 76.8, 77.8, 107.7; HR-EIMS (70 eV) *m*/*z* (relative intensity) 369.3375 $[M - H]^{+\bullet}$ ($C_{23}H_{45}O_3$, calcd 369.3369) (3), 355.3204 $[M - CH_3]^+$ ($C_{22}H_{43}O_3$, calcd 355.3212) (100), 340.2971 $[M - 2CH_3]^+$ ($C_{21}H_{40}O_3$, calcd 340.2977) (14), 339.3251 $[M - CH_2OH]^+$ ($C_{22}H_{43}O_2$, calcd 339.3263) (58).

(2*R*,3*S*)-2,3-*O*-Isopropylideneicosanol (21b). Amorphous solid; $[\alpha]^{25}_D$ +7.7 (*c* 0.012, $CHCl_3$). The IR, MS, and ^1H and ^{13}C NMR data were identical to those of **21a**.

General Experimental Procedure for the Preparation of Isopropylidene Acids. Alcohol **21a** (100 mg, 0.27 mmol) was dissolved in a mixture of $CH_3CN-CCl_4-H_2O$ (2:2:3) (0.54 mL: 0.54 mL:0.81 mL) and treated with sodium metaperiodate (202 mg, 0.945 mmol). To this biphasic solution, an amount of 4.3 mg (2.2 mol %, 5.9×10^{-3} mmol) of ruthenium trichloride hydrate was added, and the entire mixture was stirred vigorously for 2 h at room temperature. Then CH_2C1_2 (10 mL) was added, and the phases were separated. The upper aqueous phase was extracted three times with CH_2C1_2. The combined organic extracts were dried ($MgSO_4$) and concentrated. The resulting residue was diluted with ether (20 mL), filtered through a Celite pad, and concentrated. The crude product was purified by column chromatography, affording 40 mg (38%) of acid **22a**.

(2*R*,3*R*)-2,3-*O*-Isopropylideneicosanoic Acid (22a). Amorphous solid; $[\alpha]^{25}_D$ −15 (*c* 0.01, $CHCl_3$); IR ν_{max} (film, NaCl) 3421, 2916, 2849, 1700, 1462, 1410, 1297, 942, 721 cm^{-1}; ^1H NMR (δ, $CDCl_3$, 400 MHz) 0.85 (3H, m), 1.17−1.33 (28H, m), 1.33 (3H, s), 1.50 (3H, s), 4.26 (1H, br s), 4.52 (1H, br s); ^{13}C NMR (δ, $CDCl_3$) 13.8, 22.4, 29.1, 29.4, 29.5, 31.6, 77.0, 78.5, 108.7, 187.5; HR-FABMS (relative intensity) 385.3315 $[M + H]^+$ ($C_{23}H_{45}O_4^+$, calcd 385.3318), 384.3250 $[M]^+$ ($C_{23}H_{44}O_4^+$, calcd 384.3240), 383.3152 $[M - H]^+$ ($C_{23}H_{43}O_4^+$, calcd 383.3161), 369.2995 $[M - CH_3]^+$ ($C_{23}H_{41}O_4^+$, calcd 369.3005) (100), 339.3251 $[M - COOH]^+$ ($C_{22}H_{43}O_2^+$, calcd 339.3263) (23), 326 (6), 309.2804 $[M - COOH - 2CH_3]^+$ ($C_{20}H_{37}O_2^+$, calcd 309.2794) (8), 281 (8), 264 (6), 149 (11), 137 (11).

(2*S*,3*S*)-2,3-*O*-Isopropylideneicosanoic Acid (22b). Amorphous solid; $[\alpha]^{25}_D$ +18 (*c* 0.02, $CHCl_3$). The IR, MS, and ^1H and ^{13}C NMR data were identical to those of **22a**.

General Experimental Procedure for the Preparation of Amides 23a and 23b. Activation Using HOBt/EDCI. To a mixture of acid **22a** (22 mg 0.057 mmol), amine **4** (21.4 mg, 0.0128 mmol), and 1-hydroxybenzotriazole (HOBt) (23.2 mg, 0.17 mmol) in dry CH_2Cl_2 (2 mL) was added EDCI (16.4 mg, 0.086 mmol). The reaction mixture was stirred for 24 h, and then it was extracted with AcOEt. The organic layers were washed using a saturated solution of NaCl and dried over $MgSO_4$. Removal of the solvent afforded the crude product **23a**, which was further purified by silica gel column chromatography to yield 14 mg (33%) of the coupling product.

Acid Activation Using Hydroxysuccinimide. To a solution of acid **22a** (25 mg, 0.065 mmol) and *N*-hydroxysuccinimide (9 mg, 0.078 mmol) in dry CH_2Cl_2 (0.8 mL) at 0 °C was added EDCI (13 mg, 0.070 mmol) in dry CH_2Cl_2 (1.0 mL). The solution was stirred for 12 h at room temperature and then filtered, and the solvent was removed in vacuo. The remaining solid was dissolved in CH_2-Cl_2 and filtered and the solvent was removed in vacuo to give a crude product that was used after purification. Sphingosine **4** (21 mg, 0.056 mmol) was dissolved in THF (1 mL), followed by addition of Et_3N (27 μL, 2 equiv) and the solution of *N*-succinimidyl derivative (3.72 mmol) in THF. After the mixture was stirred for 15 h, the precipitate was removed by filtration. The organic layer was then concentrated under reduced pressure, and the crude product

was purified by column chromatography to give 22 mg of a colorless solid (53%).

(2*S*,3*S*,4*R*,2′*R*,3′*R*)-2-(2′,3′-*O*-Isopropylideneicosanoylamino)-1,3,4-docosanetriol (23a). Amorphous solid; $[\alpha]^{25}_D$ −11.8 (*c* 0.022, $CHCl_3$); IR ν_{max} (film, NaCl) 2917, 2850, 1658, 1529, 1467, 1216, 1081 cm^{-1}; ^1H NMR (δ, $CDCl_3$, 400 MHz) 0.87 (6H, m), 1.21−1.35 (62H, m), 1.37 (3H, s), 1.35−1.60 (2H, m), 1.60−1.80 (2H, m), 1.56 (3H, s), 3.55−3.70 (2H, m), 3.75 (1H, dd, *J* = 5.7, 11.5 Hz), 3.88 (1H, dd, *J* = 2.4, 11.5 Hz), 4.12 (1H, m), 4.36 (1H, m), 4.46 (1H, d, *J* = 7.2 Hz), 7.33 (1H, d, *J* = 8.0 Hz); ^{13}C NMR (δ, $CDCl_3$) 14.1, 22.7, 24.7, 25.7, 26.6, 27.4, 29.4, 29.7, 30.4, 31.9, 33.2, 52.6, 61.4, 72.4, 76.5, 77.6, 77.7, 109.4, 170.7; HR-FABMS (relative intensity) 740.6797 $[M + H]^+$ ($C_{49}H_{90}NO_6^+$, calcd 740.6768) (22), 682 (16), 664 (17), 356 (10), 338 (16).

(2*S*,3*S*,4*R*,2′*S*,3′*S*)-2-(2′,3′-*O*-Isopropylideneicosanoylamino)-1,3,4-docosanetriol (23b). Amorphous solid; $[\alpha]^{25}_D$ −5 (*c* 0.018, $CHCl_3$); IR ν_{max} (film, NaCl) 2917, 2849, 1660, 1530, 1468, 1371, 1214, 1066 cm^{-1}; ^1H NMR (δ, $CDCl_3$, 400 MHz) 0.88 (6H, m), 1.15−1.37 (62H, m), 1.38 (3H, s), 1.40−1.80 (4H, m), 1.55 (3H, s), 3.63 (3H, m), 3.75 (1H, dd, *J* = 5.8, 11.1 Hz), 3.93 (1H, b dd, *J* = 2.5, 11.4 Hz), 4.12 (1H, m), 4.33−4.39 (1H, m), 4.47 (1H, d, *J* = 7.4 Hz), 7.35 (1H, d, *J* = 7.7 Hz); ^{13}C NMR (δ, $CDCl_3$) 13.8, 22.4, 24.4, 25.4, 26.3, 27.1, 29.1, 29.2, 29.3, 29.42, 29.46, 30.0, 31.6, 33.0, 52.4, 61.6, 72.5, 76.0, 77.4, 77.5, 109.2, 170.4; HR-FABMS (relative intensity) 740.6732 $[M + H]^+$ ($C_{49}H_{90}NO_6^+$, calcd 740.6768) (100), 682 (32), 664 (52), 398 (45), 356 (34), 338 (26).

General Experimental Procedure for the Preparation of Pentaacetate Ceramides 24 and 25. The acetonide **23a** (13 mg, 0.017 mmol) was treated with 3% HCl−MeOH (3 mL) and stirred at room temperature for 12 h. Then the mixture was neutralized with Et_3N. After removal of the MeOH in vacuo, the obtained white solid was dissolved in pyridine (2 mL) and an excess of Ac_2O was added. After 8 h, the reaction product was extracted with CH_2Cl_2 (3 × 10 mL) and the organic layer was washed with brine, dried ($MgSO_4$), and filtered. The solvent was removed in vacuo to give a white solid, which was purified by column chromatography to yield pure **24** (10 mg, 65%).

(2*S*,3*S*,4*R*,2′*R*,3′*R*)-2-(2′,3′-Diacetoxyeicosanoylamino)-1,3,4-triacetoxydocosane (24). Amorphous solid; $[\alpha]_D$ −7.5 (*c* 0.02, $CHCl_3$). Anal. ($C_{52}H_{95}NO_{11}$) C, H. N: calcd, 10.52; found, 10.07. The IR, MS, and ^1H and ^{13}C NMR data were identical to those of **2a**.

(2*S*,3*S*,4*R*,2′*S*,3′*S*)-2-(2′,3′-Diacetoxyeicosanoylamino)-1,3,4-triacetoxydocosane (25). Amorphous solid; $[\alpha]^{25}_D$ −2.0 (*c* 0.035, $CHCl_3$); IR ν_{max} (film, NaCl) 2918, 2850, 1746, 1698, 1523, 1467, 1371, 1225, 1047 cm^{-1}; ^1H NMR (δ, $CDCl_3$) 0.87 (6H, m), 1.15−1.35 (62H, m), 1.55−1.75 (4H, m), 2.04 (9H, br s), 2.08 (3H, s), 2.22 (3H, s), 4.07 (1H, dd, *J* = 3.2, 11.7 Hz), 4.20 (1H, dd, *J* = 5.6, 11.6 Hz), 4.44−4.50 (1H, m), 4.81−4.85 (1H, m), 5.04 (1H, dd, *J* = 3.6, 7.5 Hz), 5.19−5.26 (1H, m), 5.33 (1H, d *J* = 3.0 Hz), 6.76 (1H, d *J* = 9.2 Hz); ^{13}C NMR (δ, $CDCl_3$) 13.9, 20.5, 20.6, 20.8, 22.4, 25.2, 25.2, 28.4, 29.1, 29.2, 29.3, 2935, 31.7, 47.3, 62.3, 72.1, 72.5, 72.8, 73.8, 166.4, 169.2, 170.0, 170.1, 170.5, 170.8; HR-FABMS *m*/*z* (relative intensity) 932 (6), 910.6927 $[M + H]^+$ ($C_{52}H_{96}NO_{11}^+$, calcd 910.6983) (12), 850 (20), 790 (22), 320 (22). Anal. ($C_{52}H_{95}NO_{11}$) C, H. N: calcd, 10.52; found, 9.97.

General Experimental Procedure for the Preparation of Pentaacetate Ceramides 26−27. To a mixture of acid **17a** (8 mg, 0.0128 mmol), amine **4** (5.5 mg, 0.0128 mmol), and 1-hydroxybenzotriazole (HOBt) (5 mg, 0.037 mmol) in dry CH_2Cl_2 (2 mL) was added EDCI (3.68 mg, 0.0192 mmol). The reaction mixture was stirred for 48 h, and then it was extracted with AcOEt. The organic layers were washed using a saturated solution of NaCl and dried over $MgSO_4$. This residue was dissolved in pyridine. Acetic anhydride was added, and the solution was stirred for 24 h at room temperature. The product was dried in vacuo to furnish **26**.

(2*S*,3*S*,4*R*,2′*S*,3′*R*)-2-(2′,3′-Diacetoxyeicosanoylamino)-1,3,4-triacetoxydocosane (26). Amorphous solid (6.8 mg, 0.0074 mmol, 58%); $[\alpha]^{25}_D$ +8.5 (*c* 0.02, $CHCl_3$); IR ν_{max} (film, NaCl) 3285, 2918, 2850, 1746, 1698, 1469, 1372, 1220, 1044 cm^{-1}; ^1H NMR (δ, $CDCl_3$) 0.87 (6H, t, *J* = 6.5 Hz, Me-22 and Me-20′), 1.20−1.40 (62H, br s, 31-CH_2), 1.60 (4H, m, CH_2-5 and CH_2-4′), 2.03 (3H, s, OAc), 2.04 (6H, s, OAc), 2.08 (3H, s, OAc), 2.27 (3H, s, OAc), 4.04 (1H, dd, *J* = 3.1, 11.6 Hz, H_a-1), 4.13 (1H, dd, *J* = 5.4, 11.7 Hz, H_b-1), 4.45 (1H, m, H-2), 4.80 (1H, dd, *J* = 6.7, 9.7 Hz, H-4), 5.05 (1H, dd, *J* = 3.4, 7.9 Hz, H-3), 5.23 (1H, d, *J* = 3.1 Hz, H-3′), 5.31 (1H, m, H-2′), 6.62 (1H, d, *J* = 9.4 Hz, N−H); ^{13}C NMR (δ, $CDCl_3$) 14.1 (C-22 and C-20′), 20.6 (2 × OAc), 20.7 (OAc), 20.9 (2 × OAc), 25.1−31.9 [C−(5−21) and C−(4′-19′)], 47.6 (C-2), 62.7 (C-1), 72.0 (C-3), 73.3 (C-3′), 72.8 (C-4), 74.0 (C-2′), 167.4 (C-1′), 169.3 (C═O), 169.8 (C═O), 170.3 (C═O), 170.7 (C═O), 171.0 (C═O); HR-EIMS (70 eV) *m*/*z* (relative intensity) $[M]^+$ (absent), 790.6172 $[M - C_5H_{11}O_3]^+$ ($C_{47}H_{84}NO_8^+$, calcd 790.6197) (83), 776 (42), 747 (36), 730 (26), 687 (13), 669 (26); 656 (27), 627 (18), 599 (11), 512.3546 ($C_{28}H_{50}NO_7^+$, calcd 512.3587) (86), 484.3729 ($C_{28}H_{52}O_6^+$, calcd 484.3764) (75), 452 (44), 428 (24), 424 (19), 411.3085 ($C_{24}H_{43}O_5^+$, calcd 411.3110) (46), 392 (100), 383 (33), 369 (42), 364 (12), 341 (39), 320 (20). Anal. ($C_{52}H_{95}NO_{11}$) C, H. N: calcd, 10.52; found, 11.0.

(2*S*,3*S*,4*R*,2′*R*,3′*S*)-2-(2′,3′-Diacetoxyeicosanoylamino)-1,3,4-triacetoxydocosane (27). Amorphous solid (7.1 mg, 0.0074 mmol, 44%); $[\alpha]^{25}_D$ +15.3 (*c* 0.004, $CHCl_3$); IR ν_{max} (film, NaCl) 3286, 2917, 2852, 1744, 1699, 1470, 1370, 1220, 1044 cm^{-1}; ^1H NMR (δ, $CDCl_3$) 0.86 (6H, t, *J* = 6.5 Hz, Me-22 and Me-20′), 1.20−1.40 (62H, br s, 31-CH_2), 1.59 (4H, m, CH_2-5 and CH_2-4′), 2.00 (3H, s, OAc), 2.06 (3H, s, OAc), 2.07 (3H, s, OAc), 2.08 (3H, s, OAc), 2.27 (3H, s, OAc), 4.01 (1H, dd, *J* = 3.6, 11.7 Hz, H_a-1), 4.33 (1H, dd, *J* = 7.1, 11.7 Hz, H_b-1), 4.46 (1H, m, H-2), 4.95 (1H, td, *J* = 3.4, 7.5 Hz, H-4), 5.01 (1H, dd, *J* = 4.3, 6.0 Hz, H-3), 5.24 (1H, d, *J* = 3.6 Hz, H-3′), 5.33 (1H, m, H-2′), 6.68 (1H, d, *J* = 9.1 Hz, N−H); ^{13}C NMR (δ, $CDCl_3$) 14.1 (C-22 and C-20′), 20.6 (2OAc), 20.7 (OAc), 20.8 (OAc), 21.0 (OAc), 25.1−31.9 [C-(5−21) and C-(4′−19′)], 48.4 (C-2), 62.1 (C-1), 72.3 (C-3), 72.6 (C-3′), 72.9 (C-4), 73.7 (C-2′), 167.4 (C-1′), 169.3 (C═O), 169.7 (C═O), 170.3 (C═O), 170.6 (C═O), 171.1 (C═O); EIMS (70 eV) *m*/*z* (relative intensity) $[M]^+$ (absent), 792 (14), 790 (84), 777 (22), 776 (41), 748 (21), 747 (36), 730 (26), 729 (23), 716 (7), 687 (12), 669 (23); 657 (12), 599 (12), 424 (19), 411 (46), 392 (100), 383 (33), 369 (43). Anal. ($C_{52}H_{95}NO_{11}$) C, H, N.

Cell Culture. Human SK-MEL-1 melanoma cells (DSMZ No. ACC 303, DSMZ, German Collection of Microorganisms and Cell Cultures, Braunschweig, Germany) were grown in RPMI 1640 (Sigma) supplemented with 10% (v/v) heat-inactivated fetal bovine serum (Sigma) and 100 units/mL penicillin and 100 μg/mL streptomycin at 37 °C in a humidified atmosphere containing 5% CO_2. The cell numbers were counted by a hematocytometer, and the viability was always greater than 95% in all experiments as assayed by the 0.025% trypan blue exclusion method. Stock solutions of 10 mM ceramides were made in ethanol/dodecane (49:1), and aliquots were frozen at −20 °C. Further dilutions were made in culture media just before use. In all experiments, the final concentration of ethanol/dodecane (49:1) did not exceed 0.5% (v/v), a concentration that is nontoxic to the cells. Cells were resuspended in fresh medium 24 h before each treatment.

Assay for Growth Inhibition and Cell Viability. The cytotoxicity of ceramides was assessed using the 3-[4,5-dimethylthiazol-2-yl]-2,5-diphenyltetrazolium bromide assay.[23] Briefly, 1 × 10^4 exponentially growing cells were seeded in 96-well microculture plates with various ceramide concentrations in a volume of 100 μL for 72 h at 37 °C. Controls were always treated with the same amount of ethanol−dodecane (49:1) as used in the corresponding experiments. Surviving cells were detected on the basis of their ability to metabolize 3-[4,5-dimethylthiazol-2-yl]-2,5-diphenyltetrazolium bromide (MTT) into formazan crystals. Optical density at 570 nm was used as a measure of cell viability. Cell survival was calculated as the fraction of cells alive relative to control for each point:

$$\text{cell survival (\%)} = \frac{\text{mean absorbance in treated cells}}{\text{mean absorbance in control wells}} \times 100$$

Concentrations inducing a 50% inhibition of cell growth (IC_{50}) were determined graphically for each experiment using the curve-fitting

routine of the computer software Prism 2.0 (GraphPad) and the equation derived by DeLean et al. (1978).[24]

Western Blot for PARP. Cells were treated with ceramides **1a** and **24**−**27**. After different times cells were pelleted by centrifugation and washed with ice-cold phosphate-buffered saline. Western blot analysis for PARP was performed as described (Rivero et al., 2003).[25]

Analysis of DNA Fragmentation. The presence of apoptosis was evaluated by agarose gel electrophoresis of DNA extracted from SK-MEL-1 melanoma cells. Briefly, cells (4×10^5) were washed with phosphate-buffered saline and incubated in 20 μL of 50 mM Tris-HCl (pH 8.0), 10 mM EDTA, 0.5% SDS, and 1 μg/μL RNase A (Sigma) at 37 °C for 1 h. Then 10 μg/μL proteinase K (Sigma) (2 μL) was added, and the mixture was incubated at 50 °C for 2 h more. DNA was extracted with 100 μL of phenol−chloroform−isoamyl alcohol and mixed with 5 μL of loading buffer. Samples were separated by electrophoresis at 40 V for 4 h through a 2% agarose gel in TAE buffer (40 mM Tris-acetate and 1.0 mM EDTA, pH 8.3). DNA bands were visualized under UV light after staining with ethidium bromide (0.5 μg/mL), and the images were captured by a digital camera (Kodak).

Acknowledgment. This work was supported in part by the Instituto Canario de Investigación del Cáncer (Grant G-05-09 to J.B. and F.L.), Programa de Iniciativa Comunitaria INTERREG IIIB Açores-Madeira-Canarias (Grant 04/MAC/3.5/C5), the Ministerio de Educación y Ciencia of Spain, and FEDER (Grant SAF 2004-07928 to F.E.), and the Dirección General de Universidades e Investigación of the Canary Islands Government (Grants GRUP-2004/44 and INFRA 2004:59 to F.E. and F.T. for a research studenship).

Supporting Information Available: ^{1}H NMR spectra of compounds **1a**, **2a**, and **24**−**27** and enlargement of the ^{1}H NMR spectra of compounds **1a** and **24**. This material is available free of charge via the Internet at http://pubs.acs.org.

References

(1) Bratton, S. B.; Walker, G.; Srinivasula, S. M.; Sun, X. M.; Butterworth, M.; Alnemri, E. S.; Cohen, G. M. Recruitment, activation and retention of caspases-9 and -3 by Apaf-1 apoptosome and associated XIAP complexes. *EMBO J.* **2001**, *20*, 998−1009.

(2) (a) Cohen, G. M. Caspases: the executioners of apoptosis. *Biochem. J.* **1997**, *326*, 1−16. (b) Earnshaw, W. C.; Martins, L. M.; Kaufmann, S. H. Mammalian caspases: structure, activation, substrates, and functions during apoptosis. *Annu. Rev. Biochem.* **1999**, *68*, 383−424.

(3) (a) Perry, D. K.; Hannun, Y. A. The role of ceramide in cell signalling. *Biochim. Biophys. Acta* **1998**, *1436*, 233−243. (b) Andrieu-Abadie, N.; Gouazé, V.; Salvayre, R.; Levade, T. Ceramide in apoptosis signaling: relationship with oxidative stress. *Free Radical Biol. Med.* **2001**, *31*, 717−728. (c) Mimeault, M. New advances on structural and biological functions of ceramide in apoptotic/necrotic cell death and cancer. *FEBS Lett.* **2002**, *530*, 9−16. (d) Reynolds, C. P.; Maurer, B. J.; Kolesnick, R. N. Ceramide synthesis and metabolism as a target for cancer therapy. *Cancer Lett.* **2004**, *206*, 169−180.

(4) Luberto, C.; Kraveka, J. M.; Hannun, Y. A. Ceramide regulation of apoptosis versus differentiation: A walk on a fine line. Lessons from neurobiology. *Neurochem. Res.* **2002**, *27*, 609−617.

(5) Kolesnick, R.; Fuks, Z. Radiation and ceramide-induced apoptosis. *Oncogene* **2003**, *22*, 5897−5906.

(6) Gulbins, E.; Kolesnick, R. Raft ceramide in molecular medicine. *Oncogene* **2003**, *22*, 7070−7077.

(7) Birbes, H.; Luberto, C.; Hsu, Y. T.; El Bawab, S.; Hannun, Y. A.; Obeid, L. M. A mitochondrial pool of sphingomyelin is involved in TNFα-induced Bax translocation to mitochondria. *Biochem. J.* **2005**, *386*, 445−451.

(8) Anishkin, A.; Sukharev, S.; Colombini, M. Searching for the molecular arrangement of transmembrane ceramide channels. *Biophys. J.* **2006**, *90*, 2414−2426.

(9) (a) Thon, L.; Mohlig, H.; Mathieu, S.; Lange, A.; Bulanova, E.; Winoto-Morbach, S.; Schutze, S.; Bulfone-Paus, S.; Adam, D. Ceramide mediates caspase-independent programmed cell death. *FASEB J.* **2005**, *19*, 1945−1956. (b) Rotolo, J. A.; Zhang, J.; Donepudi, M.; Lee, H.; Fuks, Z.; Kolesnick, R. Caspase-dependent and -independent activation of acid sphingomyelinase signaling. *J. Biol. Chem.* **2005**, *280*, 26425−34.

(10) González, A. G.; León, F.; Rivera, A.; Muñoz, C. M.; Bermejo, J. Lanostanoids triterpenes from *Ganoderma lucidum. J. Nat. Prod.* **1999**, *62*, 1700−1701.

(11) González, A. G.; León, F.; Rivera, A.; Padrón, J. I.; González-Plata, J.; Zuluaga, J.; Quintana, J.; Estévez, F.; Bermejo, J. New lanostanoids from *Ganoderma concinna. J. Nat. Prod.* **2002**, *65*, 417−421.

(12) León, F.; Valencia, M.; Rivera, A.; Nieto, I.; Quintana, J.; Estévez, F.; Bermejo, J. Novel cytostatic lanostanoid triterpenes from *Ganoderma australe. Helv. Chim. Acta* **2003**, *86*, 3088−3095.

(13) León, F.; Quintana, J.; Rivera, A.; Estévez, F.; Bermejo, J. Isolation of lanostane triterpenes from *Laetiporus sulphureus* that induce apoptosis in human myeloid leukemia cells. *J. Nat. Prod.* **2004**, *67*, 2008−2011.

(14) Setliff, E. C.; Ryvarden, L. Los hongos de Colombia VII: Some aphyllophoraceous wood-inhabiting fungi. *Mycotaxon* **1983**, *28*, 509−525.

(15) Zjawiony, J. K. Biologically active compounds from aphyllophorales (polypore) fungi. *J. Nat. Prod.* **2004**, *67*, 300−310.

(16) Lourenço, A.; Lobo, A. M.; Rodríguez, B.; Jimeno, M. L. Ceramides from the fungus *Phellinus pini. Phytochemistry* **1996**, *43*, 617−620.

(17) (a) Zhan, Z. J.; Yue, J. M. New glycosphingolipids from the fungus *Catathelasma ventricosa. J. Nat. Prod.* **2003**, *66*, 1013−1016. (b) Gao, J. M.; Zhang, A. L.; Zhang, C. L.; Liu, J. K. Paxillamide: A novel phytosphingosine derivative from the fruiting of *Paxillus panuoides. Helv. Chim. Acta* **2004**, *87*, 1483−1487.

(18) Asai, N.; Fusetani, N.; Matsunaga, S. Sex pheromones of the hair crab *Erimacrus isenbeckii.* II. Synthesis of ceramides. *J. Nat. Prod.* **2001**, *64*, 1210−1215.

(19) Gelas, J.; Horton, D. Acetonation of D-ribose and D-arabinose with alkyl isopropenyl ethers. *Carbohydr. Res.* **1975**, *45*, 181−195.

(20) Fokina, N. A.; Kornilov, A. M.; Kulik, I. B.; Kukhar, V. P. Towards optically pure mono- and difluorinated amino acids: common methodology based on (*R*)-2,3-*O*-isopropylideneglyceraldehyde. *Synthesis* **2002**, *17*, 2589−2596.

(21) Chang, Y. T.; Choi, J.; Ding, S.; Prieschl, E. E.; Baumruker, T.; Lee, J. M.; Chung, S. K.; Schultz, P. G. The synthesis and biological characterization of a ceramide library. *J. Am. Chem. Soc.* **2002**, *124*, 1856−1857.

(22) Duclos, R. I., Jr. The total syntheses of D-*erythro*-sphingosine, *N*-palmitoylshingosine (ceramide), and glucosylceramide (cerebroside) via an azidosphingosine analog. *Chem. Phys. Lipids* **2001**, *111*, 111−138.

(23) Mosmann, T. Rapid colorimetric assay for cellular growth and survival: application to proliferation and cytotoxicity assays. *J. Immunol. Methods* **1983**, *65*, 55−63.

(24) DeLean, A.; Munson, P. J.; Rodbard, D. Simultaneous analysis of families of sigmoidal curves: application to bioassay, radioligand assay and physiological dose-response curves. *Am. J. Physiol.* **1978**, *235*, E97−E102.

(25) Rivero, A.; Quintana, J.; Eiroa, J. L.; López, M.; Triana, J.; Bemejo, J.; Estévez, F. Potent induction of apoptosis by germacranolide sesquiterpene lactones on human myeloid leukemia cells. *Eur. J. Pharmacol.* **2003**, *482*, 77−84.

JM0605334

A New Ceramide from *Suillus luteus* and Its Cytotoxic Activity against Human Melanoma Cells

by **Francisco León**[a][b], **Ignacio Brouard**[a], **Fernando Torres**[b][c], **José Quintana**[b][c], **Augusto Rivera**[d], **Francisco Estévez**[c], and **Jaime Bermejo***[a]

[a]) Instituto de Productos Naturales y Agrobiología, C.S.I.C., Instituto Universitario de Bio-Orgánica 'Antonio González', Av. Astrofísico F. Sánchez 3, E-38206 La Laguna, Tenerife (phone: +34-922-250-766; fax: +34-922-318-571; e-mail: jbermejo@ull.es)

[b]) Instituto Canario de Investigación del Cáncer (ICIC), Av. Astrofísico F. Sánchez 2, E-38206 La Laguna, Tenerife

[c]) Departamento de Bioquímica, Centro de Ciencias de la Salud, Universidad de Las Palmas de Gran Canaria, E-35016 Las Palmas de Gran Canaria

[d]) Departamento de Química, Universidad Nacional de Colombia, Apartado Aéreo 14490, Bogotá, D.C., Colombia

A new phytosphingosine-type ceramide, suillumide (**1**), was isolated from the EtOH extract of the basidiomycete *Suillus luteus* (L.) S. F. Gray, along with ten known compounds: ergosta-4,6,8(14),22-tetraen-3-one, ergosterol, ergosterol peroxide, suillin, (*E*)-3,4,5-trimethoxycinnamic alcohol, 5α,6α-epoxyergosta-8,22-diene-3β,7β-diol, (*R*)-1-palmitoylglycerol, ergosta-7,9(11),22-triene-3β,5α,6β-triol, cerevisterol, and 4-hydroxybenzoic acid. The structure of **1** was determined on the basis of spectroscopic and mass-spectrometric analyses, as well as by chemical methods. Compound **1** and its synthetic diacetyl derivative **2** were tested for their cytotoxic activities against the human melanoma cell line SK-MEL-1. Both drugs showed IC_{50} values of *ca.* 10 μM after 72 h of exposure.

Introduction. – As a part of our research program on biologically active compounds isolated from Basidiomycetes from Colombia [1–3], we have studied the ectomycorrize fungus *Suillus luteus* (L.) S. F. Gray. The *Suillus* genus, included in the Boletal order, is widely distributed throughout the world and has been used as a model in the exclusive symbiotic interaction with pines [4]. Additionally, *Suillus* fungi show a special capacity to degrade soil contaminants (polycyclic and aromatic hydrocarbons) [5] as well as heavy metals [6]. In previous chemical studies of this genus, precedents of quinone-type compounds isolated from *Suillus granulatus*, *S. luteus*, and *S. placidus* [7], as well as tetraprenylphenols from *S. granulatus* and *S. bovinus*, with antibacterial activity and cytotoxicity against KB cells [8], have been described. The MeOH extract from *S. luteus* exhibited potent antioxidant [9] and cytotoxic activities [10].

Herein, we report on the isolation and characterization of a new phytosphingosine-type ceramide, suillumide (**1**), from *S. luteus*, together with ten known compounds, ergosta-4,6,8(14),22-tetraen-3-one [11], ergosterol and ergosterol peroxide [12], suillin [8], (*E*)-3,4,5-trimethoxycinnamic alcohol [13], 5α,6α-epoxyergosta-8,22-diene-3β,7β-diol [14], (*R*)-1-palmitoylglycerol [15], ergosta-7,9(11),22-triene-3β,5α,6β-triol [16], cerevisterol [2], and 4-hydroxybenzoic acid [17]. These metabolites were separated by column chromatography on silica gel from the EtOH extract of the fresh fruiting bodies

© 2008 Verlag Helvetica Chimica Acta AG, Zürich

of the fungus. The structures of the known compounds were determined by a combination of spectroscopic analysis and comparison with reported data. The cytotoxicity of ceramide **1** and its acetyl derivative **2** was assayed against the human melanoma SK-MEL-1 cell line.

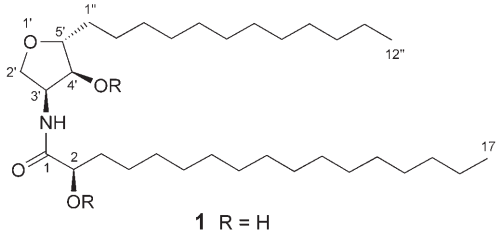

1 R = H
2 R = Ac

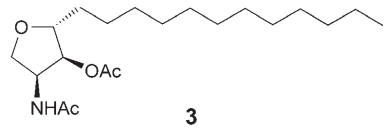

3

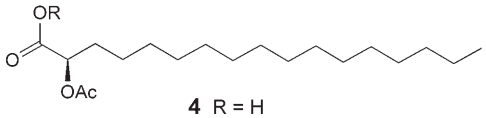

4 R = H
5 R = Me

Results and Discussion. – 1. *Compound Isolation and Characterization*. Compound **1** was obtained as a colorless, amorphous solid. The IR spectrum of **1** exhibited absorptions at 3463, 1638, and 1719 cm^{-1}, indicating OH, amide, and C=O groups, respectively, as well as characteristic signals for a tetrahydrofuran ring (1074 and 912 cm^{-1}) [18].

The ^{1}H-NMR spectrum of **1** (*Table 1*) showed a *doublet* at δ(H) 6.98 (1 H), which was exchangeable upon addition of D_2O, confirming the presence of a secondary amide function. In addition, signals for five H-atoms at δ(H) 3.55–4.17, and four oxygenated C-atoms at δ(C) 70.11, 72.40, 77.40, and 84.93 in the ^{13}C-NMR spectrum (*Table 1*) pointed to the presence of OH and/or other oxygenated groups. The overlapped signals at δ(H) 1.27–1.41 in the ^{1}H-NMR spectrum, and the signals at δ(C) 22.67–31.91 in the ^{13}C-NMR spectrum inferred the presence of long aliphatic chains [19].

A consecutive sequence of ^{1}H,^{1}H-COSY correlations (*Fig. 1*), starting from CH_2(2′) and going to CH_2(1″), as well as correlations from the terminal Me signal with aliphatic $(CH_2)_n$ signals in the carbon skeleton allowed us to establish the connectivity $CH_2-CH(NH)-CH(-O)-CH(-O)-CH_2-(CH_2)_n-Me$, a partial structure of sphingosine. In addition, a second partial structure, $CO-CH(-O)-(CH_2)_n-Me$ was evident from the ^{1}H,^{1}H-COSY experiment, which indicated the presence of two long aliphatic chains.

Table 1. *^{1}H- and ^{13}C-NMR Data of* **1** *and* **2**. At 400/100 MHz, resp., in $CDCl_3$; δ in ppm, J in Hz. Assignments were confirmed by DEPT, ^{1}H,^{1}H-COSY, HSQC, and HMBC experiments. Arbitrary atom numbering.

Position	**1**		**2**	
	δ(C)	δ(H)	δ(C)	δ(H)
1	174.94	–	174.94	–
2	72.40	4.13 (*dd*, *J* = 3.6, 8.1)	74.11	5.13 (*dd*, *J* = 4.7, 7.4)
3	34.77	1.39–1.66 (*m*) 1.70–1.90 (*m*)	34.77	1.70–1.92 (*m*)
4–16	22.67–31.91	1.27–1.41 (*m*)	22.63–33.74	1.27–1.41 (*m*)
17	14.10	0.87 (*t*, *J* = 6.7)	14.06	0.87 (*t*, *J* = 6.7)
2′	70.11	3.55 (*dd*, *J* = 7.3, 9.0) 4.17 (*dd*, *J* = 7.0, 9.0)	69.90	3.53 (*dd*, *J* = 8.4, 8.5) 4.20 (*dd*, *J* = 7.0, 8.4)
3′	51.56	4.34–4.43 (*m*)	49.67	4.60 (*ddd*, *J* = 6.1, 7.0, 8.4)
4′	77.40	3.99 (*t*, *J* = 4.8)	77.20	4.90 (*dd*, *J* = 3.0, 6.1)
5′	84.93	3.71 (*dd*, *J* = 5.1, 12.2)	83.77	3.86 (*dd*, *J* = 5.2, 8.0)
1″	33.42	1.39–1.66 (*m*)	33.74	1.70–1.92 (*m*)
2″–11″	22.67–31.91		22.63–33.74	1.27–1.41 (*m*)
12″	14.10	–	14.06	0.87 (*t*, *J* = 6.7)
NH	–	6.98 (*d*, *J* = 7.8)	–	6.25 (*d*, *J* = 8.4)
AcO	–	–	169.8 (2C) 20.70, 20.85	2.10, 2.15 (2*s*)

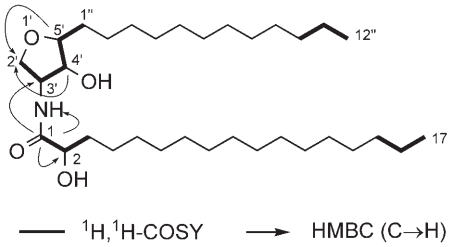

Fig. 1. *^{1}H,^{1}H-COSY and HMBC Correlations for* **1**

An HMBC experiment (*Fig. 1*) showed correlations between H–C(2′) and both C(4′) and C(5′), indicating the presence of an ether group between C(2′) and C(5′), belonging to a tetrahydrofuranyl ring. The C=O group at δ(C) 174.94 was assigned to C(1) on the basis of an HMBC correlation with H–C(2) at δ(H) 4.13. Both fragments were connected based on correlations between the amide H-atom and H–C(3′) at δ(H) 6.98 and 4.34–4.43, respectively, with the C=O C-atom.

To confirm the number of OH groups, compound **1** was acetylated with Ac_2O in pyridine at room temperature to afford the diacetate **2**. This compound showed two AcO signals [δ(H) 2.15, 2.10; δ(C) 20.70, 20.85, and 169.80 (two Me*C*O)] (*Table 1*), thereby confirming the presence of two OH groups in the original structure **1**.

The relative configuration at the tetrahydrofuranyl ring of **2** was deduced by a NOESY experiment (*Fig. 2*), which showed correlations between H_a–C(2′) and

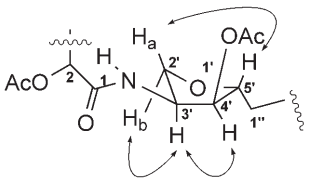

Fig. 2. *Key NOE correlations for* **2**

H−C(5′), and between H−C(3′) and both H−C(4′) and H_b−C(2′), indicating *cis*-configuration for the substituents at positions 3′ and 4′ of the tetrahydrofuranyl ring.

Basic hydrolysis of **1** (KOH, MeOH, H_2O) afforded a crude mixture, which was acetylated *in situ* (Ac_2O/pyridine) to yield the diacetate **3** and the mono-acetylated acid **4**; the latter was isolated as its methyl ester **5** upon exposure to an etheral solution of diazomethane. HR-EI-MS Analysis of **3** and **5** exhibited ion peaks at *m*/*z* 355.2756 and 342.2489, corresponding to the molecular formulae $C_{20}H_{37}NO_4$ and $C_{20}H_{38}O_4$, respectively. The chain lengths of both the amine and acyl units in **1** were, thus, unambiguously determined. The structure of **3** was further elucidated by ^{1}H-NMR and HR-EI-MS analyses. The optical rotation of the ester **5** ($[\alpha]_D^{20} = -2.53$), indicated the (*R*)-isomer [20].

From the above data, compound **1** was identified as (2*R*)-*N*-[(3*S**,4*S**,5*R**)-5-dodecyl-4-hydroxytetrahydrofuran-3-yl]-2-hydroxyheptadecanamide, and named *suillumide*. To the best of our knowledge, ceramides with a tetrahydrofuranyl ring are unusual, and some representatives have been found only in fungi [18][21].

2. *Cytotoxicity Assay.* We have assessed the cytotoxicity of suillumide (**1**) and its acetyl derivative **2** against human melanoma SK-MEL-1 cells, using the 3-(4,5-dimethylthiazol-2-yl)-2,5-diphenyltetrazolium bromide (MTT) dye-reduction assay. Both ceramides showed similar IC_{50} values of *ca.* 10 μM (*Table 2*), indicating that the introduction of an Ac group in the ceramide skeleton does not play a crucial role in their cytotoxicity. Etoposide was used as a positive control.

Table 2. *Effects of* **1** *and* **2** *on the Growth of Human Melanoma Cells* (SK-MEL-1). The data represent means ± S.E.M. of three independent experiments with three determinations each. For details, see *Exper. Part*.

Compound	IC_{50} [μM]
1	9.7 ± 2.4
2	11.6 ± 1.7
Etoposide[a])	16.1 ± 4.0

[a]) Positive control.

This work was supported, in part, by grants from the Instituto Canario de Investigación del Cáncer (G-04-09, to *J. B.*), the *Ministerio de Educación y Ciencia* of Spain, and *FEDER* (SAF 2004-07928, to *F. E.*), and the *Dirección General de Universidades e Investigación* of the Canary Islands Government (GRUP-2004/44 and EQU2005/078, to *F. E.*). *F. T.* was supported by a research studentship from the *Dirección General de Universidades e Investigación* of the Canary Islands Government.

Experimental Part

General. Column chromatography (CC): silica gel *60* (230–400 mesh; *Merck*). Thin-layer chromatography (TLC): silica gel *60* $PF_{254+366}$ plates (1 mm thickness; *Merck*) and *Sephadex LH-20* (*Aldrich*). M.p.: *Büchi B-540* apparatus; uncorrected. Optical rotations: *Perkin-Elmer-343* polarimeter. IR Spectra: *Bruker IFS55* spectrophotometer; in cm^{-1}. ^1H- and ^{13}C-NMR Spectra: *Bruker AMX-400* spectrometer, standard pulse sequences, at 400/100 MHz, resp., in $CDCl_3$ soln.; δ in ppm rel. to Me_4Si, J in Hz. EI-MS and HR-EI-MS: *Micromass Autospec* (70 eV) mass spectrometer; in m/z (rel. %).

Plant Material. The fungus *Suillus luteus* (L.) S. F. Gray was collected in the *Parque Nacional Natural del Embalse del Neusa*, Colombia, in May 2000, and was identified by Prof. *Luis G. Henao*, Instituto de Ciencias Naturales, Universidad Nacional de Colombia, where a voucher specimen was deposited (Col. 444).

Extraction and Isolation. The body fungi (117 g) were ground and steeped in EtOH (96%) for 7 d. The EtOH extract (30 g) was subjected to CC (SiO_2; hexane/AcOEt 9:1, 8:2; 7:3; 1:1; 2:3, 0:1; then AcOEt/MeOH 9:1, 200 ml each) to yield seven fractions: *Fr. 1–Fr. 7. Fr. 1* (1.2 g), eluted with hexane/AcOEt 9:1, was purified by CC (1. SiO_2, benzene/Et_2O 48:2; 2. *Sephadex LH-20*, hexane/$CHCl_3$/MeOH 1:1:1) to yield ergosta-4,6,8(14),22-tetraen-3-one (20 mg) and ergosterol (900 mg). *Fr. 2* (300 mg), eluted with hexane/AcOEt 8:2, was subjected to CC (SiO_2; hexane/AcOEt 4:1) to afford ergosterol peroxide (30 mg). *Fr. 3* (400 mg), eluted with hexane/AcOEt 7:3, was subjected to CC (1. SiO_2, CH_2Cl_2/acetone 48:2; 2. *Sephadex LH-20*, hexane/AcOEt/MeOH 1:1:1) to yield suillin (12 mg) and (*E*)-3,4,5-trimethoxycinnamic alcohol (5 mg). *Fr. 4* (150 mg), eluted with hexane/AcOEt 1:1), was purified by prep. TLC (SiO_2; hexane/AcOEt 3:2; two runs) to afford pure **1** (20 mg). *Fr. 5* (1.0 g), eluted with hexane/AcOEt 2:3, was purified by CC (1. SiO_2, CH_2Cl_2/acetone gradient; 2. *Sephadex LH-20*, CH_2Cl_2/MeOH 1:1) to yield 5α,6α-epoxyergosta-8,22-diene-3β,7β-diol (9 mg) and (*R*)-1-palmitoylglycerol (20 mg). *Fr. 6* (1.2 g), eluted with AcOEt, was subjected to CC (SiO_2; CH_2Cl_2/MeOH 10:0→10:1) followed by prep. TLC (SiO_2; CH_2Cl_2/MeOH 9:1) to yield ergosta-7,9(11),22-triene-3β,5α,6β-triol (3 mg) and cerevisterol (20 mg). *Fr. 7* (1.3 g), eluted with AcOEt/MeOH 9:1, was purified by CC (1. SiO_2, $CHCl_3$/MeOH 10:0→10:2; 2. *Sephadex LH-20*, CH_2Cl_2/MeOH 2:1) and finally by repeated prep. TLC (SiO_2; hexane/AcOEt 9:1) to yield 4-hydroxybenzoic acid (15 mg).

Suillumide (=*(2*R*)*-N-*[(3*S**,4*S**,5*R**)-5-Dodecyl-4-hydroxytetrahydrofuran-3-yl]-2-hydroxyheptadecanamide*; **1**). Colorless, amorphous solid. $C_{33}H_{65}NO_4$ (539.87 g/mol). $[\alpha]_D^{25} = +16.3$ ($c = 0.1$, $CHCl_3$). IR (film, NaCl): 3463, 2964, 2925, 2856, 1719, 1638, 1597, 1540, 1455, 1382, 1255, 1074, 912. ^1H- and ^{13}C-NMR: *Table 1*. EI-MS: 539 (absent, M^+), 339 (14), 300 (30), 299 (17), 286 (19), 285 (82), 283 (10), 253 (21), 241 (16), 240 (23), 239 (100), 237 (21), 211 (21), 197 (48). Anal. calc. for $C_{33}H_{65}NO_4$: C 73.42, H 12.14, N 2.59; found: C 73.50, H 12.22, N 2.63.

Hydrolysis of **1** *and Derivatization*. A soln. of 1N KOH (5 ml) in MeOH/H_2O 9:1 was added to **1** (3 mg), and the mixture was maintained at 80° under Ar atmosphere with constant stirring. After 2 h, the mixture was diluted with H_2O and extracted with CH_2Cl_2. The org. phase was concentrated *in vacuo*, and the residue was acetylated in the usual manner with Ac_2O/pyridine. The resulting mixture was purified by prep. TLC (SiO_2; $CHCl_3$/MeOH 5:1) to yield *phytosphingosine* (**3**; 0.6 mg) as an oil. The above aq. phase was acidified with 5% H_2SO_4, extracted with CH_2Cl_2, and treated with CH_2N_2 in Et_2O at r.t. for 12 h. Solvent removal followed by acetylation furnished *methyl (2*R*)-2-acetoxyheptadecanoate* (**5**; 0.6 mg).

Data of **3**. Oil. $[\alpha]_D^{25} = +8.0$ ($c = 0.007$, $CHCl_3$). ^1H-NMR (400 MHz, $CDCl_3$): 5.54 (*m*, NH); 5.40 (*m*, 1 H); 4.90 (*m*, 1 H); 4.17 (*m*, 1 H); 3.86 (*m*, 1 H); 3.62 (*m*, 1 H); 2.14 (*s*, AcO); 2.11 (*s*, AcO); 1.80–1.25 (br. *s*, CH_2); 0.97 (*t*, $J = 6.26$, 3 H). EI-MS: 355 (2, M^+), 239 (4), 111 (29). HR-EI-MS: 355.2756 (M^+, $C_{20}H_{37}NO_4^+$; calc. 355.2723).

Data of **5**. Oil. $[\alpha]_D^{25} = -2.53$ ($c = 0.01$, $CHCl_3$). ^1H-NMR (400 MHz, $CDCl_3$): 4.98 (*t*, $J = 6.7$, 1 H); 3.58 (*s*, MeO); 2.04 (*s*, AcO); 1.60 (*m*, CH_2); 1.25 (br. *s*, CH_2); 0.80 (*t*, $J = 7.4$, Me). EI-MS: 342 (7, M^+), 341 (6), 323 (35), 217 (100), 189 (14). HR-EI-MS: 342.2489 (M^+, $C_{20}H_{38}O_4^+$; 342.2770).

Acetylation of **1**. Compound **1** (14 mg) was treated in the usual manner with Ac_2O/pyridine to afford the diacetate **2** (12 mg).

Data of **2**. Colorless, amorphous solid. $C_{37}H_{69}NO_6$ (623.95 g/mol). M.p. 96–98°. $[\alpha]_D^{25} = +19.4$ ($c = 0.09$, $CHCl_3$). IR (film, NaCl): 3285, 2918, 2850, 1740, 1665, 1577, 1464, 1234, 1071, 721. ^1H- and

^{13}C-NMR: see *Table 1*. EI-MS: 623 (absent, M^+), 441 (18), 399 (8), 326 (4), 300 (13), 285 (35), 266 (14), 264 (10), 256 (11), 253 (27), 251 (20), 239 (45), 237 (36), 209 (11), 197 (31).

Cell Culture. Human SK-MEL-1 melanoma cells (DSMZ No. ACC 303, DSMZ, German Collection of Microorganisms and Cell Cultures, Braunschweig, Germany) were cultured in suspension using *RPMI-1640* medium (*Sigma*) supplemented with 10% (*v*/*v*) heat-inactivated fetal bovine serum (FBS; *Sigma*), 100 U/ml penicillin, and 100 μg/ml streptomycin, at 37° in a humidified atmosphere containing 5% CO_2. Cells were maintained at a density less than 5×10^5 cells/ml. The cell numbers were counted by a hematocytometer, and the viability was always greater than 95% in all experiments, as assayed by the Trypan Blue (0.025%) exclusion method. To ensure exponential growth, cells were resuspended in fresh medium 24 h before each treatment. Stock solns. of 10 mM ceramides were prepared in EtOH/dodecane 49:1, and aliquots were frozen at −20°. Further dilutions were made in culture medium immediately prior to use. In all experiments, the final concentration of EtOH/dodecane 49:1 did not exceed 0.5% (*v*/*v*), a concentration that is nontoxic to the cells.

Cytotoxicity Assay. The cytotoxicities of **1** and **2** were determined by the MTT assay [22]. Briefly, 1×10^4 exponentially growing cells were seeded in 96-well microculture plates with various ceramide concentrations in a volume of 100 μl for 72 h at 37°. Controls were treated with the same amount of EtOH/dodecane 49:1 as used in the corresponding drug experiments. Surviving cells were detected based on their ability to metabolize MTT into formazan crystals. The optical density at 570 nm was used as a measure of cell viability. Cell survival was calculated as the fraction of cells alive relative to control for each point: cell survival [%] = (mean absorbance in treated wells/mean absorbance in control wells) × 100. Concentrations inducing 50% inhibition of cell growth (IC_{50}) were determined graphically for each experiment using the curve-fitting routine of the computer software Prism 2.0™ (*GraphPad*) and the equation derived by *DeLean et al.* [23].

REFERENCES

[1] A. G. González, F. León, A. Rivera, J. I. Padrón, J. González-Platas, J. C. Zuluaga, J. Quintana, F. Estévez, J. Bermejo, *J. Nat. Prod*. **2002**, *65*, 417.
[2] F. León, J. Quintana, A. Rivera, F. Estévez, J. Bermejo, *J. Nat. Prod*. **2004**, *67*, 2008.
[3] F. León, I. Brouard, A. Rivera, F. Torres, S. Rubio, J. Quintana, F. Estévez, J. Bermejo, *J. Med. Chem*. **2006**, *49*, 5830.
[4] P. Bonfante, R. Balestrini, E. Martino, S. Perotto, C. Plassard, D. Mousain, *Mycorrhiza* **1998**, *8*, 1.
[5] A. Braun-Lullemann, A. Huttermann, A. Majcherczyk, *Appl. Microbiol. Biotechnol*. **1999**, *53*, 127.
[6] P. H. Grazzioti, J. O. Siquiera, F. M. Moreira, D. Carvalho, *Rev. Bras. Ciencia Solo* **2001**, *25*, 839.
[7] H. Besl, I. Michler, R. Preuss, W. Steglish, *Z. Naturforsch., B*. **1974**, *29*, 784.
[8] C. Tringali, C. Geraci, G. Nicolosi, J. F. Verbist, C. Roussakis, *J. Nat. Prod.* **1989**, *52*, 844.
[9] S. M. Badalyan, *Int. J. Med. Mushrooms* **2003**, *5*, 153.
[10] S. Tomassi, F. Lohezic-LeDevehat, P. Sauleau, C. Bezivin, J. Boustie, *Pharmazie* **2004**, *59*, 290.
[11] A. G. González, J. B. Bermejo, F. J. M. Toledo, *Phytochemistry* **1983**, *22*, 1049.
[12] J. Rösecke, W. A. König, *Phytochemistry* **2000**, *54*, 757.
[13] M. Hattori, X. W. Yang, Y. Z. Shu, N. Kakiuchi, Y. Tezuka, T. Kikuchi, T. Namba, *Chem. Pharm. Bull.* **1988**, *36*, 648.
[14] Y. Yasunori, E. Makiko, T. Yoshino, M. Kaori, A. Keiko, F. Katsuyuki, K. Masao, *Chem. Pharm. Bull.* **1999**, *47*, 847.
[15] L. Misra, S. A. Siddiqui, *Z. Naturforsch., C* **2000**, *55*, 500.
[16] T. Ishizuka, Y. Yaoita, M. Kikuchi, *Chem. Pharm. Bull.* **1997**, *45*, 1756.
[17] R. B. Cain, R. F. Bilton, J. A. Darrah, *Biochem. J.* **1968**, *108*, 797.
[18] J. W. ApSimon, A. J. Hannaford, W. B. Whalley, *J. Chem. Soc.* **1965**, 4164.
[19] M. Meyer, M. Guyot, *J. Nat. Prod.* **2002**, *65*, 1722.
[20] W. Jin, K. L. Rinehart, E. A. Jares-Erijman, *J. Org. Chem.* **1994**, *59*, 144.
[21] Y. Kishimoto, M. Hoshi, C. Hignite, *Biochemistry* **1974**, *13*, 3992.
[22] T. Mosmann, *J. Immunol. Methods* **1983**, *65*, 55.
[23] A. DeLean, P. J. Munson, D. Rodbard, *Am. J. Physiol.* **1978**, *235*, E97.

Received April 24, 2007

Cytotoxic Activities of Flavonoid Glycoside Acetates from *Consolida oliveriana*

Author **Jesús G. Díaz**[1], **Armando J. Carmona**[1], **Fernando Torres**[2], **José Quintana**[2], **Francisco Estévez**[2], **Werner Herz**[3]

Affiliation
[1] Instituto Universitario de Bio-Orgánica "Antonio González", La Laguna, Tenerife, Spain
[2] Departamento de Bioquímica, Biología Molecular y Fisiologia, Centro de Ciencias de la Salud, Universidad de las Palmas de Gran Canaria, Gran Canaria, Spain
[3] Department of Chemistry and Biochemistry, The Florida State University, Tallahassee, Florida, USA

Key words
- *Consolida oliveriana*
- Ranunculaceae
- flavonoids
- flavonoid acetates
- cytoxicity

Abstract

The flavonoids kaempferol, quercetin, trifolin, hyperoside 2″- and 6″- acetates, 7-glucotrifolin, biorobin and robinin were isolated from the aerial parts of *Consolida oliveriana*. Their derivatives kaempferol tetraacetate, quercetin pentaacetate, trifolin heptaacetate and hyperoside octaacetate exhibited significant cytotoxicity *in vitro* against three human cell lines HL-60, U937 and SK-MEL-1 while hyperoside 2″-acetate, hyperoside-6″-acetate, glucotrifolin decaacetate and heptamethyltrifolin were inactive.

Supporting information available online at http://www.thieme-connect.de/ejournals/toc/plantamedica

received October 8, 2007
revised November 7, 2007
accepted December 3, 2007

Bibliography
DOI 10.1055/s-2008-1034278
Planta Med © Georg Thieme Verlag KG Stuttgart · New York
Published online 2008
ISSN 0032-0943

Correspondence
Professor Werner Herz
Department of Chemistry and Biochemistry
The Florida State University
Tallahassee
Florida 32306-4390
USA
Tel.: +1-850-644-2774
Fax: +1-850-644-8281
jdulin@chem.fsu.edu

Introduction

Consolida, a highly specialized genus of Ranunculaceae closely allied to *Delphinium* with its center of diversity in Anatolia, is like its relatives a rich source of alkaloids. Previous studies of the aerial parts of *Consolida oliveriana* (DC) Schrod., a species used medicinally in parts of Anatolia, have concentrated on the isolation of its constituent alkaloids [1], [2]. A large number of publications has dealt with the diterpenoid alkaloids of other *Consolida* species but reports on the flavonoid content of members of this genus are sparse [3], [4]. As part of our ongoing research on flavonoids in the genus *Delphinium* and related genera [5], [6] we have investigated the most polar fraction of the ethanol extract of the aerial parts of *C. oliveriana*. We now report isolation of the flavonoids kaempferol (**1**), quercetin (**2**), trifolin (**3**) [7], hyperoside (**4**) [7], 2″-acetylhyperoside (**5**) [8], 6″-acetylhyperoside (**6**) [7], 7-glucotrifolin (**7**) [9], biorobin (**8**) [10], [11] and robinin (**9**) [12] from this fraction. Compounds were identified by HR-MS as well as ^{1}H- and ^{13}C-NMR spectrometry.

The availability of these relatively polar flavonoids allowed us to follow up earlier work by the Las Palmas de Gran Canaria group on substituent effects governing cytotoxicities with flavonoids [15]. It had been shown that acetylation of certain polyhydroxyflavonoids, among which were quercetin derivatives containing a methoxy group on C-3, increased the antiproliferative activities of the parent compounds against HL-60 and other cell lines. While quercetin itself was modestly active against the HL-60 cell line the earlier results indicated that the increased activities of the acetate derivatives were not due to hydrolysis of the parent compounds. Methylation of kaempferol at the 3-position also appeared to bestow a modest degree of activity since earlier work [14] had shown that kaempferol itself only slightly affects HL-60 cells. It was therefore of interest to determine how peracetylation of not only kaempferol and quercetin but also peracetylation of some of the more highly substituted glycosides from *Consolida oliveriana* affects cytotoxicity. Compounds **1 – 4** and **7 – 9** were therefore converted to the corresponding polyacetates **1a – 4a** and **7a – 9a** and trifolin (**3**) was also converted to heptamethyltrifolin (**3b**). Known compounds **1, 1a, 2, 2a, 3 – 9** were identified by HR-MS as well as ^{1}H- and ^{13}C-NMR spectrometry. The ^{1}H- and ^{13}C-NMR spectra of the new compounds **3a**, **3b**, **4a**, **7a – 9a** as well as the previously unreported ^{13}C-NMR spectra of compounds **7**, **8** and **9** are available as Supporting Information.

Materials and Methods

General

The ^{1}H- and ^{13}C-NMR spectra were measured using a Bruker AMX-400 or a Bruker MAX-500 in-

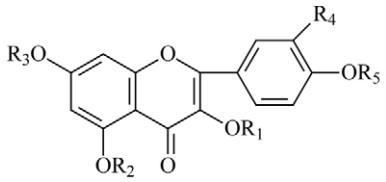

1a	Kaempferol tetraacetate: R_1, R_2, R_3, R_5 = Ac, R_4 = H
2a	Quercetin pentaacetate: R_1, R_2, R_3, R_5 = Ac, R_4 = OAc
3	Trifolin: R_1 = Gal, R_2, R_3, R_4, R_5 = H
3a	Trifolin heptaacetate: R_1 = Gal Ac, R_2, R_3, R_5 = Ac, R_4 = H
3b	Heptamethyltrifolin: R_1 = Gal OMe, R_2, R_3, R_5 = Me, R_4 = H
4	Hyperoside: R_1 = Gal, R_2, R_3, R_5 = H, R_4 = OH
4a	Hyperoside acetate: R_1 = Gal Ac, R_2, R_3, R_5 = Ac, R_4 = OAc
5	2"-Acetylhyperoside: R_1 = Gal-2"-Ac, R_2, R_3, R_5 = H, R_4 = OH
6	6"-Acetylhyperoside: R_1 = Gal-6"-Ac, R_2, R_3, R_5 = H, R_4 = OH
7	7-Glucotrifolin: R_1 = Gal, R_3 = Glu, R_2, R_4, R_5 = H
7a	Glucotrifolin decaacetate: R_1 = GalAc, R_2, R_5 = Ac, R_3 = GluAc, R_4 = H
8	Biorobin: R_1 = rbinoside, R_2, R_3, R_4, R_5 = H
8a	Biorobin acetate: R_1 = rbinoside Ac, R_2, R_3, R_5 = Ac, R_4 = H
9	Robinin: R_1 = Robinoside, R_3 = Rha, R_2, R_4, R_5 = H
9a	Robinin acetate: R_1 = rbinoside Ac; R_3 = Rha Ac, R_2, R_5 = Ac, R_4 = H

Gal = β-galactopyranosyl; Glu = β-glucopyranosyl; Rha = α-rhamnopyranosyl; rbinoside = α-rhamnopyranosyl-(1→6)-β-galactopyranoside.

strument. FAB5 and exact mass measurements were determined using a Micromass Autospec instrument at 70 eV. ESI-IT mass spectral data were obtained by tandem electrospray ion trap mass spectrometry (ESI-IT-MS) (LCQ Deca XP Plus; ThermoFinnigan; San Jose, CA, USA). Column chromatography was performed over Sephadex LH-20 Pharmacia (ref. 17-0090-01; Upsala, Sweden); silica gel 60 (Merck 230–400 mesh; Darmstadt, Germany) and analytical TLC, Merck Kieselgel 60 F 254. HPLC separations were performed on a JASCO Pu-980 series pumping system equipped with a JASCO UV-975 ultraviolet detector and with a Waters Kromasil 5 (5 mm × 250 mm) column. A Macherey-Nagel VP 250/10 nucleodur Sphinx RP 5 mm column (Düren, Germany) was used for HPLC-RP chromatography; chromatograms were visualized under UV light at 255 and 366 nm and/or sprayed with oleum followed by heating. All solvents were distilled before use; the purity of all compounds was 99.0% as judged by HPLC. Stock solutions of 10 mM flavonoids were made in DMSO and aliquots were frozen at –20 °C. Tissue culture media and standard analyzed grade laboratory reagents were obtained from Sigma (St. Louis, MO, USA).

Plant material

Aerial parts of *Consolida oliveriana* (DC) Schrod. were collected and identified near Pazarkik in eastern Turkey at an altitude of 980 m by Prof. Julian Molero Briones, Department of Botany, Faculty of Pharmacy, University of Barcelona where a voucher specimen (BCF-37 810) has been deposited.

Extraction and isolation

Dried and powdered aerial parts of *Consolida oliveriana* (2.23 kg) were defatted with hexane (6 L) during one month and subsequently extracted repeatedly with 80% EtOH (7 L) at room temperature for two weeks. The extract was filtered and concentrated at reduced pressure. The remaining aqueous layer was exhaustively extracted with *n*-BuOH to give, after removal of the solvent, 36 g of a brown viscous residue. The aqueous layer was concentrated and filtered through a column of Amberlite XAD-2 resin (8 × 40 cm) to remove the polar compounds while the flavonoids remaining on the column were eluted with MeOH (see below).

10 g of the viscous *n*-BuOH extract were fractionated on a 50 × 8 cm column packed with Sephadex LH-20 and eluted with hexane-CH_2Cl_2-MeOH, 1 : 1 : 2, 15 500-mL fractions (S_1 – S_{15}) being collected. Frs S_1 – S_{15} contained mainly alkaloids contaminated by material exhibiting no UV absorption and frs S_4 – S_8 contained mixtures of glycosides. Frs S_9 and S_{10} and frs S_{11} – S_{13} gave after recrystallization from MeOH-EtAc quercetin (**2**, 556 mg), respectively, kaempferol (**1**, 472 mg). Frs S_4 – S_8 were chromatographed over a 40 × 4 cm Sephadex LH-20 column using hexane-CH_2Cl_2-MeOH (1 : 1 : 1), the elution being monitored by TLC analysis. This resulted in three fractions A (430 mg) B (70 mg) and C (55 mg). Fr B afforded after recrystallization from MeOH 90 mg of trifolin (**3**) and fr C 49 mg of hyperoside (**4**). Rechromatography of fr A over silica gel using 40 mL hexane-EtOAc mixtures of increasing polarity afforded from frs 64–77 (hexane-EtOAc 2 : 8) 24 mg of 6″-acetylhyperoside (**6**) after further purification over Sephadex LH-20 (hexane-MeOH-CH_2Cl_2, 2 : 1 : 1). Frs 86–90 (hexane-EtOHc, 1 : 9) yielded 21 mg of 2″-acetylhyperoside (**5**).

The material eluted from the Amberlite XAD-2 column with methanol was further purified over a 50 × 8 cm column packed with Sephadex LH-20 and eluted with CH_2Cl_2-MeOH (1 : 1), six frs (J_1 – J_6) of 500 mL each being collected. Frs J_1 – J_3 containing mainly alkaloids and other components exhibiting no UV absorption were combined with frs S_1 – S_3. Frs J_4 – J_6 (2 g) were subjected to gel filtration on Sephadex LH-20 using 42 200-mL frs of H_2O-MeOH (1 : 1). Frs 14 – 22 afforded after recrystallization from MeOH 260 mg of 7-glucotrifolin (**7**). Frs 28 – 31 yielded 45 mg of trifolin (**3**), frs 33 – 38 18 mg of hyperoside (**4**). Frs. 5 – 12 on RP-HPLC on a C-18 Sphinx column (100 × 10 mm, flow rate 1.4 mL min^{-1}) using MeOH-H_2O (1 : 1) afforded 7 mg of robinin (**9**, t_r 12 min) and 5 mg at biorobin (**8**, t_r 16 min).

General method for acetylation

Dry phenolic material was dissolved in the minimum volume of pyridine. Twice the amount of acetic anhydride was added and the solution was allowed to stand overnight at ambient temperature. The mixture was diluted with H_2O and extracted three times with EtOAc. The extract was evaporated under vacuum and the residue containing the polyacetate was further purified by column chromatography over silica gel using hexane-EtOAc as eluent. Mass spectra of the polyacetylated compounds, all gums, are listed below.

Kaempferol tetraacetate (**1a**): EI-MS: *m/z* = 412 (M^+ – $C_2H_3O_2$, 23), 370 (M^+ – 2 $C_2H_3O_2$, 57) 286 (M^+ - 4 $C_2H_3O_2$, 100).

Quercetin pentaacetate (**2a**): HR-EI-MS: *m/z* = 513.0997, calcd. for $C_{25}H_{20}O_2 + H^+$: 513.1033.

Trifolin heptaacetate (**3a**): HR-FAB-MS: *m/z* = 743.1784, calcd. for $C_{35}H_{34}O_{18} + H^+$: 743.1823.

Hyperoside octaacetate (**4a**): HR-FAB-MS: *m/z* = 823.1687, calcd. for $C_{37}H_{36}O_{20}Na$: 823.1698.

Glucotrifolin decaacetate (**7a**): HR-FAB-MS: *m/z* = 1030.2592, calcd. for $C_{47}H_{50}O_{26}$: 1030.2590.

Biorobin nonaacetate (**8a**): HR-FAB-MS: *m/z* = 972.2583, calcd. for $C_{45}H_{48}O_{24}$: 972.2536.

Robinin undecaacetate (**9a**): HR-FAB-MS: *m/z* = 1226.3344, calcd. for $C_{55}H_{63}O_{30}Na$: 1226.3302, m/z = 1202.3344, calcd. for $C_{55}H_{62}O_{30}$: 1202.3326.

Methylation of trifolin

To a solution of **3** (14 mg) in DMSO (2 mL) was added aqueous 50% NaOH (2 mL) and 2 mL of methyl iodide. The mixture was stirred at room temperature overnight, poured into H_2O and extracted with ethyl acetate. The organic extract was dried over Na_2SO_4, filtered and evaporated at reduced pressure. The residue was purified by HPLC (SiO2, EtOAc : hexane 3 : 2, flow rate 2 mL/min) to afford 10 mg of heptamethoxytrifolin **3b** (TR 62 min) as a gum. HR-FAB-MS: *m/z* = 569.1981, 547.2155 calcd. for $C_{28}H_{34}O_{11}Na$: 569.1999, calcd. for $C_{28}H_{35}O_{11}$: 547.2179.

Tumor cell growth assay

Human HL-60 and U 937 cells were obtained from the European Collection of Cell Cultures (Salisbury, UK) and human SK-MEL-1 melanoma cells (DSMZ No ACC 303) from the German Collection of Microorganisms and Cell Cultures, Braunschweig, Germany. HL-60 and U 937 were grown as described [15]. HL-60, U 937 and SK-MEL-1 cells were cultured suspended in RPMI 1640 (Sigma) with L-glutamine cell culture medium supplemented with 10% heat-inactivated fetal bovine serum (FBS) medium and antibiotics (100 units/mL of penicillin and 100 μg/mL of streptomycin) in 250 cm^3 culture vessels at 37 °C in a humidified atmosphere containing 5% CO_2. The cells were routinely kept in the logarithmic growth phase at 0.1 – 0.9 × 10^6 cells/mL by dilution with fresh medium at least every third day. Cells were counted by a hematocytometer; the viability was always greater than 95% as assayed by the 0.025% trypan blue exclusion method. Stock solutions of the flavonoids were further diluted with culture medium just before use. In all experiments the final concentration of DMSO did not exceed 0.5% (v/v), a concentration which is non-toxic to the cells.

Cytotoxicity assays were performed using a colorimetric 3-[4,5-dimethylthiazol-2-yl-]-2,5 diphenyl-2*H*-tetrazolium bromide (MTT) assay as described [15]. Briefly, 10^4 exponentially growing cells were seeded on 96-well microculture plates with various flavonoid concentrations (0.1 – 10 μM) in a 200 μL volume for 72 h. Surviving cells were detected based on their ability to metabolize 3-[4,5-dimethylthiazol-2-yl]-2,5 diphenyltetrazolium bromide (Sigma) into formazan crystals. The optical density at 570 nm was used as a measure of cell viability. Cell survival was calculated as fraction of cells relative to control for each point: Cell survival (%) = mean absorbance in treated cells/mean absorbance in control wells × 100. Concentrations inducing 50% inhibition of cell growth (IC_{50}) were determined graphically for each experiment using the curve fitting routine of the computer software Prism 2.0™. (GraphPad) and the equation derived by DeLean et al. Etoposide (Sigma) was used as a positive control (IC_{50} = 0.32 ± 0.02 mM in HL-60 cells, IC_{50} = 1.25 ± 0.25 mM in U937 cells, not determined in SK-MEL-1 cells).

Supporting information

^{1}H- and ^{13}C-NMR spectra of the new compounds **3a**, **3b**, **4a**, **7a-9a** as well as the previously unreported ^{13}C-NMR spectra of compounds **7**, **8** and **9** are available as Supporting Information.

Results and Discussion

Kaempferol tetraacetate (**1a**), quercetin pentaacetate (**2a**), the polyacetates **3a**, **4a**, the monoacetates **5** and **6** as well as the methylated derivative **3b** were screened for *in vitro* cytotoxicity against the human myeloid leukemia HL-60 and U937 cell lines and against the human melanoma SK-MEL-1 cell line. The results, given in concentrations causing 50% growth inhibition (IC_{50}), are summarized in **Table 1**. Polyacetates **1a**, **2a**, **3a** and **4a** inhibited growth and viability of human HL-60 and U937 cells in a dose-dependent manner as determined by the 3-[4,5-dimethylthiazol-2-yl]-2,5-diphenyltetrazolium bromide (MTT dye re-

Table 1 Effect of flavonoid acetates on the growth of three human cell lines

Compound	IC_{50} (μM)		
	HL-60	U937	SK-MEL-1
1a	45 ± 3	48 ± 17	37 ± 8
2a	38 ± 6	25 ± 11	58 ± 7
3a	21 ± 8	10 ± 2	15 ± 2
3b	88 ± 9	> 100	> 100
4a	15 ± 1	19 ± 2	23 ± 2
5	> 100	> 100	> 100
6	> 100	> 100	> 100
7a	> 100	> 100	> 100

Cells were cultured for 72 h. IC_{50} values were calculated as described in the Materials and Merthods section. Data shown represent the mean ± SEM of 2 – 3 independent experiments with three determinations in each.

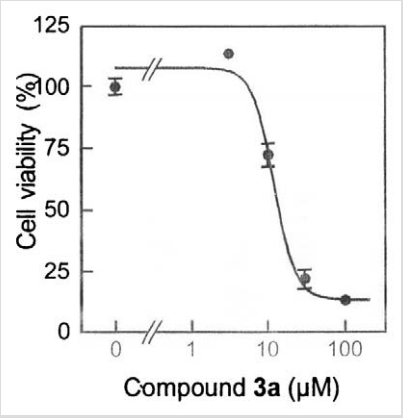

Fig. 1 The effect of trifolin heptaacetate on human U 937 cell viability. Cells were cultured in the presence of the indicated doses of **3a** for 72 h; thereafter cell viability was determined by the MIT assay as described. Results of a representative experiment are shown. Each point represents the average of triplicate determinations.

duction) assay. An example of a dose-response curve is shown in **Fig. 1**. Similar results were obtained with the human melanoma cell line. Glycoside polyacetates **3a** and **4a** were most effective against all lines, although not spectacularly so. Quercetin pentaacetate (**2a**) was also modestly active but no more so that quercetin itself [13] in agreement with the earlier suggestion that antiproliferative activity may actually decrease with increasing installation of acetate functions on C-5 and C-4′ of the flavone nucleus. Kaempferol tetraacetate (**2a)**, on the other hand, displayed increased, but still only very modest, activity compared with kaempferol itself [14]. Finally, as permethylation of betuletol 3-methyl ether, the most active naturally occurring flavonoid studied by our group earlier, had eliminated the compound's activity we were also interested in the effect of permethylation of **3** whose peracetate **3a** was the most active of our compounds. Indeed, the relatively non-polar heptamethyltrifolin (**3b**) containing no acetate function was inactive as were the isomeric monoacetylhyperosides **5** and **6** and, somewhat surprisingly, glucotrifolin acetate. However, it needs to be pointed out that none of the flavonol derivatives included in the present study were 3-methyl ethers which served as the basis for the generalizations in the earlier study [13].

Acknowledgments

Financial support in the form of grants to FE from the Ministerio de Educación y Ciencia (Spain) (SAF 2004-07928) and the Consejeria de Educación del Gobierno de Canarias (GRUP-2004-44). FT was supported by a research studentship from the Dirección General de Universidades e Investigacion del Gobierno del Canarias is gratefully acknowledged.

References

1 *Ulubelen A, Desai H, Haridutt K, Hart BP, Joshi BS, Pelletier SW et al.* Diterpenoid alkaloids from *Consolida oliveriana.* J Nat Prod 1996; 59: 907 – 10
2 *Grandez M, Madinaveitia A, Gavin JA, Alva A, De La Fuente G.* Alkaloids from *Consolida oliveriana.* J Nat Prod 2002; 65: 513 – 6
3 *Melnichuk GG. Consolida regalis* flavonoids (*C. regalis* [*Delphinium consolida*]). Inst Bot Kiev, USSR. Ukrains'ki Botanichnii Zhurnal 1971; 28 : 525; Chem Abstr 1972; 7: 32 233
4 *Kucukislamoglu M, Yayli N, Senturk HB, Genc H, Özden S.* Flavonol glycosides from *Consolida armeniaca.* Turk J Chem 2000; 24 : 191 – 7; Chem Abstr 2001; 134: 16 017
5 *Díaz JG, Ruiz JG, Dias BR, Sazatornil JAG, Herz W.* Flavonol 3,7-glycosides and dihydroxyphenethyl glycosides from *Aconitum napellum* ssp *lusitanicum.* Biochem Syst Ecol 205; 33: 201 – 5
6 *Luis JC, Valdes F, Martin R, Carmona AJ, Díaz JG.* DPPH radical scavenging activity of two flavonol glycosides from *Aconitum napellus* ssp *lusitanicum.* Fitoterapia 2006; 77: 469 – 71
7 *Foo LUY, Molan AL, Woodfield DR, McNabb WC.* The phenols and prodelphinidins of white clover flowers. Phytochemistry 2000; 54: 539 – 48
8 *Juergenliemk G, Nahrstedt A.* Phenolic compounds from *Hypericum perforatum.* Planta Med 2002; 68: 88 – 91
9 *Park H-J, Lim CE, Park C-W, Cha H-C.* Analysis of flavonols extracted from leaves of various grapevine cultivars by HPLC. J Korean Soc Hortic Sci 2004; 45: 138 – 42
10 *Hou WC, Lin RD, Lee TH, Huang YH, Hsu FL, Lee MH.* The phenolic constituents and free radical scavenging activities of *Gynura formosana* Kiamura. J Sci Food Agric 2005; 85: 615 – 21
11 *Yahara S, Kohjyouma M, Kohoda H.* Flavonoid glycosides and saponins from *Astragalus shikokianus.* Phytochemistry 2000; 53: 469 – 71
12 *Rivero A, Quintana J, Eiroa JL, Lopez M, Triana J, Bermejo J et al.* Potent induction of apoptosis by germacranolide sesquiterpene lactones on human myeloid leukemia cells. Eur J Pharmacol 2003; 482: 77 – 84
13 *Wang I-K, Lin-Sjoai S-Y, Lin J-K.* Induction of apoptosis by apigenin and related flavonoids through cytochrome 6 release and activation of caspase-9 and caspase-3 in leukemia HL-60 cells. Eur J Cancer 1999; 35: 1517 – 25
14 *Rubio S, Quintana J, López M, Eiroa JL, Triana J, Estévez F.* Phenylbenzylpyrones structure activity studies identify betuletol derivatives as potential antitumoral agents. Eur J Pharmacol 2006; 548: 9 – 20
15 *DeLean A, Munson PJ, Rodbard D.* Simultaneous analysis of families of sigmoidal curves: Application to bioassay, radioligand assay and physiological dose-response curves. Am J Physiol 1978; 235: E97 – 102

Available online at www.sciencedirect.com
ScienceDirect
Bioorganic & Medicinal Chemistry 16 (2008) 2063–2076
Bioorganic & Medicinal Chemistry

Synthesis of novel spirostanic saponins and their cytotoxic activity

Juan C. Hernández,[a,b] Francisco León,[a,b] Ignacio Brouard,[a] Fernando Torres,[b,c] Sara Rubio,[b,c] José Quintana,[b,c] Francisco Estévez[b,c] and Jaime Bermejo[a,*]

[a]*Instituto de Productos Naturales y Agrobiología-C.S.I.C., Instituto Universitario de Bio-Orgánica, "Antonio González", Av. Astrofísico F. Sánchez 3, 38206 La Laguna, Tenerife, Spain*
[b]*Instituto Canario de Investigación del Cáncer (ICIC), Av. Astrofísico F. Sánchez 2, 38206 La Laguna, Tenerife, Spain*
[c]*Department of Biochemistry, Molecular Biology and Physiology, University of Las Palmas de Gran Canaria, Plaza Dr. Pasteur s/n, 35016 Las Palmas de Gran Canaria, Spain*

Received 2 July 2007; revised 23 October 2007; accepted 30 October 2007
Available online 4 November 2007

Dedicated to the memory of Professor Antonio G. González.

Abstract—This study was carried out to assess the cytotoxicity of several new synthetic steroidal saponins against the human myeloid leukemia cell lines (HL-60 and U937) and against human melanoma cells (SK-MEL-1). Several diosgenyl glycosides analyzed showed strong cell growth inhibition which was associated with alterations in cell cycle progression and induction of apoptosis. Studies of cytochrome *c* release and caspase-9 activation suggest a main role of the intrinsic pathway of apoptosis in the mechanism of cytotoxicity caused by this kind of compounds.
© 2007 Elsevier Ltd. All rights reserved.

1. Introduction

Saponins are a very large group of glycosylated secondary metabolites isolated primarily from plants, but also found in lower marine organisms.[1] Saponins are believed to be some of the principal constituents of many plant drugs and traditional medicines worldwide, and are described as being responsible for most of the observed biological effects. Although the biological role of saponins in plants is not yet fully understood, they are considered to be a part of the natural chemical defense mechanism of plants against attack by pathogens.[2] Saponins consist of a hydrophobic aglycone, which may have a triterpenoid or steroid structure, linked by a glycosidic bond to a sugar moiety normally including glucose, rhamnose, galactose, or xylose, among others. Steroidal saponins are amphipathic molecules of special interest due to the biological activities they exhibit. In recent years several research groups have evaluated their cytotoxic activities.[3–11]

Consequently, various syntheses of steroidal saponins have been successfully developed.[12–15] As a part of our research focused on the cytotoxicity of several steroidal saponins isolated from *Dracaena draco*,[5,16] we designed the synthesis of ten analogs containing a diosgenyl α-L-rhamnopyranosyl-(1 → 2)-β-D-glucopyranoside skeleton. Mimaki et al.,[17] employing molecular models and molecular dynamic studies, suggested that the three-dimensional structure of the diglycoside moiety contributed to the cytotoxic activity of the molecule. In that study, they revealed that in the diosgenyl α-L-rhamnopyranosyl-(1 → 2)-β-D-glucopyranoside derivative, which is cytotoxic, the diglycoside exists in a vertically oriented conformation against the steroid plane. However, in the diosgenyl α-L-rhamnopyranosyl-(1 → 4)-β-D-glucopyranoside derivative, which presents a conformation with the diglycoside and the steroid in the same plane, the activity was not relevant.

Starting from this hypothesis, we proposed the synthesis of several saponins analogous to those obtained from *Dracaena draco*,[5,16] always having the diosgenyl β-D-glucopyranoside basic structure and including different monosaccharides (Glc, Gal, Man, Ara, Xyl, and Fuc) as well as the same derivative with rhamnose, linked through the C-2′ of the glucose. Then, the most potent

Keywords: Synthesis; Spirostanic saponins; Cytotoxicity; Apoptosis; Leukemia; Human melanoma cells; Cytochrome *c* release; Caspase.
* Corresponding author. Tel.: +34 922318583; fax: +34 922318571; e-mail: jbermejo@ull.es

0968-0896/$ - see front matter © 2007 Elsevier Ltd. All rights reserved.
doi:10.1016/j.bmc.2007.10.089

cytotoxic compound was submitted to additional modifications.

Some chemotherapeutic drugs have been shown to use apoptotic pathways to mediate their cytotoxic effects. An important goal in chemotherapy is to find new cytotoxic agents that are able to increase or restore the ability of tumor cells to undergo apoptosis. Apoptotic cell death is characterized by morphological and biochemical changes, which largely result from the activation of a family of cysteine proteases known as caspases. There are two primary caspase activation pathways, involving either stimulation of cell surface death receptors (the extrinsic pathway) or perturbation of mitochondria (the intrinsic pathway). Many anti-cancer drugs induce apoptosis by activating the intrinsic pathway. This cell death pathway involves the release of cytochrome *c* and the activation of the apoptosome-catalyzed caspase cascade. The apoptosome is a protein complex consisting of cytochrome *c*, apoptotic protease-activating factor 1, and caspase-9. Apoptosome assembly processes and activates the initiator caspase-9. Active caspase-9 then triggers a caspase cascade to induce apoptosis.

This study was undertaken to investigate the effects of synthetic diosgenyl glycosides on cell growth and death in human tumor cells, and associated biological events such as induction of apoptosis and impairment of cell cycle progression.

2. Results and discussion

Chemistry: In order to develop the synthesis of a set of new steroidal saponins, we initially decided to prepare the common precursor diosgenyl β-D-glucopyranoside, known as trillin (**3**), suitably protected as 4,6-*O*-benzylidene-3-*O*-pivaloyl-β-D-glucopyranoside **4a**. Compound **3**, as shown in Scheme 1, was prepared starting from 2,3,4,6-tetra-*O*-benzoyl-α-D-glucopyranosyl bromide (**1**) and commercially available diosgenin, using AgOTf as coupling promoter with high stereoselectivity and was prepared in good yield (67%). Hydrolysis of the ester groups of **2** under basic conditions yielded **3**, which was protected as the *O*-benzylidene derivative **4**. Attempts at selective monoprotection of the hydroxyl group located at C-3′ under conditions described by Li et al.[18] using TBDMSCl and imidazole in DMF were unrewarded in our case because starting material was recovered.

A report was found in the literature on the difficulty of accomplishing the selective monoprotection of the hydroxyl groups at C-2′ and C-3′ of a glucopyranosyl unit.[18,19] As an alternative, treatment of the above-mentioned *O*-benzylidene derivative **4** with pivaloyl chloride[19] provided a mixture of protected alcohols at the desired C-3′ position (45%, **4a**), at C-2′ (9.5%, **4b**), and at both C-2′ and C-3′ (5%, **4c**). Compound **4a**, which has the free –OH group at C-2′, was submitted to glycosylation reaction with the trichloroacetamidate partners (**5-11**, Table 1) obtained from their corresponding natural monosaccharides.[20]

The use of boron trifluoride-diethyl etherate complex as Lewis acid[18] and trichloroacetonitrile as leaving group allowed the coupling of the monosaccharides in a stereoselective manner and with acceptable yields affording the corresponding coupling products **12–18** (Scheme 2).

Finally, a two-step deprotection protocol employing AcOH (80%), followed by basic deacetylation with NaOMe in MeOH, gave the desired new spirostane-type steroidal saponins **20**, **21**, **23**, and **24**, and the known natural ones **19**, **22**, and **25**. The physical data of the known compounds were in accordance with those reported in the literature.[21–23] Analysis of the ^{1}H and ^{13}C NMR spectra of **20**, **21**, **23** and **24** together with homonuclear correlation (COSY) and heteronuclear multiple coherence (HMQC and HMBC) and TROESY experiments allowed the structure of these new compounds to be unambiguously deduced. Correlations between C-2′ of the glucopyranoside unit and H-1″ of the second monosaccharide unit as well as the ROE effect between H-2′ and H-1″ confirmed the interglycosidic linkage. The connection between the aglycone moiety and the saccharide portion was confirmed by a correlation between the C-1′ of glucose and H-3 of the aglycone and the ROE effect between H-1′ and H-3.

Preliminary results on cytotoxicity bioassays showed that compound **25** was the most potent cytotoxic agent against the three tumor cell lines tested (Table 2), and thus subsequent modifications were developed over this structure. It has been reported that the presence of acetyl groups usually increases cytotoxic potency.[17]

Thus, following the methodology described by Yu et al.,[24] the selective introduction of acetyl groups employing the lipase Novozyme 435 was performed (Scheme 3). This procedure afforded a mono- and a diacetyl derivative named diosgenyl α-L-rhamnopyranosyl-(1 → 2)-6-*O*-acetyl-β-D-glucopyranoside (**27**) and diosgenyl 4-*O*-acetyl-α-L-rhamnopyranosyl-(1 → 2)-6-*O*-acetyl-β-D-glucopyranoside (**26**), respectively.

It is noteworthy that trisaccharides with pharmacological activity are reported in the literature.[3,5] We therefore synthesized, starting from **4a**, a novel derivative **30**, containing a trisaccharide core attached to diosgenin, taking advantage of a 'one-pot' procedure.[25] In this method, trichloroacetamidate glycosyl and thioglycoside were used as sequential glycosyl donors and two glycosidic linkages (Scheme 4).[26]

3. Biological evaluation

3.1. Diosgenyl glycosides inhibit growth of human tumor cell lines

Initial studies on the cytotoxicity of diosgenyl α-L-rhamnopyranosyl-(1 → 2)-β-D-glucopyranoside (**25**) showed that this compound was a potent cytotoxic agent against HL-60 cells.[17] In the present report, we describe the chemical modifications that were developed

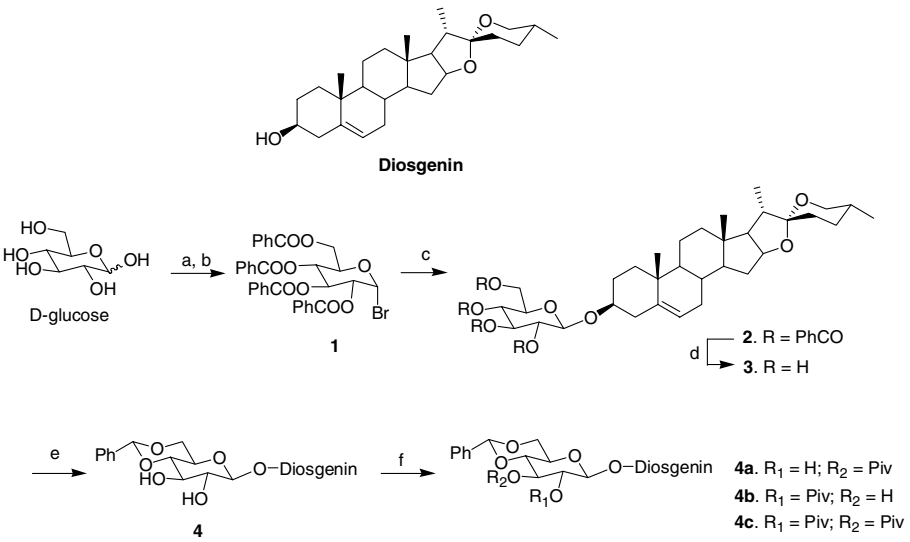

Scheme 1. Reagents and conditions: (a) PhCOCl, DMAP, Py; (b) HBr/AcOH (30:70), CH_2Cl_2; (c) diosgenin, AgOTf, CH_2Cl_2, −20 °C–rt, 4 Å MS; (d) NaOMe in MeOH 0.5 M; (e) $PhCH(OMe)_2$, CSA, DMF, 50 °C; (f) PivCl, Py, rt.

over this basic structure to obtain new semi-synthetic diosgenyl glycosides and the effect of these chemical changes on the growth of human myeloid (HL-60 and U937) and melanoma (SK-MEL-1) cell lines (Table 2).

Growth inhibition of human tumor cells in culture was determined by the 3-(4,5-dimethylthiazol-2-yl)-2,5-diphenyl-2*H*-tetrazolium bromide (MTT) dye-reduction assay. Antiproliferative studies of compound **25** indicated that these diosgenyl glycosides displayed strong cytotoxic properties in all assayed cell lines, with an IC_{50} of about 5–7 μM. Interestingly this compound was more potent than etoposide, a chemotherapy drug for the treatment of some types of cancer, against SK-MEL-1 melanoma cells (results not shown). Since an important structural component of compound **25** is rhamnose, we next decided to evaluate the role of this monosaccharide. Therefore, saponin glycosides containing different hexoses were synthesized. The results indicated that those compounds containing glucose (**19**), galactose (**20**), mannose (**21**) or fucose (**24**) instead of rhamnose were, in general, less cytotoxic in all cell lines tested. However, a certain cell-type dependence was also observed with some chemical changes. For example, compounds **21** and **24** presented IC_{50}s similar to those of compound **25** ($IC_{50} \sim 5$ to 11 μM) on HL-60 cells. However, these substances were completely ineffective on SK-MEL-1 cells if compared to **25** ($IC_{50} > 100$ μM vs $IC_{50} = 7$ μM). Selective acetylation was also performed on compound **25** to yield the mono- and diacetylated derivatives **27** and **26**, respectively. Compound **27** was highly cytotoxic (Fig. 1A and B) and no impact on the IC_{50}s was observed when compared with its deacetylated counterpart **25**. This result indicated that the hydroxyl group at C-6′ of glucose may not play a significant role in the cytotoxicity of this compound. Contrarily, a significant decrease in cytotoxic potency was observed for the diacetylated derivative **26** in all cell lines tested, which suggests that the free hydroxyl group linked to C-4″ on the rhamnose unit is relevant for antiproliferative activity. In consonance with these results, compound **30**, which contains the hydroxyl group at C-4″ attached to a second rhamnose, was also significantly less cytotoxic than **25** but similar to **26**, with no noteworthy differences among cell lines. Next, we decided to determine the influence of a pentose instead of rhamnose on the cytotoxicity of the diosgenyl glycosides. Therefore, compounds **22** and **23**, containing arabinose and xylose, respectively, were synthesized. The results indicated that the presence of these pentoses did not improve cytotoxicity. Contrarily, the antiproliferative capability of both compounds was decreased, as compared to compound **25**, in all human cell lines. As occurs with other substitutions, these chemical changes affected the cell lines under study to different degrees. A dramatic decrease in growth inhibitory activity was specifically observed on SK-MEL-1 in response to the above compounds ($IC_{50} > 100$ μM). These results support the role of rhamnose as a necessary structural requirement for diosgenyl glycosides' cytotoxicity.

3.2. Effect of diosgenyl glycosides on cell cycle progression

A detailed inspection of Table 2 reveals that of the three human cell lines used in this study, the growth of promyelocytic HL-60 cells was, in general, highly susceptible to the cytotoxicity induced by diosgenyl glycosides and, therefore, further studies were performed in this cell line. Thus, only those compounds with low IC_{50} ($\leqslant 15$ μM) were selected to explore the mechanism through which diosgenyl glycosides decrease cell viability. Therefore, we first analyzed whether cell growth inhibition induced by compounds **20**, **21**, **24**, **25**, and **27** is mediated via alteration in cell cycle progression.

Consistent with growth inhibitory effects, the cytometric flow studies (Table 3) reveal that compounds **21** and **24** in-

Table 1. Synthesis of disaccharide saponins by coupling reaction

Donor	Acceptor	Coupling product	Yield	Deprotection product	Yield
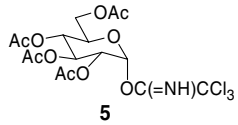 **5**	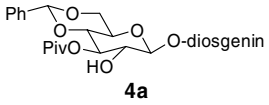 **4a**	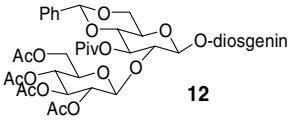 **12**	**77**	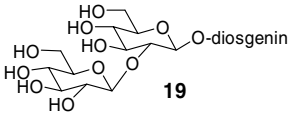 **19**	**58**
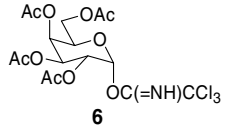 **6**	**4a**	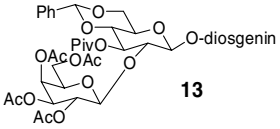 **13**	**50**	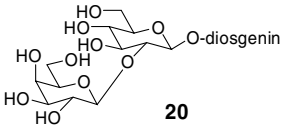 **20**	**38**
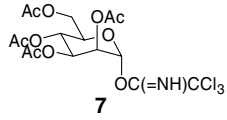 **7**	**4a**	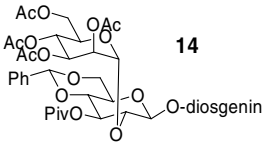 **14**	**52**	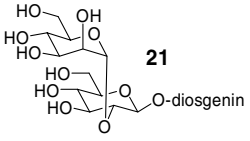 **21**	**41**
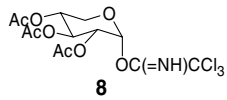 **8**	**4a**	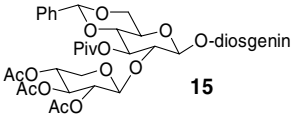 **15**	**64**	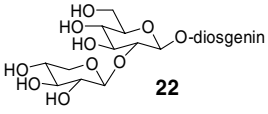 **22**	**49**
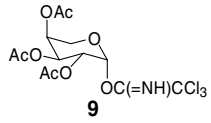 **9**	**4a**	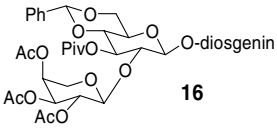 **16**	**56**	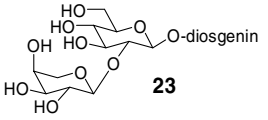 **23**	**47**
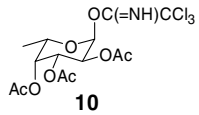 **10**	**4a**	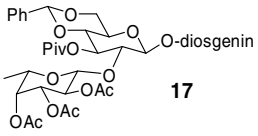 **17**	**58**	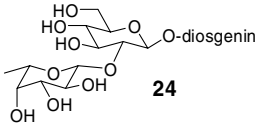 **24**	**40**
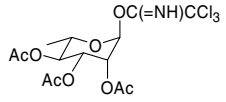 **11**	**4a**	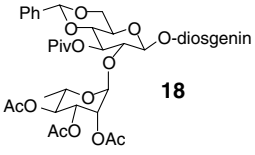 **18**	**49**	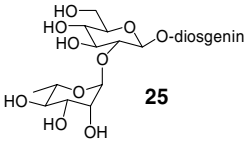 **25**	**41**

duce significant G_1 arrest at the expense of S- and G_2/M-phase cell population following treatment over 16 h with concentrations from 10 to 30 μM. Concentrations of 30 μM were used to demonstrate that the effects on cell cycle progression were dose-dependent. Doses higher than the antiproliferative IC_{50} were used to identify the primary targets and early mechanism of action of diosgenyl glycosides.

Moreover, the IC_{50} values were determined at 72 h of treatment, while the experiments of flow cytometry were analyzed after a short incubation time. Interestingly, compounds **25** and **27** also produced alterations in cell cycle progression although they induced G_2–M arrest at the expense of G_1 phase cell number. A significant increase in the S-phase was also observed at 30 μM of compounds. Taken together, the results indicated that compounds **21** and **24** versus **25** and **27** displayed antiproliferative activities through different mechanisms that involve cell cycle alteration. Selective modulation of different cell cycle-regulatory proteins could explain the differences among them, although other possibilities cannot be ruled out. No evidence of change in the phases of the cell cycle was observed in response to compound **20**. In this context it is important to note that galactose present in **20** is a diastereomer of mannose, which is the monosaccharide present in **21**. The results suggest that not only the configuration of the hydroxyl group in compound **21** plays an important role in the cell cycle arrest but also the configuration of the glycosidic bond between the monosaccharides.

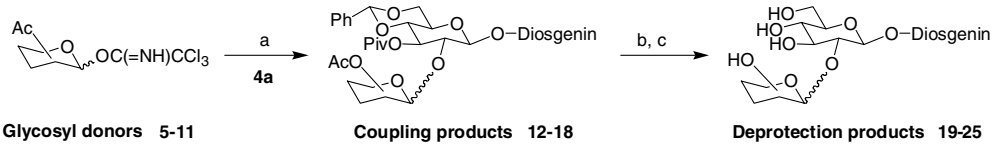

Scheme 2. Reagents: (a) $BF_3{\cdot}Et_2O$; (b) AcOH (80%); (c) NaOMe, MeOH.

Table 2. Effects of synthetic steroidal saponins on the growth of human tumor cell lines[a]

Compound	IC_{50} (μM)		
	HL-60	U937	SK-MEL-1
19	88 ± 12	>100	>100
20	15 ± 3	43 ± 12	>100
21	11 ± 4	12 ± 1	>100
22	38 ± 10	56 ± 4	>100
23	41 ± 4	80 ± 21	>100
24	10 ± 4	28 ± 8	>100
25	5 ± 1	6 ± 1	7 ± 2
26	33 ± 8	18 ± 3	17 ± 4
27	7 ± 2	5 ± 1	4 ± 2
30	22 ± 3	21 ± 2	37 ± 8

[a] Cells were cultured for 72 h and the IC_{50} values were calculated as described in Section 5. The data shown represent means ± SEM of 3–5-independent experiments with three determinations in each.

These data indicate a considerable effect on the extent as well as the nature of the cell cycle arrest in HL-60 cells when the diosgenyl β-D-glucopyranoside skeleton is modified by substitution at C-2′ with different glycosyl moieties.

3.3. Diosgenyl glycosides induce apoptosis in human myeloid leukemia cells

To determine whether diosgenyl glycosides decrease HL-60 cell viability through apoptosis activation, quantification of the number of hypodiploid cells (i.e., apoptotic cells) by flow cytometry was performed.

The results indicate that the percentage of apoptotic cells increased from 5 ± 1% (control) to 12.5 ± 0.5% (2.5-fold increase) and 18 ± 0.5% (3.6-fold increase) after 16 h of treatment with 10 μM of diosgenyl glycosides **25** and **27**, respectively (Fig. 2A). Using a higher concentration (30 μM) of compounds **21** and **24** the percentage of apoptotic cells increased from 4.5 ± 1% to 22 ± 1% (5-fold) and to 18 ± 2% (fourfold), respectively (Fig. 2B and C). Doses of 10–30 μM were used to demonstrate that the induction of apoptosis was dose-dependent.

Compound **20** did not induce apoptosis at either concentration tested (Fig. 2A and B). Etoposide, which induces morphological changes and internucleosomal DNA fragmentation characteristic of apoptotic cell death in human leukemia cells, was used as a positive

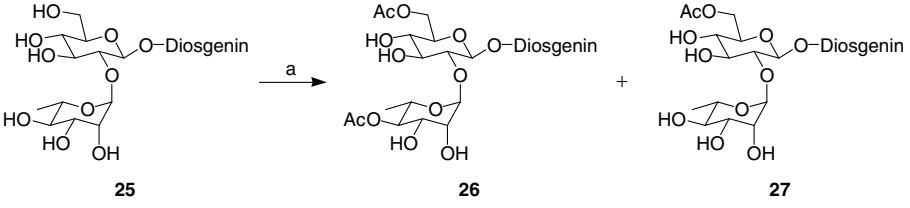

Scheme 3. Reagents: (a) Novozyme 435, vinyl acetate, THF.

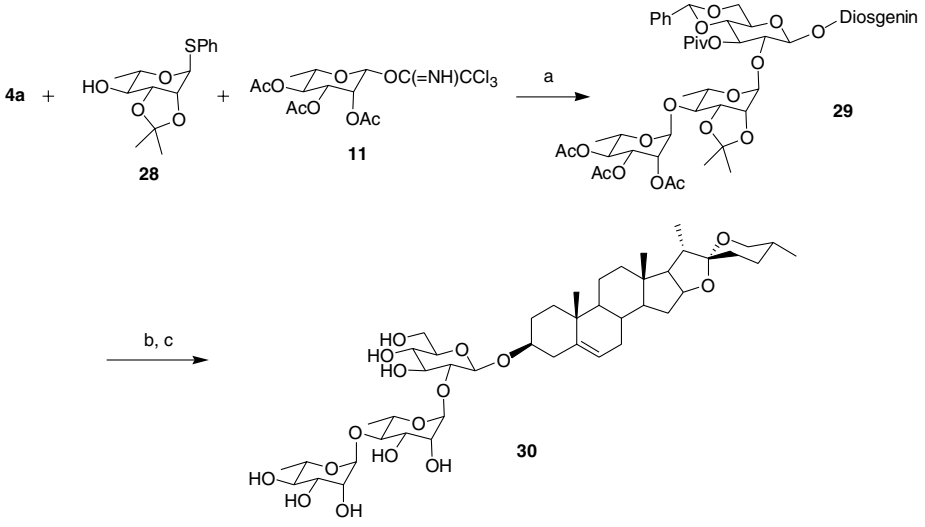

Scheme 4. Reagents and conditions: (a) 4 Å MS, TMSOTf, NIS, CH_2Cl_2, −20 °C; (b) AcOH (80%), 70 °C; (c) NaOH, MeOH/THF/H_2O (1:1:1).

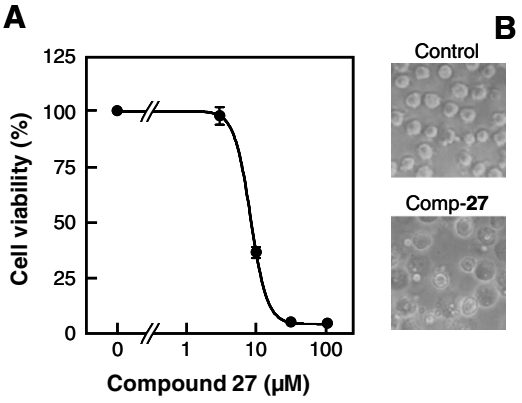

Figure 1. (A) Effect of diosgenyl glycoside **27** on human HL-60 cell viability. Cells were cultured in the presence of the indicated doses of compound **27** for 72 h, and thereafter cell viability was determined by the MTT assay as described in Section 5. The results of a representative experiment are shown. Each point represents the average of triplicate experiments. (B) Effects of diosgenyl glycoside **27** on the morphology of HL-60 cells as visualized by phase contrast microscopy. The cells were untreated (control) or treated with 10 μM of compound **27** (lower panel) for 16 h.

control and induced 48.6 ± 2.6% of apoptotic cells (data not shown). Morphological changes characteristic of apoptotic cells (fragmented and condensed chromatin) were visualized by fluorescent microscopy. Figure 2D shows a representative field of cells exposed to 10 μM of compound **25** for 6 h displaying such morphological changes and etoposide was also included as a positive control.

3.4. Involvement of caspase-3 activation in diosgenyl glycoside induced cell death

Next, we examined whether these diosgenyl glycosides (compounds **21**, **24**, **25**, and **27**) induce pro-caspase-3 cleavage since caspase-3 is the most active effector caspase to be involved in apoptosis induced by cytotoxic agents. Cleavage of procaspase-3 by diosgenyl glycosides was determined by immunoblotting using a polyclonal antihuman caspase-3 antibody that recognized the M_r 32,000 proenzyme (procaspase-3). The results indicate that these compounds at 10 μM promote the cleavage of procaspase-3 (Fig. 3, upper panel). An

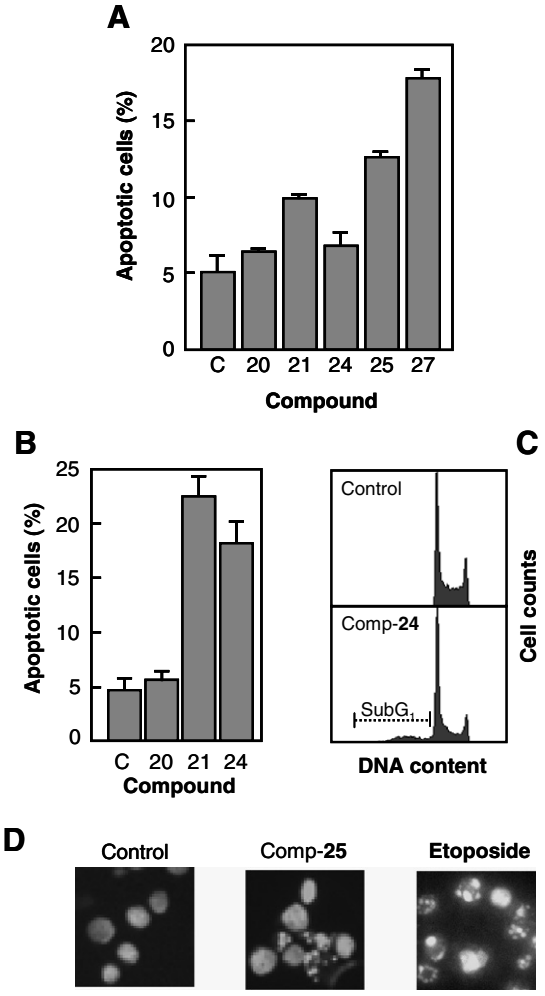

Figure 2. Induction of apoptosis in HL-60 cells by diosgenyl glycosides. (A) Cells were incubated with 10 μM of the indicated compounds for 16 h, and the percentages of apoptotic cells were determined by flow cytometry. The results of a representative experiment are shown, and each point represents the average ± SE of triplicate determinations. (B) Cells were treated with 30 μM of the indicated compounds and the percentages of apoptotic cells were determined by flow cytometry as above. (C) HL-60 cells were treated with 30 μM of **24**, harvested at 16 h, and subjected to DNA flow cytometry. (D) Cells were cultured in the absence (control) or presence of 10 μM of compound **25** for 6 h; then they were stained with Hoechst 33258 and nuclei were visualized using fluorescence microscopy. Etoposide was used as a positive control.

Table 3. Effect of synthetic steroidal saponins on cell cycle distribution of HL-60 cells

		%G_0/G_1	%S	%G_2-M
Control		49.1 ± 1.2	22.4 ± 1.0	28.5 ± 1.8
20	10 μM	50.8 ± 0.1	21.7 ± 0.8	27.5 ± 0.5
	30 μM	49.9 ± 1.2	22.1 ± 0.8	28.0 ± 0.7
21	10 μM	52.0 ± 0.2	20.8 ± 0.2	27.1 ± 0.7
	30 μM	61.5 ± 1.0	17.4 ± 2.0	21.1 ± 3.5
24	10 μM	52.2 ± 0.7	21.6 ± 0.5	26.2 ± 0.1
	30 μM	58.9 ± 4.5	17.4 ± 0.1	23.7 ± 0.9
25	10 μM	46.7 ± 0.2	22.7 ± 1.1	30.5 ± 0.1
	30 μM	41.7 ± 3.1	23.1 ± 0.1	35.2 ± 0.4
27	10 μM	44.9 ± 0.4	22.8 ± 0.1	32.3 ± 0.4
	30 μM	33.8 ± 4.5	25.2 ± 3.5	41.0 ± 6.4

The cells were cultured with the indicated compounds for 16 h and the cell cycle distribution was determined by flow cytometry. The results of a representative experiment are expressed as means ± SE of duplicate determinations

important processing of procaspase-3 was observed at 30 μM concentration, indicating that this effect was dose-dependent (results not shown).

Since poly(ADP-ribose) polymerase (PARP) is a typical substrate for caspase-3, we also examined whether these compounds induce PARP cleavage. Western blot analysis using a polyclonal antibody which recognizes the M_r 85,000 cleaved form of PARP shows the generation of the 85 kDa fragment in diosgenyl glycoside-treated cells after 6 h of treatment (Fig. 3, middle panel). Membranes were stripped and reprobed with β-actin antibody as loading control (Fig. 3, lower panel).

3.5. Diosgenyl glycoside-induced apoptosis involves mitochondrial cytochrome *c* release, but does not affect the expression of *Bcl*-2

The vast majority of conventional anti-cancer agents indirectly exploit mitochondria to exert their cytotoxic action. In order to evaluate whether apoptosis induced by diosgenyl glycosides **21**, **24**, **25**, and **27** in HL-60 and U937 cells involves cytochrome *c* release from mitochondria to cytosol, we subjected cytosolic preparations to immunoblot analysis. The exposure of HL-60 cells to these diosgenyl glycosides resulted in increased cytosolic cytochrome *c* and this response was observed at 6 h of treatment (Fig. 4A). Similar results were obtained with compounds **21** and **27** on U937 cells (Fig. 4B). Since the Bcl-2 family proteins are the central regulator of cytochrome *c* release and caspase activation,[27] we tested whether Bcl-2 is involved in the apoptosis induction by diosgenyl glycosides. The results indicate that the expression of Bcl-2 was unchanged after exposure to compounds **21**, **24**, **25**, and **27** (results not shown).

3.6. Diosgenyl glycoside-induced cell death involves caspase-9 activation

Once cytochrome *c* is in the cytoplasm, it binds to apoptotic protease-activating factor-1 (Apaf-1), which then permits recruitment of procaspase-9. Oligomerization results in autoactivation of procaspase-9. In the mitochondrial pathway, the complex of cytochrome *c*, Apaf-1, and caspase-9, called the 'apoptosome', is a critical activator of effector caspases. Incubation of HL-60 cells with 10 μM diosgenyl glycosides **21**, **24**, **25**, and **27** for 6 h promoted cleavage of the inactive pro-caspase-9 to the active 37 kDa fragment (Fig. 5).

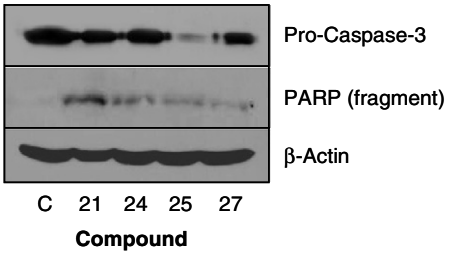

Figure 3. Western blot analysis for the cleavage of procaspase-3 and for the cleavage of poly (ADP-ribose) polymerase. Cells were treated with 10 μM of the indicated diosgenyl glycosides for 6 h and whole cell lysates were subjected to sodium dodecyl sulfate–polyacrylamide gel electrophoresis followed by blotting with an anti-procaspase-3 antibody (upper panel) or with an anti-poly(ADP-ribose) polymerase (PARP) antibody which recognizes the 85 kDa fragment (middle panel). The migration positions of full-length procaspase-3, as well as of PARP cleavage product p85, are indicated. Data shown are representative of two experiments performed. β-Actin was used as loading control (lower panel). Control lane (C) refers to untreated cells.

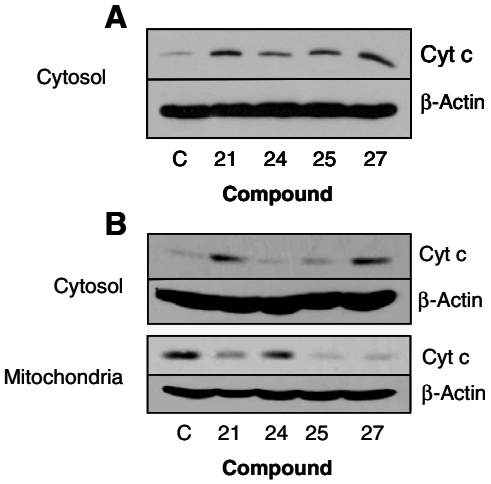

Figure 4. Analysis of cytochrome *c* release from mitochondria induced by diosgenyl glycosides. (A) HL-60 cells were treated with 10 μM of the indicated diosgenyl glycosides and harvested at 6 h. After treatment, cytosolic extracts were prepared, separated by sodium dodecyl sulfate–polyacrylamide gel electrophoresis, and cytochrome *c* was detected by immunoblotting. β-Actin was used as loading control. (B) U937 cells were treated as above and cytosolic or mitochondrial lysates were analyzed by immunoblotting with an anti-cytochrome *c* antibody.

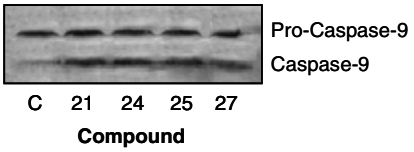

Figure 5. Western blot analysis for the cleavage of procaspase-9. HL-60 cells were cultured in the presence of 10 μM of the indicated diosgenyl glycosides and harvested at 6 h. Total cell lysates were subjected to sodium dodecyl sulfate–polyacrylamide gel electrophoresis followed by immunoblotting with an anti-procaspase-9 antibody that also recognizes the proteolytic fragments generated.

Taken together, these results allow us to conclude that the mitochondria play an important role in the activation of caspase-3, proteolytic cleavage of poly(ADP-ribose) polymerase, and induction of apoptosis triggered by diosgenyl glycosides in human myeloid cells.

4. Conclusions

In conclusion, we have synthesized a series of diosgenyl glycosides binding different monosaccharide units to

diosgenyl β-glucopyranoside (trillin) and evaluated the cytotoxicity against three different human cell lines (HL-60, U937, and SK-MEL-1). Not all diosgenyl glycosides were equally cytotoxic to the three cell lines. SK-MEL-1 cells were resistant to compounds **19**–**24**, while compounds **25** and **27** were the most cytotoxic toward all cell lines assayed. Induction of cell death by diosgenyl glycosides **21** and **24** in human leukemia cells was associated with cell cycle delays at the G_1 (and S) phase. However, compounds **25** and **27** induced G_2/M arrest like most DNA-damaging agents that arrest cells at the G_2/M transition. Cell death induced by diosgenyl glycosides **21**, **24**, **25**, and **27** was preceded by a rapid release of cytochrome *c* from mitochondria into the cytosol and subsequent caspase activation involving caspase-9 and -3 to cleave poly (ADP-ribose) polymerase. These findings suggest that these diosgenyl glycosides present anti-tumor activity, which may be mediated by apoptosis caused by cytochrome *c* release and caspase activation in human leukemia cells. Our data should contribute to the development of diosgenyl glycosides or related drugs as potential cancer chemotherapeutic or chemopreventive agents.

5. Experimental

5.1. General experimental procedures

Optical rotations were recorded in a Perkin-Elmer 343 polarimeter. ^{1}H NMR and ^{13}C NMR spectra were obtained on Bruker AMX-400, Avance 400, and Avance 300 spectrometers with standard pulse sequences operating at 400, 300 MHz in ^{1}H NMR and 100, 75 MHz in ^{13}C NMR. Chemical shifts are given in δ values (ppm) using tetramethylsilane as the internal standard. EIMS, HREIMS, FABS, and HRFABS were taken on a Micromass Autospec (70 eV) spectrometer. Column chromatography was carried out on silica gel 60 (Merck 230–400 mesh), and preparative TLC on silica gel 60 $PF_{254+366}$ plates (20 × 20 cm, 1 mm thickness), and Sephadex LH-20 (Aldrich). IR data reported in cm^{-1} were obtained using a Bruker IFS 55 spectrophotometer. Elemental analyses (C, H, N) were performed on a Fisons EA 1108 analyzer.

5.2. General conditions for coupling

To a mixture of diosgenyl 4,6-*O*-benzylidene-3-*O*-pivaloyl-β-D-glucopyranoside **4a** (360 mg, 0.48 mmol) and 4 Å MS (0.6 g) in dry CH_2Cl_2 (12 mL) at −78 °C, under N_2, $BF_3{\cdot}OEt_2$ (0.07 mL, 0.57 mmol) was added, followed by a solution of imidate **5** (349 mg, 0.71 mmol) in dry CH_2Cl_2 (4 mL). The mixture, warmed up to room temperature for 7 h, was neutralized with Et_3N (≈0.1 mL) to yield saponin **12** (Table 1).

5.2.1. Diosgenyl 2,3,4,6-tetra-*O*-acetyl-β-D-glucopyranosyl-(1 → 2)-4,6-*O*-benzylidene-3-*O*-pivaloyl-β-D-glucopyranoside (12). White amorphous solid, $[\alpha]_D^{20}$ −44° (*c* 0.100, $CHCl_3$). ^{1}H NMR (δ, $CDCl_3$, 400 MHz): 0.76 (6H, CH_3-18, CH_3-27), 0.95 (d, 3H, *J* = 6.7 Hz, CH_3-21), 1.00 (s, 3H, CH_3-19), 1.22 (s, 9H, CH_3-Piv), 1.97 (s, 3H, –OAc), 1.99 (s, 3H, –OAc), 2.03 (s, 3H, –OAc), 2.05 (s, 3H, –OAc), 3.38 (t, 1H, *J* = 10.8 Hz, H-26), 3.45 (m, 3H, H-26, H-3, H-5′), 3.57 (t, 1H, *J* = 9.4 Hz, H-4′), 3.67 (m, 2H, H-5″, H-2′), 3.71 (m, 1H, H-6′), 4.09 (m, 1H, H-6″), 4.29–4.42 (m, 3H, H-6′, H-6″, H-16), 4.61 (d, 1H, *J* = 8.0 Hz, H-1′), 4.67 (d, 1H, *J* = 7.9 Hz, H-1″), 4.97 (t, 1H, *J* = 7.2 Hz, H-2″), 5.08 (m, 2H, H-3″, H-4″), 5.26 (t, 1H, *J* = 7.9 Hz, H-3′), 5.35 (br d, 1H, H-6), 5.43 (s, 1H, Ph-*CH*), 7.29–7.35 (m, 5H, Ph). ^{13}C NMR (δ, $CDCl_3$, 75 MHz): 177.0 (*C*O-Piv), 170.7 (*C*O-Ac), 170.2 (*C*O-Ac), 169.8 (*C*O-Ac), 169.4 (*C*O-Ac), 140.4 (C-5), 128.2 (Ph), 125.8 (Ph), 121.8 (C-6), 109.3 (C-22), 101.1 (Ph*C*H), 100.7 (C-1″), 100.2 (C-1′), 80.80 (C-16), 80.20 (C-3), 78.9 (C-4′), 78.7 (C-2′), 73.6 (C-3′), 73.0 (C-3″), 71.0 (C-5″), 71.0 (C-2″), 68.8 (C-6′), 68.4 (C-4″), 66.85 (C-26), 65.4 (C-5′), 62.19 (C-17), 62.0 (C-6″), 56.51 (C-14), 50.07 (C-9), 41.62 (C-20), 40.27 (C-13), 39.78 (C-12), 38.69 (C-4), 37.12 (C-1), 36.81 (C-10), 32.05 (C-7), 31.83 (C-2), 31.42 (C-15), 31.40 (C-8), 30.30 (C-25), 29.56 (C-23), 28.81 (C-24), 27.16 (CH_3-Piv), 20.86 (C-11), 20.76 (*C*H_3-Ac), 20.55 (*C*H_3-Ac) and 19.36 (C-19), 17.12 (C-27), 16.28 (C-18), 14.51 (C-21). HRFABMS: 1079.5514 $(M+H)^+$ (calcd for $C_{59}H_{83}O_{18}$, 1079.5579) (5), 665 (12), 398 (14), 397 (56), 331 (36). Anal. Calcd for $C_{59}H_{82}O_{18}$: C, 65.66; H, 7.66. Found: C, 65.66; H, 7.28.

5.2.2. Diosgenyl 2,3,4,6-tetra-*O*-acetyl-β-D-galactopyranosyl-(1 → 2)-4,6-*O*-benzylidene-3-*O*-pivaloyl-β-D-glucopyranoside (13). White amorphous solid, $[\alpha]_D^{20}$ −38° (*c* 0.102, $CHCl_3$). ^{1}H NMR (δ, $CDCl_3$, 400 MHz): 0.76 (m, 6H, CH_3-18, CH_3-27), 0.95 (d, 3H, *J* = 6.7 Hz, CH_3-21), 1.00 (s, 3H, CH_3-19), 1.20 (s, 9H, CH_3-Piv), 1.95 (s, 3H, –OAc), 2.02 (s, 3H, –OAc), 2.04 (s, 3H, –OAc), 2.11 (s, 3H, –OAc), 3.35 (t, 1H, *J* = 10.9 Hz, H-26), 3.48 (m, 3H, H-26, H-3, H-5′), 3.59 (t, 1H, *J* = 9.5 Hz, H-4′), 3.68–3.73 (m, 2H, H-2′, H-6′), 3.86 (t, 1H, *J* = 7.0 Hz, H-5″), 4.0 (dd, 1H, *J* = 10.5; 5.0 Hz, H-6′), 4.12 (m, 2H, H-6″), 4.39 (dd, 1H, *J* = 14.2; 6.6 Hz, H-16), 4.63 (m, 2H, H-1′, H-1″), 4.89 (dd, 1H, *J* = 10.5; 3.3 Hz, H-3″), 5.14 (dd, 1H, *J* = 10.4; 8.0 Hz, H-2″), 5.26 (t, 1H, *J* = 8.5 Hz, H-3′), 5.35 (m, 2H, H-6, H-4″), 5.43 (s, 1H, Ph-C*H*), 7.29–7.35 (m, 5H, Ph). ^{13}C NMR (δ, $CDCl_3$, 75 MHz): 177.0 (*C*O-Piv), 170.4, 170.2 and 169.9 (*C*O-Ac), 140.6 (C-5), 128.2 (Ph), 125.8 (Ph), 121.7 (C-6), 109.3 (C-22), 101.1 (Ph*C*H), 100.9 (C-1″), 100.3 (C-1′), 80.82 (C-16), 80.16 (C-3), 78.80 (C-4′), 78.23 (C-2′), 73.58 (C-3′), 71.05 (C-3″), 70.41 (C-5″), 68.88 (C-6′), 68.73 (C-2″), 66.88 (C-4″), 66.88 (C-26), 65.50 (C-5′), 62.15 (C-17), 60.9 (C-6″), 56.50 (C-14), 50.07 (C-9), 41.63 (C-20), 40.28 (C-13), 39.77 (C-12), 38.79 (C-4), 37.07 (C-1), 36.84 (C-10), 32.06 (C-7), 31.85 (C-2), 31.47 (C-8), 31.41 (C-15), 30.30 (C-25), 29.51 (C-23), 28.82 (C-24), 27.16 (*C*H_3-Piv), 20.86 (C-11), 20.73, 20.65 and 20.54 (*C*H_3-Ac), 19.40 (C-19), 17.12 (C-27), 16.28 (C-18), 14.51 (C-21). HRFABMS: 1079 $(M+H)^+$, 1078.5470 (M^+) (calcd. for $C_{59}H_{83}O_{18}$, 1078.5501) (5), 665 (14), 398 (17), 397 (57), 331 (74). Anal. Calcd for $C_{59}H_{82}O_{18}$: C, 65.66; H, 7.66. Found: C, 65.91; H, 7.40.

5.2.3. Diosgenyl 2,3,4,6-tetra-*O*-acetyl-α-D-mannopyranosyl-(1 → 2)-4,6-*O*-benzylidene-3-*O*-pivaloyl-β-D-glucopyranoside (14). White amorphous solid, $[\alpha]_D^{20}$ −43° (*c*

0.020, $CHCl_3$). ^1H NMR (δ, $CDCl_3$, 400 MHz): 0.76 (m, 6H, CH_3-18, CH_3-27), 0.89 (d, 3H, J = 5.5 Hz, CH_3-21), 0.99 (s, 3H, CH_3-19), 1.16 (s, 9H, CH_3-Piv), 3.35 (t, 1H, J = 10.9 Hz, H-26), 3.44 (d, 1H, J = 3.4 Hz, H-26), 3.50 (m, 1H, H-5′), 3.56 (t, 1H, J = 9.6 Hz, H-4′), 3.61 (m, 1H, H-3), 3.70 (m, 1H, H-2′), 3.56 (m, 1H, H-4′), 3.74 (t, 1H, J = 10.2 Hz, H-6′$_b$), 3.99 (m, 1H, H-5′), 4.33 (dd, 1H, J = 10.4; 4.8 Hz, H − 6′$_a$), 4.38 (dd, 1H, J = 14.4, 7.1 Hz, H-16), 4.71 (d, 1H, J = 7.5 Hz, H-1′), 5.22 (dd, 1H, J = 10.1; 2.7 Hz, H-3″), 5.29 (m, 1H, H-2″), 5.30 (m, 1H, H-4″), 5.33 (t, 1H, J = 9.7 Hz, H-3′), 5.36 (br d, 1H, H-6), 5.44 (s, 1H, H-1″), 5.45 (s, 1H, PhC*H*), 7.33–7.40 (m, 5H, Ph). ^{13}C RMN (δ, $CDCl_3$, 75 MHz): 177.0 (*C*O-Piv), 170.7, 169.7, 169.6 and 169.5 (*C*O-Ac), 140.0 (C-5), 125.8 and 128.2 (Ph), 122.1 (C-6), 109.3 (C-22), 101.5 (C-1′), 101.1 (Ph*C*H), 97.2 (C-1″), 80.81 (C-16), 79.25 (C-4′), 79.25 (C-3), 76.48 (C-2′), 72.43 (C-3′), 69.33 (C-2″), 68.89 (C-3″), 68.63 (C-6′), 68.63 (C-5″), 66.82 (C-26), 65.95 (C-5′), 65.79 (C-4″), 62.13 (C-17), 62.13 (C-6″), 56.47 (C-14), 50.07 (C-9), 41.62 (C-20), 40.26 (C-13), 39.79 (C-12), 38.07 (C-4), 37.17 (C-1), 36.85 (C-10), 32.10 (C-7), 31.84 (C-2), 31.84 (C-15), 31.40 (C-8), 30.29 (C-25), 29.63 (C-23), 28.81 (C-24), 27.16 (*C*H_3-Piv), 20.80 (C-11), 20.71 and 20.63 (*C*H_3-Ac), 19.18 (C-19), 17.12 (C-27), 16.24 (C-18), 14.51 (C-21). HRFABMS: 1079.5623 $(M+H)^+$ (calcd for $C_{59}H_{83}O_{18}$, 1079.5579), 661 (6), 398 (9), 397 (39), 331 (32). Anal. Calcd for $C_{59}H_{82}O_{18}$: C, 65.66; H, 7.66. Found: C, 65.35; H, 7.61.

5.2.4. Diosgenyl 2,3,4-tri-*O*-acetyl-β-D-xilopyranosyl-(1 → 2)-4,6-*O*-benzylidene-3-*O*-pivaloyl-β-D-glucopyranoside (15). White amorphous solid, $[\alpha]_D^{20}$ −57° (*c* 0.100, $CHCl_3$). ^1H NMR (δ, $CDCl_3$, 400 MHz): 0.77 (m, 6H, CH_3-18, CH_3-27), 0.96 (d, 3H, J = 6.7 Hz, CH_3-21), 1.02 (s, 3H, CH_3-19), 1.21 (s, 9H, CH_3-Piv), 2.05 (s, 3H, –OAc), 2.08 (s, 3H, –OAc), 2.16 (s, 3H, –OAc), 3.35 (m, 1H, H-26), 3.38 (1H, H-5″), 3.44–3.55 (m, 4H, H-26, H-3, H-5′, H-4′), 3.69–3.76 (m, 2H, H-2′, H-6′), 4.25 (dd, 1H, J = 12.2; 4.7 Hz, H-5″), 4.31 (dd, 1H, J = 10.5; 4.9 Hz, H-6′), 4.40 (dd, 1H, J = 14.7; 6.9 Hz, H-16), 4.62 (d, 1H, J = 7.2 Hz, H-1′), 4.75 (d, 1H, J = 6.1 Hz, H-1″), 4.85–4.93 (m, 2H, H-2″, H-4″), 5.06 (t, 1H, J = 7.9 Hz, H-3″), 5.29 (t, 1H, J = 8.9 Hz, H-3′), 5.37 (br d, 1H, H-6), 5.44 (s, 1H, Ph-*CH*), 7.29–7.35 (m, 5H, Ph). ^{13}C RMN (δ, $CDCl_3$, 75 MHz): 177.0 (*C*O-Piv), 169.9 and 169.6 (*C*O-Ac), 140.2 (C-5), 128.2 and 125.8 (Ph), 121.9 (C-6), 109.3 (C-22), 101.1 (Ph*C*H), 101.0 (C-1″), 100.1 (C-1′), 80.80 (C-16), 79.73 (C-3), 78.91 (C-4′), 77.25 (C-2′), 73.74 (C-3′), 70.89 (C-3″), 70.19 (C-2″), 69.05 (C-4″), 68.79 (C-6′), 66.81 (C-26), 65.59 (C-5′), 62.06 (C-17), 61.78 (C-5″), 56.47 (C-14), 50.04 (C-9), 41.58 (C-20), 40.24 (C-13), 39.74 (C-12), 38.63 (C-4), 37.12 (C-1), 36.82 (C-10), 32.04 (C-7), 31.81 (C-2), 31.37 (C-8), 31.37 (C-15), 30.27 (C-25), 29.53 (C-23), 28.77 (C-24), 27.16 (CH_3-Piv), 20.83 (C-11), 20.77, 20.70 and 20.63 (*C*H_3-Ac), 19.40 (C-19), 17.10 (C-27), 16.27 (C-18), 14.49 (C-21). FABMS: 1008 $(M+H)^+$($C_{56}H_{79}O_{16}$), 1005 $(M-H)^+$, 604 (10), 593 (16), 523 (24), 398 (24), 397 (54), 396 (21). Anal. Calcd for $C_{56}H_{79}O_{16}$: C, 66.78; H, 7.81. Found: C, 66.91; H, 7.35.

5.2.5. Diosgenyl 2,3,4-tri-*O*-acetyl-β-L-arabinopyranosyl-(1 → 2)-4,6-*O*-benzylidene-3-*O*-pivaloyl-β-D-glucopyranoside (16). White amorphous solid, $[\alpha]_D^{20}$ −33° (*c* 0.105, $CHCl_3$). ^1H NMR (δ, $CDCl_3$, 400 MHz): 0.75 (m, 6H, CH_3-18, CH_3-27), 0.94 (d, 3H, J = 6.7 Hz, CH_3-21), 0.98 (s, 3H, CH_3-19), 1.17 (s, 9H, CH_3-Piv), 2.00 (s, 3H, –OAc), 2.03 (s, 3H, –OAc), 2.05 (s, 3H, –OAc), 3.35 (t, 1H, J = 10.9 Hz, H-26), 3.43–3.60 (m, 5H, H-26, H-3, H-5′, H-5″, H-4′), 3.66–3.73 (m, 2H, H-2′, H-6′), 4.12 (dd, 1H, J = 12.7; 4.8 Hz, H-5″), 4.29 (dd, 1H, J = 10.5; 4.9 Hz, H-6′), 4.40 (dd, 1H, J = 14.7; 6.9 Hz, H-16), 4.63 (d, 1H, J = 7.0 Hz, H-1′), 4.65 (d, 1H, J = 5.7 Hz, H-1″), 4.98 (dd, 1H, J = 8.2; 3.4 Hz, H-3″), 5.04 (dd, 1H, J = 8.1; 5.8 Hz, H-2″), 5.16 (m, 1H, H-4″), 5.25 (t, 1H, J = 8.5 Hz, H-3′), 5.36 (br d, 1H, H-6), 5.42 (s, 1H, Ph-*CH*), 7.29–7.35 (m, 5H, Ph). ^{13}C RMN (δ, $CDCl_3$, 75 MHz): 177.0 (*C*O-Piv), 170.2 and 170.1 (*C*O-Ac), 140.5 (C-5), 128.2 (Ph) and 125.8 (Ph), 121.8 (C-6), 109.3 (C-22), 101.1 (Ph*C*H), 100.2 (C-1′), 99.9 (C-1″), 80.78 (C-16), 79.70 (C-3), 78.87 (C-4′), 77.40 (C-2′), 73.63 (C-3′), 69.46 (C-3″), 69.10 (C-2″), 68.87 (C-6′), 66.99 (C-4″), 66.81 (C-26), 65.54 (C-5′), 62.10 (C-17), 61.73 (C-5″), 56.47 (C-14), 50.07 (C-9), 41.60 (C-20), 40.25 (C-13), 39.74 (C-12), 38.79 (C-4), 37.09 (C-1), 36.83 (C-10), 32.05 (C-7), 31.82 (C-2), 31.43 (C-8), 31.38 (C-15), 30.27 (C-25), 29.51 (C-23), 28.79 (C-24), 27.16 (CH_3-Piv), 20.86 (C-11), 20.74 and 20.63 (*C*H_3-Ac), 19.34 (C-19), 17.13 (C-27), 16.29 (C-18), 14.52 (C-21) FABMS: 1008 $(M+H)^+$ ($C_{56}H_{79}O_{16}$), 397 (64). Anal. Calcd for $C_{56}H_{79}O_{16}$: C, 66.78; H, 7.81. Found: C, 66.85; H, 7.43.

5.2.6. Diosgenyl 2,3,4-tri-*O*-acetyl-β-L-fucopyranosyl-(1 → 2)-4,6-*O*-benzylidene-3-*O*-pivaloyl-β-D-glucopyranoside (17). White amorphous solid, $[\alpha]_D^{20}$ −34° (*c* 0.095, $CHCl_3$). ^1H NMR (δ, $CDCl_3$, 400 MHz): 0.73 (m, 6H, CH_3-18, CH_3-27), 0.91 (d, 3H, J = 6.7 Hz, CH_3-21), 1.00 (s, 3H, CH_3-19), 1.11 (d, 3H, J = 6.2 Hz, H-6″), 1.19 (s, 9H, CH_3-Piv), 1.91 (s, 3H, –OAc), 1.97 (s, 3H, –OAc), 2.05 (s, 3H, –OAc), 3.31 (t, 1H, J = 10.9 Hz, H-26), 3.41–3.56 (m, 4H, H-26, H-3, H-5′, H-4′), 3.66–3.73 (m, 3H, H-2′, H-6′, H-5″), 4.26 (dd, 1H, J = 10.5; 4.8 Hz, H-6′), 4.36 (dd, 1H, J = 14.7; 6.9 Hz, H-16), 4.59 (d, 1H, J = 7.9 Hz, H-1′), 4.86 (d, 1H, J = 7.6 Hz, H-1″), 4.90–4.98 (m, 2H, H-3″, H-4″), 5.12–5.19 (m, 2H, H-2″, H-3′), 5.32 (br d, 1H, H-6), 5.41 (s, 1H, Ph-C*H*), 7.29–7.35 (m, 5H, Ph). ^{13}C RMN (δ, $CDCl_3$, 75 MHz) 177.0 (*C*O-Piv), 170.7, 170.2 169.8 and 169.4 (*C*O-Ac), 140.4 (C-5), 128.2 and 125.8 (Ph). 121.8 (C-6), 109.3 (C-22), 101.1 (Ph*C*H), 100.97 (C-1′), 99.08 (C-1″), 80.80 (C-16), 79.90 (C-3), 78.92 (C-4′), 75.49 (C-2′), 71.79 (C-4″), 70.94 (C-2″), 70.28 (C-3′), 69.56 (C-3″), 68.80 (C-5″), 68.66 (C-6′), 66.81 (C-26), 66.11 (C-5′), 62.10 (C-17), 56.51 (C-14), 50.07 (C-9), 41.62 (C-20), 40.27 (C-13), 39.78 (C-12), 38.80 (C-4), 37.10 (C-1), 36.81 (C-10), 32.05 (C-7), 31.79 (C-2), 31.42 (C-8), 31.42 (C-15), 30.30 (C-25), 29.56 (C-23), 28.81 (C-24), 27.16 (*C*H_3-Piv), 20.97 (C-6″), 20.86 (C-11), 20.76 and 20.55 (*C*H_3-Ac), 19.39 (C-19), 17.12 (C-27), 16.28 (C-18), 14.51 (C-21). HRFABMS: 1021.5515 $(M+H)^+$ (calcd. for $C_{57}H_{81}O_{16}$, 1021.5525) (5), 607 (14), 398 (14), 397 (50), 396 (13). Anal. Calcd for $C_{57}H_{80}O_{16}$: C, 67.04; H, 7.90. Found: C, 67.05; H, 7.93.

5.2.7. Diosgenyl 2,3,4-tri-*O*-acetyl-α-L-rhamnopyranosyl-(1 → 2)-4,6-*O*-benzylidene-3-*O*-pivaloyl-β-D-glucopyranoside (18). White amorphous solid, $[\alpha]_D^{20}$ −45° (*c* 0.090, $CHCl_3$). ^1H NMR (δ, $CDCl_3$, 400 MHz): 0.77 (m, 6H, CH_3-18, CH_3-27), 0.96 (d, 3H, *J* = 6.7 Hz, CH_3-21), 1.01 (s, 3H, CH_3-19), 1.19 (d, 3H, *J* = 6.1 Hz, CH_3-6′), 1.12 (s, 9H, CH_3-Piv), 1.95 (s, 3H, –OAc), 2.00 (s, 3H, –OAc), 2.09 (s, 3H, –OAc), 3.36 (t, 1H, *J* = 10.8 Hz, H-26), 3.45–3.54 (m, 3H, H-26, H-5′, H-4′), 3.63 (m, 1H, H-3), 3.71–3.80 (m, 2H, H-2′, H-6′), 4.32 (dd, 1H, *J* = 10.5; 4.8 Hz, H-6′), 4.37–4.48 (m, 2H, H-16, H-5″), 4.70 (d, 1H, *J* = 7.6 Hz, H-1′), 4.93 (s, 1H, H-1″), 5.04 (t, 1H, *J* = 9.9 Hz, H-4″), 5.17 (d, 1H, *J* = 1.4 Hz, H-2″), 5.23 (dd, 1H, *J* = 9.9; 3.3 Hz, H-3″), 5.37–5.41 (m, 2H, H-6, H-3′), 5.43 (s, 1H, Ph-C*H*), 7.29–7.35 (m, 5H, Ph). ^{13}C RMN (δ, $CDCl_3$, 75 MHz): 177.0 (*C*O-Piv), 170.55, 170.27 and 169.27 (*C*O-Ac), 140.09 (C-5), 128.2 and 125.8 (Ph), 122.03 (C-6), 109.22 (C-22), 101.1 (Ph*C*H), 99.6 (C-1′), 97.6 (C-1″), 80.74 (C-16), 79.04 (C-4′), 78.61 (C-3), 75.39 (C-2′), 73.84 (C-3′), 71.22 (C-4″), 69.60 (C-2″), 68.84 (C-3″), 68.65 (C-6′), 66.77 (C-26), 66.40 (C-5″), 66.02 (C-5′), 62.09 (C-17), 56.44 (C-14), 50.06 (C-9), 41.57 (C-20), 40.26 (C-13), 39.72 (C-12), 38.15 (C-4), 37.16 (C-1), 36.82 (C-10), 32.03 (C-7), 31.83 (C-2), 31.40 (C-15), 31.35 (C-8), 30.24 (C-25), 29.74 (C-23), 28.78 (C-24), 27.16 (CH_3-Piv), 20.89 (C-11), 20.97, 20.89 and 20.52 (*C*H_3-Ac), 19.41 (C-19), 17.21 (C-6″), 17.13 (C-27), 16.00 (C-18), 14.52 (C-21). HRFABMS: 1021.5549 $(M+H)^+$ (calcd for $C_{57}H_{81}O_{16}$, 1021.5525) (4), 607 (17), 398 (19), 397 (65), 396 (17). Anal. Calcd for $C_{57}H_{81}O_{16}$: C, 67.04; H, 7.90. Found: C, 67.09; H, 7.89.

5.3. General procedure to obtain compounds 19–25

A solution of **12** (269.5 mg, 0.25 mmol) in AcOH (20 mL, 80%) was stirred at 70 °C for 2 h, then concentrated and dissolved in CH_2Cl_2/MeOH (1:1) (8 mL) and NaOH (0.1 equiv for each ester) was added and stirred overnight at 40 °C. The mixture was neutralized with acid resin Dowex-50 (H^+), the residue was filtered, and the solvent was evaporated to yield compound **19** (Table 1).

5.3.1. Diosgenyl β-D-glucopyranosyl-(1 → 2)-β-D-glucopyranoside (19). White amorphous solid, $[\alpha]_D^{20}$ −38° (*c* 0.011, EtOH); IR ν_{max} (film, NaCl) 3363, 2926, 1376, 1075, 982, 898 cm^{-1}; ^1H NMR (δ, pyridine, 400 MHz): 0.66 (d, 3H, *J* = 4.3 Hz, CH_3-27), 0.78 (s, 3H, CH_3-18), 0.95 (s, 3H, CH_3-19), 1.10 (d, 3H, *J* = 6.8 Hz, CH_3-21), 1.77 (m, 1H, H-17), 3.45 (t, 1H, *J* = 9.9 Hz, H-26), 3.54 (m, 1H, H-26), 3.80 (m, 1H, H-3), 3.87 (m, 1H, H-5′), 3.95 (m, 1H, H-5″), 4.11 (m, 2H, H-2′, H-2″), 4.21 (m, 2H, H-3″, H-4″), 4.31 (m, 2H, H-3′, H-4′), 4.31–4.50 (dd, 1H, *J* = 14.4, 7.1 Hz, H-16), 4.51 (m, 2H, H-6′, H-6″), 5.03 (d, 1H, *J* = 7.5 Hz, H-1′), 5.24 (d, 1H, *J* = 7.6 Hz, H-1″), 5.30 (br d, 1H, *J* = 4.6 Hz, H-6). ^{13}C NMR (δ, pyridine, 75 MHz): 141.0 (C-5), 121.6 (C-6), 109.3 (C-22), 106.5 (C-1″), 101.4 (C-1′), 84.42 (C-2′), 81.83 (C-16), 79.35 (C-3), 78.73 (C-5′), 78.16 (C-5″), 77.96 (C-3″), 77.84 (C-3′), 76.95 (C-2″), 71.42 (C-4′), 71.36 (C-4″), 66.84 (C-26), 62.84 (C-17), 62.84 (C-6″), 62.62 (C-6′), 56.65 (C-14), 50.24 (C-9), 41.97 (C-20), 40.45 (C-13), 39.89 (C-12), 39.22 (C-4), 37.32 (C-1), 37.02 (C-10), 32.18 (C-2), 32.18 (C-7), 31.79 (C-8), 31.61 (C-15), 30.58 (C-25), 30.21 (C-23), 29.24 (C-24), 21.11 (C-11), 19.49 (C-19), 17.34 (C-27), 16.37 (C-18), 15.05 (C-21). FABMS *m*/*z* 761 $(M+Na)^+$, 413, 397. HRFABMS *m*/*z* 761.4117, calcd for $C_{39}H_{62}O_{13}Na$, 761.4088; Anal. Calcd for $C_{39}H_{62}O_{13}$: C, 63.39; H, 8.46. Found: C, 63.32; H, 8.74.

5.3.2. Diosgenyl β-D-galactopyranosyl-(1 → 2)-β-D-glucopyranoside (20). White amorphous solid, $[\alpha]_D^{20}$ −27° (*c* 0.041, EtOH); IR ν_{max} (film, NaCl) 3363, 2925, 1462, 1080, 897 cm^{-1}; ^1H NMR (δ, pyridine, 400 MHz): 0.65 (d, 3H, *J* = 4.7 Hz, CH_3-27), 0.78 (s, 3H, CH_3-18), 0.94 (s, 3H, CH_3-19), 1.09 (d, 3H, *J* = 6.8 Hz, CH_3-21), 3.45 (t, 1H, *J* = 9.9 Hz, H-26), 3.53 (m, 1H, H-26), 3.79–3.84 (m, 2H, H-3, H-5′), 3.95 (m, 1H, H-5″), 4.08 (m, 2H, H-2′, H-2″), 4.15 (m, 1H, H-3″), 4.19 (m, 1H, H-4′), 4.27–4.33 (m, 2H, H-3′, H-6″), 4.44–4.54 (m, 3H, H-6′, H-6″) 4.55 (m, 1H, H-5″), 4.58 (m, 1H, H-2″), 5.02 (d, 1H, *J* = 7.5 Hz, H-1′), 5.11 (d, 1H, *J* = 7.7 Hz, H-1″), 5.33 (br d, 1H, H-6). ^{13}C NMR (δ, pyridine, 75 MHz): 140.8 (C-5), 121.3 (C-6), 109.0 (C-22), 107.3 (C-1″), 101.2 (C-1′), 85.00 (C-2′), 81.87 (C-16), 79.12 (C-3), 77.93 (C-5′), 77.67 (C-3′), 76.97 (C-4″), 74.80 (C-3″), 74.35 (C-2″), 71.12 (C-4′), 69.64 (C-5″), 62.65 (C-17), 66.64 (C-26), 62.64 (C-6″), 62.33 (C-6′), 56.42 (C-14), 50.01 (C-9), 41.73 (C-20), 40.21 (C-13), 39.65 (C-12), 39.05 (C-4), 37.18 (C-1), 36.81 (C-10), 32.04 (C-2), 32.04 (C-7), 31.58 (C-8), 31.40 (C-15), 30.36 (C-25), 30.00 (C-23), 29.03 (C-24), 20.88 (C-11), 19.27 (C-19), 17.10 (C-27), 16.12 (C-18), 14.80 (C-21). FABMS *m*/*z* 761 $(M+Na)^+$, 397; HRFABMS *m*/*z* 761.4053, calcd for $C_{39}H_{62}O_{13}Na$, 761.4088; Anal. Calcd for $C_{39}H_{62}O_{13}$: C, 63.39; H, 8.46. Found: C, 63.34; H, 8.71.

5.3.3. Diosgenyl α-D-mannopyranosyl-(1 → 2)-β-D- glucopyranoside (21). White amorphous solid, $[\alpha]_D^{20}$ −34 ° (*c* 0.013, EtOH); IR ν_{max} (film, NaCl) 3427, 2930, 1645, 979 cm^{-1}; ^1H NMR (δ, pyridine, 400 MHz): 0.65 (d, 3H, *J* = 4.3 Hz, CH_3-27), 0.79 (s, 3H, CH_3-18), 0.81 (s, 3H, CH_3-19), 1.09 (d, 3H, *J* = 6.9 Hz, CH_3-21), 3.45 (t, 1H, *J* = 10.4 Hz, H-26), 3.54 (m, 1H, H-26), 3.76 (m, 1H, H-5′), 3.85 (m, 1H, H-3), 3.95 (m, 1H, H-5″), 4.10–4.17 (m, 3H, H-2′, H-3′, H-4′), 4.27–4.55 (m, 3H, H-6″, H-6′, H-16), 4.68 (dd, 1H, *J* = 3.2; 9.1 Hz, H-3″), 4.75–4.79 (m, 2H, H-2″, H-4″), 4.94 (d, 1H, *J* = 7.3 Hz, H-1′), 5.13 (m, 1H, H-5″), 5.19 (br d, 1H, *J* = 4.8 Hz, H-6), 6.07 (s, 1H, H-1″). ^{13}C NMR (δ, pyridine, 75 MHz): 141.0 (C-5), 121.6 (C-6), 109.3 (C-22), 106.5 (C-1″), 101.4 (C-1′), 84.42 (C-2′), 81.83 (C-16), 79.35 (C-3), 78.73 (C-5′), 78.16 (C-5″), 77.96 (C-3″), 77.84 (C-3′), 76.95 (C-2″), 71.42 (C-4′), 71.36 (C-4″), 66.84 (C-26), 62.84 (C-17), 62.84 (C-6″), 62.80 (C-6′), 56.65 (C-14), 50.24 (C-9), 41.97 (C-20), 40.45 (C-13), 39.89 (C-12), 39.22 (C-4), 38.32 (C-1), 37.02 (C-10), 32.18 (C-2), 32.18 (C-7), 31.79 (C-8), 31.61 (C-15), 30.58 (C-25), 30.21 (C-23), 29.24 (C-24), 21.11 (C-11), 19.49 (C-19), 17.34 (C-27), 16.37 (C-18), 15.05 (C-21). FABMS *m*/*z* 761 $(M+Na)^+$, 513, 397; HRFABMS *m*/*z*

761.4088, calcd for $C_{39}H_{62}O_{13}Na$, 761.4088; Anal. Calcd for $C_{39}H_{62}O_{13}$: C, 63.39; H, 8.46. Found: C, 63.41; H, 8.42.

5.3.4. Diosgenyl β-D-xylopyranosyl-(1 → 2)-β-D-glucopyranoside (22). White amorphous solid, $[\alpha]_D^{20}$ −39 ° (*c* 0.022, EtOH); IR ν_{max} (film, NaCl) 3271, 2928, 1046, 982, 833 cm^{-1}; ^1H NMR (δ, pyridine, 400 MHz): 0.66 (d, 3H, *J* = 4.3 Hz, CH_3-27), 0.80 (s, 3H, CH_3-18), 0.92 (s, 3H, CH_3-19), 1.10 (d, 3H, *J* = 6.8 Hz, CH_3-21), 3.45 (t, 1H, *J* = 9.5 Hz, H-26), 3.55 (m, 1H, H-26), 3.72 (t, 1H, *J* = 10.2 Hz, H-5″), 3.86 (m, 2H, H-3, H-5′), 4.04–4.10 (m, 2H, H-2′, H-2″), 4.14–4.19 (m, 3H, H-4′, H-3″, H-4″), 4.29 (m, 2H, H-3′, H-6′), 4.40–4.51 (m, 3H, H-6′, H-5″, H-16), 5.00 (d, 1H, *J* = 7.4 Hz, H-1′), 5.18 (m, 1H, H-1″), 5.29 (br d, 1H, H-6). ^{13}C NMR (δ, pyridine, 75 MHz): 140.8 (C-5), 121.46 (C-6), 109.0 (C-22), 106.5 (C-1″), 100.7 (C-1′), 83.32 (C-2′), 81.86 (C-16), 78.80 (C-3), 78.04 (C-5′), 77.95 (C-3′), 77.43 (C-3″), 75.79 (C-2″), 71.09 (C-4′), 70.79 (C-4″), 67.12 (C-5″), 62.65 (C-17), 66.62 (C-26), 62.33 (C-6′), 56.44 (C-14), 50.02 (C-9), 41.73 (C-20), 40.23 (C-13), 39.66 (C-12), 39.00 (C-4), 37.16 (C-1), 36.84 (C-10), 32.01 (C-2), 31.96 (C-7), 31.58 (C-8), 31.43 (C-15), 30.36 (C-25), 29.90 (C-23), 29.03 (C-24), 20.89 (C-11), 19.20 (C-19), 17.10 (C-27), 16.14 (C-18), 14.81 (C-21); FABMS *m*/*z* 731 $(M+Na)^+$, 415, 397. HRFABMS *m*/*z* 731.3962, calcd for $C_{38}H_{60}O_{12}Na$, 731.3982; Anal. Calcd for $C_{38}H_{60}O_{12}$: C, 64.38; H, 8.53. Found: C, 64.45; H, 8.46.

5.3.5. Diosgenyl β-L-arabinopyranosyl-(1 → 2)-β-D-glucopyranoside (23). White amorphous solid, $[\alpha]_D^{20}$ −21° (*c* 0.038, EtOH); IR ν_{max} (film, NaCl) 3442, 2360, 1054, 835 cm^{-1}; ^1H NMR (δ, pyridine, 400 MHz): 0.72 (d, 3H, *J* = 4.3 Hz, CH_3-27), 0.86 (s, 3H, CH_3-18), 0.98 (s, 3H, CH_3-19), 1.16 (d, 3H, *J* = 6.8 Hz, CH_3-21), 3.52 (t, 1H, *J* = 9.5 Hz, H-26), 3.62 (m, 1H, H-26), 3.84–3.91 (m, 3H, H-5′, H-6″, H-3), 4.22 (t, 1H, *J* = 10.2 Hz, H-4′), 4.27–4.37 (m, 3H, H-3′, H-3″, H-6′), 4.44–4.52 (m, 2H, H-6′, H-6″), 4.56–4.62 (m, 2H, H-2″, H-16), 5.05 (d, 1H, *J* = 7.2 Hz, H-1′), 5.30 (d, 1H, *J* = 5.8 Hz, H-1″), 5.34 (br d, 1H, H-6). ^{13}C NMR (δ, pyridine, 75 MHz): 140.9 (C-5), 121.76 (C-6), 109.3 (C-22), 105.7 (C-1″), 100.9 (C-1′), 82.85 (C-2′), 81.12 (C-16), 78.92 (C-3), 78.13 (C-3′), 78.13 (C-5′), 74.06 (C-3″), 73.09 (C-2″), 71.30 (C-4′), 68.58 (C-4″), 66.85 (C-26), 66.14 (C-5″), 62.79 (C-17), 62.48 (C-6′), 56.64 (C-14), 50.22 (C-9), 41.94 (C-20), 40.44 (C-13), 39.86 (C-12), 39.12 (C-4), 37.40 (C-1), 37.02 (C-10), 32.15 (C-2), 32.15 (C-7), 31.76 (C-8), 31.62 (C-15), 30.55 (C-25), 29.94 (C-23), 29.21 (C-24), 21.09 (C-11), 19.42 (C-19), 17.31 (C-27), 16.36 (C-18), 15.02 (C-21). FABMS *m*/*z* 731 $(M+Na)^+$ 415, 397. HRFABMS *m*/*z* 731.3977, calcd for $C_{38}H_{60}O_{12}Na$, 731.3982; Anal. Calcd for $C_{38}H_{60}O_{12}$: C, 64.38; H, 8.53. Found: C, 64.25; H, 8.59.

5.3.6. Diosgenyl β-L-fucopyranosyl-(1 → 2)-β-D-glucopyranoside (24). White amorphous solid, $[\alpha]_D^{20}$ −54° (*c* 0.024, EtOH); IR ν_{max} (film, NaCl) 3388, 2940, 1052, 900, 865 cm^{-1}; ^1H NMR (δ, pyridine, 400 MHz): 0.65 (d, 3H, *J* = 4.3 Hz, CH_3-27), 0.79 (s, 3H, CH_3-18), 0.94 (s, 3H, CH_3-19), 1.10 (d, 3H, *J* = 6.7 Hz, CH_3-21), 1.45 (d, 3H, *J* = 6.2 Hz, CH_3-6″), 3.45 (t, 1H, *J* = 9.5 Hz, H-26), 3.55 (m, 1H, H-26), 3.78–3.86 (m, 3H, H-5″, H-5′, H-3), 3.98–4.02 (m, 2H, H-2′, H-2″), 4.05 (m, 1H, H-3″), 4.13 (t, 1H, *J* = 8.8 Hz, H-3′), 4.21 (t, 1H, *J* = 8.9 Hz, H-4′), 4.31–4.38 (m, 1H, H-16), 4.47–4.58 (m, 2H, H-16, H-6′), 4.96 (d, 1H, *J* = 7.7 Hz, H-1′), 5.14 (d, 1H, *J* = 7.7 Hz, H-1″), 5.31 (br d, 1H, H-6). ^{13}C NMR δ (δ, pyridine, 75 MHz): 140.9 (C-5), 121.4 (C-6), 109.0 (C-22), 104.6 (C-1″), 100.4 (C-1′), 82.30 (C-2′), 81.86 (C-16), 78.94 (C-3), 77.95 (C-5′), 76.63 (C-3′), 74.95 (C-3″), 72.33 (C-4″), 72.23 (C-2″), 71.49 (C-5″), 71.16 (C-4′), 62.65 (C-17), 66.62 (C-26), 62.36 (C-6′), 56.46 (C-14), 50.06 (C-9), 41.73 (C-20), 40.23 (C-13), 39.66 (C-12), 39.01 (C-4), 37.21 (C-1), 36.82 (C-10), 32.07 (C-2), 31.96 (C-7), 31.58 (C-8), 31.45 (C-15), 30.36 (C-25), 30.08 (C-23), 29.02 (C-24), 20.89 (C-11), 19.25 (C-19), 17.09 (C-27), 16.90 (C-6″), 16.14 (C-18), 14.81 (C-21); FABMS *m*/*z* 723 $(M+H)^+$, 416, 397. HRFABMS *m*/*z* 723.4362, calcd for $C_{39}H_{63}O_{12}$, 723.4320; Anal. Calcd for $C_{39}H_{62}O_{12}$: C, 64.80; H, 8.64. Found: C, 64.39; H, 8.98.

5.3.7. Diosgenyl α-L-rhamnopyranosyl-(1 → 2)-β-D-glucopyranoside (25). White amorphous solid, $[\alpha]_D^{20}$ −56° (*c* 0.034, EtOH); IR ν_{max} (film, NaCl) 3365, 2936, 1455, 1050, 900, 873 cm^{-1}; ^1H NMR (δ, pyridine, 400 MHz) 0.66 (d, 3H, *J* = 3.8 Hz, CH_3-27), 0.78 (s, 3H, CH_3-18), 1.01 (s, 3H, CH_3-19), 1.10 (d, 3H, *J* = 6.7 Hz, CH_3-21), 1.73 (d, 3H, *J* = 6.7 Hz, CH_3-6″), 3.46 (t, 1H, *J* = 9.5 Hz, H-26), 3.55 (m, 1H, H-26), 3.81–3.91 (m, 2H, H-3, H-5′), 4.13 (m, 1H, H-3′), 4.24–4.28 (m, 3H, H-2′, H-4′, H-4″), 4.45–4.53 (m, 2H, H-16, H-5″), 4.59 (dd, 1H, *J* = 9.1; 3.1 Hz, H-3″), 4.76 (br s, 1H, H-2″), 5.00 (m, 1H, H-1′), 5.27 (br d, 1H, *J* = 3.8 Hz, H-6), 6.34 (s, 1H, H-1″). ^{13}C NMR (δ, pyridine, 75 MHz): 140.9 (C-5), 121.8 (C-6), 109.0 (C-22), 101.8 (C-1″), 100.1 (C-1′), 79.50 (C-16), 79.32 (C-2′), 77.96 (C-5′), 77.65 (C-3′), 77.65 (C-3), 73.87 (C-4″), 72.54 (C-3″), 72.27 (C-2″), 71.53 (C-4′), 69.23 (C-5″), 66.58 (C-26), 62.59 (C-17), 62.36 (C-6′), 56.35 (C-14), 49.99 (C-9), 41.69 (C-20), 40.18 (C-13), 39.58 (C-12), 38.70 (C-4), 37.23 (C-1), 36.86 (C-10), 32.03 (C-2), 31.53 (C-7), 31.40 (C-8), 30.31 (C-15), 29.90 (C-25), 29.69 (C-23), 28.97 (C-24), 20.82 (C-11), 19.14 (C-19), 18.39 (C-6″), 17.05 (C-27), 16.06 (C-18), 14.76 (C-21). FABMS *m*/*z* 723 $(M+H)^+$, 413, 397; Anal. Calcd for $C_{39}H_{62}O_{12}$: C, 64.80; H, 8.64. Found: C, 64.74; H, 8.67.

5.3.8. Diosgenyl 4-*O*-acetyl-α-L-rhamnopyranosyl-(1 → 2)-6-*O*-acetyl-β-D-glucopyranoside (26)[24]. White amorphous solid, $[\alpha]_D^{20}$ −29° (*c* 0.015, EtOH); IR ν_{max} (film, NaCl) 3421, 2934, 1734, 1041, 900, 872 cm^{-1}; ^1H NMR (δ, pyridine, 400 MHz) 0.66 (d, 3H, *J* = 5.2 Hz, CH_3-27), 0.83 (s, 3H, CH_3-18), 1.06 (s, 3H, CH_3-19), 1.23 (d, 3H, *J* = 6.9 Hz, CH_3-21), 1.46 (d, 3H, *J* = 6.3 Hz, CH_3-6″), 1.88 (s, 3H, Ac), 2.06 (s, 3H, Ac), 3.46 (t, 1H, *J* = 9.5 Hz, H-26), 3.55 (m, 1H, H-26), 3.92–4.01 (m, 3H, H-3, H-4′, H-5′), 4.12–4.24 (m, 2H, H-2′, H-3′), 4.53 (dd, 1H, *J* = 14.5; 7.4 Hz, H-16), 4.63 (dd, 1H, *J* = 9.5; 3.1 Hz, H-3″), 4.69–4.84 (m, 3H, H-6′, H-2″), 4.99–5.01 (m, 1H, H-1′), 5.85 (t, 1H, *J* = 9.8 Hz, H-4″), 6.37 (s, 1H, H-1″). ^{13}C NMR (δ, pyridine, 75 MHz): 171.581 and 171.51 (*C*O-Ac), 140.50

(C-5), 121.81 (C-6), 109.0 (C-22), 101.30 (C-1′), 99.83 (C-1″), 81.87 (C-16), 79.05 (C-2′), 77.77 (C-3), 76.52 (C-3′), 75.94 (C-4″), 74.68 (C-4′), 72.24 (C-2″), 71.16 (C-5′), 69.96 (C-3″), 66.63 (C-26), 65.23 (C-5″), 64.23 (C-6′), 62.66 (C-17), 56.41 (C-14), 50.08 (C-9), 41.74 (C-20), 40.25 (C-13), 39.63 (C-12), 38.78 (C-4), 37.20 (C-1), 36.92 (C-10), 32.08 (C-2), 31.99 (C-7), 31.58 (C-8), 31.50 (C-15), 30.36 (C-25), 29.03 (C-23), 29.03 (C-24), 20.93 (C-11), 20.93 and 20.48 (–*OAc*), 19.18 (C-19), 17.77 (C-6″), 17.09 (C-27), 16.17 (C-18), 14.82 (C-21). FABMS *m*/*z* 829 $(M+Na)^+$ 413, 397. Anal. Calcd for $C_{43}H_{66}O_{14}$: C, 64.00; H, 8.24. Found: C, 64.10; H, 8.33.

5.3.9. Diosgenyl α-L-rhamnopyranosyl-(1 → 2)-6-*O*-acetyl-β-D-glucopyranoside (27)[24]. White amorphous solid, $[\alpha]_D^{20}$ −22 ° (*c* 0.009, EtOH); IR ν_{max} (film, NaCl) 3277, 2934, 1648, 1419, 1052, 872 cm^{-1}; ^1H NMR (δ, pyridine, 400 MHz): 0.66 (d, 3H, *J* = 4.9 Hz, CH_3-27), 0.85 (s, 3H, CH_3-18), 1.02 (s, 3H, CH_3-19), 1.12 (d, 3H, *J* = 6.9 Hz, CH_3-21), 1.75 (d, 3H, *J* = 6.3 Hz, CH_3-6″), 1.91 (s, 3H, Ac), 3.47 (t, 1H, *J* = 9.5 Hz, H-26), 3.56 (m, 1H, H-26), 3.93–3.99 (m, 3H, H-3, H-4′, H-5′), 4.21–4.26 (m, 2H, H-2′, H-3′), 4.34 (t, 1H,*J* = 9.5 Hz, H-4″), 4.53 (dd, 1H, *J* = 14.5; 7.4 Hz, H-16), 4.62 (dd, 1H, *J* = 9.3; 3.0 Hz, H-3″), 4.75 (dd, 1H, *J* = 11.7; 5.1 Hz, H-6′), 4.79 (br s, 1H, H-2″), 4.84 (m, 1H, H-6′), 4.95 (m, 1H, H-1′), 4.99 (m, 1H, H-5″), 5.28 (d, 1H, *J* = 4.5 Hz, H-6), 6.38 (s, 1H, H-1″). ^{13}C NMR (δ, pyridine, 75 MHz): 171.0 (*C*O-Ac), 141.0 (C-5), 121.9 (C-6), 109.4 (C-22), 102.7 (C-1′), 102.3 (C-1″), 81.3 (C-16), 79.5 (C-2′), 77.6 (C-3), 76.8 (C-3′), 75.9 (C-4′), 73.87 (C-4″), 72.7 (C-2″), 70.5 (C-5′), 70.5 (C-3″), 67.0 (C-26), 67.0 (C-5″), 64.7 (C-6′), 61.5 (C-17), 56.8 (C-14), 50.4 (C-9), 40.6 (C-20), 40.0 (C-13), 39.5 (C-4), 39.2 (C-12), 37.2 (C-1), 37.2 (C-10), 32.0 (C-2), 32.0 (C-7), 31.9 (C-15), 31.8 (C-8), 30.0 (C-25), 29.4 (C-24), 29.3 (C-23), 21.3 (C-11), 20.9 (*C*H_3-Ac), 19.6 (C-19), 17.5 (C-27), 117.5 (C-6″), 6.5 (C-18), 15.2 (C-21). FABMS *m*/*z* 787 $(M+Na)^+$. HRFABMS *m*/*z* 787.4210, calcd for $C_{41}H_{64}O_{13}Na$, 787.4245; Anal. Calcd for $C_{41}H_{64}O_{13}$: C, 64.38; H, 8.43. Found: C, 64.05; H, 8.72.

5.3.10. Diosgenyl 2,3,4-tri-*O*-acetyl-α-L-rhamnopyranosyl-(1 → 4)-2,3-*O*-isopropylidene-α-L-rhamnopyranosyl-(1 → 2)-4,6-*O*-benzylidene-3-*O*-pivaloyl-β-D-glucopyranoside (29). To a stirred mixture of imidate (350 mg, 0.80 mmol), **28**[20] (158 mg, 0.53 mmol), and 4 Å MS in dry CH_2Cl_2 (12 mL) at −70 °C under N_2, TMSOTf (0.05 M in CH_2Cl_2, 1.0 mL) was added dropwise. After stirring for 1 h, compound **4a** (258 mg, 0.34 mmol) was added. The resulting mixture was stirred at −20 °C for 1.5 h, before the addition of Et_3N to quench the reaction. The mixture was filtered through a pad of Celite. The filtrate was concentrated and applied to a silica gel column chromatography (CH_2Cl_2/acetone; 40:1) to provide the desired saponin **29** as a white solid (0.19 mmol, 55%). White amorphous solid, $[\alpha]_D$ −88° (*c* 0.095, $CHCl_3$). ^1H NMR (δ, $CDCl_3$, 400 MHz): 0.80 (m, 6H, CH_3-18, CH_3-27), 0.98 (d, 3H, *J* = 6.9 Hz, CH_3-21), 1.04 (s, 3H, CH_3-19), 1.21 (d, 3H, *J* = 6.3 Hz, CH_3-6‴), 1.22 (s, 9H, CH_3-Piv), 1.33 (d, 3H, *J* = 6.2 Hz, CH_3-6″), 1.51 (s, 3H, (CH_3)$_2$–C), 1.67 (s, 3H, (CH_3)$_2$–C), 1.96 (s, 3H, –OAc), 2.03 (s, 3H, –OAc), 2.11 (s, 3H, –OAc), 3.38 (t, 1H, *J* = 10.9 Hz, H-26), 3.47–3.53 (m, 3H, H-26, H-5′, H-2″), 3.60–3.65 (m, 2H, H-3, H-4′), 3.78–3.87 (m, 3H, H-2′, H-6′, H-5‴), 4.03 (d, 1H, *J* = 5.5 Hz, H-2″), 4.14–4.17 (m, 2H, H-3″, H-5″), 4.35 (dd, 1H, *J* = 10.9, 5.5 Hz, H-6′), 4.41 (dd, 1H, *J* = 14.4, 7.1 Hz, H-16), 4.66 (d, 1H, *J* = 7.6 Hz, H-1′), 5.09 (t, 1H, *J* = 9.8 Hz, H-4″), 5.15 (s, 1H, H-1‴), 5.23 (dd, 1H, *J* = 10.0; 3.4 Hz, H-3″), 5.28 (m, 1H, H-2″), 5.33 (d, 1H, *J* = 1.5 Hz, H-1″), 5.39 (t, 1H, *J* = 9.4 Hz, H-3′), 5.44 (br d, 1H, H-6), 5.49 (s, 1H, Ph-CH), 7.33–7.42 (m, 5H, Ph). ^{13}C NMR (δ, $CDCl_3$, 75 MHz): 177.1 (*C*O-Piv), 169.7 and 169.3 (*C*O-Ac), 139.6 (C-5), 136.7, 128.6 and 125.6 (Ph), 122.1 (C-6), 109.2 ((CH_3)$_2$-*C*), 109.0 (C-22), 100.7 (Ph*CH*), 99.7 (C-1′), 97.4 (C-1‴), 95.8 (C-1″), 80.58 (C-16), 78.58 (C-3), 78.58 (C-4′), 77.59 (C-3″), 76.79 (C-5′), 75.96 (C-2′), 75.64 (C-4″), 73.81 (C-3′), 70.90 (C-4‴), 69.63 (C-2‴), 69.03 (C-3‴), 66.53 (C-5‴), 68.67 (C-6′), 65.91 (C-2″), 64.02 (C-5″), 61.87 (C-17), 60.60 (C-26), 56.62 (C-14), 49.83 (C-9), 41.37 (C-20), 40.03 (C-13), 39.55 (C-12), 38.70 (C-Piv), 38.05 (C-4), 36.88 (C-1), 36.64 (C-10), 31.85 (C-2), 31.62 (C-7), 31.14 (C-8), 31.14 (C-15), 30.06 (C-25), 29.30 (C-23), 28.56 (C-24), 27.61 and 26.10 ((CH_3)$_2$–C), 26.86 (*C*H_3-Piv), 20.8 (C-11), 20.72, 20.57 and 20.40 (*C*H_3-Ac), 18.93 (C-19), 17.82 (C-6‴), 17.13 (C-6″), 16.89 (C-27), 15.99 (C-18), 14.28 (C-21). HRFABMS: 1207.6401 $(M+H)^+$ (calcd for $C_{66}H_{95}O_{20}$, 1207.6417), 793 (6), 397 (17), 395 (9). Anal. ($C_{66}H_{94}O_{20}$) C, H. Anal. Calcd for $C_{66}H_{95}O_{20}$: C, 65.65; H, 7.85. Found: C, 65.70; H, 7.36.

5.3.11. Diosgenyl α-L-rhamnopyranosyl-(1 → 4)-α-L-rhamnopyranosyl-(1 → 2)-β-D-glucopyranoside (30). 120.0 mg (0.09 mmol) of **29** in 10 mL of AcOH (80%) was heated for 3 h at 70 °C. The residue was concentrated, dissolved in a mixture of MeOH/THF/H_2O (1:1:1) and NaOH (38 mg, 0.95 mmol) was added. The solution was heated at 40 °C for 7 h, then neutralized with an acid resin Dowex-50 (H^+), filtered, concentrated, and purified in CC using CH_2Cl_2/MeOH (8:2) to yield **30** (15.1 mg, 0.017 mmol, 19%). White amorphous solid, $[\alpha]_D^{20}$ −48° (*c* 0.015, EtOH); IR ν_{max} (film, NaCl) 3418, 2360, 1050, 891 cm^{-1}; ^1H NMR (δ, pyridine, 400 MHz): 0.65 (d, 3H, *J* = 4.9 Hz, CH_3-27), 0.76 (s, 3H, CH_3-18), 1.10 (d, 3H, *J* = 6.9 Hz, CH_3-21), 1.15 (s, 3H, CH_3-19), 1.59 (d, 3H, *J* = 6.3 Hz, CH_3-6″), 1.69 (d, 3H, *J* = 6.3 Hz, CH_3-6‴), 3.46 (t, 1H, *J* = 9.5 Hz, H-26), 3.55 (m, 1H, H-26), 3.83–3.93 (m, 2H, H-3, H-5′), 4.13 (t, 1H,*J* = 9.0 Hz, H-4′), 4.21–4.25 (m, 2H, H-2′, H-3′), 4.29 (m, 1H, H-6′), 4.39 (m, 1H, H-5‴), 4.45–4.52 (m, 5H, H-6′, H-3″, H-4‴, H-3‴, H-16), 4.65 (br s, 1H, H-2″), 4.80 (br s, 1H, H-2‴), 4.99 (m, 1H, H-1′), 5.05 (m, 1H, H-5′), 5.33 (d, 1H, *J* = 3.7 Hz, H-6), 6.34 (s, 1H, H-1″), 6.36 (s, 1H, H-1‴). ^{13}C NMR (δ, pyridine, 75 MHz): 140.48 (C-5), 121.66 (C-6), 109.0 (C-22), 102.71 (C-1‴), 101.24 (C-1″), 99.71 (C-1′), 80.88 (C-16), 79.36 (C-2′), 79.05 (C-4″), 78.05 (C-5′), 77.72 (C-3′), 77.48 (C-3), 73.80 (C-4‴), 73.39 (C-2‴), 72.93 (C-3‴), 72.67 (C-3″), 72.28 (C-2″), 71.53 (C-4′), 70.07 (C-5″), 67.40 (C-5‴), 66.63 (C-26), 62.65 (C-17), 62.37 (C-6′), 56.50 (C-14), 50.20 (C-9), 41.74 (C-20), 40.22 (C-13),

39.67 (C-12), 38.73 (C-4), 37.26 (C-1), 36.92 (C-10), 32.07 (C-2), 31.96 (C-7), 31.60 (C-8), 30.39 (C-15), 30.36 (C-25), 29.90 (C-23), 29.03 (C-24), 20.94 (C-11), 19.39 (C-19), 18.91 (C-6‴), 18.25 (C-6″), 17.09 (C-27), 16.22 (C-18), 14.76 (C-21). FABMS *m/z* 891 $(M+Na)^+$, 413 (3), 397 (4). Anal. ($C_{45}H_{72}O_{16}$) C, H. Anal. Calcd for $C_{45}H_{72}O_{16}$: C, 62.19; H, 8.35. Found: C, 62.15; H, 8.54.

5.4. Biological activity

5.4.1. Cell culture. Human HL-60 and U937 myeloid leukemia cells and human SK-MEL-1 melanoma cells were grown in RPMI 1640 (Sigma) supplemented with 10% (v/v) heat-inactivated fetal bovine serum (Sigma) and 100 U/mL penicillin and 100 μg/mL streptomycin at 37 °C in a humidified atmosphere containing 5% CO_2. The cell numbers were counted by a hematocytometer, and the viability was always greater than 95% in all experiments as assayed by the 0.025% Trypan blue exclusion method. Stock solutions of 100 mM diosgenyl glycosides were made in dimethylsulfoxide (DMSO), and aliquots were frozen at −20 °C.

5.4.2. Assay for growth inhibition and cell viability. The cytotoxicity of diosgenyl glycosides was assessed using a 3-(4,5-dimethylthiazol-2-yl)-2,5-diphenyl-2*H*-tetrazolium bromide (MTT) assay.[28] Briefly, 1×10^4 exponentially growing cells were seeded in 96-well microculture plates with various diosgenyl glycoside concentrations (0.3–100 μM) in a volume of 200 μL. DMSO concentration was the same in all the treatments and did not exceed 0.1% (v/v). After 72 h, surviving cells were detected based on their ability to metabolize 3-(4,5-dimethylthiazol-2-yl)-2,5-diphenyl-2*H*-tetrazolium bromide (Sigma) into formazan crystals. Optical density was read with an ELISA reader at a wavelength of 570 nm and was used as a measure of cell viability. The MTT dye-reduction assay measures mitochondrial respiratory function and can detect the onset of cell death earlier than dye-exclusion methods. Cell survival was calculated as the fraction of cells alive relative to control for each point: cell survival (%) = mean absorbance in treated cells/mean absorbance in control wells × 100. Concentrations inducing a 50% inhibition of cell growth (IC_{50}) were determined graphically for each experiment. Parameters describing the concentration–response curves (IC_{50}) were determined using the curve fitting routine of the computer software Prism™ (GraphPad) and the equation derived by DeLean et al.[29]

5.4.3. Flow cytometry analysis for cell cycle distribution. After 16 h of treatment, cells were harvested and quickly washed twice with ice-cold phosphate-buffered saline (PBS), and cell pellets were collected and resuspended in 50 μL of PBS. Following dropwise addition of 1 mL of ice-cold 75% ethanol, fixed cells were stored at −20 °C for 1 h. Samples were then centrifuged at 500*g* for 10 min at 4 °C and washed with PBS before resuspension in 1 mL containing 50 μg/mL propidium iodide and 100 μg/mL RNase A and incubation for 1 h at 37 °C in the dark. Cell cycle distribution was then analyzed by flow cytometry using a Coulter EPICS™ cytometer (Beckman–Coulter). Histograms were analyzed with the Expo 32 ADC Software™ (Beckman–Coulter). The quantitative data presented are means ± SE of percentage of cells in different phases of cell cycle from triplicate samples in each treatment, and were reproducible in 2–3-independent experiments.

5.4.4. Immunoblot analysis of procaspase-3, procaspase-9, and Bcl-2. HL-60 or U937 cells (1×10^6) were treated with diosgenyl glycosides at the indicated concentrations in RPMI 1640 medium. Cells were pelleted by centrifugation, washed with phosphate-buffered saline and lysed in lysis buffer containing 125 mM Tris–HCl, pH 6.8, 2% sodium dodecyl sulfate, 5% glycerol, and 1% β-mercaptoethanol, and boiled for 5 min. The samples were separated on 12% sodium dodecyl sulfate–polyacrylamide gel, electrotransferred to a polyvinylidene difluoride membrane. The membrane was probed first with a polyclonal anti-procaspase-3 (Stressgen, 1:2000 dilution), anti-procaspase-9 (Stressgen, 1:1000) or anti-Bcl-2 (Santa Cruz Biotechnology, 1:1000) and then with anti-rabbit (pro-caspase-3) or anti-mouse (pro-caspase-9 and Bcl-2) antibody conjugated to horseradish peroxidase (HRP). Protein bands were detected by chemiluminescence (SuperSignal West Pico Chemiluminescent Substrate, Pierce) using the manufacturer's protocol.

5.4.5. Immunoblotting of poly(ADP-ribose) polymerase. Induction of apoptosis was also examined by proteolytic cleavage of poly(ADP-ribose) polymerase. Briefly, 1×10^6 exponentially growing HL-60 or U937 cells were treated with diosgenyl glycosides at the indicated concentrations for 6 h at 37 °C. Cells were pelleted by centrifugation, washed twice with phosphate-buffered saline resuspended in lysis buffer, and subjected to Western blot analysis as described previously.[28] Proteins were separated on 7.5% sodium dodecyl sulfate–polyacrylamide mini gels and electrotransferred to polyvinylidene difluoride membrane. The membrane was probed with polyclonal anti-poly(ADP-ribose) polymerase (Stressgen, 1:1000 dilution) and then with anti-rabbit antibody conjugated to horseradish peroxidase (HRP). Protein bands were detected by chemiluminescence (SuperSignal West Pico Chemiluminescent Substrate, Pierce) as described above.

5.4.6. Release of cytochrome *c* from mitochondria in diosgenyl glycoside-treated cells. Untreated and diosgenyl glycosides-treated cells were harvested by centrifugation at 1000*g* for 5 min at 4 °C. Cell pellets were washed twice with ice-cold phosphate-buffered saline and resuspended with 20 mM Hepes–KOH (pH 7.5), 10 mM KCl, 1.5 mM $MgCl_2$, 1 mM EDTA, 1 mM EGTA, 1 mM dithiothreitol, 0.1 mM phenylmethylsulfonylfluoride (PMSF), and 250 mM sucrose. After 15-min incubation on ice, cells were lysed by pushing them several times through a 22-gauge needle and the lysate spun down at 1000*g* for 5 min at 4 °C. The supernatant fraction was centrifuged at 105,000*g* for 45 min at 4 °C and the resulting supernatant was used as the soluble cytosolic fraction. Cytosolic proteins (50 μg) were resolved on a sodium dodecyl sulfate/15% polyacrylamide gel and elec-

trotransferred onto a polyvinylidene difluoride membrane (Millipore). Membrane was blocked with 5% nonfat milk in Tris-buffered saline containing 0.1% Tween 20 (TBST) for 1 h, followed by incubation with anti-cytochrome *c* monoclonal antibody (BD Pharmingen; 1:1000) overnight. After washing and incubation with horseradish peroxidase-conjugated anti-mouse antibody (Amersham Biosciences), the antigen–antibody complexes were visualized by SuperSignal West Pico Chemiluminescent Substrate (Pierce) as described above. The same membrane was probed with monoclonal anti-β-actin (Sigma, 1:3000 dilution) as loading control.

Acknowledgments

This work was supported in part by grants from the Programa de Iniciativa Comunitaria INTERREG IIIB Azores-Madeira-Canarias (04/MAC/3.5/C5), from the Instituto Canario de Investigación del Cáncer (G-05-09 to J.B. and F.L.), from FEDER (Grant No. 1FD1997-1831 to J.B.), and from the Dirección General de Universidades e Investigación of the Canary Islands Government (Grants TR2003/002 and GRUP-2004-44 to F.E.). J.C.H. thanks the Cabildo Insular de Tenerife (Spain) and the Town Council of Icod de los Vinos (Tenerife, Spain). F.T. was supported by a research studentship from the Dirección General de Universidades e Investigación of the Canary Islands Government. We thank Mr. José Estévez (Hospital Universitario Insular de Gran Canaria) for his collaboration in the Western blot assays and Mr. Lennart Loven for his encouragement and support.

Supplementary data

Supplementary data associated with this article can be found, in the online version, at doi:10.1016/j.bmc.2007.10.089.

References and notes

1. Hostettmann, K.; Marston, A. *Saponin*; Cambridge Univ. Press, 1995.
2. Bowyer, H.; Clarke, B. R.; Lunness, P.; Daniels, M. J.; Osbourn, A. E. *Science* **1995**, *267*, 371–374.
3. Ke, H.; Xinsheng, Y. *Anti-Cancer Drugs* **2001**, *12*, 541–547.
4. Watanabe, K.; Mimaki, Y.; Sakagami, H.; Sashida, Y. *J. Nat. Prod.* **2003**, *66*, 236–241.
5. Hernández, J. C.; León, F.; Estévez, F.; Quintana, J.; Bermejo, J. *Bioorg. Med. Chem.* **2004**, *12*, 4423–4429.
6. Ma, X.; Yu, B.; Hui, Y.; Miao, Y.; Ding, J. *Bioorg. Med. Chem. Lett.* **2001**, *11*, 2153–2156.
7. Shi, B.; Wu, H.; Yu, B.; Wu, J. *Angew. Chem., Int. Ed.* **2004**, *43*, 4324–4327.
8. Deng, L.; Wu, H.; Yu, B.; Jiang, M.; Wu, J. *Bioorg. Med. Chem. Lett.* **2004**, *14*, 2781–2785.
9. Morzycki, J. W.; Wojtkielewicz, A. *Phytochem. Rev.* **2005**, *4*, 259–277.
10. Shi, B.; Tang, P.; Wu, X.; Liu, J. O.; Yu, B. *J. Org. Chem.* **2005**, *70*, 10354–10367.
11. Tang, P.; Mamdani, F.; Hu, X.; Liu, J. O.; Yu, B. *Bioorg. Med. Chem. Lett.* **2007**, *17*, 1003–1007.
12. Zou, C.; Hou, S.; Shi, Y.; Lei, P.; Liang, X. *Carbohydr. Res.* **2003**, *338*, 721–727.
13. Cheng, M. S.; Wang, Q. L.; Tian, Q.; Song, H. Y.; Liu, Y. X.; Li, Q.; Xu, X.; Miao, H. D.; Yao, X. S.; Yang, Z. *J. Org. Chem.* **2003**, *68*, 3658–3662.
14. Cheng, M. S.; Wang, Q. L.; Tian, Q.; Song, H. Y.; Liu, Y. X.; Li, Q.; Xu, X.; Miao, H. D.; Yao, X. S.; Yang, Z. *Chem. Lett.* **2005**, *34*, 1220–1221.
15. Hou, S.; Xu, P.; Zhou, L.; Yu, D.; Lei, P. *Bioorg. Med. Chem. Lett.* **2006**, *16*, 2454–2458.
16. Hernández, J. C.; León, F.; Estévez, F.; Quintana, J.; Bermejo, J. *Chem. Biodiver.* **2006**, *3*, 62–68, and references cited therein.
17. Mimaki, Y.; Yokosuka, A.; Kuroda, M.; Sashida, Y. *Biol. Pharm. Bull.* **2001**, *24*, 1286–1289.
18. Li, C.; Yu, B.; Liu, M.; Hui, Y. *Carbohydr. Res.* **1998**, *306*, 189–195.
19. Deng, S.; Yu, B.; Hui, Y.; Yu, H.; Han, X. *Carbohydr. Res.* **1999**, *317*, 53–62.
20. De la Fuente, J. M.; Penadés, S. *Tetrahedron Asymmetry* **2002**, *13*, 1879–1888.
21. Takechi, M.; Kousaka, Y.; Uno, C.; Tanaka, Y. *Planta Med.* **1998**, *64*, 179–180.
22. Takechi, M.; Doi, K.; Wakayama, Y. *Phytother. Res.* **2003**, *17*, 83–85.
23. Espejo, O.; Llavot, J. C.; Jung, H.; Giral, F. *Phytochemistry* **1982**, *21*, 413–416.
24. Yu, B.; Xing, G.; Huia, Y.; Han, X. *Tetrahedron Lett.* **2001**, *42*, 5513–5516.
25. Yu, B.; Yu, H.; Hui, Y.; Han, X. *Tetrahedron Lett.* **1999**, *40*, 8591–8594.
26. Crich, D.; Li, H. *J. Org. Chem.* **2002**, *67*, 4640–4646.
27. Borner, C. *Mol. Immunol.* **2003**, *39*, 615–647.
28. Rivero, A.; Quintana, J.; Eiroa, J. L.; López, M.; Triana, J.; Bermejo, J.; Estévez, F. *Eur. J. Pharmacol.* **2003**, *482*, 77–84.
29. DeLean, A.; Munson, P. J.; Rodbard, D. *Am. J. Physiol.* **1978**, *235*, E97–E102.

Apoptosis (2008) 13:716–728
DOI 10.1007/s10495-008-0202-0

ORIGINAL PAPER

Trifolin acetate-induced cell death in human leukemia cells is dependent on caspase-6 and activates the MAPK pathway

Fernando Torres · José Quintana · Jesús G. Díaz · Armando J. Carmona · Francisco Estévez

Published online: 5 April 2008
© Springer Science+Business Media, LLC 2008

Abstract In the present study we demonstrated that the flavonoid derivative trifolin acetate (TA), obtained by acetylation of naturally occurring trifolin, induces apoptosis. Associated downstream signaling events were also investigated. TA-induced cell death was prevented by the non-specific caspase inhibitor z-VAD-fmk and reduced by the presence of the selective caspase inhibitors z-LEHD-fmk (caspase-9), z-DEVD-fmk (caspase-3) and z-VEID-fmk (caspase-6). The apoptotic effect of TA was associated with (i) the release of cytochrome *c* from mitochondria which was not accompanied by dissipation of the mitochondrial membrane potential ($\Delta\Psi_m$), (ii) the activation of the mitogen-activated protein kinases (MAPKs) pathway and (iii) abrogated by the over-expression of Bcl-2 or Bcl-x_L. TA-induced cell death was attenuated by inhibition of extracellular signal-regulated kinases (ERK) 1/2 with U0126 and inhibition of $p38^{MAPK}$ with SB203580. In contrast, inhibition of c-Jun NH_2-terminal kinase (JNK) by SP600125 significantly enhanced apoptosis. Although reactive oxygen species (ROS) increased in response to TA, this did not seem to play a pivotal role in the apoptotic process since different anti-oxidants were unable to provide cell protection. The present study demonstrates that TA-induced cell death is mediated by an intrinsic-dependent apoptotic event involving mitochondria and MAPK, and through a mechanism independent of ROS generation.

Keywords Apoptosis · Flavonoids · Mitogen-activated protein kinase · $p38^{MAPK}$ · Extracellular signal-regulated kinases

F. Torres · J. Quintana · F. Estévez (✉)
Department of Biochemistry, Instituto Canario de Investigación del Cáncer (I.C.I.C.), University of Las Palmas de Gran Canaria, Plaza Dr. Pasteur s/n, 35016 Las Palmas de Gran Canaria, Spain
e-mail: festevez@dbbf.ulpgc.es

J. G. Díaz · A. J. Carmona
Department of Chemistry, University of La Laguna, Instituto Universitario de Bio-Orgánica "Antonio González", 38206 La Laguna, Teneriffe, Spain

Introduction

Most antitumoral compounds induce apoptosis, a kind of cell death defined by characteristic changes in the nuclear morphology. This form of cell death can occur with or without the activation of caspases [1]: a family of cysteine proteases which are constitutively expressed as inactive zymogens [2]. Two pathways of caspase activation during apoptosis have been described [3]. The extrinsic pathway involves apoptosis mediated by death receptors, such as Fas or tumor necrosis factor receptors [4], that is dependent on the initiator caspase-8. Active caspase-8 activates the downstream effector caspases (caspase-3, -6 and -7), inducing a cascade of caspases. In the intrinsic pathway, diverse proapoptotic signals provoke the translocation of cytochrome *c* from mitochondria to cytoplasm and caspase-9 activation, which cleaves and activates downstream caspases. This mitochondrial pathway of apoptosis may be inhibited by anti-apoptotic factors of the Bcl-2 family, which interfere with the relocalization of cytochrome *c* resulting in inhibition of the binding of this protein to Apaf-1-apoptotic protease activating factor-1- [5, 6]. Although caspase-3 is the main effector caspase, it seems to be dispensable for cell death induced by a variety of stimuli, such as tumor necrosis factor or anticancer drugs, since other effector caspases, such as caspase-6 or -7 can compensate for the lack of caspase-3 [7].

Members of the mitogen-activated protein kinases (MAPKs) family are involved in apoptotic signaling, as well as in control of growth and differentiation. Three major MAPKs cascades have been well characterized: the extracellular signal-regulated kinases (ERK) 1/2, the c-Jun NH_2-terminal kinases/stress-activated protein kinases (JNK/SAPK) and the p38 mitogen-activated protein kinases ($p38^{MAPK}$). Although exceptions exist, the bulk of evidence suggests that activation of JNK/SAPK and $p38^{MAPK}$ cascades promote apoptosis [8] whereas ERK 1/2 activation exerts a cytoprotective effect [9].

Flavonoids are phenylbenzo-γ-pyrones that are relatively abundant in the human diet and are among the most promising anticancer agents [10–12]. The flavonoid trifolin (kaempferol-3-*O*-galactoside) has been isolated from the aerial parts of *Consolida oliveriana* [13]. We have previously shown that trifolin acetate (TA), obtained by acetylation of the natural product trifolin, is cytotoxic on human leukaemia—(HL-60 and U937) and melanoma—(SK-MEL-1) cell lines and displays similar potency among different cell lines [13]. Here we have studied the effect of this compound on apoptosis induction on the above tumor cell lines as well as human myeloid cells over-expressing the anti-apoptotic proteins Bcl-2 and Bcl-x_L.

Materials and methods

Reagents

Trifolin was isolated from *Consolida oliveriana*. The acetyl derivative of trifolin (TA) was obtained by treatment of the corresponding alcohol (trifolin) with acetic anhydride in pyridine for 12 h at room temperature. TA was purified by chromatography on a silica gel column and eluted with hexane, and hexane-ethyl acetate mixtures (8:2). Purity of this compound was 99.0% as judged by high-performance liquid chromatography. Structural identity of this compound was determined spectroscopically (PMR and ^{13}C NMR, i.r. and UV/Visible spectroscopy and mass spectrometry). The details of the isolation have been published recently [13]. Stock solutions of 10 mM TA were made in dimethyl sulfoxide (DMSO) and aliquots were frozen at −20°C. Poly (vinylidene difluoride) (PVDF) membranes were purchased from Millipore (Billerica, MA, USA). The inhibitors benzyloxycarbonyl-Val-Ala-Asp(OMe) fluoromethyl ketone (z-VAD-fmk), benzyloxycarbonyl-Asp(OMe)-Glu(O-Me)-Val-Asp(O-Me) fluoromethyl ketone (z-DEVD-fmk), benzyloxycarbonyl-Ile-Glu-Thr-Asp(OMe) fluoromethyl ketone (z-IETD-fmk), benzyloxycarbonyl-Leu-Glu-His-Asp(OMe) fluoromethyl ketone (z-LEHD-fmk), benzyloxycarbonyl-Val-Asp(OMe)-Val-Ala-Asp(OMe) fluoromethyl ketone (z-VDVAD-fmk), SB203580, SP600125 and U0126 were purchased from Sigma (Saint Louis, MO, USA). The caspase inhibitors benzyloxycarbonyl-Tyr-Val-Ala-Asp(OMe) fluoromethyl ketone (z-YVAD-fmk) and benzyloxycarbonyl-Val-Glu(OMe)-Ile-Asp(OMe)-fluoromethyl ketone (z-VEID-fmk) were from Calbiochem (Darmstadt, Germany). Acrylamide, bisacrylamide, ammonium persulfate and *N*,*N*,*N*′,*N*′-tetramethylethylenediamine were from Bio-Rad (Hercules, CA, USA). Antibodies for poly(ADP-ribose) polymerase (PARP), caspase-3, and caspase-9 were purchased from Stressgen (Victoria, British Columbia, Canada). Antibody for cytochrome *c* was purchased from BD PharMingen (San Diego, CA, USA). Anti-caspase-6 monoclonal antibody was from Medical & Biological Laboratories (Nagoya, Japan). Anti-JNK/SAPK, anti-p44/42 MAP Kinase, anti-Phospho-p44/42 MAP Kinase (T202/Y204), anti-$p38^{MAPK}$ and a phosphorylated form (T180/Y182) of $p38^{MAPK}$ antibodies were purchased from New England BioLabs (Cell Signaling Technology, Beverly, MA, USA). Anti-JNK/SAPK (phosphor T183 + Y185) and anti-cytochrome *c* oxidase (Cox IV) antibodies were purchased from Abcam (Cambridge, UK). Secondary antibodies were from Amersham Biosciences (Freiburg, Germany). All other chemicals were obtained from Sigma (Saint Louis, MO, USA).

Cell culture

HL-60 and U937 cells were cultured in RPMI 1640 medium containing 10% (v/v) heat-inactivated fetal bovine serum, 100 units/ml penicillin and 100 μg/ml streptomycin at 37°C in a humidified atmosphere containing 5% CO_2. The cultures were passed twice weekly exhibiting characteristic doubling times of ∼24 h. The cell numbers were counted by a hematocytometer, and the viability was always greater that 95% in all experiments as assayed by the trypan blue exclusion method. Further dilutions of stock solutions of TA were made in culture media just before use. In all experiments, the final concentration of DMSO did not exceed 0.3% (v/v), a concentration which is non-toxic to the cells. The same concentration was present in control groups. These cell lines were obtained from the European Collection of Cell Cultures (Salisbury, UK).

HL-60 cells transfected with the pSFFV-neo plasmid (HL-60/neo) and/or pSFFV-bcl-x_L plasmid (HL-60/Bcl-x_L) (donated by Dr. Angelika Vollmar, Department of Pharmacy, Center of Drug Research, University of Munich, Germany, and which were established by Dr. KN Bhalla, Medical College of Georgia Cancer Center, GA, USA) were cultured as described for HL-60 cells except that 0.1 mM non-essential amino acids and 1 mM sodium pyruvate (Invitrogen) were added to the culture medium. Geneticin (1 mg/ml) was added to the culture medium every fifth passage. Cells which were exposed to geneticin

were not used for experiments. The U937 cell line over-expressing human Bcl-2 (kindly provided by Dr. Jacqueline Bréard, INSERM U749, Faculté de Pharmacie Paris-Sud, Châtenay-Malabry, France) was cultured as described [14].

Human peripheral blood mononuclear cells (PBMC) were isolated from heparin-anticoagulated blood of healthy volunteers by centrifugation with Ficoll-Paque Plus (Amersham Biosciences). PBMCs were also stimulated with phytohemagglutinine (PHA, 2 μg/ml) for 48 h before experimental treatment.

Cytotoxicity of TA on human tumor cells and human normal peripheral mononuclear cells

The cytotoxicity of TA on human tumor and human PBMC cells was analyzed by colorimetric 3-(4,5-dimethyl-2-thiazolyl-)-2,5-diphenyl-2*H*-tetrazolium bromide (MTT) assay as described [15]. Briefly, 1×10^4 exponentially growing cells were seeded in 96-well microculture plates with various TA concentrations. After the addition of MTT (0.5 mg/ml) cells were incubated at 37°C for 4 h. Sodium dodecyl sulfate (SDS) (10% w/v) in 0.05 M HCl was added to the wells and then incubated at room temperature overnight under dark conditions. The extension of reduction of MTT was quantified by absorbance measurement at 570 nm.

Evaluation of apoptosis

The rate of apoptotic cell death was analyzed by fluorescent microscopy and by flow-cytometric analysis of propidium iodide (PI)-stained nuclei as described below.

Fluorescent microscopy analysis

Cells were harvested and fixed in 3% paraformaldehyde and incubated at room temperature for 10 min. The fixative was removed and the cells were washed with PBS, resuspended in 30–50 μl of PBS containing 20 μg/ml bisbenzimide trihydrochloride (Hoechst 33258) and incubated at room temperature for 15 min. Stained nuclei were visualized using Zeiss fluorescent microscopy.

Quantification of apoptosis by flow cytometry

To study changes in the cell DNA content, histogram measurements of hypodiploid DNA formation was performed by flow cytometry using a Coulter EPICS™ cytometer (Beckman Coulter). Histograms were analyzed with the Expo 32 ADC Software™. Cells were collected and centrifuged at 500 × *g*, washed with PBS and resuspended in 50 μl of PBS. Following dropwise addition of 1 ml of ice-cold 75% ethanol, fixed cells were stored at −20°C for 1 h. Samples were then centrifuged at 500 × *g* and washed with PBS before resuspension in 1 ml of PBS containing 50 μg/ml propidium iodide and 100 μg/ml RNase A and incubation for 1 h at 37°C in the dark. The percentage of cells with decreased DNA staining, composed of apoptotic cells resulting from either fragmentation or decreased chromatin, was determined of a minimum of 10,000 cells per experimental condition. Cell debris was excluded from analysis by selective gating based on anterior and right angle scattering.

Analysis of DNA fragmentation

A late biochemical hallmark of apoptosis is the fragmentation of the genomic DNA. It is an irreversible event and occurs before changes in plasma membrane permeability. DNA isolation and gel electrophoresis were performed as described previously [15]. Briefly, cells (3×10^5) were collected by centrifugation, washed with PBS and incubated in 30 μl of lysis buffer [50 mM Tris-HCl (pH 8.0), 10 mM EDTA, 0.5% sodium dodecyl sulfate], containing 1 μg/μl RNase A at 37°C for 1 h. Then, 3 μl of proteinase K (10 μg/μl) was added and the mixture was incubated at 50°C for an additional 2 h. DNA was extracted with 100 μl of phenol-chloroform-isoamyl alcohol (24:24:1) and mixed with 5 μl of loading solution [10 mM EDTA, 1% (w/v) low melting-point agarose, 0.25% bromophenol blue and 40% sucrose, pH 8.0]. Samples were separated by electrophoresis in 2% agarose gels in TAE buffer [40 mM Tris-acetate (pH 8.0), 1 mM EDTA], visualized by ultraviolet illumination after ethidium bromide (0.5 μg/ml) staining and the images were captured by a digital camera (Digi Doc system, Bio-Rad).

Western blot analysis

Cells (1×10^6/ml) were treated in the absence or presence of TA (3–10 μM) for various time periods as indicated and harvested by centrifugation at 500 × *g* for 10 min. Cell pellets were resuspended in lysis buffer [20 mM Tris-HCl (pH 7.4), 2 mM EDTA, 137 mM NaCl, 10% glycerol, 1% Triton X-100, 2 mM tetrasodium pyrophosphate, 20 mM sodium *β*-glycerophosphate, 10 mM sodium fluoride, 2 mM sodium orthovanadate], supplemented with protease inhibitors phenylmethylsulfonyl fluoride (PMSF, 1 mM), leupeptin, aprotinin and pepstatin A (5 μg/ml each) for 15 min at 4°C. The cells were sonicated on ice (five times for 5 s each at 40 W, with 20 s intervals between each sonication) with a Braun Labsonic 2000 microtip sonifier (Braun, Melsungen, Germany) and centrifuged at 11,000 × *g* for 10 min at 4°C. Protein concentration of supernatants was measured by the Bradford method [16]

and samples containing equal amounts of proteins were boiled in sodium dodecyl sulfate sample buffer for 5 min before loading on an sodium dodecyl sulfate-polyacrylamide gel (7.5% for PARP, 10% for MAPKs and 12.5% for caspases). Proteins were electrotransferred to poly(vinylidene difluoride) (PVDF) membranes, blocked with 5% fat-free dry milk in Tris-buffered saline [50 mM Tris-HCl (pH 7.4), 150 mM NaCl] with 0.1% Tween 20 and then incubated with specific antibodies against PARP, caspase-9, caspase-6, caspase-3, β-actin, $p38^{MAPK}$, phospho-$p38^{MAPK}$ (Thr^{180}/Tyr^{182}), JNK/SAPK, phospho-JNK (Thr^{183}/Tyr^{185}), ERK 1/2 and phospho-ERK1/2 overnight at 4°C. After washing and incubation with an appropriate horseradish peroxidase-conjugated secondary antibody, the antigen-antibody complexes were visualized by enhanced chemiluminescence (ECL, Amersham Biosciences) using the manufacturer's protocol.

Detection of cytochrome *c*

Release of cytochrome *c* from mitochondria was detected by Western blot analysis. After treatments, cells were washed twice with PBS and then resuspended in ice-cold buffer [20 mM HEPES (pH 7.5), 1.5 mM $MgCl_2$, 10 mM KCl, 1 mM EDTA, 1 mM EGTA, 1 mM dithiothreitol, 0.1 mM phenylmethylsulfonylfluoride and 5 μg/ml leupeptin, aprotinin, and pepstatin A] containing 250 mM sucrose. After 15 min incubation on ice, cells were lysed by pushing them several times through a 22-gauge needle and the lysate spun down at 1,000 × *g* for 5 min at 4°C to eliminate nuclei and unbroken cells. The supernatant fraction was centrifuged at 15,000 × *g* for 20 min at 4°C, and the resulting pellet was designated as the mitochondrial fraction. The supernatant was further centrifuged at 105,000 × *g* for 45 min at 4°C and the resulting supernatant was designated as the cytosolic fraction. Cytosolic and mitochondrial proteins (50 μg) were resolved on a 15% sodium dodecyl sulfate/polyacrylamide gel and cytochrome *c* was detected by chemiluminescence as described above.

Analysis of mitochondrial membrane potential $\Delta\Psi_m$

Cells were treated with TA (10 μM) for different time periods and incubated with the fluorescent probe 5,5′,6,6′-tetrachloro-1,1′,3,3′-tetraethylbenzimidazolylcarbocyanine iodide (JC-1, 10 μM) for the last 30 min. JC-1 exists as a monomer at low values of $\Delta\Psi_m$ (green fluorescence; emission, 527 nm) while it forms aggregates at high $\Delta\Psi_m$ (orange fluorescence; emission, 590 nm). As a positive control, cells were treated with 10 μM of the protonophore CCCP (carbonyl cyanide m-chlorophenylhydrazone). Flow cytometric analysis was carried out using a Coulter EPICS^{TM} cytometer (Beckman Coulter).

Intracellular reactive oxygen species (ROS) determination

Intracellular reactive oxygen species (ROS) were detected by flow cytometry using 2′,7′-dichlorodihydrofluorescein diacetate (H_2-DCF-DA). This compound is deacetylated by intracellular esterase and converted to non fluorescent 2′,7′-dichlorodihydrofluorescein (H_2-DCF), which is rapidly oxidized to the highly fluorescent compound 2′,7′-dichlorofluorescein (DCF) in the presence of ROS (especially hydrogen peroxide and lipid hydroperoxides). HL-60 cells were treated with or without 10–30 μM TA for 1–6 h. Then 20 μM H_2-DCF-DA was added to the TA-treated cells, which were further incubated for 30 min. The cells were then washed and resuspended in 1 ml PBS. Flow cytometric analysis was carried out within 1 h using a Coulter EPICS^{TM} cytometer (Beckman Coulter). In each study, 10,000 cells were counted. Fluorescence of DCF was detected at an excitation and emission wavelengths of 485 and 530 nm, respectively.

Statistical analysis

Statistical significance of differences between control and treated samples were calculated using Student's *t*-test. *P* values of <0.05 were considered significant.

Results

TA induces apoptosis on human myeloid leukaemia cells

We have previously observed that human myeloid leukaemia HL-60 and U937 cell lines and also the human SK-MEL-1 melanoma cell line were highly sensitive to the antiproliferative effect of TA (Fig. 1a), a flavonoid derivative which was obtained by acetylation of the natural product trifolin [13]. Antiproliferative studies on TA indicate that this compound displays similar cytotoxic properties in all cell lines assayed ($IC_{50} \sim 10$ μM at 72 h). The IC_{50} value in U937 cells was 10 ± 2 μM, similar to the obtained value for SK-MEL-1 cells ($IC_{50} = 15 \pm 2$ μM) [13]. However, the naturally occurring trifolin is not an effective antiproliferative agent because the IC_{50} value increased to >100 μM in all cell lines.

Degradation of DNA into a specific fragmentation pattern is a characteristic feature of apoptosis. In contrast to the random fragmentation in necrosis, apoptosis-associated DNA fragmentation is characterized by cleavage of the DNA at regular intervals, visualized on agarose gel electrophoresis as a DNA ladder consisting of multimers of approximately 200 base pairs. When cells were incubated

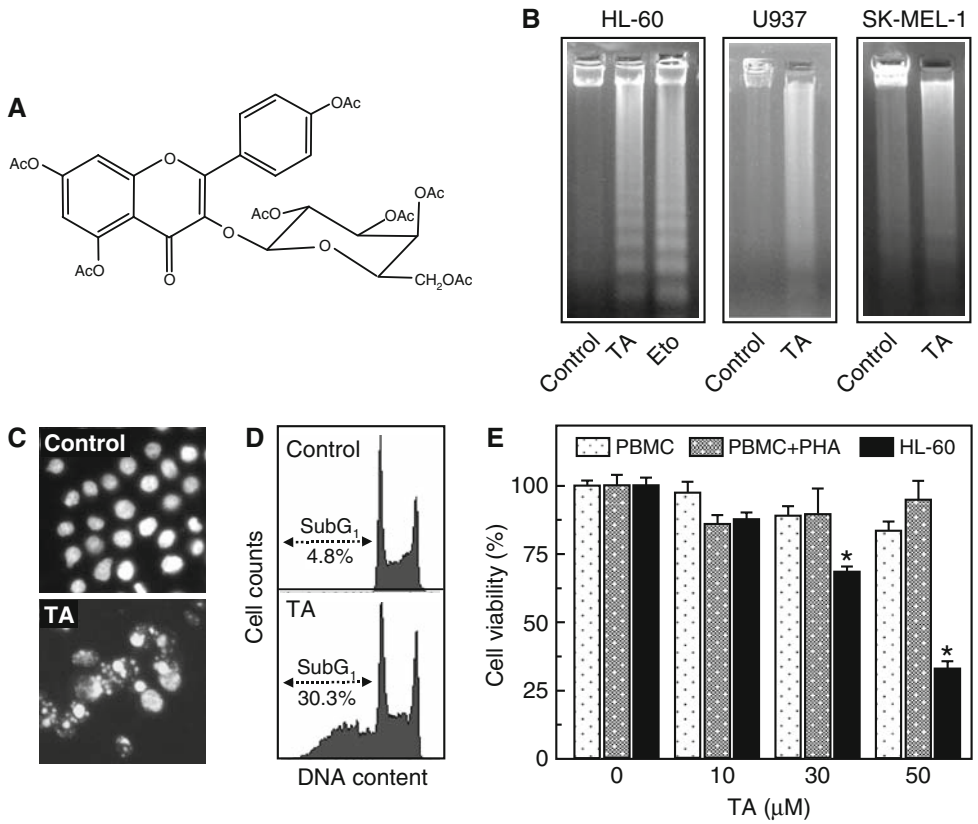

Fig. 1 (**a**) Chemical structure of TA. (**b**) Effects of TA on DNA fragmentation in human tumoral cells. Cells were treated with TA (10 μM) and genomic DNA was extracted, separated on an agarose gel and visualized under UV light by ethidium bromide staining. Etoposide (Eto) was included as a positive control. (**c**) Photomicrographs of representative fields of HL-60 cells stained with bisbenzimide trihydrochloride to evaluate nuclear chromatin condensation (i.e. apoptosis) after treatment of TA. (**d**) HL-60 cells were incubated as above and subjected to DNA flow cytometry using propidium iodide labeling. Hypodiploid cells (apoptotic cells) are shown in region marked with an arrow. (**e**) Differential effect of TA on proliferation of normal peripheral blood mononuclear cells (PBMC) versus HL-60 cells. Proliferation of HL-60 cells, quiescent PBMC and phytohemagglutinine (PHA)-activated healthy human PBMC cultured in presence of the indicated concentrations of TA for 24 h. Values represent means ± SEM. of two independent experiments each performed in triplicate. $*P < 0.05$, significantly different from untreated control

with TA, the DNA showed the typical fragmentation patterns formed by internucleosomal hydrolysis of chromatin in the human HL-60 and U937 cells, thus confirming the apoptosis-inducing effects (Fig. 1b). However, in SK-MEL-1 cells there was not a clear DNA laddering which suggests that other factors may be involved. In this regard, the mitochondrial flavoprotein apoptosis-inducing factor (AIF) has been demonstrated to cause chromatin condensation and high molecular weight DNA fragmentation without DNA laddering in response to certain apoptotic stimuli [17]. Whether AIF plays a role in TA-induced SK-MEL-1 cell death remains to be elucidated.

Next, we used fluorescent microscopy to analyze the morphological changes of cells treated with TA and observed condensed and fragmented chromatin characteristic of apoptotic cell death (Fig. 1c). Evaluation of the number of hypodiploid cells by flow cytometry showed that the percentage of apoptotic cells increased about approximately 6-fold in TA-treated HL-60 cells after 6 h exposure (Fig. 1d).

Since an ideal anti-cancer agent should have no effect on normal, non-tumoral cells, we investigated whether TA was also cytotoxic for human PBMC. No cytotoxicity (up 50 μM) to either fresh or proliferating PBMC was observed. However, there was an important reduction in the proliferation of HL-60 cells which were included in the experiment as a positive control (Fig. 1e).

TA-induced cell death is mediated by a caspase-dependent pathway

To demonstrate that TA-triggered apoptosis requires the activation of caspases, HL-60 cells were pretreated with increasing concentrations of the broad-spectrum caspase inhibitor z-VAD-fmk. As shown in Fig. 2a, the results indicated that apoptosis was completely suppresed,

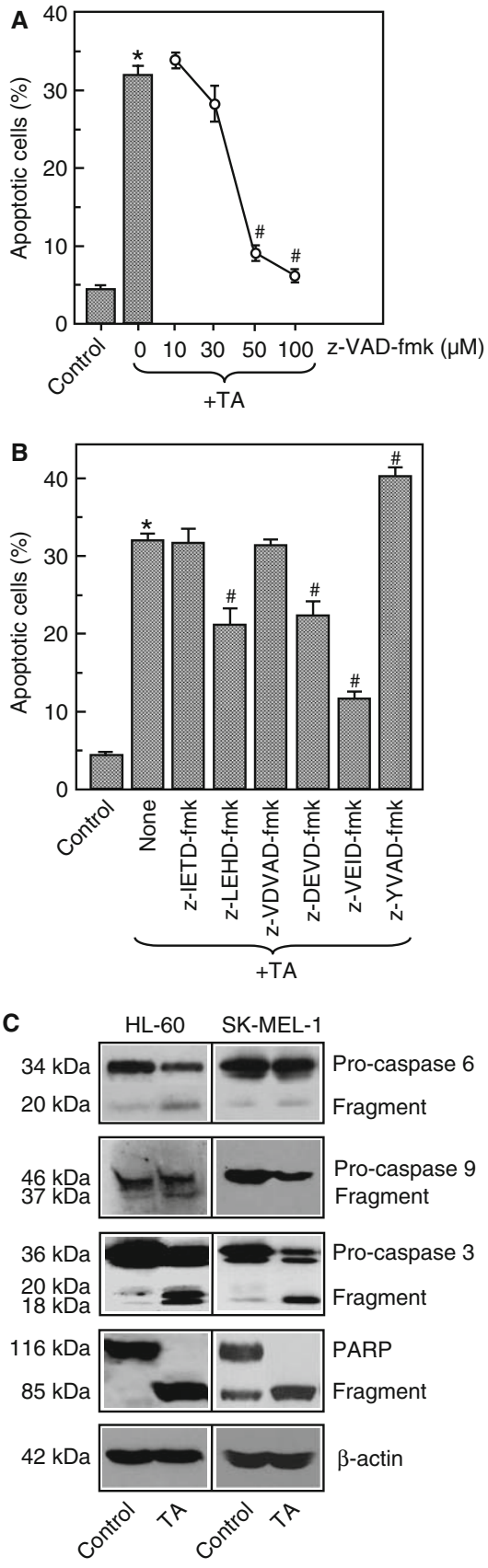

◀**Fig. 2** Involvement of caspases in the induction of apoptosis in human leukaemia cells. (**a**) Cells were pretreated with increasing concentrations of z-VAD-fmk before addition of TA and apoptotic cells were analyzed by flow cytometry. Values represent means ± SEM. of two independent experiments each performed in duplicate. $^{*}P < 0.05$, significantly different from untreated control. $^{\#}P < 0.05$, significantly different from TA treatment alone. (**b**) Effect of cell-permeable caspase inhibitors on TA-stimulated apoptosis. HL-60 cells were incubated with 10 μM TA for 12 h, in absence or presence of the caspase-8 inhibitor z-IETD-fmk (50 μM), the caspase-2 inhibitor z-VDVAD-fmk (50 μM), the caspase-9 inhibitor z-LEHD-fmk (50 μM), the caspase-6 inhibitor z-VEID-fmk (50 μM), the caspase-3 and -7 inhibitor z-DEVD-fmk (50 μM) and the caspase-1 inhibitor z-YVAD-fmk (50 μM). Apoptotic cells were determined and quantified by flow cytometry. The results are means ± SEM of three independent experiments. $^{*}P < 0.05$, significantly different from untreated control. $^{\#}P < 0.05$, significantly different from TA treatment alone. (**c**) Cells were incubated in the presence of TA and cell lysates were assayed by immunoblotting for the cleavage of procaspase-9, -6, -3 and poly(ADP-ribose) polymerase (PARP) on HL-60 and SK-MEL-1 cells. β-Actin was used as a loading control

indicating that TA induced cell death by a caspase dependent mechanism.

To identify which caspases were important in TA-induced cytotoxicity, the effects of cell-permeable caspase inhibitors were examined. These included z-LEHD-fmk (caspase-9-selective inhibitor), z-DEVD-fmk (caspase-3 and -7-selective inhibitor), z-YVAD-fmk (caspases-1-selective inhibitor), z-VDVAD-fmk (caspase-2-selective inhibitor), z-VEID-fmk (caspase-6-selective inhibitor) and z-IETD-fmk (caspase-8-selective inhibitor). The results (Fig. 2b) indicated that the pretreatment of cells with z-LEHD-fmk, z-DEVD-fmk and z-VEID-fmk significantly reduced the percentage of TA-mediated apoptotic cells. The percentage of apoptotic cells decreased from 33 ± 2% in TA-treated cells to approximately 20 ± 2% in cells pretreated with z-LEHD-fmk and z-DEVD-fmk. The effect of z-VEID-fmk was quantitatively greater and reduced the percentage of TA-induced cell death to 10 ± 1%. In contrast, z- IETD-fmk and z-VDVAD-fmk did not show any effect, which indicated that caspase-8 and caspase-2 were not involved in TA-induced cell death. Surprisingly, z-YVAD-fmk sensitized the HL-60 cells to TA-induced cell death. No impact on basal apoptosis level was detected in cells incubated with z-YVAD-fmk. Specific inhibitors for selected caspases were used at 50 μM, the lower concentration which showed to be effective in decreasing the percentage of apoptotic cells induced by TA (results not shown).

Since the proteolytic processing of caspases is an important event in caspase-dependent apoptotic cell death, we decided to evaluate the effect of this compound on caspases in accordance with the inhibition experiments. To this end, HL-60 and SK-MEL-1 cells were treated with TA

and the initiator (caspase-9) and executioners (caspases-6 and 3) caspases were determined by western blot using specific antibodies that bind both the proenzyme (caspase precursors) and the cleaved caspases. As expected, TA significantly promoted the cleavage of inactive procaspase-9, -6 and -3 in both cell lines (Fig. 2c).

To determine whether the procaspase-3 processing was associated with an increase in enzymatic activity we examined poly(ADP-ribose) polymerase (PARP) cleavage, a known substrate of caspase-3 that plays an important role in the DNA repair. Hydrolysis of the 116 kDa PARP protein to the 85 kDa fragment was detected in TA treated cells suggesting that PARP cleavage was involved in apoptosis induced by this compound (Fig. 2c).

Release of cytochrome *c* from mitochondria to cytosol is a central event in apoptotic signaling. To determine whether this key molecule is involved in TA-induced apoptosis on HL-60 and SK-MEL-1 cells, time course experiments were performed and cytosolic preparations were analyzed by immunoblotting. The results show a significant increase in the amount of cytochrome *c* in the cytosol, early detected at 6 h of treatment (Fig. 3a). To examine whether a disruption of the $\Delta\Psi_m$ is required for the release of cytochrome *c*, HL-60 cells were left untreated or treated with TA for different times (3, 6, 12 and 24 h), stained with JC-1 and analyzed by flow cytometry. The results indicate that $\Delta\Psi_m$ remained intact for at least 24 h of treatment, which suggests that the disruption of the mitochondrial membrane potential is not involved in TA-induced apoptosis. In this study, the protonophore CCCP was used as a positive control (Fig. 3b).

Since Bcl-2 and Bcl-x_L are known to inhibit apoptosis by regulating mitochondrial membrane potential and cytochrome *c* release needed for the activation of caspase-9 [9], we decided to clarify whether these proteins protect the cells against the effects of TA. To this end we used cell lines over-expressing Bcl-x_L (HL-60/Bcl-x_L) or Bcl-2 (U937/Bcl-2). Results indicate that over-expression of both factors blocked the apoptosis induction by TA on these cell lines (Fig. 3c).

TA activates MAPKs

MAPK pathways can mediate signals that either promote or suppress the growth of malignant hematopoietic cells. In view of evidence that the ERK, JNK/SAPK and $p38^{MAPK}$ play a critical role in cell fate, the effects of TA on the activation of these kinases were examined (Fig. 4a). The results show a fast phosphorylation (<15 min) of ERK1/2, JNK/SAPK and $p38^{MAPK}$ in HL-60 and U937 cells. Phosphorylation of ERK1/2 and JNK/SAPK remained elevated for at least 6 h, while the activation of $p38^{MAPK}$ decreased in HL-60 cells after 4 h

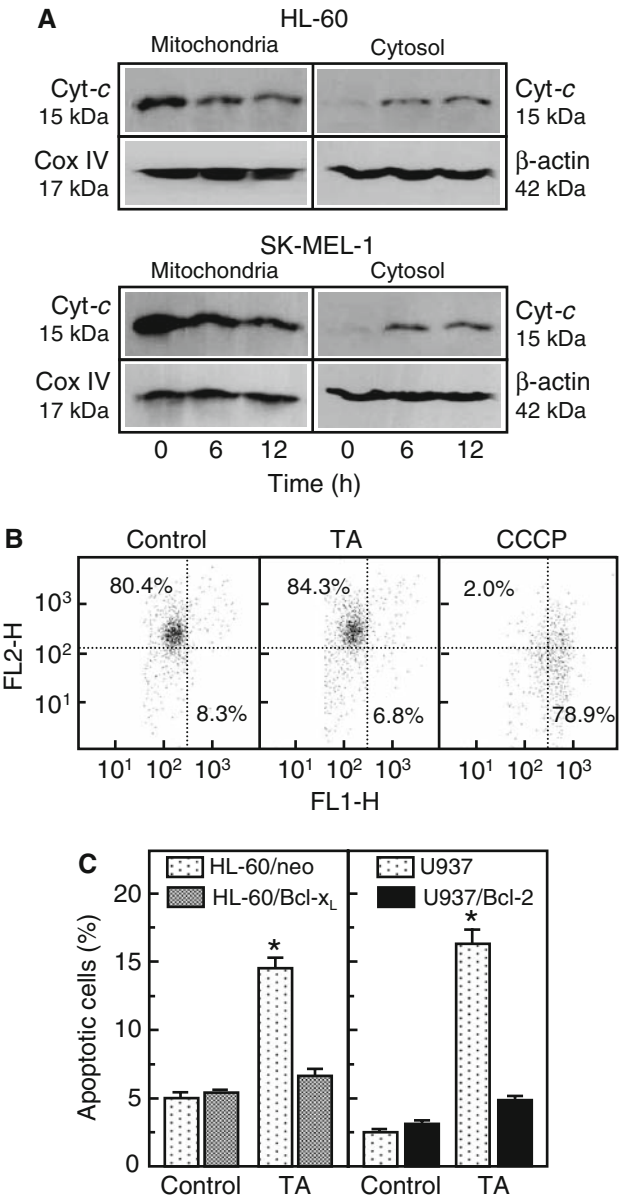

Fig. 3 (**a**) Cytochrome *c* release occurs after TA-treatment. The cells were incubated in the presence of TA (10 μM) and harvested at the indicated times and cytosolic or mitochondrial extracts were assayed by immunoblotting for cytochrome *c* release on HL-60 and SK-MEL-1 cells. *β*-actin and Cox IV (cytochrome *c* oxidase) were used as loading controls in cytosol and mitochondria, respectively. The cytosolic and mitochondria-enriched fractions were prepared and western blot analyses were performed as described in the Materials and Methods. (**b**) TA does not reduce the mitochondrial membrane potential ($\Delta\Psi_m$). Cells were treated with TA for 24 h and $\Delta\Psi_m$ analyzed with JC-1. The intensity of JC-1 fluorescence was analyzed by flow cytometry as described in the Materials and Methods. Similar results were obtained in two separate experiments each performed in triplicate. As a positive control, aliquots of cells were stained in the presence of 10 μM of CCCP. (**c**) Effect of TA on cells over-expressing Bcl-x_L and Bcl-2. Comparison of TA treatment in HL-60/neo and HL-60/Bcl-x_L cells, and also in U937 and U937/Bcl-2 cells. The percentage of hypodiploid cells was determined by flow cytometry in absence or presence of TA. Values represent means ± SEM. of three different experiments. *$P < 0.05$, significantly different from untreated control

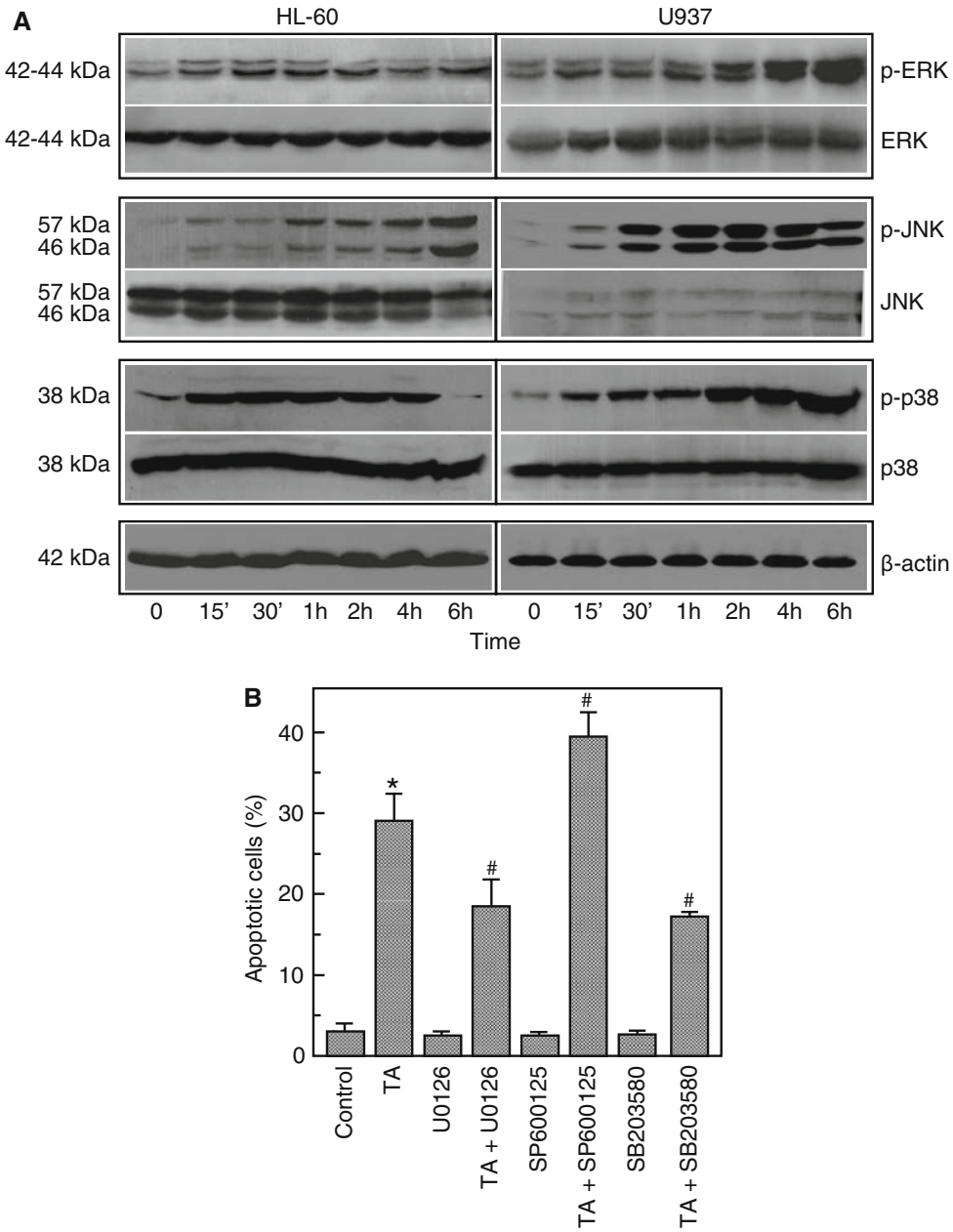

Fig. 4 TA induces phosphorylation of MAPKs and impact of MAPKs inhibitors on TA-induced apoptosis. (**a**) Representative Western blots show the time-dependent phosphorylation of ERK 1/2, JNK/SAPK and $p38^{MAPK}$ by TA. Cells were incubated with TA for the indicated time points. Protein extracts were prepared and analysed on western blots probed with specific antibodies to ascertain the phosphorylation of MAPKs. Membranes were stripped and reprobed with total ERK 1/2, JNK/SAPK, $p38^{MAPK}$ and β-actin antibodies as loading controls. (**b**) HL-60 cells were preincubated with U0126 (10 μM), SP600125 (10 μM) and SB203580 (2 μM) for 1 h and then treated with TA. Apoptosis was quantified by flow cytometry as described in the Materials and Methods. Bars represent the means ± SEM. of three independent experiments each performed in triplicate. $^{*}P < 0.05$, significantly different from untreated control. $^{\#}P < 0.05$, significantly different from TA treatment alone

under the same experimental conditions. These results indicate that TA treatment of HL-60 and U937 cells leads to activation of ERK1/2, JNK/SAPK and $p38^{MAPK}$ following similar kinetics. To determine whether the phosphorylation of MAPKs plays a key role in TA-induced apoptosis, we examined the effects of specific inhibitors of ERK1/2, JNK/SAPK and $p38^{MAPK}$ (Fig. 4b). Treatment of HL-60 cells with U0126, a specific inhibitor of mitogen-activated extracellular kinase 1/2 (MEK1/2) which blocks the activation of ERK1/2, partially decreased the TA-induced apoptosis which strongly suggests that ERK 1/2 is required for its cytotoxicity. In contrast with the above results, previous studies have demonstrated synergistic effects of chemotherapeutic agents and drugs that inhibit MAPK activation in inducing growth suppression and apoptosis of acute leukemia cells [18, 19]. We have recently described that specific inhibitors of ERK 1/2 may serve as sensitizers towards quercetin 3-methyl ether tetracetate-mediated apoptosis in human leukaemia cells [20].

Pharmacological inhibition of the $p38^{MAPK}$ using SB 203580 inhibitor was found to significantly attenuate TA-induced cell death from 30% of apoptotic cells to 15% in the combination group (TA + SB203580). These data suggest that activation of $p38^{MAPK}$ is involved in TA-induced apoptosis.

Interestingly, pretreatment of human myeloid leukaemia HL-60 cells with the specific JNK/SAPK inhibitor SP600125 amplified TA-mediated apoptosis. Similar results were obtained in U937 cells (results not shown). Therefore, the inhibition of the JNK/SAPK pathway might be a valuable strategy in increasing the sensitivity of cells toward TA. This result is surprising since JNK/SAPK pathway has been described to be activated by various chemotherapeutic agents which induce apoptosis and are usually used in the treatment of acute myelogenous leukaemia [21, 22].

Reactive oxygen species (ROS) were not required for TA-induced cell death

Most apoptosis-inducing agents release ROS, which is considered one of the key mediators of apoptotic signaling. Since increased ROS production in leukemic cells may lead to the activation of MAPKs and cell death [23–26], we decided to investigate whether ROS is involved in TA-induced apoptosis. To this end, TA-treated cells were loaded with the fluorescent dye 2′,7′-dichlorodihydrofluorescein diacetate and then analyzed by flow cytometry. As shown in Fig. 5a, ROS formation was detected within 1 h of TA treatment. To determine whether the generation of ROS is involved in TA-induced cell death we also investigated the effect of the following antioxidants: ascorbic acid (vitamin C, 100 μM), the glutathione precursor *N*-acetyl-L-cysteine (NAC, 10 mM), α-tocopherol (vitamin E, 25 μM), trolox (2 mM), the inhibitor of xanthine oxidase allopurinol (100 μM) and superoxide dismutase (SOD, 400 units/ml). None of these antioxidants blocked cell death as assessed by flow cytometry indicating that TA-induced apoptosis is independent of ROS production (Fig. 5b).

Discussion

Plant-derived active principles and their semi-synthetic and synthetic analogs have served as a major route to new anticancer compounds [27]. Current conventional chemotherapy treatments are very expensive, toxic, and less effective in treating the disease. Compounds from natural sources therefore require investigation in further detail to mitigate the increasing incidence of cancer. Flavonoids are naturally occurring phenylbenzo-γ-pyrones found in abundance in diets rich in fruits, vegetables and plant-derived beverages [11] and appear to have anticancer properties [10]. In previous studies with natural and semi-synthetic phenylbenzo-γ-pyrones, we have documented that some derivatives induce cytotoxicity in human myeloid leukemia HL-60 cells [15]. Anti-proliferative studies of TA indicated that this compound displays similar cytotoxic properties in all assayed cell lines, with an IC_{50} value of about 10–15 μM, although the mechanism by which the flavonoid derivative leads to decreased cell growth has not yet been assessed. Studies performed with the naturally occurring flavonoid trifolin indicated that this compound did not display any cytotoxic activity in all cell lines tested (data not shown). Therefore, further studies were carried out with TA instead of trifolin. As for all of the agents used or developed for cancer treatment, selectivity toward cancer cells is an important criterion. We therefore compared the effects of TA between human tumor cells and human PBMC. Interestingly, dose-response studies revealed that

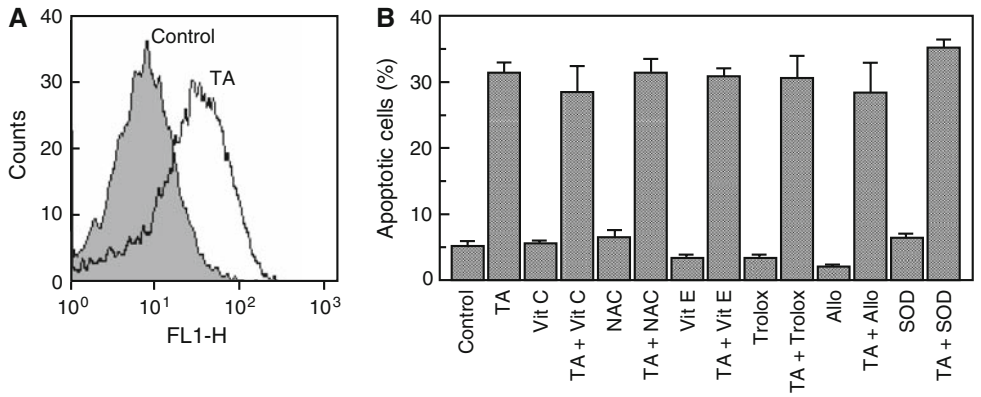

Fig. 5 (**a**) TA increases ROS generation in HL-60 cells. Cells were treated with TA for 1 h and the fluorescence of oxidized H_2DCF was determined by flow cytometry. Similar results were obtained from three independent experiments. (**b**) Lack of apoptosis inhibition by scavengers of ROS in TA-treated HL-60 cells. Cells were incubated with the anti-oxidants ascorbic acid (vit C, 100 μM), *N*-acetyl-L-cysteine (NAC, 10 mM), α-tocopherol (vit E, 25 μM), trolox (2 mM), allopurinol (Allo, 100 μM) and superoxide dismutase (SOD, 400 units/ml) for 1 h and then treated with TA. Cells were also incubated with each antioxidant only. Apoptosis was quantified by flow cytometry after staining with propidium iodide. Bars represent the means ± SEM. of two independent experiments each performed in triplicate

quiescent PBMC and proliferating PBMC were highly resistant toward TA.

Since many antitumoral compounds are apoptotic inducers we initiated studies to evaluate whether TA stimulates apoptosis in human cell lines. Ours results clearly indicate that TA induces cell death by apoptosis. This form of cell death that can occur with or without activation of caspases, a family of cysteine proteases that plays critical roles in mammalian apoptosis or proteolytic activation of cytokine. Thus, the utilization of these mechanisms is stimulus- and cell type-dependent. In order to know whether the cell death is associated to caspase activation, a general caspase inhibitor (z-VAD-fmk) was used. The results indicate that TA-induced apoptosis was completely abolished in z-VAD-fmk pretreated cells which supported a caspase dependent cell death mechanism. There are two well-characterized apoptotic pathways in mammalian cells, referred to as the death receptor (extrinsic) and mitochondrial (intrinsic) pathways. They are widely considered as being responsible for most, if not all, caspase-dependent apoptosis. Therefore, we decided to evaluate which apoptotic pathway was involved in TA-induced cell death by using selective inhibitors against caspase-8 (z-IETD-fmk) and caspase-9 (z-LEHD-fmk), the main initiator (apical) caspases for the extrinsic- and intrinsic- pathway, respectively. We demonstrated that the death receptor pathway does not play any role since z-IETD-fmk was unable to prevent TA-induced cell death. This result is also concordant with those obtained from immunoblotting analyses which indicated absence of hydrolysis of inactive procaspase-8 (data not shown). In contrast, the percentage of apoptotic cells significantly decreased in the presence of z-LEHD-fmk which indicated that the mitochondrial pathway plays an important role in TA-induced cell death. This result is consistent with an increase in the hydrolysis of the inactive pro-caspase-9 observed in lysates from TA-treated cells. In a previous study of HL-60 cells we showed an effective blockage of betuletol 3-methyl ether induced-apoptosis by z-IETD-fmk, but not by z-LEHD-fmk, supporting a caspase-8 mediated mechanism [15]. Therefore, different apoptotic pathways can be activated in this cell line in response to compounds containing the same basic structure (phenylbenzo-γ-pyrones) such as TA and betuletol 3-methyl ether.

We also evaluated whether caspase-2 is involved in TA-induced cell death since this caspase appears to act upstream of mitochondria to promote cytochrome *c* release in different cell systems [28–30]. Our results, by using the specific inhibitor z-VDVAD-fmk, indicate that caspase-2 is not necessary for TA-induced apoptosis and that its involvement in caspase-9 activation can be ruled out. It also supports a preeminent function of caspase-9 as the apical caspase which is activated in response to TA. Thus, caspase-2 is the only pro-caspase constitutively present in the nucleus and appears to be necessary for the onset of apoptosis triggered by agents that promote DNA damage such as etoposide, cis-platin and ultraviolet-light [28, 31]. Although more experimental evidences are necessary, the results showed herein also suggest that TA triggers cell death through a mechanism that seems to be independent of DNA damage.

Once activated, most initiator caspases proteolytically activate the downstream effector caspases, which in turn cleave specific cellular substrates resulting in chromatin condensation, membrane blebbing and cell shrinkage. To further characterize the effector caspases that are involved in TA-induced apoptotic process, selective inhibitors against caspase-3 (z-DEVD-fmk) and caspase-6 (z-VEID-fmk) were used. Therefore, we demonstrated that both caspases are important to promote apoptosis triggered by TA. Interestingly we found that z-VEID-fmk was significantly more effective than z-DEVD-fmk to prevent apoptosis upon treatment with TA. This result suggests that caspase-6 might play an important upstream role, as previously described for resveratrol-induced apoptosis in human T-cell leukaemia cell lines [32] and in contrast with a large number of studies which suggest that caspase-6 is an effector caspase that is activated downstream of caspase-3 during apoptosis [33, 34]. However, other explanations can not be ruled out and could be related to differences in the accessibilities of inhibitors to cellular caspases [35] and/or implication of non identified apical protease with caspase-like activity, as recently suggested for heat shock induced-apoptosis in Jurkat cells [36].

In this context caspase-1, in addition to the well-characterized function in the processing of proinflammatory cytokines IL-1β and IL-18 [37], appears to be involved in cell death as demonstrated in fibroblasts [38], neuronal cells [39] and is also required for the induction of apoptosis in macrophages by certain bacteria [40]. Moreover, previous work has shown that caspase-1 activates caspase-6 in serum-deprived human neurons and results in neuronal cell death [41]. Paradoxically, we find that the percentage of hypodiploid cells significantly increased in presence of the caspase-1 inhibitor z-YVAD-fmk, which suggests a survival role of caspase-1 in TA-stimulated cells. Interestingly, caspase-1 has been recently reported to promote cell survival through a mechanism that involves activation of sterol regulatory element binding proteins (SREBPs) and lipid biogenesis. Thus, selective inhibition of caspase-1 by z-YVAD-fmk or si-RNA mediated knockdown resulted in higher levels of cell death in response to pore-forming toxins [42]. Whether caspase-1 is activated in TA-stimulated cells and displays a mechanism that involves lipid biogenesis remains to be elucidated.

As expected, given the roles of caspases-3 and -6 in TA-induced cell death, there was also an increase in the proteolytic processing of both pro-enzymes to form activated enzymes. Thus, apoptosis was accompanied by cleavage of the nuclear protein PARP, a recognized caspase-3 substrate which is involved in DNA repair and it is important for maintaining cell viability [43–45]. Therefore, hydrolysis of PARP guarantees cellular disassembly and supports a role for this protein as a key regulator of apoptosis in TA-treated cells [45].

Mitochondria play a key role in cell death when their membranes become permeabilized [46]. Outer mitochondrial membrane permeabilization is regulated by different members of the Bcl-2 family which constitutes a critical cellular checkpoint in the intrinsic pathway of apoptosis [47].

Here we have shown that TA initiated redistribution of cytochrome *c* into the cytosol which was already detected at 6 h. However, this early event is not associated with a loss in $\Delta\Psi_m$ which remains unchanged for at least 24 h. In this regard, previous studies have shown that changes in $\Delta\Psi_m$ are not required for the complete release of cytochrome *c* upon the mitochondrial outer membrane permeabilization [48]. This latter effect occurs as a consequence of the activation of Bax and/or Bak and the formation of openings in the outer membrane [49].

To further investigate the role of mitochondria upon treatment with TA, HL-60 and U937 cells over-expressing anti-apoptotic factors were included in the study. HL-60/Bcl-x_L and U937/Bcl-2 were completely resistant compared with the parental cell lines, which suggest a central role of mitochondria in TA-induced cell death. Taken together, our results suggest that TA induces apoptosis through a mechanism that involves the mitochondrial pathway in which caspase-6 seems to operate upstream to caspase-9.

In addition to apoptosis, MAP kinases regulate diverse cellular programs including proliferation and differentiation. Although the JNK/SAPK has generally been associated with pro-apoptotic actions [8] and growth inhibitory signals [50], here we show that TA induces JNK/SAPK activation and its inhibition by SP600125 enhances apoptotic cell death. Previous studies have shown that the pro-apoptotic effect of the histone deacetylase inhibitor D1 increased in the presence of SP600125 in human acute myeloid leukaemia cell lines [51]. Additional evidence that JNK can be a prosurvival signal has been also demonstrated in hepatocellular carcinoma cells [52] and in gastric and a colorectal cancer cell lines [53].

Cell death is promoted by $p38^{MAPK}$ signaling in some cell lines, and also enhances survival, cell growth and differentiation. Therefore, the role of $p38^{MAPK}$ in apoptosis is dependent on cell type and stimulus [54]. The $p38^{MAPK}$ appears to be involved in the activation of TA-induced apoptosis, since the specific inhibitor SB203580 attenuated cell death. Activation of $p38^{MAPK}$ is also a prerequisite for apoptosis induced by cadmium, trophic factor withdrawal and ischemia [55–58]. However, the activation of $p38^{MAPK}$ is not involved in apoptosis induced by ultraviolet radiation in U937 cells [59] or by *S*-nitrosoglutathione in RAW 264.7 macrophages [60] and/or in Fas- and ultraviolet-treated Jurkat T cells [61].

Our data also indicate that the inhibitor U0126 attenuated the apoptotic effects of TA, which suggested that ERK 1/2 is involved in cell death signals. Our results are in agreement with previous work that has shown that inhibition of MEK-ERK activation with U0126 or PD98059 abolishes quercetin-induced apoptosis in A549 cells [62]. In addition, the suppression of MEK-ERK signal pathway by the MEK inhibitor PD98059 resulted in an increase in cisplatin-resistance in human cervical carcinoma SiHa cells and hepatoblastoma HepG2 cells [63]. Moreover, acrolein, a highly reactive α,β-unsaturated aldehyde generated by lipid peroxidation, induced phosphorylation of ERK and the inhibition of its activity by PD98059 and U0126 blocked acrolein-induced apoptosis [64].

Quercetin 3-methyl ether acetate, which is chemically similar to TA, enhances the activation of the MEK/ERK pathway [20]. In contrast, ERK inhibitors potentiate the apoptotic effects of quercetin 3-methyl ether. Therefore, different pathways can be activated in the same cell line by these similar compounds.

Previous reports have demonstrated that production of ROS in leukaemic cells may lead to cell death via MAPKs activation [23–26]. Although intracellular ROS generation was observed within 1 h after exposure to TA, different anti-oxidants were unable to abrogate cell death. These results indicate that ROS generation does not seem to be involved in TA triggered apoptosis.

Conclusion

In summary, our results show that TA induces apoptosis through a caspase-dependent mechanism which is associated with cytochrome *c* release and is inhibited by over-expression of Bcl-2 and Bcl-x_L. Although cleavage of procaspase-9, -6 and -3 is detected in TA-treated cells by immunoblotting, the inhibition data indicate that caspase-6 almost fully accounts for cell death. In this scenario the MAP kinases pathway plays an important role in which ERK1/2 and $p38^{MAPK}$ display pro-apoptotic function while JNK/SAPK promotes cell survival. We show that TA triggers a fast phosphorylation of MAPKs (ERK1/2, JNK/SAPK and $p38^{MAPK}$) through a mechanism independent of ROS generation. Since these cells are p53 null, our results

clearly demonstrate that TA-induced apoptosis occurs independently of p53-mediated cellular events. Detailed mechanistic studies are required to define the effect of TA on several other human leukemia cells. However, based on the present findings it is tempting to suggest that TA has strong potential for development as a chemopreventive and possibly as a therapeutic agent against cancer.

Acknowledgments We thank Dr. Angelika Vollmar and Dr. Jacqueline Bréard for supplying HL-60/neo, HL-60/Bcl-x_L and U937/Bcl-2 cells, respectively. We thank J. Estévez (Hospital Universitario Insular de Gran Canaria) for his collaboration in the Western blot assays. This work was supported by a Grant from the Ministry of Education and Science of Spain and from the European Regional Development Fund (SAF2004-07928) to FE. FT was supported by a research studentship from the Canary Islands Government.

References

1. Kroemer G, El-Deiry WS, Golstein P et al (2005) Nomenclature committee on cell death. Classification of cell death: recommendations of the nomenclature committee on cell death. Cell Death Differ 12:1463–1467
2. Thornberry NA, Lazebnik Y (1998) Caspases: enemies within. Science 281:1312–1316
3. Boatright KM, Salvesen GS (2003) Mechanisms of caspase activation. Curr Opin Cell Biol 15:725–731
4. Nagata S (1997) Apoptosis by death factor. Cell 88:355–365
5. Kluck RM, Bossy-Wetzel E, Green DR, Newmeyer DD (1997) The release of cytochrome *c* from mitochondria: a primary site for Bcl-2 regulation of apoptosis. Science 275:1132–1136
6. Yang J, Liu X, Bhalla K et al (1997) Prevention of apoptosis by Bcl-2: release of cytochrome *c* from mitochondria blocked. Science 275:1129–1132
7. Essmann F, Engels IH, Totzke G, Schulze-Osthoff K, Jänicke RU (2004) Apoptosis resistance of MCF-7 breast carcinoma cells to ionizing radiation is independent of p53 and cell cycle control but caused by the lack of caspase-3 and a caffeine-inhibitable event. Cancer Res 64:7065–7072
8. Cross TG, Scheel-Toellner D, Henriquez NV, Deacon E, Salmon M, Lord JM (2000) Serine/threonine protein kinases and apoptosis. Exp Cell Res 256:34–41
9. Kang C-D, Yoo S-D, Hwang B-W et al (2000) The inhibition of ERK/MAPK not the activation of JNK/SAPK is primarily required to induce apoptosis in chronic myelogenous leukemic K562 cells. Leuk Res 24:527–534
10. Middleton E, Kandaswami C, Theoharides TC (2000) The effects of plant flavonoids on mammalian cells: implications for inflammation, heart disease, and cancer. Pharmacol Rev 52:673–751
11. Havsteen BH (2002) The biochemistry and medical significance of the flavonoids. Pharmacol Therapeut 96:67–202
12. Ren W, Qiao Z, Wang H, Zhu L, Zhang L (2003) Flavonoids: promising anticancer agents. Med Res Rev 23:519–534
13. Díaz JG, Carmona AJ, Torres F, Quintana J, Estévez F, Herz W (2008) Cytotoxic activities of flavonoid glycoside acetates from *Consolida oliveriana*. Planta Med 74:171–174
14. Paris C, Bertoglio J, Bréard J (2007) Lysosomal and mitochondrial pathways in miltefosine-induced apoptosis in U937 cells. Apoptosis 12:1257–1267
15. Rubio S, Quintana J, López M, Eiroa JL, Triana J, Estévez F (2006) Phenylbenzopyrones structure-activity studies identify betuletol derivatives as potential antitumoral agents. Eur J Pharmacol 548:9–20
16. Bradford MM (1976) A rapid and sensitive method for the quantitation of microgram quantities of protein utilizing the principle of protein-dye binding. Anal Biochem 72:248–254
17. Susin SA, Lorenzo HK, Zamzami N et al (1999) Molecular characterization of mitochondrial apoptosis-inducing factor. Nature 397:441–446
18. Jarvis WD, Fornari FA Jr, Tombes RM et al (1998) Evidence for involvement of mitogen-activated protein kinase, rather than stress-activated protein kinase, in potentiation of 1-beta-D-arabinofuranosylcytosine-induced apoptosis by interruption of protein kinase C signaling. Mol Pharmacol 54:844–856
19. Yu C, Wang S, Dent P, Grant S (2001) Sequence-dependent potentiation of paclitaxel-mediated apoptosis in human leukemia cells by inhibitors of the mitogen-activated protein kinase kinase/mitogen-activated protein kinase pathway. Mol Pharmacol 60:143–154
20. Rubio S, Quintana J, Eiroa JL, Triana J, Estévez F (2007) Acetyl derivative of quercetin 3-methyl ether-induced cell death in human leukemia cells is amplified by the inhibition of ERK. Carcinogenesis 28:2105–2013
21. Laurent G, Jaffrézou JP (2001) Signaling pathways activated by daunorubicin. Blood 98:913–924
22. Yu R, Shtil AA, Tan TH, Roninson IB, Kong AN (1996) Adriamycin activates c-jun N-terminal kinase in human leukaemia cells: a relevance to apoptosis. Cancer Lett 107:73–81
23. Chen YR, Wang W, Kong AN, Tan TH (1998) Molecular mechanisms of c-Jun N-terminal kinase-mediated apoptosis induced by anticarcinogenic isothiocyanates. J Biol Chem 273:1769–1775
24. Shiah SG, Chuang SE, Chau YP, Shen SC, Kuo ML (1999) Activation of c-Jun NH2-terminal kinase and subsequent CPP32/Yama during topoisomerase inhibitor β-lapachone-induced apoptosis through an oxidation-dependent pathway. Cancer Res 59:391–398
25. Watabe M, Kakeya H, Osada H (1999) Requirement of protein kinase (Krs/MST) activation for MT-21-induced apoptosis. Oncogene 18:5211–5220
26. Zhuang S, Demirs JT, Kochevar IE (2000) p38 mitogen-activated protein kinase mediates bid cleavage, mitochondrial dysfunction, and caspase-3 activation during apoptosis induced by singlet oxygen but not by hydrogen peroxide. J Biol Chem 275:25939–25948
27. Lee K-H (1999) Novel antitumor agents from higher plants. Med Res Rev 19:569–596
28. Lassus P, Opitz-Araya X, Lazebnik Y (2002) Requirement for caspase-2 in stress-induced apoptosis before mitochondrial permeabilization. Science 297:1352–1354
29. Guo Y, Srinivasula SM, Druilhe A, Fernandes-Alnemri T, Alnemri ES (2002) Caspase-2 induces apoptosis by releasing proapoptotic proteins from mitochondria. J Biol Chem 277:13430–13437
30. Robertson JD, Enoksson M, Suomela M, Zhivotovsky B, Orrenius S (2002) Caspase-2 acts upstream of mitochondria to promote cytochrome *c* release during etoposide-induced apoptosis. J Biol Chem 277:29803–29809
31. Zhivotovsky B, Samali A, Gahm A, Orrenius S (1999) Caspases: their intracellular localization and translocation during apoptosis. Cell Death Differ 6:644–651
32. Bernhard D, Tinhofer I, Tonko M et al (2000) Resveratrol causes arrest in the S-phase prior to Fas-independent apoptosis in CEM-C7H2 acute leukemia cells. Cell Death Differ 7:834–842
33. Srinivasula SM, Ahmad M, Fernandes-Alnemri T, Alnemri ES (1998) Autoactivation of procaspase-9 by Apaf-1-mediated oligomerization. Mol Cell 1:949–957

34. Slee EA, Harte MT, Kluck RM et al (1999) Ordering the cytochrome *c*-initiated caspase cascade: hierarchical activation of caspases-2, -3, -6, -7, -8, and -10 in a caspase-9-dependent manner. J Cell Biol 144:281–292
35. Scoltock AB, Cidlowski JA (2004) Activation of intrinsic and extrinsic pathways in apoptotic signaling during UV-C-induced death of Jurkat cells: the role of caspase inhibition. Exp Cell Res 297:212–223
36. Milleron RS, Bratton SB (2006) Heat shock induces apoptosis independently of any known initiator caspase-activating complex. J Biol Chem 281:16991–17000
37. Gracie JA, Robertson SE, McInnes IB (2003) Interleukin-18. J Leukoc Biol 73:213–224
38. Miura M, Zhu H, Rotello R, Hartwieg EA, Yuan J (1993) Induction of apoptosis in fibroblasts by IL-1 beta-converting enzyme, a mammalian homolog of the C. elegans cell death gene ced-3. Cell 75:653–660
39. Friedlander RM (2003) Apoptosis and caspases in neurodegenerative diseases. N Engl J Med 348:1365–1375
40. Saleh M (2006) Caspase-1 builds a new barrier to infection. Cell 126:1028–1030
41. Guo H, Pétrin D, Zhang Y, Bergeron C, Goodyer CG, LeBlanc AC (2006) Caspase-1 activation of caspase-6 in human apoptotic neurons. Cell Death Differ 13:285–292
42. Gurcel L, Abrami L, Girardin S, Tschopp J, van der Goot FG (2006) Caspase-1 activation of lipid metabolic pathways in response to bacterial pore-forming toxins promotes cell survival. Cell 126:1135–1145
43. Virág L, Szabó C (2002) The therapeutic potential of poly(ADP-ribose) polymerase inhibitors. Pharmacol Rev 54:375–429
44. Oliver FJ, de la Rubia G, Rolli V, Ruiz-Ruiz MC, de Murcia G, Murcia JM (1998) Importance of poly(ADP-ribose) polymerase and its cleavage in apoptosis. Lesson from an uncleavable mutant. J Biol Chem 273:33533–33539
45. Nicholson DW, Thornberry NA (1997) Caspases: killer proteases. Trends Biochem Sci 22:299–306
46. Green DR, Kroemer G (2004) The pathophysiology of mitochondrial cell death. Science 305:626–629
47. Danial NK, Korsmeyer SJ (2004) Cell death: critical control points. Cell 116:205–219
48. Goldstein JC, Muñoz-Pinedo C, Ricci J-E et al (2005) Cytochrome *c* is released in a single step during apoptosis. Cell Death Differ 12:453–462
49. Green DR, Evan GI (2002) A matter of life and death. Cancer Cell 1:19–30
50. Platanias LC (2003) Map kinase signaling pathways and hematologic malignancies. Blood 101:4667–4679
51. Rovida E, Gozzini A, Barbetti V, Giuntoli S, Santini V, Dello Sbarba P (2006) The c-Jun-N-terminal-Kinase inhibitor SP600125 enhances the butyrate derivative D1-induced apoptosis via caspase 8 activation in Kasumi 1 t(8;21) acute myeloid leukaemia cells. Br J Haematol 135:653–659
52. Kuntzen C, Sonuc N, De Toni EN et al (2005) Inhibition of c-Jun-N-terminal-kinase sensitizes tumor cells to CD95-induced apoptosis and induces G2/M cell cycle arrest. Cancer Res 65:6780–6788
53. Xia HH, He H, De Wang J et al (2006) Induction of apoptosis and cell cycle arrest by a specific c-Jun NH2-terminal kinase (JNK) inhibitor, SP-600125, in gastrointestinal cancers. Cancer Lett 241:268–274
54. Zarubin T, Han J (2005) Activation and signaling of the p38 MAP kinase pathway. Cell Res 15:11–18
55. Galán A, García-Bermejo ML, Troyano A et al (2000) Stimulation of p38 mitogen-activated protein kinase is an early regulatory event for the cadmium-induced apoptosis in human promonocytic cells. J Biol Chem 275:11418–11424
56. Rockwell P, Martinez J, Papa L, Gomes E (2004) Redox regulates COX-2 upregulation and cell death in the neuronal response to cadmium. Cell Signal 16:343–353
57. Kummer JL, Rao PK, Heidenreich KA (1997) Apoptosis induced by withdrawal of trophic factors is mediated by p38 mitogen-activated protein kinase. J Biol Chem 272:20490–20494
58. Mackay K, Mochly-Rosen D (1999) An inhibitor of p38 mitogen-activated protein kinase protects neonatal cardiac myocytes from ischemia. J Biol Chem 274:6272–6279
59. Franklin CC, Srikanth S, Kraft AS (1998) Conditional expression of mitogen-activated protein kinase phosphatase-1, MKP-1, is cytoprotective against UV-induced apoptosis. Proc Natl Acad Sci USA 95:3014–3019
60. Callsen D, Brüne B (1999) Role of mitogen-activated protein kinases in S-nitrosoglutathione-induced macrophage apoptosis. Biochemistry 38:2279–2286
61. Juo P, Kuo CJ, Reynolds SE et al (1997) Fas activation of the p38 mitogen-activated protein kinase signalling pathway requires ICE/CED-3 family proteases. Mol Cell Biol 17:24–35
62. Nguyen TTT, Tran E, Nguyen TH, Do PT, Huynh TH, Huynh H (2004) The role of activated MEK-ERK pathway in quercetin-induced growth inhibition and apoptosis in A549 lung cancer cells. Carcinogenesis 25:647–659
63. Yeh PY, Chuang SE, Yeh KH, Song YC, Ea CK, Cheng AL (2002) Increase of the resistance of human cervical carcinoma cells to cisplatin by inhibition of the MEK to ERK signaling pathway partly via enhancement of anticancer drug-induced NF kappa B activation. Biochem Pharmacol 63:1423–1430
64. Tanel A, Averill-Bates DA (2007) P38 and ERK mitogen-activated protein kinases mediate acrolein-induced apoptosis in Chinese hamster ovary cells. Cell Signal 19:968–977

Available online at www.sciencedirect.com
ScienceDirect
Cancer Letters 269 (2008) 139–147
CANCER Letters
www.elsevier.com/locate/canlet

Induction of G_2-M phase arrest and apoptosis by α-methylene-γ-butyrolactones in human leukemia cells

Fernando Torres [a,b], José Quintana [a,b], Javier Cabrera [b], Juan F. Loro [b], Francisco León [b,c], Jaime Bermejo [c], Francisco Estévez [a,b,*]

[a] *Department of Biochemistry, University of Las Palmas de Gran Canaria, Plaza Dr. Pasteur s/n, 35016 Las Palmas de Gran Canaria, Spain*
[b] *Instituto Canario de Investigación del Cáncer, University of Las Palmas de Gran Canaria, Plaza Dr. Pasteur s/n, 35016 Las Palmas de Gran Canaria, Spain*
[c] *Instituto de Productos Naturales y Agrobiología, C.S.I.C., Instituto Universitario de Bio-Orgánica "Antonio González", Universidad de La Laguna, Av. Astrofísico F. Sánchez 3, 38206 La Laguna, Tenerife, Spain*

Received 30 January 2008; received in revised form 30 January 2008; accepted 22 April 2008

Abstract

In this study, we investigated the effect of three synthetic α-methylene-γ-butyrolactones (MBL) on viability of 10 human tumor cell lines and found that these lactones were highly cytotoxic against leukemia cells. Studies performed on HL-60 cells indicate that MBL induce G_2-M arrest and apoptosis through a caspase-dependent mechanism. Apoptosis was associated to cytochrome *c* release, cleavage of procaspases-9 and -3, and hydrolysis of PARP. Intracellular reactive oxygen species (ROS) seem to play a key role since high levels of ROS were produced early (<15 min) and apoptosis was completely abrogated by the free radical scavenger *N*-acetyl-L-cysteine (NAC).
© 2008 Elsevier Ireland Ltd. All rights reserved.

Keywords: α-Methylene-γ-butyrolactones; Apoptosis; Caspases; DNA fragmentation; PARP cleavage; Reactive oxygen species

1. Introduction

Many anticancer compounds have been shown to cause the death of sensitive cells through the induction of apoptosis. Essential executioners of apoptosis are the caspases, a family of conserved cysteine aspartate-specific proteases [1], generally synthesized as zymogens which are activated via proteolytic cleavage. In general, two major pathways for apoptosis have been described [2]. In the extrinsic (or death receptor) pathway, apoptosis is mediated by death receptors (such as Fas or tumor necrosis factor receptors) [3] and involves caspase-8 activation, while in the intrinsic (or mitochondrial) pathway diverse proapoptotic signals stimulate the translocation of cytochrome *c* from mitochondria to cytoplasm that promotes caspase-9 activation. Since caspase-3 is responsible for cleaving specific cellular proteins during apoptosis [4] both pathways converge to this level and therefore caspases-8 and -9 cleave and activate

* Corresponding author. Address: Department of Biochemistry, University of Las Palmas de Gran Canaria, Plaza Dr. Pasteur s/n, 35016 Las Palmas de Gran Canaria, Spain. Tel.: +34 928 451443; fax: +34 928 451441.
E-mail address: festevez@dbbf.ulpgc.es (F. Estévez).

0304-3835/$ - see front matter © 2008 Elsevier Ireland Ltd. All rights reserved.
doi:10.1016/j.canlet.2008.04.028

the proenzyme. A great number of studies indicate that apoptosis can be mediated by the endoplasmic reticulum signaling pathway [5] and it may also occur independently of caspase activation [6].

α-Methylene-γ-butyrolactones (MBL) have attracted much attention during the last decade because they display a wide range of biological activities, including antitumor properties. Many natural products are known to contain an α-methylene-γ-butyrolactone moiety, mainly sesquiterpene lactones. The structural requirement for the biological activities of these compounds is associated with the exocyclic, conjugated double bond (the O=C—C=CH_2 moiety), which acts as alkylating agent in a Michael-type reaction with nucleophiles. Thus, MBL are believed to exert their numerous biological activities through inhibition of enzymes and other functional proteins by forming covalent bonds with free cysteine residues in these macromolecules or by conjugation with glutathione [7].

In a previous report, we described a synthetic compound containing an α-methylene-γ-butyrolactone group that showed strong cytotoxic properties against human myeloid tumor cells (HL-60) but not against human normal peripheral mononuclear cells [8]. Since the substituent at γ-position (C-5) of the lactones may play an important role in the biological properties [9] we decided to synthesize new derivatives, to explore the impact on cytotoxicity against several human cancer cell lines and to investigate the mechanism of cell death triggered by these compounds. In this regard, compounds which possess a phenyl substituent at the γ-position of the α-methylene-γ-butyrolactone moiety were found to have both the strongest and broadest antiproliferative activity against a variety of cancer cell lines [10]. In this study, we demonstrate that MBL induce cytotoxicity in human leukemia cell lines which involves apoptosis induction and a fast production of ROS.

2. Materials and methods

2.1. Reagents

MBL-1 and MBL-2 are described for the first time and were synthesized following established protocols [8], while MBL-3 was obtained as previously described [8]. Their chemical structures were determined spectroscopically (proton nuclear magnetic resonance and ^{13}C nuclear magnetic resonance and mass spectrometry).

MBL-1: ^1H NMR (δ, $CDCl_3$): 1.30 (3H, d, $J = 6.7$ Hz, CH_3-7), 2.86 (1H, m, CH-4), 3.85 (3H, s, OCH_3), 3.87 (6H, s, 2× OCH_3), 4.52 (1H, m, CH-5), 5.57 (1H, d, $J = 2.3$ Hz, CH_a-6), 6.11 (1H, d, $J = 15.5$ Hz, CH-1′), 6.28 (1H, d, $J = 2.3$ Hz, CH_b-6), 6.62 (2H, s, CH-2″ and C-6″), 6.64 (1H, d $J = 15.5$ Hz, CH-2′); ^{13}CNMR (δ, $CDCl_3$): 15.7 (C-7), 41.4 (C-4), 56.1 (O*C*H3), 60.9 (2× O*C*H3), 85.2 (C-5), 104.0 (C-2″ and C-6″), 121.0 (C-6), 124.9 (C-1′), 131.2 (C-1″), 134.1 (C-2′), 138.6 (C-4″), 140.2 (C-3), 153.4 (C-3″ and C-5″), 169.9 (C-2); EIMS (70 eV) *m/z* (I. rel.): 304 $[M]^+$ (100), 245 (5), 221 (5), 205 (15), 181 (20), 168 (7), 82 (29); HREIMS 304.1302 ($C_{17}H_{20}O_5$, calc. 304.1310).

MBL-2: ^1H NMR (δ, $CDCl_3$): 1.29 (3H, d, $J = 6.6$ Hz, CH_3-7), 2.88 (1H, m, CH-4), 3.80 (3H, s, OCH_3), 3.83 (6H, s, 2× OCH_3), 4.79 (1H, d, $J = 7.7$ Hz, CH-5), 5.55 (1H, d, $J = 2.3$ Hz, CH_a-6), 6.25 (1H, d, $J = 2.3$ Hz, CH_b-6), 6.51 (2H, s, CH-2′ and C-6′); ^{13}CNMR (δ, $CDCl_3$): 15.9 (C-7), 43.4 (C-4), 56.2 (2× O*C*H3), 60.8 (O*C*H_3), 86.0 (C-5), 103.0 (C-2′ and C-6′), 121.0 (C-6), 133.9 (C-1′), 140.2 (C-4′), 153.4 (C-3′ and C-5′), 169.9 (C-2); EIMS (70 eV) *m/z* (I. rel.): 278 $[M]^+$ (100), 257 (23), 161 (5), 82 (99), 54 (72); HREIMS 278.1149 ($C_{15}H_{18}O_5$, calc. 278.1154). Antibodies for poly(ADP-ribose) polymerase (PARP), caspases-3 and -9 were purchased from Stressgen (Victoria, British Columbia, Canada). Antibody for cytochrome *c* was purchased from BD PharMingen (San Diego, CA, USA). Secondary antibodies were from Amersham Biosciences (Freiburg, Germany). All other chemicals were obtained from Sigma (Saint Louis, MO, USA).

2.2. Cell culture

The human breast cancer cell line MCF-7 and human adenocarcinoma A549 were cultured in Dulbecco's modified Eagle's medium containing 10% (v/v) heat-inactivated fetal bovine serum, 2 mM L-glutamine, 100 U/ml penicillin, 100 μg/ml streptomycin. The human leukaemia HL-60 and U937 cells, human cervix carcinoma HeLa and human osteosarcoma HOS cells were grown as previously described [11,12]. Human leukaemia Jurkat, K-562 and THP-1 cells were cultured in RPMI 1640 containing 2 mM L-glutamine supplemented with 10% (v/v) heat-inactivated fetal bovine serum. Human SK-MEL-1 melanoma cells were grown as previously described [13]. Human peripheral blood mononuclear cells (PBMC) were isolated from heparin-anticoagulated blood of healthy volunteers by centrifugation with Ficoll-Paque Plus (GE Healthcare Bio-Sciences AB, Uppsala, Sweden) as described [11].

2.3. Cytotoxicity of MBL on human tumor cells and human normal peripheral blood mononuclear cells

The cytotoxicity of MBL on human tumor and human PBMC cells was analyzed as previously described [11]. Concentrations inducing a 50% inhibition of cell growth (IC_{50}) were determined graphically using the curve fitting

algorithm of the computer software Prism™ 2.0 (GraphPad). Values are means ± SE from at least three-independent experiments, each performed in triplicate.

2.4. Evaluation of apoptosis

Fluorescent microscopy, flow cytometric analysis of propidium iodide-stained nuclei and DNA fragmentation assay were performed as described [12]. Apoptosis was also determined by translocation of phosphatidylserine to the cell surface using an Annexin V-FITC apoptosis detection kit (BD Pharmingen) according to the manufacturer's protocol.

2.5. Western blot analysis

Immunoblot analysis of caspase-9, caspase-3 and PARP was performed as previously described [12]. Release of cytochrome *c* from mitochondria was detected as described [11].

2.6. Intracellular reactive oxygen species (ROS) determination

Intracellular ROS were detected by flow cytometry using 2′,7′-dichlorodihydrofluorescein diacetate (H_2-DCF-DA). This compound is deacetylated by intracellular esterase and converted to non fluorescent 2′,7′-dichlorodihydrofluorescein (H_2-DCF), which is rapidly oxidized to the highly fluorescent compound 2′,7′-dichlorofluorescein (DCF) in the presence of ROS (especially hydrogen peroxide and lipid hydroperoxides). HL-60 cells were treated with or without MBL for 15–120 min, and then H_2-DCF-DA (8 μM) was added and incubated for 30 min. The cells were then washed and resuspended in 1 ml PBS. Flow cytometric analysis was carried out within 1 h using a Coulter EPICS™ cytometer (Beckman–Coulter). In each study, 10,000 cells were counted. Fluorescence of DCF was detected at an excitation and emission wavelengths of 488 and 530 nm, respectively.

2.7. Statistical analysis

Statistical significance of differences between means of control and treated samples were calculated using Student's *t*-test. *P* values of <0.05 were considered significant.

3. Results

3.1. MBL inhibit cell viability of human tumor cell lines and lack of cytotoxicity on normal human lymphocytes

In the present study, we examined the effects of the MBL derivatives (Fig. 1) on the growth of 10 human tumor cell lines and found that they display strong cytotoxic properties (Table 1). Human myeloid cell lines

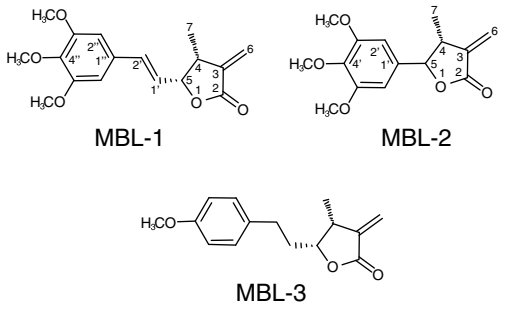

Fig. 1. Chemical structures of synthetic MBL.

(HL-60, U937, K-562 and THP-1), including the lymphoid Jurkat cell line were, in general, the most sensitive to MBL-induced cytotoxicity while HeLa and MCF-7 cells were highly resistant. Control experiments with normal lymphocytes show no appreciable toxicity at 10 μM MBL. As a positive control, Jurkat cells were also included in the experiment and, as expected, there was an important reduction in the proliferation of these cells (Fig. 2A). Since HL-60 cell line was especially sensitive to the antiproliferative effect of MBL, further studies were performed on this cell line.

3.2. MBL induce G_2-M arrest and apoptosis on human myeloid leukemia cells

In order to determine the mechanism involved in MBL-induced cytotoxicity, nuclear morphology was evaluated by fluorescent microscopy (Fig. 2B). The results on HL-60 cells clearly demonstrate an increase of condensed and fragmented chromatin (i.e. apoptotic bodies), which is typical of apoptotic cells. A significant number of apoptotic cells was already detected at 6 h of treatment and increased in a time-dependent manner (Fig. 2C). Maximal levels of apoptotic cells were observed at 24 h in response to MBL-1 (55.1 ± 10%) and MBL-3 (69 ± 8%) which represent 14- and 17-fold increase with respect to control (4 ± 1%), respectively. However, the time-frame for MBL-2 is different since the percentage of apoptotic cells peaked at 12 h (38 ± 7%) and decreased at 24 h (15 ± 4%). As expected, DNA fragmentation which is considered a hallmark of apoptosis markedly increased in MBL-treated cells, particularly in response to MBL-1 and MBL-3 (Fig. 2D). MBL-1 treatment also led to the exposure of phosphatidylserine on the outside of the plasma membrane as detected by Annexin V-FITC staining (Fig. 2E). Similar results were obtained with MBL-2 and MBL-3 (results not shown). To determine whether MBL-induced cytotoxicity involves alterations in cell cycle progression, flow cytometric analyses were included in this study. As shown (Table 2, Fig. 2F) MBL caused a significant G_2-M arrest following 12 h of treatment. Cell cycle phase distribution was especially sensitive to MBL-

Table 1
Effects of α-methylene-γ-butyrolactones on the growth of human tumor cell lines

Compound	IC_{50} (μM)									
	HL-60	K-562	THP-1	U-937	Jurkat	HOS	HeLa	MCF-7	SK-MEL-1	A-549
MBL-1	0.8 ± 0.1	6.5 ± 2.1	7.2 ± 0.7	2.6 ± 0.8	4.0 ± 1.0	24.2 ± 11	69.5 ± 6.4	>100	6.4 ± 1.3	17.1 ± 4.3
MBL-2	1.0 ± 0.4	10.2 ± 0.7	6.6 ± 1.6	9.0 ± 0.2	4.9 ± 0.7	19.2 ± 7.6	60.0 ± 14.1	>100	11.8 ± 3.0	19.0 ± 3.0
MBL-3	4.0 ± 1.1	2.1 ± 1.2	1.6 ± 0.3	1.0 ± 0.2	1.1 ± 0.1	9.5 ± 3.0	20.0 ± 4.2	85.4 ± 12.7	27.4 ± 12.7	15.3 ± 6.4

Cells were cultured for 72 h and the IC_{50} values were calculated as described in Section 2. The data shown represent the means ± SE of three- to five-independent experiments with three determinations in each.

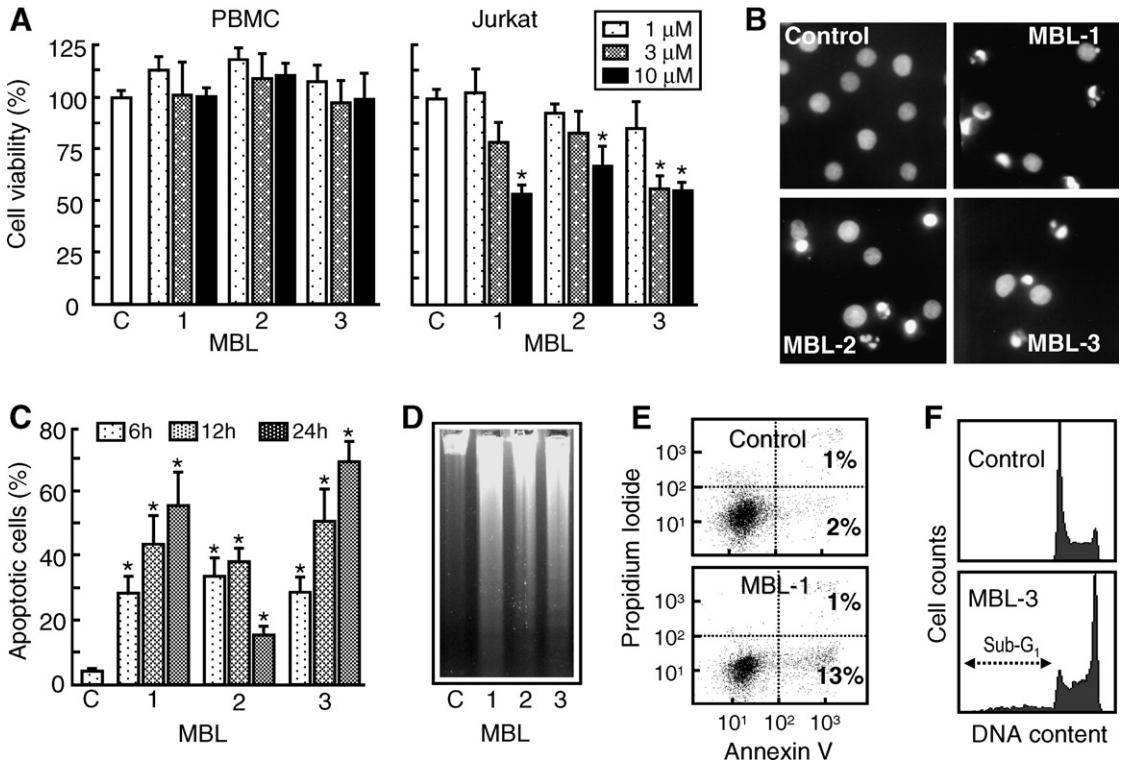

Fig. 2. Effects of MBL on human leukemia cells. (A) Differential effect of MBL on proliferation of normal peripheral blood mononuclear cells (PBMC) vs Jurkat cells. Proliferation of PBMC and Jurkat cells cultured in presence of the indicated concentrations of each MBL for 24 h. Values represent means ± SE of three-independent experiments each performed in triplicate. $^{*}P < 0.05$, significantly different from the untreated control. (B) Photomicrographs of representative fields of cells stained with Hoechst 33258 to evaluate nuclear chromatin condensation (i.e. apoptosis) after treatment with MBL. (C) HL-60 cells were treated with 10 μM of indicated MBL and apoptosis was evaluated by fluorescence microscopy. Values represent means ± SE of three-independent experiments each performed in triplicate. $^{*}P < 0.05$, significantly different from untreated control. (D) HL-60 cells were incubated as in (C) and genomic DNA was extracted, separated on an agarose gel and visualized under UV light by ethidium bromide staining. (E) FACS analysis of Annexin V-FITC and propidium iodide (PI)-stained HL-60 cells after 24 h of treatment with 5 μM MBL-1. Cells appearing in the lower right quadrant show positive Annexin V-FITC staining, which indicates phosphatidylserine translocation to the cell surface, and negative PI staining, which demonstrates intact cell membranes, both features of early apoptosis. Cells in the top right quadrant are double positive for Annexin V-FITC and PI and are undergoing necrosis. Data are representative of three separate experiments. (F) HL-60 cells were incubated as above and subjected to flow cytometric analysis. Hypodiploid cells (apoptotic cells) are shown in region marked with an arrow.

3 since this lactone induced the highest ratio in G_2-M arrest (34.8% vs 18.4% in control cells) and also stimulated accumulation of the cells in the S phase (33.1% vs 25.6% in control cells). When the subdiploid (sub-G_1) portions of the histograms were excluded from the analyses, the relative increases in the G_2-M phase of the cell cycle in MBL-1 and MBL-2-treated HL-60 cells were 30% and 40%, respectively, when compared to the untreated

Table 2
Effects of α-methylene-γ-butyrolactones on cell cycle phase distribution of HL-60 cells

	%SubG$_1$	%G$_1$	%S	%G$_2$-M
Control	3.3 ± 1.2	53.4 ± 0.9	25.6 ± 0.1	18.4 ± 0.4
MBL-1	12.8 ± 1.9	50.8 ± 3.0	14.9 ± 0.8	21.3 ± 0.4*
MBL-2	11.1 ± 0.1	49.5 ± 0.8	16.0 ± 0.2	23.2 ± 0.8*
MBL-3	14.9 ± 1.4	15.3 ± 0.1	33.1 ± 2.4	34.8 ± 0.7*

Cells were cultured with the indicated concentration for 12 h and the cell cycle phase distribution was determined by flow cytometry. The values are means ± SE of two-independent experiments with two determinations in each. *$P < 0.05$, significantly different from untreated control.

control. In accordance with the above results, the percentage of hypodiploid cells (i.e. sub-G$_1$ fraction) increased about fourfold in MBL-treated cells compared with control (Fig. 2C). In order to identify the primary targets and early mechanism of action of MBL on HL-60 cells we used doses 2- to 10-fold higher than the antiproliferative IC$_{50}$ values, which were determined at 72 h of treatment, while the flow cytometry and DNA laddering experiments were analyzed after a shorter incubation time. However, concentrations close to the IC$_{50}$ values of MBL were sufficient to trigger apoptosis and there was no evidence of gross cytolysis or other changes indicative of necrosis for up to at least 20 μM of each MBL (results not shown).

3.3. Effects of MBL on mitochondrial cytochrome c release, procaspases-9 and -3 cleavage and PARP processing

To determine whether MBL-triggered apoptosis requires the activation of caspases, HL-60 cells were pre-treated with the broad-spectrum caspase inhibitor benzyloxycarbonyl-Val-Ala-Asp(OMe) fluoromethyl ketone (z-VAD-fmk). Apoptosis was completely suppressed in the presence of the inhibitor (Fig. 3A), which suggests that MBL induce cytotoxicity by a caspase-dependent mechanism. Moreover, immunoblotting studies suggest that apoptosis induction occurs via the intrinsic pathway since MBL-induced cytochrome *c* release from mitochondria and stimulated the cleavage of inactive pro-caspase-9 to the active 35–37 kDa fragments (Fig. 3B), but did not significantly promote procaspase-8 hydrolysis (results not shown). As caspase-3 is the main effector caspase that is involved in apoptosis we also analyzed whether these lactones induce hydrolysis of the zymogen by immunoblotting. Cleavage of pro-caspase-3 into 17–19 kDa fragments significantly increased in MBL-treated cells (Fig. 3B) and in accordance with this result, poly(ADP-ribose) polymerase protein (PARP) which is normally involved in DNA repair and a known substrate for caspase-3, was effectively hydrolyzed to the 85 kDa fragment.

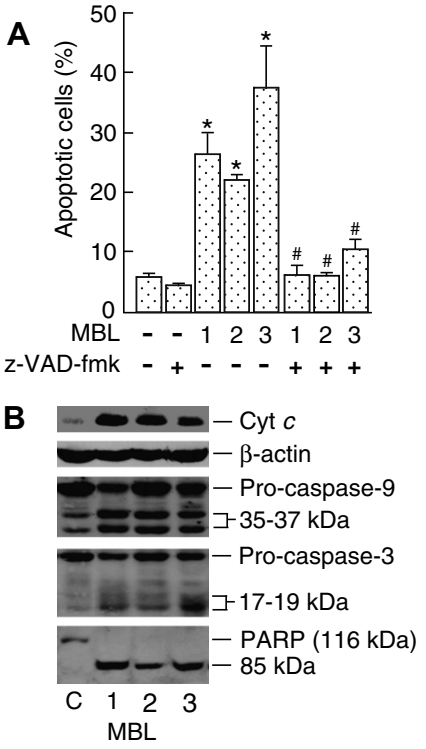

Fig. 3. Involvement of caspases in the induction of apoptosis triggered by MBL on human leukaemia cells. (A) Cells were pre-treated with z-VAD-fmk (100 μM) before the addition of the indicated MBL (10 μM) and apoptotic cells were analyzed by flow cytometry. Bars represent means ± SE of two-independent experiments each performed in duplicate. *$P < 0.05$, significantly different from untreated control. #$P < 0.05$, significantly different from the corresponding MBL treatment alone. (B) The cells were incubated in the presence of MBL and cell lysates (or cytosolic extracts in the case of cytochrome *c*) were assayed by immunoblotting for cytochrome *c* release, the cleavage of procaspases-9 and -3, and PARP. β-Actin was used as a loading control.

3.4. MBL increase intracellular ROS levels

Generation of intracellular reactive oxygen species (ROS) is considered one of the key mediators of apoptotic signaling for the most antitumoral agents. Therefore, the redox status of HL-60 cells treated with MBL-1 was monitored by the oxidation-sensitive fluorescent dye 2′,7′-dichlorodihydrofluorescein diacetate (H$_2$-DCF-DA). An increase in DCF fluorescence was detected in MBL-1-treated cells, in dose- (Fig. 4A) and time-dependent manner (Fig. 4B). Similar results were obtained with MBL-2 and MBL-3 (results not shown). A fast generation of ROS was detected at 15 min after treatment although the highest levels (>3-fold increase compared with control) were not reached until 2 h (Fig. 4B). For comparison, exposure to H$_2$O$_2$ (100 μM) was associated with a marked increase in ROS levels at 5 min that decreased at 1 h (results not

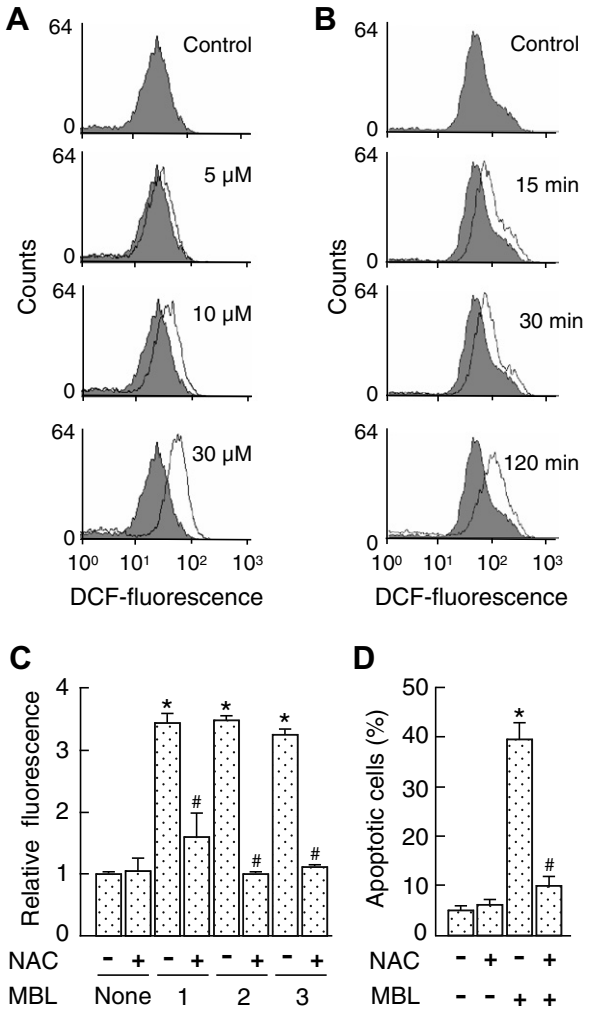

Fig. 4. MBL-induced ROS generation and apoptosis is blocked by NAC. HL-60 cells were incubated for 2 h in the presence of the indicated concentrations of MBL-1 (A) or with 10 μM of MBL-1 for the indicated time points (B) and the fluorescence of oxidized H_2DCF was determined by flow cytometry. Similar results were obtained from three-independent experiments. (C) Cells were pre-treated with NAC (10 mM) for 1 h and then incubated with the indicated MBL for 1 h and intracellular ROS levels were determined as above. Values represent means ± SE of two-independent experiments each performed in triplicate. $^{*}P < 0.05$, significantly different from untreated control. $^{\#}P < 0.05$, significantly different from the corresponding MBL treatment alone. (D) Cells were pre-treated with NAC and then exposed to MBL-1 for 24 h. DNA content was analyzed by flow cytometry, and the results shown as the percentage of the cells with sub-G_1 DNA (mean ± SE) of three different experiments. $^{*}P < 0.05$, significantly different from untreated control. $^{\#}P < 0.05$, significantly different from MBL treatment alone.

shown). We next investigated whether oxidative stress is essential for MBL-mediated apoptosis. To explore this possibility cells were pre-treated with NAC (a precursor of reduced glutathione and a free radical scavenger). As shown, NAC completely inhibited the generation of ROS (Fig. 4C) and apoptosis (Fig. 4D). These findings suggest that ROS generation is crucial for MBL-induced cell death.

4. Discussion

While there are effective treatments for acute lymphocytic leukemia and for chronic myelogenous leukemia, more effective treatments for other forms of acute leukemia are needed. It is widely believed that α-methylene-γ-butyrolactones exert their biological effect by acting as alkylating agents. These lactones can form covalent adducts *in vivo* with proteins and other nucleophilic biomolecules, via a Michael-type addition of a free sulfhydryl or amine group [7].

In this study, we have synthesized three compounds containing an α-methylene-γ-butyrolactone group linked to an aromatic ring and evaluated their potential cytotoxic properties using a wide number of tumor cell lines. Interestingly, we found that MBL display cytotoxic properties in a cell-type specific manner. Human leukaemia cells (HL-60, U937, K-562, THP-1 and Jurkat) were highly sensitive to MBL cytotoxicity while, at the other extreme, MCF-7 cells were almost completely resistant. Dose–response studies revealed that PBMC were resistant to MBL.

In general, MBL-1 and MBL-2 displayed similar potency which suggests that the length of the chain that links the aromatic ring and the α-methylene-γ-butyrolactone functional group did not significantly affect cytotoxicity. MBL-1 and MBL-2 showed a small but significant difference in U937 cells, with IC_{50} values of 2.6 and 9.0 μM, respectively. The IC_{50} values were usually higher than 10 μM to non-leukaemic cell lines, although human melanoma SK-MEL-1 cells were especially sensitive to MBL-1 ($IC_{50} \sim 6$ μM). This result is extremely interesting taking into account that melanoma is the most aggressive form of skin cancer and frequently resists chemotherapy. Further studies are needed to determine the mechanisms involved in SK-MEL-1 cell death. All human leukaemia cells (evaluated in this study) were especially sensitive to the cytotoxic effects of MBL-3.

Cell cycle analysis revealed that inhibition of cell viability by MBL was caused by a significant cell cycle arrest at the G_2-M phase, accompanied by an increase in sub-G_1 fraction, indicating apoptotic

cell death. Interestingly, MBL-3 also induced accumulation of cells in the S phase, which suggests that this lactone binds to other biological targets than those used by MBL-1 and MBL-2. Similar results were recently reported by the sesquiterpene lactone 1,6-*O,O*-diacetylbritannilactone in HL-60 cells [14].

Although MBL-3 displays the most dramatic effects on cell cycle progression and apoptosis in HL-60 cells, both MBL-1 and MBL-2 show higher cytotoxic properties only in this leukaemic cell line, as evaluated by the MTT reduction assay. As demonstrated, neither MBL-induced necrotic cell death at doses used in this study. This indicates that in addition to cell cycle arrest and apoptosis other mechanisms that induce cell growth inhibition may be triggered by these lactones on HL-60 cells. In this regard, it is interesting to note that TTFA (2-thenoyltrifluoroacetone), a conventional complex II inhibitor, prolonged the duration of each phase of the cell cycle which was caused by ROS overproduction [15]. However, other mechanisms such as autophagic cell death (i.e. cell death with autophagy) [16] can not be ruled out and needs to be evaluated in the future.

Previous studies have shown apoptosis is induced by compounds containing an α-methylene-γ-butyrolactone group, such as sesquiterpene lactones. Thus, Dirsch et al. [17] have documented that helenalin, a sesquiterpene lactone of the pseudoguaianolide type, induces apoptosis in the human leukemia Jurkat cells, and we have recently assessed the ability of sesquiterpene lactones containing a germacranolide skeleton to induce cell death in the hematopoietic cell lines HL-60 and U937 [18]. However, the compounds included in the present study are simple and more easily available by organic synthesis than the sesquiterpene lactones which also will allow us to add new substituents in order to improve the cytotoxicity.

Our results also indicate that MBL's antiproliferative effect involves a caspase-dependent apoptosis induction. These compounds induce cytochrome *c* release and activation of caspases-9 and -3, emphasizing that the intrinsic pathway plays an important role in the cell death. However, the mechanism of cytotoxicity displayed by MBL is clearly different to previously described sesquiterpene lactones. For example, arucanolide induces apoptosis in HL-60 cells by a caspase-independent mechanism since caspase inhibitors were unable to reverse the cell death, caspase-9 is not activated and cytochrome *c* release is not detected [19]. In contrast, isocostunolide, a sesquiterpene lactone isolated from *Inula helenium*, triggers apoptosis via the cooperative effects of both the extrinsic and the intrinsic pathway [20].

The reactive oxygen species (ROS) have been implicated as second messengers in multiple signaling pathways [21]. The antiproliferative effect of synthetic α-methylene-γ-butyrolactones included in this study is associated with an increase in the intracellular level of ROS which was detectable at 15 min of treatment and remained elevated for at least 120 min. Moreover, ROS seem to play a critical role since pre-incubation with NAC suppressed the increase of ROS and apoptosis on HL-60 cells. This result also suggests that MBL change the redox status of cells via binding to thiol containing molecules that are involved in the maintenance of redox balance, such as glutathione. However, further studies will be needed to evaluate this possibility.

Our results are consistent which those derived from studies with the sesquiterpene lactone parthenolide, one of the most important components in Feverfew (*Tanacetum parthenium*), which displays anticancer properties and induces apoptosis both *in vitro* [22–26] and on animal models [27,28]. Interestingly, parthenolide-induced apoptosis in multiple myeloma cells and in acute myelogenous leukaemia cells is dependent on ROS generation and was completely inhibited by NAC, indicating the crucial role of oxidative stress in the mechanism [29,30]. However, the generation of ROS is not a general feature of compounds containing the α-methylene-γ-butyrolactone functional group. In this regard, isocostunolide induces apoptosis in human melanoma cells by a ROS-independent mechanism [20].

Recent studies suggest that mitogen-activated protein kinases (MAPKs) such as c-Jun N-terminal kinases/stress activated protein kinases (JNK/SAPK 1/2) and $p38^{MAPK}$ play a key role in triggering apoptosis in response to various cellular stressors including oxidative stress [31]. Further studies are, therefore, necessary to determinate whether the MAPKs play a similar role in MBL-induced apoptosis on leukaemia cells. Interestingly, the sesquiterpene lactone 1,6-*O,O*-diacetylbritannilactone (OODBL) induces apoptosis, ROS generation and also JNK/SAPK 1/2- and $p38^{MAPK}$ -activation on HL-60 cells [14]. However, in this report the authors did not determine whether ROS and/or the MAPKs pathway are involved in OODBL-induced cell death.

In conclusion, the α-methylene-γ-butyrolactones evaluated in the present study are strongly cytotoxic

against human leukemia cell lines, involving cell cycle perturbation and caspase-dependent apoptosis by a ROS-mediated mechanism. The chemical synthesis of this kind of compounds might allow the discovery of new and highly specific antitumor agents against leukemia cells.

Conflict of interest statement

None declared.

Acknowledgments

This work was supported by Grants from the Ministerio de Educación y Ciencia of Spain and FEDER (SAF2004-07928 and SAF2007-62536 to F.E.) and from the Dirección General de Universidades e Investigación of the Canary Islands Government (PI042005/172 to J.Q.). We thank J. Estévez (Hospital Universitario Insular de Gran Canaria) for his collaboration in the Western blot assays. F.T. was supported by a research studentship from the Dirección General de Universidades e Investigación of the Canary Islands Government.

References

[1] N.A. Thornberry, Y. Lazebnik, Caspases: enemies within, Science 281 (1998) 1312–1316.
[2] K.M. Boatright, G.S. Salvesen, Mechanisms of caspase activation, Curr. Opin. Cell Biol. 15 (2003) 725–731.
[3] S. Nagata, Apoptosis by death factor, Cell 88 (1997) 355–365.
[4] G.M. Cohen, Caspases: the executioners of apoptosis, Biochem. J. 326 (1997) 1–16.
[5] D.G. Breckenridge, M. Germain, J.P. Mathai, M. Nguyen, G.C. Shore, Regulation of apoptosis by endoplasmic reticulum pathways, Oncogene 22 (2003) 8608–8618.
[6] J.E. Chipuk, D.R. Green, Do inducers of apoptosis trigger caspase-independent cell death?, Nat Rev. Mol. Cell Biol. 6 (2005) 268–275.
[7] J. Heilmann, M.R. Wasescha, T.J. Schmidt, The influence of glutathione and cysteine levels on the cytotoxicity of helenanolide type sesquiterpene lactones against KB cells, Bioorg. Med. Chem. 9 (2001) 2189–2194.
[8] A.G. González, M. Hernández Silva, J.I. Padrón, F. León, E. Reyes, M. Álvarez-Mon, J.P. Pivel, J. Quintana, F. Estévez, J. Bermejo, Synthesis and antiproliferative activity of a new compound containing an α-methylene-γ-lactone group, J. Med. Chem. 45 (2002) 2358–2361.
[9] C.C. Tzeng, K.H. Lee, T.C. Wang, C.H. Han, Y.L. Chen, Synthesis and cytotoxic evaluation of a series of γ-substituted γ-aryloxymethyl-α-methylene-γ-butyrolactones against cancer cells, Pharm. Res. 17 (2000) 715–719.
[10] P.G. Baraldi, M.C. Nunez, M.A. Tabrizi, E. De Clercq, J. Balzarini, J. Bermejo, F. Estévez, R. Romagnoli, Design, synthesis, and biological evaluation of hybrid molecules containing α-methylene-γ-butyrolactones and polypyrrole minor groove binders, J. Med. Chem. 47 (2004) 2877–2886.
[11] S. Rubio, J. Quintana, J.L. Eiroa, J. Triana, F. Estévez, Acetyl derivative of quercetin 3-methyl ether-induced cell death in human leukemia cells is amplified by the inhibition of ERK, Carcinogenesis 28 (2007) 2105–2113.
[12] S. Rubio, J. Quintana, M. López, J.L. Eiroa, J. Triana, F. Estévez, Phenylbenzopyrones structure-activity studies identify betuletol derivatives as potential antitumoral agents, Eur. J. Pharmacol. 548 (2006) 9–20.
[13] F. León, J. Quintana, A. Rivera, F. Torres, S. Rubio, J. Quintana, F. Estévez, J. Bermejo, Isolation, structure elucidation, total synthesis, and evaluation of new natural and synthetic ceramides on human SK-MEL-1 melanoma cells, J. Med. Chem. 49 (2006) 5830–5839.
[14] M.-H. Pan, Y.S. Chiou, A.C. Cheng, N. Bai, C.Y. Lo, D. Tan, C.T. Ho, Involvement of MAPK, Bcl-2 family, cytochrome *c*, and caspases in induction of apoptosis by 1,6-*O,O*-diacetilbritannilactone in human leukemia cells, Mol. Nutr. Food Res. 51 (2007) 229–238.
[15] H.-O. Byun, H.Y. Kim, J.J. Lim, Y.-H. Seo, G. Yoon, Mitochondrial dysfunction by complex II inhibition delays overall cell cycle progression via reactive oxygen species production, J. Cell. Biochem. (2008), doi:10.1002/jcb.21741.
[16] M. Enomoto, A. Tsuchida, K. Miyazawa, T. Yokoyama, H. Kawakita, H. Tokita, M. Naito, M. Ito, K. Ohyashiki, T. Aoki, Vitamin K2-induced cell growth inhibition via autophagy formation in cholangiocellular carcinoma cell lines, Int. J. Mol. Med. 20 (2007) 801–808.
[17] V.M. Dirsch, H. Stuppner, A.M. Vollmar, Cytotoxic sesquiterpene lactones mediate their death-inducing effect in leukemia T cells by triggering apoptosis, Planta Med. 67 (2001) 557–559.
[18] A. Rivero, J. Quintana, J.L. Eiroa, M. López, J. Triana, J. Bermejo, F. Estévez, Potent induction of apoptosis by germacranolide sesquiterpene lactones on human myeloid leukemia cells, Eur. J. Pharmacol. 482 (2003) 77–84.
[19] Y. Nakagawa, M. Inuma, N. Matsuura, K. Yi, M. Naoi, T. Nakayama, Y. Nozawa, Y. Akao, A potent apoptosis-inducing activity of a sesquiterpene lactone, arucanolide, in HL-60 cells:a crucial role of apoptosis-inducing factor, J. Pharmacol. Sci. 97 (2005) 242–252.
[20] C.N. Chen, H.H. Huang, C.L. Wu, C.P.C. Lin, J.T.A. Hsu, H.P. Hsieh, S.E. Chuang, G.M. Lai, Isocostunolide, a sesquiterpene lactone, induces mitochondrial membrane depolarization and caspase-dependent apoptosis in human melanoma cells, Cancer Lett. 246 (2007) 237–252.
[21] K. Apel, H. Hirt, Reactive oxygen species: metabolism, oxidative stress, and signal transduction, Annu. Rev. Plant Biol. 55 (2004) 373–399.
[22] S. Zhang, Y.K. Won, C.N. Ong, H.M. Shen, Anti-cancer potential of sesquiterpene lactones: bioactivity and molecular mechanisms, Curr. Med. Chem. Anticancer Agents 5 (2005) 239–249.
[23] S. Zhang, C.N. Ong, H.M. Shen, Critical roles of intracellular thiols and calcium in parthenolide-induced apoptosis in human colorectal cancer cells, Cancer Lett. 208 (2004) 143–153.
[24] M.T. Yip-Schneider, H. Nakshatri, C.J. Sweeney, M.S. Marshall, E.A. Wiebke, C.M. Schmidt, Parthenolide and sulindac cooperate to mediate growth suppression and

inhibit the nuclear factor-κB pathway in pancreatic carcinoma cells, Mol. Cancer Ther. 4 (2005) 587–594.
[25] M.C. Ralstin, E.A. Gage, M.T. Yip-Schneider, P.J. Klein, E.A. Wiebke, C.M. Schmidt, Parthenolide cooperates with NS398 to inhibit growth of human hepatocellular carcinoma cells through effects on apoptosis and G_0–G_1 cell cycle arrest, Mol. Cancer Res. 4 (2006) 387–399.
[26] J.H. Kim, L. Liu, S.O. Lee, Y.T. Kim, K.R. You, D.G. Kim, Susceptibility of cholangiocarcinoma cells to parthenolide-induced apoptosis, Cancer Res. 65 (2005) 6312–6320.
[27] Y.K. Won, C.N. Ong, X. Shi, H.M. Shen, Chemopreventive activity of parthenolide against UVB-induced skin cancer and its mechanisms, Carcinogenesis 25 (2004) 1449–1458.
[28] C.J. Sweeney, S. Mehrotra, M.R. Sadaria, S. Kumar, N.H. Shortle, Y. Roman, C. Sheridan, R.A. Campbell, D.J. Murry, S. Badve, H. Nakshatri, The sesquiterpene lactone parthenolide in combination with docetaxel reduces metastasis and improves survival in a xenograft model of breast cancer, Mol. Cancer Ther. 4 (2005) 1004–1112.
[29] W. Wang, M. Adachi, R. Kawamura, H. Sakamoto, T. Hayashi, T. Ishida, K. Imai, Y. Shinomura, Parthenolide-induced apoptosis in multiple myeloma cells involves reactive oxygen species generation and cell sensitivity depends on catalase activity, Apoptosis 11 (2006) 2225–2235.
[30] M.L. Guzman, R.M. Rossi, L. Karnischky, X. Li, D.R. Peterson, D.S. Howard, C.T. Jordan, The sesquiterpene lactone parthenolide induces apoptosis of human acute myelogenous leukaemia stem and progenitor cells, Blood 105 (2005) 4163–4169.
[31] K. Tobiume, A. Matsuzawa, T. Takahashi, H. Nishitoh, K. Morita, K. Takeda, O. Minowa, K. Miyazono, T. Noda, H. Ichijo, ASK1 is required for sustained activations of JNK/p38 MAP kinases and apoptosis, EMBO Rep. 2 (2001) 222–228.

Sesquiterpene Lactones from *Gonospermum gomerae* and *G. fruticosum* and Their Cytotoxic Activities

Jorge Triana,[†] José Luis Eiroa,[†] Juan José Ortega,[†] Francisco León,[‡] Ignacio Brouard,[⊥] Fernando Torres,[§,‡] José Quintana,[§,‡] Francisco Estévez,[§,‡] and Jaime Bermejo*[,⊥]

Departamento de Química, Universidad de Las Palmas de Gran Canaria, Campus de Tafira, 35017 Las Palmas de Gran Canaria, Canary Islands, Spain, Instituto de Productos Naturales y Agrobiología-CSIC-Instituto Universitario de Bio-Orgánica "Antonio González", Universidad de La Laguna, Avenida Astrofísico F. Sánchez 3, 38206 La Laguna, Tenerife, Spain, Departamento de Bioquímica, Centro de Ciencias de la Salud, Universidad de las Palmas de Gran Canaria, 35016, Las Palmas de Gran Canaria, Spain, and Instituto Canario de Investigación del Cáncer (ICIC), Hospital Universitario de La Candelaria, Carretera del Rosario 45, 38010, Tenerife, Spain

Received July 31, 2008

Four new sesquiterpene lactones (**1**−**4**) and a new sesquiterpene (**5**) together with 20 known compounds were isolated from two *Gonospermum* species (*G. gomerae* Bolle and *G. fruticosum* Less). Their structures were determined by analysis of spectroscopic data, including 1D and 2D NMR. The cytotoxicity of several new and known natural and semisynthetic sesquiterpene lactones was also assessed against human myeloid leukemia cell lines (HL-60 and U937), human melanoma cells (SK-MEL-1), and human adenocarcinoma (A549).

The genus *Gonospermum*, which belongs to the subtribe Gonosperminae (Anthemideae, family Asteraceae) and is endemic to the Canary Islands, contains four species distributed throughout the most westerly islands. This genus has been the subject of previous chemical research in which the presence of sesquiterpenes and sesquiterpene lactones was described.[1−3]

The present work describes the isolation and structural elucidation of four new sesquiterpene lactones, two from *G. gomerae* (**1** and **2**) and the other ones from *G. fruticosum* (**3** and **4**), as well as a new sesquiterpene (**5**) along with 20 known compounds (**6**−**25**). The structures of the known compounds were confirmed by comparison of their spectroscopic properties with data published in the literature.

Compounds containinig the α-methylene-γ-lactone functional group, such as sesquiterpene lactones, have attracted much attention during the last 50 years because they display a wide range of biological activities, including antitumor properties.[4] For this reason, the sesquiterpene lactones **1a**, **6a**, **7a**, and **7b** were assessed for cytotoxicity against several human tumor cell lines and for apoptosis induction in human myeloid leukemia cells.

Results and Discussion

Purification of an ethanolic extract of aerial parts of *G. gomerae* gave two new sesquiterpene lactones with a germacrane skeleton (**1** and **2**), as well as 18 known compounds, dentatin A (**6**),[5] 1β,4α,6α-trihydroxyeudesm-11-en-8α,12-olide (**7**),[6] 1α-hydroxy-deacetyltulirinol-4α,5β-epoxide (**8**),[7] tatridin A (**9**),[8] tatridin B (**10**),[8] tamirin (**11**),[9] β-cyclopyrethrosin (**12**),[10] desacetyl-β-cyclopyrethrosin (**13**),[11] desacetyl-β-cyclopyrethrosin 6-*O*-angelate (**14**),[7] spiciformin (**15**),[12] 5β-hydroxycostic acid (**16**),[13] crocinervolide (**17**),[14] stigmasterol (**18**),[15] scoparone (**19**),[16] scopoletin (**20**),[2] sesamin (**21**),[17] axillarin (**22**),[18] and 5,7,4′-trihydroxy-3,6-dimethoxyflavone (**23**).[19]

An ethanolic extract of *G. fruticosum* yielded two new sesquiterpene lactones (**3** and **4**), one new sesquiterpene (**5**), and the known compounds **8**−**11**, **13**, **17**, **19**, **20**, **23**, desacetyl-β-cyclopyrethrosin 6-*O*-angelate acetate (**24**),[20] and 6-hydroxy-6-methylocta-3,7-dien-2-one (**25**)[21] (see Supporting Information for structures of known compounds).

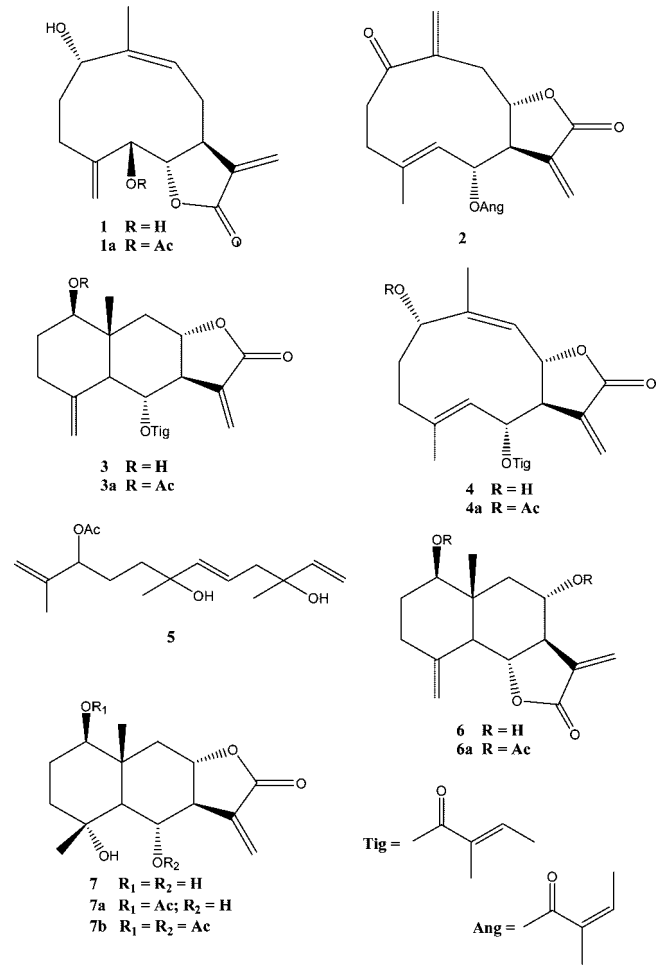

Compound **1** was acetylated for the purpose of purification, affording the acetyl derivative **1a** as colorless oil. Its IR spectrum showed the presence of γ-lactone (1770 cm^{-1}), carbonyl ester (1742 cm^{-1}), and double-bond (1648 and 967 cm^{-1}) absorptions. Its

* To whom correspondence should be addressed. Tel: (34)-922-318583. Fax: (34)-922-318571. E-mail: jbermejo@ull.es.
[†] Departamento de Química, Universidad de Las Palmas de Gran Canaria.
[⊥] Instituto de Productos Naturales y Agrobiología-CSIC.
[§] Departamento de Bioquímica, Universidad de las Palmas de Gran Canaria.
[‡] Instituto Canario de Investigación del Cáncer.

10.1021/np800474v CCC: $40.75 © 2008 American Chemical Society and American Society of Pharmacognosy
Published on Web 11/21/2008

Table 1. ^{1}H NMR Data of Compounds **1a**, **2**, **3**, **4a**, and **5** (300 MHz in $CDCl_3$)[a]

H	1a	2	3	4a	5
1	5.86 dd (4.0, 11.6)		3.59 dd (4.6, 11.3)	5.48 dd (4.2, 10.0)	5.05 d (10.7); 5.20 *d* (17.2)
2α	1.70 m	3.26 m	1.91 m		5.93 dd (10.7, 17.0)
2*β*	2.23 m		1.60 m		
3α	2.59 m	2.30−2.60 m	2.07 m		
3*β*	1.67 m		2.31 m		
4					2.28 ddd (5.5, 13.3, 19)
5	4.85 d (9.3)	4.99 d (5.9)	2.24 d (10.5)	4.90 d (11.3)	5.61 m
6	5.07 dd (9.3, 10.5)	5.21 dd (10.0, 10.0)	5.58 dd (10.5, 10.5)	5.48 dd (9.7, 10.5)	5.59 s
7	2.92 d (10.6)	2.99 m	2.79 m	2.78 m	
8	5.34 d (10.7)	4.05 m	4.08 ddd (3.5, 10.5, 10.5)	4.80 t (9.2)	1.49 m
9α	5.28 d (11.4)	3.44 d (11.0)	2.58 dd (3.5,12.0)	5.39 d (9.7)	1.65 m
9*β*		2.16 m	1.60 m		
10					5.14 t (6.6)
12a					4.88 s
12b					4.93 s
13a	5.72 s	5.80 d (2.4)	5.39 d (3.0)	5.71 d (3.3)	1.70 s
13b	6.37 s	6.34 d (2.7)	6.11 d (3.0)	6.24 d (2.9)	
14a	1.76 s	5.81 s	0.87 s	1.82 s	1.27 s
14b		5.85 d (2.4)			
15a	5.61 d (1.8)	1.79 s	4.63 d (4.5)	1.95 s	1.27 s
15b	5.63 d (1.8)		4.86 d (4.5)		
OAc	2.00 s			2.01 s	2.05
	2.03 s				
	2.08 s				
OAng		6.13 m			
		1.98 d (7.1)			
		1.91 s			
OTigl			6.84 m	6.97 m	
			1.81 s	1.83 s	
			1.88 s	1.88 s	

[a] Spectra were run at room temperature, and TMS was used as internal standard. Chemical shifts are recorded in ppm to TMS. Coupling constants (*J*) are given in parentheses.

molecular formula was established as $C_{21}H_{26}O_8$ from the EIMS at *m/z* 364.15 $[M - C_2H_2O]^+$ and the ^{1}H, ^{13}C, and DEPT NMR data. The ^{1}H NMR spectrum of **1a** (Table 1) exhibited three acetyl methyl singlets (δ_H 2.00, 2.03, and 2.08), a vinyl methyl singlet (δ_H 1.76), and signals consistent with two exocyclic double bonds [δ_H 5.61 (1H, d, J = 1.8 Hz, H-15a), 5.63 (1H, d, J = 1.8 Hz, H-15b), 5.72 (1H, s, H-13a), and 6.37 (1H, s, H-13b)]. The ^{13}C NMR and DEPT data indicated the presence of one carbonyl group corresponding to a γ-lactone, three ester carbonyl groups, six olefinic carbons, and five methine carbons. The relationships between the proton signals in **1a** were established from its ^{1}H−^{1}H COSY spectrum, which disclosed the following connectivities: H-1/H-2, H-5/H-6, H-6/H-7, H-7/H-8, and H-8/H-9. The above data, together with the HMBC experiment, placed the acetate groups at C-1, C-5, and C-8 and the lactone group at C-6. The relative configuration of **1a** was confirmed by a ROESY experiment (see Supporting Information) in which correlations observed between H-1 and H-8 and between H-6 and H-8 clearly showed that these protons were on the same face. Correlations were also observed between H-5 and H-7 and between Me-14 and H-9. Thus, the structure and relative configuration of **1** was proposed as 1α,5*β*,8α-trihydroxygermacra-4(15),9(*Z*),11(13)-trien-6α,12-olide.

Compound **2** showed IR absorption bands due to the carbonyl of a γ-lactone (1769 cm^{-1}) and olefinic bonds (1660 and 961 cm^{-1}). The EIMS did not show the molecular ion, but a fragment was observed at *m/z* 244 $[M - HOAng]^+$, corresponding to the molecular formula $C_{20}H_{24}O_5$. The ^{1}H NMR spectrum of compound **2** (Table 1) exhibited six olefinic proton signals at δ_H 4.99 (1H, d, J = 5.9 Hz, H-5), 5.80 (1H, d, J = 2.4 Hz, H-13a), 5.81 (1H, brs, H-14a), 5.85 (1H, d, J = 2.4 Hz, H-14b), 6.13 (1H, m, H-Ang), and 6.34 (1H, d, J = 2.7 Hz, H-13b). These assignments were similar to those of the known germacranolide tamirin,[9] while the low-field resonance of the C-6 proton (δ_H 5.21) located the angeloxy group at this carbon. Thus, **2** was deduced to be tamirin 6-*O*-angelate.

The IR spectrum of compound **3** showed absorption bands due to an OH group (3458 cm^{-1}) and two carbonyl bands from a γ-lactone (1770 cm^{-1}) and from an ester (1715 cm^{-1}). The EIMS showed a molecular ion peak at *m/z* 346 in agreement with the empirical formula $C_{20}H_{26}O_5$. The ^{1}H NMR spectrum of **3** (Table 1) exhibited five olefinic proton signals at δ_H 4.63 (1H, d, J = 4.5 Hz, H-15a), 4.86 (1H, d, J = 4.5 Hz, H-15b), 5.39 (1H, d, J = 3.0 Hz, H-13a), 6.11 (1H, d, J = 3.8 Hz, H-13b), and 6.84 (1H, m, tiglate). These assignments were similar to those of deacetyl-*β*-cyclopyrethrosin[11] with the exception of the signal of H-6 at δ_H 5.58 (1H, dd, J = 10.5, 10.5 Hz, H-6), which allowed assignment of the tigloyloxy group to C-6. Treatment of **3** with Ac_2O and pyridine afforded the acetyl derivative **3a**. Its NMR spectrum showed two doublets at δ_H 6.12 (J = 2.7 Hz) and 5.38 (J = 2.7 Hz) (methylene lactone), a multiplet at δ_H 6.84 and two singlets at δ_H 1.88 and 1.81 characteristic of a tiglate group, two protons geminal to tiglate, and acetate groups were assigned to the signals at δ_H 5.60 (m) and 4.83 (dd, J = 4.6 and 4.7 Hz), respectively. In addition, a singlet at δ_H 2.06 confirmed the presence of the acetyl methyl group. An exocyclic methylene group was indicated by doublets at δ_H 4.88 (J = 5.0 Hz) and 4.65 (J = 5.9 Hz) and assigned to C-15. Thus, **3** was deduced to be 6α-tigloyloxy-1*β*-hydroxy-4(15),11-eudesmadien-8α,12-olide.

Compound **4** was purified by acetylation, affording compound **4a**. Its IR and ^{1}H NMR spectra were quite similar to those of tatridin A,[8] indicating the presence of α-methylene-γ-lactone (1754 cm^{-1}), ester (1735 cm^{-1}), and olefinic groups (1139, 999, and 960 cm^{-1}). Prominent fragments at *m/z* 328 $[M - CH_3COOH]^+$ and 228 $[M - CH_3COOH - C_5H_8O_2]^+$ in the MS, in addition to a molecular ion at *m/z* 388, were consistent with the molecular formula $C_{22}H_{28}O_6$ and indicated that **4a** was a sesquiterpene lactone bearing an acetate and a tiglate group. The NMR spectrum of **4a** (Table 1) exhibited four olefinic proton signals at δ_H 4.90 (d, J = 11.3 Hz, H-5), 5.39 (d, J = 9.7 Hz, H-9), 5.71 (d, J = 3.3 Hz, H-13a), and 6.24 (d, J = 2.9 Hz, H-13b). Four vinylic methyl singlets (δ_H 1.82, 1.83, 1.88, and 1.95) and an acetyl methyl singlet (δ_H 2.01) were also observed. These assignments were similar to those of tatridin A acetate angelate[22] with the exception of H-3′ (m, δ_H 6.97) and Me-4′ (s,

Table 2. Effects of Lactones Isolated from *Gonospermum* on the Growth of Human Tumor Cell Lines[a]

	IC_{50} (μM)			
lactone	HL-60	U937	SK-MEL-1	A549
1a	16.0 ± 3.6	10.0 ± 0.3	19.5 ± 3.7	56.6 ± 15.1
6a	9.4 ± 0.7	9.2 ± 1.1	14.3 ± 3.2	72.4 ± 13.7
7a	>100	>100	>100	>100
7b	13.3 ± 2.5	10.4 ± 1.0	27.9 ± 4.1	>100
etoposide	0.25 ± 0.04	0.92 ± 0.24	>30	5.9 ± 1.7

[a] Cells were cultured for 72 h, and the IC_{50} values were calculated as described in the Experimental Section. The data shown represent the mean ± SEM of three independent experiments with three determinations in each.

δ_H 1.83). Thus, **4** was deduced to be 6α-tigloyloxy-1α-hydroxygermacra-4*E*,9*Z*,11-trien-8α,12-olide.

Compound **5** was assigned the molecular formula $C_{17}H_{26}O_3$ on the basis of the mass fragment $[M - H_2O]^+$ at *m*/*z* 278 in the EIMS. The IR spectrum showed OH (3429 cm^{-1}), acetoxy group (1738 cm^{-1}), and double-bond (1651 cm^{-1}) absorptions. The ^1H NMR spectrum (Table 1) showed seven olefinic protons [δ_H 4.88 (1H, s, H-12a), 4.93 (1H, s, H-12b), 5.05 (1H, d, J = 10.7 Hz, H-1a), 5.20 (1H, d, J = 17.2 Hz, H-1b), 5.59 (1H, m, H-6), 5.61 (1H, m, H-5), and 5.93 (1H, dd, J = 17.0 and 10.7 Hz, H-2)], an oxygenated methine [δ_H 5.14 (1H, t, J = 6.6 Hz, H-10)], and four methyl signals [δ_H 1.27 (6H, s, CH_3-14 and CH_3-15), 1.70 (3H, s, CH_3-13), and 2.05 (3H, s, OAc)]. Considering the above data, **5** was an acyclic geranylgeraniol-derived sesquiterpene with a structure similar to that of crocinervolide.[23] These observations together with the $^1H-^1H$ COSY and HMBC correlations established the structure of **5**, which was characterized as 10-acetoxy-3,7,11-trimethyldodeca-1,5,11-triene-3,7-diol.

It is widely believed that sesquiterpene lactones exert their biological effect by acting as alkylating agents. These compounds can form adducts *in vivo* with proteins and other nucleophilic biomolecules, via a Michael-type addition of a free sulfhydryl or amine group. Sesquiterpene lactones can overcome the cells' protection by high intracellular glutathione concentrations to alkylate protein molecules, leading to their numerous biological effects. Although under intracellular conditions (i.e., at neutral pH and high glutathione concentration) sesquiterpene lactones are largely transformed into the glutathione adducts, their inhibitory activity can be explained by instability of the thioether groups at physiological pH. Previous studies have demonstrated how sesquiterpene lactones are able to exert their biological activity in spite of the presence of glutathione, and this can be explained by the reversibility of glutathione addition.[24]

We also were interested in determining whether these compounds display cytotoxic properties in a cell-type specific manner. For this reason, we examined the effects of several sesquiterpene lactones on the growth of four human tumor cell lines: human leukemia cells (HL-60 and U-937), A549 lung cancer cells, and human melanoma SK-MEL-1 cells. We used the leukemia cells because they are prone to apoptosis (especially HL-60). The cell line SK-MEL-1 was used since melanoma is the most aggressive form of skin cancer and frequently resists chemotherapy, and the A549 lung cancer cells were selected since they are apoptotic-reluctant. Initial studies showed that compounds **1a**, **6a**, and **7b** were relatively cytotoxic agents against human myeloid leukemia HL-60 and U937 cells. Interestingly, compounds **1a** and **6a** were equally potent against human SK-MEL-1 melanoma cells. In the present report we describe the effect of these compounds on the growth of human myeloid (HL-60 and U937) and melanoma (SK-MEL-1) cell lines (Table 2). Growth inhibition of human tumor cells in culture was determined by the 3-(4,5-dimethylthiazol-2-yl)-2,5-diphenyl-2*H*-tetrazolium bromide (MTT) dye-reduction assay. Etoposide was used as a positive control. Antiproliferative studies on compounds **1a** and **6a** indicated that they were cytotoxic against human myeloid (HL-60 and U937) and melanoma (SK-MEL-1) cell lines, with an IC_{50} about 10 μM. However, **7b** was less potent than **1a** and **6a** only against SK-MEL-1 cells. Human adenocarcinoma A549 cells were resistant to all lactones tested.

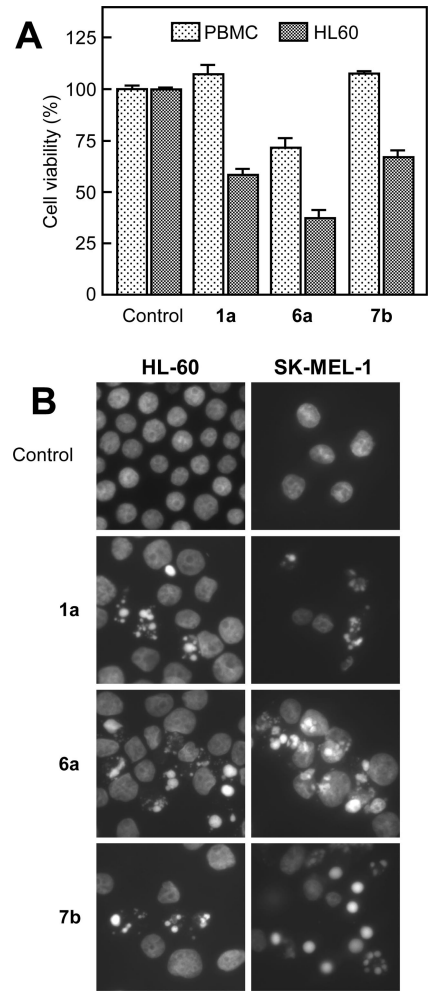

Figure 1. (A) Differential effect of compounds **1a**, **6a**, and **7b** on proliferation of normal peripheral blood mononuclear cells (PBMC) versus HL-60 cells. Proliferation of PBMC and HL-60 cells cultured in the presence of 30 μM of each compound for 24 h. Values represent means ± SE of three independent experiments, each performed in triplicate. (B) Photomicrographs of representative fields of HL-60 and SK-MEL-1 cells stained with bisbenzimide trihydrochloride to evaluate nuclear chromatin condensation (i.e., apoptosis) after treatment with compounds **1a**, **6a**, and **7b**.

Control experiments with normal lymphocytes showed no appreciable toxicity of compounds **1a** and **7b** and only weak toxicity with **6a** at 30 μM. As a positive control, HL-60 cells were also included in the experiment, and as expected, there was an important reduction in the proliferation of these cells (Figure 1A).

Inspection of Table 2 revealed that the growth of leukemia cells was, in general, highly susceptible to the cytotoxicity induced by sesquiterpene lactones. Therefore, further studies were performed on HL-60 cells. Only those compounds with low IC_{50} (≤15 μM)

Table 3. Effects of Sesquiterpene Lactones Isolated from *Gonospermum* on Cell Cycle Distribution of HL-60 Cells[a]

	% sub G_0/G_1	% G_0/G_1	%S	%G_2-M
control	2.9 ± 0.3	47.9 ± 0.6	21.4 ± 1.1	27.8 ± 0.8
1a	12.2 ± 2.8	35.6 ± 5.8	20.0 ± 1.0	29.6 ± 1.5
6a	30.0 ± 3.5	26.8 ± 6.7	22.0 ± 0.4	18.5 ± 2.6
7b	11.8 ± 1.9	39.3 ± 3.6	21.5 ± 0.7	21.8 ± 2.7
etoposide	47.7 ± 2.5	29.4 ± 1.5	17.1 ± 2.1	2.6 ± 0.9

[a] The cells were cultured with 30 μM of the indicated compounds for 48 h, and the cell cycle distribution was determined by flow cytometry. The results are expressed as mean ± SEM of two different experiments with two determinations in each.

were selected to explore the mechanism through which these selected sesquiterpenes lactones decrease cell viability.

We first analyzed whether cell growth inhibition induced by these compounds was mediated via alteration in cell cycle progression. Consistent with growth inhibitory effects, the cytometric flow studies (Table 3) revealed that compounds **6a** and **7b** induce significant S arrest at the expense of G1 phase cell population following treatment (over 24−48 h) with concentrations of 30 μM. Concentrations of 30 μM were used to demonstrate that the effects on cell cycle progression were dose dependent. Concentrations higher than the antiproliferative IC_{50} were used to identify the primary targets and early mechanism of action of sesquiterpene lactones. The IC_{50} values were determined at 72 h of treatment, and the flow cytometry experiments were analyzed after a short incubation time. However, the sesquiterpene lactone **1a** induced G_2-M arrest at the expense of G_1 phase cell number.

Taken together, the results indicated that compound **1a** versus **6a** and **7b** displayed antiproliferative activities through different mechanisms that involve cell cycle alteration. Selective modulation of different cell cycle-regulatory proteins could explain the differences among them, although other possibilities cannot be ruled out.

Although we did not identify the targets of these compounds, we showed that compounds **6a** and **7b** induce significant S arrest and that **1a** induced G2-M arrest. These results show that **6a** and **7b** have different targets than **1a**. The progression through the cell cycle is due to the timely regulated activation of serine/threonine cyclin-dependent kinases, the CDKs, a family of protein kinases that are in turn controlled by a complex array of proteins including the cyclins. These compounds could affect different sets of CDKs or CDK inhibitors. Further studies are needed to determine the effect of these compounds on specific regulators of each phase (S or G2-M) of the cell cycle.

To elucidate the possible mechanism(s) of action-mediated cell growth inhibition, we tested the effects of **1a**, **6a**, and **7b** to induce apoptosis using HL-60 cells. As shown in Figure 1B, compounds **1a**, **6a**, and **7b** induced morphological changes characteristic of apoptotic cells (fragmented and condensed chromatin), as visualized by fluorescence microscopy. In the left panel, the control HL-60 cells appeared normal, with the nuclei round and homogeneous, while cells exposed to compounds **1a**, **6a**, and **7b** displayed condensation of chromatin and the appearance of apoptotic bodies by fluorescence microscopy after DNA staining with Hoechst 33258. Similar results were obtained on SK-MEL-1 cells.

A biochemical hallmark of apoptosis is the fragmentation of genomic DNA into integer multiples of 180-bp units, resulting in a characteristic ladder on agarose gel electrophoresis. Therefore, we also examined whether these compounds induced chromosomal DNA fragmentation, which is considered the end point of the apoptotic pathway. The results demonstrated that exposure to 30 μM **1a**, **6a**, and **7b** resulted in endonucleolytic DNA cleavage, which then leads to DNA ladder formation in HL-60 cells (Figure 2A). Using QFM (quantitative fluorescence microscopy) the least potent compound was **7b**, while compound **6a** was the most potent (Figure 2B) at the times and concentrations assayed.

To confirm that the selected sesquiterpene lactones decrease HL-60 cell viability through apoptosis activation, quantification of the

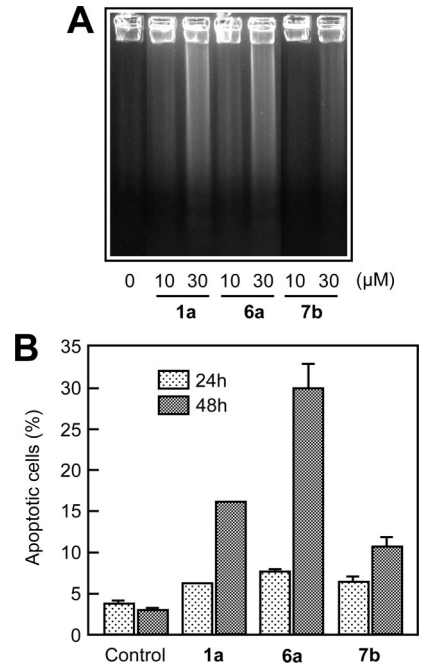

Figure 2. Induction of apoptosis in HL-60 cells by sesquiterpene lactones. (A) HL-60 cells were treated with the indicated compounds (30 μM) for 24 h, and total cellular DNA was isolated and stained with ethidium bromide after electrophoresis on a 2% agarose gel. Internucleosomal DNA fragmentation was visualized under UV light. (B) Cells were incubated with the indicated compounds (for 16 h), and the percentages of apoptotic cells were determined by flow cytometry. The results of a representative experiment are shown, and each point represents the average ± SE of triplicate determinations.

number of hypodiploid cells (i.e., apoptotic cells) by flow cytometry was performed. The results indicated that the percentage of apoptotic cells increased from 4 ± 1% (control) to 16 ± 0.5% (4-fold increase), 30 ± 0.5% (~8-fold increase), and 12 ± 0.5% (~3-fold) after 48 h of treatment with 30 μM **1a**, **6a**, and **7b**, respectively (Figure 2B). The other sesquiterpene lactones described in this paper did not induce apoptosis at either concentration tested (up 30 μM).

Next, we examined whether compounds **1a**, **6a**, and **7b** induce pro-caspase-3, -6, and -7 cleavage. Caspases have been shown to be key mediators of cell death in biological and biochemical analyses. Downstream effector caspases include caspases-3, -6, and -7. Since the proteolytic processing of caspases is an important event in caspase-dependent apoptotic cell death, we evaluated the effect of selected sesquiterpene lactones on executioner caspases by Western blot using specific antibodies. Cleavage of procaspases-3, -6, and -7 by sesquiterpene lactones was determined by immunoblotting using a polyclonal anti-human caspase-3 antibody (Stressgen) that recognized the M_r 32 000 proenzyme (procaspase-3), a monoclonal anti-human caspase-7 antibody (BD Pharmingen), and an anti-caspase-6 monoclonal antibody (MBL). The results indicate that these compounds (at 30 μM) promote an important cleavage of procaspases-3, -6, and -7 (Figure 3). Caspase-3 is the most active effector caspase to be involved in apoptosis induced by cytotoxic agents.

Since poly(ADP-ribose)polymerase (PARP) is a typical substrate for caspases-3 and -7, we also examined whether these compounds induce poly(ADP-ribose) polymerase cleavage. Western blot analysis using a polyclonal antibody that recognizes the M_r 85 000 cleaved form of PARP showed the generation of the 85 kDa fragment in sesquiterpene lactones-treated cells after 16 h of treatment (Figure 5). Equal protein loading was controlled by staining membranes with Ponceau S. Control lane (C) refers to untreated cells.

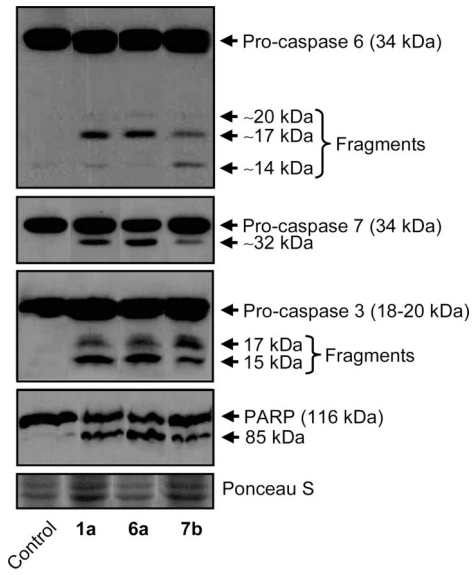

Figure 3. Cells were incubated with the indicated compounds, and cell lysates were assayed by immunoblotting for the cleavage of pro-caspases-6, -7, and -3 and PARP. One representative blot of three is shown. Equal protein loading was controlled by staining membranes with Ponceau S (a representative section of the stained membrane is shown).

In conclusion, this study demonstrates the cytotoxic activities of several sesquiterpene lactones against human myeloid leukemia HL-60 and U937 cells. Interestingly, compounds **1a** and **6a** were equally potent against human SK-MEL-1 melanoma cells. However, human lung carcinoma A549 cells were resistant to all lactones tested. Cell growth inhibition in HL-60 cells was associated with alterations in cell cycle progression and induction of apoptosis through a caspase-dependent mechanism.

Experimental Section

General Experimental Procedures. Optical rotations were recorded in a Perkin-Elmer model 343 polarimeter. IR spectra were recorded using a Bruker model IFS-55 spectrophotometer. ^{1}H and ^{13}C NMR spectra were obtained on a Bruker model AMX-300 spectrometer with standard pulse sequences operating at 300 MHz in ^{1}H and 75 MHz in ^{13}C NMR. $CDCl_3$ was used as solvent. EIMS were taken on a Micromass model Autospec (70 eV) spectrometer. Open column chromatography (1500 × 85 mm, fraction volumes 1 L) was performed using Si gel (particle size 0.2−0.5 mm, Merck Co.), and the low-pressure liquid chromatography was carried out using Ace Glass columns (300 × 21 and 250 × 8 mm, fraction volumes 50 and 25 mL, respectively) packed with Si gel (particle size 0.04−0.60 mm, Merck Co.) with a FMI QSY (Fluid Metering Inc.) pump. Preparative TLC used silica gel 60 $PF_{254+366}$ plates (20 × 20 cm, 1 mm thickness, Merck Co.).

Plant Material. The aerial parts of *Gonospermum gomerae* Bolle and *G fruticosum* Less were collected by Prof. José L. Eiroa in Barranco de Agulo and Alojera, respectively (La Gomera, Canary Islands), in April 1999. The plant material was identified by Dra. Rosa Febles, and a voucher specimen has been deposited at the Herbarium of the Viera y Clavijo Botanical Garden (Gran Canaria) (*G. gomerae* No. 19422 and *G. fruticosum* No. 19421).

Extraction and Isolation. The aerial parts of *G. gomerae* (2950 g) were exhaustively extracted with 95% EtOH in a Soxhlet apparatus for 72 h. The solvent was removed *in vacuo* to yield 410 g of a viscous mass, which was submitted to silica gel CC using *n*-hexane−EtOAc mixtures of increasing polarity (7:3; 3:2, and 1:1 v/v), affording three fractions (1−3). Fraction 1, eluted with *n*-hexane−EtOAc (4:1), gave two fractions (1A and 1B). Fraction 1A yielded **14** (25 mg), **10** (50 mg), **8** (35 mg), and **18** (30 mg) and a nonseparable mixture (125 mg), which was treated with pyridine (1 mL) and acetic anhydride (2 mL) at room temperature for 12 h. Purification of the acetylated mixture by preparative TLC afforded **6a** (15 mg), **7a** (12 mg), **7b** (17 mg), and **1a** (21 mg). Fraction 1B was chromatographed on silica gel (*n*-hexane−EtOAc, 4:1) to give **20** (25 mg), **19** (30 mg), and a residue that was purified after acetylation under the usual conditions, yielding **15a** (22 mg). Fraction 2 was eluted with *n*-hexane−EtOAc (4:1) to give subfractions 2A, 2B, and 2C. Fraction 2A eluted with benzene−EtOAc (4:1) yielded **12** (23 mg) and **22** (35 mg). Fraction 2B eluted with benzene−EtOAc (4:1) gave **2** (10 mg) and **21** (12 mg). Fraction 2C was purified using preparative TLC with *n*-hexane−EtOAc (7:3) to afford **16** (30 mg). Fraction 3, eluting with *n*-hexane−EtOAc (7:3), yielded **17** (45 mg) and **23** (29 mg) along with a mixture that was submitted to preparative TLC with *n*-hexane−EtOAc (4:1) to yield **13** (40 mg), **9** (15 mg), and **11** (28 mg). See Supporting Information for structures of compounds **6**−**25**.

Compound 1a: colorless oil; $[\alpha]^{25}_D$ +18.3 (*c* 0.06, $CHCl_3$); IR (KBr) ν_{max} 1770, 1742, 1648, 1276, 1242, 967 cm^{-1}; ^{1}H NMR, see Table 1; ^{13}C NMR (75 MHz, $CDCl_3$) δ 69.9 (C-1), 26.5 (C-2), 29.7 (C-3), 142.5 (C-4), 77.2 (C-5), 73.2 (C-6), 47.3 (C-7), 74.0 (C-8), 125.9 (C-9), 137.3 (C-10), 133.9 (C-11), 170.0 (C-12), 127.3 (C-13), 17.7 (C-14), 114.8 (C-15), 20.7, 20.9, 21.1 (3 × CH_3CO), 169.0, 169.1, 169.7 (3 × CH_3CO); EIMS *m/z* (%) 364 $[M - C_2H_2O]^+$ (7.4), 347 $[M - C_2H_3O_2]^+$ (100), 304 $[M - C_2H_3O_2 - C_2H_2O]^+$ (51); HRESIMS *m/z* 364.1513 $[M - C_2H_2O]^+$ (calcd for $C_{19}H_{24}O_7$, 364.1522).

Compound 2: colorless oil; $[\alpha]^{25}_D$ +10.2 (*c* 0.40, $CHCl_3$); IR (KBr) ν_{max} 1769, 1732, 1660, 1229, 961 cm^{-1}; ^{1}H NMR, see Table 1; ^{13}C NMR (75 MHz, $CDCl_3$) δ 203.0 (C-1), 31.9 (C-3), 139.6 (C-4), 135.4 (C-5), 71.6 (C-6), 76.6 (C-8), 40.2 (C-9), 147.0 (C-10), 139.1 (C-11), 169.2 (C-12), 126.0 (C-13), 126.0 (C-14), 17.3 (C-15), 169.2, 139.6, 127.0, 20.6, and 15.9 (Ang); EIMS *m/z* (%): 244 $[M - HOAng]^+$ (21.6); HRESIMS *m/z* 344.1624 $[M]^+$ (calcd for $C_{20}H_{24}O_5$, 344.1624).

The extraction of *G. fruticosum* (1295 g) gave 200 g of a viscous mass that afforded, by CC on silica gel using *n*-hexane−EtOAc in increasing polarity, five fractions. Fraction 1 eluted with *n*-hexane−EtOAc (9:1) to give **20** (52 mg), **19** (12 mg), and **25** (23 mg). Fraction 2, using *n*-hexane−EtOAc (7:3), gave **17** (26 mg) and **23** (19 mg). Fraction 3, using *n*-hexane−EtOAc (7:3), yielded **9** (24 mg) and **8** (16 mg). Fraction 4, using *n*-hexane−EtOAc (3:2), afforded **10** (21 mg), **13** (13 mg), and **11** (34 mg) and, by preparative TLC using *n*-hexane−EtOAc (3:2), **3** (5.3 mg). Finally, fraction 5 eluted with *n*-hexane−EtOAc (1:1) gave two subfractions. The less polar fraction was subjected to CC using *n*-hexane−EtOAc (2:3) to give **5** (40 mg). The other fraction was acetylated with pyridine (1 mL) and Ac_2O (2 mL) overnight to afford a mixture, which was separated on CC with *n*-hexane−EtOAc (9:1), giving **4a** (4 mg) and **24** (30 mg).

Compound 3: colorless oil, $[\alpha]_D$ +31.5 (*c* 0.13, $CHCl_3$); IR (KBr) ν_{max} 3458, 1770, 1715, 1645, 1265, 973 cm^{-1}; ^{1}H NMR, see Table 1; EIMS *m/z* (%) 346 $[M]^+$ (1.1).

Compound 3a: Compound **3** (4 mg) was acetylated with acetic anhydride (2 mL) and pyridine (2 mL) at room temperature overnight. Evaporation of the reagents under vacuum yielded the corresponding monoacetate **3a** (2.2 mg) as a colorless oil: IR (KBr) ν_{max} 1776, 1731, 1651, 1242, 977, 907, 814, 756, 667, 607 cm^{-1}; ^{1}H NMR (300 MHz, $CDCl_3$) δ 0.95 (3H, s, CH_3-14), 1.60 (1H, m, H-2β), 1.60 (1H, m, H-9β), 1.81 (3H, s, OTigl), 1.87 (1H, m, H-2α), 1.88 (3H, s, OTigl), 2.05 (1H, m, H-3α), 2.06 (3H, s OAc), 2.30 (1H, m, H-3β), 2.30 (1H, m, H-9α), 2.34 (1H, d J = 10.0 Hz, H-5), 2.78 (1H, m, H-7), 4.05 (1H, m, H-8), 4.65 (1H, d, J = 5.9 Hz, H-15a), 4.83 (1H, dd, J = 4.6, 11.5 Hz, H-1), 4.88 (1H, d, J = 5.0 Hz, H-15b), 5.38 (1H, d, J = 2.7 Hz, H-13a), 5.60 (1H, m, H-6), 6.12 (1H, d, J = 2.7 Hz, H-13b), 6.84 (1H, m, OTigl); EIMS *m/z* (%) 388 (0.7); HRESIMS *m/z* 288.1338 $[M - TigOH]^+$ (calcd for $C_{17}H_{20}O_4$, 288.1362).

Compound 4a: colorless oil, $[\alpha]^{25}$ −8.3 (*c* 0.15, $CHCl_3$); IR (KBr) ν_{max} 1754, 1735, 1241, 1139, 999, 960 cm^{-1}; ^{1}H NMR, see Table 1. ^{13}C NMR (75 MHz, $CDCl_3$) δ 68.0 (C-1), 24.5 (C-2), 34.8 (C-3), 138.0 (C-4), 132.0 (C-5), 72.7 (C-6), 49.2 (C-7), 74.2 (C-8), 128.0 (C-9), 137.0 (C-10), 138.0 (C-11), 169.5 (C-12), 122.5 (C-13), 17.3 (C-14), 15.3 (C-15), OAc: 168.0 and 20.9; OTigl: 162,0; 140.0; 128.2; 14.3 and 11.8; EIMS *m/z* (%) 388 $[M]^+$ (3.6); HRESIMS *m/z* 411.1787 $[M + Na]^+$ (calcd for $C_{22}H_{28}O_6Na$, 411.1784).

Compound 5: colorless oil, $[\alpha]^{25}_D$ +2.0 (*c* 0.30, $CHCl_3$); IR (KBr) ν_{max} 3429, 1738, 1651, 1242, 920 cm^{-1}; ^{1}H NMR see Table 1; ^{13}C NMR (75 MHz, $CDCl_3$) δ 18.00 (C-13), 21.20 (CH_3CO), 27.07 (C-4), 27.40 (C-14), 28.46 (C-15), 37.76 (C-5), 45.09 (C-9), 72.44 (C-6), 72.58 (C-10), 77.40 (C-3), 111.97 (C-12), 112.90 (C-1), 122.87 (C-8), 140.91 (C-7), 142.81 (C-2), 144.68 (C-11), 170.31 ($COCH_3$); EIMS *m/z* (%)

278 $[M - H_2O]^+$ (1.7); HRESIMS *m/z* 218.1671 $[M - C_2H_2O - 2\times H_2O]^+$ (calcd for $C_{15}H_{22}O$, 218.1671).

Cell Culture. Human HL-60 and U937 myeloid leukemia cells and human SK-MEL-1 melanoma cells were grown in RPMI 1640 (Sigma) supplemented with 10% (v/v) heat-inactivated fetal bovine serum (Sigma) and 100 units/mL penicillin and 100 μg/mL streptomycin at 37 °C in a humidified atmosphere containing 5% CO_2. The cell numbers were counted by a hematocytometer, and the viability was greater than 95% in all experiments as assayed by the 0.025% trypan blue exclusion method. Stock solutions of 100 mM sesquiterpene lactones were made in dimethyl sulfoxide (DMSO), and aliquots were frozen at −20 °C. Human peripheral blood mononuclear cells (PBMC) were isolated from heparin-anticoagulated blood of healthy volunteers by centrifugation with Ficoll-Paque Plus (GE Healthcare Bio-Sciences AB, Uppsala, Sweden).

Assay for Growth Inhibition and Cell Viability. Cytotoxicity was assessed using a 3-(4,5-dimethylthiazol-2-yl)-2,5-diphenyl-2*H*-tetrazolium bromide (MTT) assay. Briefly, 1×10^4 exponentially growing cells were seeded in 96-well microculture plates with various sesquiterpene lactone concentrations (0.3−100 μM) in a volume of 200 μL. DMSO concentration was the same in all the treatments and did not exceed 0.1% (v/v). After 72 h, surviving cells were detected on the basis of their ability to metabolize 3-(4,5-dimethylthiazol-2-yl)-2,5-diphenyl-2*H*-tetrazolium bromide (Sigma) into formazan crystals. Optical density was read with an ELISA reader at 570 nm and was used as a measure of cell viability. The MTT dye reduction assay measures mitochondrial respiratory function and can detect the onset of cell death earlier than dye-exclusion methods. Cell survival was calculated as the fraction of cells alive relative to control for each point: cell survival (%) = mean absorbance in treated cells/mean absorbance in control wells × 100. Concentrations inducing a 50% inhibition of cell growth (IC_{50}) were determined graphically using the curve-fitting algorithm of the computer software Prism 2.0 (GraphPad). Values are means ± SE from three independent experiments, each performed in triplicate.

Flow Cytometry Analysis for Cell Cycle Distribution. After 24−48 h of treatment, cells were harvested and quickly washed twice with ice-cold phosphate-buffered saline (PBS), and cell pellets were collected and resuspended in 50 μL of PBS. Following dropwise addition of 1 mL of ice-cold 75% ethanol, fixed cells were stored at −20 °C for 1 h. Samples were then centrifuged at 500*g* for 10 min at 4 °C and washed with PBS before resuspension in 1 mL containing 50 μg/mL propidium iodide and 100 μg/mL RNase A and incubation for 1 h at 37 °C in the dark. Cell cycle distribution was then analyzed by flow cytometry using a Coulter EPICS cytometer (Beckman Coulter). Histograms were analyzed with the Expo 32 ADC Software (Beckman Coulter). The quantitative data presented are mean ± SE of percentage of cells in different phases of cell cycle from triplicate samples in each treatment and were reproducible in two independent experiments.

Immunoblot Analysis of Procaspases-3, -6, and -7. HL-60 or U937 cells (1×10^6) were treated with sesquiterpene lactone derivatives at the indicated concentrations in RPMI 1640 medium. Cells were pelleted by centrifugation, washed with phosphate-buffered saline, lysed in lysis buffer containing 125 mM Tris-HCl pH 6.8, 2% sodium dodecyl sulfate, 5% glycerol, and 1% β-mercaptoethanol, and boiled for 5 min. The samples were separated on 12% sodium dodecyl sulfate-polyacrylamide gel and electrotransferred to a polyvinylidene fluoride membrane. The membrane was probed first with a polyclonal anti-procaspase-3 (Stressgen, 1:2000 dilution), anti-caspase-6 monoclonal antibody (MBL), anti-caspase-7 monoclonal antibody (BD Pharmingen), or procaspase-9 (Stressgen, 1:1,000) and then with anti-rabbit (pro-caspase-3) or anti-mouse (caspase-6, caspase-7, pro-caspase-9) antibody conjugated to horseradish peroxidase (HRP). Protein bands were detected by chemiluminescence (SuperSignal West Pico chemiluminescent substrate, Pierce) using the manufacturer's protocol.

Immunoblotting of Poly(ADP-ribose) Polymerase. Induction of apoptosis was also examined by proteolytic cleavage of poly(ADP-ribose) polymerase. Briefly, 1×10^6 exponentially growing HL-60 cells were treated with the selected sesquiterpene lactones at the indicated concentrations for 16 h at 37 °C. Cells were pelleted by centrifugation, washed twice with phosphate-buffered saline, resuspended in lysis buffer, and subjected to Western blot analysis. Proteins were separated on 7.5% sodium dodecyl sulfate-polyacrylamide minigels and electrotransferred to polyvinylidene difluoride membrane. The membrane was probed with polyclonal anti-poly(ADP-ribose) polymerase (Stressgen, 1:3000 dilution) and then with anti-rabbit antibody conjugated to horseradish peroxidase (HRP). Protein bands were detected by chemiluminescence (SuperSignal West Pico chemiluminescent substrate, Pierce) as described above.

Acknowledgment. This work was supported in part by grants from the Ministerio de Educación y Ciencia of Spain and Fondo Europeo de Desarrollo Regional (SAF2004-07928 and SAF2007-62536), from the Programa de Iniciativa Comunitaria INTERREG IIIB Azores-Madeira-Canarias (04/MAC/3.5/C5), and from the Instituto Canario de Investigación del Cáncer (G-05-09 to J.B. and F.L.). F.T. was supported by a research studentship from the Dirección General de Universidades e Investigación of the Canary Islands Government. We thank Mr. José Estévez (Hospital Universitario Insular de Gran Canaria) for his collaboration in the Western blot assays.

Supporting Information Available: ^1H and ^{13}C NMR, COSY, HMBC, and ROESY spectra of compounds **1**−**5**. Structures of known compounds **6**−**25**. This material is available free of charge via the Internet at http://pubs.acs.org.

References and Notes

(1) González, A.; Bermejo, J.; Triana, J.; López, M.; Eiroa, J. L. *Phytochemistry* **1992**, *31*, 1816–1817.
(2) Triana, J.; López, M.; Eiroa, J. L.; González, A.; Bermejo, J. *Biochem. Syst. Ecol.* **2000**, *28*, 95–96.
(3) Triana, J.; López, M.; Rico, M.; González, J.; Quintana, J.; Estévez, F.; León, F.; Bermejo, J. *J. Nat. Prod.* **2003**, *66*, 943–948.
(4) Zhang, S.; Wong, Y. K.; Ong, C. N.; Shen, H. M. *Curr. Med. Chem. Anticancer Agents* **2005**, *5*, 239–249.
(5) Bohlmann, F.; Jakupovic, J.; Ahmed, M.; Schuster, A. *Phytochemistry* **1983**, *22*, 1623–1636.
(6) Goren, N.; Ulubelen, A.; Bozok-Johansson, C.; Tahtasakal, E. *Phytochemistry* **1993**, *33*, 1157–1159.
(7) Triana, J.; Eiroa, J. L.; López, M.; Ortega, J. J.; González, A.; Bermejo, J. *Biochem. Syst. Ecol.* **2001**, *29*, 869–871.
(8) Sashida, Y.; Nakata, H.; Shimomura, H.; Kagaya, M. *Phytochemistry* **1983**, *22*, 1219–1222.
(9) Goren, N.; Woerdenbag, H. J.; Bozok-jonansson, C. *Planta Med.* **1996**, *62*, 419–422.
(10) Doskotch, R. W.; El-Feraly, F. S. *Can. J. Chem.* **1969**, *47*, 1139–1142.
(11) Konstantinopoulou, M.; Karioti, A.; Skaltsas, S.; Skaltsa, H. *J. Nat. Prod.* **2003**, *66*, 699–702.
(12) González, A. G.; Bermejo, J.; Triana, J.; López, M.; Eiroa, J. L. *Phytochemistry* **1992**, *31*, 1821–1822.
(13) Mahmoud, A. A. *Phytochemistry* **1997**, *45*, 1633–1638.
(14) Ortega, A.; López, J. C.; Maldonado, E. *Phytochemistry* **1989**, *28*, 2735–2736.
(15) Wilkomirski, B.; Kucharska, E. *Phytochemistry* **1992**, *31*, 3915–3916.
(16) Herz, W.; Bhat, S. V.; Santhanam, P. S. *Phytochemistry* **1970**, *9*, 891–894.
(17) Kuropka, G.; Glombitza, K. W. *Planta Med.* **1987**, *53*, 440–442.
(18) Kamanzi, K.; Voirin, B.; Raynaud, J. *Plantes Med. Phytother.* **1983**, *17*, 52–56.
(19) Van Hereden, F. R.; Viljoen, A. M.; Van Wyk, B. E. *Fitoterapia* **2000**, *71*, 602–604.
(20) Yunusov, A. I.; Kasymov, S. Z.; Sidyakin, G. P. *Khim. Prir. Soedinenii* **1976**, *2*, 261–262.
(21) Bohlmann, F.; Gupta, R. K.; Jakupovic, J.; King, R. M.; Robinson, H. *Phytochemistry* **1981**, *20*, 1635–1637.
(22) Bohlmann, F.; Schmeda-Hirschmann, G.; Jakupovic, J.; King, R. M.; Robinson, H. *Phytochemistry* **1984**, *23*, 1989–1993.
(23) Ortega, A.; Del, C.; López, J.; Maldonado, E. *Phytochemistry* **1989**, *28*, 2735–2736.
(24) Schmidt, T. J.; Lyss, G.; Pahl, H. L.; Merfort, I. *Bioorg. Med. Chem.* **1999**, *7*, 2849–2855.

NP800474V

Author Proof

MOLECULAR CARCINOGENESIS 9999:1–12 (2010)

5,7,3′-Trihydroxy-3,4′-Dimethoxyflavone-Induced Cell Death in Human Leukemia Cells Is Dependent on Caspases and Activates the MAPK Pathway[Q1]

Fernando Torres,[1,2] José Quintana,[1,2] and Francisco Estévez[1,2]*

[1]Department[Q3] *of Biochemistry and Molecular Biology, University of Las Palmas de Gran Canaria, Las Palmas de Gran Canaria, Spain*
[2]*Instituto Canario de Investigación del Cáncer, Las Palmas de Gran Canaria, Spain*

Flavonoids are polyphenolic compounds which display a vast array of biological activities and are promising anticancer agents. In this study we investigated the effect of 5,7,3′-trihydroxy-3,4′-dimethoxyflavone (THDF) on viability of nine human tumor cell lines and found that it was highly cytotoxic against leukemia cells. THDF induced G_2–M phase cell-cycle arrest and apoptosis through a caspase-dependent mechanism involving cytochrome *c* release, processing of multiple caspases (caspase-3, -6, -7, and -9) and cleavage of poly(ADP-ribose) polymerase. Overexpression of the protective mitochondrial proteins Bcl-2 and Bcl-x_L conferred partial resistance to THDF-induced apoptosis. This flavonoid induced the phosphorylation of members of the mitogen-activated protein kinases (MAPKs) family and cell death was attenuated by inhibition of c-*jun* N-terminal kinases/stress-activated protein kinases (JNK/SAPK) and of extracellular signal-regulated kinases (ERK) 1/2. In the present study we report that THDF-induced cell death is mediated by an intrinsic dependent apoptotic event involving mitochondria and MAPKs, and through a mechanism independent of the generation of reactive oxygen species. The results suggest that THDF could be useful in the development of novel anticancer agents. © 2010 Wiley-Liss, Inc.

Key words: apoptosis; flavonoids; cell-cycle arrest; mitogen-activated protein kinases; c-*jun* N-terminal kinases; extracellular signal-regulated kinases

INTRODUCTION

Flavonoids are phenylbenzo-γ-pyrones derivatives which display a vast array of biological activities and are among the most promising anticancer agents [1]. One of the best-studied bioflavonoids is quercetin (3,3′,4′,5,7-pentahydroxyflavone). This compound potentiates the cytotoxic action of 1-β-D-arabinofuranosylcytosine [2] and inhibits cell invasion and induces apoptosis [3]. Many anticancer compounds have been shown to cause the death of sensitive cells through the induction of apoptosis. Essential executioners of apoptosis are the caspases, a family of conserved cysteine aspartate-specific proteases [4], generally synthesized as inactive proenzymes or zymogens which are activated by proteolytic cleavage. In general, two major pathways for apoptosis have been described [5]. In the extrinsic (or death receptor) pathway, apoptosis is mediated by death receptors (such as tumor necrosis factor or Fas receptors) [6] and involves caspase-8 activation, while in the intrinsic (or mitochondrial) pathway diverse proapoptotic signals lead to the release of cytochrome *c* from mitochondria to cytoplasm that promotes the assembly of apoptosome and caspase-9 activation. Since caspase-3 is responsible for cleaving specific cellular proteins during apoptosis [7] both pathways converge to this level and therefore caspase-8 and -9 cleave and activate the proenzyme. A great number of studies indicate that apoptosis can also be mediated by the endoplasmic reticulum signaling pathway [8] and it may occur independently of caspase activation [9].

Mitogen-activated protein kinases (MAPKs) are a family of serine/threonine protein kinases that are activated by mitogens or stress conditions and play an essential role in a diverse array of cellular functions, including proliferation, differentiation, stress responses, and apoptosis [10]. Mammalian

Abbreviations: MAPKs, mitogen-activated protein kinases; ERK, extracellular signal-regulated kinases; JNK, c-*jun* N-terminal kinases; SAPK, stress-activated protein kinase; $p38^{MAPK}$, p38 mitogen-activated protein kinases; THDF, 5,7,3′-trihydroxy-3,4′-dimethoxyflavone; ROS, reactive oxygen species; PARP, poly(ADP-ribose) polymerase; PBMC, peripheral blood mononuclear cells; IC_{50}, 50% inhibition of cell growth; JC-1, 5,5′,6,6′-tetrachloro-1,1′,3,3′-tetraethylbenzimidazolylcarbocyanine iodide; $\Delta\Psi_m$, mitochondrial membrane potential; H_2-DCF-DA, 2′,7′-dichlorodihydrofluorescein diacetate; MEK, mitogen-activated extracellular kinases; MKPs, MAPK phosphatases.

*Correspondence to: Plaza Drs Pasteur s/n, Las Palmas de Gran Canaria 35016, Spain.

Received 11 September 2009; Revised 4 December 2009; Accepted 28 December 2009

DOI 10.1002/mc.20619

Published online 00 Month 2010 in Wiley InterScience (www.interscience.wiley.com)

© 2010 WILEY-LISS, INC.

Author Proof

MAPKs comprise three major groups, which are classified on the basis of sequence similarity, differential activation by agonists, and substrate specificity. These are the extracellular signal-regulated kinases (ERK) 1/2, the c-*jun* N-terminal kinases/stress-activated protein kinases (JNK/SAPK), and the p38 MAPKs ($p38^{MAPK}$). Activation of MAPKs requires dual phosphorylation of threonine and tyrosine residues in the catalytic domain by specific MAPK kinases (MAPKKs). ERK1/2 is predominantly activated by growth factors or mitogens leading to cell differentiation, growth, and survival. In contrast, JNK/SAPK and $p38^{MAPK}$ are preferentially activated in response to stress conditions and are often associated with apoptosis [11], although under certain conditions both kinases may induce anti-apoptotic, proliferative, and cell survival signals [12].

In a previous report, we described the cytotoxicity of 22 flavonoids in five human tumor cell lines and reported that the methylation of hydroxyl group at position C3 of quercetin yields a compound with a higher antiproliferative activity [13]. In the present study we have found that a derivative of quercetin, 3′,5,7-trihydroxy-3,4′-dimethoxyflavone (THDF), displays higher cytotoxic properties than the natural flavonoid in human leukemia cell lines and induces cell death by caspase activation which is associated with cytochrome *c* release. We have also evaluated whether the MAPK cascade and the reactive oxygen species (ROS) generation are involved in the mechanism of action.

MATERIALS AND METHODS

Reagents

THDF was from Extrasynthese (Genay Cedex, France). Antibodies for poly(ADP-ribose) polymerase (PARP), caspase-3, -8, and -9 were purchased from Stressgen (Victoria, British Columbia, Canada). Antibodies for cytochrome *c*, Bax, and caspase-7 were purchased from BD Pharmingen (San Diego, CA). Anticaspase-6 monoclonal antibody was from Medical and Biological Laboratories (Nagoya, Japan). Anti-Bcl-2 monoclonal antibody was from Santa Cruz Biotechnology (Santa Cruz, CA). Anticytochrome *c* oxidase (Cox IV) antibody was purchased from Abcam (Cambridge, UK). Anti-JNK/SAPK, antiphospho-JNK/SAPK (phospho T183 + Y185), anti-p44/42 MAPK, antiphospho-p44/p42 MAPK (T202/Y204), anti-$p38^{MAPK}$, and antiphospho-$p38^{MAPK}$ (T180/Y182) antibodies were purchased from New England BioLabs (Cell Signaling Technologies, Beverly, MA). Secondary antibodies were from GE Healthcare (Little Chalfont, UK). All other chemicals were obtained from Sigma (St. Louis, MO).

Cell Culture

The human leukemia HL-60, U937, and Jurkat cells and human SK-MEL-1 melanoma cells were grown as previously described [13–15]. Human leukemia Molt-3 cells were cultured in RPMI 1640 containing 2 mM L-glutamine supplemented with 10% (v/v) heat-inactivated fetal bovine serum. The human adenocarcinoma A549 cell line was cultured in Dulbecco's modified Eagle's medium containing 10% (v/v) heat-inactivated fetal bovine serum, 2 mM L-glutamine, 100 U/mL penicillin, 100 μg/mL streptomycin. Human peripheral blood mononuclear cells (PBMC) were isolated from heparin-anticoagulated blood of healthy volunteers by centrifugation with Ficoll-Paque Plus (GE Healthcare BioSciences AB, Uppsala, Sweden). PBMC are normal cells in a physiological G_0 state. PBMC grow in size, synthesize DNA, and eventually proliferate in the presence of phytohemagglutinin (PHA, 2 μg/mL for 48 h) [16].

HL-60 cells transfected with the pSFFV-neo plasmid (HL-60/neo) and/or pSFFV-bcl-x_L plasmid (HL-60/Bcl-x_L) (donated by Dr. Angelika Vollmar, Department of Pharmacy, Center of Drug Research, University of Munich, Germany, and which were established by Dr. K.N. Bhalla, Medical College of Georgia Cancer Center, GA) and the U937 cell line overexpressing human Bcl-2 (kindly provided by Dr. Jacqueline Bréard, INSERM U749, Faculté de Pharmacie Paris-Sud, Châtenay-Malabry, France) were cultured as described [17].

Cytotoxicity of THDF on Human Tumor Cells and Human Normal Peripheral Blood Mononuclear Cells

The cytotoxicity of THDF on human tumor and human PBMC cells was analyzed as previously described [13]. Concentrations inducing a 50% inhibition of cell growth (IC_{50}) were determined graphically for each experiment by a nonlinear regression using the curve-fitting routine of the computer software Prism™ 2.0 (GraphPad) and the equation derived by De Lean and co-workers [18]. Values are means ± SE from at least three independent experiments, each performed in triplicate.

Evaluation of Apoptosis

Fluorescent microscopy, flow cytometric analysis of propidium iodide-stained nuclei, and DNA fragmentation assay were performed as described [17]. Apoptosis was also determined by translocation of phosphatidylserine to the cell surface using an Annexin V-FITC apoptosis detection kit (BD Pharmingen) according to the manufacturer's protocol.

Analysis of DNA Fragmentation

A late biochemical hallmark of apoptosis is the fragmentation of the genomic DNA. It is an irreversible event and occurs before changes in plasma membrane permeability. DNA isolation and gel electrophoresis were performed as described previously [13].

Author Proof

Transmission Electron Microscopy (TEM)

Cells were treated with THDF for 24 h, harvested, and fixed (2.5% glutaraldehyde in 0.2 M sodium phosphate buffer, pH 7.2) for 24 h at 4°C. Then, cells were washed three times with sodium phosphate buffer, postfixed in 1% OsO_4 for 4 h at 4°C, and washed with distilled water. Cells were embedded in Epon 812 after dehydratation in ethanol. Ultrathin sections were counterstained with uranyl acetate and lead citrate before observations with a Zeiss EM 912 transmission electron microscope. Pictures were taken with a Proscan Slow-scan CCD-Camera for TEM.

Western Blot Analysis

Immunoblot analysis of caspase-9, -8, -7, -6, -3, PARP, and MAPKs was performed as previously described [17]. Release of cytochrome *c* from mitochondria was detected as described [15].

Assay of Caspase Activity

Caspase activity was performed as described previously [13].

Analysis of Mitochondrial Membrane Potential $\Delta\Psi_m$

The membrane potential was measured by FACS using the fluorochrome 5,5′,6,6′-tetrachloro-1,1′,3,3′-tetraethylbenzimidazolylcarbocyanine iodide (JC-1) as previously described [17]. Cells were treated with THDF (10 μM) for different time periods and incubated with the fluorescent probe JC-1 (10 μM) for the last 30 min. JC-1 exists as a monomer at low values of $\Delta\Psi_m$ (green fluorescence; emission, 527 nm) while it forms aggregates at high $\Delta\Psi_m$ (orange fluorescence; emission, 590 nm). Flow cytometric analysis was carried out using a Coulter EPICS^{TM} cytometer (Beckman Coulter, Miami, FL).

Intracellular Reactive Oxygen Species (ROS) Determination

Intracellular ROS were detected by flow cytometry using 2′,7′-dichlorodihydrofluorescein diacetate (H_2-DCF-DA). This compound is deacetylated by intracellular esterase and converted to nonfluorescent 2′,7′-dichlorodihydrofluorescein (H_2-DCF), which is rapidly oxidized to the highly fluorescent compound 2′,7′-dichlorofluorescein (DCF) in the presence of ROS (especially hydrogen peroxide and lipid hydroperoxides). HL-60 cells were treated with or without THDF for 15–120 min, and then H_2-DCF-DA (8 μM) was added and incubated for 30 min. The cells were then washed and resuspended in 1 mL phosphate-buffered saline (PBS). Flow cytometric analysis was carried out within 1 h using a Coulter EPICS^{TM} cytometer. In each study, 10 000 cells were counted. Fluorescence of DCF was detected at an excitation and emission wavelengths of 488 and 530 nm, respectively.

Statistical Analysis

Statistical significance of differences between means of control and treated samples were calculated using Student's *t*-test. *P*-values of <0.05 were considered significant.

RESULTS

THDF Inhibits Cell Viability of Human Tumor Cell Lines and Lack of Cytotoxicity on Normal Human Lymphocytes

In the present study, we examined the effects of THDF (Figure 1A) on the growth of nine human tumor cell lines and found that it displays strong cytotoxic properties (Table 1). Human myeloid (HL-60 and U937) and lymphoid (Jurkat and Molt-3) leukemia cell lines and cell lines overexpressing Bcl-2 (U937/Bcl-2) and Bcl-x_L proteins (HL-60/Bcl-x_L) were, in general, the most sensitive to THDF-induced cytotoxicity while human adenocarcinoma A549 ($IC_{50} = 10.8 \pm 2.4$ μM) and human melanoma SK-MEL-1 cell lines ($IC_{50} = 13.9 \pm 2.5$ μM) were more resistant (Figure 1B). Control experiments with normal quiescent lymphocytes showed no appreciable toxicity up to 10 μM THDF for 24 h (Figure 1C). Since HL-60 and U937 cells were especially sensitive to the antiproliferative effect of THDF, further studies were performed on these cell lines.

THDF Induces G_2–M Arrest and Apoptosis on Human Myeloid Leukemia Cells

To determine whether THDF-induced cytotoxicity involves alterations in cell-cycle progression, flow cytometric analyses were included in this study. As shown (Table 2, Figure 2A) THDF caused a significant G_2–M arrest at the expense of G_1 phase cell population at 6–12 h of treatment on both cell lines and this effect invariably diminished with increased treatment time (24 h) in HL-60 cells. The percentage of cells in G_2–M phase increased from ~25% in control cells to 44% after treatment with THDF for 12 h. Moreover, the percentage of hypodiploid cells (i.e., sub-G_1 fraction) increased about fivefold in THDF-treated HL-60 compared with control cells after 24 h exposure at a concentration as low as 1 μM (Figure 2A). THDF showed a similar trend in G_2–M arrest in U937 cells and this effect was sustained until 24 h. Maximal levels of apoptotic cells (approximately fivefold increase with respect to control) were observed at 12 h with 3 μM THDF in U937 or at 24 h with 1 μM THDF in HL-60 (Table 2). Taken together, these results indicate that THDF induces cell-cycle arrest in the G_2–M phase and apoptosis on human myeloid leukemia HL-60 and U937 cells.

When cells were incubated with THDF, the DNA showed the typical fragmentation patterns formed by internucleosomal hydrolysis of chromatin thus confirming the apoptosis-inducing effects (Figure 2B). Fluorescence microscopy experiments on HL-60 and U937 cells clearly demonstrate an increase of

Author Proof

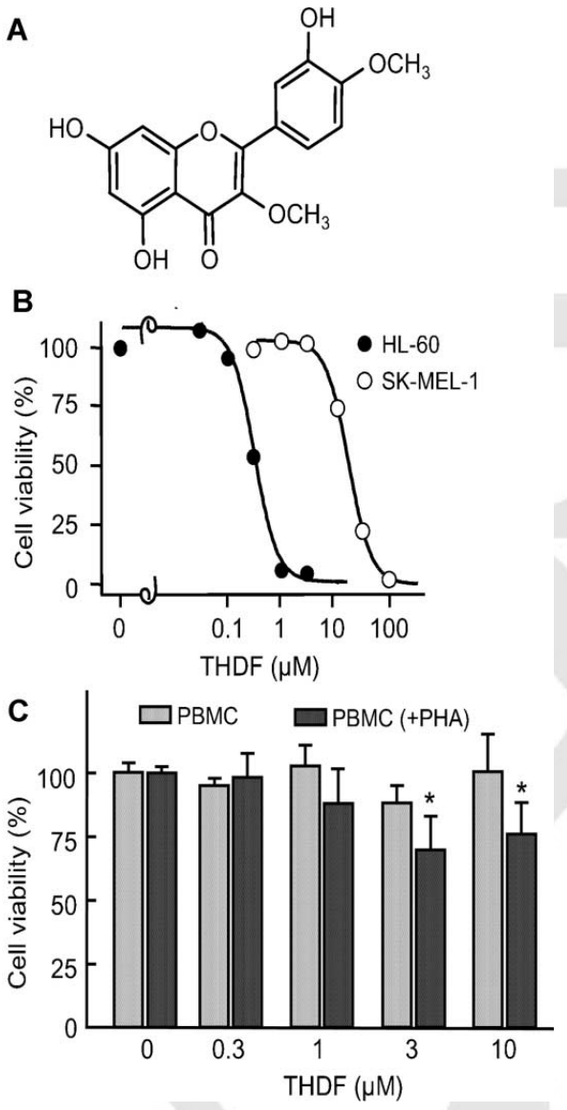

Figure 1. (A) Chemical structure of THDF. (B) Effect of THDF on human HL-60 and SK-MEL-1 cell viability. Cells were cultured in the presence of the indicated concentrations of THDF for 72 h, and thereafter cell viability was determined by the 3-(4,5-dimethyl-2-thyazolyl-)-2,5-diphenyl-2*H*-tetrazolium bromide assay (MTT). The results of a representative experiment are shown. Each point represents the mean of triplicate determinations. (C) Effect of THDF on proliferation of normal PBMCs. Quiescent and phytohemagglutinin-activated healthy human PBMC were cultured in presence of the indicated concentrations of THDF for 24 h. Values represent mean ± SE of three independent experiments each performed in triplicate. $*P < 0.05$, significantly different from untreated control.

condensed and fragmented chromatin, which is typical of apoptotic cells (Figure 2C). A significant number of apoptotic cells was already detected at 12 h of treatment and increased in a time-dependent manner (results not shown). THDF treatment also led to the exposure of phosphatidylserine on the outside of the plasma membrane as detected by Annexin V-FITC staining in both cell lines (Figure 2D). We also used transmission electronic microscopy to visualize the apoptosis-associated ultrastructural changes. Cells with fragmented and/or condensed nuclei characteristic of apoptotic cells were clearly visible as shown in Figure 2E. THDF-treated cells showed a dense perinuclear condensation and also abundant vacuoles.

Effects of THDF on Mitochondrial Cytochrome *c* Release and on Caspases and PARP Processing

To determine whether caspases were involved in the response of the cells to THDF, we examined whether this flavonoid induces proteolytic processing of caspases and PARP cleavage. To this end, HL-60 and U937 cells were treated with 3 μM THDF for various time durations or with increasing concentrations of this compound, and initiators (caspase-9 and -8) and executioners (caspase-7, -6, and -3) caspases were determined by Western blot using antibodies that bind both the proenzyme (caspase precursors) and the cleaved caspases. We used concentrations 3- to 10-fold higher than the antiproliferative IC_{50} values in order to identify the primary targets and early mechanism of action of THDF. The results indicate that THDF stimulates the cleavage of inactive procaspase-9 to the active 35–37 kDa fragment. This was clearly visible at 12 h of treatment in both cell lines. We also evaluated the potential contribution of the extrinsic apoptotic pathway. As shown in Figure 3A, THDF did not induce a significant procaspase-8 processing. Hydrolysis of this zymogen was only detected at longer incubation times (24 h) for treatments with the highest concentration (10 μM).

As caspase-3 is the main effector caspase we also analyzed whether THDF induces hydrolysis of the zymogen. Cleavage of procaspase-3 into 17–19 kDa fragments significantly increased in THDF-treated cells (Figure 3A) and in accordance with this result, PARP protein which is normally involved in DNA repair and a known substrate for caspase-3, was effectively hydrolyzed to the 85 kDa fragment. As shown in Figure 3A, concentrations of THDF as low as 3 μM significantly promote procaspase-7, -6, and -3 hydrolysis. Protein loading was checked by reprobing the membranes with β-actin antibody.

Release of cytochrome *c* from mitochondria to cytosol is a central event in apoptotic signaling. To determine whether THDF-induced apoptosis involves cytochrome *c* release, cytosolic and mitochondrial preparations were analyzed by immunoblotting on HL-60 and U937 cell lines. The results show a significant increase in the amount of cytochrome *c* in the cytosol, which was correlated with a decrease in the mitochondria, in a concentration- and time-dependent manner (Figure 3A).

The intrinsic pathway is controlled by the Bcl-2 protein family. Bcl-2 itself and Bax inhibits and promotes apoptosis, respectively. We also investi-

Author Proof

Table 1. Effects of THDF on the Growth of Human Tumor Cell Lines

IC_{50} (μM)								
HL-60	HL-60/neo	HL-60/Bcl-x_L	U-937	U-937/Bcl-2	Jurkat	Molt-3	SK-MEL-1	A-549
0.30 ± 0.02	0.59 ± 0.02	3.0 ± 1.2	1.4 ± 0.5	4.3 ± 1.7	0.43 ± 0.05	0.27 ± 0.01	13.9 ± 2.5	10.8 ± 2.4

Cells were cultured for 72 h and the IC_{50} values were calculated as described in the Materials and Methods Section. The data shown represent the means ± SE of 3–5 independent experiments with three determinations in each.

gated the expression of these proteins in THDF-treated cells. Although, there were no clear changes in Bcl-2 levels, cleavage of this antiapoptotic factor was observed in both cell lines (Figure 3A, central panel). Bax may play a crucial role in the apoptotic process via a number of different mechanisms. For instance, Bcl-2 or Bcl-x_L counteracts the effect of Bax by forming heterodimers with it. Previous studies have shown that the ratio between proapoptotic and antiapoptotic Bcl-2 families plays a major role in determining susceptibility of cells to apoptotic stimuli [19,20]. When HL-60 and U937 cells were exposed to THDF a clear decrease in Bax levels in the cytosolic fraction was observed, but there were no significant changes in the mitochondrial fraction in the assayed conditions (Figure 3A, central panel).

As processing does not always correlate with activity, enzymatic activity of caspase-3-like protease (caspase-3/7) was also investigated in extracts of HL-60 cells treated during different time durations or with different concentrations of THDF. Cell lysates were assayed for cleavage of the tetrapeptide substrate DEVD-*p*NA as specific substrate for caspase-3/7. As shown (Figure 3B), induction of caspase-3 like activity was significantly detectable after 12 h of treatment and increased with the incubation time. Dose–response experiments show that a low concentration (1 μM) of THDF was sufficient to induce caspase-3/7 activation (Figure 3C). To confirm that THDF-triggered apoptosis requires the activation of caspases, cells were pretreated with the broad-spectrum caspase inhibitor z-VAD-fmk. The results (Figure 3D) show that apoptosis was almost completely suppressed in the presence of the inhibitor, which suggests that THDF induces cytotoxicity by a caspase-dependent mechanism.

Overexpression of the Mitochondrial Proteins Bcl-2 and Bcl-x_L Confers Partial Resistance to THDF-Induced Apoptosis

Since Bcl-2 and Bcl-x_L are known to inhibit apoptosis by regulating mitochondrial membrane potential and cytochrome *c* release needed for the activation of caspase-9, we decided to clarify whether these proteins protect cells against the effects of THDF. To this end we used cell lines overexpressing Bcl-x_L (HL-60/Bcl-x_L) or Bcl-2 (U937/Bcl-2). Our results indicate that the overexpression of both factors partially blocked THDF-induced cell death and apoptosis, as determined by the 3-(4,5-dimethyl-2-thyazolyl-)-2,5-diphenyl-2*H*-tetrazolium bromide (MTT) assay (Table 1) and flow cytometry experiments (Figure 3E).

The dissipation of the electrochemical gradient ($\Delta\Psi_m$) created by the proteins of the respiratory chain located on the inner mitochondrial membrane

Table 2. Effect of Different Durations of Treatment With THDF on Cell-Cycle Phase Distribution of HL-60 and U937 Cells

		% Sub-G_1	% G_1	% S	% G_2–M
HL-60 (h)					
6	Control	5.7 ± 0.6	40.6 ± 2.4	21.6 ± 0.8	33.3 ± 3.6
	THDF	6.3 ± 2.2	28.4 ± 4.5*	23.1 ± 2.2	42.8 ± 4.8*
12	Control	4.3 ± 1.5	46.6 ± 3.3	24.9 ± 2.6	25.1 ± 3.1
	THDF	11.3 ± 3.4*	22.5 ± 2.5*	16.5 ± 5.1	44.3 ± 0.5*
24	Control	4.4 ± 1.8	46.8 ± 3.1	23.9 ± 2.3	25.4 ± 2.9
	THDF	21.5 ± 3.8*	30.6 ± 1.7*	17.8 ± 3.9*	26.5 ± 1.0*
U937 (h)					
6	Control	4.9 ± 1.9	48.8 ± 3.6	20.4 ± 1.5	24.1 ± 4.6
	THDF	5.0 ± 1.3	36.5 ± 2.1*	22.6 ± 0.8	33.4 ± 5.3*
12	Control	4.8 ± 1.1	51.8 ± 5.2	20.3 ± 2.5	22.4 ± 3.0
	THDF	23.6 ± 4.8*	20.5 ± 5.5*	10.1 ± 3.6	38.6 ± 8.7*
24	Control	5.4 ± 1.5	51.3 ± 3.6	19.7 ± 2.4	22.6 ± 2.1
	THDF	21.4 ± 0.6*	20.9 ± 0.6*	14.6 ± 4.6	35.8 ± 3.2*

Cells were cultured with 3 μM THDF for the indicated period of times and the cell-cycle phase distribution was determined by flow cytometry. The values are means ± SE of two independent experiments with two determinations in each. Asterisks indicate a significant difference ($P < 0.05$) compared with the corresponding controls.

Author Proof

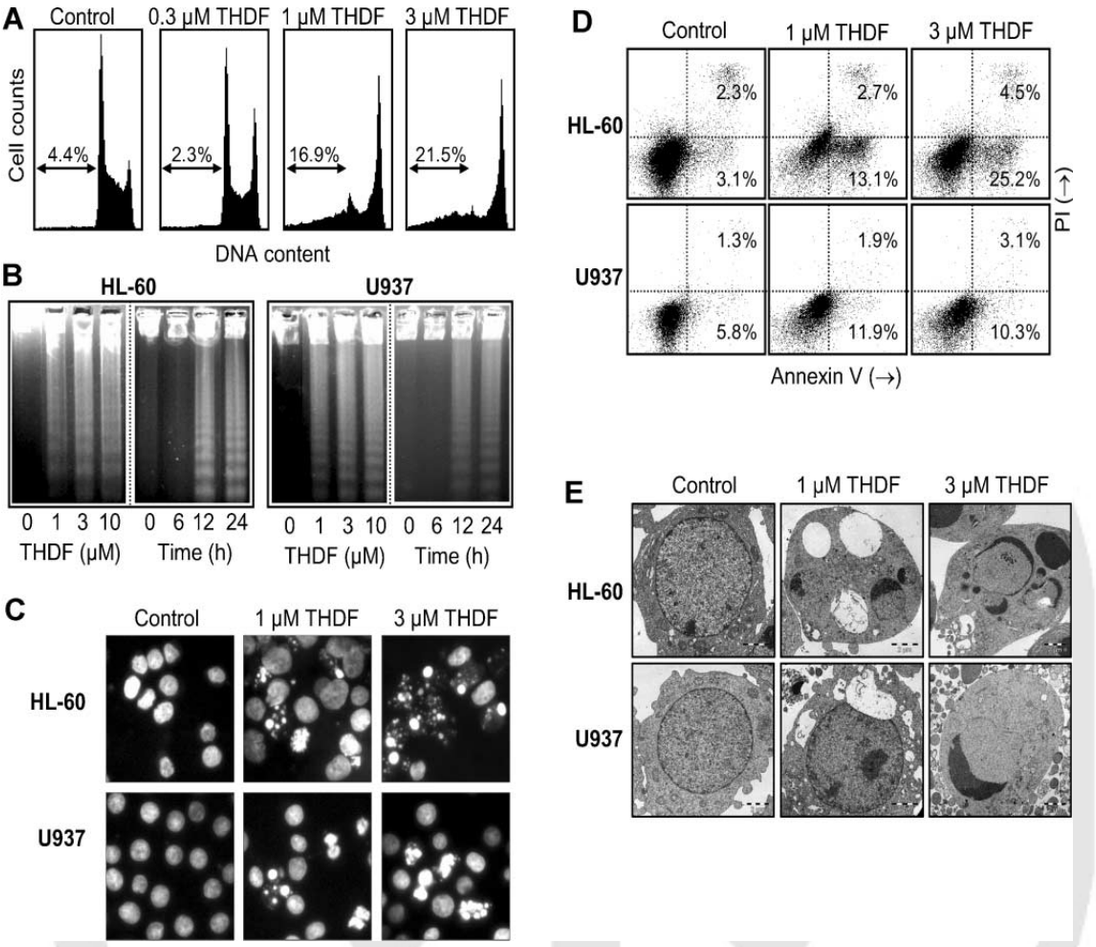

Figure 2. Effects of THDF on apoptosis on human myeloid leukemia HL-60 and U937 cells. (A) HL-60 cells were incubated in the presence of the indicated concentrations of THDF and subjected to flow cytometric analysis. Hypodiploid cells (apoptotic cells) are shown in region marked with an arrow. (B) Dose–response and kinetics of DNA fragmentation in response to THDF. HL-60 and U937 cells were incubated in the presence of the indicated concentrations of THDF for 24 h or were treated with 3 μM THDF and harvested at the indicated times and genomic DNA was extracted, separated on an agarose gel, and visualized under UV light by ethidium bromide staining. (C) Photomicrographs of representative fields of HL-60 and U937 cells stained with Hoechst 33258 to evaluate nuclear chromatin condensation (i.e., apoptosis) after treatment with THDF. (D) FACS analysis of Annexin V-FITC and propidium iodide (PI)-stained HL-60 and U937 cells after 24 h of treatment with the indicated concentrations of THDF. Cells appearing in the lower right quadrant show positive Annexin V-FITC staining, which indicates phosphatidylserine translocation to the cell surface, and negative PI staining, which demonstrates intact cell membranes, both features of early apoptosis. Cells in the top right quadrant are double positive for Annexin V-FITC and PI and are undergoing necrosis. Data are representative of three separate experiments. (E) Transmission electron micrographs of HL-60 and U937 cells after 24 h incubation with the indicated concentrations of THDF.

Figure 3. Evaluation of apoptotic pathways triggered by THDF on human leukemia cells. (A) HL-60 and U937 cells were incubated in the presence of 3 μM THDF for the indicated times or incubated with the indicated concentrations of THDF for 24 h. Cell lysates were assayed by immunoblotting. β-Actin and Cox IV (cytochrome c oxidase) were used as loading controls in cytosol and mitochondria, respectively. The cytosolic and mitochondria-enriched fractions were prepared and Western blot analyses were performed as described in the Materials and Methods Section. (B) HL-60 cells were treated with 3 μM THDF and harvested at the indicated times. Cell lysates were assayed for caspase-3 and -7 activity using the DEVD-*p*NA colorimetric substrates. Results are expressed as factorial increases in caspase activity compared with the control. Values represent means ± SE of two independent experiments each performed in triplicate. (C) Dose–response experiments of caspase-3/7 activation in response to THDF. HL-60 cells were treated with the indicated concentrations of THDF and cell lysates were assayed for caspase-3 and -7 activities as above. (D) HL-60 and U937 cells were pretreated with z-VAD-fmk (100 μM) before the addition of THDF (3 μM) for 24 h, and apoptotic cells were analyzed by flow cytometry after staining with propidium iodide. Values represent the means ± SE of three independent experiments each performed in triplicate. $^{*}P < 0.05$, significantly different from untreated control. $^{\#}P < 0.05$, significantly different from THDF treatment alone. (E) Effect of THDF on cells overexpressing Bcl-x_L and Bcl-2. Comparison of THDF treatment in HL-60/neo and HL-60/Bcl-x_L cells, and also in U937 and U937/Bcl-2 cells. The percentage of hypodiploid cells was determined by flow cytometry at 24 h in the absence or presence of 3 μM THDF. Values represent means ± SE of three different experiments. $^{*}P < 0.05$, significantly different from untreated control. (F) THDF reduces the mitochondrial membrane potential ($\Delta\Psi_m$). HL-60 and U937 cells were treated with 1 μM THDF and harvested at indicated times and $\Delta\Psi_m$ analyzed with JC-1. The intensity of JC-1 fluorescence was analyzed by flow cytometry as described in the Materials and Methods Section. Similar results were obtained in two separate experiments each performed in triplicate.

Author Proof

is also a key event in mitochondria-controlled apoptotic pathways. To examine whether a disruption of the $\Delta\Psi_m$ is required for the release of cytochrome *c*, cells were treated with THDF for different times (6, 12, and 24 h), stained with JC-1 and analyzed by flow cytometry. The results (Figure 3F) indicate that $\Delta\Psi_m$ dropped at 12 h of treatment, which suggests that the disruption of the

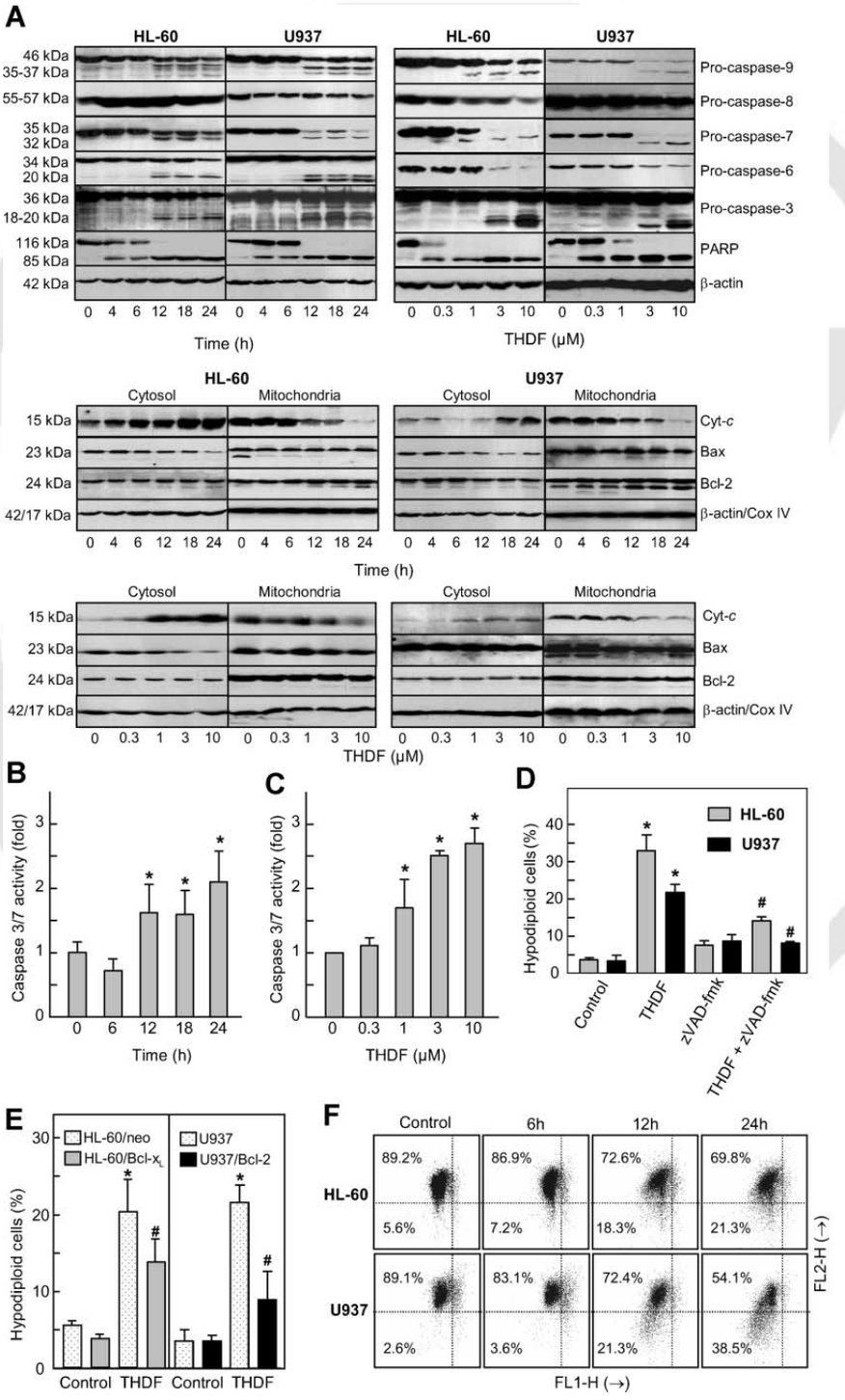

Figure 3.

Author Proof

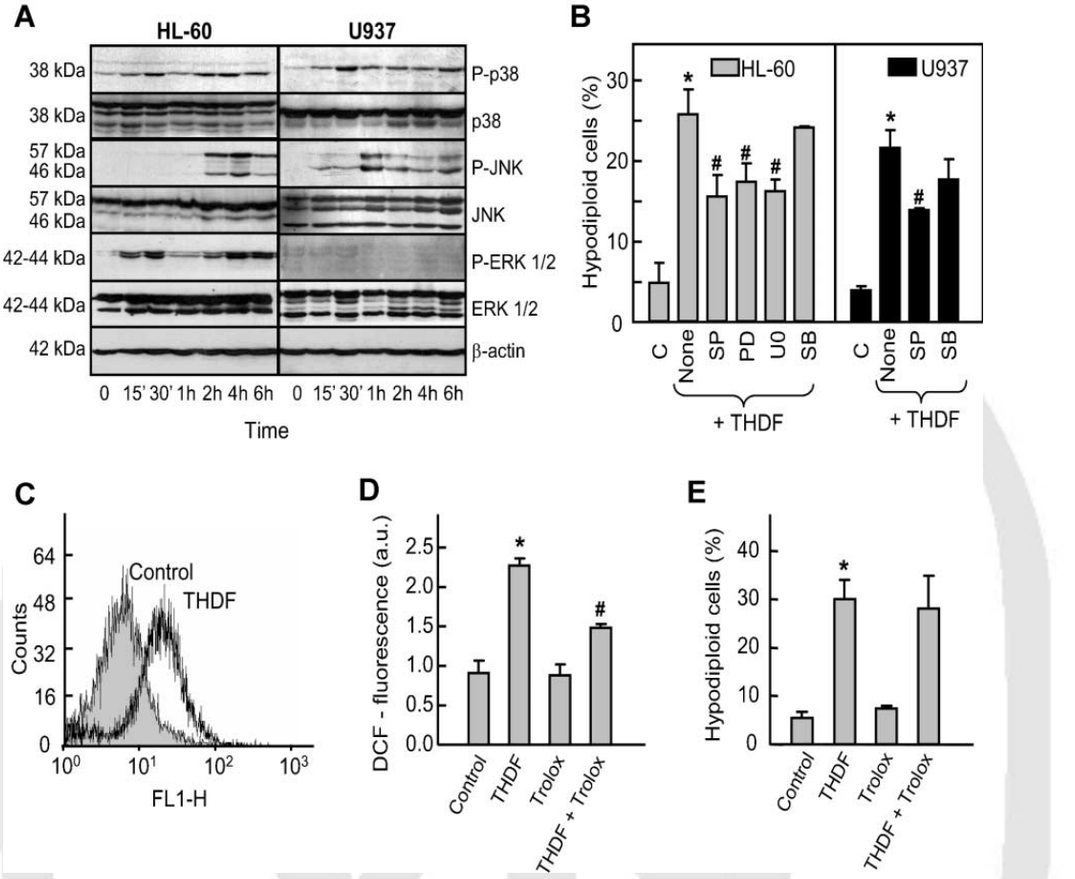

Figure 4. THDF induces phosphorylation of MAPKs and ROS generation. (A) Representative Western blots show the time-dependent phosphorylation of $p38^{MAPK}$, JNK/SAPK, and ERK1/2 by THDF. HL-60 and U937 cells were incubated with THDF for the indicated time points. Protein extracts were prepared and analyzed on Western blots probed with specific antibodies to ascertain the phosphorylation of MAPKs. Membranes were stripped and reprobed with total $p38^{MAPK}$, JNK/SAPK, ERK1/2, and β-actin antibodies as loading controls. (B) Cells were preincubated with SP600125 (SP, 10 μM), PD98059 (PD, 10 μM), U0126 (U0, 10 μM), and SB203580 (SB, 2 μM) for 1 h and then treated with THDF. Apoptosis was quantified by flow cytometry and bars represent the means ± SE of three independent experiments each performed in triplicate. (C) THDF increases ROS generation. HL-60 cells were treated with 10 μM THDF for 1 h and the fluorescence of oxidized H_2-DCF was determined by flow cytometry. Similar results were obtained from three independent experiments. (D) Cells were pretreated with Trolox (2 mM) for 1 h and then incubated with THDF for 24 h and intracellular ROS levels were determined as above. (E) Cells were pretreated with Trolox and then exposed to THDF (3 μM) for 24 h. Hypodiploid cells were determined by flow cytometry. Values represent means ± SE of three independent experiments each performed in triplicate. $^{*}P < 0.05$, significantly different from untreated control. $^{\#}P < 0.05$, significantly different from THDF treatment alone.

mitochondrial membrane potential is associated in THDF-induced apoptosis.

THDF Activates Mitogen-Activated Protein Kinases (MAPKs)

In view of evidence that the MAPKs play a critical role in cell fate, the effects of THDF on the activation of these signaling pathways were examined. As shown (Figure 4A) this compound leads to phosphorylation of JNK/SAPK, p38 MAPKs ($p38^{MAPK}$) on HL-60 and U937, while phosphorylation of ERK1/2 was only observed in HL-60. Phosphorylation of $p38^{MAPK}$ was detected 15 min after THDF addition and remained elevated for at least 6 h (Figure 4A). However, the activation of JNK/SAPK was not observed until 1 and 2 h in U937 and HL-60 cells, respectively, under the same experimental conditions (Figure 4A). The level of phosphorylated ERK1/2 increased after 15 min and returned to the control level at 1 h (initial peak). Two hours after THDF addition, the levels of phosphorylated ERK1/2 increased again for at least 6 h (Figure 4A). These results indicate that the ERK1/2 pathway is activated rapidly in response to THDF in HL-60 cells, and that this activation occurs in a biphasic manner. Therefore, THDF leads to activation of JNK/SAPK, $p38^{MAPK}$, and ERK1/2 following different kinetics. It is important to note that the changes in the phosphorylation state of MAPKs were only investigated until 6 h after exposure to THDF. Taking into account that THDF induces significant cell death after 12 h, we analyzed the changes in the phosphorylation state of MAPKs

Author Proof

prior to this in order to evaluate the early changes caused by THDF rather nonspecific changes associated with apoptosis. To determine whether the phosphorylation of MAPKs plays a key role in THDF-induced apoptosis, we examined the effects of specific inhibitors. Therefore, pretreatment of cells with SB203580 (2 μM) did not alter significantly the rate of THDF-mediated apoptosis (Figure 4B), which suggest that $p38^{MAPK}$ activation is not involved. However, preincubation with the specific JNK/SAPK inhibitor SP600125 (10 μM) partially blocked THDF-mediated apoptosis in both cell lines.

We also investigated the putative impact of ERK1/2 on the signal transduction pathway leading to THDF-mediated cell death. For this purpose, we used specific mitogen-activated extracellular kinase 1/2 (MEK1/2) inhibitors in order to block the activation of ERK1/2. The results indicate that PD98059 and U0126 significantly attenuated THDF-induced cell death (Figure 4B).

THDF Increases Intracellular ROS Levels

Generation of intracellular ROS is considered one of the key mediators of apoptotic signaling for the most antitumoral agents. Therefore, the redox status of HL-60 cells was monitored by the oxidation-sensitive fluorescent dye H_2-DCF-DA. The results show a fast generation of ROS after 15 min (results not shown) of treatment with THDF, although the highest levels (~2.2-fold increase compared with control) were not reached until 1 h (Figure 4C). For comparison, exposure to H_2O_2 (100 μM) was associated with a quick increase in ROS levels (5 min) that decreased after 1 h of treatment (results not shown). We next investigated whether oxidative stress is essential for THDF-mediated apoptosis. To explore this possibility cells were pretreated with different antioxidants, including trolox (2 mM), the glutathione precursor *N*-acetyl-L-cysteine (NAC, 10 mM), α-tocopherol (vitamin E, 25 μM), the inhibitor of xanthine oxidase allopurinol (100 μM), ascorbic acid (vitamin C, 100 μM), and the ROS degrading enzymes catalase (400 U/mL) and superoxide dismutase (SOD, 400 U/mL). Trolox was the only antioxidant in decreasing the generation of ROS, but it was unable to block cell death (Figure 4D and E). These findings suggest that THDF-induced apoptosis is independent of ROS generation.

DISCUSSION

While there are effective treatments for acute lymphocytic leukemia and for chronic myelogenous leukemia, more effective treatments for other forms of acute leukemia are needed. Polyphenolic compounds are of great current interest due to their possible anticancer activities [1]. In previous studies with naturally occurring and semisynthetic phenylbenzo-γ-pyrones, we showed that methylation of hydroxyl group at position C3 of quercetin yields a compound with a higher antiproliferative activity in several cancer cell lines [13]. We have also demonstrated that betuletol 3-methyl ether, a natural flavonoid, is a potent inhibitor of proliferation which displays high cytotoxic activity on human myeloid leukemia HL-60 cells [13].

In this study we have specifically selected an analog of quercetin 3-methyl ether, THDF, which contains an additional methoxyl group on position 4′ of the phenylbenzo-γ-pyrone core and evaluated its potential cytotoxic properties using nine tumor cell lines. Interestingly, we found that THDF displays cytotoxic properties in a cell-type specific manner. Human leukemia cells (HL-60, U937, Molt-3, and Jurkat) were highly sensitive to THDF cytotoxicity while SK-MEL-1 and A549 cells were more resistant than hematopoietic cells. Moreover, dose–response studies revealed that PBMC were more resistant to THDF than PBMC treated with PHA. Cell-cycle analysis showed that inhibition of cell viability by THDF was caused by a significant cell-cycle arrest at the G_2–M phase, accompanied by an increase in sub-G_1 fraction and phosphatidylserine externalization, indicating apoptotic cell death. Similar results were recently reported by the semisynthetic quercetin 3-methyl ether tetracetate in human leukemia cells [15], although the potency of THDF was the highest, both in arresting the cells at the G_2–M phase and as an apoptotic inducer. The arrest of cells in the G_2–M phase of the cell cycle induced by THDF might be explained by the inhibition of microtubule formation or by changes in the expression and/or activity of G_2–M cell-cycle regulators. Further studies are needed to determine the effect of this compound on these regulators such as the cyclin-dependent kinase-1, cyclin-dependent kinase inhibitor $p21^{Cip1}$, B-type cyclin isoforms, and cdc25C.

Our results also indicate that THDF's antiproliferative effect is dependent on caspase, since cell death was inhibited by the general caspase inhibitor z-VAD-fmk. The intrinsic apoptotic pathway (mitochondrial pathway) involves the release of cytochrome *c* and the assembly of apoptosome. THDF initiated redistribution of cytochrome *c* into the cytosol which was correlated with the dissipation of $\Delta\Psi_m$ and caspase-3 activation. We also observed a concentration- and time-dependent activation of caspase-9 and -3, in accordance with the cytochrome *c* release experiments, emphasizing that the intrinsic pathway plays an important role in the cell death. Moreover, THDF induced PARP cleavage, a hallmark of apoptosis that indicates activation of caspase. Although PARP is also degraded in other forms of cell death like necrosis [21], this did not seem to be the case with THDF in accordance with the fluorescence microscopy and the flow cytometric analyses of Annexin V-FITC and propidium-iodide-stained cells experiments. The results clearly demonstrate that

Author Proof

THDF also stimulates the proteolytic processing of other executioner caspases, namely caspase-7 and -6 to form activated enzymes.

There was also a clear concentration- and time-dependent decrease of the Bax levels in the cytosol in both cell lines. However, the levels of Bcl-2 in mitochondria and in cytosol remain unchanged. Therefore, it appears that the mechanism of cytotoxicity displayed by THDF is clearly different to that caused by previously described phenylbenzo-γ-pyrones, such as betuletol 3-methyl ether which induces apoptosis in HL-60 cells by a caspase-8-dependent mechanism [13]. In contrast, quercetin 3-methyl ether tetracetate, a flavonoid obtained by acetylation of the natural product quercetin 3-methyl ether, triggers apoptosis which is prevented by the general caspase inhibitor z-VAD-fmk, but not by the specific caspase-8 inhibitor [15].

Previous studies have shown that increased expression of Bcl-2 and/or Bcl-x_L is associated with chemoresistance particularly in the case of hematologic malignancies [22] and there is also poor prognostic outcome with increased Bcl-x_L expression [23]. To further investigate the role of mitochondria in THDF-induced cytotoxicity, HL-60 and U937 cells overexpressing antiapoptotic factors were included in this study. Our results indicate that HL-60/Bcl-x_L and U937/Bcl-2 were partially resistant compared with the parental cell lines, which suggest that mitochondria play an important role in THDF-induced cell death. However, the partial protection by these proteins could be explained by various mechanisms, including inactivation of Bcl-2 or the activation of the extrinsic apoptotic pathway. The fact that THDF induces cell death also in leukemic cells overexpressing Bcl-2 and Bcl-x_L could have important clinical implications for the use of this compound as potential therapeutic agent.

Recent studies suggest that MAPKs such as JNK/SAPK and $p38^{MAPK}$ play a key role in triggering apoptosis in response to various cellular stressors including oxidative stress [24]. The $p38^{MAPK}$ is activated by a variety of cellular stresses including ultraviolet light, hyperosmolarity, heat shock, and proinflammatory cytokines, and acts at early step prior to dysfuction of mitochondria and caspase activation. Moreover, $p38^{MAPK}$ is a potential upstream regulator of Bax [25] and a mediator of the G_2–M checkpoint response [26]. In this regard, activation of $p38^{MAPK}$ in mammalian cells in response to the disruption of the microtubule cytoskeleton initiates G_2–M checkpoint [27] and also previous studies have shown that flavonoids containing a 3-methoxyl group may inhibit tubulin polymerization [28]. Although our studies indicate that the activation of $p38^{MAPK}$ is not involved in THDF-induced cell death, this could be involved in the initiation of the G_2–M checkpoint through a perturbation of the microtubules.

A proapoptotic role of JNK has been described in apoptosis induced by different chemotherapeutic agents, such as vinblastine, doxorubicin, and etoposide [29,30]. Furthermore, 2-methoxyestradiol-induced apoptosis was inhibited by SP600125 in multiple myeloma cells [31]. In this study we show that THDF-induced cell death was also associated with the phosphorylation of the members of MAPKs following different kinetics and this effect was cell specific, since ERK1/2 activation was observed in HL-60 but not in U937 cells. Moreover, THDF induced a biphasic phosphorylation of ERK1/2. Although the mechanisms by which THDF caused this response is unknown, one possible explanation could be the involvement of dual specificity threonine/tyrosine MAPK phosphatases (MKPs) because some of these MKPs are encoded by genes that are transcriptionally activated by ERK1/2 and this can provide a feedback loop to downregulate ERK1/2 activity [32]. In addition, the enzymatic activity of MKPs is sensitive to reversible oxidation and inactivation due to the presence of the catalytic cysteine residue in the catalytic cleft [33]. The reversible oxidation of this cysteine residue that inactivates the phosphatase may be mediated by the generation of ROS such as H_2O_2 [34]. THDF induces ROS and might inhibit the MKPs and therefore explain the second peak of ERK activation triggered by THDF. Another possible explanation could be that the early activation of ERK1/2 may enhance the expression of potential targets, which amplify the THDF response and induce a secondary phosphorylation of ERK1/2, as previously reported for transforming growth factor-β-1 [35].

Although the JNK pathway has been shown to be closely linked to apoptosis [12], its exact role seems to depend on the cell type and stimulus. Interestingly, in HL-60 the percentage of hypodiploid cells in response to THDF was attenuated by inhibition of JNK/SAPK and by inhibition of ERK1/2, which suggests that both MAPKs are required for cell death.

Our results also indicate that the MEK1/2 inhibitors PD98059 and U0126 attenuated the apoptotic effects of THDF, which suggest that ERK1/2 is involved in cell death signals. These findings are in agreement with previous work that has shown that inhibition of MEK-ERK activation with U0126 or PD98059 abolishes quercetin-induced apoptosis in A549 cells [36]. In addition, we have recently shown that inhibition of ERK1/2 attenuates cell death induced by the acetyl derivative of the flavonoid trifolin [17] and by the naturally occurring flavonoid betuletol 3-methyl ether [37].

ROS have been implicated as second messengers in multiple signaling pathways [38]. Although the antiproliferative effect of THDF is associated with an increase in the intracellular level of ROS, this did not seem to play a pivotal role in the apoptotic process. The generation of ROS is not a general feature of

Author Proof

polyphenolic compounds containing a phenylbenzo-γ-pyrone core. In this regard, we have previously demonstrated that quercetin 3-methyl ether tetracetate induces apoptosis in human leukemia cells without ROS formation [15], while that trifolin acetate induces ROS, but they are not necessary to trigger cell death [17].

In conclusion, we describe a potent analog of quercetin that induces cytotoxicity via G_2–M phase cell-cycle arrest and apoptosis through a caspase-dependent mechanism involving mitochondria and MAPK. Our study reveals details about the signaling pathways triggered by THDF in human leukemia cells. Based on the present findings, we suggest that this flavonoid may be useful in the development of new therapeutic agents against cancer.

ACKNOWLEDGMENTS

We thank J. Estévez (Hospital Universitario Insular de Gran Canaria) for his collaboration in the Western blot assays and to the Electronic Microscopy Service of the University of Las Palmas de Gran Canaria. F.T. was supported by a research studentship from the Canary Islands Government. This work was supported by Grants from the Ministry of Education and Science of Spain and from the European Regional Development Fund (SAF2007-62536) and from the Canary Islands Government (PI 2007/045 to J.Q.).

REFERENCES

1. Middleton E, Kandaswami C, Theoharides TC. The effects of plant flavonoids on mammalian cells: Implications for inflammation, heart disease, and cancer. Pharmacol Rev 2000;52:673–751.
2. Teofili L, Pierelli L, Iovino MS, et al. The combination of quercetin and cytosine arabinoside synergistically inhibits leukemic cell growth. Leuk Res 1992;16:497–503.
3. Wei YQ, Zhao X, Kariya Y, Fukata H, Teshigawara K, Uchida A. Induction of apoptosis by quercetin: Involvement of heat shock protein. Cancer Res 1994;54:4952–4957.
4. Thornberry NA, Lazebnik Y. Caspases: Enemies within. Science 1998;281:1312–1316.
5. Boatright KM, Salvesen GS. Mechanisms of caspase activation. Curr Opin Cell Biol 2003;15:725–731.
6. Nagata S. Apoptosis by death factor. Cell 1997;88:355–365.
7. Cohen GM. Caspases: The executioners of apoptosis. Biochem J 1997;326:1–16.
8. Breckenridge DG, Germain M, Mathai JP, Nguyen M, Shore GC. Regulation of apoptosis by endoplasmic reticulum pathways. Oncogene 2003;22:8608–8618.
9. Chipuk JE, Green DR. Do inducers of apoptosis trigger caspase-independent cell death? Nat Rev Mol Cell Biol 2005; 6:268–275.
10. Raman M, Chen W, Cobb MH. Differential regulation and properties of MAPKs. Oncogene 2007;26:3100–3112.
11. Verheij M, Bose R, Lin XH, et al. Requirement for ceramide-initiated SAPK/JNK signalling in stress-induced apoptosis. Nature 1996;380:75–79.
12. Davis RJ. Signal transduction by the JNK group of MAP kinases. Cell 2000;103:239–252.
13. Rubio S, Quintana J, López M, Eiroa JL, Triana J, Estévez F. Phenylbenzopyrones structure-activity studies identify betuletol derivatives as potential antitumoral agents. Eur J Pharmacol 2006;548:9–20.
14. Torres F, Quintana J, Cabrera J, et al. Induction of G_2–M phase arrest and apoptosis by α-methylene-γ-butyrolactones in human leukaemia cells. Cancer Lett 2008;269:139–147.
15. Rubio S, Quintana J, Eiroa JL, Triana J, Estévez F. Acetyl derivative of quercetin 3-methyl ether-induced cell death in human leukemia cells is amplified by the inhibition of ERK. Carcinogenesis 2007;28:2105–2113.
16. Kaczmarek L, Calabretta B, Baserga R. Expression of cell-cycle-dependent genes in phytohemagglutinin-stimulated human lymphocytes. Proc Natl Acad Sci USA 1985;82:5375–5379.
17. Torres F, Quintana J, Díaz JG, Carmona AJ, Estévez F. Trifolin acetate-induced cell death in human leukaemia cells is dependent on caspase-6 and activates the MAPK pathway. Apoptosis 2008;13:716–728.
18. De Lean A, Munson PJ, Rodbard D. Simultaneous analysis of families of sigmoidal curves: Application to bioassay, radioligand assay, and physiological dose-response curves. Am J Physiol 1978;235:E97–E102.
19. Zhang L, Yu J, Park BH, Kinzler KW, Vogelstein B. Role of BAX in the apoptotic response to anticancer agents. Science 2000;290:989–992.
20. Perlman H, Zhang X, Chen MW, Walsh K, Buttyan R. An elevated bax/bcl-2 ratio corresponds with the onset of prostate epithelial cell apoptosis. Cell Death Differ 1999;6: 48–54.
21. Soldani C, Scovassi AI. Poly(ADP-ribose) polymerase-1 cleavage during apoptosis: An update. Apoptosis 2002;7: 321–328.
22. Amundson SA, Myers TG, Scudiero D, Kitada S, Reed JC, Fornace AJ, Jr. An informatics approach identifying markers of chemosensitivity in human cancer cell lines. Cancer Res 2000;60:6101–6110.
23. Addeo R, Caraglia M, Baldi A, et al. Prognostic role of bcl-xL and p53 in childhood acute lymphoblastic leukemia (ALL). Cancer Biol Ther 2005;4:32–38.
24. Tobiume K, Matsuzawa A, Takahashi T, et al. ASK1 is required for sustained activations of JNK/p38 MAP kinases and apoptosis. EMBO Rep 2001;2:222–228.
25. Ghatan S, Larner S, Kinoshita Y, et al. p38 MAP kinase mediates bax translocation in nitric oxide-induced apoptosis in neurons. J Cell Biol 2000;150:335–347.
26. Bulavin DV, Higashimoto Y, Popoff IJ, et al. Initiation of a G2/M checkpoint after ultraviolet radiation requires p38 kinase. Nature 2001;411:102–107.
27. Matsusaka T, Pines J. Chfr acts with the p38 stress kinases to block entry to mitosis in mammalian cells. J Cell Biol 2004; 166:507–516.
28. Beutler JA, Hamel E, Vlietinck AJ, et al. Structure-activity requirements for flavone cytotoxicity and binding to tubulin. J Med Chem 1998;41:2333–2338.
29. Brantley-Finley C, Lyle CS, Du L, et al. The JNK, ERK and p53 pathways play distinct roles in apoptosis mediated by the antitumor agents vinblastine, doxorubicin, and etoposide. Biochem Pharmacol 2003;66:459–469.
30. Mingo-Sion AM, Marietta PM, Koller E, Wolf DM, Van Den Berg CL. Inhibition of JNK reduces G2/M transit independent of p53, leading to endoreduplication, decreased proliferation, and apoptosis in breast cancer cells. Oncogene 2004; 23:596–604.
31. Chauhan D, Li G. JNK-dependent release of mitochondrial protein, Smac, during apoptosis in multiple myeloma (MM) cells. J Biol Chem 2003;278:17593–17596.
32. Owens DM, Keyse SM. Differential regulation of MAP kinase signalling by dual-specificity protein phosphatases. Oncogene 2007;26:3203–3213.
33. Kamata H, Honda S, Maeda S, Chang L, Hirata H, Karin M. Reactive oxygen species promote TNFα-induced death and sustained JNK activation by inhibiting MAP kinase phosphatases. Cell 2005;120:649–661.
34. Tonks NK. Redox redux: Revisiting PTPs and the control of cell signaling. Cell 2005;121:667–670.